

Fall 2003

# Synthetic, structural, and stability studies of metal complexes of cross -bridged tetraamine macrocycles

Weijun Niu

*University of New Hampshire, Durham*

Follow this and additional works at: <https://scholars.unh.edu/dissertation>

---

## Recommended Citation

Niu, Weijun, "Synthetic, structural, and stability studies of metal complexes of cross -bridged tetraamine macrocycles" (2003). *Doctoral Dissertations*. 182.

<https://scholars.unh.edu/dissertation/182>

This Dissertation is brought to you for free and open access by the Student Scholarship at University of New Hampshire Scholars' Repository. It has been accepted for inclusion in Doctoral Dissertations by an authorized administrator of University of New Hampshire Scholars' Repository. For more information, please contact [nicole.hentz@unh.edu](mailto:nicole.hentz@unh.edu).

**SYNTHETIC, STRUCTURAL, AND STABILITY STUDIES OF  
METAL COMPLEXES OF CROSS-BRIDGED TETRAAMINE  
MACROCYCLES**

**BY**

**WEIJUN NIU**

**B.S., Hangzhou Teachers College, 1992  
M.S., Hangzhou University, 1995**

**DISSERTATION**

**Submitted to the University of New Hampshire  
In Partial Fulfillment of  
the Requirements for the Degree of**

**Doctor of Philosophy**

**in**

**Chemistry**

**SEPTEMBER, 2003**

UMI Number: 3097788

**UMI**<sup>®</sup>

---

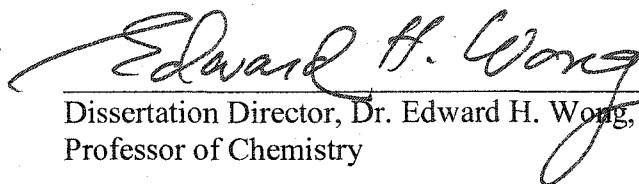
UMI Microform 3097788

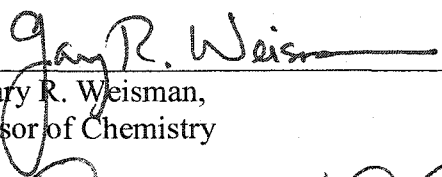
Copyright 2003 by ProQuest Information and Learning Company.

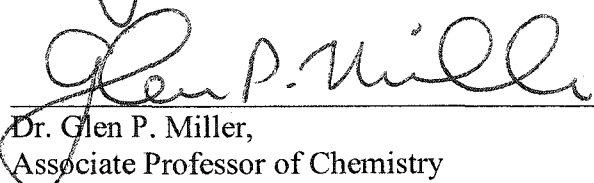
All rights reserved. This microform edition is protected against  
unauthorized copying under Title 17, United States Code.


ProQuest Information and Learning Company  
300 North Zeeb Road  
P.O. Box 1346  
Ann Arbor, MI 48106-1346

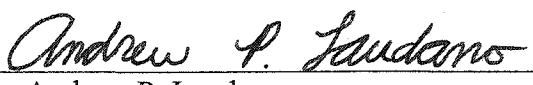
This dissertation has been examined and approved.

  
Dissertation Director, Dr. Edward H. Wong,  
Professor of Chemistry

  
Dr. Gary R. Weisman,  
Professor of Chemistry

  
Dr. Glen P. Miller,  
Associate Professor of Chemistry

  
Dr. Roy P. Planalp  
Associate Professor of Chemistry

  
Dr. Andrew P. Laudano  
Associate Professor of Biochemistry

06/12/03  
Date: June 12, 2003

## **DEDICATION**

**To my wife Xiuqin Gao, my daughter Emily Niu  
and my parents Hualin Niu and Aafen Hu  
for their understanding, love and support throughout  
the pursuit of my Ph.D. degree here**

**Special appreciation to our American host-family  
Mr. Baldwin and Mrs. Baldwin for their continuous help to my family throughout  
the pursuit of my Ph.D. degree at UNH**

## ACKNOWLEDGEMENTS

I would like to give my heartfelt and deepest appreciation to my research adviser, Professor Edward Wong, for his professional guidance, support, patience and innovative research ideas as well as his invaluable help during the pursuit of my Ph.D. degree here. My heartfelt and deepest appreciation is also made to my coadviser, Professor Gary Weisman, for his useful suggestions in my research and all other helps that he has given to me. Both of my two advisers have taught me to perform scientific, organized, and safe research work which I intend to carry on through my chemistry career life. I'd also like to acknowledge my graduation committee, Professor Glen Miller, Professor Andrew Laudano, and Professor Roy Planalp for their help to me to fulfill my Ph.D. requirements. My gratitude goes to Professor Charles Zercher for his help to me. My special acknowledgement is given to Kathy Gallagher for her professional instruction in the use of NMR instruments and her kindness to me. Thanks to John Wilderman, Anne Gorham, Nancy Cherim, and Jeff Simpson at UIC for their technical assistance in the use of instruments. I'm grateful to Cindi Rohwer, Peggy Torch, Robert Constantine, and Sabrina Kirwan for their helps. The friendship, understanding, and encouragement of both Professor Wong's and Professor Weisman's group members are appreciated. I also appreciate many graduate students in the chemistry department such as Susanne Lewis, John Mabry, Weimin Lin, and Yijie Peng for their friendship. Finally, I really appreciate Professor Arnold L. Rheingold and his group for their help to solve more than 30 X-ray structures of the metal complexes that I synthesized.

## TABLE OF CONTENTS

	Page
DEDICATION -----	iii
ACKNOWLEDGEMENTS -----	iv
LIST OF TABLES -----	x
LIST OF SCHEMES -----	xiv
LIST OF FIGURES -----	xvi
ABSTRACT -----	xxxi
CHAPTER I GENERAL INTRODUCTION -----	1
1. Coordination Chemistry of Cyclam, Cyclen and their Derivatives and Potential Applications of these Complexes -----	2
1.1 General Information on their Coordination Chemistry -----	3
1.2 Zinc(II) Complexes of Cyclen, Cyclam and their Derivatives -----	5
1.3 Cd(II) and Hg(II) Complexes of Cyclen, Cyclam and their Derivatives -----	23
1.4 Co(III) Complexes of Cyclen and its Derivatives -----	28
1.5 Complexes of Cyclen, Cyclam and their Derivatives with Cu(II) -----	31

1.6 Complexes of Cyclen, Cyclam and their Derivatives with Ga(III) and In(III) -----	41
2. Coordination Chemistry of Cross-bridged Tetraazamacrocyclic Ligands -----	46
2.1 Our Ethylene Cross-bridged Tetraazamacrocyclic Ligands -----	47
2.2 Other Cross-bridged Tetraazamacrocyclic Ligands -----	60
3. General Aspects of this Dissertation -----	66

## CHAPTER II Zn(II), Cd(II) AND Hg(II) COMPLEXES OF CROSS-BRIDGED TETRAAZAMACROCYCLIC

LIGANDS 1-4 -----	69
1. Synthesis and Characterization of Zn(II), Cd(II) and Hg(II) Complexes -----	69
1.1 General Synthetic Methods -----	69
1.2 Synthesis of Zn(II) and Cd(II) Complexes -----	70
1.3 Synthesis of Hg(II) Complexes -----	73
1.4 Comparison of the Solubility of Metal Complexes -----	75
2. Spectral Data -----	75
2.1 Infrared Spectra -----	76
2.2 Solution $^1\text{H}$ and $^{13}\text{C}\{^1\text{H}\}$ NMR Spectra -----	78
(a) Zinc Complexes of Ligands 1-4 -----	79



(b) Cadmium Complexes of Ligands 1-4 -----	96
(c) Mercury Complexes of Ligands 1 and 2 -----	105
2.3 N-H/N-D Exchange in D <sub>2</sub> O and CD <sub>3</sub> OD -----	106
3. X-ray Structural Data -----	108
3.1 The Five Zn(II) Complexes -----	108
3.2 The Five Cd(II) Complexes -----	122
3.3 The Three Hg(II) Complexes -----	131
3.4 Summary of Structural Data -----	141

## CHAPTER III Zn(II), Cd(II) AND Hg(II) COMPLEXES OF

### PENDANT-ARMED CROSS-BRIDGED

#### TETRAAMINES LIGANDS 5-8 ----- 144

1. General Comments on the Synthesis and Characterization of Zn(II), Cd(II) and Hg(II) Complexes of Ligands 5-8 -----	144
1.1 Synthesis of Zn(II) and Cd(II) Complexes of Ligands 5 and 6 -----	145
1.2 Synthesis of Zn(II), Cd(II) and Hg(II) Complexes of Ligands 7 and 8 -----	146
2. Spectral Data -----	147
2.1 Infrared Spectra -----	147
2.2 Solution <sup>1</sup> H and <sup>13</sup> C{ <sup>1</sup> H} NMR Spectra -----	148
(a) Zn(II) and Cd(II) Complexes of Ligands 5 and 6 -----	149
(b) Zn(II), Cd(II) and Hg(II) Complexes of Ligands 7 and 8 -----	154

2.3 Variable-temperature $^1\text{H}$ and $^{13}\text{C}\{^1\text{H}\}$ NMR Spectral Studies in $\text{CD}_3\text{OD}$ -----	161
3. X-ray Structural Data -----	166

## CHAPTER IV Ga(III), In(III) AND Cu(II) COMPLEXES OF

CROSS-BRIDGED LIGANDS -----	181
1. Ga(III) and In(III) Complexes of Cross-bridged Ligands	
1, 2, and 8 -----	181
1.1. Synthesis and Characterization -----	181
1.2. Spectral Data -----	185
(a) Infrared Spectra -----	185
(b) Solution $^1\text{H}$ and $^{13}\text{C}\{^1\text{H}\}$ NMR Spectra -----	186
1.3 X-ray Structural Data -----	197
2. Cu(II) Complexes of Ligands 1-4 -----	207
2.1 Preparation and Characterization of Copper Complexes -----	207
2.2 Infrared Spectra -----	210
2.3 Electronic Spectra -----	214
2.4 X-ray Structural Data -----	217
3. Cu(II) Complexes of Ligands 5-8 -----	230
3.1 Preparation and Characterization of Copper Complexes -----	230
3.2 Infrared Spectra -----	231
3.3 Electronic Spectra -----	232
3.4 X-ray Structural Data -----	234

CHAPTER V KINETIC STABILITY OF METAL COMPLEXES OF CROSS-BRIDGED LIGANDS -----	244
1. Introduction -----	244
2. Results and Discussion -----	245
2.1 Relative Kinetic Inertness of Ga(III) and In(III) Complexes -----	245
2.2 Relative Kinetic Inertness of Zn(II), Cd(II) and Hg(II) Complexes -----	249
2.3 Preliminary Results on Relative Kinetic Inertness of Cu(II) Complexes -----	262
3. Experimental for Kinetic Studies -----	269
EXPERIMENTAL SECTION -----	271
LIST OF REFERENCES -----	312
Appendix Table Selected Bond Distances (Å) and Bond Angles (deg) in [Ni•1(μ-Cl)] <sub>2</sub> Cl <sub>2</sub> (167) -----	326
Appendix Figure Structure of the [Ni(μ-Cl)•1] <sub>2</sub> <sup>2+</sup> dimer in [Ni(μ-Cl)•1] <sub>2</sub> Cl <sub>2</sub> (167) -----	327

## LIST OF TABLES

		Page
<b>Table 1.1</b>	Comparison of the 'fit' of metal ions inside cross-bridged ligands	58
<b>Table 1.2</b>	Comparison of the 'fit' of metal ions inside tri-methylene cross-bridging ligands	64
<b>Table 1.3</b>	Kinetic data for the acid decomplexation of metal complexes of some cross-bridged ligands in 5N HCl reported by Springborg	65
<b>Table 2.1</b>	CHN elemental results of $(\text{HgCl}_2)_{11}(\mathbf{2})_6$	75
<b>Table 2.2</b>	Comparison of NH stretches in the IR spectra of Zn(II), Cd(II) and Hg(II) complexes of ligands <b>1</b> and <b>2</b>	76
<b>Table 2.3</b>	The assignment of proton and $^{13}\text{C}\{^1\text{H}\}$ NMR spectra of $[\text{Zn}\cdot\mathbf{1}(\mu\text{-Cl})]_2\text{Cl}_2$ in $\text{CD}_3\text{OD}$	86
<b>Table 2.4</b>	The assignment of proton and $^{13}\text{C}\{^1\text{H}\}$ NMR spectra of $\text{ZnCl}_2\cdot\mathbf{2}$ in $\text{CD}_3\text{OD}$ (N-D complex)	93
<b>Table 2.5</b>	Comparison of $^1\text{H}$ and $^{13}\text{C}\{^1\text{H}\}$ NMR data of Cd(II) $\cdot\mathbf{1}$ complexes (all N-D complexes) in $\text{D}_2\text{O}$	101
<b>Table 2.6</b>	Half-lives for the NH/ND exchange in Zn(II), Cd(II) and Hg(II) complexes of ligands <b>1</b> and <b>2</b> in $\text{D}_2\text{O}$ or $\text{CD}_3\text{OD}$	107
<b>Table 2.7</b>	(a) Selected Bond Distances (Å) and Bond Angles (deg) in $[\text{Zn}\cdot\mathbf{1}(\text{OH}_2)(\mu\text{-Cl})\text{ZnCl}_3]$ ( <b>115</b> )	110
	(b) Selected Bond Distances (Å) and Bond Angles (deg) in $[\text{Zn}\cdot\mathbf{1}(\mu\text{-Cl})]_2\text{Cl}_2(\text{CH}_3\text{OH})_4$ ( <b>116</b> )	113
	(c) Selected Bond Distances (Å) and Bond Angles (deg) in $[\text{Zn}\cdot\mathbf{1}(\mu\text{-Cl})]_2\text{Cl}_2$ ( <b>116a</b> )	115
	(d) Selected Bond Distances (Å) and Bond Angles (deg) in $\text{Zn}\cdot\mathbf{3}(\mu\text{-Cl})_2\text{-ZnCl}_2$ ( <b>120</b> )	117

<b>Table 2.7</b>	(e) Selected Bond Distances (Å) and Bond Angles (deg) in $[\text{Zn}\cdot\mathbf{2}(\text{H}_2\text{O})_2](\text{ClO}_4)_2$ ( <b>122</b> )	119
	(f) Selected Bond Distances (Å) and Bond Angles (deg) in $\text{ZnCl}_2\cdot\mathbf{4}$ ( <b>124</b> )	121
	(g) Selected Bond Distances (Å) and Bond Angles (deg) in $\text{CdCl}_2\cdot\mathbf{1}$ ( <b>125</b> )	123
	(h) Selected Bond Distances (Å) and Bond Angles (deg) in $\text{CdCl}_2\cdot\mathbf{2}$ ( <b>129</b> )	125
	(i) Selected Bond Distances (Å) and Bond Angles (deg) in $[\text{Cd}\cdot\mathbf{2}(\eta^2\text{-NO}_3)_2]$ ( <b>130</b> )	127
	(j) Selected Bond Distances (Å) and Bond Angles (deg) in $\text{CdCl}_2\cdot\mathbf{3}$ ( <b>128</b> )	129
	(k) Selected Bond Distances (Å) and Bond Angles (deg) in $\text{CdCl}_2\cdot\mathbf{4}$ ( <b>132</b> )	131
	(l) Selected Bond Distances (Å) and Bond Angles (deg) in $[\text{HgCl}_2(\mu\text{-1})]_2$ ( <b>133</b> )	133
	(m) Selected Bond Distances (Å) and Bond Angles (deg) in $\text{HgCl}_2\cdot\mathbf{2}$ ( <b>134</b> )	136
	(n) Selected Bond Distances (Å) and Bond Angles (deg) in cationic $[\text{Hg}\cdot\mathbf{2}(\mu\text{-Cl})]_2^{2+}$ part of $(\text{HgCl}_2)_6\cdot\mathbf{(2)}_4$ ( <b>135</b> )	139
	(o) Selected Bond Distances (Å) and Bond Angles (deg) in anionic $[\text{Hg}\cdot\mathbf{2Cl}(\mu\text{-Cl})(\text{HgCl}_3)]^-$ part of $(\text{HgCl}_2)_6\cdot\mathbf{(2)}_4$ ( <b>135</b> )	140
<b>Table 2.8</b>	Comparison of Zn(II), Cd(II) and Hg(II) fit inside cross-bridged ligand clefts	142
<b>Table 3.1</b>	Comparison of C=O stretches in the IR spectra of Zn(II), Cd(II) and Hg(II) complexes of ligands 5-8	147
<b>Table 3.2</b>	(a) Selected Bond Distances (Å) and Bond Angles (deg) in $[\text{Zn}\cdot\mathbf{5}](\text{ClO}_4)_2$ ( <b>136</b> )	168
	(b) Selected Bond Distances (Å) and Bond Angles (deg) in $[\text{Zn}\cdot\mathbf{6}](\text{ClO}_4)_2$ ( <b>137</b> )	170

	(c) Selected Bond Distances (Å) and Bond Angles (deg) in $[\text{Cd}\cdot 6(\eta^1\text{-NO}_3)](\text{NO}_3)$ (140)	172
	(d) Selected Bond Distances (Å) and Bond Angles (deg) in $[\text{Zn}\cdot(7\text{-2H})](\text{NaClO}_4)$ (141)	175
	(e) Selected Bond Distances (Å) and Bond Angles (deg) in $[\text{Hg}\cdot(7\text{-2H})]_2(\text{HgCl}_2)_3$ (148a)	178
<b>Table 3.3</b>	Structural comparison of Zn(II), Cd(II) and Hg(II) complexes of ligands 5-8	180
<b>Table 4.1</b>	NH stretches in the IR spectra of Ga(III) and In(III) complexes of ligands 1 and 2	186
<b>Table 4.2</b>	(a) Selected Bond Distances (Å) and Bond Angles (deg) in $[\text{GaCl}_2\cdot 1]\text{Cl}$ (149)	199
	(b) Selected Bond Distances (Å) and Bond Angles (deg) in $[\text{InBr}_2\cdot 1]\text{Br}$ (150)	201
	(c) Selected Bond Distances (Å) and Bond Angles (deg) in $[\text{InBr}_2\cdot 2]\text{Br}$ (152)	202
	(d) Selected Bond Distances (Å) and Bond Angles (deg) in $[\text{Ga}\cdot(8\text{-2H})](\text{NO}_3)$ (153)	204
<b>Table 4.3</b>	Comparison of Ga(III) and In(III) 'fit' inside cross-bridged ligand clefts	206
<b>Table 4.4</b>	Summary of electronic spectral data for the copper complexes of ligands 1-4	215
<b>Table 4.5</b>	(a) Selected Bond Distances (Å) and Bond Angles (deg) in $[\text{Cu}\cdot 2(\mu\text{-Cl})]_2\text{Cl}_2$ (155)	218
	(b) Selected Bond Distances (Å) and Bond Angles (deg) in $[\text{Cu}(2)(\text{CH}_3\text{OH})](\text{ClO}_4)_2$ (156a)	220
	(c) Selected Bond Distances (Å) and Bond Angles (deg) in $[\text{Cu}(3)(\text{CH}_3\text{CN})](\text{ClO}_4)_2$ (157a)	223
	(d) Selected Bond Distances (Å) and Bond Angles (deg) in $\text{CuCl}_2\cdot 4$ (158)	225

	(e) Selected Bond Distances (Å) and Bond Angles (deg) in $[\text{Cu}_2(\mu\text{-}\eta^1\text{:}\eta^2\text{-CO}_3)(\mathbf{4})_2](\text{ClO}_4)_2$ ( <b>159</b> )	227
<b>Table 4.6</b>	Summary of axial N-Cu-N angles and equatorial N-Cu-N angles in Cu(II) complexes of cross-bridged ligands <b>2</b> , <b>3</b> and <b>4</b>	229
<b>Table 4.7</b>	Summary of C=O stretches in the IR spectra of Cu(II) complexes of ligands <b>5-8</b>	231
<b>Table 4.8</b>	Summary of electronic spectral data for the copper complexes of ligands <b>5-8</b>	233
<b>Table 4.9</b>	(a) Selected Bond Distances (Å) and Bond Angles (deg) in $[\text{Cu}\cdot\mathbf{5}](\text{NO}_3)_2$ ( <b>161</b> )	236
	(b) Selected Bond Distances (Å) and Bond Angles (deg) of the five-coordinate Cu(II) center in $[\text{Cu}\cdot\mathbf{6}](\text{ClO}_4)_2$ ( <b>162</b> )	238
	(c) Selected Bond Distances (Å) and Bond Angles (deg) of the five-coordinate Cu(II) center involving MeOH hydrogen bonding in $[\text{Cu}\cdot\mathbf{6}](\text{ClO}_4)_2$ ( <b>162</b> )	240
	(d) Selected Bond Distances (Å) and Bond Angles (deg) of the six-coordinate Cu(II) center in $[\text{Cu}\cdot\mathbf{6}](\text{ClO}_4)_2$ ( <b>162</b> )	241
<b>Table 4.10</b>	Summary of axial N-Cu-N angles and equatorial N-Cu-N angles in Cu(II) complexes of cross-bridged ligands <b>5</b> and <b>6</b>	243
<b>Table 5.1</b>	Acid decomplexation data for Zn(II) and Cd(II) complexes of ligands <b>1</b> and <b>2</b>	249
<b>Table 5.2</b>	Acid decomplexation data for Zn(II), Cd(II), and Hg(II) complexes of ligands <b>1</b> and <b>2</b> and $\text{Zn}(\text{NO}_3)_2\cdot(\text{Me}_4\text{Cyclam})$ in buffered $\text{D}_2\text{O}$ at pD 5.9	250
<b>Table 5.3</b>	Acid decomplexation data for Cu(II) complexes of cross-bridged ligands and the reference copper complex of ligand <b>tet a</b> in 5N HCl	263
<b>Table 5.4</b>	Acid decomplexation data for $[\text{Cu}\cdot(\mathbf{7-2H})](\text{NaClO}_4)(\text{NaCF}_3\text{COO})_{0.5}(\text{H}_2\text{O})_{1.5}$ in 5N HCl	265

## LIST OF SCHEMES

		Page
<b>Scheme 1.1</b>	The dynamic process of $[\text{Zn}(\text{Me}_4\text{Cyclam})(\text{Cl})](\text{ClO}_4)$ ( <b>13</b> ) in nitromethane solution	7
<b>Scheme 1.2</b>	Carbon dioxide fixation by the $\text{Zn}^{\text{II}}$ -cyclam complex in MeOH	8
<b>Scheme 1.3</b>	The formation of the Zn(II) complex of a phenol pendant-armed cyclam	9
<b>Scheme 1.4</b>	The equilibrium between the carboxylate-bound and the carboxylate-unbound forms of Zn(II) complexes of carboxylate pendant-armed cyclens	12
<b>Scheme 1.5</b>	An overall reaction mechanism for 4-nitrophenyl acetate hydrolysis catalyzed by an alcohol pendant-armed cyclen zinc(II) complex	14
<b>Scheme 1.6</b>	The reaction of <b>34</b> with bis(4-nitrophenyl) phosphate yielded a "phosphoryl-transfer" intermediate <b>36</b> which was isolated	14
<b>Scheme 1.7</b>	Zn(II) complexes of carboxamide pendant-armed cyclens (Type one)	15
<b>Scheme 1.8</b>	Zn(II) complexes of carboxamide pendant-armed cyclens (Type two)	16
<b>Scheme 1.9</b>	The synthesis of a protonated ligand <b>49</b> •5HCl	17
<b>Scheme 1.10</b>	Helicity reversal in the approximately square anti-prismatic Zn(II) and Cd(II) complexes of ligand DOTAM in solution	24
<b>Scheme 1.11</b>	Proposed mechanism of $\text{CH}_3\text{CN}$ hydration catalyzed by a Co(III) cyclen complex, <b>78</b>	28
<b>Scheme 1.12</b>	Stepwise mechanism for proton exchange and inversion at a coordinated secondary amine center	31



<b>Scheme 1.13</b>	NH/ND exchange at a coordinated secondary amine center	31
<b>Scheme 1.14</b>	Structural rearrangement $[\text{Cu(II)99}](\text{ClO}_4)_2$ in aqueous solution	39
<b>Scheme 1.15</b>	General synthetic route to make cross-bridged ligands	47
<b>Scheme 1.16</b>	An alternative method to synthesize cross-bridged ligand <b>108</b>	48
<b>Scheme 1.17</b>	An alternative method to synthesize cross-bridged ligand <b>2</b>	48
<b>Scheme 1.18</b>	An alternative method to synthesize cross-bridged ligand <b>110</b>	60
<b>Scheme 2.1</b>	The NH/ND exchange observed for Zn(II), Cd(II) and Hg(II) complexes of Cross-bridged ligands <b>1</b> and <b>2</b> in $\text{D}_2\text{O}$ or $\text{CD}_3\text{OD}$	79

## LIST OF FIGURES

	Page
<b>Figure 1.1</b> Cross-bridged ligands studied in this research	2
<b>Figure 1.2</b> A family of macrocyclic tetraamines	3
<b>Figure 1.3</b> Cyclam and cyclen	3
<b>Figure 1.4</b> Five possible configurations of cyclam in its metal complexes	4
<b>Figure 1.5</b> Four possible configurations of cyclen in its metal complexes	4
<b>Figure 1.6</b> The metal-to-ligand bond distances and bite angles that produce the minimum-strain energy structures for chelate rings of sizes five and six	4
<b>Figure 1.7</b> The X-ray structure of [Zn(cyclam)(NCS) <sub>2</sub> ] ( <b>11</b> )	5
<b>Figure 1.8</b> The X-ray structure of [Zn(5,12-dimethyl-cyclam)(Cl)](ClO <sub>4</sub> ) ( <b>12</b> )	6
<b>Figure 1.9</b> The X-ray structure of [Zn(Me <sub>4</sub> Cyclam)(Cl)](ClO <sub>4</sub> ) ( <b>13</b> )	7
<b>Figure 1.10</b> The X-ray structure of a dimeric Zn(II) Xylyl-bicyclam complex ( <b>14</b> )	7
<b>Figure 1.11</b> The X-ray structure of [Zn(cyclen)-Imidazolate-Zn(cyclen)] ( <b>20</b> )	10
<b>Figure 1.12</b> The X-ray structure of complex [Zn(II) <b>21</b> (H <sub>2</sub> O)] <sup>2+</sup>	10
<b>Figure 1.13</b> The X-ray structure of complex [Zn(II) <b>22</b> ] <sup>2+</sup>	11
<b>Figure 1.14</b> The p <i>K</i> <sub>a</sub> values for Zn(II) complexes of cyclam, Me <sub>4</sub> Cyclam, and cyclen	12
<b>Figure 1.15</b> The solid-state structure of <b>29</b>	13
<b>Figure 1.16</b> Cation parts of two Zn(II) cyclen complexes	18

<b>Figure 1.17</b>	The structure of a ternary zinc(II) complex, <b>54</b>	18
<b>Figure 1.18</b>	Lipophilic Zn(II) cyclen derivative complexes	19
<b>Figure 1.19</b>	Zn(II) complexes of two pendant-armed cyclen derivatives	20
<b>Figure 1.20</b>	Ternary Zn(II) complexes of two pendant-armed cyclen derivatives and deprotonated 1-methylthymine	20
<b>Figure 1.21</b>	The structure of $[\text{Zn}(\text{DOTAM})]^{2+}$ ( <b>65</b> )	21
<b>Figure 1.22</b>	The structures of a seven-coordinated Zn(II) complex of ligand <b>66</b>	21
<b>Figure 1.23</b>	Ligand DO2A ( <b>68</b> ) and the X-ray structure of $[\text{Zn}(\text{H}_2\text{DOTA})]$ ( <b>69</b> )	23
<b>Figure 1.24</b>	The X-ray structure of $[\text{Zn}(\text{H}_2\text{TETA})]$ ( <b>70</b> ) and ligand <b>71</b>	23
<b>Figure 1.25</b>	The structure of $[\text{Cd}(\text{DOTAM})]^{2+}$ ( <b>72</b> )	24
<b>Figure 1.26</b>	The X-ray structure of the Cd(II) complex of a cyclam derivative, complex <b>73</b>	25
<b>Figure 1.27</b>	The X-ray structure of $[\text{Cd}_3(\text{cyclam})_3(\text{CO}_3)](\text{ClO}_4)_4$ ( <b>74</b> )	25
<b>Figure 1.28</b>	The X-ray structure of $[\{\text{Cd-cyclen}\}\{\text{Pt}(\text{CH}_3)_2(\text{bpy})\}](\text{ClO}_4)_2$ ( <b>75</b> )	26
<b>Figure 1.29</b>	The X-ray structure of a Hg(II) complex with a hexamethyl cyclam	27
<b>Figure 1.30</b>	The X-ray structure of Hg(II) complex of a cyclam derivative	27
<b>Figure 1.31</b>	Three Co(III) complexes of cyclen and $\text{Me}_2\text{Cyclen}$	28
<b>Figure 1.32</b>	The eight possible configurational isomers of $[\text{Co}(\text{Mecyclen})(\text{S-AlaO})]^{2+}$	30
<b>Figure 1.33</b>	The four possible configurational isomers of $[\text{Co}(\text{cyclen})(\text{S-AlaO})]^{2+}$	30
<b>Figure 1.34</b>	The X-ray structure of $[\text{Cu}(\text{cyclam})(\text{MeCN})_2]^{2+}$	32

<b>Figure 1.35</b>	The molecular structure of [Cu(Me <sub>4</sub> Cyclam)Br]Br ( <b>90</b> )	33
<b>Figure 1.36</b>	The molecular structure of a Cu(II) complex with <i>trans</i> -6,13-Diammonio-5,7,12,14-tetramethyl-cyclam	33
<b>Figure 1.37</b>	The molecular structure of [Cu <sub>2</sub> (Me <sub>4</sub> Cyclam) <sub>2</sub> (1,3-μ-N <sub>3</sub> )] <sup>3+</sup> ( <b>92</b> )	34
<b>Figure 1.38</b>	The molecular structure of Cu(II) complex of a cyclam derivative	34
<b>Figure 1.39</b>	The molecular structure of [Cu(tet b)(o-SC <sub>6</sub> H <sub>4</sub> CO <sub>2</sub> )]	35
<b>Figure 1.40</b>	The X-ray structure of a copper complex of cyclen derivative	36
<b>Figure 1.41</b>	The X-ray structure of [Cu(Me <sub>4</sub> Cyclen)(H <sub>2</sub> O)] <sup>2+</sup>	36
<b>Figure 1.42</b>	The X-ray structure of [Cu(Cage L)] <sup>2+</sup>	37
<b>Figure 1.43</b>	The X-ray structure of [Cu(H <sub>2</sub> dota)] ( <b>98</b> )	37
<b>Figure 1.44</b>	The X-ray structure of copper(II) complex of a carboxylate pendant-armed cyclam	38
<b>Figure 1.45</b>	The X-ray structure of copper(II) complex of a carbamoyl pendant-armed cyclam	40
<b>Figure 1.46</b>	The X-ray structure of [Cu(HDO3A)] ( <b>101</b> )	40
<b>Figure 1.47</b>	Methanephosphonate derivatives of cyclen	41
<b>Figure 1.48</b>	The X-ray structure of [(CH <sub>3</sub> )GaCyclam]Cl <sub>2</sub>	42
<b>Figure 1.49</b>	Cyclen and cyclam derivatives tested for potential metal-based radiopharmaceutical application by Kaden <i>et al.</i>	43
<b>Figure 1.50</b>	The X-ray structure of an In(III) complex of a cyclen derivative, ligand <b>104a</b>	43
<b>Figure 1.51</b>	Two cyclen derivatives for bioconjugation towards potential metal-based radiopharmaceutical application	44
<b>Figure 1.52</b>	The X-ray structure of a Ga(III) complex of a cyclen derivative, ligand <b>106</b>	45

<b>Figure 1.53</b>	The X-ray structure of an Y(III) complex of a cyclen derivative, ligand <b>106</b>	45
<b>Figure 1.54</b>	Adjacent-bridged cyclam and cyclen	46
<b>Figure 1.55</b>	Cross-bridged ligands used to form metal complexes	47
<b>Figure 1.56</b>	<i>cis</i> -folded configuration (V) adopted by cross-bridged ligands in their metal complexes	49
<b>Figure 1.57</b>	Equatorial and axial nitrogen atoms are labeled as N <sub>eq</sub> and N <sub>ax</sub> respectively in the metal complexes of these cross-bridged ligands	50
<b>Figure 1.58</b>	The X-ray structure of a Cu(II) complex of cross-bridged cyclam, ligand <b>1</b>	50
<b>Figure 1.59</b>	The X-ray structure of a Cu(II) complex of N,N' dibenzyl cross-bridged cyclam, ligand <b>3</b>	51
<b>Figure 1.60</b>	The X-ray structure of a Cu(II) complex of a dicarboxylate pendant-armed cross-bridged cyclam, ligand <b>7-2H</b>	51
<b>Figure 1.61</b>	The X-ray structure of the dimeric Zn(II) complex of ligand <b>1</b>	52
<b>Figure 1.62</b>	The X-ray structure of an In(III) complex of cross-bridged cyclen, ligand <b>2</b>	53
<b>Figure 1.63</b>	The X-ray structure of Cu(II) complex of a cross-bridged cyclam derivative	53
<b>Figure 1.64</b>	The X-ray structure of a Cu(I) complex of N,N' dibenzyl cross-bridged cyclam, ligand <b>3</b>	54
<b>Figure 1.65</b>	The X-ray structure of [Cu(II)(MeCN)• <b>3</b> ] <sup>2+</sup>	55
<b>Figure 1.66</b>	The X-ray structure of Cu(II) complex of a cross-bridged cyclam derivative	56
<b>Figure 1.67</b>	Trimethylene cross-bridged ligands	60
<b>Figure 1.68</b>	The X-ray structure of a Cu(II) complex of a trimethylene cross-bridged ligand <b>112</b>	61

<b>Figure 1.69</b>	The X-ray structure of a Co(II) complex of a trimethylene cross-bridged ligand <b>114</b>	63
<b>Figure 1.70</b>	Tetra-, penta-, hepta-, octa-methylene cross-bridged ligands	66
<b>Figure 2.1</b>	Cross-bridged ligands <b>1-4</b>	69
<b>Figure 2.2</b>	(a) The IR (KBr) spectrum of monoprotonated <b>3</b> obtained from the failed complexation of $\text{Zn}(\text{ClO}_4)_2 \cdot 6\text{H}_2\text{O}$ with ligand <b>3</b>	71
	(b) The IR (KBr) spectrum of $\text{ZnCl}_2 \cdot \mathbf{3}$	71
<b>Figure 2.3</b>	The $^1\text{H}$ NMR spectra of monoprotonated <b>3</b> obtained from the failed complexation of $\text{Zn}(\text{ClO}_4)_2 \cdot 6\text{H}_2\text{O}$ with ligand <b>3</b> and $\text{ZnCl}_2 \cdot \mathbf{3}$	72
<b>Figure 2.4</b>	The IR (KBr) spectra of $\text{HgCl}_2 \cdot \mathbf{2}$ , $(\text{HgCl}_2)_6 \cdot (\mathbf{2})_4$ , and $(\text{HgCl}_2)_{11} \cdot (\mathbf{2})_6$	77
<b>Figure 2.5</b>	Comparison of $^1\text{H}$ NMR spectra of three Zn(II) complexes of <b>1</b> in $\text{CD}_3\text{OD}$	80
<b>Figure 2.6</b>	Comparison of $^{13}\text{C}\{^1\text{H}\}$ NMR spectra of three Zn(II) complexes of <b>1</b> in $\text{CD}_3\text{OD}$	81
<b>Figure 2.7</b>	A 2D [ $^1\text{H}, ^1\text{H}$ ] gCOSY spectrum of $[\text{Zn} \cdot \mathbf{1}(\mu\text{-Cl})]_2\text{Cl}_2$ in $\text{CD}_3\text{OD}$	82
<b>Figure 2.8</b>	A 2D [ $^1\text{H}, ^{13}\text{C}$ ] gHSQC NMR spectrum of $[\text{Zn} \cdot \mathbf{1}(\mu\text{-Cl})]_2\text{Cl}_2$ (0.050 M N-D complex) in $\text{CD}_3\text{OD}$	83
<b>Figure 2.9</b>	Comparison of $^1\text{H}$ NMR spectra of the NH complex and the ND complex of $[\text{Zn} \cdot \mathbf{1}(\mu\text{-Cl})]_2\text{Cl}_2$ in $\text{CD}_3\text{OD}$	84
<b>Figure 2.10</b>	(a) Comparison of $^1\text{H}$ NMR spectra of the three Zn(II) complexes of <b>1</b> in $\text{CD}_3\text{CN}$	87
	(b) Comparison of $^{13}\text{C}\{^1\text{H}\}$ NMR spectra of three Zn(II) complexes of <b>1</b> in $\text{CD}_3\text{CN}$	88
<b>Figure 2.11</b>	Comparison of $^1\text{H}$ NMR spectra of the four Zn(II) complexes of <b>1</b> in $\text{D}_2\text{O}$	88

<b>Figure 2.12</b>	<b>(a)</b> Comparison of $^1\text{H}$ NMR spectra of the three Zn(II) complexes of <b>2</b> in $\text{CD}_3\text{OD}$ (N-H complexes)	90
	<b>(b)</b> Comparison of $^{13}\text{C}\{^1\text{H}\}$ NMR spectra of the three Zn(II) complexes of <b>2</b> in $\text{CD}_3\text{OD}$ (N-D complexes)	91
<b>Figure 2.13</b>	Comparison of $^1\text{H}$ NMR spectra of NH complex and ND complex of $\text{ZnCl}_2\cdot\mathbf{2}$ in $\text{CD}_3\text{OD}$	91
<b>Figure 2.14</b>	<b>(a)</b> A 2D [ $^1\text{H}, ^1\text{H}$ ] COSY spectrum of $\text{ZnCl}_2\cdot\mathbf{2}$ (N-D complex) in $\text{CD}_3\text{OD}$	92
	<b>(b)</b> A 2D [ $^1\text{H}, ^{13}\text{C}$ ] HMQC NMR spectrum of $\text{ZnCl}_2\cdot\mathbf{2}$ (N-D complex) in $\text{CD}_3\text{OD}$	93
<b>Figure 2.15</b>	<b>(a)</b> Comparison of $^1\text{H}$ NMR spectra of the three Zn(II) complexes of <b>2</b> in $\text{D}_2\text{O}$ (N-D complexes)	94
	<b>(b)</b> Comparison of $^{13}\text{C}\{^1\text{H}\}$ NMR spectra of the three Zn(II) complexes of <b>2</b> in $\text{D}_2\text{O}$ (N-D complexes)	95
<b>Figure 2.16</b>	The proton NMR spectrum of $\text{ZnCl}_2\cdot\mathbf{3}$ in $\text{D}_2\text{O}$	96
<b>Figure 2.17</b>	The proton NMR spectrum of $\text{ZnCl}_2\cdot\mathbf{4}$ in $\text{CDCl}_3$	96
<b>Figure 2.18</b>	Comparison of $^1\text{H}$ NMR spectra of the three Zn(II), Cd(II) and Hg(II) complexes of <b>2</b> in $\text{CD}_3\text{OD}$ (N-D complexes)	97
<b>Figure 2.19</b>	The proton NMR spectrum of $\text{CdCl}_2\cdot\mathbf{4}$ in $\text{CDCl}_3$	98
<b>Figure 2.20</b>	Detailed comparison of $^1\text{H}$ NMR spectra of the three Cd(II) complexes of <b>1</b> in $\text{D}_2\text{O}$	99
<b>Figure 2.21</b>	Detailed comparison of $^1\text{H}$ NMR spectra of the three Cd(II) complexes (all N-D complexes) of <b>2</b> in $\text{D}_2\text{O}$	99
<b>Figure 2.22</b>	<b>(a)</b> The $^1\text{H}$ NMR spectrum of a 1:1 mixture of 0.10 M $\text{CdCl}_2\cdot\mathbf{1}$ and 0.10 M $\text{Cd}\cdot\mathbf{1}(\text{NO}_3)_2$ in $\text{D}_2\text{O}$	100
	<b>(b)</b> The $^{13}\text{C}\{^1\text{H}\}$ NMR spectrum of a 1:1 mixture of 0.10 M $\text{CdCl}_2\cdot\mathbf{1}$ and 0.10 M $\text{Cd}\cdot\mathbf{1}(\text{NO}_3)_2$ in $\text{D}_2\text{O}$	100
<b>Figure 2.23</b>	The $^1\text{H}$ NMR spectrum of the mixture obtained by the addition of 10 equivalents of NaCl into a 1:1 mixture of 0.10 M $\text{CdCl}_2\cdot\mathbf{1}$ and 0.10 M $\text{Cd}\cdot\mathbf{1}(\text{NO}_3)_2$ in $\text{D}_2\text{O}$	101

<b>Figure 2.24</b>	A 2D [ <sup>1</sup> H, <sup>1</sup> H] gCOSY spectrum of CdCl <sub>2</sub> •2 (N-D complex) in CD <sub>3</sub> OD	103
<b>Figure 2.25</b>	A 2D [ <sup>1</sup> H, <sup>13</sup> C] gHSQC NMR spectrum of CdCl <sub>2</sub> •2 (N-D complex) in CD <sub>3</sub> OD	104
<b>Figure 2.26</b>	X-ray structure of [Zn•1(OH <sub>2</sub> )(μ-Cl)ZnCl <sub>3</sub> ] (115)	109
<b>Figure 2.27</b>	Hydrogen bonding interactions in the crystal structure of [Zn•1(OH <sub>2</sub> )(μ-Cl)ZnCl <sub>3</sub> ] (115)	109
<b>Figure 2.28</b>	Structure of the [Zn•1(μ-Cl)] <sub>2</sub> <sup>2+</sup> dimer in [Zn•1(μ-Cl)] <sub>2</sub> Cl <sub>2</sub> •4CH <sub>3</sub> OH (116)	112
<b>Figure 2.29</b>	Hydrogen bonding interactions in the crystal structure of [Zn•1(μ-Cl)] <sub>2</sub> Cl <sub>2</sub> •4CH <sub>3</sub> OH (116)	112
<b>Figure 2.30</b>	Structure of [Zn•1(μ-Cl)] <sub>2</sub> Cl <sub>2</sub> (116a)	114
<b>Figure 2.31</b>	X-ray structure of Zn•3((μ-Cl) <sub>2</sub> -ZnCl <sub>2</sub> ) (120)	116
<b>Figure 2.32</b>	X-ray structure of [Zn•2(H <sub>2</sub> O) <sub>2</sub> ](ClO <sub>4</sub> ) <sub>2</sub> (122)	118
<b>Figure 2.33</b>	X-ray structure of ZnCl <sub>2</sub> •4 (124)	120
<b>Figure 2.34</b>	X-ray structure of CdCl <sub>2</sub> •1 (125)	122
<b>Figure 2.35</b>	X-ray structure of CdCl <sub>2</sub> •2 (129)	124
<b>Figure 2.36</b>	X-ray structure of [Cd•2(η <sup>2</sup> -NO <sub>3</sub> ) <sub>2</sub> ] (131)	126
<b>Figure 2.37</b>	X-ray structure of CdCl <sub>2</sub> •3 (128)	128
<b>Figure 2.38</b>	X-ray structure of CdCl <sub>2</sub> •4 (132)	130
<b>Figure 2.39</b>	X-ray structure of [HgCl <sub>2</sub> (μ-1)] <sub>2</sub> (133)	132
<b>Figure 2.40</b>	An ORTEP view of the X-ray structure of HgCl <sub>2</sub> •2 (123)	135
<b>Figure 2.41</b>	Structure of the cationic [Hg•2(μ-Cl)] <sub>2</sub> <sup>2+</sup> part of (HgCl <sub>2</sub> ) <sub>6</sub> •(2) <sub>4</sub> (135)	137
<b>Figure 2.42</b>	X-ray Structure of the anionic [Hg•2Cl(μ-Cl)(HgCl <sub>3</sub> )] <sup>-</sup> part of (HgCl <sub>2</sub> ) <sub>6</sub> •(2) <sub>4</sub> (135)	137
<b>Figure 3.1</b>	Pendant-armed cross-bridged ligands 5-8	144



<b>Figure 3.2</b>	<b>(a)</b> The $^{13}\text{C}\{^1\text{H}\}$ NMR spectrum of the $\text{Cd}(\text{ClO}_4)_2$ complex of <b>5</b> in $\text{D}_2\text{O}$	149
	<b>(b)</b> The carboxylate carbonyl resonance in the $^{13}\text{C}\{^1\text{H}\}$ NMR spectrum of the $\text{Cd}(\text{ClO}_4)_2$ complex of <b>5</b> in $\text{D}_2\text{O}$	150
<b>Figure 3.3</b>	<b>(a)</b> Comparison of $^1\text{H}$ NMR spectra of the two Zn(II) complexes of <b>6</b> in $\text{D}_2\text{O}$	150
	<b>(b)</b> Comparison of $^1\text{H}$ NMR spectra of the two Zn(II) complexes of <b>6</b> in $\text{CD}_3\text{OD}$	151
<b>Figure 3.4</b>	<b>(a)</b> $^1\text{H}$ NMR spectra of $\text{Cd}\cdot\mathbf{6}(\text{ClO}_4)_2$ (top) and $[\text{Cd}\cdot\mathbf{6}(\eta^1\text{-NO}_3)](\text{NO}_3)$ (bottom) in $\text{CD}_3\text{OD}$	152
	<b>(b)</b> $^1\text{H}$ NMR spectrum of $[\text{Cd}\cdot\mathbf{6}(\eta^1\text{-NO}_3)](\text{NO}_3)$ in $\text{CD}_3\text{CN}$	152
<b>Figure 3.5</b>	$^1\text{H}$ NMR spectrum of $\text{Cd}\cdot\mathbf{6}(\text{ClO}_4)_2$ in $\text{CD}_3\text{CN}$	153
<b>Figure 3.6</b>	A doublet satellite around the amide carbonyl resonance in the $^{13}\text{C}\{^1\text{H}\}$ NMR spectrum of $\text{Cd}\cdot\mathbf{6}(\text{ClO}_4)_2$ in $\text{CD}_3\text{CN}$	153
<b>Figure 3.7</b>	Comparison of $^1\text{H}$ NMR spectra of the two Zn(II) complexes of <b>7-2H</b> in $\text{D}_2\text{O}$	155
<b>Figure 3.8</b>	Comparison of $^1\text{H}$ NMR spectra of the two Zn(II) complexes of <b>8-2H</b> in $\text{D}_2\text{O}$	155
<b>Figure 3.9</b>	$^1\text{H}$ NMR spectra of $[\text{Cd}\cdot(\mathbf{7-2H})](\text{NaNO}_3)$ and $[\text{Cd}\cdot(\mathbf{7-2H})](\text{NaClO}_4)$ in $\text{D}_2\text{O}$	156
<b>Figure 3.10</b>	The satellites around the carboxylate carbonyl resonance in the $^{13}\text{C}\{^1\text{H}\}$ NMR spectrum of $[\text{Cd}\cdot(\mathbf{7-2H})](\text{NaNO}_3)$ in $\text{D}_2\text{O}$	157
<b>Figure 3.11</b>	<b>(a)</b> $^1\text{H}$ NMR spectrum of $[\text{Cd}\cdot(\mathbf{7-2H})](\text{NaClO}_4)$ in $\text{CD}_3\text{OD}$	157
	<b>(b)</b> $^{13}\text{C}\{^1\text{H}\}$ NMR spectrum of $[\text{Cd}\cdot(\mathbf{7-2H})](\text{NaClO}_4)$ in $\text{CD}_3\text{OD}$	158
<b>Figure 3.12</b>	$^1\text{H}$ NMR spectrum of $[\text{Cd}\cdot(\mathbf{8-2H})](\text{NaClO}_4)$ in $\text{D}_2\text{O}$	158

<b>Figure 3.13</b>	Satellites around the carboxylate carbonyl resonance in the $^{13}\text{C}\{^1\text{H}\}$ NMR spectrum of $[\text{Cd}\cdot(\mathbf{8-2H})](\text{NaClO}_4)$ in $\text{D}_2\text{O}$	159
<b>Figure 3.14</b>	(a) $^1\text{H}$ NMR spectrum of $[\text{Cd}\cdot(\mathbf{8-2H})](\text{NaClO}_4)$ in $\text{CD}_3\text{OD}$	159
	(b) $^{13}\text{C}\{^1\text{H}\}$ NMR spectrum of $[\text{Cd}\cdot(\mathbf{8-2H})](\text{NaClO}_4)$ in $\text{CD}_3\text{OD}$ .	159
<b>Figure 3.15</b>	$^{13}\text{C}\{^1\text{H}\}$ NMR spectrum of $[\text{Hg}\cdot(\mathbf{7-2H})](\text{K}_2\text{HgCl}_4)$ in $\text{D}_2\text{O}$	160
<b>Figure 3.16</b>	Doublet satellites at the sides of both resonances in the $^{13}\text{C}\{^1\text{H}\}$ NMR spectrum of $[\text{Hg}\cdot(\mathbf{7-2H})](\text{K}_2\text{HgCl}_4)$ in $\text{D}_2\text{O}$	160
<b>Figure 3.17</b>	(a) A possible non-dissociative mechanism for the averaged $C_{2v}$ symmetry in the Zn(II) complex of $\mathbf{8-2H}$ in $\text{CD}_3\text{OD}$	161
	(b) A dissociative mechanism for the averaged $C_{2v}$ symmetry in the Zn(II) complex of $\mathbf{8-2H}$ in $\text{CD}_3\text{OD}$	162
<b>Figure 3.18</b>	Variable-temperature $^1\text{H}$ NMR spectra of $[\text{Zn}\cdot(\mathbf{7-2H})](\text{NaClO}_4)$ in $\text{CD}_3\text{OD}$ at room temperature and at $-80^\circ\text{C}$	163
<b>Figure 3.19</b>	Variable-temperature $^1\text{H}$ NMR spectra of $[\text{Cd}\cdot(\mathbf{7-2H})](\text{NaClO}_4)$ in $\text{CD}_3\text{OD}$ at room temperature and at $-80^\circ\text{C}$	163
<b>Figure 3.20</b>	Variable-temperature $^1\text{H}$ NMR spectra of $[\text{Zn}\cdot\mathbf{6}](\text{ClO}_4)_2$ in $\text{CD}_3\text{OD}$ at $15^\circ\text{C}$ and at $-80^\circ\text{C}$	164
<b>Figure 3.21</b>	Variable-temperature $^1\text{H}$ NMR spectra of $[\text{Zn}\cdot(\mathbf{8-2H})](\text{NaClO}_4)$ in $\text{CD}_3\text{OD}$ at room temperature and at $-80^\circ\text{C}$	165
<b>Figure 3.22</b>	Variable-temperature $^{13}\text{C}\{^1\text{H}\}$ NMR spectra of $[\text{Zn}\cdot(\mathbf{8-2H})](\text{NaClO}_4)$ in $\text{CD}_3\text{OD}$ at room temperature and at $-80^\circ\text{C}$	165
<b>Figure 3.23</b>	X-ray structure of $[\text{Zn}\cdot\mathbf{5}](\text{ClO}_4)_2$ (136)	167
<b>Figure 3.24</b>	X-ray structure of $[\text{Zn}\cdot\mathbf{6}](\text{ClO}_4)_2$ (138)	169
<b>Figure 3.25</b>	X-ray structure of $[\text{Cd}\cdot\mathbf{6}(\eta^1\text{-NO}_3)](\text{NO}_3)$ (140)	171

<b>Figure 3.26</b>	X-ray structure of $[\text{Zn}\cdot(7\text{-}2\text{H})](\text{NaClO}_4)$ ( <b>141</b> )	173
<b>Figure 3.27</b>	Hydrogen bonding interactions in the crystal structure of $[\text{Zn}\cdot(7\text{-}2\text{H})](\text{NaClO}_4)$ ( <b>141</b> )	173
<b>Figure 3.28</b>	X-ray structure of $[\text{Zn}\cdot(8\text{-}2\text{H})](\text{NaClO}_4)$ ( <b>143</b> )	176
<b>Figure 3.29</b>	X-ray structure of $[\text{Hg}\cdot(7\text{-}2\text{H})]_2(\text{HgCl}_2)_3$ ( <b>148a</b> )	177
<b>Figure 4.1</b>	Proton NMR spectrum of the crystalline solid from $[\text{InBr}_2\cdot 2]\text{Br}$ synthesis in $\text{CD}_3\text{CN}$	182
<b>Figure 4.2</b>	Proton NMR spectra of a protonated <b>1</b> and of an attempted complexation product of $\text{InBr}_3$ with <b>1</b> in methanol in $\text{D}_2\text{O}$	182
<b>Figure 4.3</b>	Proton NMR spectrum of an attempted complexation product between $\text{Ga}(\text{NO}_3)_3$ hydrate and <b>1</b> in methanol ( $\text{D}_2\text{O}$ )	183
<b>Figure 4.4</b>	IR (KBr) spectrum of the product of an attempted complexation of $\text{Ga}(\text{NO}_3)_3$ hydrate with $7\cdot(\text{TFA})_2$	184
<b>Figure 4.5</b>	(a) Top: Proton NMR spectrum of $7\cdot(\text{HCl})_2$ in $\text{D}_2\text{O}$ . Bottom: Proton NMR spectrum of an attempted complexation product of $\text{Ga}(\text{acac})_3$ with $7\cdot(\text{TFA})_2$ in $\text{D}_2\text{O}$	185
	(b) Top: $^{13}\text{C}\{^1\text{H}\}$ NMR spectrum of $7\cdot(\text{HCl})_2$ in $\text{D}_2\text{O}$ . Bottom: $^{13}\text{C}\{^1\text{H}\}$ NMR spectrum of an attempted complexation product of $\text{Ga}(\text{acac})_3$ with $7\cdot(\text{TFA})_2$ in $\text{D}_2\text{O}$	185
<b>Figure 4.6</b>	(a) Proton NMR spectrum of $[\text{GaCl}_2\cdot\mathbf{1}]\text{Cl}$ (N-D complex) in $\text{D}_2\text{O}$	186
	(b) Top: $^{13}\text{C}\{^1\text{H}\}$ NMR spectrum of $[\text{GaCl}_2\cdot\mathbf{1}]\text{Cl}$ (N-D complex) in $\text{D}_2\text{O}$ . Bottom: $^{13}\text{C}\{^1\text{H}\}$ NMR spectrum of $[\text{Zn}\cdot\mathbf{1}(\mu\text{-Cl})]_2\text{Cl}_2$ ( <b>116a</b> ) in $\text{D}_2\text{O}$	187
<b>Figure 4.7</b>	$^1\text{H}$ NMR spectrum of $[\text{GaCl}_2\cdot\mathbf{1}]\text{Cl}$ (N-D complex) in acidic $\text{D}_2\text{O}$	187
<b>Figure 4.8</b>	Expansion of the two doublets of pentets at $\delta$ 1.84 and 1.76 in the $^1\text{H}$ NMR spectrum of $[\text{GaCl}_2\cdot\mathbf{1}]\text{Cl}$ (N-D complex) in acidic $\text{D}_2\text{O}$	188

<b>Figure 4.9</b>	$^{13}\text{C}\{^1\text{H}\}$ NMR spectrum of $[\text{GaCl}_2\cdot\mathbf{1}]\text{Cl}$ in acidic $\text{D}_2\text{O}$ . Top: N-D complex. Bottom: a 1:1 N-H and N-D complex mixture	188
<b>Figure 4.10</b>	Expansion of two peaks at $\delta$ 19.7 and 19.4 in the $^{13}\text{C}\{^1\text{H}\}$ NMR spectrum of $[\text{GaCl}_2\cdot\mathbf{1}]\text{Cl}$ in acidic $\text{D}_2\text{O}$	189
<b>Figure 4.11</b>	Comparison of the changes of the two sets of proton doublet of pentets at $\delta$ 1.84 and 1.76 with increased KCl concentration (pD = 1.07)	189
<b>Figure 4.12</b>	Comparison of the changes of the two $^{13}\text{C}\{^1\text{H}\}$ resonances at $\delta$ 19.7 and 19.4 with the increase of KCl concentration (pD = 1.07)	190
<b>Figure 4.13</b>	Comparison of $^{13}\text{C}\{^1\text{H}\}$ NMR spectral change of $[\text{GaCl}_2\cdot\mathbf{1}]\text{Cl}$ in acidic $\text{D}_2\text{O}$ (pD = 1.07) with the increase of KCl concentration	191
<b>Figure 4.14</b>	Top: Proton NMR spectrum of $[\text{InBr}_2\cdot\mathbf{1}]\text{Br}$ (N-D complex) in $\text{D}_2\text{O}$ . Bottom: $^{13}\text{C}\{^1\text{H}\}$ NMR spectrum of this complex in $\text{D}_2\text{O}$	191
<b>Figure 4.15</b>	Comparison of $^1\text{H}$ NMR spectra of 0.030 M, 0.018 M and 0.0030 M $[\text{InBr}_2\cdot\mathbf{1}]\text{Br}$ in $\text{D}_2\text{O}$	192
<b>Figure 4.16</b>	(a) Proton NMR spectrum of $[\text{InBr}_2\cdot\mathbf{2}]\text{Br}$ (N-D complex) in $\text{D}_2\text{O}$	192
	(b) $^{13}\text{C}\{^1\text{H}\}$ NMR spectrum of $[\text{InBr}_2\cdot\mathbf{2}]\text{Br}$ (N-D complex) in $\text{D}_2\text{O}$	193
<b>Figure 4.17</b>	$^{13}\text{C}\{^1\text{H}\}$ NMR spectrum of $[\text{GaCl}_2\cdot\mathbf{1}]\text{Cl}$ in $\text{CD}_3\text{CN}$	193
<b>Figure 4.18</b>	$^{13}\text{C}\{^1\text{H}\}$ NMR spectrum of $[\text{InBr}_2\cdot\mathbf{2}]\text{Br}$ in $\text{CD}_3\text{CN}$	194
<b>Figure 4.19</b>	$^1\text{H}$ NMR spectrum of $[\text{InBr}_2\cdot\mathbf{2}]\text{Br}$ in $\text{CD}_3\text{CN}$	194
<b>Figure 4.20</b>	A 2D [ $^1\text{H}$ , $^{13}\text{C}$ ] HMQC NMR spectrum of $[\text{InBr}_2\cdot\mathbf{2}]\text{Br}$ in $\text{CD}_3\text{CN}$	195
<b>Figure 4.21</b>	A 2D [ $^1\text{H}$ , $^1\text{H}$ ] COSY spectrum of $[\text{InBr}_2\cdot\mathbf{2}]\text{Br}$ in $\text{CD}_3\text{CN}$	195
<b>Figure 4.22</b>	Solution structure of $[\text{InBr}_2\cdot\mathbf{2}]\text{Br}$ with a $C_{2v}$ symmetry	196
<b>Figure 4.23</b>	$^1\text{H}$ NMR spectrum of $[\text{Ga}(\mathbf{8}\text{-}2\text{H})](\text{NO}_3)$ in $\text{D}_2\text{O}$	197

<b>Figure 4.24</b>	X-ray structure of $[\text{GaCl}_2 \cdot \mathbf{1}]\text{Cl}$ ( <b>149</b> )	198
<b>Figure 4.25</b>	X-ray structure of $[\text{InBr}_2 \cdot \mathbf{1}]\text{Br}$ ( <b>150</b> )	200
<b>Figure 4.26</b>	X-ray structure of $[\text{InBr}_2 \cdot \mathbf{2}]\text{Br}$ ( <b>152</b> )	202
<b>Figure 4.27</b>	X-ray structure of $[\text{Ga} \cdot (\mathbf{8-2H})](\text{NO}_3)$ ( <b>153</b> )	203
<b>Figure 4.28</b>	IR (KBr) spectrum of the recrystallization product of $\text{Cu}(\mathbf{1})(\text{ClO}_4)_2$ from MeCN	208
<b>Figure 4.29</b>	IR (KBr) spectrum of the recrystallization product of $\text{Cu}(\mathbf{2})(\text{ClO}_4)_2$ from MeCN	208
<b>Figure 4.30</b>	A $^1\text{H}$ NMR spectrum of colorless crystals obtained from an attempted recrystallization of $\text{Cu}(\mathbf{1})(\text{ClO}_4)_2$ from refluxing MeCN	209
<b>Figure 4.31</b>	The IR (KBr) spectrum of $\text{Cu}_2(\text{OH})(\mathbf{1})_2(\text{ClO}_4)_3(\text{H}_2\text{O})$	211
<b>Figure 4.32</b>	The IR (KBr) spectrum of $\text{Cu}(\mathbf{1})(\text{ClO}_4)_2$	211
<b>Figure 4.33</b>	The IR (KBr) spectrum of $\text{Cu}(\mathbf{3})(\text{ClO}_4)_2$	212
<b>Figure 4.34</b>	(a) The IR (KBr) spectrum of $[\text{Cu}(\mathbf{3})(\text{CH}_3\text{CN})](\text{ClO}_4)_2$	213
	(b) The IR (KBr) spectrum of $\text{Cu}(\mathbf{4})(\text{CH}_3\text{CN})_2(\text{ClO}_4)_2$	213
<b>Figure 4.35</b>	(a) The IR (KBr) spectrum of $[\text{Cu}_2(\mu\text{-}\eta^1\text{:}\eta^2\text{-CO}_3)(\mathbf{4})_2](\text{ClO}_4)_2$	214
	(b) The IR (KBr) spectrum of $\text{Cu}(\mathbf{4})(\text{ClO}_4)_2$	214
<b>Figure 4.36</b>	The electronic spectrum of $\text{Cu}_2(\text{OH})(\mathbf{1})_2(\text{ClO}_4)_3(\text{H}_2\text{O})$ in acetonitrile	215
<b>Figure 4.37</b>	(a) The electronic spectrum of $[\text{Cu} \cdot \mathbf{2}(\mu\text{-Cl})]_2\text{Cl}_2$ in water	216
	(b) The electronic spectrum of $\text{Cu}(\mathbf{2})(\text{ClO}_4)_2$ in water	216
<b>Figure 4.38</b>	X-ray structure of $[\text{Cu} \cdot \mathbf{2}(\mu\text{-Cl})]_2\text{Cl}_2$ ( <b>155</b> )	217
<b>Figure 4.39</b>	X-ray structure of $[\text{Cu}(\mathbf{2})(\text{CH}_3\text{OH})(\text{ClO}_4)](\text{ClO}_4)$ ( <b>156a</b> )	219

<b>Figure 4.40</b>	X-ray structure of [Cu(3)(CH <sub>3</sub> CN)](ClO <sub>4</sub> ) <sub>2</sub> ( <b>157a</b> )	222
<b>Figure 4.41</b>	X-ray structure of CuCl <sub>2</sub> •4 ( <b>158</b> )	224
<b>Figure 4.42</b>	X-ray structure of [Cu <sub>2</sub> (μ-η <sup>1</sup> :η <sup>2</sup> -CO <sub>3</sub> )(4) <sub>2</sub> ](ClO <sub>4</sub> ) <sub>2</sub> ( <b>159</b> )	226
<b>Figure 4.43</b>	X-ray structure of [(Cu• <b>112</b> ) <sub>3</sub> (μ <sub>3</sub> -CO <sub>3</sub> )](ClO <sub>4</sub> ) <sub>4</sub> (H <sub>2</sub> O) <sub>2</sub>	228
<b>Figure 4.44</b>	The IR (KBr) spectrum of [Cu• <b>5</b> ](NO <sub>3</sub> ) <sub>2</sub> ( <b>161</b> )	231
<b>Figure 4.45</b>	The IR (KBr) spectrum of [Cu• <b>6</b> ](ClO <sub>4</sub> ) <sub>2</sub> ( <b>162</b> )	232
<b>Figure 4.46</b>	The UV-Vis spectrum of [Cu• <b>6</b> ](ClO <sub>4</sub> ) <sub>2</sub> in water	233
<b>Figure 4.47</b>	The UV-Vis spectrum of [Cu•( <b>8-2H</b> )](NaClO <sub>4</sub> ) in water	233
<b>Figure 4.48</b>	X-ray structure of [Cu• <b>5</b> ](NO <sub>3</sub> ) <sub>2</sub> ( <b>161</b> )	235
<b>Figure 4.49</b>	X-ray structure of the five-coordinate Cu(2) center in [Cu• <b>6</b> ](ClO <sub>4</sub> ) <sub>2</sub> ( <b>162</b> )	237
<b>Figure 4.50</b>	X-ray structure of the five-coordinate Cu(1) center with MeOH hydrogen bonding in [Cu• <b>6</b> ](ClO <sub>4</sub> ) <sub>2</sub> ( <b>162</b> )	239
<b>Figure 4.51</b>	X-ray structure of the six-coordinate Cu(3) center in [Cu• <b>6</b> ](ClO <sub>4</sub> ) <sub>2</sub> ( <b>162</b> )	241
<b>Figure 4.52</b>	X-ray structure of [Cu•( <b>8-2H</b> )](NaNO <sub>3</sub> ) ( <b>166</b> )	242
<b>Figure 5.1</b>	Cross-bridged ligands and ligand <b>tet-a</b> used in kinetic stability studies	245
<b>Figure 5.2</b>	<sup>1</sup> H NMR spectra recorded at different time periods for [InBr <sub>2</sub> • <b>2</b> ]Br in D <sub>2</sub> O	246
<b>Figure 5.3</b>	<sup>1</sup> H NMR spectra recorded after [InBr <sub>2</sub> • <b>1</b> ]Br was dissolved in D <sub>2</sub> O	247
<b>Figure 5.4</b>	<sup>1</sup> H NMR spectra recorded after [GaCl <sub>2</sub> • <b>2</b> ]Cl was dissolved in D <sub>2</sub> O	247
<b>Figure 5.5</b>	<sup>1</sup> H NMR spectra after [GaCl <sub>2</sub> • <b>1</b> ]Cl was dissolved in acidic D <sub>2</sub> O	248
<b>Figure 5.6</b>	<sup>1</sup> H NMR spectra after [Ga•( <b>8-2H</b> )](NO <sub>3</sub> ) was dissolved in acidic D <sub>2</sub> O	248

<b>Figure 5.7</b>	The most upfield doublets of pentets in the $^1\text{H}$ NMR spectrum of $\text{Cd}(\text{NO}_3)_2 \cdot \mathbf{1}$ in buffered $\text{D}_2\text{O}$ (pD = 5.9, MES)	250
<b>Figure 5.8</b>	A typical kinetic plot of $\ln(C_0/C)$ vs time ( $t$ ) in the acid decomplexation of $\text{Cd}(\text{NO}_3)_2 \cdot \mathbf{1}$ in buffered $\text{D}_2\text{O}$	251
<b>Figure 5.9</b>	A typical kinetic plot of $\ln(C_0/C)$ vs time ( $t$ ) in the acid decomplexation of $\text{Zn}(\text{NO}_3)_2 \cdot \mathbf{1}$ in buffered $\text{D}_2\text{O}$	252
<b>Figure 5.10</b>	Comparison of $^1\text{H}$ NMR spectra of $\text{Me}_4\text{Cyclam}$ in buffered $\text{D}_2\text{O}$ (pD = 5.0, HOAc/NaOAc)	253
<b>Figure 5.11</b>	The most downfield doublet of doublets in the $^1\text{H}$ NMR spectrum of $[\text{Zn}(\text{OH}_2)_2 \cdot \mathbf{2}](\text{ClO}_4)_2$ in buffered $\text{D}_2\text{O}$ (pD = 5.0, HOAc/NaOAc)	254
<b>Figure 5.12</b>	$^1\text{H}$ NMR spectrum of $[\text{Cd}(\eta^2\text{-NO}_3)_2 \cdot \mathbf{2}]$ in buffered $\text{D}_2\text{O}$ (pD = 5.0, HOAc/NaOAc)	254
<b>Figure 5.13</b>	$^1\text{H}$ NMR spectrum of $[\text{Cd}(\eta^2\text{-NO}_3)_2 \cdot \mathbf{2}]$ in buffered $\text{D}_2\text{O}$ (pD = 5.9, MES)	255
<b>Figure 5.14</b>	$^1\text{H}$ NMR spectrum of $\text{HgCl}_2 \cdot \mathbf{2}$ in buffered $\text{D}_2\text{O}$ (pD = 5.9, MES) recorded 14 minutes after this complex was dissolved	255
<b>Figure 5.15</b>	$^1\text{H}$ NMR spectrum of $\text{HgCl}_2 \cdot \mathbf{2}$ in buffered $\text{D}_2\text{O}$ (pD = 5.9, MES) recorded 163 minutes after dissolving	256
<b>Figure 5.16</b>	Comparison of $^1\text{H}$ NMR spectra of protonated $\mathbf{2}$ in buffered $\text{D}_2\text{O}$ (pD = 5.0, HOAc/NaOAc) and protonated $\mathbf{2}$ plus two crystals of $\text{Zn}(\text{ClO}_4)_2 \cdot 6\text{H}_2\text{O}$	257
<b>Figure 5.17</b>	$^1\text{H}$ NMR spectrum of $[\text{Zn} \cdot \mathbf{6}](\text{ClO}_4)_2$ in buffered $\text{D}_2\text{O}$ (pD = 5.0, HOAc/NaOAc) at equilibrium and that of a mixture of $[\text{Zn} \cdot \mathbf{6}](\text{ClO}_4)_2$ in buffered $\text{D}_2\text{O}$ (pD = 5.0, HOAc/NaOAc) at equilibrium plus excess protonated $\mathbf{6}$	257
<b>Figure 5.18</b>	(a) A kinetic plot of $\ln(C_0/C)$ vs time ( $t$ ) in the acid decomplexation of $[\text{Zn} \cdot \mathbf{6}](\text{ClO}_4)_2$ in buffered $\text{D}_2\text{O}$	258
	(b) A kinetic plot of $\ln(C_0/C)$ vs time ( $t$ ) in the acid decomplexation of $[\text{Zn} \cdot \mathbf{6}](\text{ClO}_4)_2$ in buffered $\text{D}_2\text{O}$ excluding two data points collected after 3000 minutes	258

<b>Figure 5.19</b>	A kinetic plot of $\ln(C_0/C)$ vs time ( $t$ ) in the acid decomplexation of $[\text{Zn}\cdot\mathbf{6}](\text{ClO}_4)_2$ in buffered $\text{D}_2\text{O}$	259
<b>Figure 5.20</b>	$^1\text{H}$ NMR spectrum of $\text{Zn}(\text{NO}_3)_2\cdot\mathbf{1}$ in acidic $\text{D}_2\text{O}$ (5 M HCl)	260
<b>Figure 5.21</b>	$^{13}\text{C}\{^1\text{H}\}$ NMR spectrum of $[\text{Hg}\cdot(\mathbf{7-2H})](\text{K}_2\text{HgCl}_4)$ ( <b>148</b> ) after it was kept in $\text{D}_2\text{O}$ for 48 days	261
<b>Figure 5.22</b>	$^1\text{H}$ NMR spectrum of $[\text{Zn}\cdot(\mathbf{7-2H})](\text{NaClO}_4)$ in acidic $\text{D}_2\text{O}$ (pD = 5.0, HOAc/NaOAc) after 70 days	261
<b>Figure 5.23</b>	$^{13}\text{C}\{^1\text{H}\}$ NMR spectrum of $[\text{Zn}\cdot(\mathbf{7-2H})](\text{NaClO}_4)$ in acidic $\text{D}_2\text{O}$ (pD = 5.0, HOAc/NaOAc) after 70 days	262
<b>Figure 5.24</b>	The electronic spectrum of $\text{Cu}_2(\text{OH})(\mathbf{1})_2(\text{ClO}_4)_3(\text{H}_2\text{O})$ in aqueous 5N HCl	263
<b>Figure 5.25</b>	The electronic spectrum of 0.00905 M $\text{CuCl}_2$ in aqueous 5N HCl	263
<b>Figure 5.26</b>	A plot of $-\ln A$ vs time ( $t$ ) in the acid decomplexation of $\text{Cu}_2(\text{OH})(\mathbf{1})_2(\text{ClO}_4)_3$ in 5N HCl	264
<b>Figure 5.27</b>	The electronic spectrum of $[\text{Cu}\cdot(\mathbf{7-2H})](\text{NaClO}_4)(\text{NaCF}_3\text{COO})_{0.5}(\text{H}_2\text{O})_{1.5}$ in aqueous 5N HCl	265
<b>Figure 5.28</b>	The electronic spectrum of $[\text{Cu}\cdot\mathbf{2}(\mu\text{-Cl})]_2\text{Cl}_2$ after 2 minutes in aqueous 5N HCl	266
<b>Figure 5.29</b>	The electronic spectrum of $[\text{Cu}\cdot(\mathbf{8-2H})](\text{NaClO}_4)$ after 2 minutes in aqueous 5N HCl	266
<b>Figure 5.30</b>	The electronic spectrum of $[\text{Cu}\cdot\mathbf{6}](\text{ClO}_4)_2$ after 3 minutes in aqueous 5N HCl	267
<b>Figure 5.31</b>	The electronic spectrum of $[\text{Cu}\cdot(\mathbf{8-2H})](\text{NaClO}_4)$ after 63 minutes in aqueous 5N HCl	267
<b>Figure 5.32</b>	The electronic spectrum of $[\text{Cu}\cdot\mathbf{6}](\text{ClO}_4)_2$ after 52 minutes in aqueous 5N HCl	268
<b>Figure 5.33</b>	A kinetic plot of $-\ln A$ vs time ( $t$ ) in the acid decomplexation of red-isomer $\text{Cu}(\text{tet } \mathbf{a})(\text{ClO}_4)_2$ in 5N HCl	268



## ABSTRACT

# SYNTHETIC, STRUCTURAL, AND STABILITY STUDIES OF METAL COMPLEXES OF CROSS-BRIDGED TETRAAMINE MACROCYCLES

BY

WEIJUN NIU

University of New Hampshire, September, 2003

Cross-bridging of tetraazamacrocyclic ligands with an ethylene unit forms a family of bicyclic tetraamine ligands originally designed and synthesized by the Weisman-Wong research group to selectively complex small metal ions such as  $\text{Li}^+$  in a *cis*-folded configuration. Cu(II), Ga(III), and In(III) complexes of these cross-bridged ligands have potential radiometal-based pharmaceutical applications. It has been generally accepted that high kinetic stability of a metal complex is important to realize this potential. Cu(II) complexes of eight cross-bridged tetraazamacrocyclic ligands have been synthesized and structurally characterized. Their relative kinetic stabilities were evaluated by monitoring acid-promoted dissociation processes using UV-Vis spectroscopy. The copper complex of a dicarboxylate pendant-armed cross-bridged cyclam (ligand 7) was the most inert, consistent with its superior *in vivo* stability. This is also in accord with the fact that copper fits best in this ligand as indicated by the largest  $\text{N}_{\text{ax}}\text{-Cu-N}_{\text{ax}}$  bond angle of this complex compared to any other six-coordinate Cu(II) complexes of cross-bridged ligands. Ga(III) and In(III) complexes of three of the ligands

have also been prepared and characterized. The indium complex of cross-bridged cyclen with the poorest fit in the solid-state showed the lowest inertness as indicated by its partial decomplexation in water. By contrast, gallium complexes of cross-bridged cyclam (ligand 1) and a dicarboxylate pendant-armed cross-bridged cyclen have been found to be stable in acidic  $D_2O$  (pD = 1.07) for more than seven months. Thus we were able to investigate the possible solution structures of the Ga(III) complex with ligand 1 in acidic  $D_2O$  using NMR techniques. Zn(II), Cd(II) and Hg(II) complexes of the eight cross-bridged ligands have been synthesized and whenever appropriate, structurally characterized. Comparison of their solid-state structures suggested the selectivity of this family of cross-bridged ligands for Zn(II) ion based on its best fit inside the cleft formed by the cross-bridged ligands. The solution structures of these metal complexes were also investigated using NMR spectroscopy. In addition, the kinetic stabilities of selected Zn(II), Cd(II) and Hg(II) complexes were studied. As with copper and indium complexes, the Zn(II) complex of cross-bridged cyclam is more inert than that of cross-bridged cyclen. These results indicate that cross-bridged cyclam and its derivatives have more potential for radiopharmaceutical applications than related cross-bridged cyclen and its derivatives.

## CHAPTER I

### GENERAL INTRODUCTION

Macrocyclic ligands are ring compounds whose structures can allow several of their donor atoms to bind to a single metal.<sup>1</sup> They are divided into two major classes. One features the oxygen donors, such as the crown ethers and oxygen-based cryptands.<sup>2,3</sup> The other contains nitrogen donor sites.<sup>4,5</sup> Compared to their acyclic analogues, macrocyclic complexes typically have higher kinetic inertness as well as higher thermodynamic stability.<sup>5,6</sup> Among macrocyclic complexes, metal complexes of cyclic tetraamines and their derivatives have played an important role in a variety of research areas. These areas include coordination chemistry,<sup>7,8</sup> cancer therapy,<sup>9,10</sup> contrast agents,<sup>11</sup> catalysis,<sup>7</sup> enzyme mimics,<sup>12,13</sup> supramolecular chemistry,<sup>14,15,16</sup> and molecular switches.<sup>17</sup>

This doctoral research focuses on the coordination chemistry of eight bicyclic tetraamine ligands with a bridging ethylene connecting nonadjacent nitrogens (**Figure 1.1**). These ligands were originally designed by our research group for selective complexation with small metal ions such as lithium(I) and copper(II).<sup>18,19</sup> The metals used for complexation here include Cu(II), Ga(III), In(III), Zn(II), Cd(II) and Hg(II). Since ligands **1-4** are ethylene-cross-bridged cyclam and cyclen and ligands **5-8** are carboxylate and carbamoyl derivatives of ethylene-cross-bridged cyclam and cyclen,

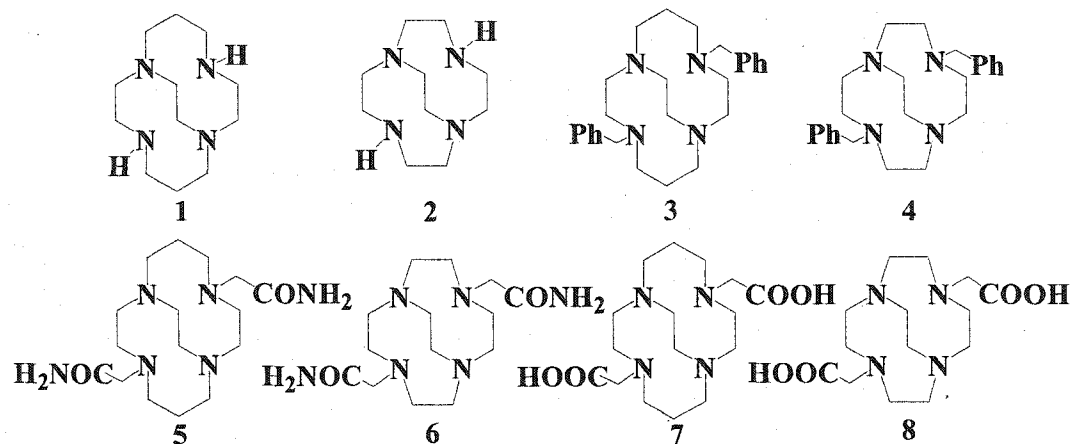


**Figure 1.1** Cross-bridged ligands studied in this research.

literature work on the coordination chemistry of cyclam, cyclen, and their derivatives including carboxylate and carbamoyl derivatives will be discussed.

## 1. Coordination Chemistry of Cyclam, Cyclen and their Derivatives and Potential Applications of these Complexes.

### 1.1 General Information on Coordination Chemistry of cyclam and cyclen.

A family of macrocyclic tetraamines is shown in **Figure 1.2**. 1,4,8,11-tetraazacyclotetradecane (cyclam, 14-ane-N<sub>4</sub>) (**9** in **Figure 1.3**) and 1,4,7,10-tetraazacyclododecane (cyclen, 12-ane-N<sub>4</sub>) (**10** in **Figure 1.3**) have been the most studied of macrocyclic tetraamines. The 14-membered cyclam and its derivatives are fairly flexible.

According to Bosnich, they can potentially adopt any of the five coordinated configurations (**I** to **V** in **Figure 1.4**) in their metal complexes featuring two five-

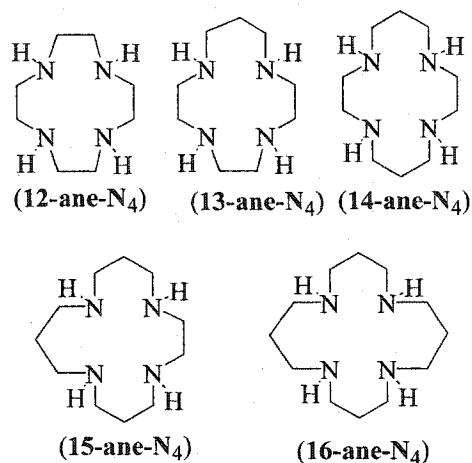


**Figure 1.2** A family of macrocyclic tetraamines.

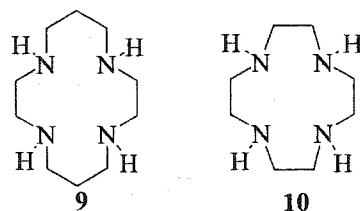


**Figure 1.3** Cyclam and Cyclen.

membered and two six-membered chelate rings.<sup>7,20,21</sup> Both *cis*-folded and *trans*-isomers are possible for the three configurations I, II and V. In their complexes with specific cations, cyclam and its derivatives may prefer one configuration over the others.<sup>22(a-d)</sup> For example, the preferred low-energy configuration of cyclam and its derivatives in their Cu(II) complexes is the *trans*-III.<sup>22(a-e)</sup> By contrast, the metallation of N', N'', N''', N''''-tetramethylcyclam (Me<sub>4</sub>Cyclam) by transition metal ions typically leads to five-coordinate *trans*-I type isomers.<sup>22(a-e)</sup> Only very recently, several Cu(II) complexes of this ligand in a *trans*-III configuration have been structurally characterized.<sup>22(c-e)</sup> The 12-membered cyclen and its derivatives may adopt any of the four coordinated configurations (I, II, III (IV) and V in Figure 1.5) in their metal complexes, giving four

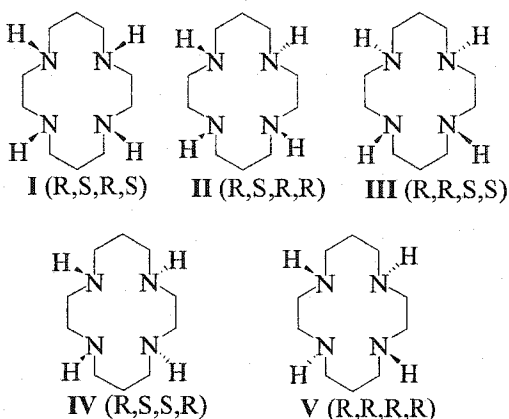


**Figure 1.4** Five possible configurations of cyclam in its metal complexes.

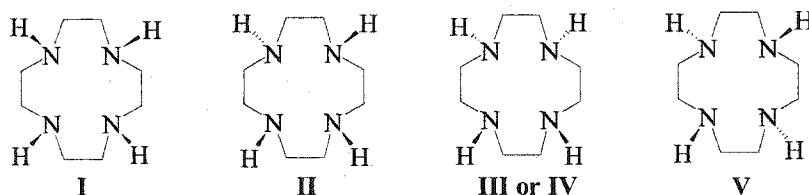


**Figure 1.5** Four possible configurations of cyclen in its metal complexes.

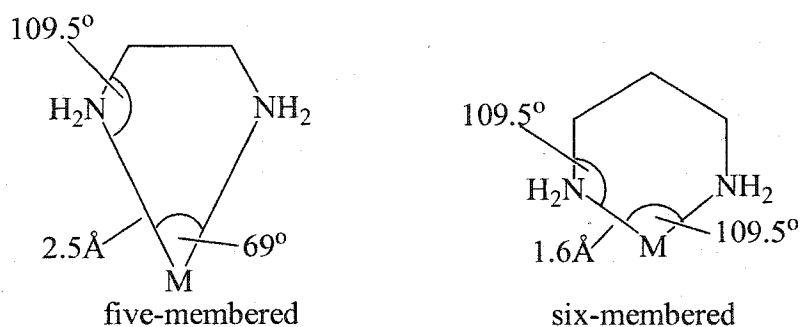


**Figure 1.6** The metal-to-ligand bond lengths and bite angles that produce the minimum-strain energy structures for chelate rings of sizes five and six with saturated chelate rings containing nitrogen donors.

five-membered chelate rings. The available crystal structures indicate that the *trans*-I configuration is dominant.<sup>22a</sup> Consistently, MM calculations have shown that the *trans*-III configuration of coordinated cyclen and its derivatives are at much higher energy than the *trans*-I configuration.<sup>22a</sup> The minimum-strain geometries (MM calculation) for

chelate rings of sizes five and six, involving neutral nitrogen donors, are shown in **Figure 1.6**.

Metal ions complexed by cyclam, cyclen and their derivatives comprise almost all the transition metals. Only the most relevant metal complexes will be discussed here.

## 1.2 Zinc(II) Complexes of Cyclen, Cyclam and their Derivatives.

One important metal cation is  $\text{Zn}^{2+}$  because of its biological relevance. A search of the *Cambridge Crystallographic Database* revealed a total of 58 X-ray structures of zinc complexes with cyclam and its derivatives. Most of these have the favored *trans-III* ligand configuration with a coordination number of six<sup>23(a-l)</sup> or five<sup>24(a-e)</sup>. The structure of a six-coordinate Zn(II) complex of cyclam (**11**)<sup>23(a)</sup> is shown in **Figure 1.7**. The

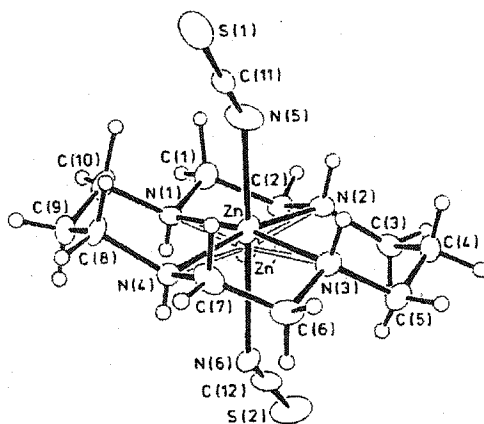


**Figure 1.7** The X-ray structure of  $[\text{Zn}(\text{cyclam})(\text{NCS})_2]$  (**11**) (Zn is disordered over two sites.).

coordination geometry around this Zn(II) center is pseudo-octahedral. The five-coordinate Zn(II) complex of meso-5,12-dimethyl-cyclam (**12**)<sup>24(c)</sup> has a distorted square pyramidal geometry (**Figure 1.8**). The adopting of a *trans*-configuration is indicated by

similar values of the N(1)-Zn-N(3) angle of  $153.7(4)^\circ$  and N(2)-Zn-N(4) angle of  $156.6(3)^\circ$  in the approximate square plane defined by the four nitrogen atoms from the macrocycle.

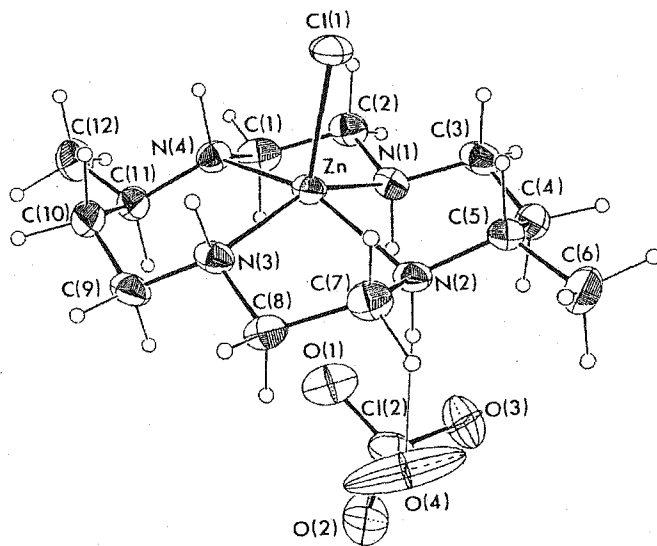


**Figure 1.8** The X-ray structure of  $[\text{Zn}(5,12\text{-dimethyl-cyclam})(\text{Cl})](\text{ClO}_4)$  (**12**).

$\text{N}'$ ,  $\text{N}''$ ,  $\text{N}'''$ ,  $\text{N}''''$ -tetramethylcyclam ( $\text{Me}_4\text{Cyclam}$ ) complexes of  $\text{Zn}(\text{II})$  have a five-coordinate *trans-I* configuration.<sup>25(a-c)</sup> The X-ray structure of such a  $\text{Zn}(\text{II})$  complex (**13**) is presented in **Figure 1.9**.<sup>25(a)</sup> The  $\text{Zn}(\text{II})$  center in **13** has square-pyramidal geometry around it. Variable-temperature  $^{13}\text{C}$  NMR spectral studies of **13** in nitromethane solution demonstrated the presence of a dynamic process (**Scheme 1.1**).<sup>25(a)</sup>

By contrast, only six *cis-V* structures are known and all of them are  $\text{Zn}(\text{II})$  complexes of cyclam derivatives.<sup>26(a-f)</sup> The X-ray structure of a dimeric  $\text{Zn}(\text{II})$  Xylyl-bicyclam complex (**14**) in such a *cis*-folded (**V**) configuration is shown in



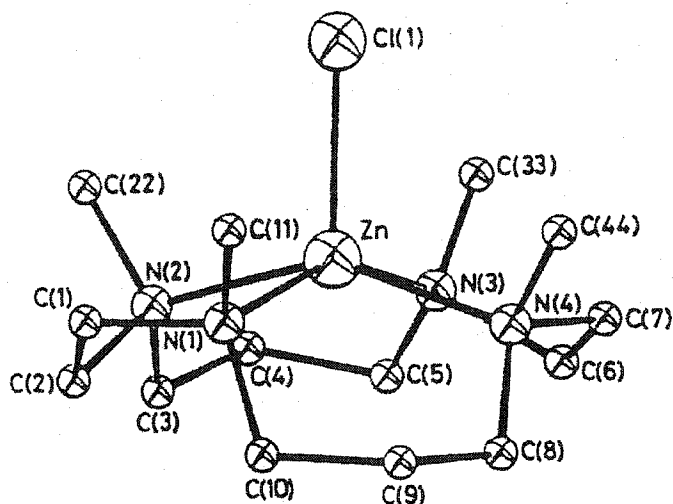
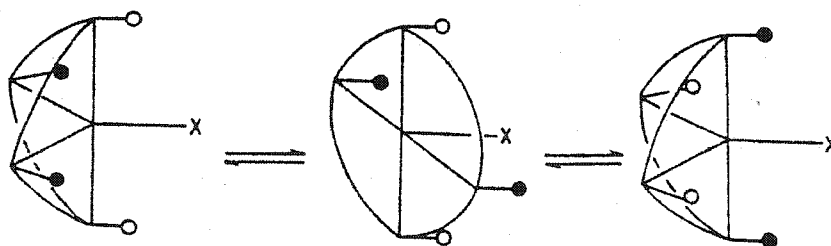


**Figure 1.9** The X-ray structure of  $[\text{Zn}(\text{Me}_4\text{Cyclam})(\text{Cl})](\text{ClO}_4)$  (13),  $\text{Me}_4\text{Cyclam} = \text{N}', \text{N}'', \text{N}''', \text{N}''''$ -tetramethylcyclam.



**Scheme 1.1** The dynamic process of  $[\text{Zn}(\text{Me}_4\text{Cyclam})(\text{Cl})](\text{ClO}_4)$  (13) in nitromethane solution.

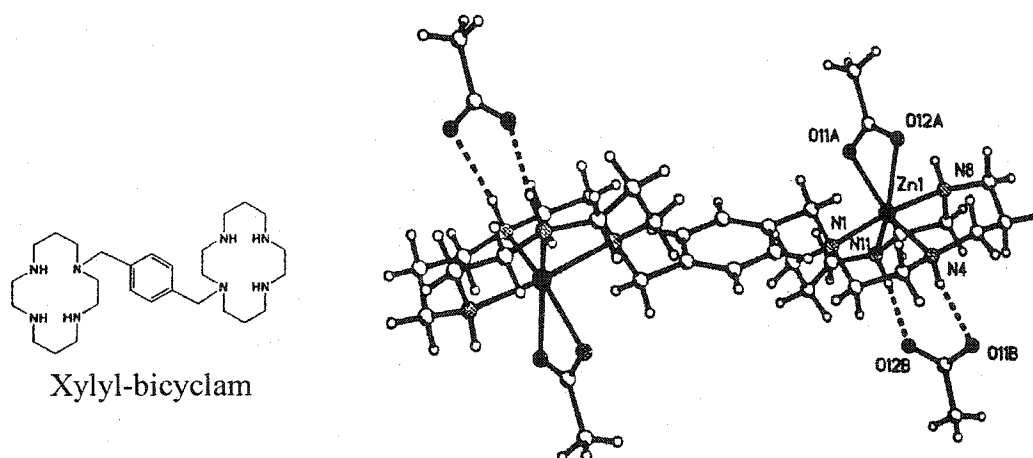
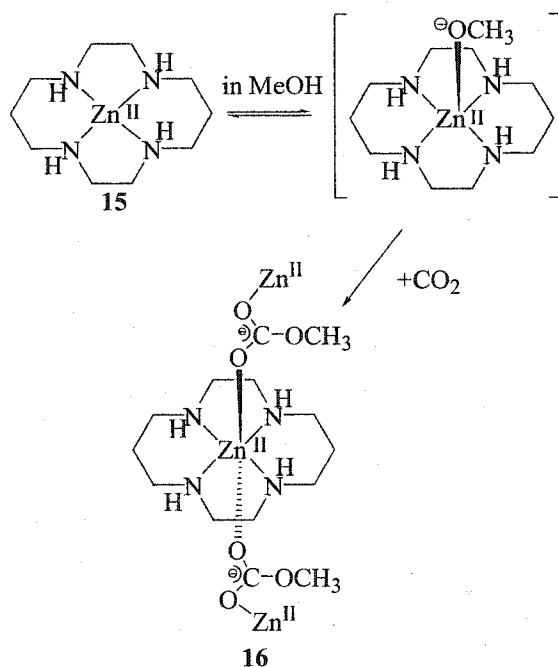


**Figure 1.10** The X-ray structure of a dimeric  $\text{Zn}(\text{II})$  Xylyl-bicyclam complex (14).

**Figure 1.10.**<sup>26(a)</sup> Here, each distorted octahedral Zn(II) center is coordinated by four nitrogen atoms from the macrocycle and a bidentate acetate. The adopting of such a *cis*-configuration is indicated by the N(1)-Zn-N(8) angle of 174.67(4)° in the axial position and N(4)-Zn-N(11) angle of 105.32(10)° in the equatorial position. In aqueous solution, the major configurations of this Zn(II) complex are *cis*-V/*trans*-I as indicated by detailed 1D and 2D NMR studies.<sup>26(a)</sup>

The coordination chemistry of Zn(II) complexes of cyclam and its derivatives has been explored in bioinorganic chemistry. In 1985, Ito and co-worker reported that carbon dioxide was fixed by the Zn(II)-cyclam complex in MeOH (**Scheme 1.2**).<sup>23(i)</sup>

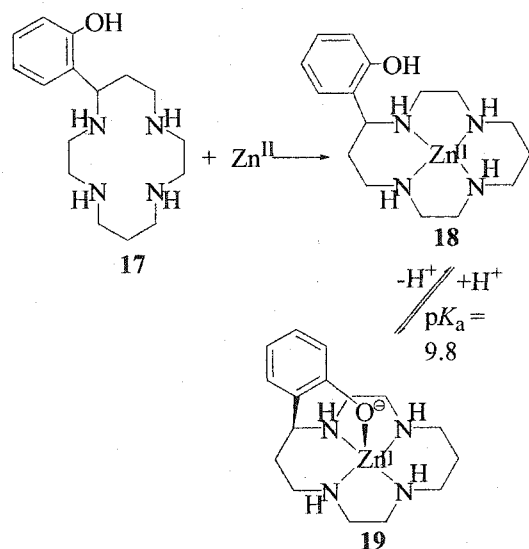


**Scheme 1.2** Carbon dioxide fixation by the Zn<sup>II</sup>-cyclam complex in MeOH.

The solid-state structure of **16** showed that pseudo-octahedral Zn<sup>2+</sup> is surrounded by cyclam in a *trans*-III configuration with two oxygen atoms from a pair of MeOCO<sub>2</sub> occupying the axial positions. The MeOCO<sub>2</sub> bridges two neighboring [Zn(cyclam)]<sup>2+</sup>

units to give a linear chain structure along the axis. More interestingly, it was found that Zn(II) complex **15** was the most effective in uptake of carbon dioxide among Ni(II), Co(II), Cu(II) and Zn(II) complexes of cyclam.<sup>27</sup> This research stimulated other research groups to use cyclen or cyclam complexes of Zn(II) to mimic the active centers in Zn(II) enzymes.

The Zn(II) complex of a phenol C-pendant-armed cyclam (**19** in Scheme 1.3) was reported by Kimura and his coworkers as a possible mimic of the anion inhibition in Carbonic Anhydrase. They were able to obtain the X-ray structure of the penta-coordinated Zn(II) complex **19**.<sup>28</sup> The coordination geometry around Zn(II) is square pyramidal. The configuration of cyclam in **19** is again the *trans*-III.



**Scheme 1.3** The formation of the Zn(II) complex of a phenol pendant-armed cyclam.

There are numerous structural reports of zinc complexes with cyclen and its pendant-armed derivatives in the literature, almost all of these have the *trans*-I ligand configuration with all four amine substituents on the same side of the macrocycle as zinc.<sup>14,15,29(a-n)</sup> Their coordination number is generally five or six<sup>14,15,29(a-m)</sup> but a higher

coordination number of seven is also found.<sup>30(a-c)</sup> An X-ray structure of a 5-coordinate Zn(II) complex of cyclen, [Zn(cyclen)-im-Zn(cyclen)](ClO<sub>4</sub>)<sub>3</sub> (**20**) (im = imidazolate) revealed that two distorted square pyramidal Zn(II) centers are bridged by an imidazolate (**Figure 1.11**)<sup>29(i)</sup>.

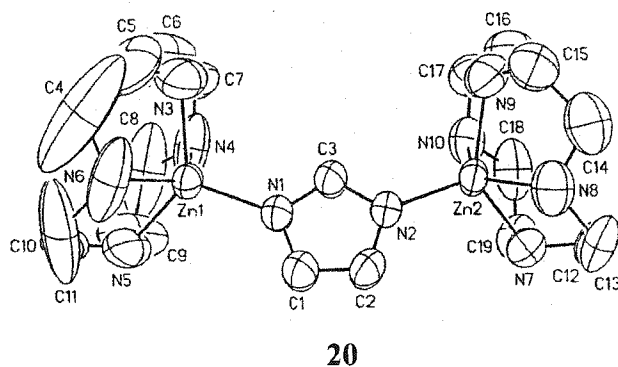


**Figure 1.11** The X-ray structure of [Zn(cyclen)-Imidazolate-Zn(cyclen)] (**20**).

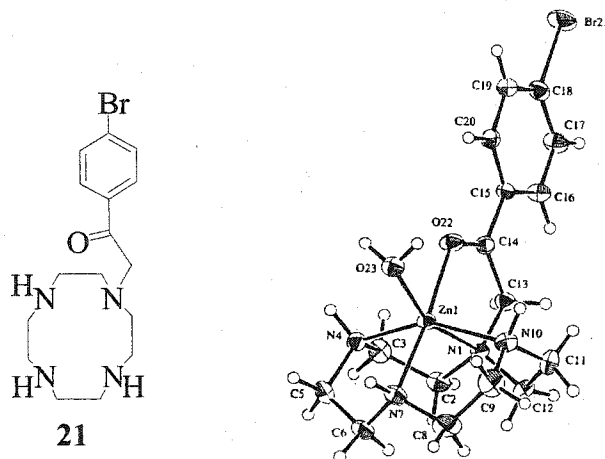


**Figure 1.12** The X-ray structure of complex [Zn(II)**21**(H<sub>2</sub>O)]<sup>2+</sup>.

The X-ray structure of a 6-coordinate Zn(II) complex with a pendant-armed cyclen derivative (ligand **21**) is shown in **Figure 1.12**.<sup>29(f)</sup> The Zn(II) atom in this complex is octahedrally coordinated by four nitrogen atoms, one carbonyl oxygen from the pendant arm and the water oxygen. An example of a seven-coordinate Zn(II) complex is the X-

ray structure of  $[\text{Zn}(\text{II})\mathbf{22}]^{2+}$  (Figure 1.13).<sup>30(a)</sup> The zinc ion is seven-coordinated by the four nitrogen atoms of the macrocycle and three N atoms of the pyrazole groups. The coordination polyhedron of  $\mathbf{22}$  may be approximately described as a pentagonal bipyramid. Zn(II) complexes of parent cyclen ( $\mathbf{10}$ ) prefer the coordination number five.<sup>29(a),(d),(h-j)</sup> Studies of Zn(II) with cyclen and its derivatives have been carried out mainly by Kimura and his coworkers. These Zn(II) complexes have been extensively examined as models for Zn(II) enzymes such as Alkaline Phosphatase (AP), Carboxypeptidase (CP), Carbonic Anhydrase (CA) and Alcohol Dehydrogenase (AD).<sup>31,32</sup>

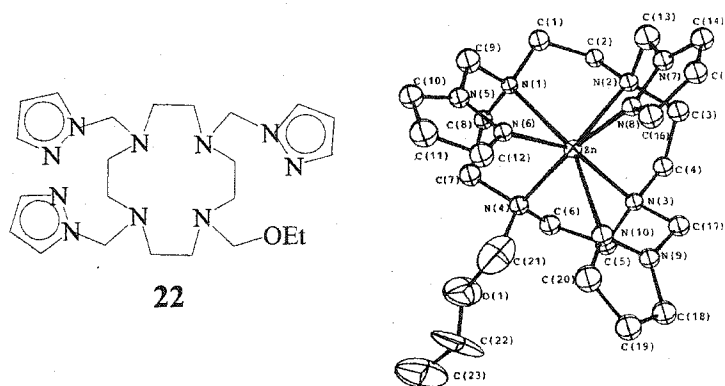


Figure 1.13 The X-ray structure of complex  $[\text{Zn}(\text{II})\mathbf{22}]^{2+}$ .

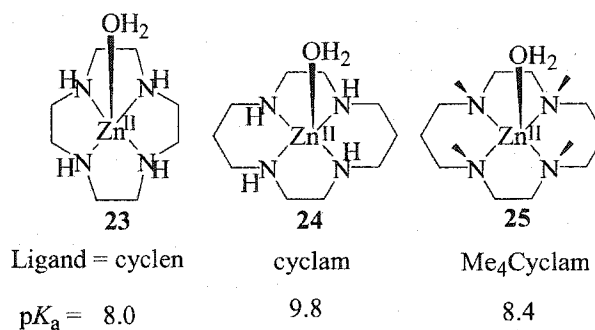
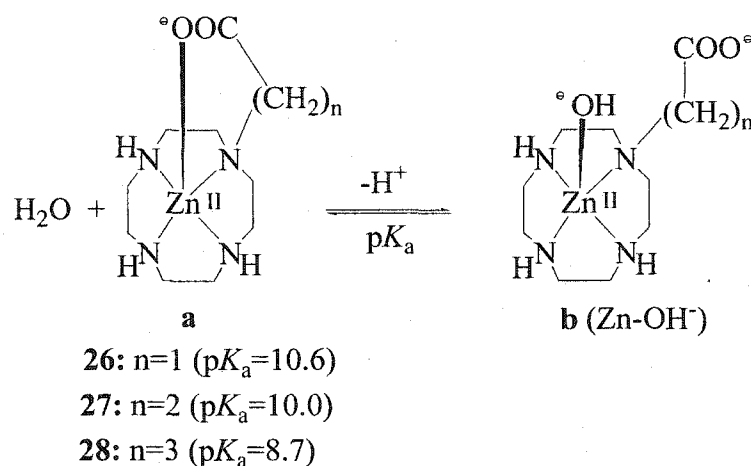


Figure 1.14 The  $\text{p}K_a$  values for  $\text{L-Zn-OH}_2^{2+} \xrightleftharpoons{K_a} \text{L-Zn-OH}^+ + \text{H}^+$ .

Since it is well established that the  $Zn^{II}-OH^-$  and/or  $Zn-OR^-$  are the most critical reactants with substrates in Zn(II) enzymes, Kimura's group has been quite interested in how coordination influences the Zn(II) Lewis acidity which promotes proton dissociation from  $[Zn^{II}-OH_2]^{2+}$  or  $[Zn^{II}-OHR]^{2+}$ . The  $pK_a$  values of  $[Zn^{II}-OH_2]^{2+}$  complexes (**23**, **24**, and **25** in **Figure 1.14**) of three cyclic tetraamines are significantly higher than those for CA ( $\sim 7$ ) and carboxypeptidase A (CPA) ( $\sim 6$ ). In fact, few model complexes showed such low  $pK_a$  values of Zn-bound  $H_2O$ . Hence, Kimura surmised since the  $Zn^{II}$  ion alone can not generate sufficient Zn(II)- $OH^-$  species at a physiological pH,<sup>33</sup> this generation may be possible only in the presence of nearby complementary strong bases such as carboxylates within the active sites.



**Scheme 1.4** The equilibrium between the carboxylate-bound and the carboxylate-unbound forms of Zn(II) complexes of carboxylate pendant-armed cyclens.

Acetate is another anionic inhibitor of CA. Zn(II) complexes of carboxymethyl-ligand **26**, carboxyethyl-ligand **27**, and carboxypropyl pendant-armed cyclen **28** (**Scheme 1.4**) were thus prepared by Kimura's group.<sup>34</sup> As shown in **Scheme 1.4**, in acidic solution, all these  $Zn^{2+}$  complexes exist in equilibrium between the carboxylate-

bound and the carboxylate-unbound forms. **28a** has the lowest  $pK_a$  value (8.7) because the seven-membered chelate ring from the carboxylate arm is not stable.  $\text{OH}^-$  can thus easily displace it to give **28b**. In fact, the solid-state structure of **28a** shows a dimeric Zn(II) complex, **29** (Figure 1.15), which is in equilibrium with the monomeric species **28a** in aqueous solution. The reactivity order in 4-nitrophenyl acetate (NA) hydrolysis at pH 9.3 was found to be **28**  $\gg$  **27**  $>$  **26**. This is consistent with the fact that **28a** has the lowest  $pK_a$  value.

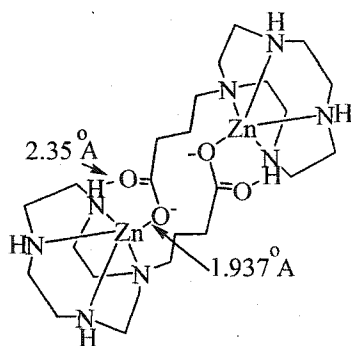
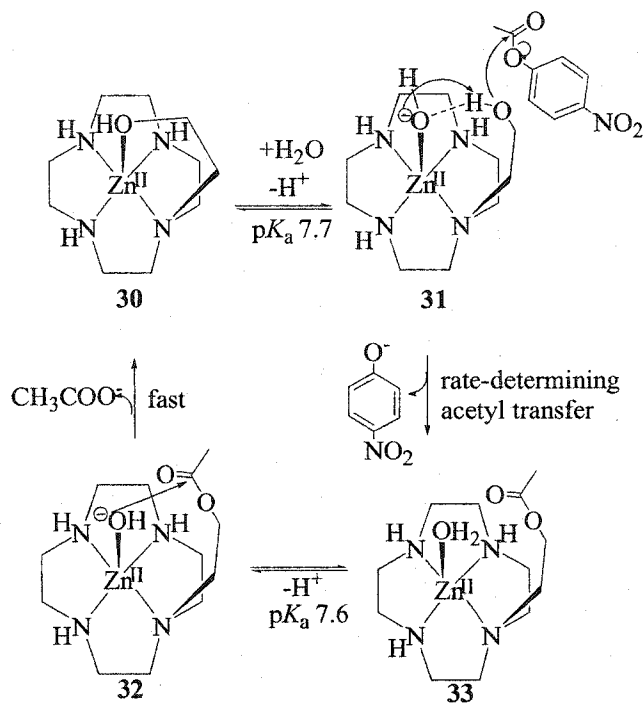
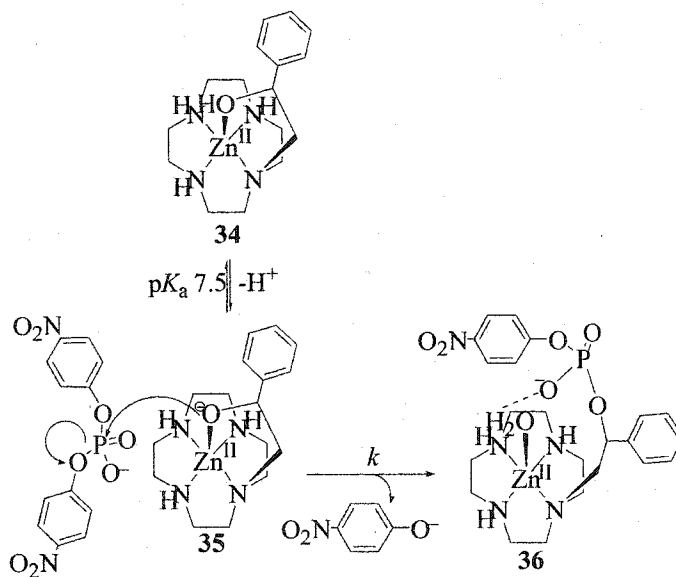


**Figure 1.15** The solid-state structure of **29**.

The neutral inhibitors of CA include weak acids such as sulfonamides, carboxamides and alcohols. Such inhibitors with high  $pK_a$  values may bind either as neutral molecules or as deprotonated anions to the active zinc center. To understand the effect of weak inhibitor alcohols on the Zn(II) center at the alkaline phosphatase active center, Kimura's group synthesized the Zn(II) complexes of an alcohol pendant-armed cyclen (**30** in Scheme 1.5). The X-ray structure of **30** indicated a distorted square pyramidal geometry. An overall reaction mechanism for NA hydrolysis catalyzed by **30** proposed by this group is shown in Scheme 1.5.<sup>29(b)</sup>



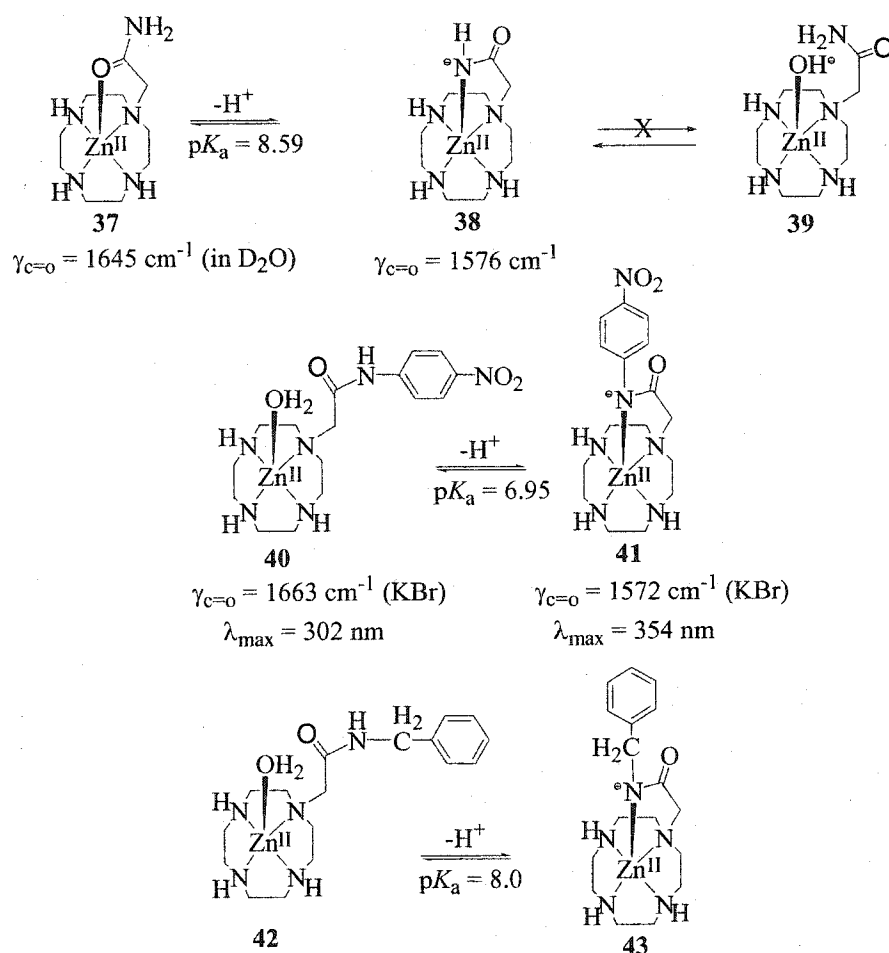
**Scheme 1.5** An overall reaction mechanism for 4-nitrophenyl acetate hydrolysis catalyzed by an alcohol pendant-armed cyclen zinc(II) complex.



**Scheme 1.6** The reaction of 34 with bis(4-nitrophenyl) phosphate yielded a "phosphoryl-transfer" intermediate 36 which was isolated.

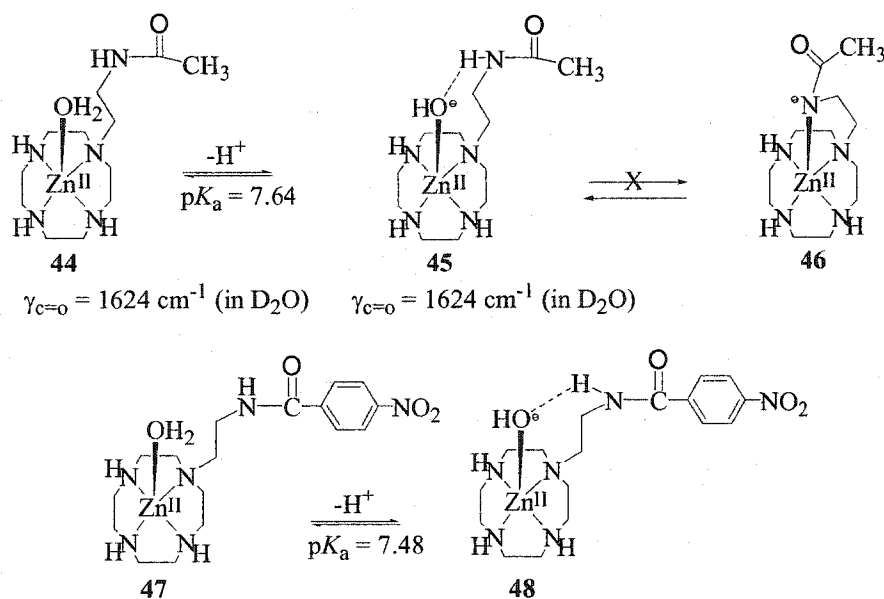


The Zn(II) complex of a benzyl alcohol pendant-armed cyclen (**34** in **Scheme 1.6**) was also synthesized and characterized by Kimura's group.<sup>36</sup> The crystal structure of the zinc(II)-bound alkoxide species **35** with a  $pK_b$  of 6.5 at 25°C showed the alkoxide closely bounded at the fifth coordination site. The direct reaction of this zinc(II) complex **35** with bis(4-nitrophenyl) phosphate yielded a "phosphoryl-transfer" intermediate **36** which was isolated.



**Scheme 1.7** Zn(II) complexes of carboxamide pendant-armed cyclens (Type one).

Interestingly, carboxamides are substrates for CPA but inhibitors for CA. Different modes of recognition of carboxamides by CA and CPA were mimicked by using various carboxamide-pendant cyclens.<sup>37</sup> Zn<sup>2+</sup> complexes of neutral carboxamides with either the carbonyl oxygen (37 in Scheme 1.7) or water molecule bound to Zn(II) were characterized by their IR and UV spectral data. The solid-state structure of 41 confirmed this assignment. Species 37, 40 and 42 represent the first models for demonstrating Zn(II)-facilitated carboxamide deprotonation. Consistent with the assumption that no Zn(II)-OH<sup>-</sup> was produced from them, none of the species in Scheme 1.7 were able to catalyze NA hydrolysis.



**Scheme 1.8** Zn(II) complexes of carboxamide pendant-armed cyclens (Type two).

In the second type of amide-pendant-armed cyclen Zn(II) complexes 44 and 47, monodeprotonation also occurred but the products were the Zn<sup>2+</sup>-OH<sup>-</sup> species 45 and 48 (Scheme 1.8) since the  $\gamma_{\text{C}=\text{O}}$  (in D<sub>2</sub>O) before (1624 cm<sup>-1</sup>) and after deprotonation (1624



the presence of large excess of other biologically important metal ions such as  $\text{Na}^+$ ,  $\text{K}^+$ ,  $\text{Ca}^{2+}$ , and  $\text{Mg}^{2+}$ .

van Eldik's group performed a detailed kinetic study of the catalytic activity of the Zn(II) complex of cyclen (**52** in **Figure 1.16**) with respect to the hydration of  $\text{CO}_2$  and dehydration of  $\text{HCO}_3^-$ .<sup>38</sup> Subsequently, an attempt to fix carbon dioxide by alcohol (ROH) to dialkyl carbonate (ROCOOR) in the presence of a base failed.<sup>29(a)</sup> During this study, they were able to obtain the X-ray structure of  $[\text{Zn}(\text{cyclen})\text{EtOH}](\text{ClO}_4)_2$  (**53** in **Figure 1.16**), which is five-coordinate with the four nitrogen donor atoms from the macrocycle and the oxygen of the coordinated ethanol. The coordination geometry around Zn(II) in **53** is distorted square pyramidal.

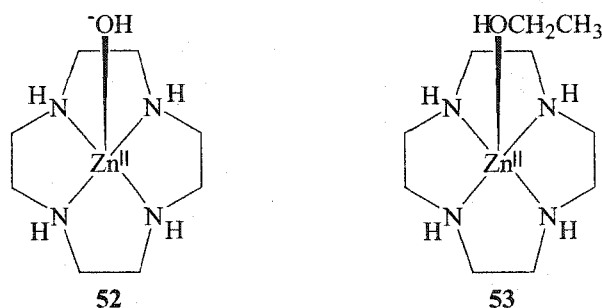


**Figure 1.16** Cation parts of two Zn(II) cyclen complexes.

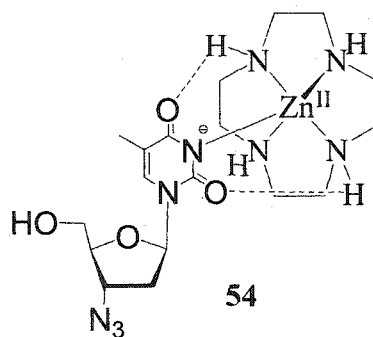


**Figure 1.17** The structure of a ternary zinc(II) complex, **54**.

Kimura's group has been interested in the selective recognition of nucleosides such as thymidine by Zn(II) complexes of cyclen derivatives.<sup>29(d),29(e),39(a-e)</sup> In 1993, they found that complex  $[\text{Zn}\cdot\text{cyclen}(\text{H}_2\text{O})](\text{ClO}_4)_2$  reacted with AZT (3'-azido-3'-deoxythymidine) in slightly basic solution to form a ternary Zn(II) complex.<sup>29(d)</sup> The crystal structure of this ternary zinc (II) complex showed that four nitrogen donors from cyclen and deprotonated  $\text{N}_a$  in AZT coordinated to Zn(II) (**54** in **Figure 1.17**). The coordination geometry around Zn(II) is again a distorted square pyramid. Such a structure might be maintained in solution as indicated by its  $^1\text{H}$  and  $^{13}\text{C}$  NMR spectra in  $d_6$ -DMSO and its solution UV absorption spectra. Several Zn(II) complexes of lipophilic cyclen derivatives (**Figure 1.18**) were also investigated as carriers for extraction of imide-containing nucleosides and nucleotides. Among these Zn(II) complexes, the most lipophilic Zn(II) complex, **58** extracted thymidine most effectively from an aqueous solution into chloroform.<sup>39(b)</sup> **58** almost quantitatively extracted more lipophilic thymidine derivatives such as AZT into chloroform.

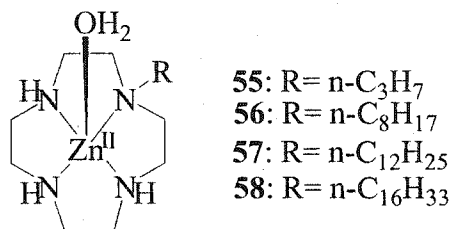


**Figure 1.18** Lipophilic Zn(II) cyclen derivative complexes.

More recently, Kimura and his coworkers found that Zn(II) complexes of cyclen derivatives with the pendant bis[(1-naphthyl)methyl] or bis[(4-quinolyl)methyl] group (**59** or **60** in **Figure 1.19**) formed the strongest binding thymine-Zn(II)-cyclen derivative

complexes.<sup>39(c)</sup> They believed that this increased binding was the result of the double  $\pi$ - $\pi$  stacking interactions between the two naphthalene rings and the zinc-bound N(3')-deprotonated 1-methylthymine in solution. Interestingly, the X-ray structure analysis of

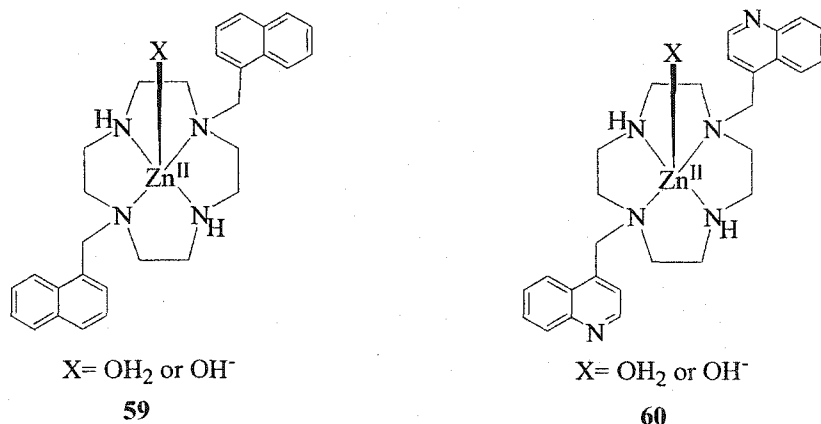


**Figure 1.19** Zn(II) complexes of two pendant-armed cyclen derivatives.

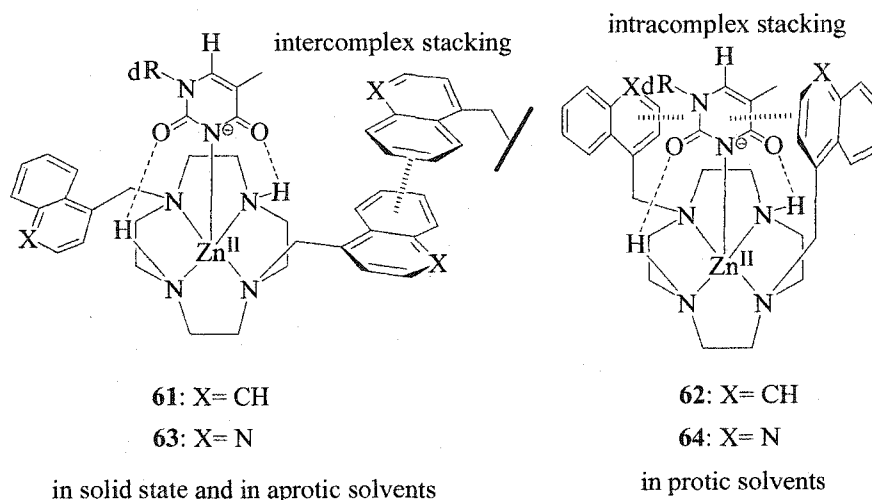


**Figure 1.20** Ternary Zn(II) complexes of two pendant-armed cyclen derivatives and deprotonated 1-methylthymine.

the ternary zinc(II) complex of N',N'''-bis[(1-naphthyl)methyl] cyclen and N(3')-deprotonated 1-methylthymine (**61** in Figure 1.20) showed that such an interaction did not exist in the solid state whereas <sup>1</sup>H NMR studies in protic and aprotic solvents

indicated that these double  $\pi$ - $\pi$  stacking interactions between the two naphthalene rings and the zinc-bound N(3')-deprotonated 1-methylthymine existed in protic solvents.<sup>39(f)</sup> The authors thus deduced that this ternary Zn(II) complex formed as **61** (or **63**) in solid or in aprotic solvents and as **62** (or **64**) in protic solvents (Figure 1.20).

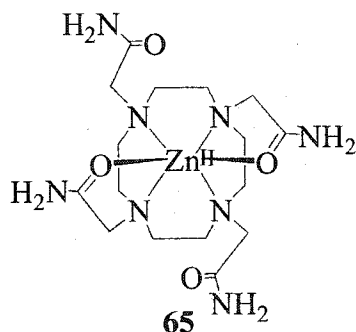


**Figure 1.21** The structure of  $[\text{Zn}(\text{DOTAM})]^{2+}$  (**65**).

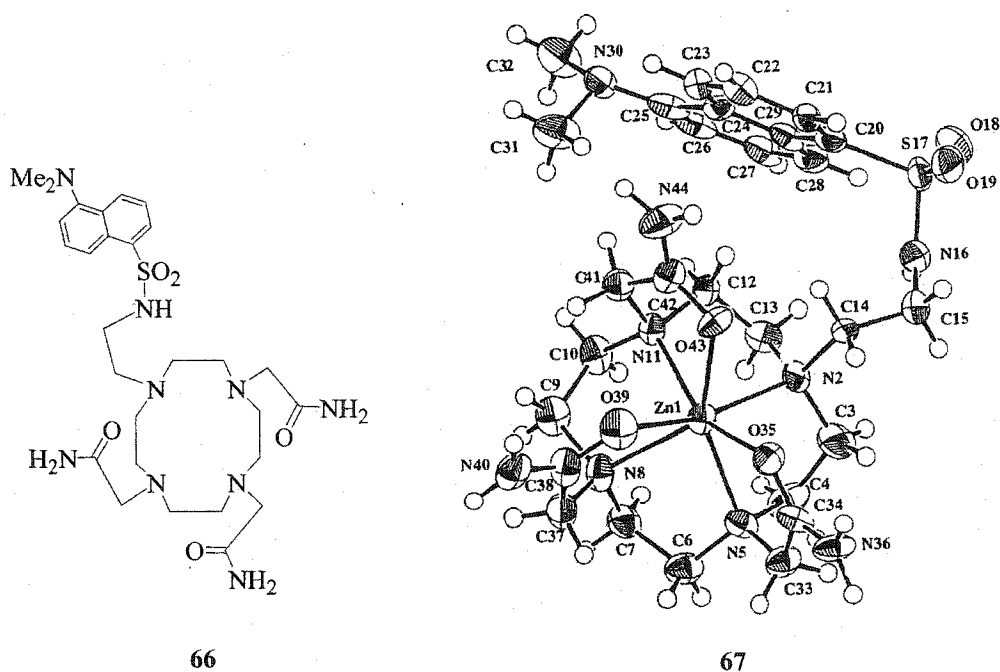


**Figure 1.22** The structures of a seven-coordinated Zn(II) complex of ligand **66** (complex **67**).

There are few reported examples featuring carboxylate and carbamoyl derivatives of cyclam and cyclen complexing with Zn(II). A Zn(II) complex of an octadentate ligand DOTAM (1,4,7,10-tetrakis(acetamido)-1,4,7,10-cyclododecane) (**65** in **Figure 1.21**) was synthesized and structurally characterized by Wainwright's group.<sup>40</sup> In this complex, zinc(II) is hexa-coordinated by four amino nitrogens of cyclen and two carbonyl oxygens of non-adjacent amides. More recently, a new pendant amide-derivative of cyclen (**66**) and its Zn(II) complex were synthesized and characterized by Kimura and coworkers.<sup>30(c)</sup> The X-ray structure of this Zn(II) complex (**67** in **Figure 1.22**) revealed a 7-coordinated Zn(II) center with four nitrogens of cyclen and three carbonyl oxygens of amides. In 2002, a rare structural example of a Zn(II) complex with a deprotonated amide (**41** in **Scheme 1.7**) was published by Kimura *et al.*<sup>29(g)</sup> Its solid-state structure showed that Zn(II) is penta-coordinate with four nitrogens from the cyclen ring and one deprotonated amide nitrogen from the pendant arm.

Several Zn(II) complexes of carboxylate derivatives of macrocyclic tetraamines have been reported.<sup>23(d),23(g),30(b),41</sup> The zinc(II) complex of a cyclen derivative, ligand DO2A (**68** in **Figure 1.23**) was prepared by Wainwright's group.<sup>41</sup> No solid-state structure of [Zn(DO2A)] has been reported. From <sup>13</sup>C{<sup>1</sup>H} NMR studies in neutral D<sub>2</sub>O, it was concluded that this Zn(II) complex has a time-averaged C<sub>2v</sub> symmetrical *cis*-octahedral structure. The X-ray structure of a Zn(II) complex of a tetrasubstituted cyclen derivative, [Zn(H<sub>2</sub>DOTA)] (**69** in **Figure 1.23**) was reported by Riesen and his coworkers.<sup>23(d)</sup> The Zn(II) center staying on a C<sub>2</sub> axis has a pseudo-octahedral coordination geometry with a coordinated *cis*-I ligand. The X-ray structure of [Zn(H<sub>2</sub>TETA)]•4H<sub>2</sub>O (**70** in **Figure 1.24**) revealed a *trans*-III octahedral arrangement of



the four planar amino nitrogen donors and of the two axial carboxylate oxygens around Zn(II). H<sub>2</sub>TETA is a tetraacetate derivative of cyclam. A similar X-ray structure to that of [Zn(H<sub>2</sub>TETA)]·4H<sub>2</sub>O was also reported on the Zn(II) complex of dicarboxylate-armed macrocyclic tetraamine derivative (71 in Figure 1.24).<sup>23(g)</sup>

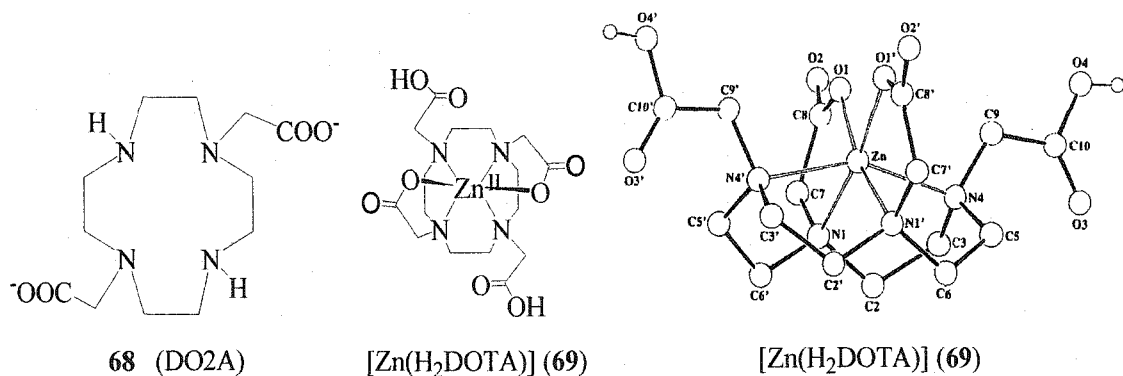


**Figure 1.23** Ligand DO2A (68) and the X-ray structure of [Zn(H<sub>2</sub>DOTA)] (69).

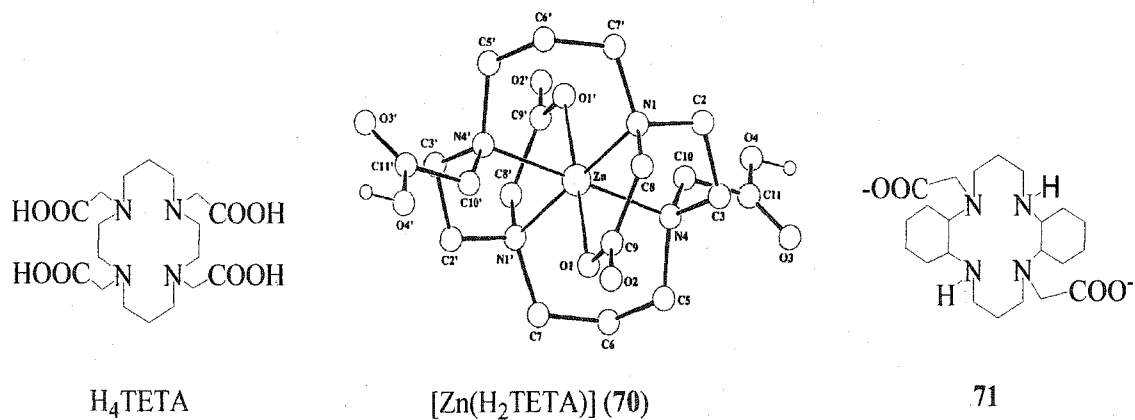


**Figure 1.24** The X-ray structure of [Zn(H<sub>2</sub>TETA)] (70) and ligand 71.

### 1.3 Cd(II) and Hg(II) Complexes of Cyclen, Cyclam and their Derivatives.

There are less than twenty well-characterized Cd(II) complexes of cyclam, cyclen and their derivatives in the literature. The majority are eight-coordinated Cd(II) complexes with tetra-N-substituted cyclam and cyclen derivatives.<sup>40,42(a-e)</sup> A good

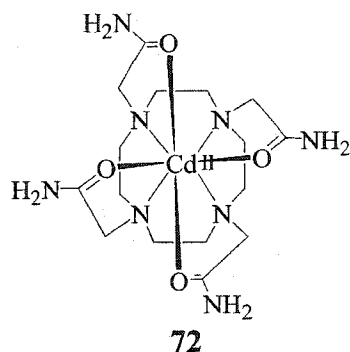
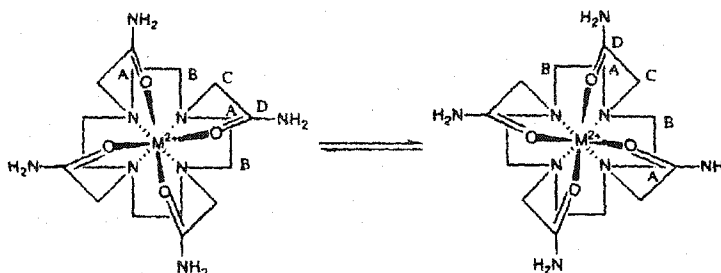


**Figure 1.25** The structure of  $[\text{Cd}(\text{DOTAM})]^{2+}$  (72).

example is the structure of a Cd(II) complex of an octadentate ligand DOTAM (72 in **Figure 1.25**).<sup>40</sup> In this complex, Cd(II) is encapsulated by the four nitrogen atoms of the macrocyclic ring and by the four oxygen atoms of the amide groups. The coordination geometry around Cd(II) is a distorted square-antiprism with two sets of Cd-O bond lengths. In  $\text{D}_2\text{O}$  or  $\text{DMF-}d_6$ , both this Cd(II) complex and Zn(II) complex (65 in **Figure 1.21**) undergo a nondissociative Bailar-twist for a dynamic process (**Scheme 1.10**) as



**Scheme 1.10** Helicity reversal in the approximately square anti-prismatic Zn(II) and Cd(II) complexes of ligand DOTAM in solution.



octahedron. The solid-state structure of  $[\text{Cd}_3(\text{cyclam})_3(\text{CO}_3)](\text{ClO}_4)_4$  (**74** in **Figure 1.27**) showed a *cis*-I configuration of coordinated cyclam. The complex contains three independent  $[\text{Cd}(\text{cyclam})]^{2+}$  units. Each unit has a distorted octahedral geometry of the *cis*- $\text{CdN}_4\text{O}_2$  set. Yet in  $\text{CD}_3\text{CN}$  solution, it adopted a *trans*-I configuration as supported by 1D and 2D  $^1\text{H}$ ,  $^{13}\text{C}$  and  $^{15}\text{N}$  NMR studies.<sup>43(b)</sup> The rest of these 6-coordinate Cd(II) complexes have the *trans*-I coordinated ligand configuration.<sup>43(c-e)</sup> Several Cd(II) complexes with coordination number five are also available.<sup>44a,44b</sup> These include a square pyramidal Cd(II) complex of cyclen,  $[\{\text{Cd}(\text{cyclen})\}\{\text{Pt}(\text{CH}_3)_2(\text{bpy})\}](\text{ClO}_4)_2$  (**75** in **Figure 1.28**).<sup>44a</sup> The most interesting feature of **75** is the existence of a  $\text{Pt}^{\text{II}} \rightarrow \text{Cd}^{\text{II}}$  bond.

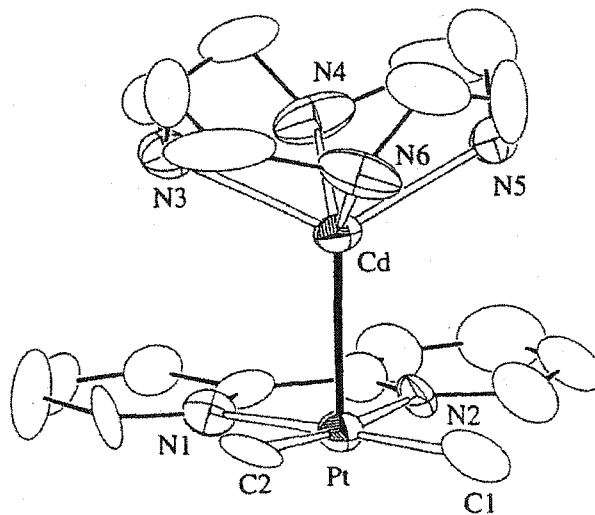


**Figure 1.28** The X-ray structure of  $[\{\text{Cd-cyclen}\}\{\text{Pt}(\text{CH}_3)_2(\text{bpy})\}](\text{ClO}_4)_2$  (**75**).

Only several examples of Hg(II) complexes with cyclam, cyclen and their derivatives are available in the literature,<sup>45(a-c)</sup> including a pseudo-octahedral Hg(II) complex of a cyclam derivative in a *cis*-folded (I) configuration (**76** in **Figure 1.29**).<sup>45c</sup> In contrast to the Cd(II) complex with the same ligand (**73**), the Hg(II) complex of *cis*-

6,13-Dimethyl-1,4,8,11-tetraazacyclotetradecane-6,13-diamine is an out-of cavity complex (77 in Figure 1.30)<sup>45b</sup> in which two separate molecular units co-exist. The first unit (77a in Figure 1.30) has two mercury ions chelated at the opposite sides of the macrocycle and the second (77b in Figure 1.30) has the Hg(II) bound to each pendant amine in a unidentate manner.

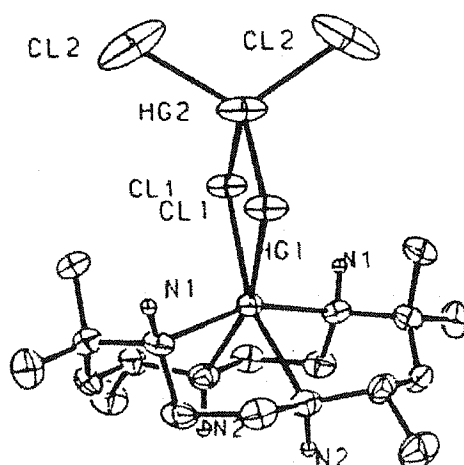


**Figure 1.29** The X-ray structure of a Hg(II) complex with a hexamethyl cyclam (76).

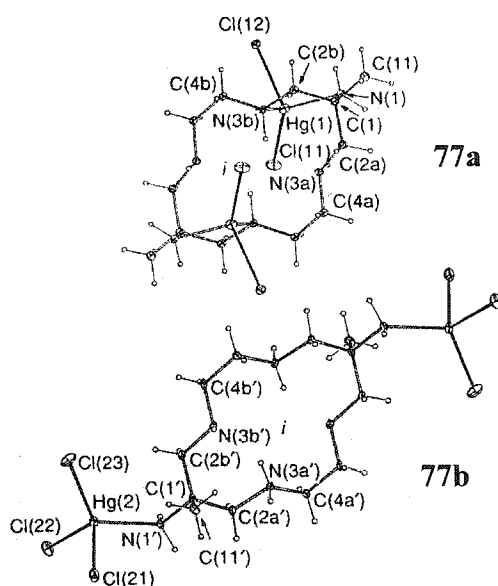


**Figure 1.30** The X-ray structure of the Hg(II) complex of L (77) (L = 6,13-Dimethyl-1,4,8,11-tetra-azacyclotetradecane-6,13-diamine).

#### 1.4 Co(III) Complexes of Cyclen and its Derivatives.

Co(III) complexes are interesting because of their slow ligand-exchange reactions and particular affinity for nitrogen donors. Co(III) complexes of cyclen and its derivatives, as well as other polyamines, have also been studied as models for the active sites of Co(III) phosphate monoesterases, diesterases, and thioesterases.<sup>46(a-c)</sup> In 1993, Chin and his coworkers reported studies on the kinetics and mechanism of nitrile hydration catalyzed by a Co(III) cyclen complex,  $[\text{Co}(\text{cyclen})(\text{OH}_2)_2](\text{ClO}_4)_3$  (**78** in Figure 1.31). Under mild conditions, **78** catalytically hydrated nitriles to amides at pH 7.

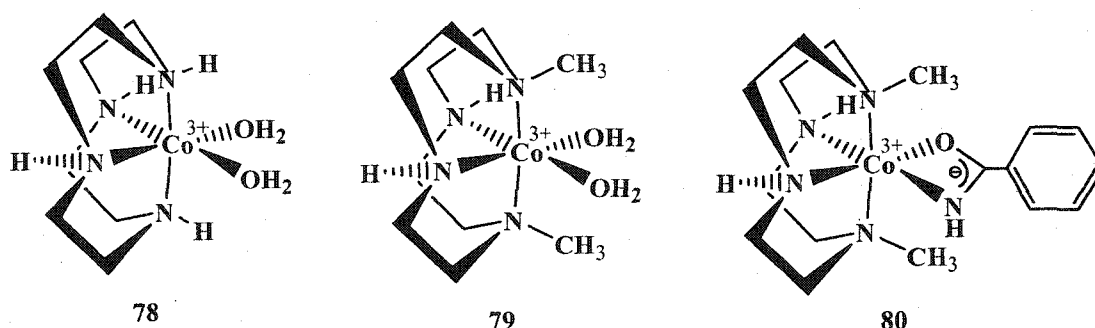
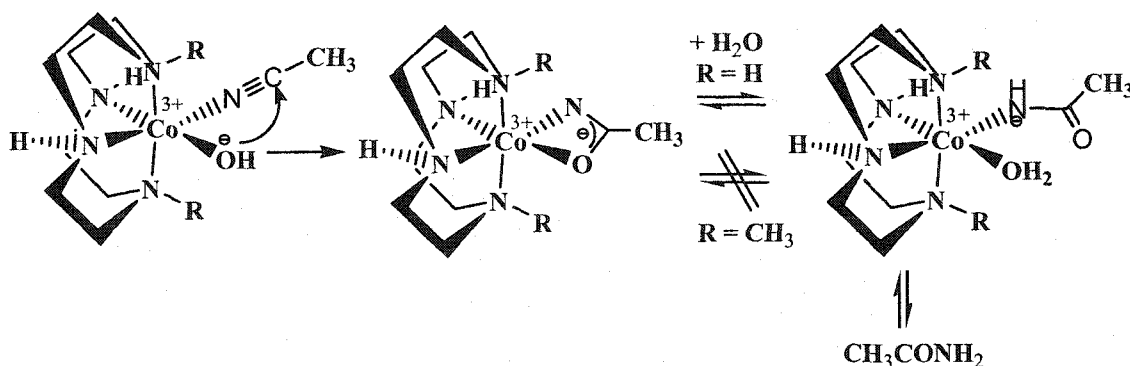
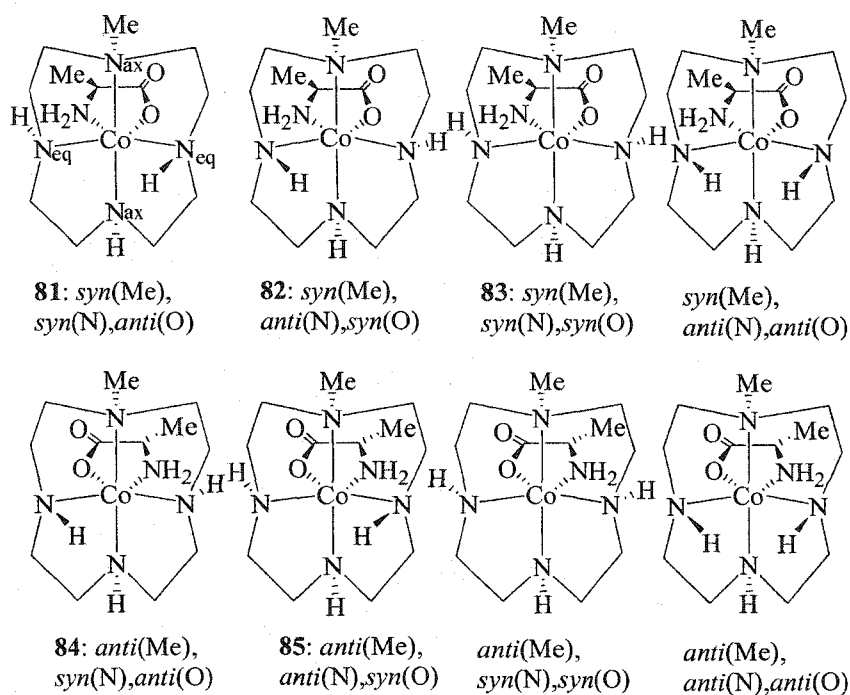


Figure 1.31 Three Co(III) complexes **78**, **79** and **80**.



Scheme 1.11 Proposed mechanism of  $\text{CH}_3\text{CN}$  hydration catalyzed by a Co(III) cyclen complex, **78**.

The mechanism of this process involved a three-step cycle (**Scheme 1.11**)<sup>47</sup> However, addition of **79** to benzonitrile yielded an isolable Co(III) complex of chelated benzonitrile (**80**) without any catalytic turnover. The authors believed that the two methyl groups in **80** prohibited the equilibrium between the bidentate and monodentate amide Co(III) complexes in **Scheme 1.11**. This led to the loss of catalytic hydration of benzonitrile by **79**. This work clearly indicates that it is important for an enzyme model complex to have two *cis*-coordinating sites available in order to have catalytic activity. In the past ten years, Buckingham and his coworkers have explored the coordination chemistry of Co(III) cyclen and 1-methyl-cyclen (Mecyclen) complexes.<sup>48(a-i)</sup> Treatment of [Co(Mecyclen)Cl<sub>2</sub>]Cl with S-alanine (S-AlaOH) gave a mixture of six [Co(Mecyclen)(S-AlaO)]<sup>2+</sup> isomers out of eight possible isomers of this octahedral Co(III) complex (**Figure 1.32**).<sup>48(a)</sup> Using both cation ion exchange chromatography and recrystallization, five isomers (**81, 82, 83, 84, 85**) were isolated and structurally assigned through a combination of nOe and COSY <sup>1</sup>H NMR spectroscopies in *d*<sub>6</sub>-DMSO solvent. The presence of separate N-H resonances was critical for the structural assignments by the <sup>1</sup>H NMR method. The X-ray structures of **81, 82** and **84** further confirmed these assignments. As shown for **81** in **Figure 1.32**, all three structures exhibited distorted octahedral coordination geometry around Co(III). One oxygen donor and one nitrogen donor from the chelating S-alanine and two secondary amine nitrogen donors from the *cis*-folded Mecyclen constituted the equatorial position and the two remaining amine nitrogen donors including the tertiary amine nitrogen donor took the axial positions. This group was also able to isolate and structurally characterize three *cis*-folded [Co(cyclen)(S-AlaO)]<sup>2+</sup> (**86, 87, 88**) out of four possible isomers (**Figure 1.33**).<sup>48(f)</sup>



**Figure 1.32** The eight possible configurational isomers of  $[\text{Co}(\text{Mecyclyen})(\text{S-AlaO})]^{2+}$ .

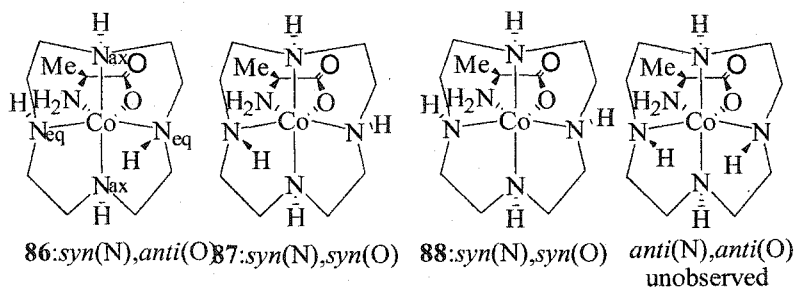
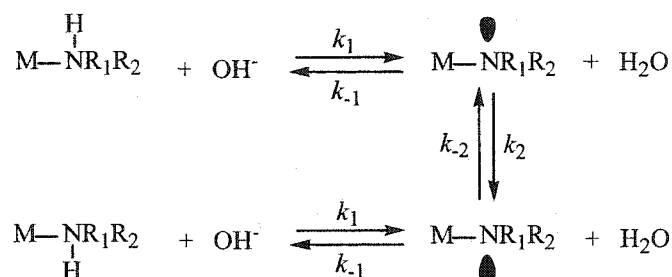


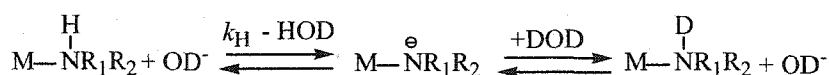
**Figure 1.33** The four possible configurational isomers of  $[\text{Co}(\text{cyclen})(\text{S-AlaO})]^{2+}$ .

The separation and characterization of these isomers enabled the authors to investigate pathways for proton exchange at a coordinated secondary amine center (**Scheme 1.12**). The *NH/ND* exchange rate constants (**Scheme 1.13**) for various *NH* protons in these isomers were obtained by following the decay of amine *NH* signals as a function of time





**Scheme 1.12** Stepwise mechanism for proton exchange and inversion at a coordinated secondary amine center.



**Scheme 1.13** NH/ND exchange at a coordinated secondary amine center.

by  $^1\text{H}$  NMR using dilute DCl solutions or  $\text{D}_2\text{O}$  buffers at  $25^\circ\text{C}$ . The second-order rate constants of isomerization (**Scheme 1.12**) were monitored by the growth or decay of the appropriate *NMe* signal. Ratios of these two rate constants suggested that the two equatorial secondary amine centers in the coordinated cyclen were very susceptible to inversion. Interestingly, when equilibrium was reached at  $25^\circ\text{C}$  ( $I \sim 0.1\text{M}$ ), the **81**: **82**: **83** ratios were 73:21:6 and the **86**: **87**: **88** ratios were 63:32:5.

### 1.5 Complexes of Cyclen, Cyclam and their Derivatives with Cu(II)

Copper(II) complexes of cyclen, cyclam and their derivatives commonly adopt six-coordinate elongated rhombic or tetragonal octahedral structure, or five-coordinate distorted square pyramidal or distorted trigonal bipyramidal geometry.<sup>49</sup>

A search of the *Cambridge Crystallographic Database* revealed hundreds of X-ray structures of copper complexes with cyclam and its derivatives. The most common configuration is the most-stable *trans*-III.<sup>22(a-c),50(a-m)</sup> Here only selected references are listed with more discussed later. As expected, the majority of these Cu(II) complexes have a coordination number of six or five.<sup>22(a-c),50(a-h)</sup> For example, complex cation  $[\text{Cu}(\text{Cyclam})(\text{MeCN})_2]^{2+}$  (**89**) has a coordination number of six as revealed by its solid-state structure (**Figure 1.34**).<sup>50(a)</sup> The Cu(II) atom is coordinated by four nitrogen donors

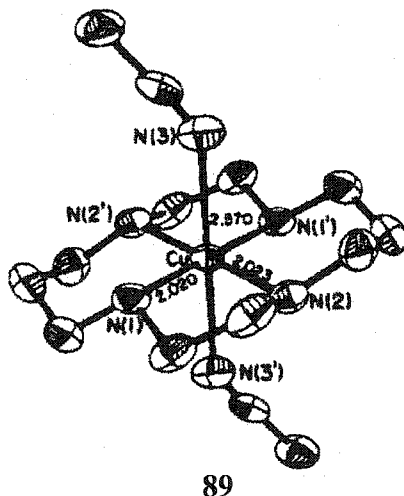
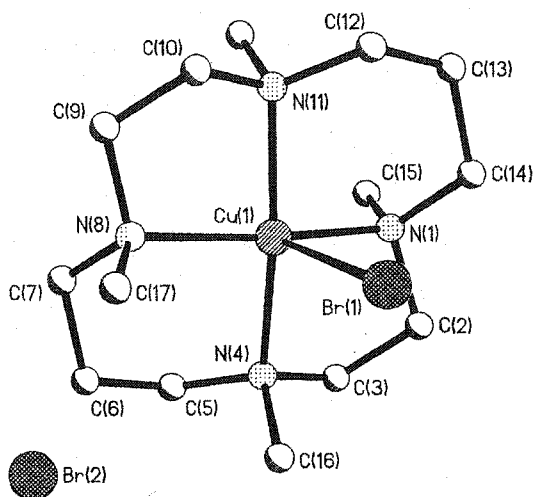


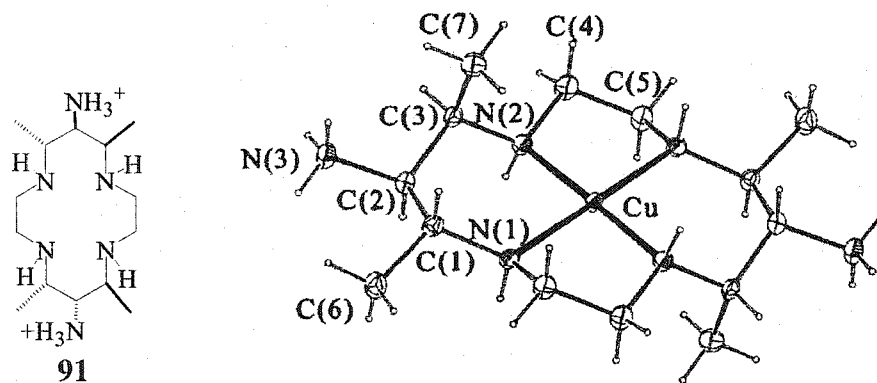
**Figure 1.34** The X-ray structure of  $[\text{Cu}(\text{Cyclam})(\text{MeCN})_2]^{2+}$  (**89**).

from cyclam in the equatorial position and two weakly-coordinated acetonitriles in axial position of a distorted octahedral geometry. The X-ray structure of a five-coordinate Cu(II) complex with  $\text{Me}_4\text{cyclam}$  is shown in **Figure 1.35**.<sup>22(d)</sup> The Cu(II) atom in this complex (**90**) has a slightly distorted square-pyramidal geometry. Several four-coordinate copper(II) complexes with cyclam derivatives have been structurally characterized.<sup>50(i-m)</sup> These include a Cu complex of *trans*-6,13-Diammonio-5,7,12,14-tetramethyl-cyclam (ligand **91**) (**Figure 1.36**).<sup>50n</sup> Here, Cu(II) only coordinates to four



90

**Figure 1.35** The molecular structure of  $[\text{Cu}(\text{Me}_4\text{Cyclam})\text{Br}]\text{Br}$  (**90**).



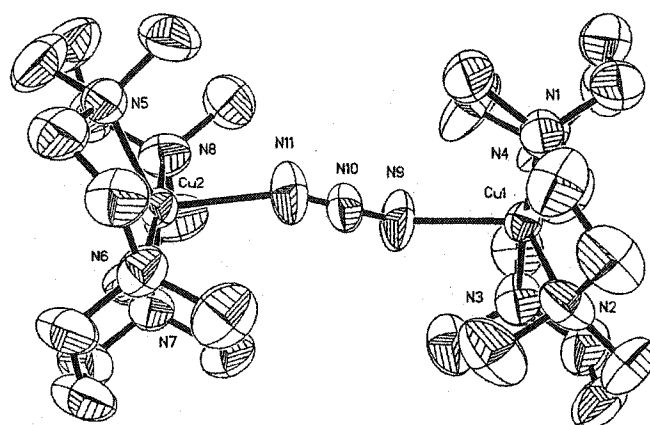
91

**Figure 1.36** The molecular structure of a  $\text{Cu}(\text{II})$  complex with *trans*-6,13-Diammonio-5,7,12,14-tetramethyl-cyclam (ligand **91**).

cyclam nitrogen donors in a square-planar geometry whereas two primary amine groups from this potential hexadentate ligand are both protonated. Some  $\text{Cu}(\text{II})$  complexes of cyclam and its derivatives with a *trans*-I configuration have also been reported.<sup>50(g),51(a-h)</sup>

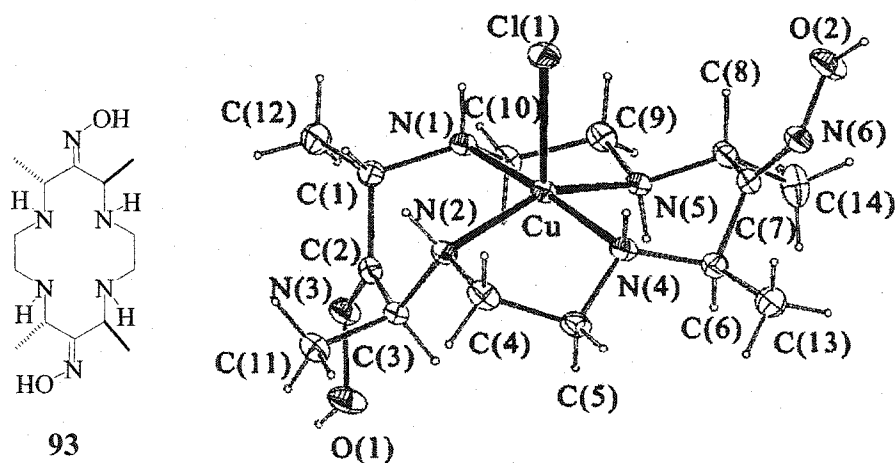
For example, the X-ray structure (**92**) in **Figure 1.37** features an azide bridging dinuclear

Cu(II) complex of Me<sub>4</sub>cyclam. Very interestingly, in the presence of excess ligand, Cu(II) complex **92** disproportionated and isomerized to yield the *trans*-III isomer and copper metal in alkaline aqueous solutions.



**92**

**Figure 1.37** The molecular structure of  $[\text{Cu}_2(\text{Me}_4\text{Cyclam})_2(1,3\text{-}\mu\text{-N}_3)]^{3+}$  (**92**).



**93**

**Figure 1.38** The molecular structure of  $[\text{Cu}(\text{II})\text{Cl}93]^+$ .

Several X-ray structures of copper(II) complexes with cyclam and its derivatives have also been found to adopt a *trans*-II configuration<sup>50(n),52(a-d)</sup> including a Cu(II)

complex of ligand **93** in **Figure 1.38**.<sup>50(n)</sup> In this structure, Cu(II) is coordinated by four nitrogen donors from the macrocycle and one terminal chloride to form a square pyramidal geometry.

Several examples of the rarer *cis*-folded Cu(II) cyclam complexes have also been reported.<sup>26(b),53(a-d)</sup> These include the X-ray structure of [Cu(tet b)(*o*-SC<sub>6</sub>H<sub>4</sub>CO<sub>2</sub>)] (**94**) in **Figure 1.39** (tet b = *rac*-5,7,7,12,14,14-Hexamethyl-cyclam and *o*-SC<sub>6</sub>H<sub>4</sub>CO<sub>2</sub> = *o*-mercaptobenzoate). In this five-coordinate Cu(II) complex, coordinated ligand tet b adopted a *cis*-folded (V) configuration. This is indicated by the N(1)-Cu-N(3) angle of 170.8(4)° in the axial position and N(2)-Cu-N(4) angle of only 103.5(4)° in the equatorial position. The coordination geometry of this Cu(II) complex is a distorted trigonal bipyramid.

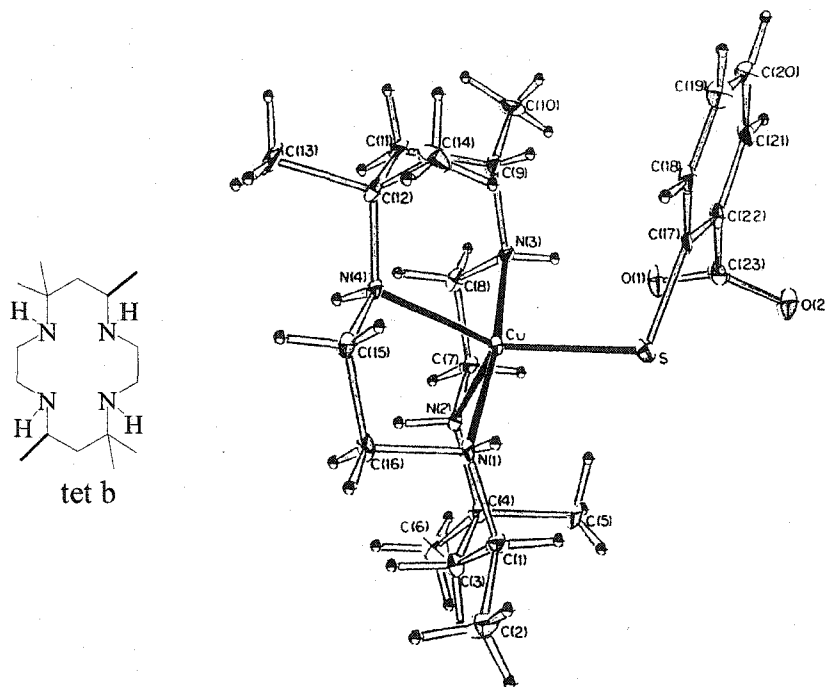


**Figure 1.39** The molecular structure of [Cu(tet b)(*o*-SC<sub>6</sub>H<sub>4</sub>CO<sub>2</sub>)] (**94**).

There are more than thirty reported X-ray structures of Cu(II) complexes with cyclen and its derivatives. The majority of these adopt the *trans-I* configuration with a coordination number of five or six.<sup>54(a-t)</sup> The X-ray structure of a six-coordinate Cu(II) complex of a pyridylmethyl pendant-armed cyclen derivative (ligand **95**) is shown in **Figure 1.40**.<sup>54(m)</sup> In this structure, Cu(II) is coordinated by four-nitrogen donors from the

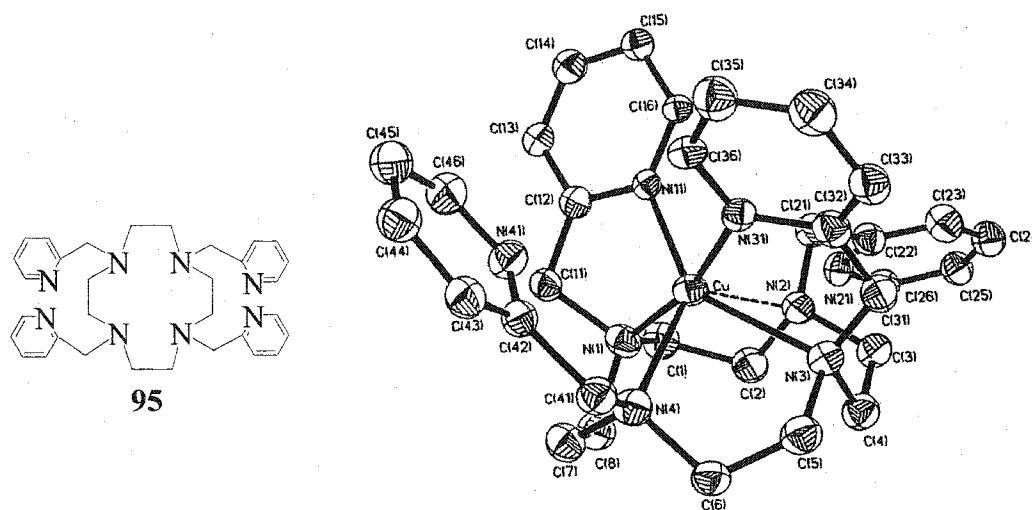


**Figure 1.40** The X-ray structure of  $[\text{Cu}(\text{II})\mathbf{95}]^{2+}$ .

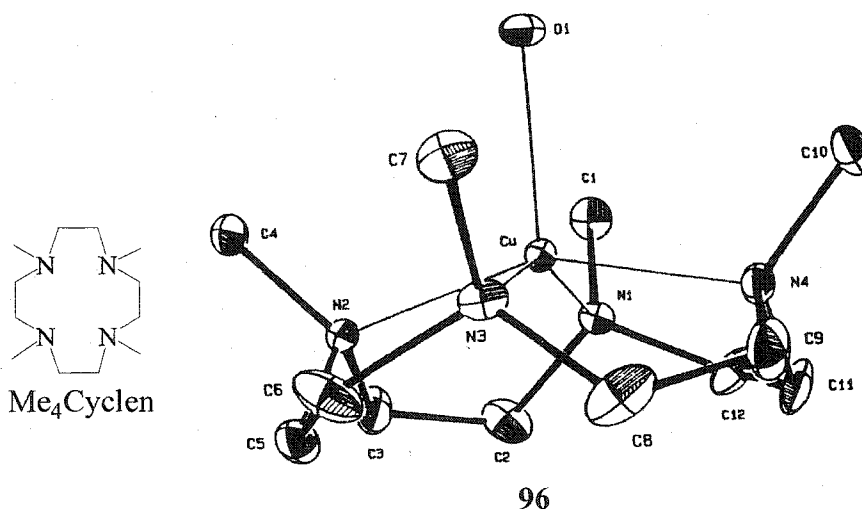


**Figure 1.41** The X-ray structure of  $[\text{Cu}(\text{Me}_4\text{Cyclen})(\text{H}_2\text{O})]^{2+}$  (**96**).

cyclen ring and two nitrogen atoms of the four pyridyl groups. It has a severely-distorted octahedral geometry around the Cu(II) atom. The X-ray structure of a five-coordinate  $[\text{Cu}(\text{Me}_4\text{cyclen})\text{H}_2\text{O}]^{2+}$  (96) is shown in Figure 1.41.<sup>54(m)</sup> The copper atom has a square pyramidal geometry. An interesting Cu(II) complex of a bicyclic cyclen derivative (cryptand Cage L) in the *cis-II* configuration (Figure 1.42) was reported by Micheloni

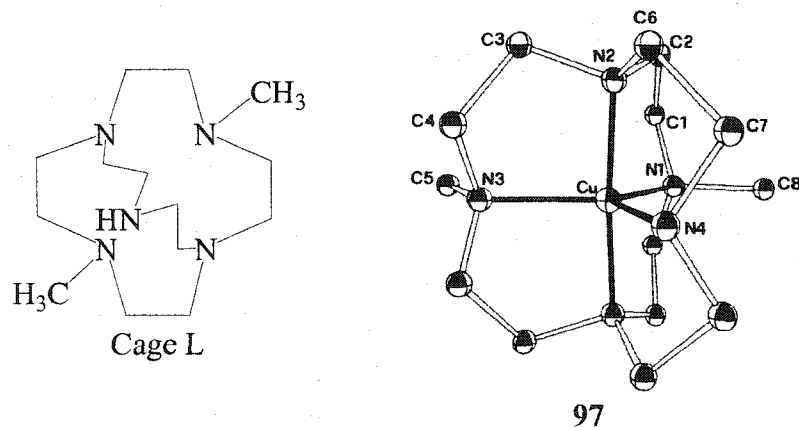


Figure 1.42 The X-ray structure of  $[\text{Cu}(\text{Cage L})]^{2+}$  (97).

*et al.*<sup>55</sup> The five-coordinate Cu(II) atom is fully coordinated by this pentadentate macrocycle, adopting a trigonal bipyramidal coordination geometry.

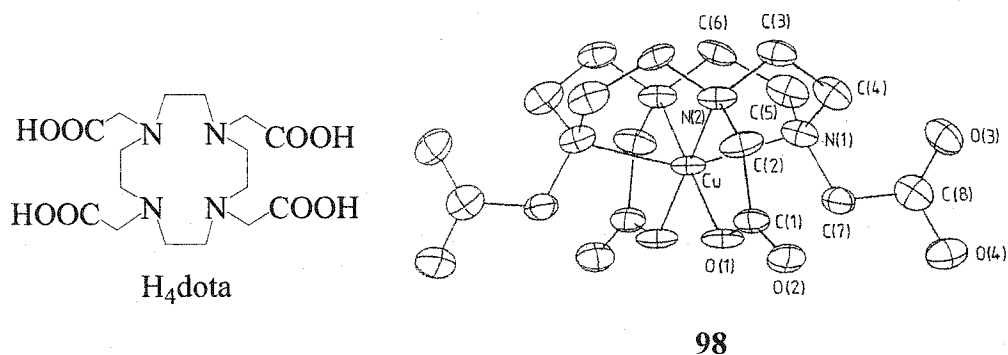
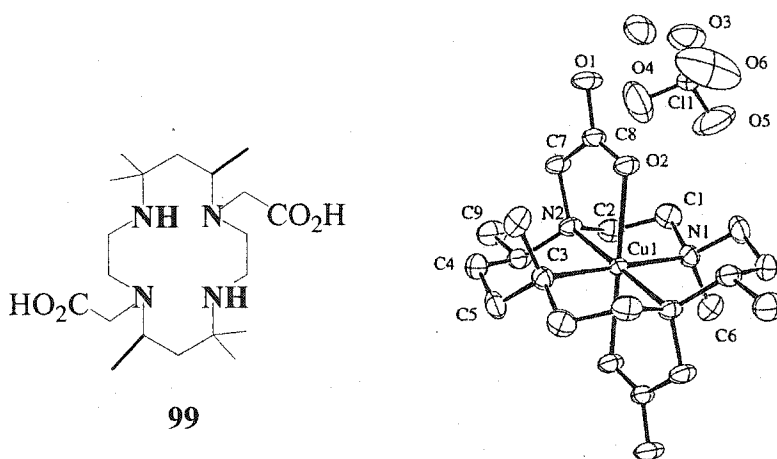


Figure 1.43 The X-ray structure of  $[\text{Cu}(\text{H}_2\text{dota})]$  (98).

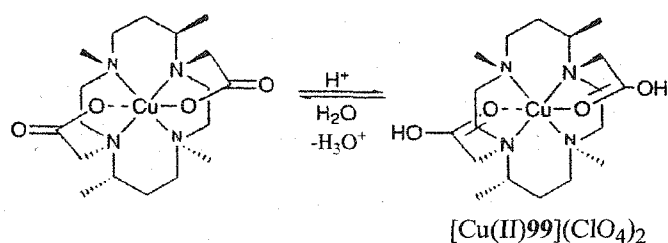
Only six-coordinate Cu(II) complexes of carboxylate-armed cyclen derivatives have their ligands in the *cis-I* configuration.<sup>56(a-c)</sup> Those include a Cu(II) complex of a tetracarboxylate-substituted ligand H<sub>4</sub>dota (complex **98** in **Figure 1.43**).<sup>56(c)</sup> The coordination geometry of this complex is a pseudo-octahedron as evidenced by the N(ax)-Cu-N(ax) angle of only 152.6(3)° and the larger N(eq)-Cu-N(eq) angle of 105.0(3)°.

Compared to the relatively few Zn(II) complexes, numerous Cu(II) complexes featuring carboxylate and carbamoyl derivatives of cyclam have been reported.<sup>50(i),53(d),57(a-o)</sup> In X-ray structures of most of these, all four nitrogen donor atoms from the macrocycle and two oxygen donors from the *trans-III* ligand generally coordinate to Cu(II) center in a distorted octahedral geometry.<sup>57(a-l)</sup> This is illustrated by the X-ray of a Cu(II) complex of a dicarboxylate-functionalized cyclam (ligand **99** in **Figure 1.44**).<sup>50(i)</sup> This structure shows that the coordinated ligand **99** adopts a *trans-III*



**Figure 1.44** The X-ray structure of complex [Cu(II)**99**](ClO<sub>4</sub>)<sub>2</sub>.





**Scheme 1.14** Structural rearrangement [Cu(II)99](ClO<sub>4</sub>)<sub>2</sub> in aqueous solution.

configuration and the Cu(II) atom is in *trans*-octahedral geometry as defined by the apical positions of two carboxylate arms. This Cu(II) atom is coordinated by the four nitrogen atoms of the macrocycle in the equatorial plane and the two carbonyl oxygens at the apical positions. Thus the two carboxylate groups from the macrocycle are in the protonated form while coordinating to the Cu(II) atom. The electronic spectra of this Cu(II) complex at different pH values are different. Specifically, it exhibited a broad band at 622 nm in aqueous solution whereas in 0.1 M HClO<sub>4</sub>, this band shifted to 595 nm. Such a change in electronic spectra can be explained by the equilibrium in **Scheme 1.14**. A tetraamide-armed cyclam derivative (ligand **100**) complex of Cu(II) (**Figure 1.45**) showed a similar coordination geometry.<sup>57(a)</sup> Several Cu(II) complexes with carboxylate derivatives of cyclen have been structurally characterized.<sup>54(e),56(a-d),58</sup> Unlike complex **98** in **Figure 1.43**, the crystal structure of a Cu(II) complex with a trisubstituted carboxylate derivative of cyclen [Cu(HDO3A)] (**101** in **Figure 1.46**) revealed that this coordinated cyclen derivative had an intermediate structure between *trans*-I and *cis*-I.<sup>58</sup> This is indicated by the pseudo-axial N-Cu-N bond angle of 138.5(1)° and pseudo-equatorial N-Cu-N angle of 115.5(2)°.

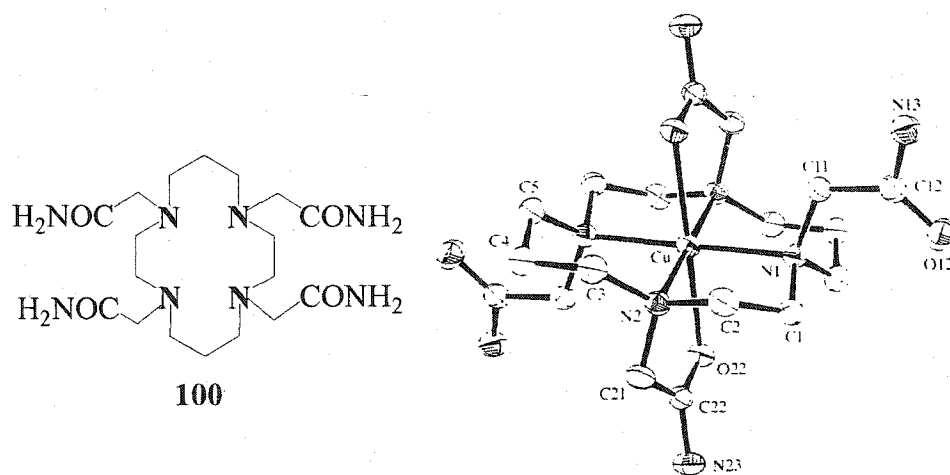


Figure 1.45 The X-ray structure of complex  $[\text{Cu}(\text{II})\mathbf{100}]^{2+}$ .

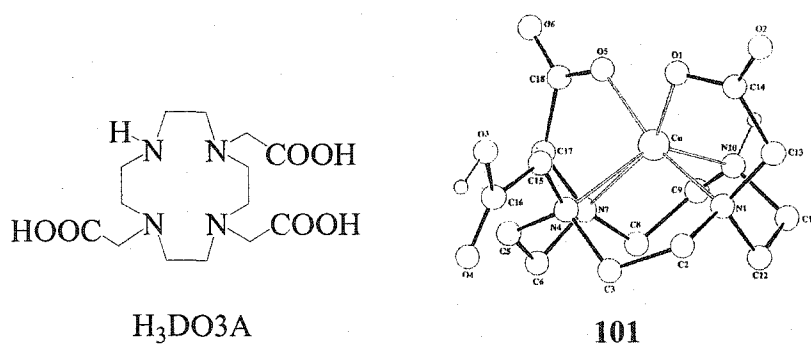
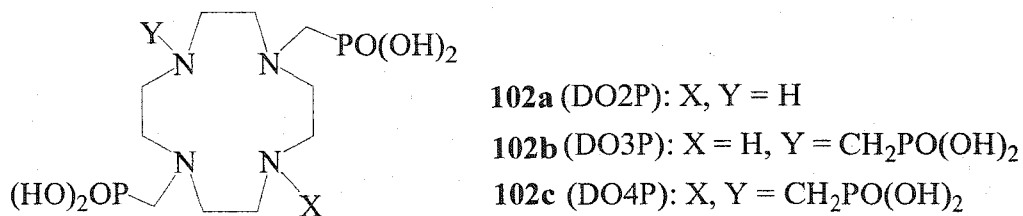


Figure 1.46 The X-ray structure of  $[\text{Cu}(\text{HDO3A})]$  (**101**).

$^{60}\text{Cu}(\text{II})$ ,  $^{61}\text{Cu}(\text{II})$ ,  $^{62}\text{Cu}(\text{II})$ ,  $^{64}\text{Cu}(\text{II})$  and  $^{67}\text{Cu}(\text{II})$  complexes have applications as radiopharmaceuticals.<sup>59</sup> For success, their *in vivo* stability is a very important factor.<sup>59</sup> This requires their very high thermodynamic stability and especially kinetic inertness to avoid transchelation with *in vivo* biological ligands such as transferrin. For this purpose,  $\text{Cu}(\text{II})$  complexes of cyclam or cyclen derivatives have been investigated.<sup>58,59</sup> The possible relationship between their structures and *in vivo* stability were also studied.<sup>58,59</sup> The metabolic studies of  $\text{Cu}$ -64-labeled methanephosphonate derivatives of cyclen



**Figure 1.47** Methanephosphonate derivatives of cyclen.

(**102a**, **102b** and **102c** in **Figure 1.47**) in rat liver by Anderson and her research group suggested that the DO2P ligand (**102a** in **Figure 1.47**) may be the most promising of these because its complex was stable in rat serum out to 24 hours and had the most optimal clearance through blood and liver among these three ligands.<sup>60</sup> The authors believed that this was due to the hexa-coordinate Cu(II)–DO2P complex. This ligand may be used as a bifunctional chelator for copper radionuclides in radiotherapy.

### 1.6 Complexes of Cyclen, Cyclam and their Derivatives with Ga(III) and In(III).

Both Ga(III) and In(III) are generally considered hard metal ions.<sup>58</sup> Indium(III) has an ionic radius of 94 pm in six-coordinate complexes and gallium(III) has an ionic radius of 76 pm. Therefore, In(III) is slightly softer than Ga(III) and can also be considered a borderline metal ion. Ga(III) prefers to coordinate to harder oxygen donor ligands whereas In(III) prefers neutral nitrogen or negative sulfur donors. In the preparation of Ga(III) and In(III) coordination complexes, a problem that always exists is that the precipitation of Ga(OH)<sub>3</sub> and In(OH)<sub>3</sub> may occur more quickly than the complexation of Ga(III) or In(III) with ligands.<sup>59</sup>

The Ga(III) and In(III) complexes of macrocyclic tetraamines are potential precursors in III-V semiconductor epitaxy and porous hybrid materials.<sup>61(a-c)</sup> Some

organometallic complexes of Ga(III) and In(III) with cyclam and cyclen have been reported for this purpose.<sup>61(a),61(b),62(a-d)</sup> For example, an X-ray structure of  $[(\text{CH}_3)\text{GaCyclam}]\text{Cl}_2$  (**103** in **Figure 1.48**) showed that this six-coordinated Ga(III) is coordinated by four amino nitrogens from cyclam with the common *trans-III* geometry and one methyl and one weakly bonded chloride *trans* to it.<sup>62(a)</sup> Several gallium phosphate complexes of cyclam have been characterized as building blocks in the construction of mesoporous materials. Cyclam in these gallium complexes again adopts the common *trans-III* configuration.<sup>62(c),63(a),63(b)</sup>

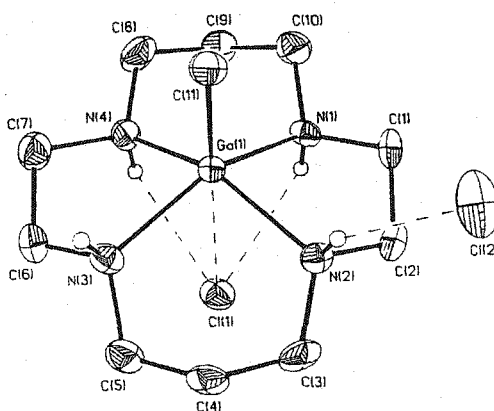


**Figure 1.48** The X-ray structure of  $[(\text{CH}_3)\text{GaCyclam}]\text{Cl}_2$  (**103**).

No well-characterized gallium and indium halide complexes of tetrazamacrocycles cyclam and cyclen have been reported. In 1981, Taylor *et al.* reported 1:2 In(III) complexes with cyclam. These In(III) complexes were formulated as  $[\text{In}(\text{cyclam})_2][\text{InX}_4]_3$  (X=halide) but characterized only by In(III) and halogen elemental analyses.<sup>64</sup> CHN elemental analyses of  $[\text{In}(\text{cyclam})_2][\text{InCl}_4]_3$ , however, failed and no structural evidence was provided.

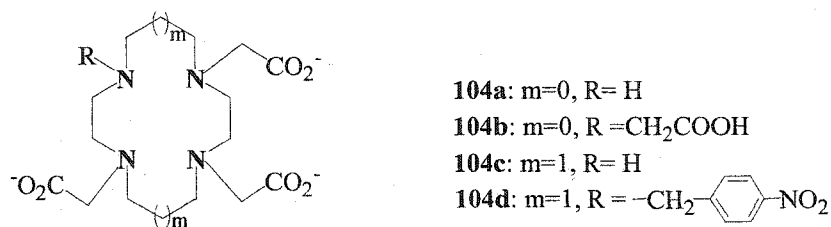


**Figure 1.49** Cyclen and cyclam derivatives tested for potential metal-based radiopharmaceutical application by Kaden *et al.*

Ga(III) and In(III) complexes of pendant-armed cyclam and cyclen derivatives are of interest<sup>60</sup> also because of their potential radiopharmaceutical application. <sup>66</sup>Ga(III), <sup>67</sup>Ga(III), <sup>68</sup>Ga(III), <sup>111</sup>In(III), <sup>113m</sup>In(III), <sup>86</sup>Y(III) and <sup>86</sup>Y(III) are the relevant radioisotopes. Four carboxymethylated cyclen and cyclam derivatives shown in **Figure 1.49 (104a-104d)** were synthesized by Kaden *et al.* The stability of their <sup>111</sup>In(III) complexes in blood serum was measured and it was demonstrated that the In(III) complex of **104a** was the most stable in blood serum.<sup>65</sup> The X-ray structure of this In(III)

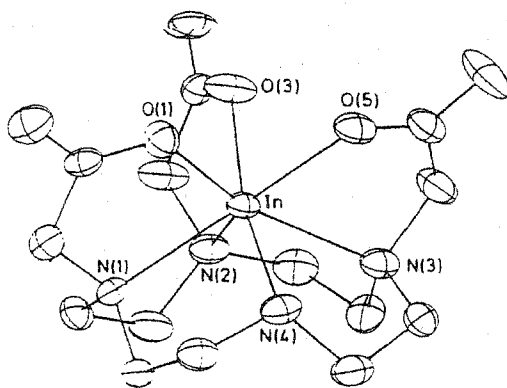


**Figure 1.50** The X-ray structure of an In(III) complex of a cyclen derivative, ligand **104a**.

complex (**Figure 1.50**) showed that the In(III) was hepta-coordinated by the four nitrogen atoms and the three carboxylate groups of ligand **104a**, which adopted a *trans-I* configuration. The X-ray structure of the In(III) complex of **104c** is very similar to that of **104a** but it is less compact and symmetrical, which may cause have lowered the stability of this complex in serum.

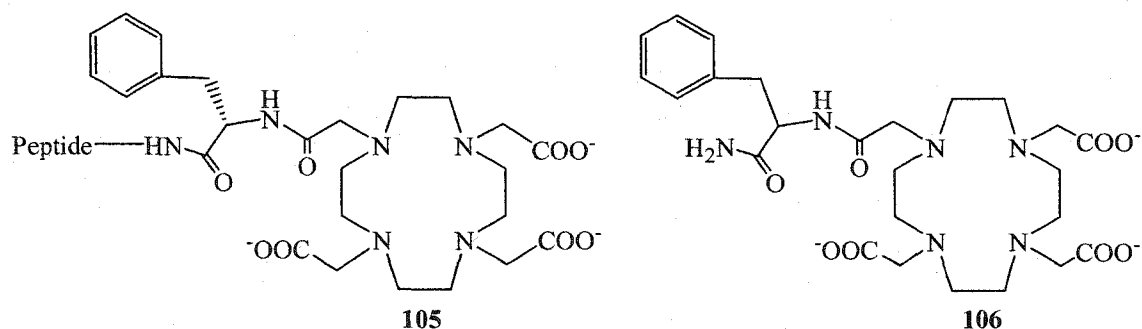


**Figure 1.51** Two cyclen derivatives for bioconjugation towards potential metal-based radiopharmaceutical application.

More recently, the same research group found that both  $^{67}\text{Ga(III)}$  and  $^{90}\text{Y}$ -labelled cyclen-derivatized somatostatin analogue (ligand **105** in **Figure 1.51**) showed high *in vivo* stability and superb tumor-targeting properties.<sup>66</sup> The  $^{67}\text{Ga(III)}$  complex of this cyclen-derivatized somatostatin analogue had much faster *in vivo* kidney clearance and higher tumor-targeting ability than the  $^{90}\text{Y}$  complex. The authors believed that the differences in the coordination chemistry of these two complexes caused the differences in biological behavior. In the X-ray structure (**Figure 1.52**) of the Ga(III) complex of a model ligand (**106** in **Figure 1.51**), the Ga(III) center is hexa-coordinated by this *cis*-folded macrocyclic ligand. The amide oxygen and one deprotonated carboxylate group are not coordinated to the metal. This structural feature likely contributed to the favorable handling of the radiopeptide by the kidneys. By contrast, in the structure

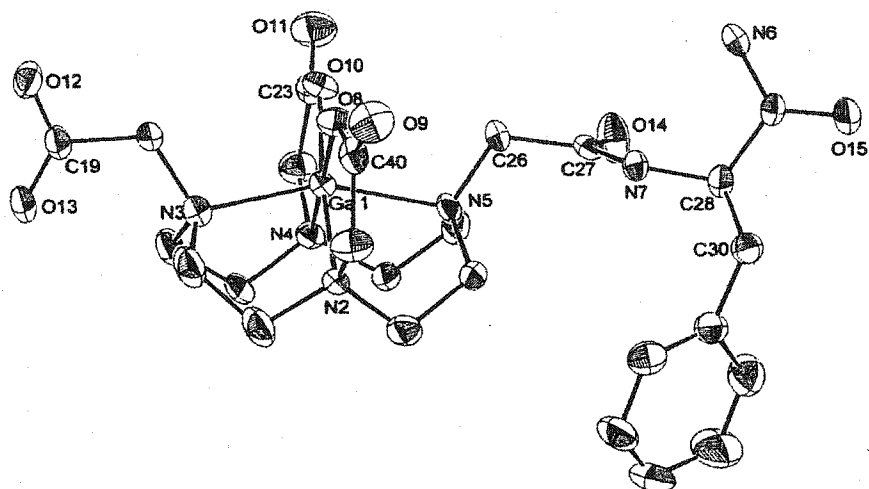


**Figure 1.52** The X-ray structure of a Ga(III) complex of a cyclen derivative, ligand 106.

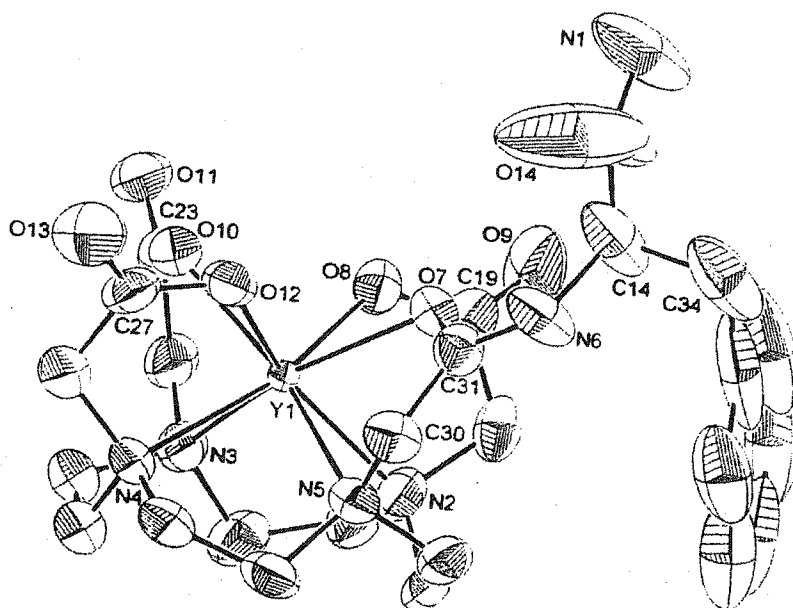


**Figure 1.53** The X-ray structure of an Y(III) complex of a cyclen derivative, ligand 106.

(Figure 1.53) of the Y(III) complex of this model ligand, the Y(III) center was octa-coordinated by all four amine nitrogens, the amide oxygen and all three carboxylate

groups. Assuming that the Y(III) complex of the original cyclen-derivatized somatostatin analogue (**105** in **Figure 1.51**) had the same coordination geometry, this would force the chelator closer to the peptide and thus introduce steric strain, possibly disturbing the proper spatial arrangement of the targeting peptide. Besides this research by Kaden's group, several pendant-armed derivatives of cyclam and cyclen have been also investigated by others for this purpose.<sup>67(a),67(b)</sup> However, fully characterized Ga(III) and In(III) complexes of pendant-armed cyclam and cyclen derivatives are still rare.

## 2. Coordination Chemistry of Cross-bridged Tetraazamacrocyclic Ligands

An important concept in macrocyclic chemistry is the ligand/cation size match selectivity, which means that a macrocyclic ligand may complex best with metal ions that fits best into the cavity of the macrocycles. Macrocyclic polyamines such as cyclam and cyclen have thus been structurally reinforced for this purpose. Wainwright made a structural modification to the parent cyclam and cyclen ligands in which two adjacent nitrogens were bridged with an ethylene unit (**Figure 1.54**). This adjacent-bridging ethylene increased the tendency towards *trans*-coordination of transition metal ions.<sup>68(a),68(b)</sup>

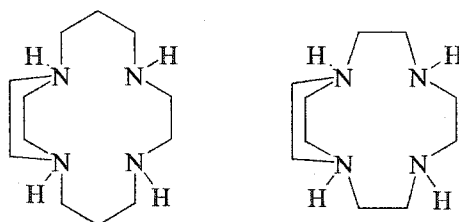


**Figure 1.54** Adjacent-bridged cyclam and cyclen.



## 2.1 Ethylene Cross-bridged Tetraazamacrocyclic Ligands.

Cross-bridging of tetraazamacrocyclic ligands with an ethylene unit formed a new family of bicyclic tetraamine ligands (**Figure 1.55**) which were first designed and

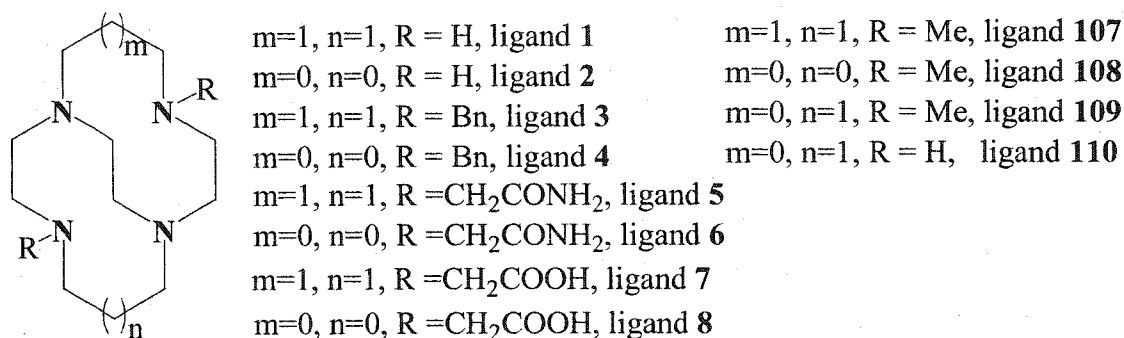
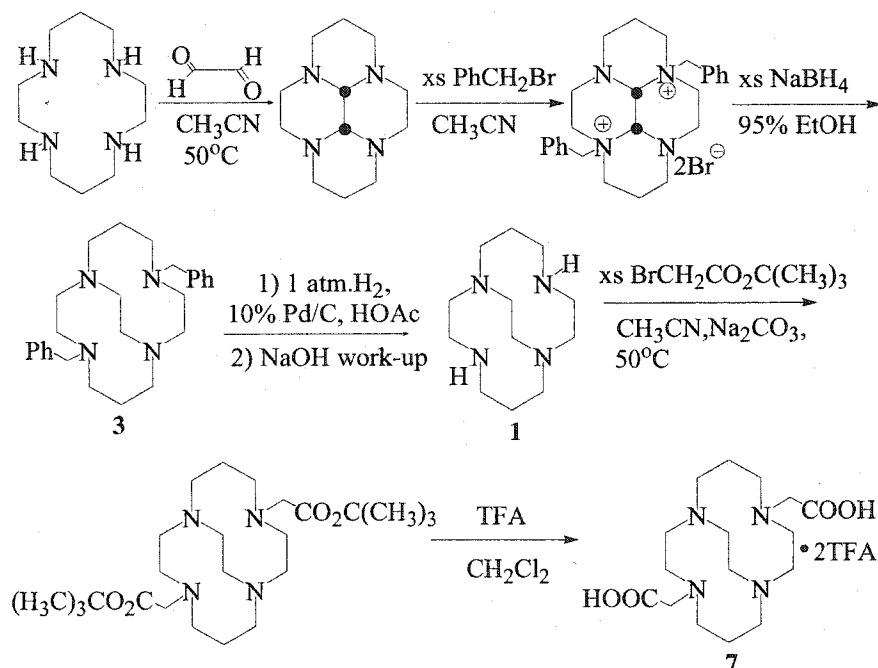
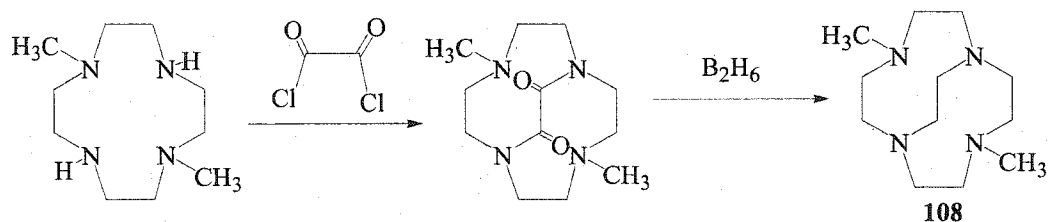


**Figure 1.55** Cross-bridged ligands used to form metal complexes.

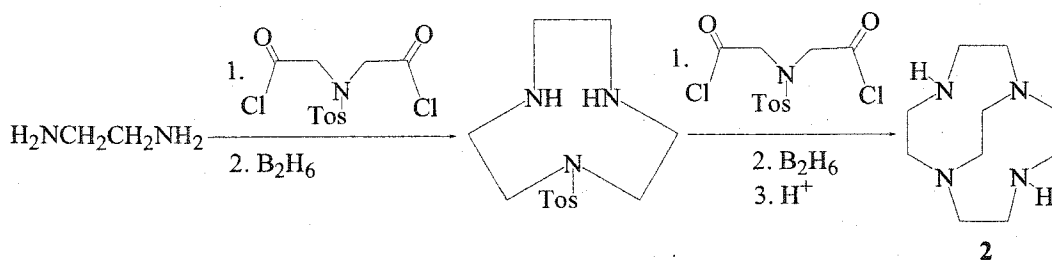


**Scheme 1.15** General synthetic route to make cross-bridged ligands.

synthesized by Weisman, Wong and coworkers.<sup>18,19</sup> A typical procedure of making these cross-bridged ligands is shown in **Scheme 1.15**,<sup>69(a),69(b)</sup> by which ligands **1**, **3** and **7** were synthesized. Ligand **108** was also produced by a less efficient route (**Scheme 1.16**).<sup>70</sup> Ligand **2** has also been synthesized using the much less efficient Schmidtchen method



**Scheme 1.16** An alternative method to synthesize ligand **108**.



**Scheme 1.17** An alternative method to synthesize ligand **2**.

(**Scheme 1.17**).<sup>71</sup> Cross-bridging cyclam or cyclen with an ethylene was anticipated to result in a higher kinetic inertness of metal complexes than those of the parent cyclam or cyclen complexes as a consequence of the highly-favored *cis*-folded (*cis*-V) ligand coordination mode. This binds a metal cation within a ligand's molecular cleft using all four convergent nitrogen lone pairs (**Figure 1.56**) and deters common decomplexation pathways. Consistent with the design by Weisman, Wong and coworkers, this family of

ligands (Figure 1.55), as shown by the Wong/Weisman group and others, yielded very stable complexes with many many group as well as first-row transition metal cations.<sup>72-75</sup> Competition NMR experiment studies indicated that the binding of Li(I) to ligand 107 was about 10,000 times better than Na(I).<sup>18,19</sup> Another common property of these cross-bridged ligands is their strong basicity.

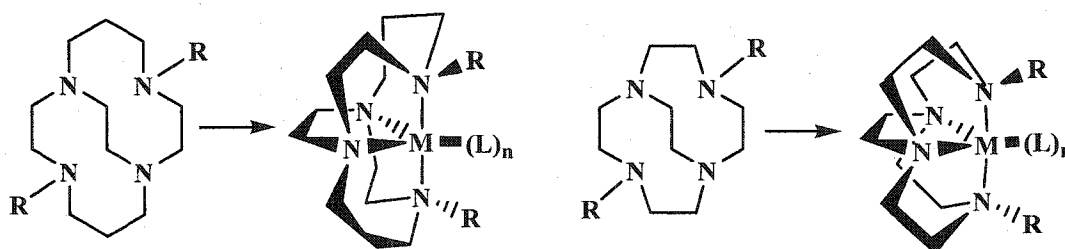


**Figure 1.56** *Cis*-folded configuration (V) adopted by cross-bridged ligands in their metal complexes.

To date, the metal ions successfully complexed with these ethylene cross-bridged ligands include Li(I), Cu(II), Cu(I), Ni(II), Co(II), Co(III), Fe(II), Fe(III), Mn(II), Mn(III), Ga(III), In(III), Pd(II) and Zn(II).<sup>76</sup> All structural and spectral studies of metal complexes of cross-bridged ligands in the literature have affirmed this single coordination mode in which octahedral, trigonal bipyramidal, square pyramidal and tetrahedral geometries were observed. To describe the “fit” of a metal ion within the cavity formed by a coordinated cross-bridged ligand, the axial bond angle between the non-bridged nitrogen atoms through the metal ion, the  $N_{ax}\text{-M-N}_{ax}$  bond angle (Figure 1.57) as well as the  $N_{eq}\text{-M-N}_{eq}$  bond angle are very useful. In five- or six-coordinate metal complexes, the closer the  $N_{ax}\text{-M-N}_{ax}$  angle is to linearity, the better of the metal

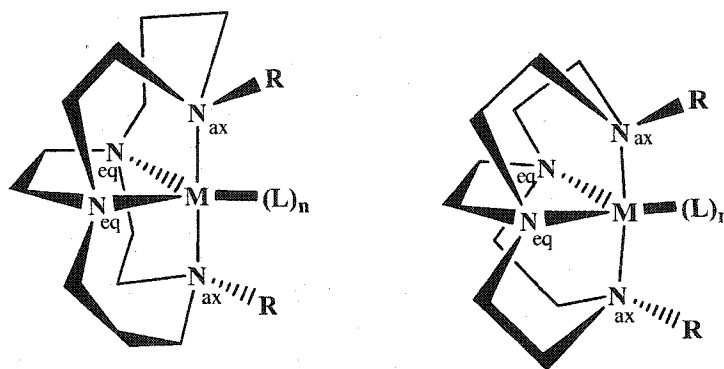


**Figure 1.57** Equatorial and axial nitrogen atoms are labeled as  $N_{eq}$  and  $N_{ax}$  respectively in the metal complexes of these cross-bridged ligands.

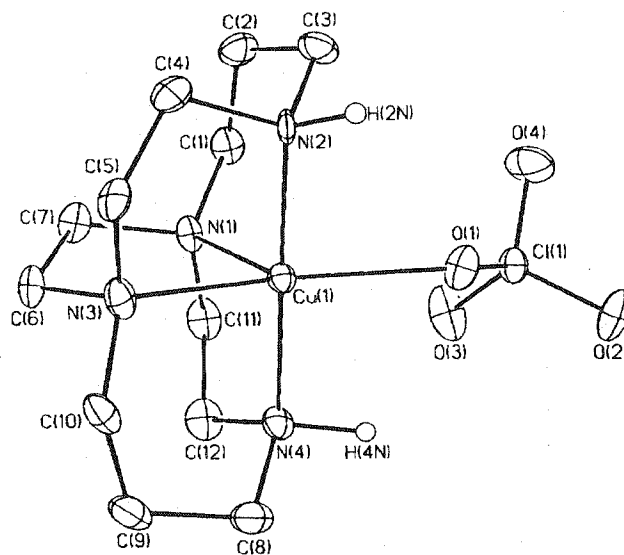


**Figure 1.58** The X-ray structure of a Cu(II) complex of ligand **1**.

ion fits inside a cross-bridged ligand's cavity. Our research group has reported the syntheses and characterization of Cu(II) complexes of ligands **1**, **3**, **5** and **7**.<sup>18,69</sup> The X-ray structures of  $[Cu(1)(ClO_4)]ClO_4$  (**Figure 1.58**),  $[Cu(1)Cl]Cl(H_2O)_3$  and  $[Cu(3)Cl]Cl(H_2O)$  (**Figure 1.59**) all exhibit five-coordinate Cu(II). The coordination geometries of  $[Cu(1)(ClO_4)]ClO_4$  and  $[Cu(1)Cl]Cl(H_2O)_3$  lie between the idealized

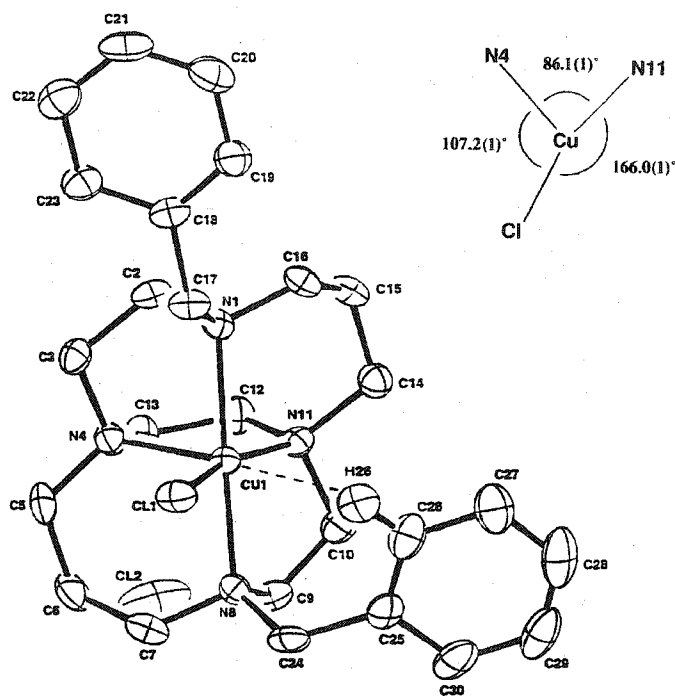


Figure 1.59 The X-ray structure of a Cu(II) complex of ligand 3.

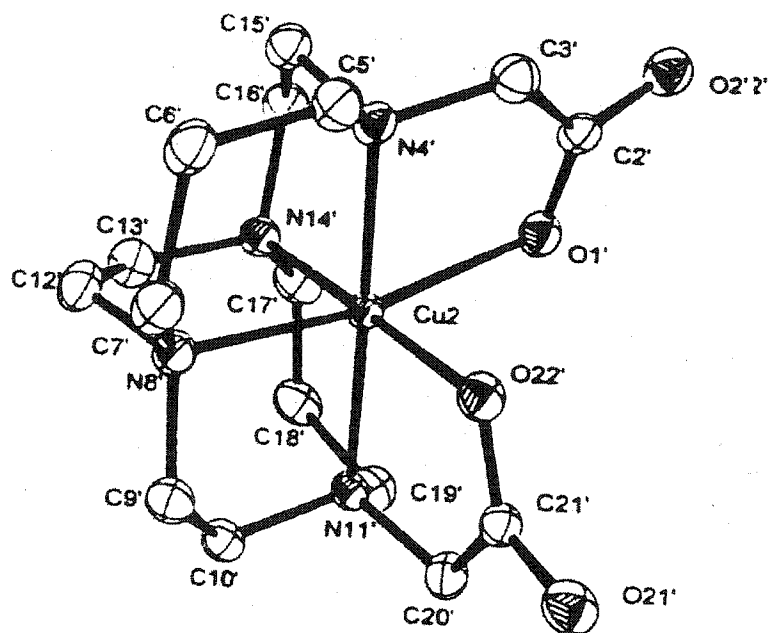
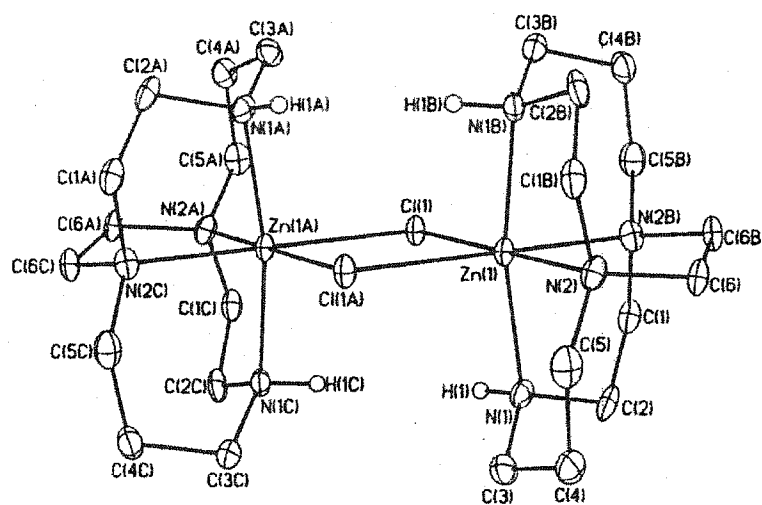
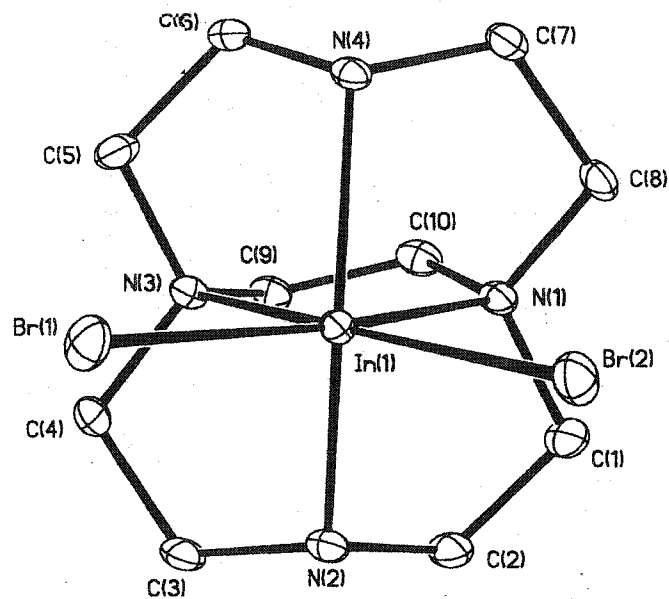


Figure 1.60 The X-ray structure of a Cu(II) complex of ligand 7-2H.

square pyramidal and the trigonal bipyramidal. The most striking crystal structure is that of a six-coordinated Cu(II) complex of deprotonated ligand 7,  $[\text{Cu}\cdot(7\text{-}2\text{H})\text{Na}(\text{H}_2\text{O})\text{ClO}_4]_2(\text{H}_2\text{O})$  (Figure 1.60). This is currently the only structurally-characterized metal complex of any pendant-armed cross-bridged ligand in the literature. Here, Cu(II) coordinates to a distorted octahedral  $\text{N}_4\text{O}_2$  donor set from 7 and is fully engulfed within the cavity formed as indicated by the  $\text{N}_{\text{ax}}\text{-Cu-N}_{\text{ax}}$  bond angle of  $179.7(3)^\circ$ . The synthesis and characterization of two six-coordinated Zn(II) complexes of ligand 1<sup>72</sup> and four six-coordinated Ga(III) and In(III) complexes of ligands 1 and 2 in this thesis were communicated recently.<sup>77</sup> In contrast to what was claimed in Busch's work,<sup>73,74</sup> these Zn(II) complexes of ligand 1 were readily synthesized in the protic solvent methanol. The structures of  $[\text{Zn}\cdot\mathbf{1}(\text{OH}_2)(\mu\text{-Cl})\text{ZnCl}_3]$ , dimeric  $[\text{Zn}\cdot\mathbf{1}(\mu\text{-Cl})]_2\text{Cl}_2(\text{CH}_3\text{OH})_4$  (Figure 1.61) and  $[\text{GaCl}_2\cdot\mathbf{1}]\text{Cl}$  all present slightly distorted octahedral coordination geometries whereas  $[\text{InBr}_2\cdot\mathbf{2}]\text{Br}$  (Figure 1.62) has a more distorted octahedral geometry as indicated by their axial bond angles (*vide infra*).



**Figure 1.61** The X-ray structure of the dimeric Zn(II) complex of ligand 1.



**Figure 1.62** The X-ray structure of an In(III) complex of ligand 2.

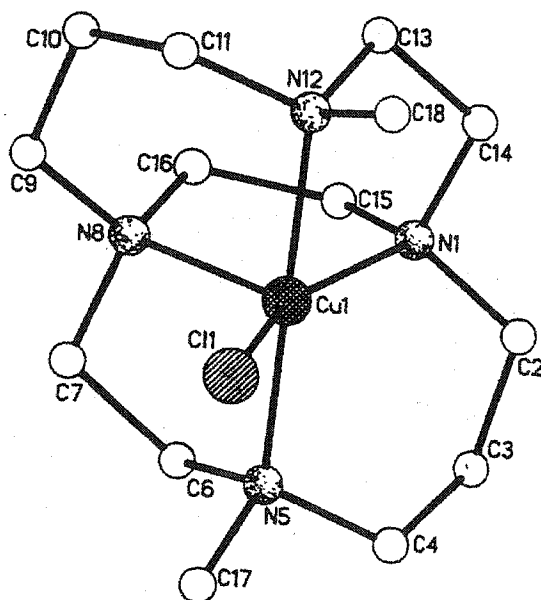


**Figure 1.63** The X-ray structure of  $[\text{Cu(II)Cl}\cdot 107]^+$ .

Since 1998, Busch and his coworkers have reported the syntheses and structural characterization of several Mn(II), Mn(III), Fe(II), Fe(III), Co(II), Co(III), Ni(II), Cu(I), Cu(II) and Pd(II) complexes of ligands **1**, **2**, **3**, **4**, **107** and **108**. A common feature for the syntheses of these complexes was the use of an aprotic solvent, anhydrous MeCN or DMF. The X-ray structure of the six-coordinate  $\text{MnCl}_2 \cdot \mathbf{107}$  showed a distorted octahedral geometry.<sup>73</sup> It was noted that the kinetic stability of Cu(II) complex of **107** was at least eight orders of magnitude larger than that of Cu(II) complex of  $\text{Me}_4\text{cyclam}$ .  $\text{Me}_4\text{cyclam}$  is the closest unbridged analogue of **107**. The X-ray structure of a Cu(II) complex of **107**,  $[\text{Cu(II)Cl} \cdot \mathbf{107}]\text{PF}_6$  was later shown to be penta-coordinate (**Figure 1.63**).<sup>74</sup> Busch's group also communicated the solid-state structures of a rare tetra-

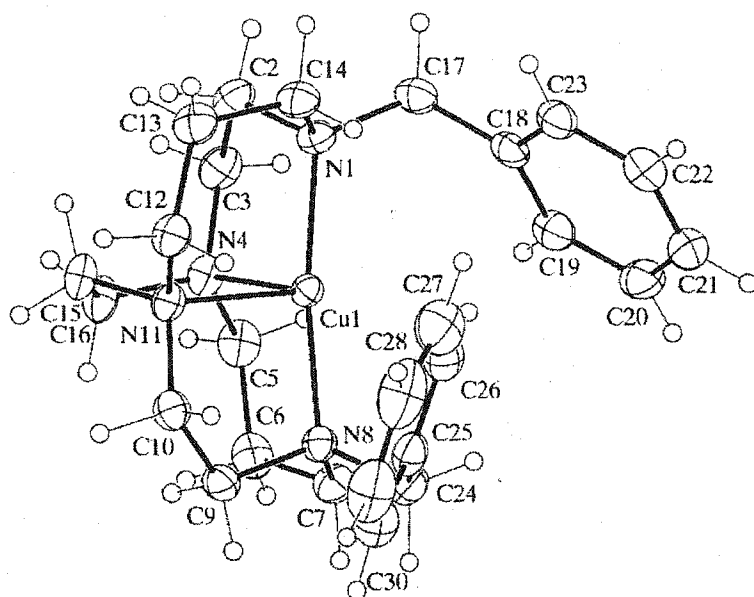


**Figure 1.64** The X-ray structure of  $[\text{Cu(I)} \cdot \mathbf{3}]^+$ .



coordinated  $[\text{Cu(I)}\cdot\mathbf{3}]\text{PF}_6$  (**Figure 1.64**) and penta-coordinated  $[\text{Pd(II)Cl}\cdot\mathbf{107}]\text{Cl}(\text{H}_2\text{O})$  in 1999<sup>78</sup> and  $[\text{Cu(II)}(\text{MeCN})\cdot\mathbf{3}](\text{PF}_6)_2$  (**Figure 1.65**) in 2000.<sup>79</sup>  $[\text{Cu(I)}\cdot\mathbf{3}]\text{PF}_6$  has a

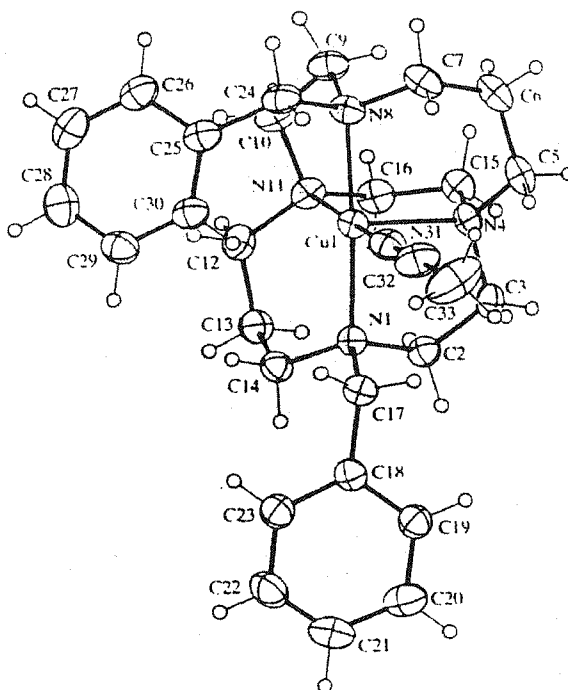


**Figure 1.65** The X-ray structure of  $[\text{Cu(II)}(\text{MeCN})\cdot\mathbf{3}]^+$ .

severely-distorted tetrahedral geometry with both benzyl groups folded toward the metal ion. In 2000, they detailed the syntheses and characterization of Mn(II) and Fe(II) complexes of ligands **107** and **108**.<sup>75</sup> These six-coordinate complexes include  $\text{MnCl}_2\cdot\mathbf{107}$ ,  $\text{MnCl}_2\cdot\mathbf{108}$ ,  $\text{FeCl}_2\cdot\mathbf{107}$  and  $\text{FeCl}_2\cdot\mathbf{108}$ . The structural data (**Table 1.1**, *vide infra*) of these complexes revealed that the 14-membered macrobicyclic in **107** engulfed the metal ion more fully than that of 12-membered macrobicyclic in **108**. To study the kinetic stability of the paramagnetic complex,  $\text{MnCl}_2\cdot\mathbf{9}$ , its protonation in 1 M DCl was monitored by measuring the integrated intensity of the protonated **107** in  $^1\text{H}$  NMR

spectra as a function of time. The dissociation of **107** from Mn(II) had a rate that is 12 orders of magnitude slower than the rate of water exchange from the hydrated Mn(II) ion. In 2001, the syntheses and characterization of Mn(III) and Fe(III) complexes of ligands **107** and **108** were also reported.<sup>80</sup> These Mn(III) and Fe(III) complexes were produced from the oxidation of respective Mn(II) and Fe(II) complexes. In aqueous solution, as suggested by conductance measurement,  $[\text{MnCl}_2 \cdot \mathbf{107}] \text{PF}_6$  was presented as  $[\text{Mn}(\text{H}_2\text{O})_2 \cdot \mathbf{107}]^{3+}$ . Titration data of this complex provided  $\text{p}K_a$ 's of 1.6(2) and 5.87(2), which were larger than the first two  $\text{p}K_a$ 's of  $[\text{Mn} \cdot (\text{H}_2\text{O})_6]^{3+}$  (0.82 and 0.94 respectively). X-ray structures of six-coordinated Ni(II) complexes,  $[\text{Ni}(\text{H}_2\text{O})_2 \cdot \mathbf{107}] \text{Cl}_2$ ,  $[\text{Ni}(\text{acac}) \cdot \mathbf{107}][\text{Ni}(\text{acac})_3] \text{THF}$  and  $[\text{Ni}(\text{acac}) \cdot \mathbf{108}][\text{Ni}(\text{acac})_3] \text{THF}$  were also reported.<sup>81</sup> The latter two Ni(II) complexes are the rare published examples of any metal ion that is hexa-coordinated by four nitrogen donors from a cross-bridged ligand as well as two donors from a bidentate ligand.

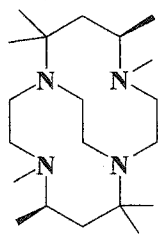


**Figure 1.66** A cross-bridged ligand, **111**.

In 2002, the structures of six-coordinated  $\text{CoCl}_2 \cdot \mathbf{107}$ ,  $\text{CoCl}_2 \cdot \mathbf{108}$  and  $[\text{CoCl}_2 \cdot \mathbf{108}] \text{PF}_6$  were reported.<sup>82</sup> Even more recently, they synthesized and structurally characterized  $\text{Mn}(\text{CF}_3\text{SO}_3)_2 \cdot \mathbf{3}$ ,  $\text{MnCl}_2 \cdot \mathbf{4}$ ,  $\text{FeCl}_2 \cdot \mathbf{4}$ ,  $[\mathbf{1} \cdot \text{FeCl}(\mu\text{-O})\text{ClFe} \cdot \mathbf{1}] \text{Cl}_2(\text{H}_2\text{O})_3$  and

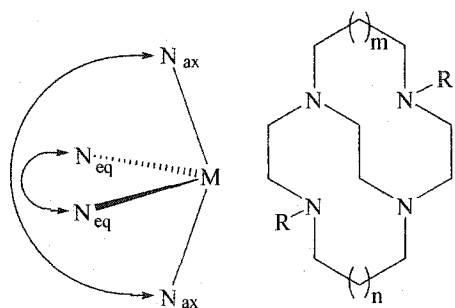
$[2 \cdot \text{FeCl}(\mu\text{-O})\text{ClFe} \cdot 2] \text{Cl}_2(\text{H}_2\text{O})_2$ .<sup>83</sup> The metal centers in these metal complexes all were found to adopt the distorted octahedron coordination geometry. A structural modified cross-bridged ligand **111** (Figure 1.66) was also synthesized by Busch's group. X-ray structures of five-coordinate metal complexes,  $[\text{CoCl} \cdot \mathbf{111}]_2(\text{CoCl}_4)$ ,<sup>82</sup>  $[\text{NiCl} \cdot \mathbf{111}]\text{PF}_6$ ,<sup>81</sup> and  $[\text{CuCl} \cdot \mathbf{111}]\text{PF}_6$ <sup>74</sup> have been reported. A summary of the  $N_{\text{ax}}\text{-Cu-}N_{\text{ax}}$  bond angles and the  $N_{\text{eq}}\text{-Cu-}N_{\text{eq}}$  bond angles of the complexes reported by both Busch and us is listed in **Table 1.1**.

As discussed above, due to their high kinetic stabilities, metal complexes of cross-bridged ligands have potential application in areas including radiopharmaceutical<sup>84</sup> and oxidation catalysis research<sup>85,86</sup>.

Studies by our collaborator, Dr. Carolyn Anderson and her group at Washington University have revealed that the <sup>64</sup>Cu(II) complex of the dicarboxylate-armed ligand, **7** has high *in vivo* stability.<sup>84</sup> This Cu(II) complex is much more stable *in vivo* than the <sup>64</sup>Cu(II) complex of 1,4,8,11-tetraazacclotetradecane-1,4,8,11-tetraacetic acid (TETA). It survived in serum for days and showed fast clearance from all tissues and organs in normal rats. This indicates that bioconjugated ligand **7** derivatives labeled with copper radionuclides may well have potential applications in diagnostic imaging and targeted radiotherapy. The Busch group has been interested in the oxidation catalysis application of their metal complexes.<sup>75,80,85,86</sup> They reported that  $\text{MnCl}_2 \cdot \mathbf{107}$  reacted with oxidizing agents to form the Mn(IV)·**107** complex. Unlike the metalloporphyrins, in the presence of  $\text{MnCl}_2 \cdot \mathbf{9}$  at pH 10, significant oxidation of carbamazepine was observed to produce the sole product, epoxide, in 7.3 % yield using  $\text{H}_2\text{O}_2$  as the oxidizing agent. Under the same conditions, the hydrogen abstraction reaction with 1,4-cyclohexadiene to form

**Table 1.1** Comparison of the 'fit' of metal ions inside cross-bridged ligands.

Complex	Coordination Geometry or coordination number	Axial N-M-N Angle	Equatorial N-M-N Angle	Reference
MnCl <sub>2</sub> • <b>107</b>	Severely distorted O <sub>h</sub>	158.0 (2) <sup>o</sup>	75.6 (2) <sup>o</sup>	75
MnCl <sub>2</sub> • <b>108</b>	Severely distorted O <sub>h</sub>	144.0 (2) <sup>o</sup>	73.7 (2) <sup>o</sup>	75
Mn(CF <sub>3</sub> SO <sub>3</sub> ) <sub>2</sub> • <b>3</b>	Distorted O <sub>h</sub>	165.25 (10) <sup>o</sup>	79.40 (14) <sup>o</sup>	83
MnCl <sub>2</sub> • <b>4</b>	Severely distorted O <sub>h</sub>	144.30 (6) <sup>o</sup>	74.56 (8) <sup>o</sup>	83
[MnCl <sub>2</sub> • <b>107</b> ]PF <sub>6</sub>	Distorted O <sub>h</sub>	170.1 (2) <sup>o</sup>	81.7 (7) <sup>o</sup>	80
[MnCl <sub>2</sub> • <b>108</b> ]PF <sub>6</sub>	Severely distorted O <sub>h</sub>	155.01 (11) <sup>o</sup>	81.29 (11) <sup>o</sup>	80
FeCl <sub>2</sub> • <b>107</b>	Distorted O <sub>h</sub>	161.88 (5) <sup>o</sup>	78.36 (5) <sup>o</sup>	75
FeCl <sub>2</sub> • <b>108</b>	Severely distorted O <sub>h</sub>	145.78 (7) <sup>o</sup>	77.31 (7) <sup>o</sup>	75
FeCl <sub>2</sub> • <b>4</b>	Severely distorted O <sub>h</sub>	147.71 (8) <sup>o</sup>	76.92 (9) <sup>o</sup>	83
[ <b>1</b> -FeCl(μ-O)ClFe <b>1</b> ]Cl <sub>2</sub> (H <sub>2</sub> O) <sub>3</sub>	Distorted O <sub>h</sub>	159.6 (2) <sup>o</sup>	79.2 (2) <sup>o</sup>	83
[ <b>2</b> -FeCl(μ-O)ClFe <b>2</b> ]Cl <sub>2</sub> (H <sub>2</sub> O) <sub>2</sub>	Severely distorted O <sub>h</sub>	146.8 (2) <sup>o</sup>	77.7 (2) <sup>o</sup>	83
CoCl <sub>2</sub> • <b>107</b>	Distorted O <sub>h</sub>	172.4 (2) <sup>o</sup>	81.11 (13) <sup>o</sup>	82
CoCl <sub>2</sub> • <b>108</b>	Severely distorted O <sub>h</sub>	149.81 (9) <sup>o</sup>	80.86 (8) <sup>o</sup>	82
[CoCl <sub>2</sub> • <b>108</b> ]PF <sub>6</sub>	Distorted O <sub>h</sub>	168.8 (4) <sup>o</sup>	87.2 (4) <sup>o</sup>	82
[Ni(H <sub>2</sub> O) <sub>2</sub> • <b>107</b> ]Cl <sub>2</sub>	Distorted O <sub>h</sub>	175.39 (5) <sup>o</sup>	85.56 (5) <sup>o</sup>	81
[Ni(acac)• <b>9</b> ][Ni(acac) <sub>3</sub> ]THF	Distorted O <sub>h</sub>	174.56 (10) <sup>o</sup>	84.84 (9) <sup>o</sup>	81
[Ni(acac)• <b>108</b> ][Ni(acac) <sub>3</sub> ]THF	Distorted O <sub>h</sub>	161.58 (13) <sup>o</sup>	81.61 (13) <sup>o</sup>	81
[CuCl• <b>1</b> ]Cl(H <sub>2</sub> O) <sub>3</sub>	Halfway between SP and TBPY	176.9 (2) <sup>o</sup>	87.8 (2) <sup>o</sup>	69(a)
[Cu(ClO <sub>4</sub> )• <b>1</b> ]ClO <sub>4</sub>	Halfway between SP and TBPY	179.7 (3) <sup>o</sup>	88.5 (3) <sup>o</sup>	69(a)
[CuCl• <b>3</b> ]Cl(H <sub>2</sub> O)	Distorted SP	176.0 (2) <sup>o</sup>	86.1 (1) <sup>o</sup>	69(a)
[Cu• <b>3</b> ]PF <sub>6</sub>	Severely distorted T <sub>d</sub>	171.85 (5) <sup>o</sup>	85.17 (5) <sup>o</sup>	78
[Cu(CH <sub>3</sub> CN)• <b>3</b> ](PF <sub>6</sub> ) <sub>2</sub>	Distorted SP	177.34 (9) <sup>o</sup>	86.96 (10) <sup>o</sup>	78
[CuCl• <b>107</b> ]PF <sub>6</sub>	Halfway between SP and TBPY	175.16 (13) <sup>o</sup>	85.30 (12) <sup>o</sup>	74
[Zn• <b>1</b> (OH <sub>2</sub> )(μ-Cl)ZnCl <sub>3</sub> ]	Distorted O <sub>h</sub>	173.5 (2) <sup>o</sup>	84.9 (2) <sup>o</sup>	72
[Zn• <b>1</b> (μ-Cl)] <sub>2</sub> Cl <sub>2</sub> (CH <sub>3</sub> OH) <sub>4</sub>	Distorted O <sub>h</sub>	168.7 (3) <sup>o</sup>	84.5 (2) <sup>o</sup>	72
[GaCl <sub>2</sub> • <b>1</b> ]Cl	Distorted O <sub>h</sub>	169.33 (7) <sup>o</sup>	84.17 (7) <sup>o</sup>	77
[InBr <sub>2</sub> • <b>2</b> ]Br	Severely distorted O <sub>h</sub>	143.95 (12) <sup>o</sup>	76.78 (12) <sup>o</sup>	77

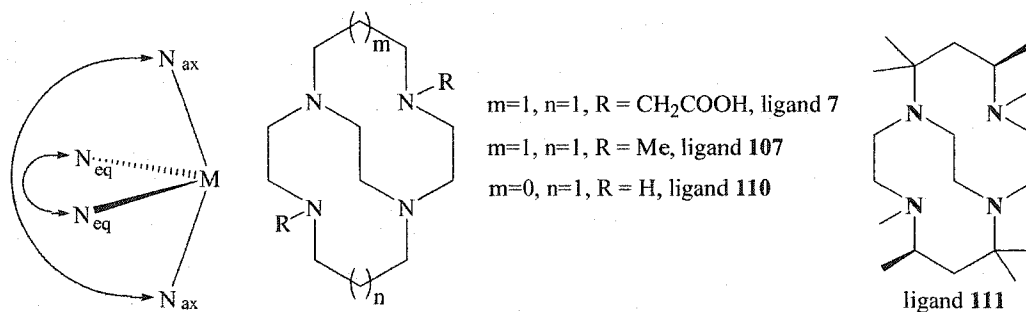


m=1, n=1, R = H, ligand **1**  
 m=0, n=0, R = H, ligand **2**  
 m=1, n=1, R = Bn, ligand **3**  
 m=0, n=0, R = Bn, ligand **4**

m=1, n=1, R = Me, ligand **107**  
 m=0, n=0, R = Me, ligand **108**

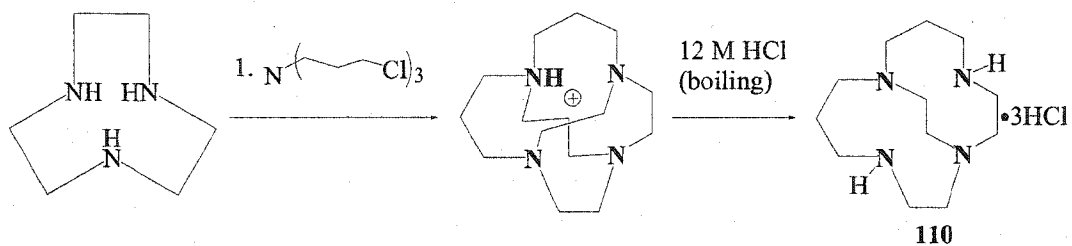
**Table 1.1** Comparison of the 'fit' of metal ions inside cross-bridged ligands (Cont.).

Complex	Coordination Geometry or coordination number	Axial N-M-N Angle	Equatorial N-M-N Angle	Reference
[PdCl•107]PF <sub>6</sub> (H <sub>2</sub> O) <sub>2</sub>	Distorted SP	171.65 (11) <sup>o</sup>	80.12 (10) <sup>o</sup>	79
[CuBr•110]ClO <sub>4</sub>	Distorted SP	176.3 (2) <sup>o</sup>	83.9 (2) <sup>o</sup>	88
[CoCl•111] <sub>2</sub> (CoCl <sub>4</sub> )	Distorted TBPY	175.0 (6) <sup>o</sup>	89.3 (5) <sup>o</sup>	82
[CuCl•111]PF <sub>6</sub>	Distorted TBPY	175.14 (8) <sup>o</sup>	87.51 (8) <sup>o</sup>	74
[Cu•(7-2H)Na(H <sub>2</sub> O)ClO <sub>4</sub> ] <sub>2</sub> H <sub>2</sub> O	Distorted O <sub>h</sub>	177.5 (1) <sup>o</sup>	84.8 (1) <sup>o</sup>	69(a)



benzene in 63.2% yield. These results revealed that this Mn(IV)•107 complex is a selective catalyst which showed moderate catalytic activity in oxygen transfer and much higher catalytic activity in hydrogen abstraction reactions. This is relevant to the development of bleaching agent technology.<sup>75,80,85,86</sup>

An alternative procedure to make ligand 110 was reported by Springborg *et al.*<sup>87</sup> Reaction of 1,4,7-triazacyclononane with tris(3-chloropropyl)amine afforded the inside monoprotonated form of the tricyclic amine 1,4,8,12-tetraazatricyclo[6.6.3.24,12]nonadecane, which was then treated with concentrated boiling hydrochloric acid to cause a slow cleavage of one trimethylene bridge to give triprotonated ligand 110 salt in 40% yield (Scheme 1.18). In 2001, they also reported the synthesis and X-ray structure of a five-coordinated Cu(II) complex, [CuBr•110]ClO<sub>4</sub>.<sup>88</sup>



**Scheme 1.18** An alternative method to synthesize ligand 110.

## 2.2 Other Cross-bridged Tetraazamacrocyclic Ligands.

Very recently, Springborg reviewed the coordination chemistry of cross-bridged tetraazamacrocyclic ligands.<sup>76</sup> Springborg *et al.* have used the reaction of the ditosylate of 1,3-propane diol with cyclen (*trans* ditosylated) to prepare three tri-methylene cross-bridged ligands, 112, 113 and 114 (Figure 1.67). Cu(II), Co(II), Co(III) and Ni(II) complexes of 112 and 114 have been synthesized and characterized by his group.

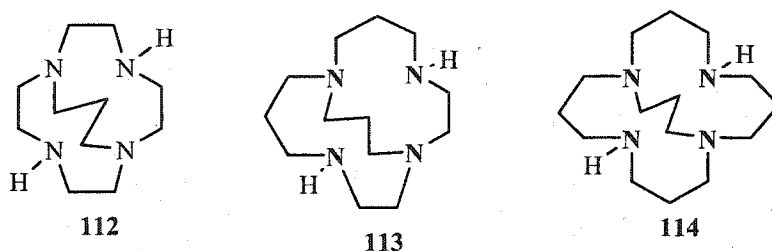


**Figure 1.67** Trimethylene cross-bridged ligands.

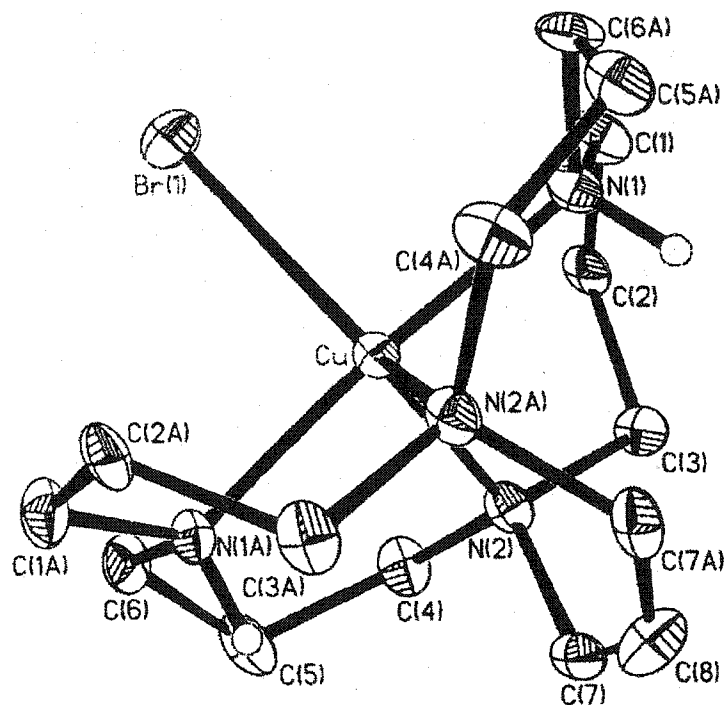


**Figure 1.68** The X-ray structure of a Cu(II) complex of ligand 114.

In 1997, Springborg and his coworkers reported two Cu(II) complexes,  $[\text{CuBr}\cdot\mathbf{112}]\text{ClO}_4$  and  $[\text{CuI}\cdot\mathbf{112}]\text{I}$ . As shown by their crystal structures, the coordination geometry of  $[\text{CuBr}\cdot\mathbf{112}]\text{ClO}_4$  can be described as being halfway between trigonal bipyramidal and square pyramidal whereas the coordination geometry of  $[\text{CuI}\cdot\mathbf{112}]\text{I}$  is a distorted trigonal bipyramid.<sup>89</sup> In a basic carbonate buffer,  $[\text{CuBr}\cdot\mathbf{112}]\text{ClO}_4$  existed as  $[\text{CuOH}\cdot\mathbf{112}]^+$ , which reacted with carbonate to form a trinuclear Cu(II) complex,  $[(\text{Cu}\cdot\mathbf{112})_3(\mu_3\text{-CO}_3)](\text{ClO}_4)_4(\text{H}_2\text{O})_2$ .<sup>90</sup> Their work further revealed that the cleavage of copper(II) nitrogen bonds in a penta-coordinated  $[\text{CuBr}\cdot\mathbf{112}]\text{ClO}_4$ , has a half-life of 130 hours in 5 N HCl.<sup>88</sup> More recently,  $[\text{CuBr}\cdot\mathbf{114}]\text{ClO}_4$  was synthesized and shown to have a trigonal bipyramidal geometry (**Figure 1.68**).<sup>89</sup>

Two dinuclear Ni(II) complexes,  $[(\text{Ni}\cdot\mathbf{112})_2(\mu\text{-Br})_2](\text{ClO}_4)_2$  and  $[(\text{Ni}\cdot\mathbf{112})_2(\mu\text{-Cl})_2](\text{ClO}_4)_2$  were also synthesized and characterized. The dinuclear structure of  $[(\text{Ni}\cdot\mathbf{112})_2(\mu\text{-Cl})_2](\text{ClO}_4)_2$ , which is similar to that of dinuclear  $[\text{Zn}\cdot\mathbf{1}(\mu\text{-Cl})_2]\text{Cl}_2(\text{CH}_3\text{OH})_4$  (Figure 1.61), was determined by a single-crystal X-ray analysis.<sup>91</sup>  $[\text{Ni}(\mu\text{-Br})_2\cdot\mathbf{112}](\text{ClO}_4)_2$  was formed from the reaction of anhydrous  $\text{NiBr}_2$  with **112** in anhydrous DMF. In dilute aqueous solution, both Ni(II) complexes exist as  $[\text{Ni}(\text{H}_2\text{O})_2\cdot\mathbf{112}]^{2+}$  which was isolated as  $[\text{Ni}(\text{H}_2\text{O})_2\cdot\mathbf{112}]\text{S}_2\text{O}_6\cdot 2\text{H}_2\text{O}$ . Two additional Ni(II) complexes,  $[\text{Ni}(\eta^2\text{-NO}_2)\cdot\mathbf{112}]\text{PF}_6$  and  $[\text{Ni}(\eta^2\text{-NO}_3)\cdot\mathbf{112}]\text{PF}_6$  were obtained by the reaction of  $[\text{Ni}(\text{H}_2\text{O})_2\cdot\mathbf{112}]\text{S}_2\text{O}_6\cdot 2\text{H}_2\text{O}$  with nitrite and nitrate respectively. The coordination geometry about Ni(II) in all five of these complexes is a distorted octahedron. In contrast to the use of anhydrous conditions in the synthesis of  $[(\text{Ni}\cdot\mathbf{112})_2(\mu\text{-Br})_2](\text{ClO}_4)_2$ ,  $[\text{Ni}(\eta^2\text{-NO}_3)\cdot\mathbf{114}]\text{NO}_3$  was obtained using the hydrated salt and **114** with ethanol as the reaction solvent.<sup>88</sup> The authors found that maintenance of excess metal ions was crucial to the high yields of this purple complex which was structurally characterized as a six-coordinated chelated nitrate complex. In the syntheses of five-coordinate  $[\text{NiCl}\cdot\mathbf{114}]\text{Cl}$  and  $[\text{NiBr}\cdot\mathbf{114}]\text{Br}$  each with a trigonal bipyramidal coordination geometry, methoxyethanol was found to be the optimal reaction solvent. Treatment of  $[\text{NiCl}\cdot\mathbf{114}]\text{Cl}$  with dilute perchlorate acid yielded the blue chelated perchlorate complex,  $[\text{Ni}(\eta^2\text{-ClO}_4)\cdot\mathbf{114}]\text{ClO}_4$ .

Springborg and his coworkers also prepared several Co(II) complexes of ligand **114**.<sup>88</sup> The reaction of  $\text{CoCl}_2\cdot 6\text{H}_2\text{O}$  with free ligand in methoxyethanol produced a high yield (83%) of  $[\text{CoCl}\cdot\mathbf{114}]\text{Cl}$ , which has a trigonal bipyramidal geometry. The crystal structure of this complex is similar to that of  $[\text{CuBr}\cdot\mathbf{114}]\text{Br}$ . Complex  $[\text{CoCl}\cdot\mathbf{114}]\text{Cl}$



formed a five-coordinate  $[\text{CoCl}\cdot\mathbf{114}]^+$  in 12M HCl and a six-coordinate  $[\text{CoXY}\cdot\mathbf{114}]^{n+}$  (X, Y = Cl<sup>-</sup> or MeOH and n = 0, 1 or 2) in MeOH. Both a six-coordinate pale green diaqua complex,  $[\text{Co}(\text{H}_2\text{O})_2\cdot\mathbf{114}](\text{ClO}_4)_2\cdot\text{H}_2\text{O}$  and a four-coordinated pink  $[\text{Co}\cdot\mathbf{114}][\text{ZnCl}_4]$  were isolated from two different aqueous solutions. The proposed structure of the pale green complex as the six-coordinated  $[\text{Co}(\text{H}_2\text{O})_2\cdot\mathbf{114}](\text{ClO}_4)_2\cdot\text{H}_2\text{O}$  was based upon spectral data. The X-ray of  $[\text{Co}\cdot\mathbf{114}][\text{ZnCl}_4]$  (Figure 1.69) revealed a

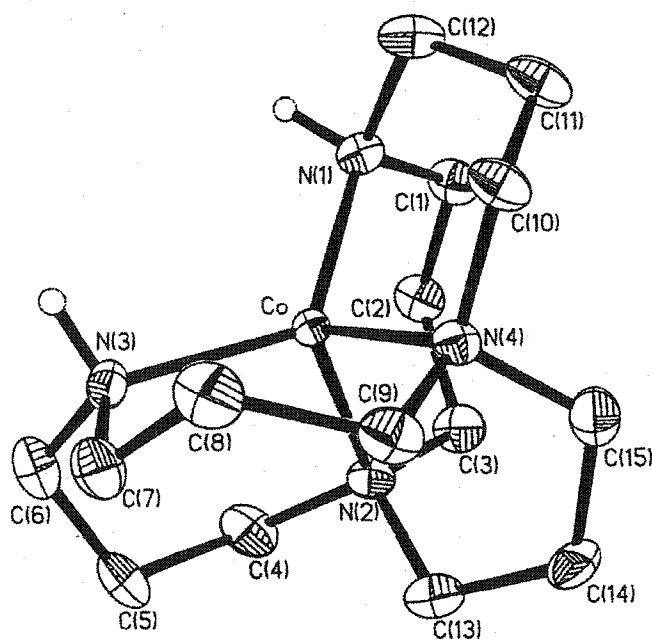
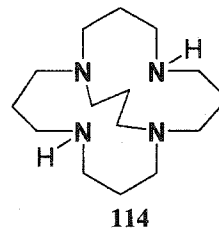
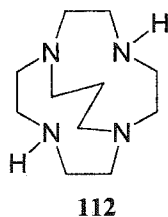
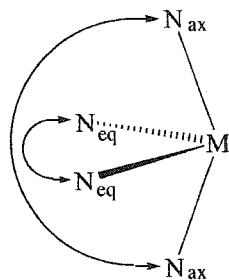


**Figure 1.69** The X-ray structure of a Co(II) complex of ligand 114.

distorted tetrahedral coordination, which was also observed in  $[\text{Zn}\cdot\mathbf{114}][\text{ZnCl}_4]$ . The high flexibility of this ligand is indicated by the dramatic change of the bond angle between the two non-bridging nitrogen atoms at Co(II), which is  $126.22(11)^\circ$  in four-coordinate  $[\text{Co}\cdot\mathbf{114}][\text{ZnCl}_4]$  and is  $173.08(9)^\circ$  in five-coordinate  $[\text{Co}\cdot\mathbf{114}\text{Cl}]\text{Cl}$ . Very

**Table 1.2** Comparison of the 'fit' of metal ions inside tri-methylene cross-bridging ligands.

Complex	Coordination Geometry or coordination number	Axial N-M-N Angle	Equatorial N-M-N Angle	Reference
[CoCl•114]Cl	Distorted TBPY	173.08 (9) <sup>o</sup>	87.78 (6) <sup>o</sup>	88
[Co•114(η <sup>2</sup> -CO <sub>3</sub> )]AsF <sub>6</sub>	Distorted O <sub>h</sub>	176.8 (3) <sup>o</sup>	103.0 (2) <sup>o</sup>	92
[Co(η <sup>2</sup> -SO <sub>4</sub> )•114]AsF <sub>6</sub> (H <sub>2</sub> O)	Distorted O <sub>h</sub>	176.02 (15) <sup>o</sup>	103.69 (15) <sup>o</sup>	92
[Co(η <sup>2</sup> -HCO <sub>3</sub> )•114](ZnBr <sub>4</sub> )(H <sub>2</sub> O)	Distorted O <sub>h</sub>	177.7 (4) <sup>o</sup>	103.4 (4) <sup>o</sup>	92
[(Ni•112) <sub>2</sub> (μ-Cl) <sub>2</sub> ](ClO <sub>4</sub> ) <sub>2</sub>	Distorted O <sub>h</sub>	166.2 (2) <sup>o</sup>	94.3 (2) <sup>o</sup>	91
[Ni(η <sup>2</sup> -NO <sub>2</sub> )•112]PF <sub>4</sub>	Distorted O <sub>h</sub>	170.0 (2) <sup>o</sup>	99.0 (2) <sup>o</sup>	91
[Ni(η <sup>2</sup> -NO <sub>3</sub> )•112]PF <sub>4</sub>	Distorted O <sub>h</sub>	170.14 (9) <sup>o</sup>	98.46 (8) <sup>o</sup>	91
[Ni(H <sub>2</sub> O) <sub>2</sub> •112]S <sub>2</sub> O <sub>6</sub> (H <sub>2</sub> O) <sub>2</sub>	Distorted O <sub>h</sub>	168.43 (5) <sup>o</sup>	94.88 (5) <sup>o</sup>	91
[NiCl•114]Cl	Distorted TBPY	173.87 (12) <sup>o</sup>	87.90 (8) <sup>o</sup>	88
[NiBr•114]Br	Distorted TBPY	174.15 (8) <sup>o</sup>	87.95 (6) <sup>o</sup>	88
[Ni(η <sup>2</sup> -NO <sub>3</sub> )•114]NO <sub>3</sub>	Distorted O <sub>h</sub>	176.5 (2) <sup>o</sup>	105.9 (2) <sup>o</sup>	88
[Ni(η <sup>2</sup> -ClO <sub>4</sub> )•114]ClO <sub>4</sub>	Distorted O <sub>h</sub>	177.34 (10) <sup>o</sup>	106.41 (9) <sup>o</sup>	88
[CuBr•112]ClO <sub>4</sub>	Halfway between SP and TBPY	170.5 (4) <sup>o</sup>	99.0 (3) <sup>o</sup>	89
[Cu•112]I	Distorted TBPY	170 (2) <sup>o</sup>	103 (2) <sup>o</sup>	89
[(Cu•112) <sub>3</sub> (μ <sub>3</sub> -CO <sub>3</sub> )](ClO <sub>4</sub> ) <sub>4</sub> (H <sub>2</sub> O) <sub>2</sub>	Distorted TBPY	169.0 (2) <sup>o</sup>	98.0 (2) <sup>o</sup>	90
[CuBr•114]Br	Distorted TBPY	174.8 (2) <sup>o</sup>	88.12 (12) <sup>o</sup>	88



interestingly, unlike most polyamine Co(II) complexes, [Co•114][ZnCl<sub>4</sub>] is not oxidized to a Co(III) complex by air. A purple Co(III) complex, [Co(η<sup>2</sup>-CO<sub>3</sub>)•114]Cl was thus prepared by the reaction of 114 with a Co(III) compound, [Co(py)<sub>3</sub>(η<sup>2</sup>-CO<sub>3</sub>)Cl] in ethanol.<sup>92</sup> When this reaction was carried out in perchloric acid, a blue complex [Co(η<sup>2</sup>-HCO<sub>3</sub>)•114][ZnBr<sub>4</sub>]•H<sub>2</sub>O was isolated. This is a rare example of a complex with a

chelated bound hydrogen carbonate. While in H<sub>2</sub>SO<sub>4</sub>, a turquoise Co(III) complex, [Co( $\eta^2$ -SO<sub>4</sub>) • 114] AsF<sub>6</sub>•H<sub>2</sub>O was obtained. The N<sub>ax</sub>-Cu-N<sub>ax</sub> bond angles and the N<sub>eq</sub>-Cu-N<sub>eq</sub> bond angles of the complexes reported by Springborg are summarized in **Table 1.2**.

The kinetic inertness of these metal complexes of ligands **112** and **114** were studied in 5 N HCl by Springborg. Data for these acid decomplexations are shown in **Table 1.3**. For comparison, the kinetic data of acidic decomplexation of [CuCl•110]<sup>+</sup> in 5N HCl is also included. The rate of cleavage in these metal complexes of **114** increased in the order Ni(II) < Cu(II) < Zn(II) < Co(II).

**Table 1.3** Kinetic data for the acid decomplexation of metal complexes of some cross-bridged ligands in 5N HCl reported by Springborg.

Complex	$k_{\text{cleavage}}/\text{s}^{-1}$	$\Delta H/\text{KJ mol}^{-1}$	$\Delta S/\text{J mol}^{-1}\text{K}^{-1}$	Ref.
[Cu•112Cl] <sup>+</sup>	1.48(2) x 10 <sup>-6</sup>	89(6)	-60(14)	91
[Cu•110Cl] <sup>+</sup>	1.79(5) x 10 <sup>-6</sup>	93(4)	-42(9)	91
[Cu•114Cl] <sup>+</sup>	2.28(6) x 10 <sup>-7</sup>	121(4)	32(14)	91
[Ni•112(H <sub>2</sub> O) <sub>2</sub> ] <sup>+</sup>	1.7(9) x 10 <sup>-9</sup>	110(5)	-45(15)	88
[Ni•114Cl] <sup>+</sup>	1.4(6) x 10 <sup>-9</sup>	126(6)	8(17)	91
[Co•114] <sup>+</sup>	1.12(2) x 10 <sup>-4</sup>	84(2)	-39(15)	91
[Zn•114] <sup>+</sup>	1.60(6) x 10 <sup>-4</sup>	82(2)	-44(7)	91

The synthesis of tetra-, penta-, hepta<sup>93,94,95</sup> and octa-methylene<sup>96,97,98</sup> cross-bridged ligands (**Figure 1.70**) have been also reported. Their coordination chemistry has been unexplored so far.

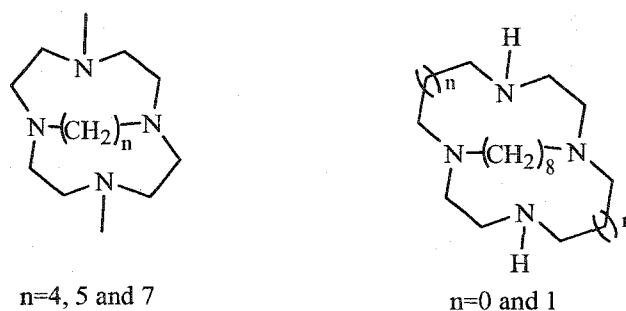


**Figure 1.70** Tetra-, penta-, hepta-, octa-methylene cross-bridged ligands.

### 3. General Aspects of this Dissertation.

As mentioned above, this doctoral dissertation research has focused on the synthesis and characterization of Cu(II), Ga(III), In(III), Zn(II), Cd(II) and Hg(II) complexes of eight cross-bridged ligands (**Figure 1.1**). In order to synthesize their metal complexes, these eight ligands were prepared according to procedures that were originally worked out by other research group members. Metal complexes were then synthesized and characterized by elemental analyses, IR (KBr), proton and  $^{13}\text{C}\{^1\text{H}\}$  NMR (or electronic spectra) and other spectroscopic techniques as well as single crystal X-ray structural analyses where appropriate. The investigation of the kinetic stability in acidic aqueous solution of selected complexes was then carried out.

Because of their potential radiopharmaceutical application, our research group have been interested in Cu(II), Ga(III) and In(III) complexes of these cross-bridged ligands, especially those with pendant-arms. In the past several years, we have cooperated with Dr Carolyn Anderson's research group in the medical school at

Washington University, St. Louis, on the synthesis of novel cross-bridged tetraamines, their metal complexes, assays of their kinetic stability, and the evaluation of their efficacy as carriers of cancer diagnostic and therapeutic copper, gallium, and indium radionuclides. As a result of the high basicity and consequent proton-sponge behavior of these cross-bridged ligands,<sup>18,81,84</sup> determination of the thermodynamic stability constants of their metal complexes in aqueous solution is problematic.<sup>81,84</sup> Studies of their kinetic stability are however possible. By studying their relative kinetic stabilities, we hoped to select the best candidate ligands for stable radionuclide carriers. In aqueous solution, the kinetic stability of a metal complex is reflected by the rate constant of its acidic decomplexation process. If pseudo-first-order reaction conditions are adopted, a complex's kinetic stability is directly related to the half-life of this decomplexation process. Therefore, the best candidate ligands for stable radionuclide carriers are those forming the longest half-life metal complexes in acidic aqueous solution.

Since Ga(III) and In(III) are diamagnetic, the kinetic stabilities of their complexes in acidic solution can thus be readily evaluated by using NMR techniques. NMR techniques can not be used to monitor kinetic stability of Cu(II) complexes. Different d-d electronic transition maxima are expected for complexed and decomplexed Cu(II), so acidic decomplexation can be followed spectrophotometrically in the UV-Vis region (370-800 nm).

We are also interested in Zn(II), Cd(II) and Hg(II) complexes of these ligands for several reasons. As shown in this introduction, macrocyclic tetraamine Zn(II) complexes can play an important role in bioinorganic chemistry.<sup>32-34</sup> Coordination chemistry of these *cis*-folded cross-bridged tetraamine Zn(II) complexes may provide useful basic

information for entry into this field. Zn(II), Cd(II) and Hg(II) are in the Group 2B triad of *d*-metals. They range from the smallest zinc(II) (six-coordinate ionic radius 88 pm) of borderline hardness through cadmium(II) (ionic radius 109 pm) to the soft mercury(II) (ionic radius 116 pm), presenting a useful series for studying variations in coordination preferences. The well-known propensity of Hg(II) to adopt lower coordination numbers may also provide alternate ligand binding modes. The diamagnetic nature of these Zn(II), Cd(II), and Hg(II) complexes renders them amenable to NMR spectroscopic studies. In acidic aqueous solution, their <sup>1</sup>H NMR spectra can be used to deduce the decomplexation rates. Their kinetic stabilities can then be correlated to the fit of a metal ion in a cross-bridged ligand as shown by their solid-state structures. <sup>1</sup>H and <sup>13</sup>C{<sup>1</sup>H} NMR spectra of these Zn(II), Cd(II) and Hg(II) complexes can also help identify the solution structures. For robust Cd(II) and Hg(II) complexes, additional structural insight could also be obtained from observations of <sup>1</sup>H and <sup>13</sup>C coupling to their NMR-active isotopes (*I* = 1/2: <sup>111</sup>Cd, 12.75% natural abundance, <sup>113</sup>Cd, 12.26%; and <sup>199</sup>Hg, 16.84%).<sup>99-103</sup>

## CHAPTER II

### Zn(II), Cd(II) AND Hg(II) COMPLEXES OF CROSS-BRIDGED TETRAAZAMACROCYCLIC LIGANDS 1-4

#### 1. Synthesis and Characterization of Zn(II), Cd(II) and Hg(II) Complexes.

##### 1.1 General Synthetic Methods.

Twenty Zn(II), Cd(II) and Hg(II) complexes of the parent and N, N'-Dibenzyl-substituted cross-bridged ligands (1, 2, 3, 4 in Figure 2.1) were synthesized and characterized by their IR,  $^1\text{H}$  and  $^{13}\text{C}$  NMR spectral data as well as CHN elemental

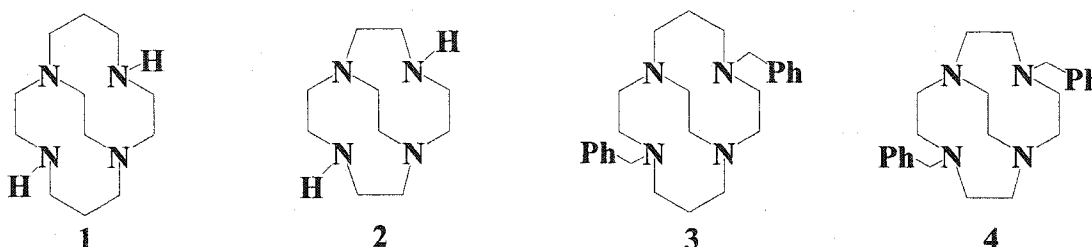


Figure 2.1 Cross-bridged ligands 1-4.

analyses. An additional complex,  $(\text{HgCl}_2)_6 \cdot (2)_4$  (135) was isolated unexpectedly but only characterized by its X-ray structure. In general, these metal complexes were prepared by refluxing a methanol or MeCN solution of the appropriate metal salt and an equivalent amount of cross-bridged ligand for a period from several hours to several days. Crystals

of the resulting complexes suitable for X-ray analyses were typically obtained by diethyl ether diffusion into a solution of the crude product in methanol, MeOH/H<sub>2</sub>O mixture, or chloroform. As mentioned in our previous communication,<sup>72</sup> specific reaction conditions are metal- and ligand-dependent.

## 1.2 Synthesis of Zn(II) and Cd(II) Complexes.

Zn(II) and Cd(II) complexes of ligands **1** and **2** were readily formed in MeOH in reasonable yields (64% - 98%) even when hydrated Zn(II) and Cd(II) salts were used as reactants.

However, attempted complexation of metal hydrate salts of Zn(II) and Cd(II) with ligands **3** and **4** yielded mainly protonated ligands as indicated by the presence of a broad NH stretch of R<sub>3</sub>NH<sup>+</sup> between 2450 and 2700 cm<sup>-1</sup> in the IR spectra and a protonated NH resonance of R<sub>3</sub>NH<sup>+</sup> at  $\delta$  larger than 9 in the <sup>1</sup>H NMR spectra of the products. For example, the unsuccessful complexation product of Zn(ClO<sub>4</sub>)<sub>2</sub>•6H<sub>2</sub>O with ligand **3** is a monoprotonated **3**. Its IR (KBr) spectrum is shown in **Figure 2.2(a)**. For comparison, the IR (KBr) spectrum of ZnCl<sub>2</sub>•**3** is shown in **Figure 2.2(b)**. The obvious difference between these two spectra is the presence of medium intensity band around 2600 cm<sup>-1</sup> indicated by an arrow in **Figure 2.2(a)**. In this spectrum, there is also a strong and broad perchlorate band around 1100 cm<sup>-1</sup>. This indicates that this monoprotonated ligand is probably [H<sub>3</sub>]<sup>+</sup>[ClO<sub>4</sub>]. The <sup>1</sup>H NMR spectrum of monoprotonated **3** obtained from this failed complexation was also compared to that of ZnCl<sub>2</sub>•**3** in the same solvent, *d*<sub>6</sub>-DMSO (**Figure 2.3**). Clearly, the downfield singlet at  $\delta$  10.4 of the monoprotonated **3** can be seen. There are several possible explanations for this problem. One is that the basicity of



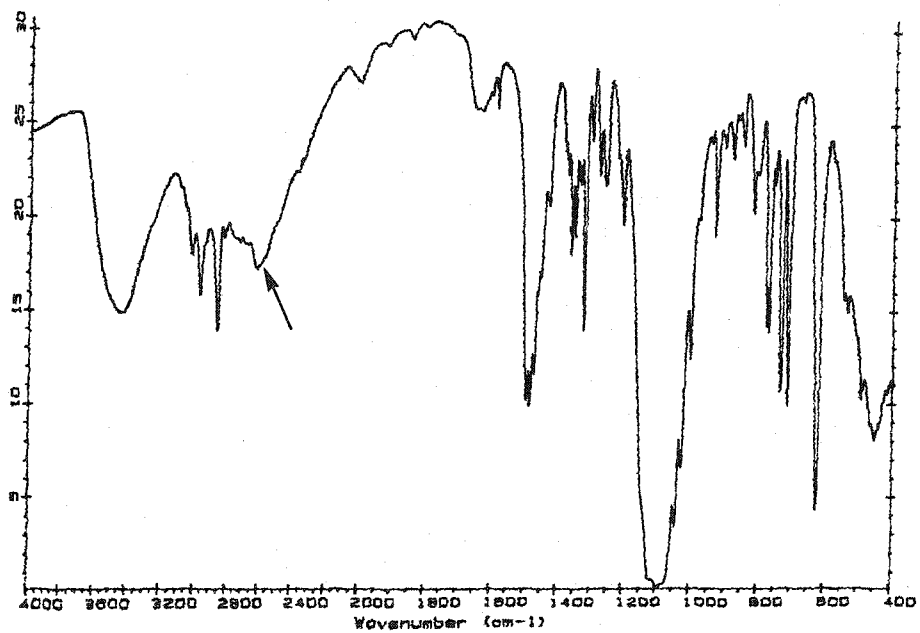


**Figure 2.2(a)** The IR (KBr) spectrum of monoprotonated **3** obtained from the failed complexation of  $\text{Zn}(\text{ClO}_4)_2 \cdot 6\text{H}_2\text{O}$  with ligand **3**.

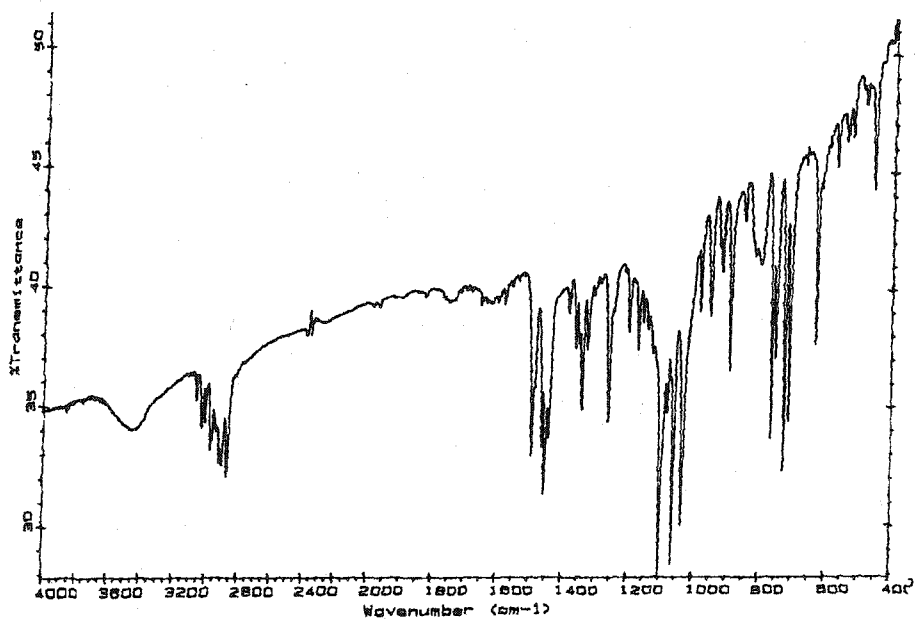


**Figure 2.2(b)** The IR (KBr) spectrum of  $\text{ZnCl}_2 \cdot 3$ .

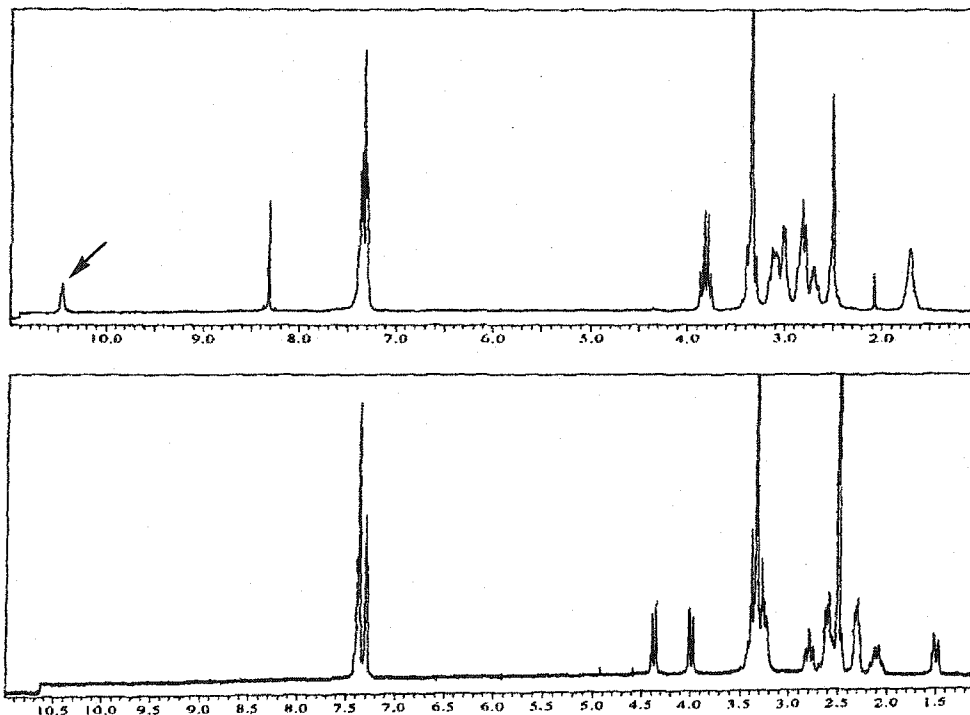


**Figure 2.3** The  $^1\text{H}$  NMR spectra of monoprotonated **3** obtained from the failed complexation of  $\text{Zn}(\text{ClO}_4)_2 \cdot 6\text{H}_2\text{O}$  with ligand **3** and  $\text{ZnCl}_2 \cdot \mathbf{3}$ . The top one is that of monoprotonated **3** in  $d_6$ -DMSO and the bottom one is that of  $\text{ZnCl}_2 \cdot \mathbf{3}$  in  $d_6$ -DMSO.

ligand **3** is higher than that of ligand **1** and the basicity of ligands **4** is probably higher than that of ligand **2**. The other is that the precipitating of protonated ligands **3** and **4** from the reaction solvent prevented successful complexation. Since ligand **1** (or **2**) has two secondary amine nitrogen donors whereas ligand **3** (or **4**) only has four tertiary amine nitrogen donors,  $\text{Zn}(\text{II})$  and  $\text{Cd}(\text{II})$  complexes of ligand **1** (or **2**) may also be thermodynamically more stable than related  $\text{Zn}(\text{II})$  complexes of ligand **3** (or **4**).<sup>104</sup>

In the complexation of  $\text{ZnCl}_2$  with ligand **3**, methanol was originally used as the solvent. But the reaction products were unpredictable due to the formation of  $\text{ZnCl}_2 \cdot \mathbf{3}$  (**119**),  $\text{Zn} \cdot \mathbf{3}(\mu\text{-Cl})_2\text{-ZnCl}_2$  (**120**) and protonated **3** (minor). An aprotic reaction solvent ( $\text{CH}_3\text{CN}$ ) and anhydrous reaction conditions were then used to successfully make

$\text{ZnCl}_2 \cdot \mathbf{3}$  and  $\text{Zn} \cdot \mathbf{3}(\mu\text{-Cl})_2\text{-ZnCl}_2$  in reasonable yields (88% and 92% respectively). In the synthesis of  $\text{ZnCl}_2 \cdot \mathbf{4}$ , when methanol was used as the reaction solvent, CHN analyses of the white precipitate formed at the end of the reaction had a varied composition of  $(\text{ZnCl}_2)_{1.2-1.7} \cdot \mathbf{4}$ . This is probably due to the presence of varying amounts of both  $\text{ZnCl}_2 \cdot \mathbf{4}$  and  $(\text{ZnCl}_2)_2 \cdot \mathbf{4}$ . Interestingly, we were able to purify  $\text{ZnCl}_2 \cdot \mathbf{4}$  (**124**) from this mixture by redissolving it in  $\text{CHCl}_3$ . This is due to the much higher solubility of  $\text{ZnCl}_2 \cdot \mathbf{4}$  in chloroform.

### 1.3 Synthesis of Hg(II) Complexes.

Attempted complexation of  $\text{HgCl}_2$  with ligand **3** (and ligand **4**) yielded white precipitates which had poor solubility even in polar NMR solvents such as  $d_6$ -DMSO,  $\text{CD}_3\text{CN}$  and  $\text{D}_2\text{O}$ . Evidence for formation of the Hg(II) complexes of ligand **3** (and ligand **4**) was the similarity of their IR spectra to these of Zn(II) and Cd(II) analogues. However, due to their poor solubility, no further characterization was carried out.

In contrast to our observation that Zn(II) and Cd(II) complexes were formed by the reactions of hydrated salts of Zn(II) and Cd(II) with either ligand **1** or ligand **2**, attempted complexation of  $\text{Hg}(\text{NO}_3)_2 \cdot \text{H}_2\text{O}$  with ligand **1** failed as indicated by the fact that the  $^1\text{H}$  and  $^{13}\text{C}\{^1\text{H}\}$  NMR spectra of the product in  $\text{D}_2\text{O}$  were the same as these of protonated **1**. This indicated that in the synthesis of Hg(II) complexes of ligand **1**, the presence of water inhibited the complexation. Anhydrous  $\text{HgCl}_2$  was thus used to react with stoichiometric amount of **1** in methanol to form the complex  $[\text{HgCl}_2(\mu\text{-1})]_2$  (**133**) in a reasonable yield (68%).

In an attempted synthesis of  $\text{HgCl}_2 \cdot \mathbf{2}$  (**134**),  $(\text{HgCl}_2)_6 \cdot (\mathbf{2})_4$  (**135**) precipitated unexpectedly from the refluxing reaction solution of an equivalent amount of ligand **2** and  $\text{HgCl}_2$ . Complex  $(\text{HgCl}_2)_6 \cdot (\mathbf{2})_4$  was characterized by its X-ray structure. An interesting feature of this complex is that all chlorides remain coordinated to Hg(II) (**Figure 2.41** and **Figure 2.42**, *vide infra*). Subsequently, under anhydrous reaction conditions and equivalent amounts of the two reactants in anhydrous methanol, a clear solution formed after reflux. Cooling of this solution to room temperature did not provide any crystals or precipitate. Diethyl ether diffusion into this solution yielded  $\text{HgCl}_2 \cdot \mathbf{2}$  as colorless crystals which was fully characterized by its CHN elemental analyses and X-ray structure (**Figure 2.40**, *vide infra*). Since the only significant change in reaction condition was the anhydrous reaction conditions, we believe the formation of  $(\text{HgCl}_2)_6 \cdot (\mathbf{2})_4$  was due to the presence of excess  $\text{HgCl}_2$ . Even though equivalent amounts of  $\text{HgCl}_2$  and **2** were used, the actual amount of  $\text{HgCl}_2$  was in excess of **2** because of two possible reasons. One is the absorbing of moisture into **2** and the other is the presence of small amount of organic impurity (< 4%) in **2**. Since complex  $(\text{HgCl}_2)_6 \cdot (\mathbf{2})_4$  has a poor solubility in MeOH, it precipitated out from the reaction solution. To test this hypothesis, a 1.5:1 mixture of  $\text{HgCl}_2$  (58.7 mg, 0.216 mmol) and **2** (29.3 mg, 0.148 mmol) were dissolved in methanol. Refluxing of this solution followed by cooling to room temperature yielded colorless crystals (40.1 mg). CHN elemental analyses of these crystals indicated the composition of  $(\text{HgCl}_2)_{11}(\mathbf{2})_6$  (or  $(\text{HgCl}_2)_{1.83}(\mathbf{2})$ ) (**Table 2.1**). Its  $^1\text{H}$  and  $^{13}\text{C}\{^1\text{H}\}$  NMR spectra in  $\text{CD}_3\text{CN}$  indicated the presence of only one coordinated **2** species on the NMR time scale. This clearly indicated that any excess  $\text{HgCl}_2$  in the reaction solution could

cause its co-precipitating with  $\text{HgCl}_2 \cdot 2$ . The formation of  $(\text{HgCl}_2)_6 \cdot (2)_4$  and  $(\text{HgCl}_2)_{11} \cdot (2)_6$  are also consistent with the high affinity of Hg(II) for chloride.

**Table 2.1** CHN elemental results of  $(\text{HgCl}_2)_{11}(2)_6$  (or  $(\text{HgCl}_2)_{1.83}(2)$ ).

Anal.	C (%)	H(%)	N(%)
Calcd.	17.26	3.19	8.05
Found	17.52 and 17.47	3.19 and 3.18	8.00 and 8.02

#### 1.4 Comparison of the Solubility of Metal Complexes.

Zn(II) and Cd(II) complexes of parent cross-bridged ligands, **1** and **2**, are freely soluble in water. Except for  $[\text{Zn} \cdot \mathbf{1}(\text{OH}_2)(\mu\text{-Cl})\text{ZnCl}_3]$  (**115**), these are also freely soluble in methanol. Their solubility in other organic solvents depends on the counter anion. Zn(II) and Cd(II) complexes with perchlorate or nitrate anions have a better solubility than those with chloride counter anions in acetonitrile.  $[\text{Zn} \cdot \mathbf{1}(\mu\text{-Cl})_2\text{Cl}_2]$  is slightly soluble in acetonitrile whereas  $\text{ZnCl}_2 \cdot 2$  is not soluble in this solvent at all. Compared to Zn(II) and Cd(II) complexes of ligands **1** and **2**, complexes of the more hydrophobic ligands, **3** and **4** have much poorer solubility in protic solvent such as  $\text{H}_2\text{O}$  and  $\text{CH}_3\text{OH}$ . Two Hg(II) complexes,  $[\text{HgCl}_2(\mu\text{-1})]_2$  (**133**) and  $\text{HgCl}_2 \cdot 2$  (**134**), have better solubility in MeOH and water than complexes of ligands **3** and **4** but are not as soluble as Zn(II) and Cd(II) complexes of ligands **1** and **2**.

## 2. Spectral Data.

## 2.1 Infrared Spectra.

As mentioned above, the IR spectral data are useful in the characterization of these Zn(II), Cd(II) and Hg(II) complexes. In the presence of acidic proton source such as water, the failure of a complexation with **1**, **2**, **3** or **4** was indicated by the presence of broad and medium-intensity  $\nu_{\text{NH}}$  of  $\text{R}_3\text{NH}^+$  varying from  $2450\text{ cm}^{-1}$  to  $2700\text{ cm}^{-1}$ . This is consistent with the absence of this band in the IR (KBr) spectra of the twenty-one characterized Zn(II), Cd(II) and Hg(II) complexes of ligands **1-4**. The different coordination modes of the  $\text{ZnCl}_2$  and  $\text{CdCl}_2$  complexes of ligand **1** compared to that of  $[\text{HgCl}_2(\mu-1)]_2$  can also be inferred from their solid-state infrared spectra. All the Zn and Cd complexes of ligands **1** and **2** have N-H stretches appearing between  $3186$  and  $3292\text{ cm}^{-1}$  (Table 2.2). By contrast, in the IR spectrum (KBr) of  $[\text{HgCl}_2(\mu-1)]_2$  (**133**), a broad

**Table 2.2** Comparison of NH stretches in the IR spectra of Zn(II), Cd(II) and Hg(II) complexes of ligands **1** and **2**.

Complex	$\nu_{\text{NH}} (\text{cm}^{-1})$	Complex	$\nu_{\text{NH}} (\text{cm}^{-1})$
$[\text{Zn}\cdot\mathbf{1}(\text{OH}_2)(\mu-\text{Cl})\text{ZnCl}_3]$	3264, 3252	$[\text{Zn}\cdot\mathbf{1}(\mu-\text{Cl})_2\text{Cl}_2]$	3216
$\text{Zn}\cdot\mathbf{1}(\text{ClO}_4)_2$	3286	$\text{Zn}\cdot\mathbf{1}(\text{NO}_3)_2$	3255
$[\text{Zn}\cdot\mathbf{2}(\text{OH}_2)_2](\text{ClO}_4)_2$	3198, 3173	$\text{ZnCl}_2\cdot\mathbf{2}$	3186
$\text{Zn}\cdot\mathbf{2}(\text{NO}_3)_2$	3199, 3173	$\text{Cd}\cdot\mathbf{1}(\text{NO}_3)_2$	3259
$\text{CdCl}_2\cdot\mathbf{1}$	3248, 3220	$\text{Cd}\cdot\mathbf{1}(\text{ClO}_4)_2$	3284
$\text{CdCl}_2\cdot\mathbf{2}$	3248	$\text{Cd}\cdot\mathbf{2}(\text{ClO}_4)_2$	3260
$[\text{Cd}\cdot\mathbf{2}(\eta^2-\text{NO}_3)_2]$	3292	$\text{HgCl}_2\cdot\mathbf{2}$	3240
$(\text{HgCl}_2)_6\cdot(\mathbf{2})_4$	3262	$[\text{HgCl}_2(\mu-1)]_2$	3078

N-H stretching band of medium intensity appeared at lower frequency ( $3078\text{ cm}^{-1}$ ) which was shifted to around  $2497\text{ cm}^{-1}$  upon deuteration. This lower-energy stretch can be attributed to the extensive intra-cleft hydrogen bonding between the N-H and the tertiary

nitrogen lone pairs, as confirmed in the X-ray study of  $[\text{HgCl}_2(\mu-1)]_2$  (Figure 2.39, *vide infra*).

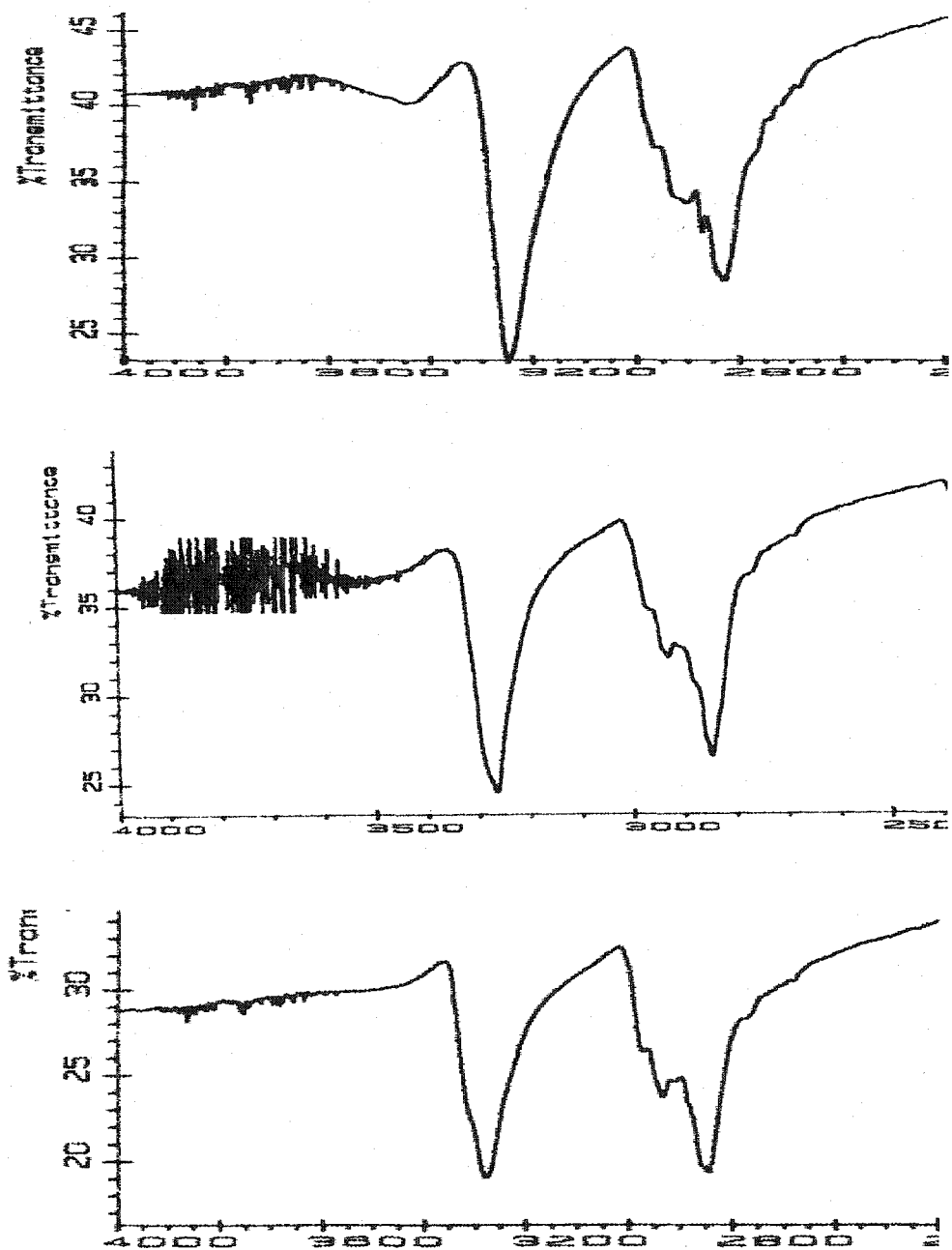


Figure 2.4 The IR (KBr) spectra of  $\text{HgCl}_2 \cdot 2$  (top),  $(\text{HgCl}_2)_6 \cdot (2)_4$  (middle), and  $(\text{HgCl}_2)_{11} \cdot (2)_6$  (bottom).

This NH stretch is also very useful in the determination of whether  $\text{HgCl}_2 \cdot 2$  formed since  $\text{HgCl}_2 \cdot 2$  has an NH stretch at  $3240 \text{ cm}^{-1}$  whereas  $(\text{HgCl}_2)_6 \cdot (2)_4$  and  $(\text{HgCl}_2)_{11} \cdot (2)_6$  presents a broad NH stretch at  $3262 \text{ cm}^{-1}$  and  $3275 \text{ cm}^{-1}$  respectively (Figure 2.4). It seems that the increased ratio of  $\text{HgCl}_2$  to **2** increased the NH stretch frequency.

## 2.2 Solution $^1\text{H}$ and $^{13}\text{C}\{^1\text{H}\}$ NMR Spectra.

Compared to the complicated NMR spectra of metal cyclam (or cyclen) complexes reported previously due to mixtures of isomers in equilibria,<sup>25(a),43(b),45(a),48(a-i)</sup> the  $^1\text{H}$  and  $^{13}\text{C}\{^1\text{H}\}$  NMR spectra of all these Zn(II), Cd(II) and Hg(II) complexes showed only one type of complexed cross-bridged ligand on the NMR timescale because of the *cis*-folded (V) ligand configuration (Figure 1.56). Interestingly, such a *cis*-folded configuration of one coordinated cyclam unit was believed to play an important role in the recognition of a Zn(II) Xylyl-bicyclam complex by an HIV coreceptor.<sup>26(a)</sup>

The  $^{13}\text{C}\{^1\text{H}\}$  NMR spectra of all characterized Zn(II), Cd(II) and Hg(II) complexes of ligands **1** and **3** indicate their actual or averaged  $C_2$  symmetry in solution at room temperature. Complexes of ligands **2** and **4** exhibit a higher-order  $C_{2v}$  symmetry as their  $^{13}\text{C}\{^1\text{H}\}$  NMR spectra contain only three carbon resonances from a total of 10 carbons in ligand **2** and eight carbon resonances from a total of 24 carbons in ligand **4**. In either  $\text{D}_2\text{O}$  or  $\text{CD}_3\text{OD}$ , the exchange between the secondary amine hydrogens from coordinated **1** or **2** and deuterium was observed for all their Zn(II), Cd(II) and Hg(II) complexes (Scheme 2.1).





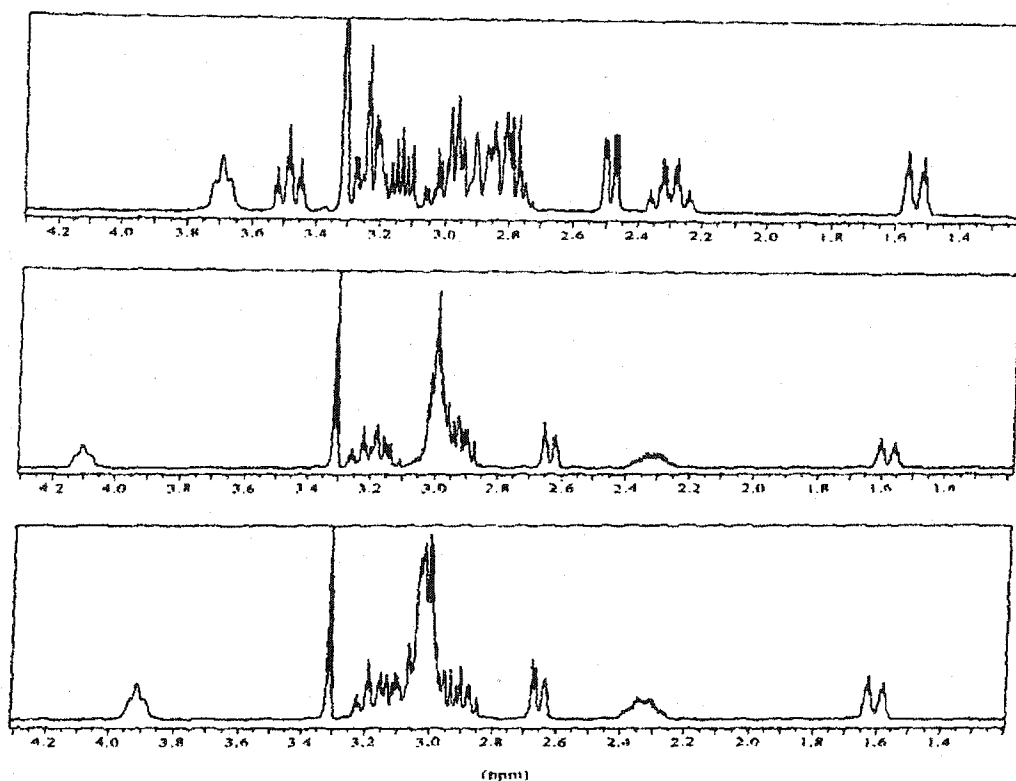
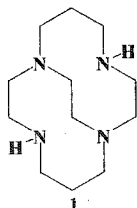


**Figure 2.5** Comparison of  $^1\text{H}$  NMR spectra of three Zn(II) complexes of **1** in  $\text{CD}_3\text{OD}$ . Top:  $[\text{Zn}\cdot\mathbf{1}(\mu\text{-Cl})]_2\text{Cl}_2$  (0.017 M), middle:  $\text{Zn}\cdot\mathbf{1}(\text{NO}_3)_2$  (0.020 M), bottom:  $\text{Zn}\cdot\mathbf{1}(\text{ClO}_4)_2$  (0.020 M).



$^{13}\text{C}\{^1\text{H}\}$  NMR spectrum of  $[\text{Zn}\cdot\mathbf{1}(\mu\text{-Cl})]_2\text{Cl}_2$  in  $\text{CD}_3\text{OD}$  also differing from those of  $\text{Zn}\cdot\mathbf{1}(\text{ClO}_4)_2$  and  $\text{Zn}\cdot\mathbf{1}(\text{NO}_3)_2$  (**Figure 2.6**). For example, the chemical shift difference in the most downfield  $^{13}\text{C}$  resonance between  $\text{Zn}\cdot\mathbf{1}(\text{ClO}_4)_2$  and  $[\text{Zn}\cdot\mathbf{1}(\mu\text{-Cl})]_2\text{Cl}_2$  is 1.05 ppm.

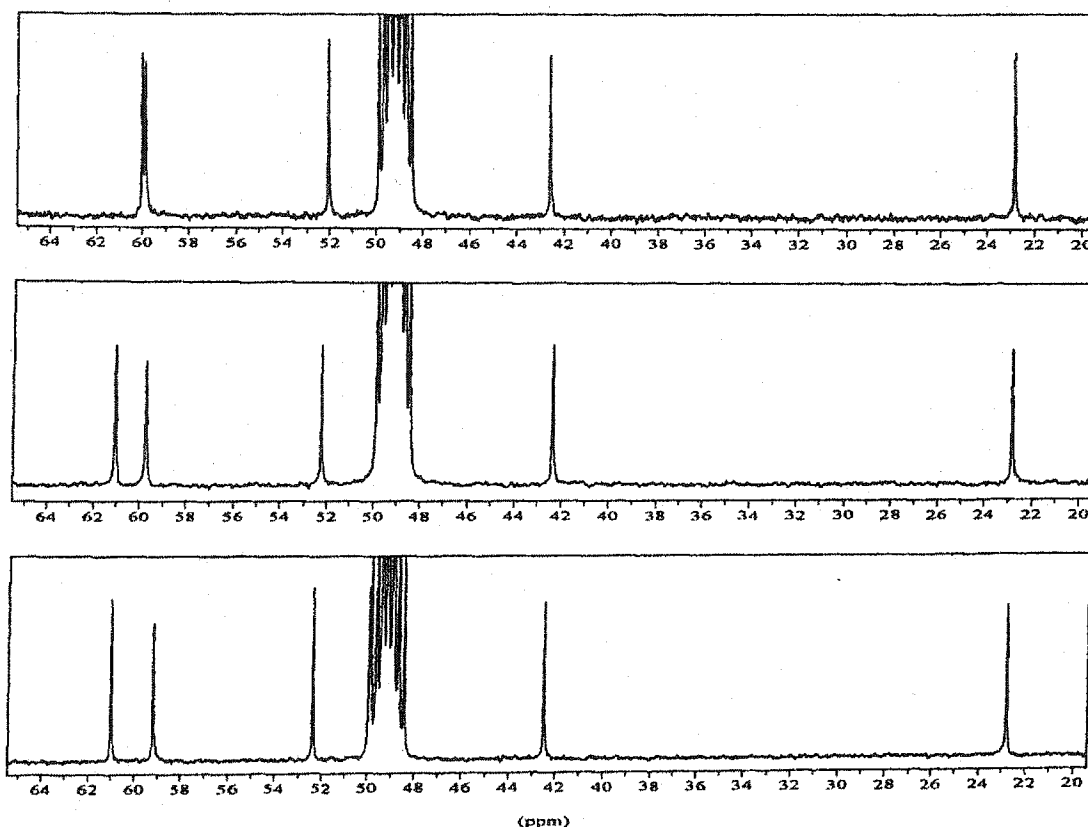


**Figure 2.6** Comparison of  $^{13}\text{C}\{^1\text{H}\}$  NMR spectra of three Zn(II) complexes of **1** in  $\text{CD}_3\text{OD}$ . Top one:  $[\text{Zn}\cdot\mathbf{1}(\mu\text{-Cl})]_2\text{Cl}_2$  (0.017 M); middle:  $\text{Zn}\cdot\mathbf{1}(\text{NO}_3)_2$  (0.020 M); and bottom:  $\text{Zn}\cdot\mathbf{1}(\text{ClO}_4)_2$  (0.020 M).

Only very limited detailed  $^1\text{H}$  and  $^{13}\text{C}$  NMR spectral analyses of the metal complexes of cyclam, cyclen and their derivatives exist in the literature. One major problem is the difficulty of analyzing complicated mixtures of possible configurational isomers in either *cis* or *trans* forms (**Figure 1.4** and **Figure 1.5**) in dynamic equilibria or slow exchange.<sup>26(a),43(b),48(a-i)</sup> By contrast, resonances in the  $^1\text{H}$  and  $^{13}\text{C}\{^1\text{H}\}$  NMR spectra of  $[\text{Zn}\cdot\mathbf{1}(\mu\text{-Cl})]_2\text{Cl}_2$  in  $\text{CD}_3\text{OD}$ , especially using the 500 MHz NMR spectrometer, can be fully interpreted using a combination of the *NH/ND* exchange (**Scheme 2.1**), 2D [ $^1\text{H}, ^1\text{H}$ ]

gCOSY and 2D [ $^1\text{H}$ ,  $^{13}\text{C}$ ] gHSQC NMR experiments. In the proton NMR spectrum of the N-H complex (Scheme 2.1), we would expect to see coupling between the amine hydrogen and hydrogens on the carbon  $\alpha$  to it. In the N-D complex, of course, such a coupling would disappear. It was also anticipated that the chemical shift of the carbon  $\alpha$  to this secondary amine nitrogen may differ significantly in the N-H and N-D complexes.

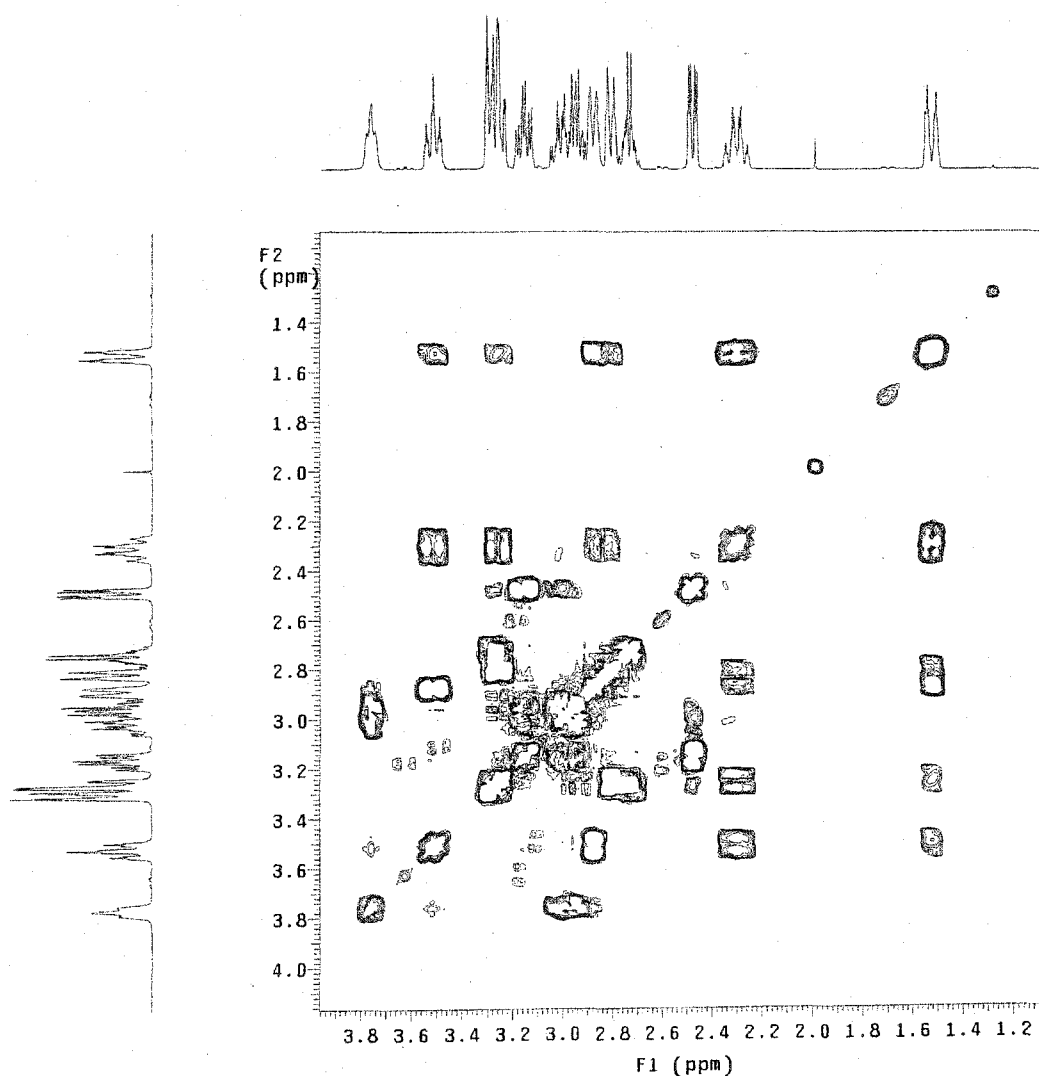


**Figure 2.7** A 2D [ $^1\text{H}$ ,  $^1\text{H}$ ] gCOSY spectrum of  $[\text{Zn}\cdot\mathbf{1}(\mu\text{-Cl})_2\text{Cl}_2]$  (0.050 M N-H complex) in  $\text{CD}_3\text{OD}$ .

In its proton NMR spectrum, the broad lowest-field resonance at  $\delta$  3.69 assigned to the axial N-H protons disappeared upon standing for days at room temperature due to this NH/ND exchange in CD<sub>3</sub>OD solvent (*vide infra*). A doublet of pentets to the highest field at  $\delta$  1.53 can be assigned to the equatorial proton of the  $\beta$ -methylene ( $\beta$ -CH<sub>eq</sub>H) in the six-membered chelate ring. The dtt at  $\delta$  2.31 can be assigned to the axial proton of this same  $\beta$ -methylene ( $\beta$ -CHH<sub>ax</sub>). As indicated by its 2D [<sup>1</sup>H, <sup>1</sup>H] gCOSY and [<sup>1</sup>H, <sup>13</sup>C] gHSQC NMR spectra (**Figure 2.7** and **Figure 2.8**), these two resonances are coupled to each other and they are also correlated to the resonance at  $\delta$  22.66 in the <sup>13</sup>C{<sup>1</sup>H} NMR spectrum which can be assigned to this  $\beta$  carbon (labeled **B** in **Table 2.3**, *vide infra*).

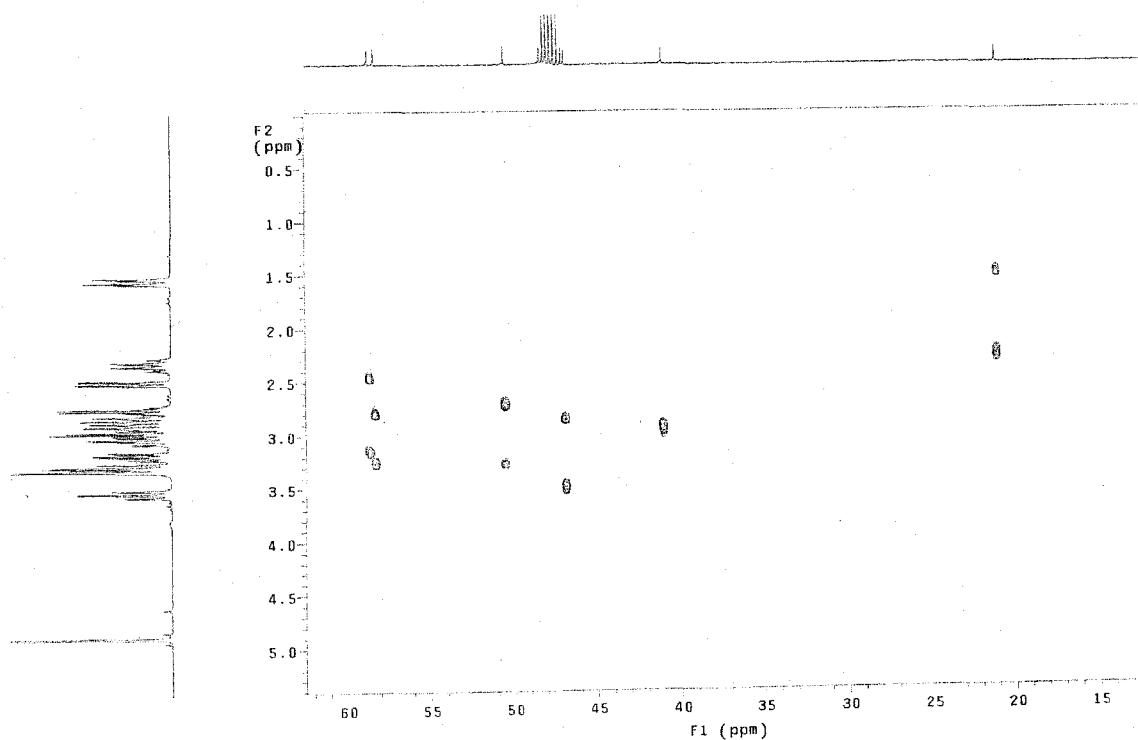


**Figure 2.8** A 2D [<sup>1</sup>H, <sup>13</sup>C] gHSQC NMR spectrum of [Zn•1( $\mu$ -Cl)]<sub>2</sub>Cl<sub>2</sub> (0.050 M N-D complex) in CD<sub>3</sub>OD.

The  $^{13}\text{C}\{^1\text{H}\}$  spectrum of  $[\text{Zn}\cdot\mathbf{1}(\mu\text{-Cl})_2\text{Cl}_2]$  in  $\text{CD}_3\text{OD}$  consists of six resonances between  $\delta$  20 and 60 for both the N-H complex and the N-D complex (**Figure 2.6**). The chemical shifts of two  $^{13}\text{C}$  resonances ( $\delta$  48.49 ppm overlapped with the solvent peak and  $\delta$  42.60 ppm) shift upfield ( $\delta$  48.35 and 42.51 ppm) upon deuteration. These two resonances can thus be assigned to the two carbons  $\alpha$  to the secondary amine nitrogens in ligand **1**. 2D  $[^1\text{H}, ^{13}\text{C}]$  gHSQC NMR data show that the  $^{13}\text{C}$  resonance at  $\delta$  42.51 couples to the proton resonance at  $\delta$  3.52. The spin pattern of this proton resonance also changed from a triplet of triplets to a triplet of doublets upon NH/ND exchange (**Figure 2.9**). As

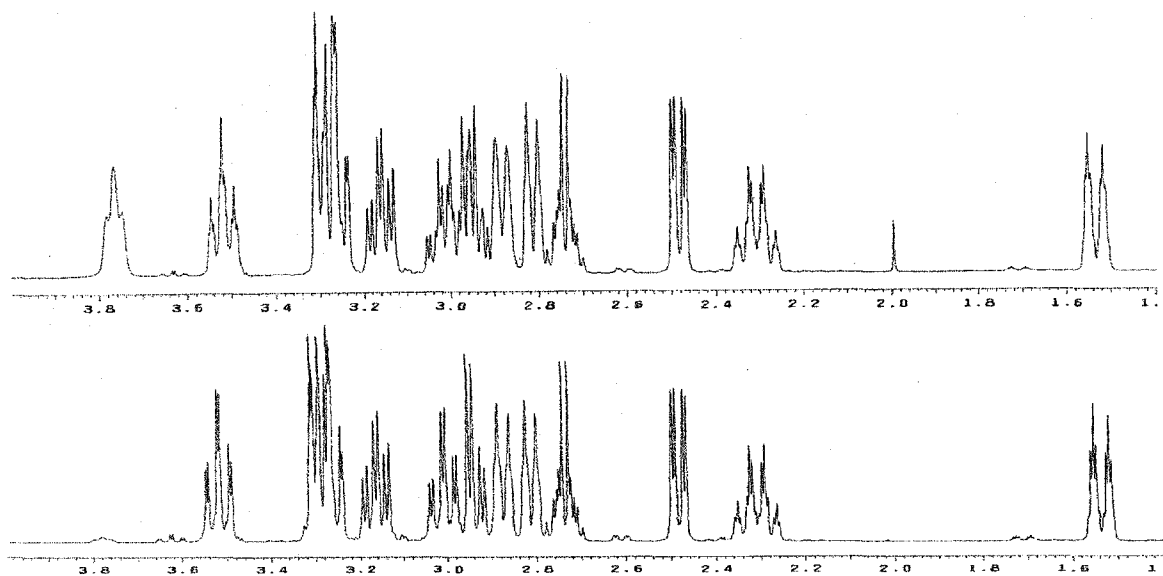


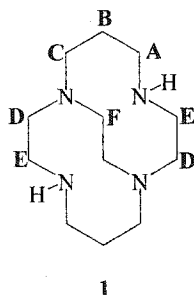
**Figure 2.9** Comparison of  $^1\text{H}$  NMR spectra of the NH complex (top) and the ND complex (bottom) of  $[\text{Zn}\cdot\mathbf{1}(\mu\text{-Cl})_2\text{Cl}_2]$  in  $\text{CD}_3\text{OD}$ .

can be seen in the 2D  $[^1\text{H}, ^1\text{H}]$  gCOSY spectrum (**Figure 2.7**), these protons are coupled to those at  $\delta$  2.30 ( $\beta\text{-CHH}_{ax}$ ). We thus assigned them as the protons at the A position in ligand **1**. They are also coupled to the proton resonance at  $\delta$  2.88 and the  $^{13}\text{C}$  resonance at

$\delta$  48.49 in the 2D [ $^1\text{H}$ ,  $^{13}\text{C}$ ] gHSQC spectrum (Figure 2.8). Both the resonance at  $\delta$  2.88 (a broad doublet) and at  $\delta$  3.52 can thus be assigned to the protons on carbon A (Table 2.3, vide infra). Thus the  $^{13}\text{C}$  resonance at  $\delta$  48.49 can be identified as this carbon A. This assignment agrees with the  $^{13}\text{C}\{^1\text{H}\}$  NMR data since this resonance at  $\delta$  48.49 shows a shift upon NH/ND exchange. As the  $^{13}\text{C}$  resonance at  $\delta$  42.60 is also significantly affected by the NH/ND exchange, it can be assigned to carbon E which in turn is coupled to the multiplet between  $\delta$  2.92 and  $\delta$  3.06 (four protons at position E). The proton multiplet at  $\delta$  2.70-2.78 (XX' of AA'XX') corresponds to the protons at F. This resonance is also coupled only to the AA' multiplet ( $\delta$  3.22-3.33). These two proton resonances only correlate to the  $^{13}\text{C}$  resonance at  $\delta$  52.0 as revealed by the 2D [ $^1\text{H}$ ,  $^{13}\text{C}$ ] gHSQC spectrum, indicating the resonance at  $\delta$  52.0 belonging to carbon F. The proton multiplet between  $\delta$  2.92 and 3.06 (E position) only couples to the dd's at  $\delta$  3.16 and 2.48. This indicates that the resonances at  $\delta$  3.16 and 2.48 belong to the protons at the D position which in turn correlates with the  $^{13}\text{C}$  resonance at  $\delta$  60.0. We can then assign this  $^{13}\text{C}$  resonance to the D position. The proton resonance at  $\delta$  2.31 is also coupled to the multiplet from  $\delta$  3.22 to 3.32 which integrates for four protons. Two of these four protons are assignable to the F protons. The other two then are attached to the C methylene, showing coupling with the broad doublet at  $\delta$  2.82. They further correlate with the  $^{13}\text{C}$  resonance at  $\delta$  59.77. We can therefore assign the proton doublet at  $\delta$  2.82, the multiplet from  $\delta$  3.22 to 3.32, and the  $^{13}\text{C}$  resonance at  $\delta$  59.7 to the C methylene. Final assignments of all these resonances are listed in Table 2.3.

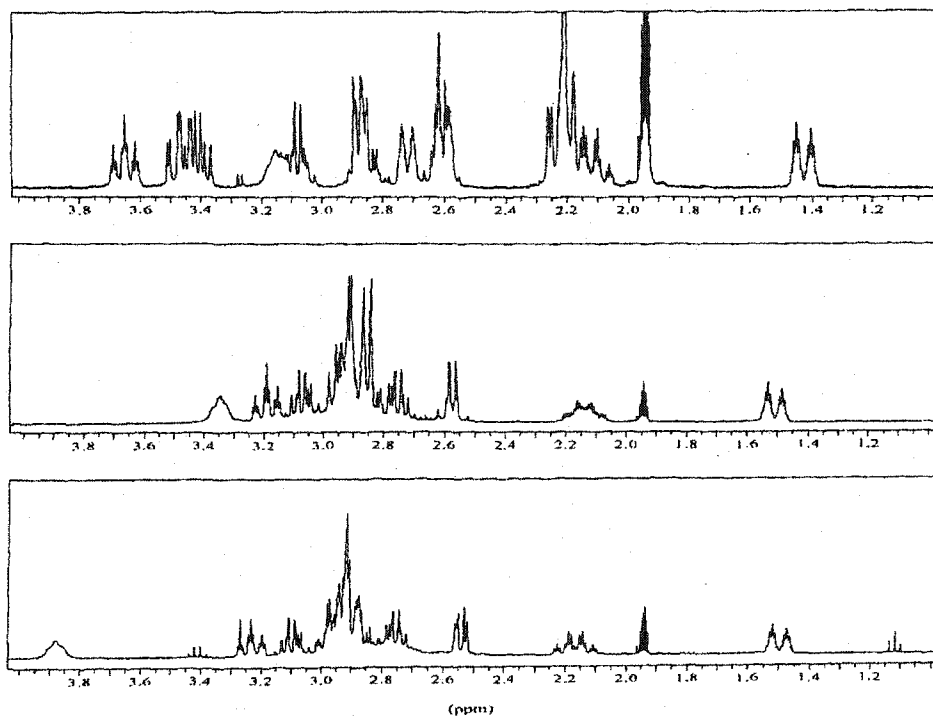
**Table 2.3** The assignment of proton and  $^{13}\text{C}\{^1\text{H}\}$  NMR spectra of 0.050 M  $[\text{Zn}\cdot\mathbf{1}(\mu\text{-Cl})]_2\text{Cl}_2$  in  $\text{CD}_3\text{OD}$  (500MHz).

Position in ligand 1	Position labeled	$\delta$ in $^1\text{H}$ NMR	Spin pattern (No. of protons)	$J_{\text{HH}}$ (Hz)	$\delta$ in $^{13}\text{C}$ NMR
$\text{HNCH}_2\text{CH}_2\text{CH}_2\text{N}$	N-H	3.77	br t (2 H)	$\sim 9$	
$\text{HNCH}_2\text{CH}_2\text{CH}_2\text{N}$	A	3.52	tt (2 H)	13.2, 3.0	48.49
$\text{HNCH}_2\text{CH}_2\text{CH}_2\text{N}$	A	2.88	d (2 H)	$\sim 13$	
$\text{HNCH}_2\text{CH}_2\text{CH}_2\text{N}$	B	2.31	dt (2 H)	16.5, 13.5, 3.0	22.66
$\text{HNCH}_2\text{CH}_2\text{CH}_2\text{N}$	B	1.53	dp (2 H)	16.5, 3.0	
$\text{HNCH}_2\text{CH}_2\text{CH}_2\text{N}$	C	3.22-3.32	m (2 H)		59.77
$\text{HNCH}_2\text{CH}_2\text{CH}_2\text{N}$	C	2.82	d (2 H)	$\sim 12$	
$\text{NCH}_2\text{CH}_2\text{NH}$	D	3.16	dd (2 H)	12.8, 5.5	60.04
$\text{NCH}_2\text{CH}_2\text{NH}$	D	2.48	dd (2 H)	12.5, 4.0	
$\text{NCH}_2\text{CH}_2\text{NH}$	E	2.92-3.06	m (4 H)		42.60
$\text{NCH}_2\text{CH}_2\text{N}$	F	3.22-3.32	AA' (2 H)		
$\text{NCH}_2\text{CH}_2\text{N}$	F	2.70-2.78	XX' (2 H)		51.98



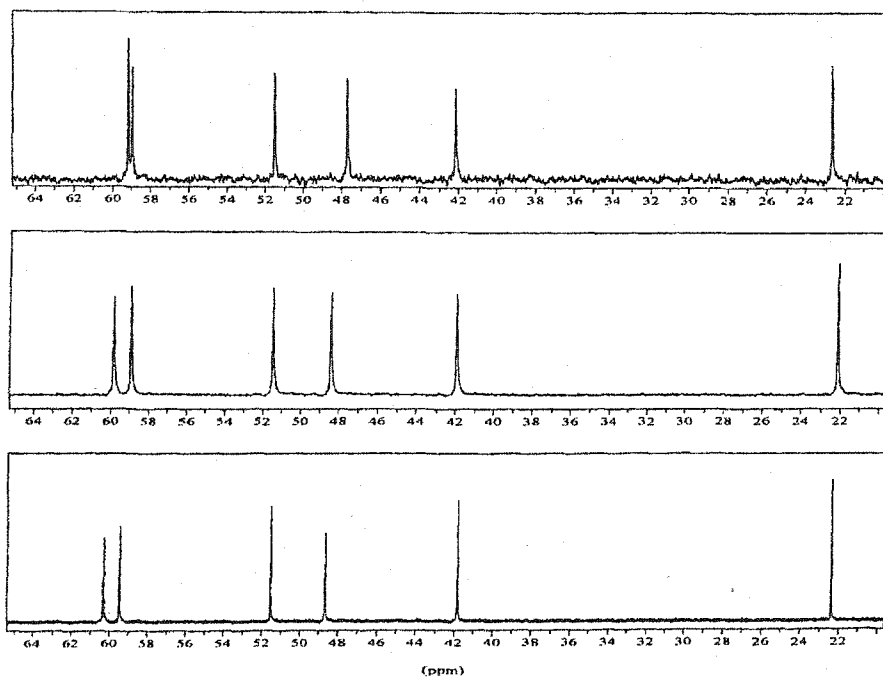
Similar to their methanol spectra, significantly different  $^1\text{H}$  NMR spectra (**Figure 2.10(a)**) were observed for the counterions  $\text{ClO}_4^-$ ,  $\text{NO}_3^-$ , and  $\text{Cl}^-$  in acetonitrile. Similarly, this is consistent with the different  $^{13}\text{C}\{^1\text{H}\}$  NMR spectrum of  $[\text{Zn}\cdot\mathbf{1}(\mu\text{-Cl})]_2\text{Cl}_2$  in  $\text{CD}_3\text{CN}$  compared to those of  $\text{Zn}\cdot\mathbf{1}(\text{ClO}_4)_2$  and  $\text{Zn}\cdot\mathbf{1}(\text{NO}_3)_2$  (**Figure 2.10(b)**). The  $^{13}\text{C}$  resonance with the largest chemical shift difference between  $\text{Zn}\cdot\mathbf{1}(\text{NO}_3)_2$  and  $[\text{Zn}\cdot\mathbf{1}(\mu\text{-Cl})]_2\text{Cl}_2$  is the most downfield one. This difference is 1.17 ppm.



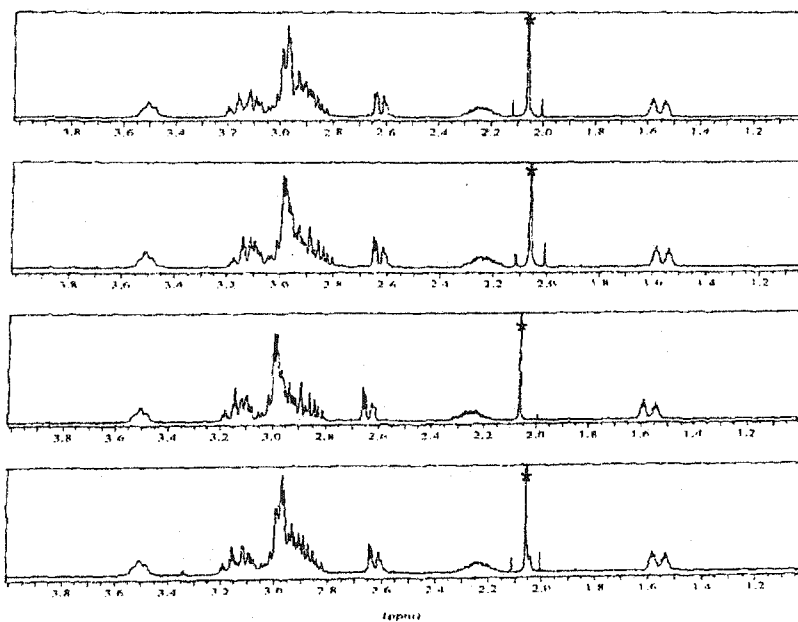


**Figure 2.10(a)** Comparison of  $^1\text{H}$  NMR spectra of the three Zn(II) complexes of **1** in  $\text{CD}_3\text{CN}$ . Top:  $[\text{Zn}\cdot\mathbf{1}(\mu\text{-Cl})]_2\text{Cl}_2$  (0.017 M); middle:  $\text{Zn}\cdot\mathbf{1}(\text{ClO}_4)_2$ ; and bottom:  $\text{Zn}\cdot\mathbf{1}(\text{NO}_3)_2$ .

In dilute ( $< 0.15\text{M}$ )  $\text{D}_2\text{O}$  solution, all zinc complexes of ligand **1** give identical  $^1\text{H}$  NMR (**Figure 2.11**) and  $^{13}\text{C}\{^1\text{H}\}$  NMR spectra regardless of counterion, suggesting a common solution species, most likely  $[\text{Zn}\cdot\mathbf{1}(\text{D}_2\text{O})_2]^{2+}$ , which is related to the X-ray structure of  $[\text{Zn}\cdot\mathbf{1}(\text{OH}_2)(\mu\text{-Cl})\text{ZnCl}_3]$  (**115**) (**Figure 2.26**, *vide infra*). There is no detectable difference between their proton NMR spectra and the largest chemical shift difference is 0.05 ppm in their  $^{13}\text{C}\{^1\text{H}\}$  NMR spectra. This is consistent with the fact that water is a better coordinating solvent than either acetonitrile or methanol resulting in full counterion dissociation. The broad lowest-field proton resonance at  $\delta$  3.50 assigned to the



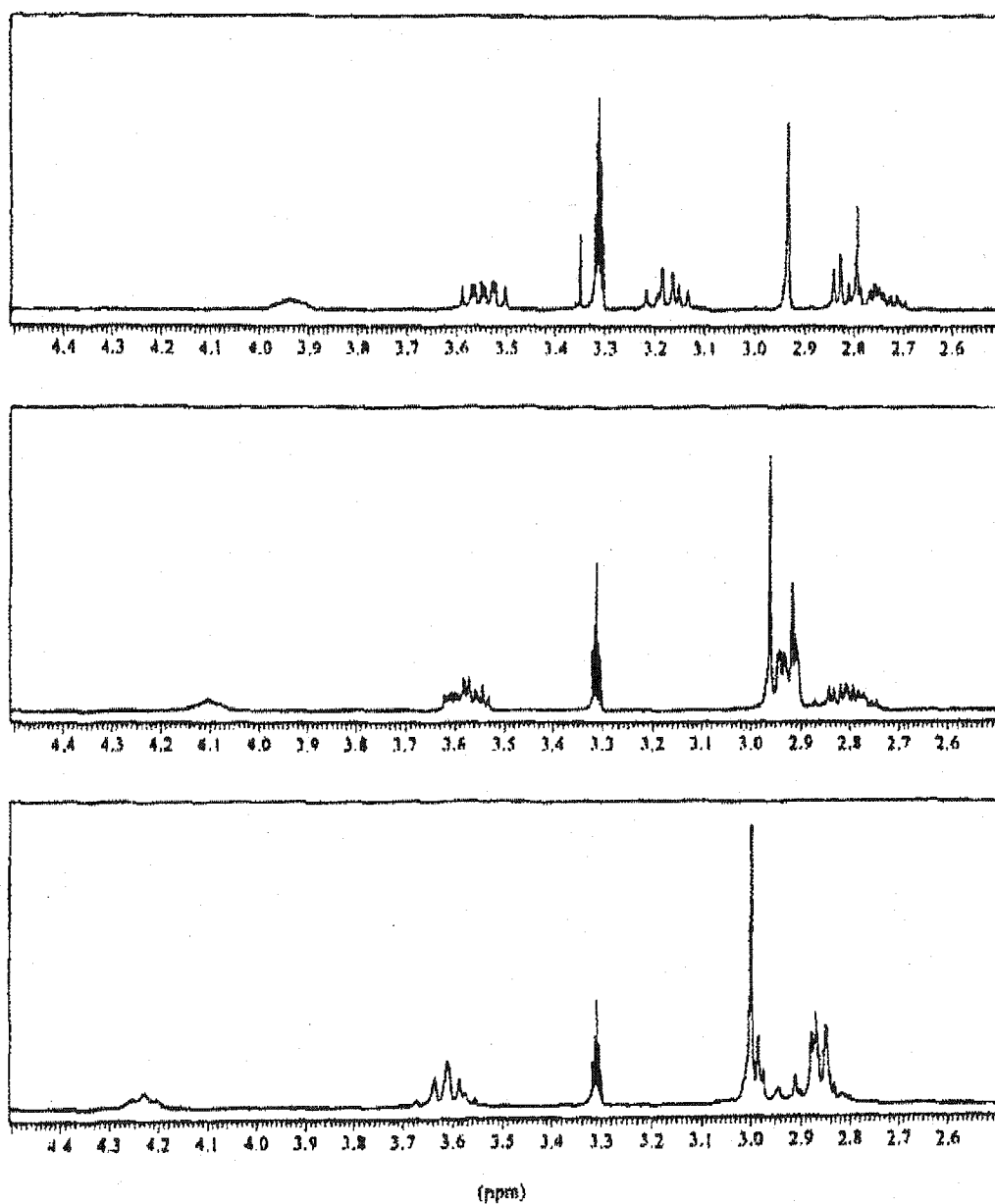
**Figure 2.10(b)** Comparison of  $^{13}\text{C}\{^1\text{H}\}$  NMR spectra of three Zn(II) complexes of **1** in  $\text{CD}_3\text{CN}$ . Top:  $[\text{Zn}\cdot\mathbf{1}(\mu\text{-Cl})_2]\text{Cl}_2$  (0.017 M); middle:  $\text{Zn}\cdot\mathbf{1}(\text{ClO}_4)_2$ ; and bottom:  $\text{Zn}\cdot\mathbf{1}(\text{NO}_3)_2$ .



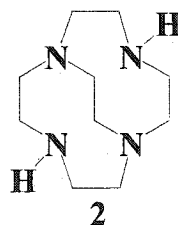
**Figure 2.11** Comparison of  $^1\text{H}$  NMR spectra of the four Zn(II) complexes of **1** in  $\text{D}_2\text{O}$ . Top:  $[\text{Zn}\cdot\mathbf{1}(\mu\text{-Cl})_2]\text{Cl}_2$ ; second:  $\text{Zn}\cdot\mathbf{1}(\text{NO}_3)_2$ ; third:  $\text{Zn}\cdot\mathbf{1}(\text{ClO}_4)_2$ ; bottom:  $[\text{Zn}\cdot\mathbf{1}(\text{OH}_2)(\mu\text{-Cl})\text{ZnCl}_3]$ . The singlet resonance marked with the asterisk belongs to reference  $\text{CH}_3\text{CN}$ .

axial N-H protons disappeared upon standing due to NH/ND exchange with the solvent (*vide infra*). The resonance at  $\delta$  2.16-2.32 can again be assigned to the axial proton of the  $\beta$ -methylene in the six-membered chelate ring ( $\beta$ -CHH<sub>ax</sub>). A doublet of pentets at the highest field at  $\delta$  1.56 belongs to the equatorial proton of this  $\beta$ -methylene ( $\beta$ -CHH<sub>eq</sub>). This is confirmed by their coupling with each other as revealed by 2D [<sup>1</sup>H,<sup>1</sup>H] gCOSY. The <sup>13</sup>C{<sup>1</sup>H} spectrum consists of six well-resolved resonances between  $\delta$  20 and 60. The proton resonances at  $\delta$  2.16-2.32 and  $\delta$  1.56 are coupled to the <sup>13</sup>C resonance at  $\delta$  21.81 which is again assigned to carbon B. The chemical shifts of two <sup>13</sup>C resonances ( $\delta$  48.49 and 41.34 ppm) shift upfield (48.35 and 41.22 ppm) upon deuteration. These two resonances can thus be assigned to the two carbons  $\alpha$  to axial N-H (either A or E). However, because of the overlapping of eighteen proton resonances within  $\delta$  2.81-3.20, no further assignments of all six carbon resonances could be made.

Similar to these three Zn(II) complexes of ligand 1, in methanol different proton spectra of zinc complexes of ligand 2 (Figure 2.12(a)) were also observed for the counterions ClO<sub>4</sub><sup>-</sup>, NO<sub>3</sub><sup>-</sup> and Cl<sup>-</sup>, again suggesting full or partial retention of the respective anion within zinc's first coordination sphere. The <sup>1</sup>H NMR spectra of [Zn•2(OH<sub>2</sub>)<sub>2</sub>](ClO<sub>4</sub>)<sub>2</sub> (122) and Zn•2(NO<sub>3</sub>)<sub>2</sub> (123) are somewhat similar to each other whereas that of ZnCl<sub>2</sub>•2 (121) is significantly different. For example, there is a triplet of doublets at  $\delta$  3.15 in the proton spectrum of ZnCl<sub>2</sub>•2 whereas no resonance was observed from  $\delta$  3.01 to  $\delta$  3.50 for the others. This is also consistent with the <sup>13</sup>C{<sup>1</sup>H} NMR spectrum of ZnCl<sub>2</sub>•2 in CD<sub>3</sub>OD which is obviously not the same as those of [Zn•2(OH<sub>2</sub>)<sub>2</sub>](ClO<sub>4</sub>)<sub>2</sub> and Zn•2(NO<sub>3</sub>)<sub>2</sub> (Figure 2.12(b)). Assignments of proton and <sup>13</sup>C



**Figure 2.12(a)** Comparison of  $^1\text{H}$  NMR spectra of the three Zn(II) complexes of **2** in  $\text{CD}_3\text{OD}$  (the N-H complexes). Top:  $\text{ZnCl}_2 \cdot \mathbf{2}$ ; middle:  $\text{Zn} \cdot \mathbf{2}(\text{NO}_3)_2$ ; bottom:  $\text{Zn} \cdot \mathbf{2}(\text{ClO}_4)_2$ .



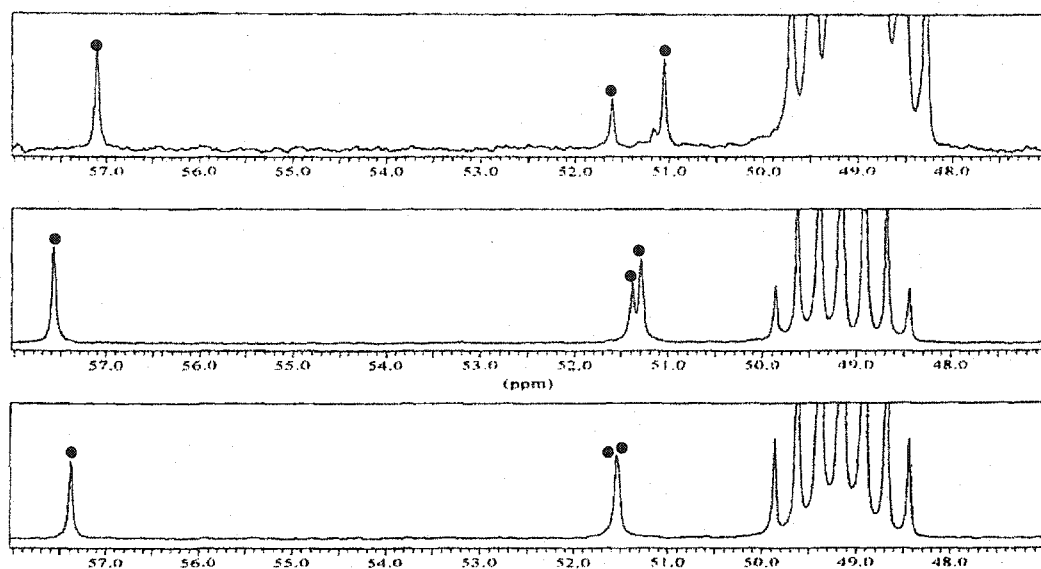


**Figure 2.12(b)** Comparison of  $^{13}\text{C}\{^1\text{H}\}$  NMR spectra of the three Zn(II) complexes of **2** in  $\text{CD}_3\text{OD}$  (the N-D complexes). Top:  $\text{ZnCl}_2\cdot\mathbf{2}$ ; middle:  $\text{Zn}\cdot\mathbf{2}(\text{NO}_3)_2$ ; bottom:  $\text{Zn}\cdot\mathbf{2}(\text{ClO}_4)_2$ . The resonances of **2** are labeled by dots.

NMR resonances of  $\text{ZnCl}_2\cdot\mathbf{2}$  in  $\text{CD}_3\text{OD}$  were also made feasible using a combination of NH/ND exchange, 2D [ $^1\text{H}, ^1\text{H}$ ] COSY, and 2D [ $^1\text{H}, ^{13}\text{C}$ ] HMQC NMR experiments.

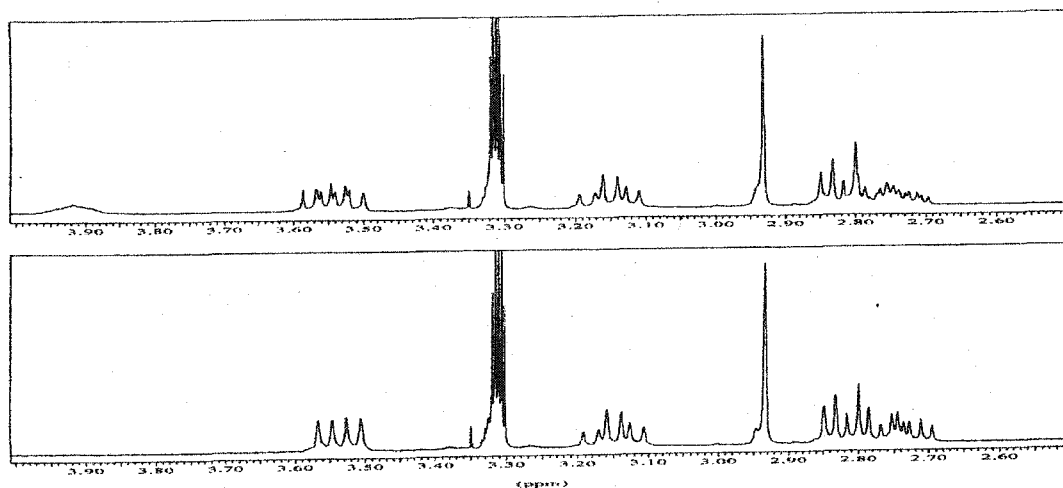


**Figure 2.13** Comparison of  $^1\text{H}$  NMR spectra of NH complex (top) and ND complex (bottom) of  $\text{ZnCl}_2\cdot\mathbf{2}$  in  $\text{CD}_3\text{OD}$ .

The broad lowest-field resonance at  $\delta$  3.9 in its proton spectrum can be assigned to the N-H protons since it disappeared upon standing due to NH/ND exchange with the solvent. Two resonances at  $\delta$  3.54 and 2.74 belong to the protons on the carbon adjacent to axial NH (carbon at **a** in Table 2.4, vide infra) since their splitting patterns simplified upon NH/ND exchange (Figure 2.13). 2D [ $^1\text{H}$ ,  $^1\text{H}$ ] COSY NMR data (Figure 2.14(a))

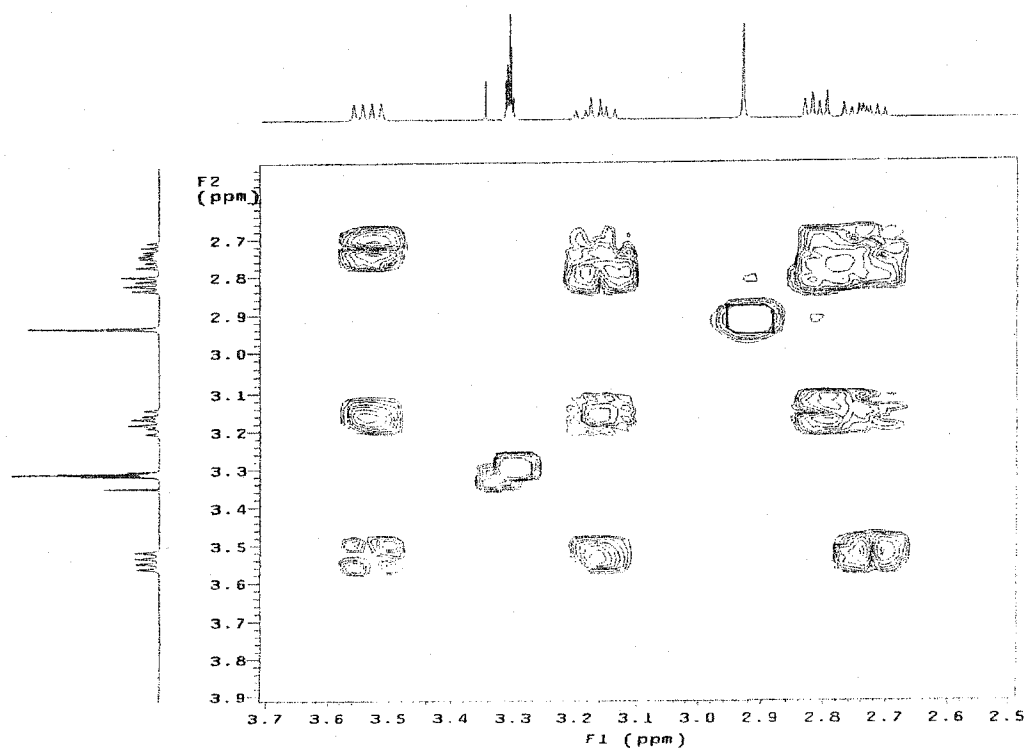


**Figure 2.14(a)** A 2D [ $^1\text{H}$ ,  $^1\text{H}$ ] COSY spectrum of  $\text{ZnCl}_2 \cdot 2$  (N-D complex) in  $\text{CD}_3\text{OD}$ .

reveal that the doublet of doublets at  $\delta$  3.54 couples to those at  $\delta$  3.15 and 2.74 while the resonance at  $\delta$  2.74 (ddd) couples to those at  $\delta$  3.15, 2.82 and 2.74. All three carbon resonances were assigned using 2D [ $^1\text{H}$ ,  $^{13}\text{C}$ ] HMQC NMR data (Figure 2.14(b)). These data indicate that the  $^{13}\text{C}$  resonance at  $\delta$  57.26 correlates to the protons at  $\delta$  3.15 and 2.82,

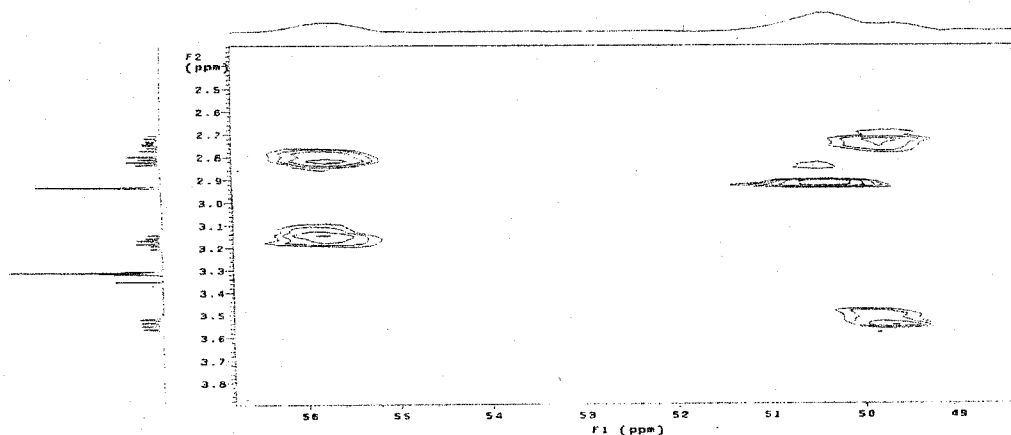
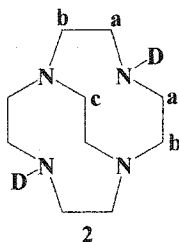


**Figure 2.14(b)** A 2D [ $^1\text{H}$ ,  $^{13}\text{C}$ ] HMQC NMR spectrum of  $\text{ZnCl}_2 \cdot 2$  (N-D complex) in  $\text{CD}_3\text{OD}$ .

while the  $^{13}\text{C}$  resonance at  $\delta$  51.77 couples to the proton singlet at  $\delta$  2.93. Finally, the resonance at  $\delta$  51.21 correlates to the proton resonances at  $\delta$  3.54 and 2.74. A full assignment of these resonances is shown in **Table 2.4**.

**Table 2.4** The assignment of proton and  $^{13}\text{C}\{^1\text{H}\}$  NMR spectra of 0.066 M  $\text{ZnCl}_2 \cdot 2$  in  $\text{CD}_3\text{OD}$  (N-D complex).

Position in ligand <b>2</b>	Position labeled	$\delta$ in $^1\text{H}$ NMR	Spin pattern (No. of protons)	$J_{\text{HH}}$ (Hz)	$\delta$ in $^{13}\text{C}$ NMR
$\text{HNCH}_2\text{CH}_2\text{N}$	<b>a</b>	3.54	dd (4 H)	14.8, 7.2	51.21
$\text{HNCH}_2\text{CH}_2\text{N}$	<b>a</b>	2.74	ddd (4 H)	14.6, 11.6, 5.9	
$\text{HNCH}_2\text{CH}_2\text{N}$	<b>b</b>	3.15	td (4 H)	11.7, 7.4	57.26
$\text{HNCH}_2\text{CH}_2\text{N}$	<b>b</b>	2.82	dd (4 H)	11.7, 5.9	
$\text{NCH}_2\text{CH}_2\text{N}$	<b>c</b>	2.93	s (4 H)		51.77



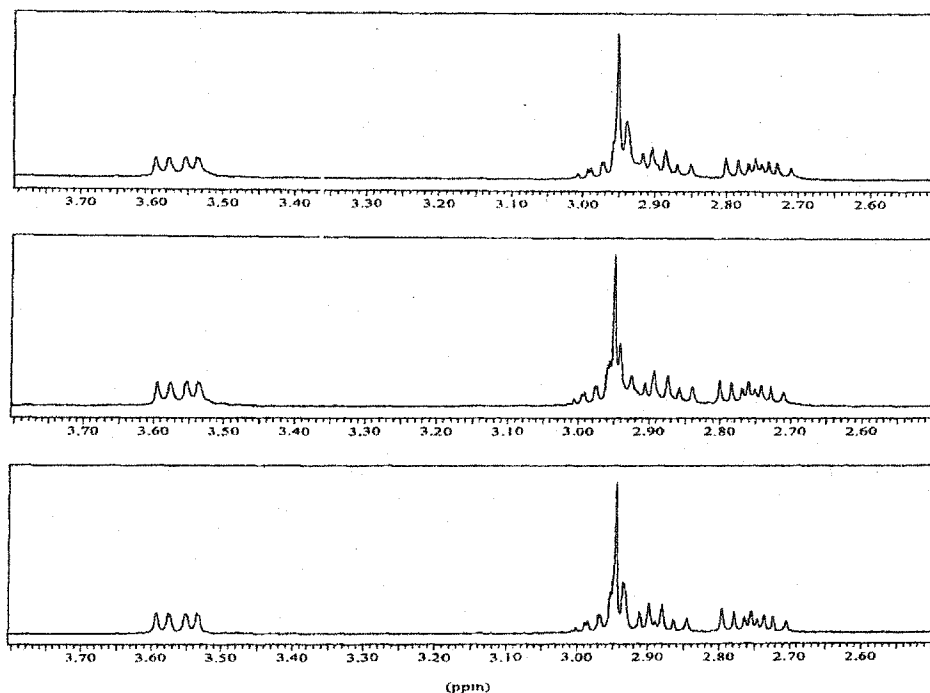


**Figure 2.15(a)** Comparison of  $^1\text{H}$  NMR spectra of the three Zn(II) complexes of **2** in  $\text{D}_2\text{O}$  (N-D complexes). Top:  $\text{ZnCl}_2 \cdot \mathbf{2}$ ; middle:  $\text{Zn} \cdot \mathbf{2}(\text{ClO}_4)_2$ ; bottom:  $\text{Zn} \cdot \mathbf{2}(\text{NO}_3)_2$ .

In dilute ( $< 0.10\text{M}$ )  $\text{D}_2\text{O}$  solution, all zinc complexes of ligand **2** give identical  $^1\text{H}$  (Figure 2.15(a)) and  $^{13}\text{C}\{^1\text{H}\}$  NMR spectra (Figure 2.15(b)) regardless of counterion, suggesting a common solution species, most likely  $[\text{Zn} \cdot \mathbf{2}(\text{D}_2\text{O})_2]^{2+}$ . The proton singlet at  $\delta$  2.94 of the N-D complex corresponds to those on the cross-bridged ethylene (position **c** in Table 2.4), correlating with the  $^{13}\text{C}$  resonance at  $\delta$  50.67 (position **c**) as revealed by a 2D  $[^1\text{H}, ^{13}\text{C}]$  gHSQC spectrum. Two proton resonances at  $\delta$  3.56 and 2.74 must be attached to the protons on the carbon adjacent to NH (**a** position) since the splitting pattern of these simplified upon complete NH/ND exchange. They are also coupled with each other as revealed by a 2D  $[^1\text{H}, ^1\text{H}]$  gCOSY. These also correlate to the  $^{13}\text{C}$  resonance at  $\delta$  50.34 as revealed by the 2D  $[^1\text{H}, ^{13}\text{C}]$  gHSQC spectrum. Thus the  $^{13}\text{C}$  resonance at



$\delta$  50.34 can be assigned the carbon at position **a**. The remaining  $^{13}\text{C}$  resonance at  $\delta$  56.36 can then be assigned to carbon **b**.

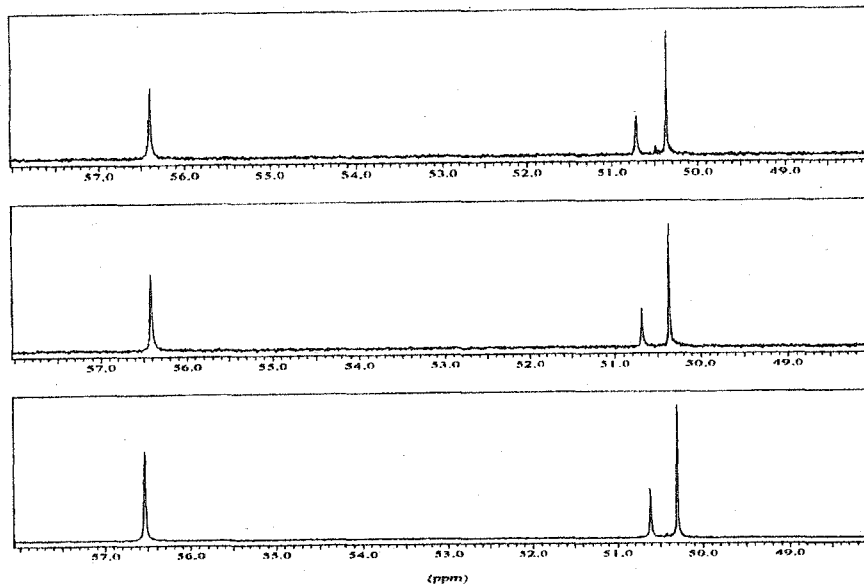


**Figure 2.15(b)** Comparison of  $^{13}\text{C}\{^1\text{H}\}$  NMR spectra of the three Zn(II) complexes of **2** in  $\text{D}_2\text{O}$  (N-D complexes). Top:  $\text{ZnCl}_2\cdot\mathbf{2}$ ; middle:  $\text{Zn}\cdot\mathbf{2}(\text{ClO}_4)_2$ ; bottom:  $\text{Zn}\cdot\mathbf{2}(\text{NO}_3)_2$ .

In the proton NMR spectra of the two Zn(II) complexes of ligand **3**, the presence of an AX splitting pattern of the benzyl methylene is consistent with an actual or averaged  $C_2$  symmetry. For example, the proton NMR spectrum of  $\text{ZnCl}_2\cdot\mathbf{3}$  (**119**) in  $\text{D}_2\text{O}$  showed an AX pattern at  $\delta$  4.24 and 3.93 (**Figure 2.16**). Both the methylenes in the two benzyl groups as well as the cross-bridged ethylene in ligand **4** also appear as singlets in the proton NMR spectra of  $\text{ZnCl}_2\cdot\mathbf{4}$  (**124**) at  $\delta$  4.62 and at  $\delta$  2.86 respectively (**Figure 2.17**). This is consistent with an actual or averaged  $C_{2v}$  symmetry of  $\text{ZnCl}_2\cdot\mathbf{4}$  in  $\text{CDCl}_3$  solution.

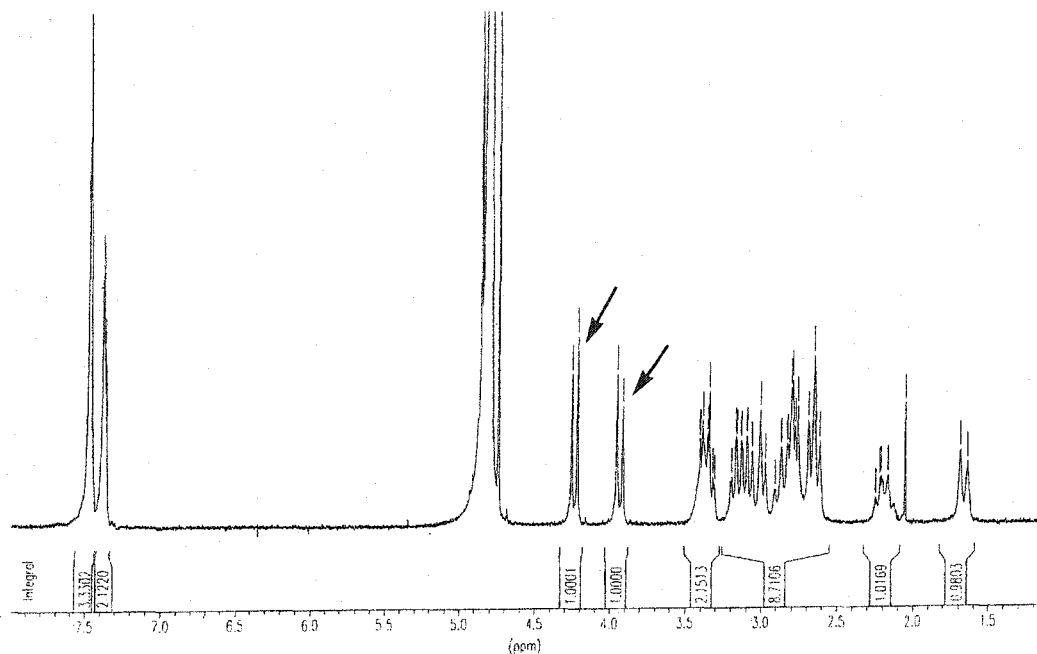


**Figure 2.16** The proton NMR spectrum of  $\text{ZnCl}_2 \cdot 3$  in  $\text{D}_2\text{O}$ . The AB of the benzyl methylene is marked by two arrows.

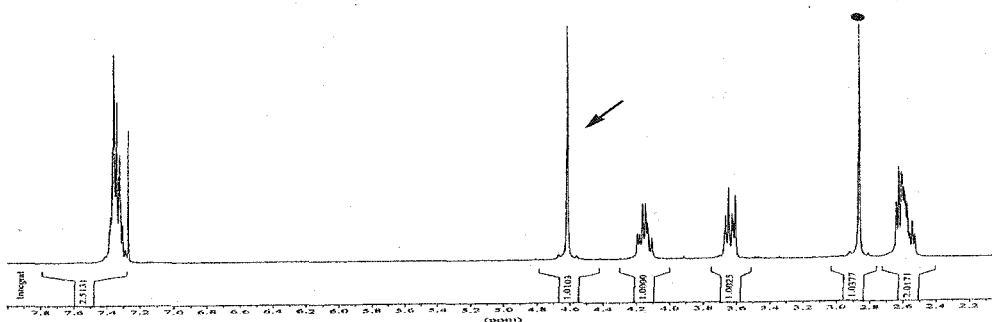


**Figure 2.17** The proton NMR spectrum of  $\text{ZnCl}_2 \cdot 4$  in  $\text{CDCl}_3$ . The benzyl methylene singlet is marked by an arrow and the cross-bridging ethylene singlet is marked by a dot.

**(b) Cadmium Complexes of Ligands 1-4.** Because the  $d^{10}$  nature of  $\text{Cd(II)}$  leads to rapid metal-ligand exchange rates, there has been a relative paucity of  $^{111,113}\text{Cd}$  coupling data with  $^1\text{H}$  and  $^{13}\text{C}$  resonances in  $\text{Cd(II)}$  complexes.<sup>102</sup> It is therefore significant that  $^{111}\text{Cd}$  and  $^{113}\text{Cd}$  doublet satellites are clearly discernable for several

proton and  $^{13}\text{C}$  resonances of our Cd(II) complexes of ligands **1** and **2**. These coupling constants vary from 6.4 Hz to 14.6 Hz. The presence of only a single doublet satellite indicates the overlap of  $^{111}\text{Cd}$  and  $^{113}\text{Cd}$  satellites and is consistent with the literature data.<sup>102</sup> This is caused by the similar magnetogyric ratios of  $^{111}\text{Cd}$  and  $^{113}\text{Cd}$ ,  $-5.9330 \times 10^{-7}$  and  $-5.6720 \times 10^{-7}$  rad/Ts, respectively.

An instructive comparison of proton NMR spectra of  $\text{ZnCl}_2 \cdot \mathbf{2}$  (**121**),  $\text{CdCl}_2 \cdot \mathbf{2}$  (**129**) and  $\text{HgCl}_2 \cdot \mathbf{2}$  (**134**) in  $\text{CD}_3\text{OD}$  (Figure 2.18) reveals that for  $\text{CdCl}_2 \cdot \mathbf{2}$ , the doublet

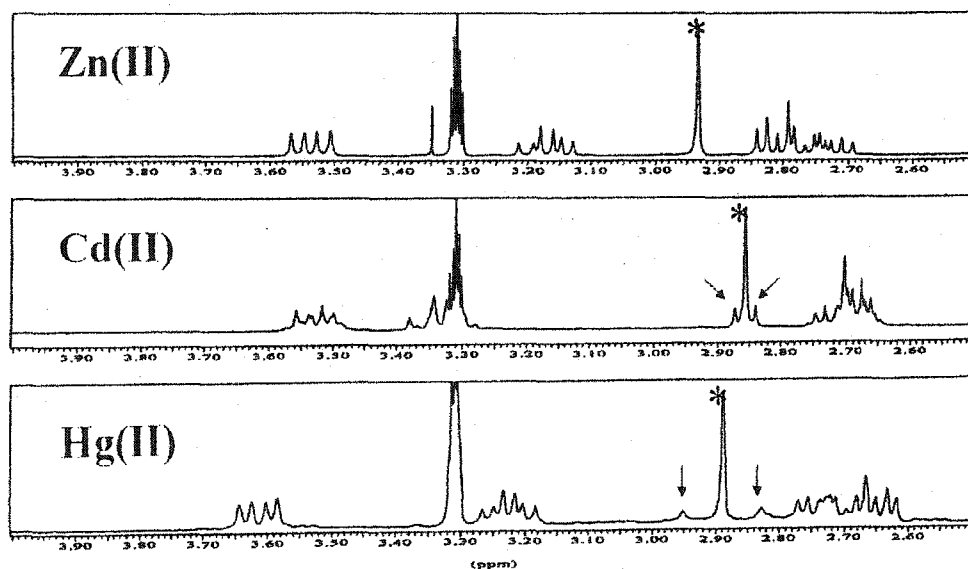


**Figure 2.18** Comparison of  $^1\text{H}$  NMR spectra of the three Zn(II), Cd(II) and Hg(II) complexes of **2** in  $\text{CD}_3\text{OD}$  (N-D complexes). Top:  $\text{ZnCl}_2 \cdot \mathbf{2}$ ; middle:  $\text{CdCl}_2 \cdot \mathbf{2}$ ; bottom:  $\text{HgCl}_2 \cdot \mathbf{2}$ . The peaks labeled with asterisks are assigned to bridging ethylene protons. The metal- $^1\text{H}$  coupling satellites are marked with arrows.

satellite around the singlet at  $\delta$  2.86 assignable to the cross-bridging  $\text{CH}_2\text{CH}_2$  is a result of  $^1\text{H}$  and  $^{111,113}\text{Cd}$  coupling. This  $^3J$  coupling constant is 11.8 Hz. Similarly, the proton NMR spectrum of  $\text{CdCl}_2 \cdot \mathbf{4}$  (**132**) in  $\text{CDCl}_3$  (Figure 2.19) also has a doublet satellite

around the cross-bridging  $CH_2CH_2$  singlet at  $\delta$  2.80. A coupling constant of 11.6 Hz is found here. In the proton spectrum of  $CdCl_2 \cdot 4$  in  $CDCl_3$ , the singlet at  $\delta$  4.66 belonging

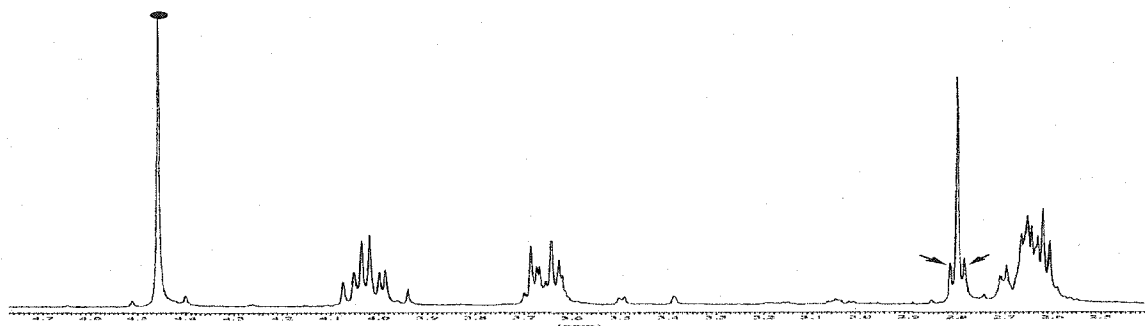


**Figure 2.19** The proton NMR spectrum of  $CdCl_2 \cdot 4$  in  $CDCl_3$ . The benzyl methylene singlet is marked by a dot and the doublet satellite around cross-bridging ethylene singlet is marked by two arrows. For clarity, only  $\delta$  2.4-4.8 region is shown.

to the methylene in the  $N,N'$ -dibenzyl arms does not show any satellites. Since a reported Karplus-type relationship between the  $^3J$  ( $^{111,113}Cd$ ,  $^1H$ ) and  $Cd-N-C-H$  dihedral angle likely applies here, the averaged coupling constant may be too small for observation.<sup>106</sup> In contrast to this, in the  $^{13}C\{^1H\}$  NMR spectra of both  $CdCl_2 \cdot 3$  and  $CdCl_2 \cdot 4$ , the tertiary carbon from the benzene ring show  $^3J$  coupling constant of 6 and 5 Hz respectively with  $^{111,113}Cd$ .

For the  $Cd(II)$  complexes of ligands **1** and **2** in  $D_2O$  solution, the specific counterion has a major effect on their aqueous solution proton spectra (**Figure 2.20** and **Figure 2.21**), again indicative of association of these counterions at the metal's first coordination sphere. These observations are different from their  $Zn(II)$  analogues' behavior. As shown in **Figure 2.20**, the  $^1H$  NMR spectrum of  $CdCl_2 \cdot 1$  (**125**) in  $D_2O$  is significantly different from these of  $Cd \cdot 1(NO_3)_2$  (**126**) and  $Cd \cdot 1(ClO_4)_2$  (**127**) which have very similar spectra. This indicates that even in  $D_2O$ ,  $CdCl_2 \cdot 1$  has partially or fully

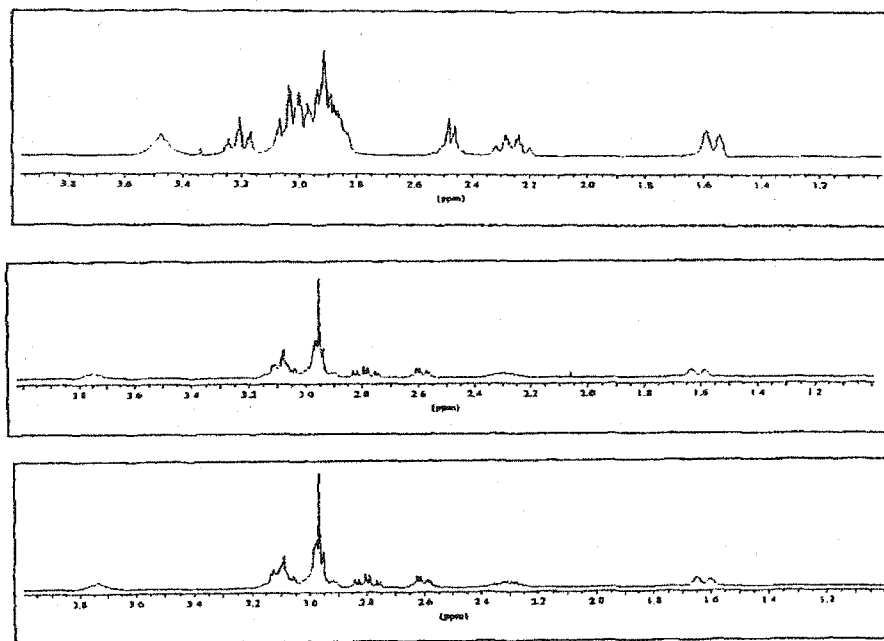


**Figure 2.20** Detailed comparison of  $^1\text{H}$  NMR spectra of the three Cd(II) complexes of **1** in  $\text{D}_2\text{O}$ . Top:  $\text{CdCl}_2 \cdot \mathbf{1}$ ; middle:  $\text{Cd} \cdot \mathbf{1}(\text{NO}_3)_2$ , bottom:  $\text{Cd} \cdot \mathbf{1}(\text{ClO}_4)_2$ .

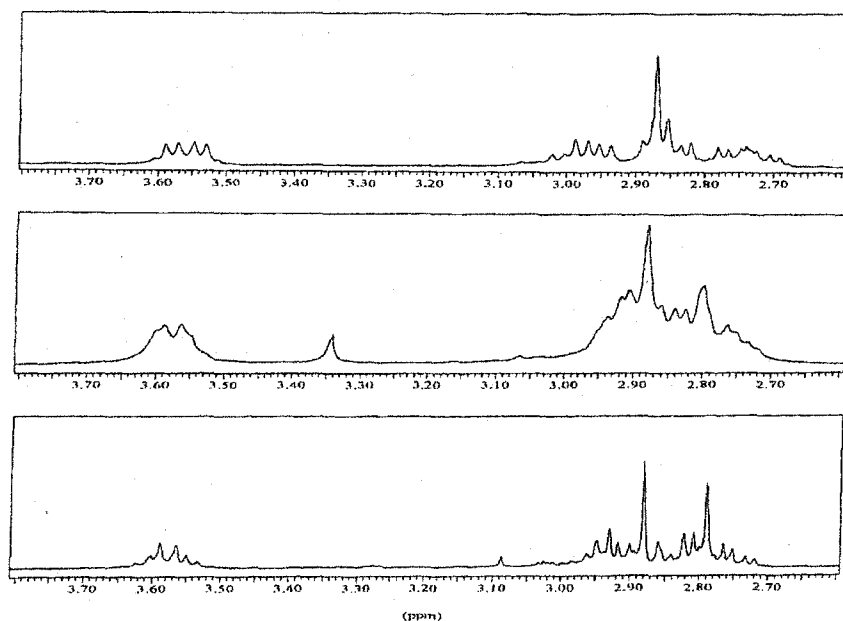


**Figure 2.21** Detailed comparison of  $^1\text{H}$  NMR spectra of the three Cd(II) complexes (all N-D complexes) of **2** in  $\text{D}_2\text{O}$ . Top:  $\text{CdCl}_2 \cdot \mathbf{2}$ ; middle:  $[\text{Cd} \cdot \mathbf{2}(\eta^2\text{-NO}_3)_2]$ ; bottom:  $\text{Cd} \cdot \mathbf{2}(\text{ClO}_4)_2$ .

coordinated  $\text{Cl}^-$  whereas  $\text{Cd}\cdot\mathbf{1}(\text{NO}_3)_2$  and  $\text{Cd}\cdot\mathbf{1}(\text{ClO}_4)_2$  share a common solution species, most likely  $[\text{Cd}\cdot\mathbf{1}(\text{D}_2\text{O})_2]^{2+}$ .  $^1\text{H}$  and  $^{13}\text{C}\{^1\text{H}\}$  NMR spectra of a 1:1 mixture of 0.10 M  $\text{CdCl}_2\cdot\mathbf{1}$  and 0.10 M  $\text{Cd}\cdot\mathbf{1}(\text{NO}_3)_2$  in  $\text{D}_2\text{O}$  (Figure 2.22(a) and Figure 2.22(b)) showed a

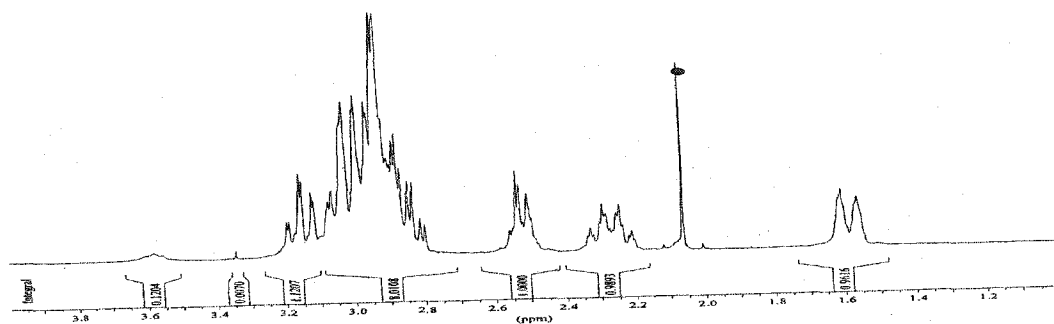


**Figure 2.22(a)** The  $^1\text{H}$  NMR spectrum of a 1:1 mixture of 0.10 M  $\text{CdCl}_2\cdot\mathbf{1}$  and 0.10 M  $\text{Cd}\cdot\mathbf{1}(\text{NO}_3)_2$  in  $\text{D}_2\text{O}$  (> 85% N-D complex). The reference  $\text{CH}_3\text{CN}$  is marked by a dot.

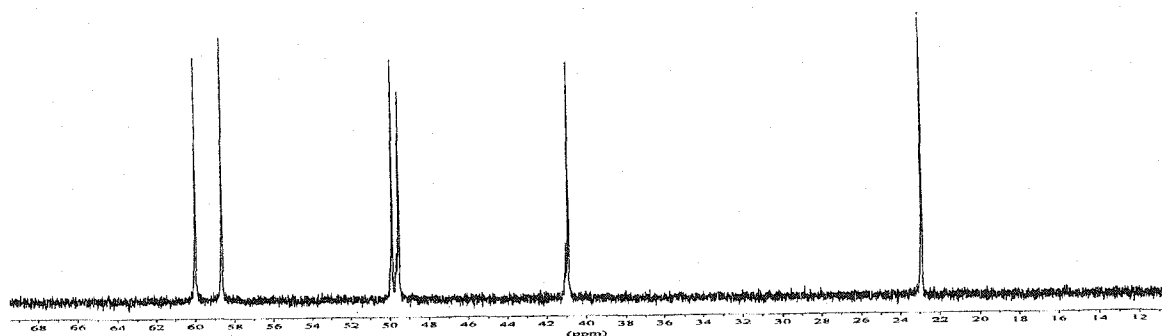


**Figure 2.22(b)** The  $^{13}\text{C}\{^1\text{H}\}$  NMR spectrum of a 1:1 mixture of 0.10 M  $\text{CdCl}_2\cdot\mathbf{1}$  and 0.10 M  $\text{Cd}\cdot\mathbf{1}(\text{NO}_3)_2$  in  $\text{D}_2\text{O}$  (N-D complex).

time-averaged spectrum whose signals lie between those of 0.10 M  $\text{CdCl}_2\cdot\mathbf{1}$  and those of 0.10 M  $\text{Cd}\cdot\mathbf{1}(\text{NO}_3)_2$  in  $\text{D}_2\text{O}$ . After addition of 10 equivalents of  $\text{NaCl}$  into this mixture, its  $^1\text{H}$  and  $^{13}\text{C}\{^1\text{H}\}$  NMR spectra are again similar to these of 0.10 M  $\text{CdCl}_2\cdot\mathbf{1}$  (Figure

2.23).  $^{13}\text{C}\{^1\text{H}\}$  NMR chemical shifts of these Cd(II) complexes (all N-D complexes) are listed in Table 2.5.

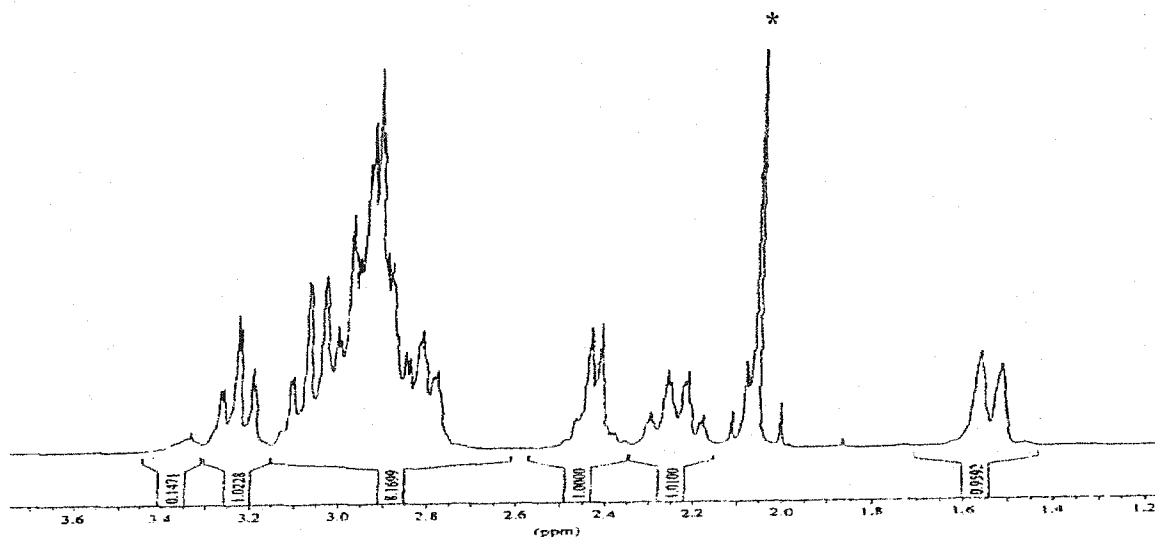


**Figure 2.23** The  $^1\text{H}$  NMR spectrum of the mixture obtained by the addition of 10 equivalents of NaCl into a 1:1 mixture of 0.10 M  $\text{CdCl}_2 \cdot \mathbf{1}$  and 0.10 M  $\text{Cd} \cdot \mathbf{1}(\text{NO}_3)_2$  in  $\text{D}_2\text{O}$  (> 85% N-D complex). The reference  $\text{CH}_3\text{CN}$  is marked by an asterisk.

**Table 2.5** Comparison of  $^1\text{H}$  and  $^{13}\text{C}\{^1\text{H}\}$  NMR data of Cd(II)•**1** complexes (all N-D complexes) in  $\text{D}_2\text{O}$ .

Complex	$^1\text{H}$ NMR in the $\delta$ 2.7 - 3.3 region	$^{13}\text{C}\{^1\text{H}\}$ NMR data $\delta$
0.10M $\text{CdCl}_2 \cdot \mathbf{1}$	3.20 (td, 2H), 2.71-2.85 (no peak)	59.69, 58.55, 49.82, 49.26, 40.93, 22.93
0.10M $\text{Cd} \cdot \mathbf{1}(\text{NO}_3)_2$	3.15-3.30 (no peak), 2.71-2.85 (m, 2H)	60.23, 58.65, 49.94, 49.84, 40.88, 22.88
0.13M $\text{Cd} \cdot \mathbf{1}(\text{ClO}_4)_2$	3.15-3.30 (no peak), 2.71-2.86 (m, 2H)	60.29, 58.71, 49.96, 49.91, 40.91, 22.89
0.10M $\text{CdCl}_2 \cdot \mathbf{1}$ + 0.10 M $\text{Cd} \cdot \mathbf{1}(\text{NO}_3)_2$	3.15 (td, 2H), 2.71-2.85 (no peak)	59.96, 58.64, 49.89, 49.53, 40.92, 22.92
0.010M $\text{CdCl}_2 \cdot \mathbf{1}$	3.16 (td, 2H), 2.71-2.85 (no peak)	59.95, 58.64, 49.89, 49.51, 40.94, 22.94
0.10M Cd(II)• <b>1</b> + 10 equivalents NaCl	3.23 (td, 2H), 2.71-2.85 (no peak)	59.37, 58.36, 49.69, 48.99, 40.88, 22.87

The  $^{113}\text{Cd}$  chemical shift has been found to be very sensitive to the number and types of donor atoms, coordination number and geometry. It also shows a wide chemical shift range ( $\sim 1100$  ppm).<sup>105(a-e)</sup> It has been reported that the deshielding of  $^{113}\text{Cd}$  increases in the order  $\text{O} < \text{N} < \text{S}$  and  $\text{I} < \text{Br} < \text{Cl}$ . Only ligands with higher donor ability than water will provide positive chemical shifts relative to that of  $[\text{Cd}(\text{H}_2\text{O})_6]^{2+}$ .  $^{113}\text{Cd}$  NMR spectra<sup>105(c),106</sup> have thus been used to elucidate the possible solution structures of Cd(II) coordination compounds.  $^{113}\text{Cd}$  NMR spectra of our three Cd(II) complexes of ligand **1** in  $\text{D}_2\text{O}$  were recorded using 3 M  $\text{CdSO}_4$  in  $\text{D}_2\text{O}$  at -3 ppm as an external reference.<sup>105(e)</sup> The chemical shifts of 0.10 M  $\text{CdCl}_2 \cdot \mathbf{1}$ , 0.10 M  $\text{Cd} \cdot \mathbf{1}(\text{NO}_3)_2$ , and 0.13 M  $\text{Cd} \cdot \mathbf{1}(\text{ClO}_4)_2$  are found to be 326, 262 and 267 ppm respectively. The solution and solid-state  $^{113}\text{Cd}$  NMR spectral studies of  $\text{Cd}(\alpha, \alpha'\text{-bipyridyl})_2\text{X}_2$  ( $\text{X}=\text{Cl}$  and  $\text{H}_2\text{O}$ ) have revealed that the chemical shift difference between a  $\text{N}_4\text{-Cd(II)-Cl}_2$  species and  $\text{N}_4\text{-Cd(II)-}(\text{OH}_2)_2$  species is -78 ppm.<sup>107</sup> The  $^{113}\text{Cd}$  NMR spectral studies also showed that the chemical shift difference is -35 ppm if a coordinated chloride in a Cd(II) complex is substituted by a coordinated water.<sup>105(c)</sup> From our data, the chemical shift difference between 0.10 M  $\text{CdCl}_2 \cdot \mathbf{1}$  and 0.10 M  $\text{Cd} \cdot \mathbf{1}(\text{NO}_3)_2$  (or 0.13 M  $\text{Cd} \cdot \mathbf{1}(\text{ClO}_4)_2$ ) is -64 (or -59) ppm. These data are thus consistent with the hypothesis that in  $\text{D}_2\text{O}$ ,  $\text{CdCl}_2 \cdot \mathbf{1}$  has partially coordinated  $\text{Cl}^-$  around its Cd(II) center with the number of coordinated chloride between one and two. Such an intermediate value is probably the result of the fast equilibria among  $[\text{Cd} \cdot \mathbf{1}(\text{OH}_2)(\text{Cl})]^+$ ,  $[\text{Cd} \cdot \mathbf{1}(\text{Cl})_2]$  and  $[\text{Cd} \cdot \mathbf{1}(\text{OH}_2)_2]^{2+}$ .

A recent report of a cadmium cyclam complex (**74** in **Figure 1.27**) assigned the highest-field multiplet (doublet of triplet of triplets) to the axial proton of the  $\beta$ -methylene within the six-membered chelate rings.<sup>43(b)</sup> This is inconsistent with our



observations here as spectra of all our synthesized Zn(II) and Cd(II) complexes in several solvents indicated the assignment to be the equatorial proton instead. This may suggest a non-chair solution conformation for the six-membered chelate ring as coordinated cyclam is more flexible than complexes of cross-bridged cyclam.<sup>43(b)</sup>

A combination of *NH/ND* exchange, 2D [<sup>1</sup>H,<sup>1</sup>H] gCOSY and 2D [<sup>1</sup>H,<sup>13</sup>C] gHSQC NMR experiments again enabled us to assign the <sup>1</sup>H and <sup>13</sup>C{<sup>1</sup>H} NMR spectra of CdCl<sub>2</sub>•2 in CD<sub>3</sub>OD. In the proton spectrum, the resonance at δ 3.49-3.55 belongs to the protons on the carbons adjacent to NH (position **a** in Table 2.4) as the spin pattern of these two resonances simplified upon complete *NH/ND* exchange. The 2D [<sup>1</sup>H,<sup>1</sup>H] gCOSY NMR spectrum (Figure 2.24) reveals that the singlet resonance at δ 2.86 does

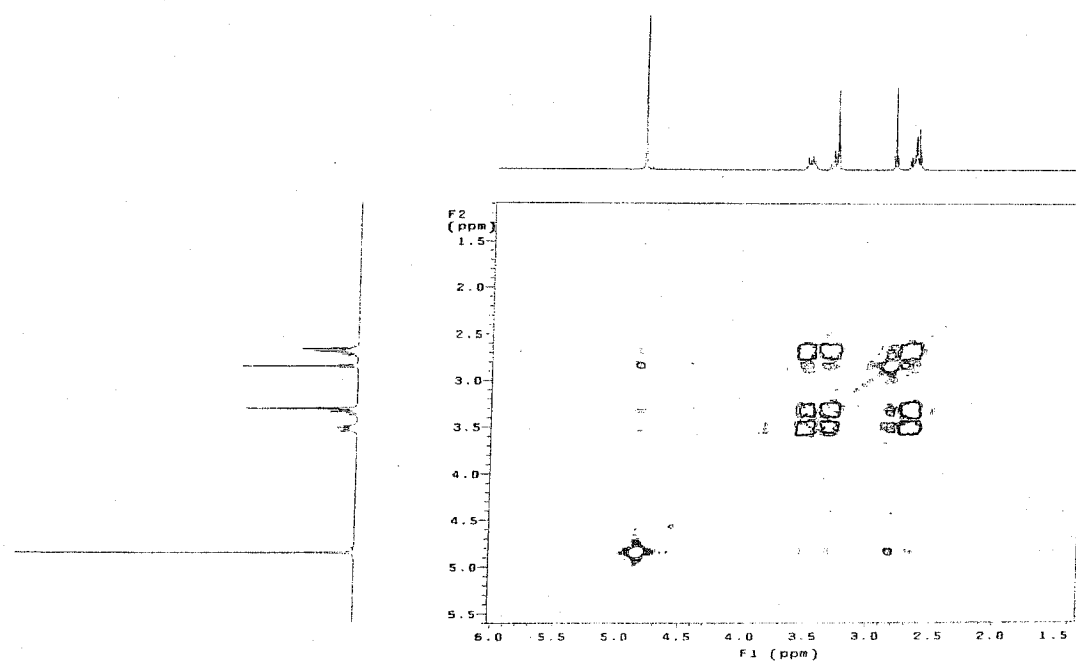


**Figure 2.24** A 2D [<sup>1</sup>H,<sup>1</sup>H] gCOSY spectrum of CdCl<sub>2</sub>•2 (N-D complex) in CD<sub>3</sub>OD.

not show any strong coupling to any other resonances so this can be assigned to that of the cross-bridging  $CH_2CH_2$ . The satellites around this singlet are from the coupling between these protons and  $^{111,113}Cd$ . All three carbon resonances were readily assigned by using 2D [ $^1H, ^{13}C$ ] gHSQC NMR (Figure 2.25). The  $^{13}C$  resonance at  $\delta$  57.82 correlates

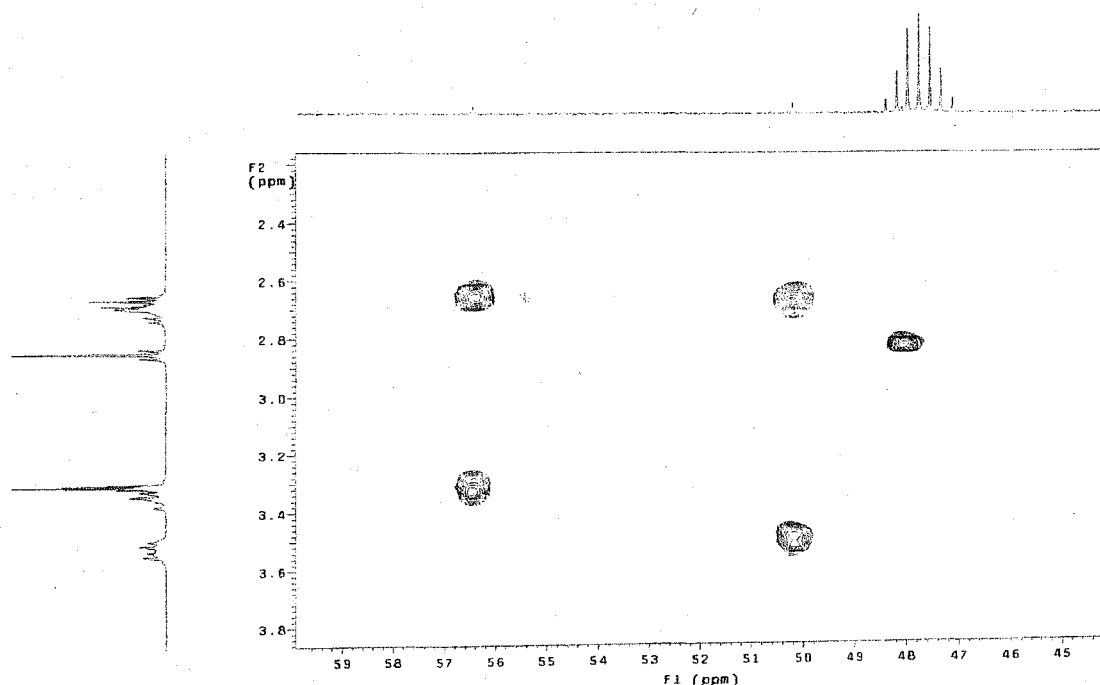


**Figure 2.25** A 2D [ $^1H, ^{13}C$ ] gHSQC NMR spectrum of  $CdCl_2 \cdot 2(N-D \text{ complex})$  in  $CD_3OD$ .

to the proton multiplet at  $\delta$  3.28-3.38 and one of the two proton resonances between  $\delta$  2.65-2.82. The  $^{13}C$  resonance at  $\delta$  57.82 can thus be assigned to carbon **b**. The  $^{13}C$  resonance at  $\delta$  49.45 belonging to carbon **c** correlates to the proton singlet at  $\delta$  2.86. Finally, the remaining  $^{13}C$  resonance at  $\delta$  51.72 can be assigned to the carbons at **a**, which is in turn coupled to the proton multiplet between  $\delta$  3.49-3.55 as well as part of the resonances between  $\delta$  2.65-2.82.

**(c) Mercury Complexes of Ligands 1 and 2.** Complex  $[\text{HgCl}_2(\mu\text{-1})]_2$  (133)

started decomplexation in  $\text{D}_2\text{O}$  immediately after it was dissolved. Nonetheless both proton and  $^{13}\text{C}\{^1\text{H}\}$  NMR data in  $\text{D}_2\text{O}$  or  $\text{CD}_3\text{OD}$  can be obtained which show only one coordinated species with retention of the ligand's  $C_2$  symmetry. Sizeable  $^{13}\text{C}$ - $^{199}\text{Hg}$  couplings of 25-52 Hz are observed as satellites in four of the six  $^{13}\text{C}$  resonances in  $\text{CD}_3\text{OD}$ . This suggests a slow exchange between coordinated **1** and free **1** in  $\text{CD}_3\text{OD}$ . We believe that in methanol the same structure is maintained as that in the solid-state (**Figure 2.39**, *vide infra*).

Again, both proton and  $^{13}\text{C}$  couplings to  $^{199}\text{Hg}$  are clearly observed in both of the  $^1\text{H}$  and  $^{13}\text{C}\{^1\text{H}\}$  NMR spectra of  $\text{HgCl}_2\cdot\mathbf{2}$  (**134**) in  $\text{D}_2\text{O}$  or  $\text{CD}_3\text{OD}$  at ambient temperature. A  $^3J$  coupling constant of 44 Hz between  $^1\text{H}$  and  $^{199}\text{Hg}$  is observed for the cross-bridging  $\text{CH}_2\text{CH}_2$  in the  $^1\text{H}$  NMR spectrum in  $\text{CD}_3\text{OD}$  (**Figure 2.18**). Compared to the analogues coupling constant of 12 Hz between  $^1\text{H}$  and  $^{111,113}\text{Cd}$  for  $\text{CdCl}_2\cdot\mathbf{2}$  (**Figure 2.18**), this coupling constant is significantly larger. This is consistent with literature data for heavy metals.<sup>102</sup> Considering the liability of most  $\text{Hg(II)}$ -polyamine complexes, there is a real paucity of such data in the literature.<sup>99,103</sup>

Similar to  $\text{HgCl}_2\cdot\mathbf{2}$ , complex  $(\text{HgCl}_2)_6\cdot(\mathbf{2})_4$  (**135**) shows a  $C_{2v}$  symmetry in  $d_6$ -DMSO due to the presence of only three carbon resonances in its  $^{13}\text{C}\{^1\text{H}\}$  NMR spectrum. This implies that even though both the cationic unit  $[\text{Hg}\cdot\mathbf{2}(\mu\text{-Cl})]_2^{2+}$  and the anionic unit  $[\text{Hg}\cdot\mathbf{2}\text{Cl}(\mu\text{-Cl})(\text{HgCl}_3)]^-$  exist in the solid-state, they must be in fast exchange in DMSO on the NMR time scale. This exchange does not include the dissociation of the ligand from  $\text{Hg(II)}$  as evidenced by the presence of  $^{13}\text{C}$ - $^{199}\text{Hg}$  couplings in all three carbon resonances in  $d_6$ -DMSO. In  $\text{CD}_3\text{CN}$ , the presence of a

proton singlet at  $\delta$  2.81 belonging to cross-bridging  $CH_2CH_2$  also indicates a  $C_{2v}$  symmetry. However, four carbon resonances including two at  $\delta$  50.46 and 50.34 appeared in its  $^{13}C\{^1H\}$  NMR spectrum in  $CD_3CN$ . This can be due to the presence of a mixture of the N-H complex ( $\delta$  50.46) and the N-D complex ( $\delta$  50.34) and is consistent with the detection of HOD in this  $CD_3CN$  solvent as indicated by the presence of a 1:1:1 triplet (3H) at  $\delta$  2.21 and also the integrated area of only about 1.2-1.5 NH protons at  $\delta$  3.09-3.30 in its  $^1H$  NMR spectrum.

### 2.3 N-H/N-D Exchange in $D_2O$ and $CD_3OD$ .

N-H/N-D exchange was observed at the secondary N-H sites for all Zn(II), Cd(II) and Hg(II) complexes of cross-bridged ligands **1** and **2** in  $D_2O$  and  $CD_3OD$  (Scheme 2.1). Generally, the resonances of protons adjacent to the axial N-H sites lose their coupling with the N-H proton upon complete deuteration. The chemical shifts of the carbons adjacent to these axial N-H sites also show a detectable upfield shift. For example, the  $^{13}C\{^1H\}$  NMR spectrum of a NH/ND mixture of  $CdCl_2 \cdot 2$  (**129**) has five peaks at  $\delta$  57.81 (**b** in N-H complex), 57.79 (**b** in N-D complex), 51.71 (**a** in N-H complex), 51.59 (**a** in N-D complex), and 49.47 (**c** in both N-H complex and N-D complex) instead of three  $^{13}C$  resonances for this  $C_{2v}$  complex. As mentioned above, these changes have been useful in assigning the respective resonances in their NMR spectra in  $D_2O$  and  $CD_3OD$ .

The NH/ND exchange rates of all detectable Zn(II) and Cd(II) complexes of ligands **1** and **2** follow a pseudo-first-order reaction rate. This exchange is so fast for the Hg(II) complexes that only the N-D complexes were detected by  $^1H$  NMR spectroscopy recorded within 30 minutes. If we assume that this exchange also follows a pseudo first-

order rate law and that the detection limit for the *NH* proton resonance in their NMR spectra is five percent, the upper limit of the half-lives for this exchange is 0.12 hour. The half-lives for the *NH/ND* exchange in all Zn(II), Cd(II) and Hg(II) complexes of ligands 1 and 2 are summarized in **Table 2.6**. As shown, these rates follows the order: Hg(II) complexes of ligand 1 (or ligand 2) > Cd(II) complexes of ligand 1 (or ligand 2) > Zn(II) complexes of ligand 1 (or ligand 2). However, due to the possible different pD values of these complexes in D<sub>2</sub>O and CD<sub>3</sub>OD even at the same starting concentration of the metal complex, these kinetic data are only the preliminary results. A more thorough investigation of a *NH/ND* exchange will require buffered D<sub>2</sub>O solutions.<sup>29(f)</sup>

**Table 2.6** Half-lives for the *NH/ND* exchange in Zn(II), Cd(II) and Hg(II) complexes of ligands 1 and 2 in D<sub>2</sub>O or CD<sub>3</sub>OD at room temperature.

Metal complex	C (mol/L)	Solvent	t <sub>1/2</sub> (hours)
ZnCl <sub>2</sub> •1	0.070	D <sub>2</sub> O	2.4 x 10 <sup>4</sup>
ZnCl <sub>2</sub> •1	no data	D <sub>2</sub> O	5.3 x 10 <sup>4</sup>
ZnCl <sub>2</sub> •1	0.0165	CD <sub>3</sub> OD	65
Zn(ClO <sub>4</sub> ) <sub>2</sub> •1	no data	CD <sub>3</sub> OD	6.5 x 10 <sup>4</sup>
CdCl <sub>2</sub> •1	no data	D <sub>2</sub> O	327
Cd(NO <sub>3</sub> ) <sub>2</sub> •1	0.029	D <sub>2</sub> O	257
Cd(NO <sub>3</sub> ) <sub>2</sub> •1	0.062	D <sub>2</sub> O	245
Cd(ClO <sub>4</sub> ) <sub>2</sub> •1	0.132	D <sub>2</sub> O	65
[HgCl <sub>2</sub> •1] <sub>2</sub>	saturated	D <sub>2</sub> O	< 0.12
[HgCl <sub>2</sub> •1] <sub>2</sub>	saturated	CD <sub>3</sub> OD	< 0.12
ZnCl <sub>2</sub> •2	0.0187	D <sub>2</sub> O	17
ZnCl <sub>2</sub> •2	0.0066	CD <sub>3</sub> OD	29
Zn(NO <sub>3</sub> ) <sub>2</sub> •2	0.018	CD <sub>3</sub> OD	23
Zn(ClO <sub>4</sub> ) <sub>2</sub> •2	0.023	CD <sub>3</sub> OD	2000
Zn(ClO <sub>4</sub> ) <sub>2</sub> •2	0.020	CD <sub>3</sub> OD	2583
CdCl <sub>2</sub> •2	0.45	D <sub>2</sub> O	0.43
CdCl <sub>2</sub> •2	0.022	CD <sub>3</sub> OD	3.0
CdCl <sub>2</sub> •2	no data	CD <sub>3</sub> OD	7.8
Cd(NO <sub>3</sub> ) <sub>2</sub> •2	0.020	CD <sub>3</sub> OD	13.5
Cd(ClO <sub>4</sub> ) <sub>2</sub> •2	0.020	CD <sub>3</sub> OD	14.7
HgCl <sub>2</sub> •2	saturated	D <sub>2</sub> O	< 0.12
HgCl <sub>2</sub> •2	saturated	CD <sub>3</sub> OD	< 0.12

### 3. X-ray Structural Data.

Thirteen X-ray structures of these Zn(II), Cd(II) and Hg(II) complexes of ligands 1-4 have been determined. A summary of relevant bond distances and angles for each of these is listed in **Tables 2.7 (a-o)**.

As mentioned in the Chapter I, the fit of a metal ion within the cavity formed by a coordinated cross-bridged ligand can be best gauged by the axial bond angle between the non-bridging nitrogen atoms at the metal ion,  $N_{ax}\text{-M-N}_{ax}$  (**Figure 1.25**).

#### 3.1 The Five Zn(II) Complexes:

**Zn•1(OH<sub>2</sub>)( $\mu$ -Cl-ZnCl<sub>3</sub>) (115)**. This complex has cross-bridged ligand **1** in the distorted diamond lattice [2323]/[2323] *cis*-folded conformation (**Figure 2.26**).<sup>108</sup> The Zn(II) center adopts a near-octahedral coordination geometry. It is coordinated by four amine nitrogens from **1**, one coordinated H<sub>2</sub>O, as well as one bridging chloride. The axial N(2)-Zn-N(4) angle of 173.5(2)° and equatorial N(1)-Zn-N(3) angle of 84.9(2)° reflect a reasonably good fit of an octahedral Zn(II) inside **1**. Consistent with literature data, the secondary N(ax)-Zn bondlength of 2.121(6)Å is marginally shorter than the tertiary N(eq)-Zn bondlength of 2.140(5)Å.<sup>269a),29(g)</sup> For comparison, most zinc complexes of cyclam and its derivatives have the *trans*-III ligand configuration.<sup>23(a-k)</sup> Only five *cis*-V structures are known and all of them are cyclam derivatives.<sup>26(a-1)</sup> These have secondary amine N-Zn distances ranging from 2.07 to 2.19Å and N(ax)-Zn-N(ax) angles between 168 and 174°. Not surprisingly, without cross-bridging, their folded N(eq)-Zn-N(eq)

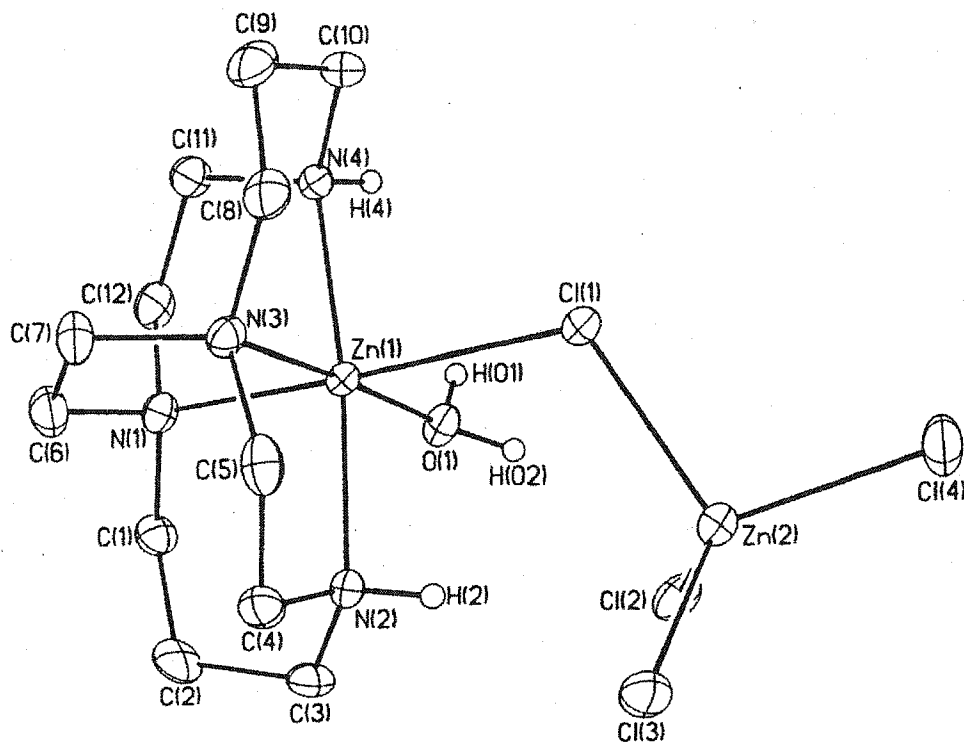


**Figure 2.26** X-ray structure of  $[\text{Zn}\cdot 1(\text{OH}_2)(\mu\text{-Cl})\text{ZnCl}_3]$  (115) showing atomic labeling scheme. Hydrogens bonded to carbons are omitted for clarity.

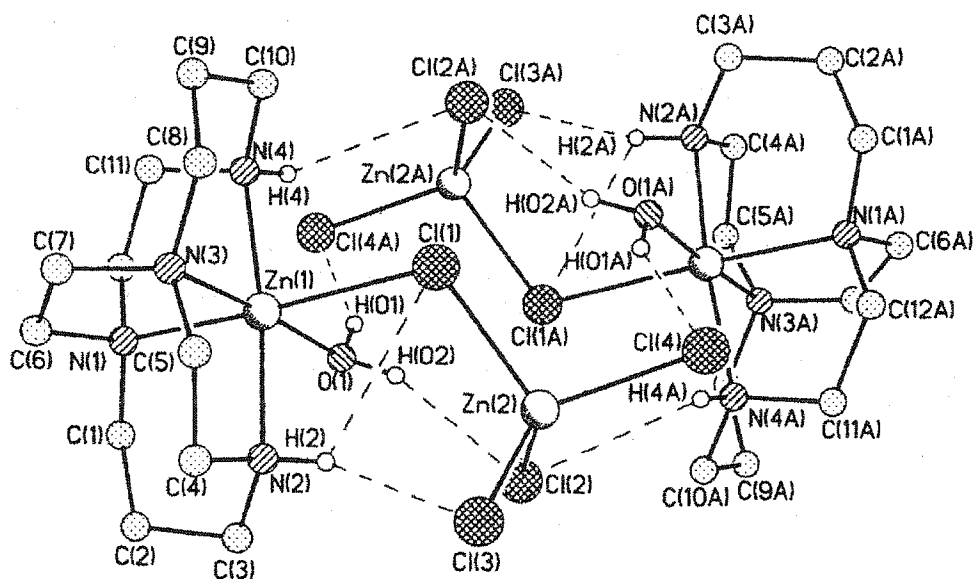


**Figure 2.27** Hydrogen bonding interactions in the crystal structure of  $[\text{Zn}\cdot 1(\text{OH}_2)(\mu\text{-Cl})\text{ZnCl}_3]$  (115).

angles have obtuse values of 102-108°. A ZnCl<sub>2</sub> complex of the N,N'-dimethyl derivative of **1** has also been communicated though without full structural detail.<sup>73</sup>

**Table 2.7(a)** Selected Bond Distances (Å) and Bond Angles (deg) in [Zn•**1**(OH<sub>2</sub>)(μ-Cl)ZnCl<sub>3</sub>] (**115**) (Hydrogen bonding interactions are included.).

Zn(1)-N(1)	2.141(5)	Zn(1)-N(2)	2.119(6)
Zn(1)-N(3)	2.140(5)	Zn(1)-N(4)	2.123(6)
Zn(1)-O(1)	2.170(5)	Zn(1)-Cl(1)	2.629(2)
Zn(2)-Cl(1)	2.309(2)	H(O1)---Cl(4A)	2.48(4)
H(O2)---Cl(2)	2.41(2)	H(2)---Cl(3)	2.70(3)
H(2)---Cl(1)	2.92(6)	H(4)---Cl(2A)	2.84(4)
N(2)-Zn(1)-N(4)	173.5(2)	N(2)-Zn(1)-N(3)	85.0(2)
N(4)-Zn(1)-N(3)	90.1(2)	N(2)-Zn(1)-N(1)	90.5(2)
N(4)-Zn(1)-N(1)	84.7(2)	N(3)-Zn(1)-N(1)	84.9(2)
N(2)-Zn(1)-O(1)	92.4(2)	N(4)-Zn(1)-O(1)	92.4(2)
N(3)-Zn(1)-O(1)	177.2(2)	N(1)-Zn(1)-O(1)	94.1(2)
N(2)-Zn(1)-Cl(1)	90.16(16)	N(4)-Zn(1)-Cl(1)	93.93(2)
N(3)-Zn(1)-Cl(1)	92.91(2)	N(1)-Zn(1)-Cl(1)	177.38(14)
O(1)-Zn(1)-Cl(1)	88.24(14)	O(1)-H(O1)-Cl(4A)	153(7)
O(1)-H(O2)-Cl(2)	158(6)	N(2)-H(2)-Cl(3)	154(6)
N(2)-H(2)-Cl(1)	115(5)	N(4)-H(4)-Cl(2A)	137(5)



Ancillary ligands in this complex include one water as well as a bridging chloride from the  $\text{ZnCl}_4^{2-}$  counterion. The inter- and intra-molecular hydrogen bonding interactions from two such units result in a pseudo-dimeric structure (**Figure 2.27**). The distances of these hydrogen bonds range from 2.25 to 2.63 Å while the Zn(1)-Cl(1) bond is quite long at 2.629(2)Å. The Zn(II)-OH<sub>2</sub> of 2.170 (5) Å is within the average Zn-O bondlength of  $2.097 \pm 0.049$  Å for a 6-coordinate Zn(II) species.<sup>109</sup> Only two previous reports were found in the *Cambridge Crystallographic Database* with this Zn(H<sub>2</sub>O)(μ-Cl-ZnCl<sub>3</sub>) structural motif. One contains triethanolamine and the other has pyridine-2-carbaldehyde as co-ligands.<sup>110,111</sup> There are two reports of 6-coordinate Zn(II) complexes of cyclam and its derivatives with coordinated water.<sup>23(j),23(l)</sup> However, the two ancillary ligands including H<sub>2</sub>O are found in the *trans* position. Since the significance of labile *cis*-coordination sites at Zn(II) centers for catalytic chemistry has often been invoked,<sup>29(a),112</sup> the potential biomimetic reactivity at this type of complex is clearly worthy of study.

**[Zn•1(μ-Cl)]<sub>2</sub>Cl<sub>2</sub>•4CH<sub>3</sub>OH (116)**. This *meso* dimer contains both enantiomers of the [Zn•1]<sup>2+</sup> core bridged by two chlorides (**Figure 2.28**). The distance between the two Zn(II) centers is 3.715 Å. The coordination geometry around each Zn(II) center is a distorted octahedron since the N(ax)-Zn-N(ax) angle is compressed from linearity to 168.7(3)° and the N(eq)-Zn-N(eq) angle from 90° to 84.5(2)°. Again, the secondary N(ax)-Zn bonds are slightly shorter (2.133(5)Å) than the tertiary N(eq)-Zn (2.185(4)Å). The N-H hydrogens are also engaged in hydrogen bonding with the methanol solvent molecules (**Figure 2.29**). All bridging Zn-Cl bonds have identical lengths of 2.5265(13) Å. For polyamine complexes of zinc, there has been only one other chloride-bridged zinc

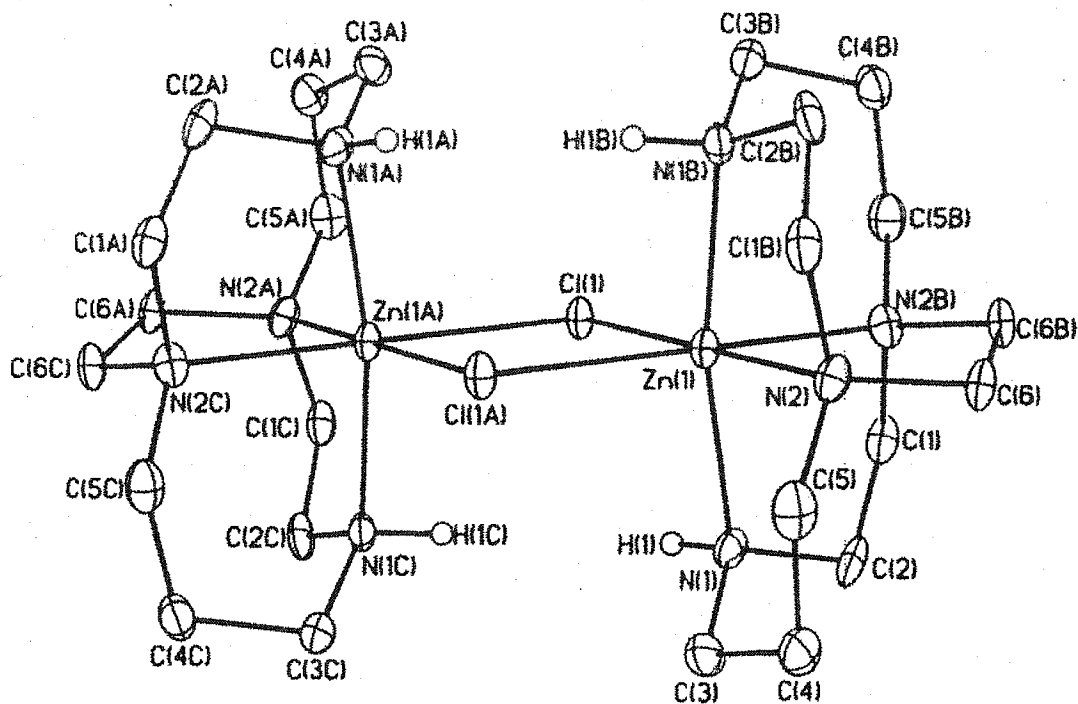


**Figure 2.28** Structure of the  $[\text{Zn}\cdot\mathbf{1}(\mu\text{-Cl})]_2^{2+}$  dimer in  $[\text{Zn}\cdot\mathbf{1}(\mu\text{-Cl})]_2\text{Cl}_2\cdot 4\text{CH}_3\text{OH}$  (**116**) showing atomic labeling scheme. Hydrogens bonded to carbons are omitted for clarity.

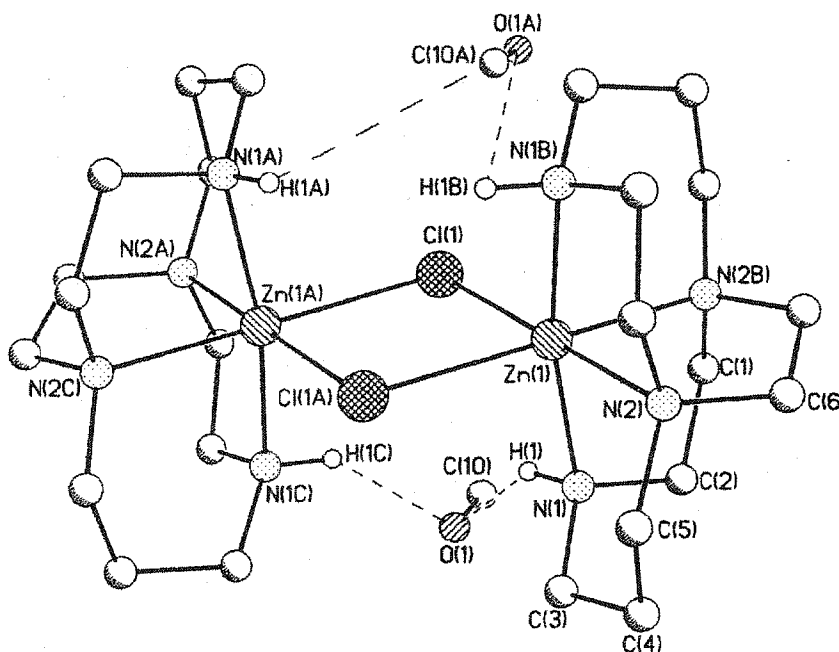


**Figure 2.29** Hydrogen bonding interactions in the crystal structure of  $[\text{Zn}\cdot\mathbf{1}(\mu\text{-Cl})]_2\text{Cl}_2\cdot 4\text{CH}_3\text{OH}$  (**116**).

complex reported.<sup>113</sup> This five-coordinate  $\text{ZnCl}_2 \cdot \text{triazacyclononane}$  dimer features rather unsymmetrical bridging Zn-Cl bonds of 2.714 Å and 2.292 Å respectively. The structure of monomeric *trans*- $\text{ZnCl}_2 \cdot \text{cyclam}$  is also known with the ligand in the common *trans*-III configuration. This has long axial Zn-Cl bondlengths of 2.664 Å and secondary N-Zn bonds of 2.090 Å and 2.103 Å.<sup>23(h)</sup>

**Table 2.7(b)** Selected Bond Distances (Å) and Bond Angles (deg) in  $[\text{Zn} \cdot \mathbf{1}(\mu\text{-Cl})]_2\text{Cl}_2(\text{CH}_3\text{OH})_4$  (**116**) (Hydrogen bonding interactions are included.).

Zn(1)-N(1)	2.133(5)	Zn(1)-N(1B)	2.133(5)
Zn(1)-N(2)	2.185(4)	Zn(1)-N(2B)	2.185(4)
Zn(1)-Cl(1)	2.5265(13)	Zn(1)-Cl(1A)	2.5265(13)
H(1)---O(1)	2.20(3)	N(1)---O(1)	2.976(6)
N(1)-Zn(1)-N(1B)	168.7(3)	N(1)-Zn(1)-N(2B)	83.51(18)
N(1)-Zn(1)-N(2)	88.10(18)	N(1B)-Zn(1)-N(2)	83.51(18)
N(2B)-Zn(1)-N(2)	84.5(2)	N(1B)-Zn(1)-N(2B)	88.10(18)
N(1)-Zn(1)-Cl(1A)	96.51(14)	N(1B)-Zn(1)-Cl(1A)	91.83(14)
N(2B)-Zn(1)-Cl(1A)	179.59(11)	N(2)-Zn(1)-Cl(1A)	95.05(12)
Cl(1A)-Zn(1)-Cl(1)	85.36(6)	Zn(1)-Cl(1)-Zn(1A)	94.64(6)
N(1)-H(1)-O(1)	143(5)		

**[Zn•1(μ-Cl)]<sub>2</sub>Cl<sub>2</sub> (116a).** [Zn•1(μ-Cl)]<sub>2</sub>Cl<sub>2</sub> was obtained when acetonitrile was used as the reaction solvent. This *meso* dimer also contains both enantiomers of the [Zn•1]<sup>2+</sup> core bridged by two chlorides (**Figure 2.30**). The N(ax)-Zn-N(ax) angle of 168.4(3)° is the same as that in [Zn•1(μ-Cl)]<sub>2</sub>Cl<sub>2</sub>•4CH<sub>3</sub>OH. Without the participation of hydrogen-bonding MeOH in this X-ray structure, this dimer becomes rather unsymmetrical with bridging Zn-Cl bonds of 2.483(2)Å and 2.515(2)Å respectively. The distance between the two Zn(II) centers is 3.60Å. This X-ray structure confirms that the formation of such a dimeric Zn(II) complex is possible without the presence of hydrogen-bonding MeOH.

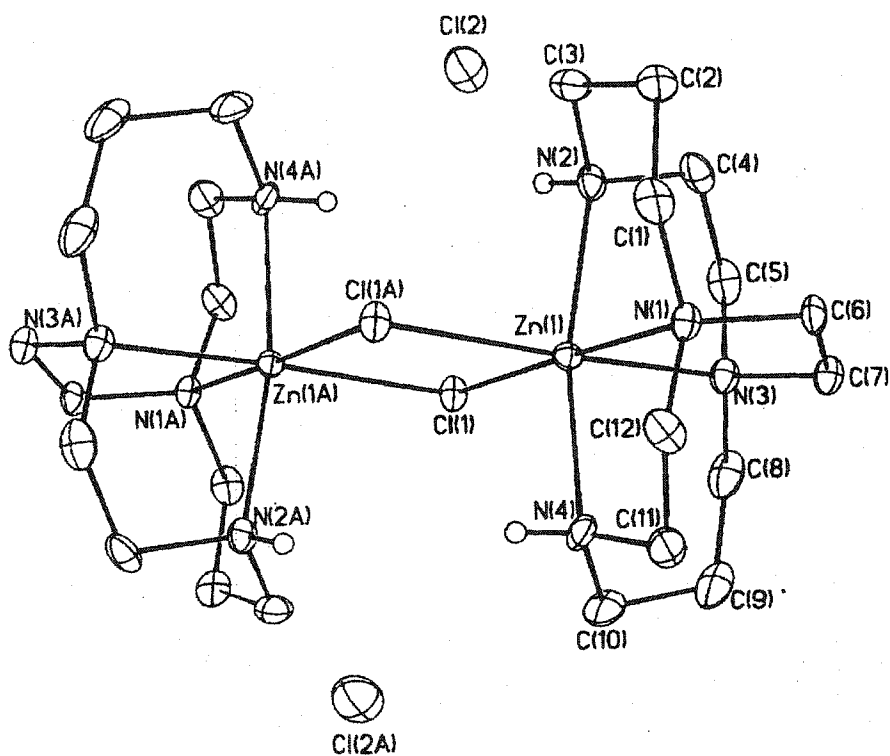


**Figure 2.30** Structure of [Zn•1(μ-Cl)]<sub>2</sub>Cl<sub>2</sub> (116a), showing atomic labeling scheme. Hydrogens bonded to carbons are omitted for clarity.

**Table 2.7(c)** Selected Bond Distances (Å) and Bond Angles (deg) in [Zn•1(μ-Cl)]<sub>2</sub>Cl<sub>2</sub> (**116a**) (Hydrogen bonding interactions are included.).

Zn(1)-N(1)	2.171(5)	Zn(1)-N(2)	2.111(6)
Zn(1)-N(3)	2.166(6)	Zn(1)-N(4)	2.171(5)
Zn(1)-Cl(1)	2.4829(18)	Zn(1)-Cl(1A)	2.515(2)
H(N2)---Cl(1)	2.91(7)	H(N2)---Cl(2)	2.50(7)
H(N4)---Cl(1)	2.88(6)	H(N4)---Cl(2)	2.70(6)
N(2)-Zn(1)-N(4)	168.3(2)	N(1)-Zn(1)-N(2)	88.3(2)
N(1)-Zn(1)-N(3)	83.4(2)	N(1)-Zn(1)-N(4)	83.0(2)
N(2)-Zn(1)-N(3)	82.8(2)	N(3)-Zn(1)-N(4)	88.3(3)
N(1)-Zn(1)-Cl(1)	178.50(16)	N(2)-Zn(1)-Cl(1)	92.86(17)
N(3)-Zn(1)-Cl(1)	95.80(15)	N(4)-Zn(1)-Cl(1)	95.73(18)
N(1)-Zn(1)-Cl(1A)	95.26(16)	N(2)-Zn(1)-Cl(1A)	95.12(17)
N(3)-Zn(1)-Cl(1A)	177.58(17)	N(4)-Zn(1)-Cl(1A)	93.5(2)
Cl(1A)-Zn(1)-Cl(1)	85.56(6)	N(2)-H(N2)-Cl(1)	113(5)
N(2)-H(N2)-Cl(2)	146(6)	N(4)-H(N4)-Cl(1)	124(6)
N(4)-H(N4)-Cl(2)	138(6)		

**Zn•3(μ-Cl)<sub>2</sub>-ZnCl<sub>2</sub> (120).** Here Zn(II) coordinates to four nitrogen donors from ligand **3** within its molecular cleft with slightly longer benzyl N(ax)-Zn bonds of 2.272(5)Å

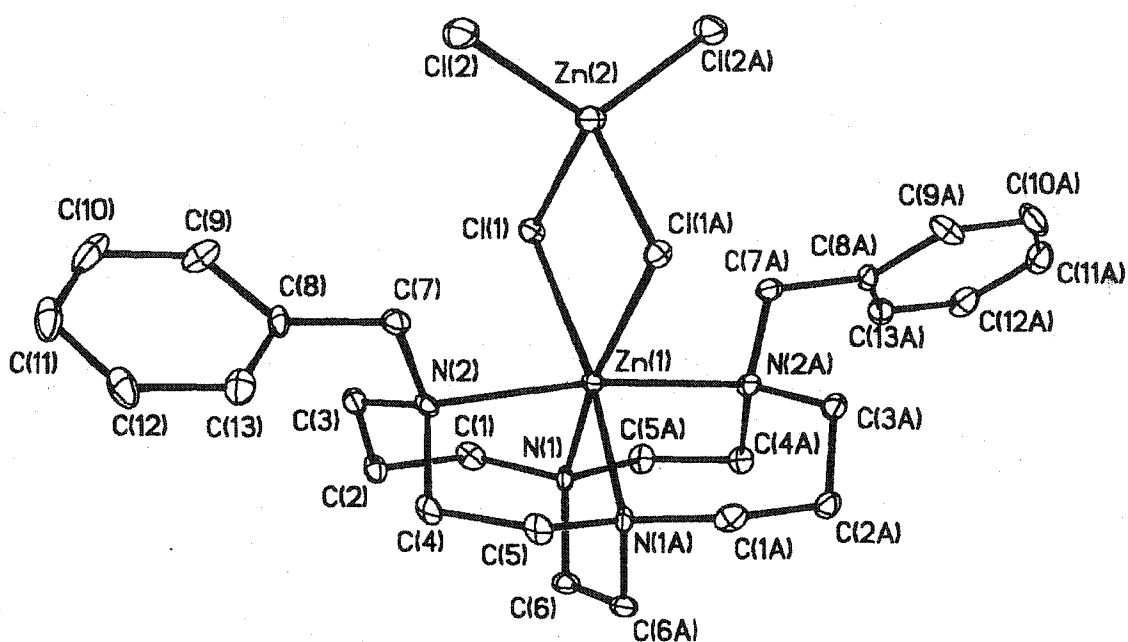


**Figure 2.31** X-ray structure of  $\text{Zn} \cdot 3(\mu\text{-Cl})_2\text{-ZnCl}_2$  (**120**) showing atomic labeling scheme. Hydrogens bonded to carbons are omitted for clarity.

compared to the N(eq)-Zn bonds of 2.124(5) Å (**Figure 2.31**). The N(ax)-Zn-N(ax) angle of 171.1(2)° is similar to those in the three Zn(II) complexes of ligand **1**. A doubly-bridging  $\text{ZnCl}_4^{2-}$  counterion completes the pseudo-octahedral metal coordination sphere. While the doubly chloride-bridged  $\text{Zn}_2\text{Cl}_6^{2-}$  anion unit has been found in X-ray structures of twenty-nine compounds,<sup>114(a-f)</sup> this variation represents the only structural form for  $\text{ZnCl}_2$  amine complexes. As can be expected, the octahedral zinc's Zn(1)-(μ-Cl) bonds, 2.518(1) Å long, are substantially weaker than the pseudo-tetrahedral Zn(2)-(μ-Cl) bonds at 2.3422(6) Å. A *Cambridge Crystallographic Database* search showed that no previous report was found for Zn(II) complexes of any mono, di, tri or tetra N-benzylated cyclam derivatives. Very recently, the X-ray structure of a Zn(II) nitrate complex of a tri N-

benzylated cyclam derivative with a *trans-I* configuration was reported.<sup>43(d)</sup> The range of Zn-N bondlengths to the tertiary amine nitrogens here is 2.109(2)-2.306(2) Å.

**Table 2.7(d)** Selected Bond Distances (Å) and Bond Angles (deg) in Zn•3(μ-Cl)<sub>2</sub>-ZnCl<sub>2</sub> (**120**).

Zn(1)-N(1A)	2.124(5)	Zn(1)-N(1)	2.124(5)
Zn(1)-N(2)	2.272(5)	Zn(1)-N(2A)	2.272(5)
Zn(1)-Cl(1A)	2.5183(15)	Zn(1)-Cl(1)	2.5183(15)
Zn(2)-Cl(2A)	2.2211(19)	Zn(2)-Cl(2)	2.2211(19)
Zn(2)-Cl(1A)	2.3422(16)	Zn(2)-Cl(1)	2.3422(16)
N(1A)-Zn(1)-N(1)	83.5(3)	N(1A)-Zn(1)-N(2)	82.87(19)
N(1)-Zn(1)-N(2)	90.45(19)	N(1A)-Zn(1)-N(2A)	90.45(19)
N(1)-Zn(1)-N(2A)	82.87(19)	N(2)-Zn(1)-N(2A)	171.1(2)
N(1A)-Zn(1)-Cl(1A)	96.88(3)	N(1)-Zn(1)-Cl(1A)	171.28(15)
N(2)-Zn(1)-Cl(1A)	98.25(13)	N(2A)-Zn(1)-Cl(1A)	88.41(13)
N(1A)-Zn(1)-Cl(1)	171.28(15)	N(1)-Zn(1)-Cl(1)	96.88(14)
N(2)-Zn(1)-Cl(1)	88.41(13)	N(2A)-Zn(1)-Cl(1)	98.25(13)
Cl(1A)-Zn(1)-Cl(1)	84.04(7)	Cl(2A)-Zn(2)-Cl(2)	118.73(10)
Cl(2A)-Zn(2)-Cl(1A)	113.85(6)	Cl(2)-Zn(2)-Cl(1A)	107.65(6)
Cl(2a)-Zn(2)-Cl(1)	107.65(6)	Cl(2)-Zn(2)-Cl(1)	113.85(6)
Cl(1A)-Zn(2)-Cl(1)	92.06(8)	Zn(2)-Cl(1)-Zn(1)	91.95(5)

$[\text{Zn}\cdot 2(\text{H}_2\text{O})_2](\text{ClO}_4)_2$  (122). The smaller cross-bridged cyclen, ligand 2, is clearly a poorer fit for the six-coordinate Zn(II) (Figure 2.32) than cross-bridged cyclam, ligand 1.

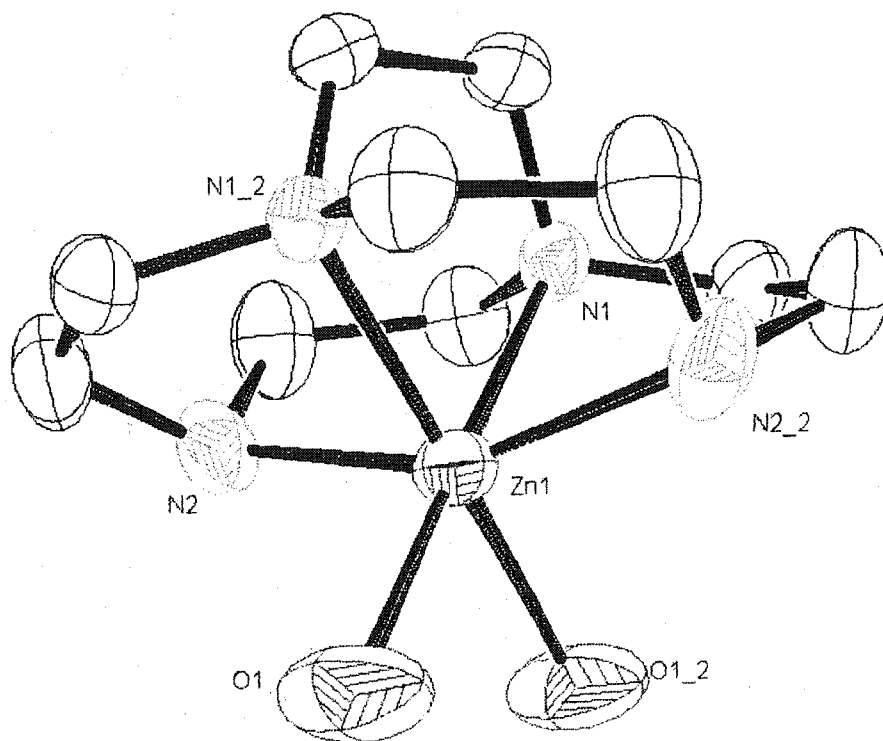


**Figure 2.32** X-ray structure of  $[\text{Zn}\cdot 2(\text{H}_2\text{O})_2](\text{ClO}_4)_2$  (122) showing atomic labeling scheme. Hydrogens bonded to carbons are omitted for clarity.

This is manifested in the increased protrusion of the cation out from the ligand cleft as the N(ax)-Zn-N(ax) angle is compressed to only  $156.8(3)^\circ$ . Contrary to previous literature data,<sup>26(a),29(g)</sup> the secondary N(ax)-Zn and tertiary N(eq)-Zn distances are essentially the same at  $2.133(5)\text{\AA}$  and  $2.139(4)\text{\AA}$  respectively. Although there are numerous structural reports of zinc complexes with cyclen and its pendant-armed derivatives in the literature, almost all of these have the *trans-I* ligand configuration with all four amine substituents on the same side of the macrocycle as zinc.<sup>29(a-l)</sup> In contrast, only two examples of *cis-I*



ligand configuration are available. These have pseudo-octahedral geometry with N(ax)-Zn-N(ax) angles of 153-154° and equatorial N-Zn-N angles of 108-109°. <sup>23(d),115</sup>

**Table 2.7(e)** Selected Bond Distances (Å) and Bond Angles (deg) in [Zn•2(H<sub>2</sub>O)<sub>2</sub>](ClO<sub>4</sub>)<sub>2</sub> (**122**).

Zn(1)-O(1)	2.123(4)	Zn(1)-O(1A)	2.123(4)
Zn(1)-N(2)	2.133(5)	Zn(1)-N(2A)	2.133(5)
Zn(1)-N(1)	2.139(4)	Zn(1)-N(1A)	2.139(4)
O(1)-Zn(1)-N(2A)	100.1(2)	O(1A)-Zn(1)-N(2)	100.1(2)
O(1)-Zn(1)-N(2)	96.7(2)	O(1A)-Zn(1)-N(2A)	96.7(2)
O(1)-Zn(1)-N(1A)	95.34(16)	O(1A)-Zn(1)-N(1)	95.34(16)
O(1)-Zn(1)-N(1)	175.83(18)	O(1A)-Zn(1)-N(1A)	175.83(18)
O(1)-Zn(1)-O(1A)	86.5(2)	N(2)-Zn(1)-N(2A)	156.8(3)
N(2)-Zn(1)-N(1)	83.40(18)	N(2A)-Zn(1)-N(1A)	83.40(18)
N(2)-Zn(1)-N(1A)	79.26(18)	N(2A)-Zn(1)-N(1)	79.26(18)
N(1)-Zn(1)-N(1A)	83.08(19)		

The favored coordination number of these cyclen Zn(II) complexes is five<sup>29(a),(d),(h-  
j)</sup> whereas six is found in the cross-bridged cyclen complex, [Zn(H<sub>2</sub>O)<sub>2</sub>•2](ClO<sub>4</sub>)<sub>2</sub>. The coordination geometry around Zn(II) center is again a pseudo-octahedron. Two *cis*-aqua

ligands complete the metal coordination sphere. Literature data of the X-ray structure of (trimethyltriazacyclononane)triazozinc(II) nitrate revealed a *cis*-N<sub>3</sub>O<sub>3</sub> coordination set.<sup>110</sup> However, no polyamine zinc complex structure with a *cis*-N<sub>4</sub>O<sub>2</sub> donor geometry has been reported. Two *bis*-phenanthroline complexes of Zn(II) with similar *cis*-aqua ligands are known.<sup>116,117</sup> These have Zn-O distances ranging from 2.04 to 2.14 Å compared to 2.123(4) Å here. Their N(ax)-Zn-N(ax) angles are less strained at 162-169° and their Zn-N bondlengths range from 2.14 to 2.21 Å.

ZnCl<sub>2</sub>•4 (124). This monomeric complex has the structure shown in Figure 2.33. Again

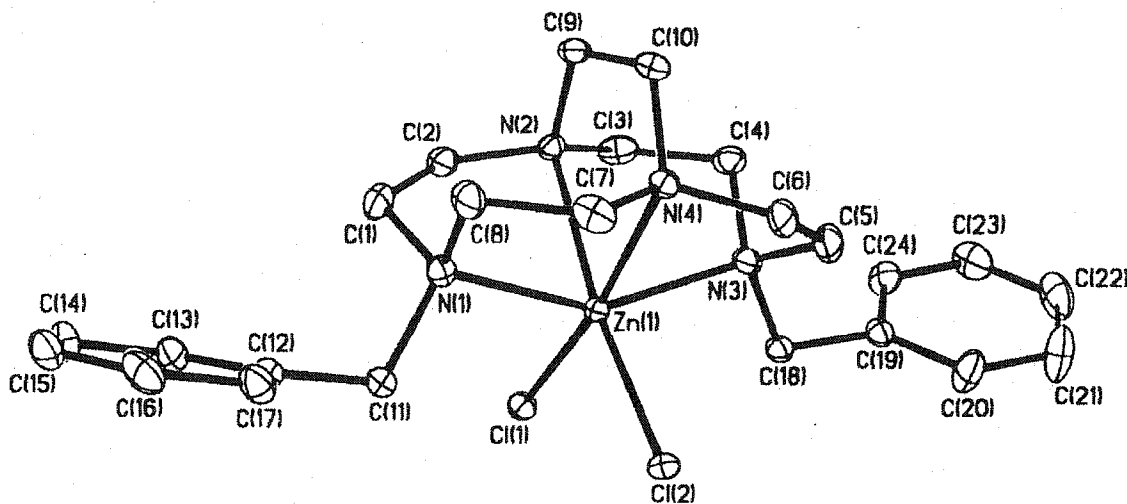


**Figure 2.33** X-ray structure of ZnCl<sub>2</sub>•4 (124) showing atomic labeling scheme. Hydrogens bonded to carbons are omitted for clarity.

the coordination geometry around this Zn(II) center is a pseudo-octahedron as evidenced by the N(ax)-Zn-N(ax) angle of only 152.6(1)° and the constrained N(eq)-Zn-N(eq) angle

of 77.61(8)°. For comparison, the corresponding angles for  $\text{Zn}\cdot\mathbf{3}(\mu\text{-Cl}_2\text{ZnCl}_2)$  are 171.1(2)° and 83.5(3)° respectively. The two terminal chlorides here are 2.36-2.39Å away from zinc and they subtend an obtuse Cl-Zn-Cl angle of 95.50(3)°. Again, a *Cambridge Crystallographic Database* search revealed no previous report for Zn(II) complexes of any mono, di, tri or tetra N-benzylated cyclen derivative.

**Table 2.7(f)** Selected Bond Distances (Å) and Bond Angles (deg) in  $\text{ZnCl}_2\cdot\mathbf{4}$  (**124**).

Zn(1)-N(1)	2.241(2)	Zn(1)-N(2)	2.231(2)
Zn(1)-N(3)	2.201(2)	Zn(1)-N(4)	2.231(2)
Zn(1)-Cl(1)	2.3874(7)	Zn(1)-Cl(2)	2.3603(7)
N(3)-Zn(1)-N(1)	152.61(9)	N(3)-Zn(1)-N(4)	77.98(8)
N(3)-Zn(1)-N(2)	81.44(9)	N(4)-Zn(1)-N(2)	77.61(8)
N(4)-Zn(1)-N(1)	81.04(9)	N(2)-Zn(1)-N(1)	77.00(9)
N(3)-Zn(1)-Cl(2)	95.37(7)	N(4)-Zn(1)-Cl(2)	92.44(6)
N(2)-Zn(1)-Cl(2)	169.96(6)	N(1)-Zn(1)-Cl(2)	102.95(7)
N(3)-Zn(1)-Cl(1)	101.04(7)	N(4)-Zn(1)-Cl(1)	172.07(6)
N(2)-Zn(1)-Cl(1)	94.46(6)	N(1)-Zn(1)-Cl(1)	97.31(7)
Cl(2)-Zn(1)-Cl(1)	95.50(3)		

### 3.2 The Five Cd(II) Complexes:

$\text{CdCl}_2 \cdot 1$  (125). The structure of this complex confirms the significantly poorer fit of this larger cation inside the ligand cleft (Figure 2.34) as shown by the N(ax)-Cd-N(ax)

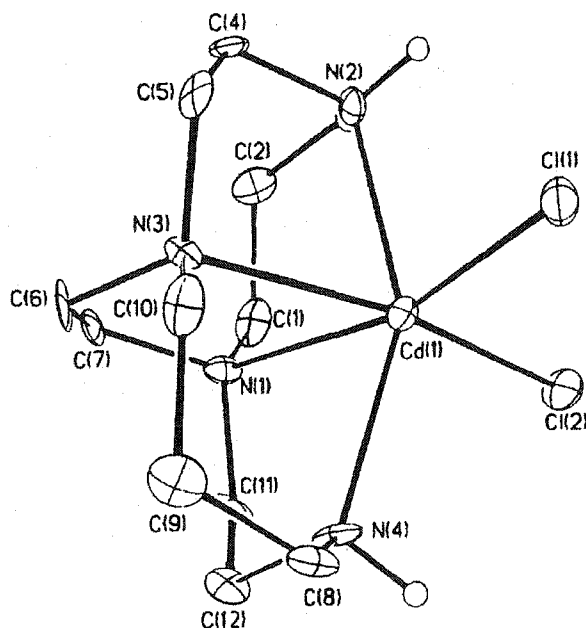


**Figure 2.34** X-ray structure of  $\text{CdCl}_2 \cdot 1$  (125) showing atomic labeling scheme. Hydrogens bonded to carbons are omitted for clarity.

angle of  $151.5(5)^\circ$  and N(eq)-Cd-N(eq) angle of  $71.5(5)^\circ$ . Its two Cd-Cl distances are similar at  $2.570(2)\text{\AA}$  and  $2.580(1)\text{\AA}$  respectively. Again, the secondary N(ax)-Cd bonds averaging  $2.33\text{\AA}$  are shorter than the tertiary N(eq)-Cd average of  $2.48\text{\AA}$ . A pentacyclic hexaamine complex of  $\text{CdCl}_2$  has been reported having the same *cis*- $\text{N}_4\text{Cl}_2$  donor set.<sup>118(a)</sup> This contains shorter Cd-Cl bonds of  $2.468(1)\text{\AA}$ , similar secondary N-Cd distances of  $2.369(2)\text{\AA}$ , and longer tertiary N-Cd bondlengths of  $2.625(2)\text{\AA}$ . However, its respective

N(ax)-Cd-N(ax) and N(eq)-Cd-N(eq) angles are even more severely distorted at 121.51(1)° and 59.8(1)°.

**Table 2.7(g)** Selected Bond Distances (Å) and Bond Angles (deg) in CdCl<sub>2</sub>•1 (125).

Cd(1)-N(1)	2.479(11)	Cd(1)-N(2)	2.329(11)
Cd(1)-N(3)	2.489(10)	Cd(1)-N(4)	2.324(12)
Cd(1)-Cl(1)	2.570(4)	Cd(1)-Cl(2)	2.530(4)
N(2)-Cd(1)-N(4)	151.5(6)	N(1)-Cd(1)-N(2)	80.2(4)
N(1)-Cd(1)-N(3)	71.5(4)	N(1)-Cd(1)-N(4)	76.6(4)
N(2)-Cd(1)-N(3)	76.2(4)	N(3)-Cd(1)-N(4)	81.0(4)
N(1)-Cd(1)-Cl(1)	162.8(3)	N(2)-Cd(1)-Cl(1)	92.0(3)
N(3)-Cd(1)-Cl(1)	91.8(3)	N(4)-Cd(1)-Cl(1)	105.50
N(1)-Cd(1)-Cl(2)	95.0(3)	N(2)-Cd(1)-Cl(2)	103.5(3)
N(3)-Cd(1)-Cl(2)	166.4(3)	N(4)-Cd(1)-Cl(2)	94.7(3)
Cl(2)-Cd(1)-Cl(1)	101.79(13)		

A cyclam derivative, 6,13,-Dimethyl-1,4,8,11-tetraazacyclotetradecane-6,13-diamine, also adopts a *cis*-folded configuration in its Cd(II) complex (73 in **Figure 1.26**).<sup>43(a)</sup> It has a very distorted N(ax)-Cd-N(ax) angle of 141.03° and a less distorted N(eq)-Cd-N(eq) angle of 91.73°. The distances between its four cyclam nitrogen atoms

and Cd range from 2.411 Å to 2.422 Å. The structures of two tetramethyl-cyclam complexes of Cd adopt the familiar *trans-I* ligand configuration with tertiary N-Cd distances of 2.34-2.38 Å, axial N-Cd-N angles in the ranges 156-157°, and equatorial angles of 129°. <sup>43(c)</sup>

**CdCl<sub>2</sub>•2 (129).** With the smaller cross-bridged cyclen **2**, the cation protrudes even further from the ligand cleft (**Figure 2.35**). An axial angle of 137.2(6)° reveals how

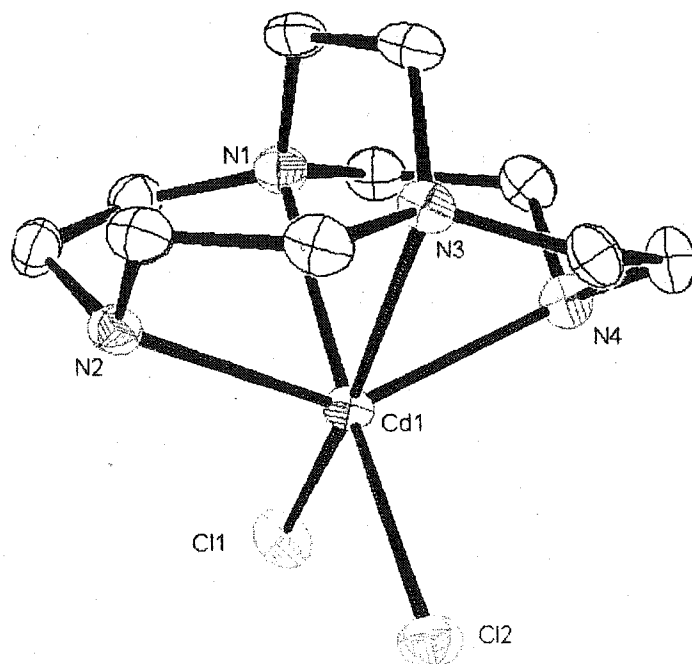


**Figure 2.35** X-ray structure of CdCl<sub>2</sub>•2 (**129**) showing atomic labeling scheme. Hydrogens bonded to carbons are omitted for clarity.

distorted this 6-coordinated geometry is away from an idealized octahedral geometry. Similar to those of CdCl<sub>2</sub>•1, the terminal Cl-Cd bond lengths average 2.525 Å while the secondary N(ax)-Cd and tertiary N(eq)-Cd distances average 2.36 Å and 2.47 Å

respectively. Four CdCl<sub>2</sub> complexes have been reported having the same *cis*-N<sub>4</sub>Cl<sub>2</sub> donor set.<sup>118(a-d)</sup> Their Cd-Cl bonds vary from 2.468 Å to 2.533 Å. Only two Cd complexes of the parent ligand cyclen have had their structures determined.<sup>44(a)</sup> Both of these feature the ligand in a *trans*-I configuration with Cd-N bonds ranging from 2.28 to 2.38Å.

**Table 2.7(h)** Selected Bond Distances (Å) and Bond Angles (deg) in CdCl<sub>2</sub>•2 (129).

Cd(1)-N(1)	2.468(2)	Cd(1)-N(2)	2.388(2)
Cd(1)-N(3)	2.456(2)	Cd(1)-N(4)	2.367(2)
Cd(1)-Cl(1)	2.4924(6)	Cd(1)-Cl(2)	2.5328(6)
N(2)-Cd(1)-N(4)	137.57(7)	N(1)-Cd(1)-N(2)	70.63(7)
N(1)-Cd(1)-N(3)	71.02(7)	N(1)-Cd(1)-N(4)	74.73(7)
N(2)-Cd(1)-N(3)	74.33(7)	N(3)-Cd(1)-N(4)	71.31(7)
N(1)-Cd(1)-Cl(1)	96.95(5)	N(2)-Cd(1)-Cl(1)	106.87(6)
N(3)-Cd(1)-Cl(1)	165.99(5)	N(4)-Cd(1)-Cl(1)	100.87(6)
N(1)-Cd(1)-Cl(2)	163.43(5)	N(2)-Cd(1)-Cl(2)	101.08(6)
N(3)-Cd(1)-Cl(2)	94.14(5)	N(4)-Cd(1)-Cl(2)	105.46(6)
Cl(2)-Cd(1)-Cl(1)	99.24(2)		

[Cd•2( $\eta^2$ -NO<sub>3</sub>)<sub>2</sub>] (131). This structure contains a nominally eight-coordinate cadmium(II) fully coordinated to ligand 2 as well as two chelating nitrate counterions (Figure 2.36). This is the only example of a metal complex of any cross-bridged ligands

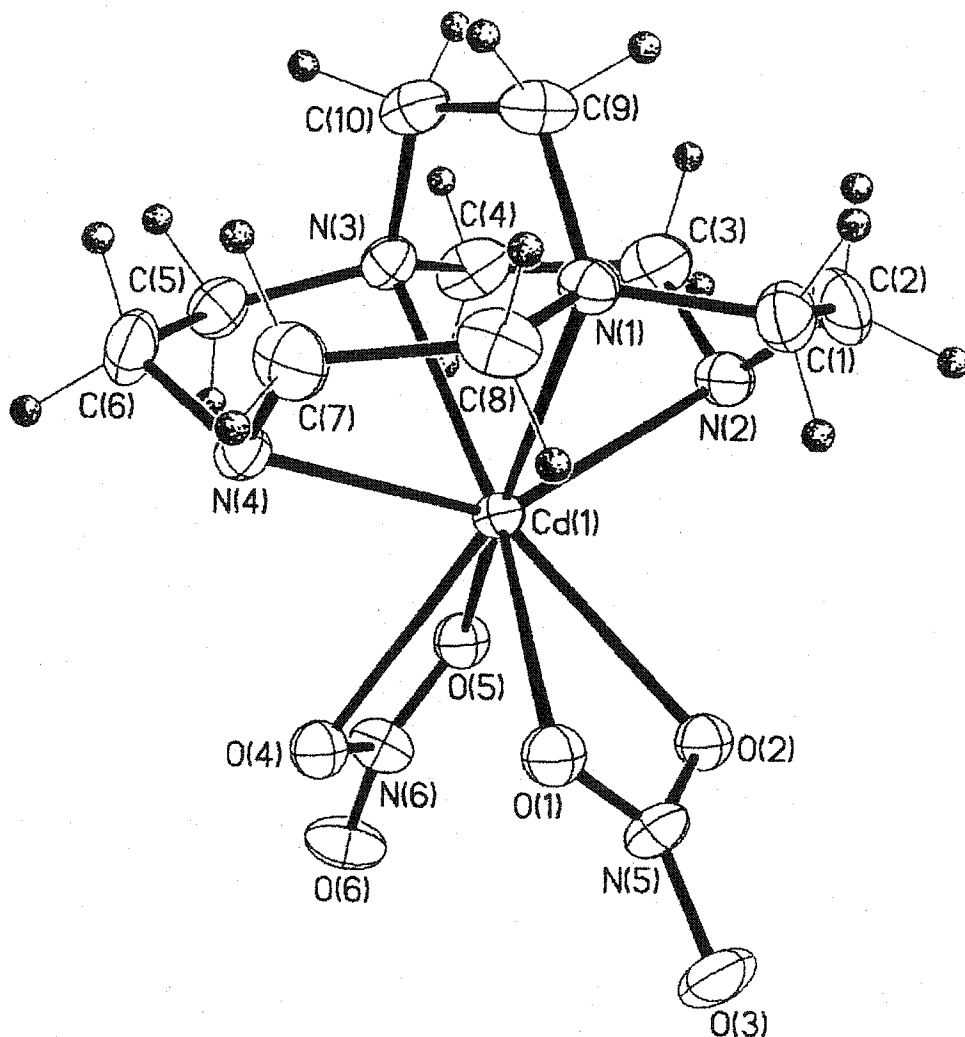


**Figure 2.36** X-ray structure of [Cd•2( $\eta^2$ -NO<sub>3</sub>)<sub>2</sub>] (131) showing atomic labeling scheme.

with a coordination number of eight. All its Cd-N distances are within 2.37-2.39 Å. Two identical bidentate nitrates here have Cd-O distances of 2.533 Å and 2.541 Å. Again, the



**Table 2.7(i)** Selected Bond Distances (Å) and Bond Angles (deg) in  $[\text{Cd}\cdot 2(\eta^2\text{-NO}_3)_2]$  (130).

Cd(1)-N(1)	2.393(4)	Cd(1)-N(2)	2.377(5)
Cd(1)-N(3)	2.393(5)	Cd(1)-N(4)	2.369(5)
Cd(1)-O(1)	2.533(11)	Cd(1)-O(2)	2.390(9)
Cd(1)-O(4)	2.511(9)	Cd(1)-O(5)	2.517(10)
N(2)-Cd(1)-N(4)	138.80(19)	N(1)-Cd(1)-N(2)	72.96(18)
N(1)-Cd(1)-N(3)	72.40(17)	N(1)-Cd(1)-N(4)	74.13(19)
N(2)-Cd(1)-N(3)	74.25(17)	N(3)-Cd(1)-N(4)	72.69(18)
N(1)-Cd(1)-O(1)	91.6(4)	N(2)-Cd(1)-O(1)	120.9(3)
N(3)-Cd(1)-O(1)	154.3(3)	N(4)-Cd(1)-O(1)	83.9(3)
N(1)-Cd(1)-O(2)	110.6(4)	N(2)-Cd(1)-O(2)	81.1(2)
N(3)-Cd(1)-O(2)	153.1(3)	N(4)-Cd(1)-O(2)	134.2(3)
N(1)-Cd(1)-O(4)	152.9(2)	N(2)-Cd(1)-O(4)	134.1(3)
N(3)-Cd(1)-O(4)	110.4(4)	N(4)-Cd(1)-O(4)	81.0(3)
N(1)-Cd(1)-O(5)	155.5(3)	N(2)-Cd(1)-O(5)	85.8(3)
N(3)-Cd(1)-O(5)	90.5(4)	N(4)-Cd(1)-O(5)	118.2(3)
O(1)-Cd(1)-O(2)	51.1(4)	O(1)-Cd(1)-O(4)	75.0(6)
O(1)-Cd(1)-O(5)	110.1(5)	O(2)-Cd(1)-O(4)	79.5(5)
O(2)-Cd(1)-O(5)	77.0(5)	O(4)-Cd(1)-O(5)	49.4(3)



**Table 2.7(j)** Selected Bond Distances (Å) and Bond Angles (deg) in CdCl<sub>2</sub>•3  
(128).

Cd(1)-N(1)	2.404(3)	Cd(1)-N(2)	2.439(3)
Cd(1)-N(1A)	2.404(3)	Cd(1)-N(2A)	2.439(3)
Cd(1)-Cl(1)	2.5268(8)	Cd(1)-Cl(1A)	2.5268(8)
N(2)-Cd(1)-N(2A)	158.51(13)	N(1)-Cd(1)-N(2)	74.79(10)
N(1)-Cd(1)-N(1A)	75.10(14)	N(1)-Cd(1)-N(2A)	88.09(10)
N(2)-Cd(1)-N(1A)	88.09(10)	N(1A)-Cd(1)-N(2A)	74.79(10)
N(1)-Cd(1)-Cl(1)	94.46(7)	N(2)-Cd(1)-Cl(1)	101.44(7)
N(1A)-Cd(1)-Cl(1)	163.67(8)	N(2A)-Cd(1)-Cl(1)	92.61(7)
N(1)-Cd(1)-Cl(1A)	163.67(8)	N(2)-Cd(1)-Cl(1A)	92.61(7)
N(1A)-Cd(1)-Cl(1A)	94.46(8)	N(2A)-Cd(1)-Cl(1A)	101.44(7)
Cl(1A)-Cd(1)-Cl(1)	98.27(4)		

structure of a Cd(II) chloride complex with (1,4,8,11-tetrakis(2-naphthylmethyl)-1,4,8,11-tetraazacyclotetradecane) has a square-pyramidal geometry in which Cd(II) is coordinated by four nitrogen donors from *trans*-I ligand and one terminal chloride. The Cd-N distances are between 2.34-2.37Å and the Cd-Cl bonds are 2.46Å long.<sup>44(b)</sup> The X-ray structure of a cadmium nitrate complex of 1,8-N,N'-dibenzylated cyclam derivative features a six-coordinated Cd(II) center. The dibenzylated cyclam in this complex has a

*trans-I* configuration.<sup>43(d)</sup> The bondlengths between the Cd(II) center and two tertiary amine nitrogens of 2.3718(16) and 2.3692(16) Å are basically the same as those in CdCl<sub>2</sub>•3. A similar Cd(II) complex of a 1,4-N,N''-dibenzylated cyclam derivative incorporating the ligand in a *trans-I* configuration has also been reported.<sup>43(d)</sup>

**CdCl<sub>2</sub>•4 (132).** The geometry of this complex is quite similar to both CdCl<sub>2</sub>•2 and CdCl<sub>2</sub>•3 with the axial N-Cd-N at 137.95(11)° and equatorial N-Cd-N of 69.77(11)° (**Figure 2.38**). All Cd-N distances are within 2.44-2.46Å and the Cd-Cl bonds are 2.056(7) Å long.

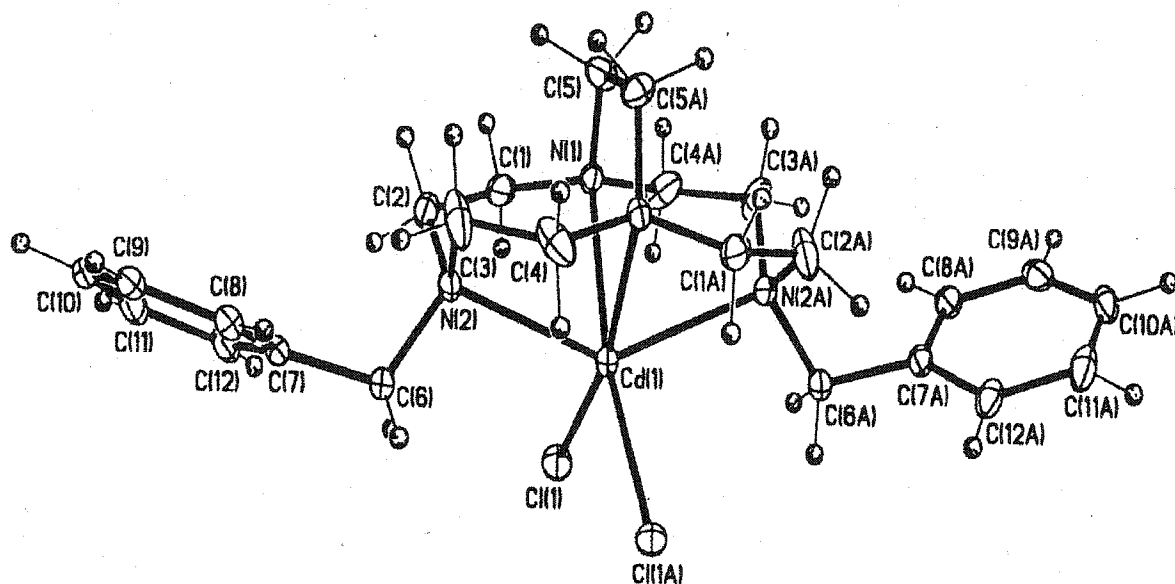


**Figure 2.38** X-ray structure of CdCl<sub>2</sub>•4 (132) showing atomic labeling scheme.

**Table 2.7(k)** Selected Bond Distances (Å) and Bond Angles (deg) in CdCl<sub>2</sub>•4 (132).

Cd(1)-N(1)	2.445(2)	Cd(1)-N(2)	2.463(2)
Cd(1)-N(1A)	2.445(2)	Cd(1)-N(2A)	2.463(2)
Cd(1)-Cl(1)	2.5056(7)	Cd(1)-Cl(1A)	2.5056(7)
<hr/>			
N(2)-Cd(1)-N(2A)	137.95(11)	N(1)-Cd(1)-N(2)	71.73(8)
N(1)-Cd(1)-N(1A)	69.77(11)	N(1)-Cd(1)-N(2A)	74.03(7)
N(2)-Cd(1)-N(1A)	74.03(8)	N(1A)-Cd(1)-N(2A)	71.73(8)
N(1)-Cd(1)-Cl(1)	96.45(6)	N(2)-Cd(1)-Cl(1)	96.98(6)
N(1A)-Cd(1)-Cl(1)	165.21(6)	N(2A)-Cd(1)-Cl(1)	110.51(6)
N(1)-Cd(1)-Cl(1A)	165.21(6)	N(2)-Cd(1)-Cl(1A)	110.51(6)
N(1A)-Cd(1)-Cl(1A)	96.45(6)	N(2A)-Cd(1)-Cl(1A)	96.98(6)
Cl(1A)-Cd(1)-Cl(1)	97.73(4)		

### 3.3 The Three Hg(II) Complexes:

[HgCl<sub>2</sub>(μ-1)]<sub>2</sub> (133). As shown by its solid-state structure (Figure 2.39), this structure represents the first confirmation of an *exo*-coordination mode for a cross-bridged tetraamine. This is a dimeric Hg(II) complex in which each ligand bridges two Hg(II) centers by using only the secondary amine nitrogens. The geometry around each cation can be described as highly-distorted tetrahedral with a small Cl-Hg-Cl angle of 103.45(8)° and large N-Hg-N angle of 138.2(2)°. The Hg-N bondlengths are 2.237(8)Å

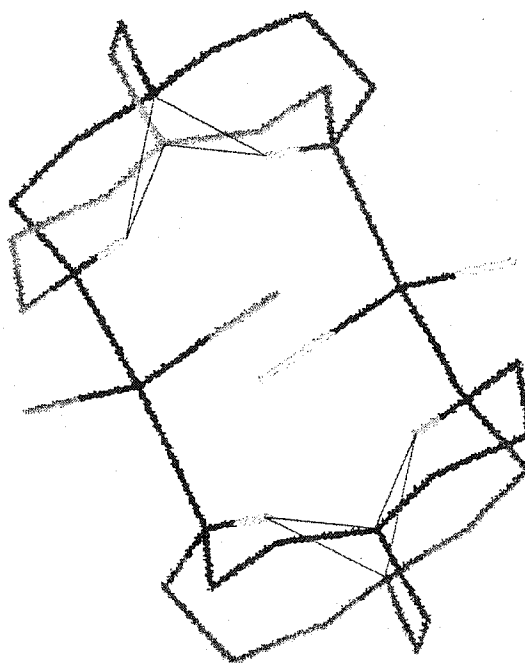
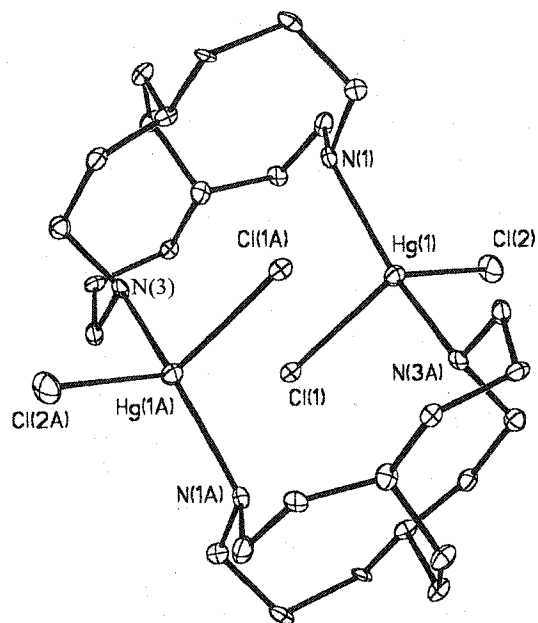


**Figure 2.39** X-ray structure of  $[\text{HgCl}_2(\mu\text{-1})]_2$  (133). The top one is an ORTEP view and the bottom one shows the intramolecular hydrogen bonding.

and 2.264(8)Å while the Hg-Cl distances are 2.522(3)Å and 2.572(2)Å. The two Hg(II) centers are 4.26Å apart. Each metal is also positioned only 3.23Å away from one chloride of the adjacent HgCl<sub>2</sub> moiety. Since three literature examples of long Hg-Cl bond distances between 3.301 Å and 3.385 Å are known,<sup>121(a-c)</sup> an alternative description of these as distorted trigonal bipyramidal Hg(II) coordination spheres is also feasible.

**Table 2.7(I)** Selected Bond Distances (Å) and Bond Angles (deg) in [HgCl<sub>2</sub>(μ-1)]<sub>2</sub> (133).

Hg(1)-N(1)	2.237(8)	Hg(1A)-N(1A)	2.237(8)
Hg(1)-N(3A)	2.264(8)	Hg(1A)-N(3)	2.237(8)
Hg(1)-Cl(1)	2.572(2)	Hg(1A)-Cl(1A)	2.572(2)
Hg(1)-Cl(2)	2.522(3)	Hg(1A)-Cl(2A)	2.522(3)
N(1)-Hg(1)-N(3A)	138.2(3)	N(1A)-Hg(1)-N(3)	138.2(3)
N(1)-Hg(1)-Cl(2)	105.8(2)	N(1A)-Hg(1A)-Cl(2A)	105.8(2)
N(3A)-Hg(1)-Cl(2)	102.9(2)	N(3)-Hg(1A)-Cl(2A)	102.9(2)
N(1)-Hg(1)-Cl(1)	101.74(19)	N(1A)-Hg(1A)-Cl(1A)	101.74(19)
N(3A)-Hg(1)-Cl(1)	100.3(2)	N(3)-Hg(1A)-Cl(1A)	100.3(2)
Cl(2)-Hg(1)-Cl(1)	103.45(8)	Cl(2A)-Hg(1A)-Cl(1A)	103.45(8)
N(1A)-Hg(1)-Cl(1A)	96.45(6)	N(2A)-Hg(1)-Cl(1A)	96.98(6)
Cl(1A)-Hg(1)-Cl(1)	97.73(4)		

Both ligand secondary N-H hydrogens lie inside the ligand cleft and are stabilized by transannular hydrogen-bonding (calculated H...N distances of 2.07-2.48 Å) with the tertiary N lone pairs. Again the distorted [2323]/[2323] diamond lattice *cis*-folded ligand configuration is adopted. A Hg(II) complex of cyclam shows a square-pyramidal geometry in which Hg(II) is coordinated by four amine nitrogen donors from a *trans-I* cyclam and one terminal chloride.<sup>45(a)</sup> The Hg-N bondlengths in this complex vary from 2.277 Å to 2.421 Å, which are all longer than those in [HgCl<sub>2</sub>(μ-1)]<sub>2</sub>. The counterion for this cationic mercury cyclam complex is HgCl<sub>4</sub><sup>2-</sup>. Though not strictly analogous, a structure of a diamine derivative of cyclam bridging two HgCl<sub>2</sub> units has also been reported (77 in **Figure 1.30**).<sup>45(b)</sup>

**HgCl<sub>2</sub>•2 (134).** Contrary to the favored formation of mercuric complexes with low coordination numbers,<sup>122</sup> the X-ray structure of HgCl<sub>2</sub>•2 features a severely distorted O<sub>h</sub> geometry. This structure contains two independent 1:1 complexes with very similar bonding details. Only one of these will be discussed here (**Figure 2.40**). It features the most distended metal cation within a cross-bridged tetraamine ligand cleft we have observed to date. The axial N-Hg-N angle is only 133.4(3)° and equatorial N-Hg-N angle is down to 66.7(3)°. The two secondary amine N(ax)-Hg bonds are 2.398(11)Å and 2.418(9)Å while the tertiary amine N(eq)-Hg distances are further lengthened to 2.556(6)Å and 2.572(7)Å. One of the two terminal *cis*-chlorides is disordered over two sites (Cl(1) and Cl(1A)). The Hg-Cl distances are 2.547(11)Å and 2.568(9)Å, relatively long for terminal Hg-Cl bondlengths which are typically between 2.32-2.54Å. No X-ray structure of Hg(II) complexes with either cyclen or its derivatives has yet been reported.



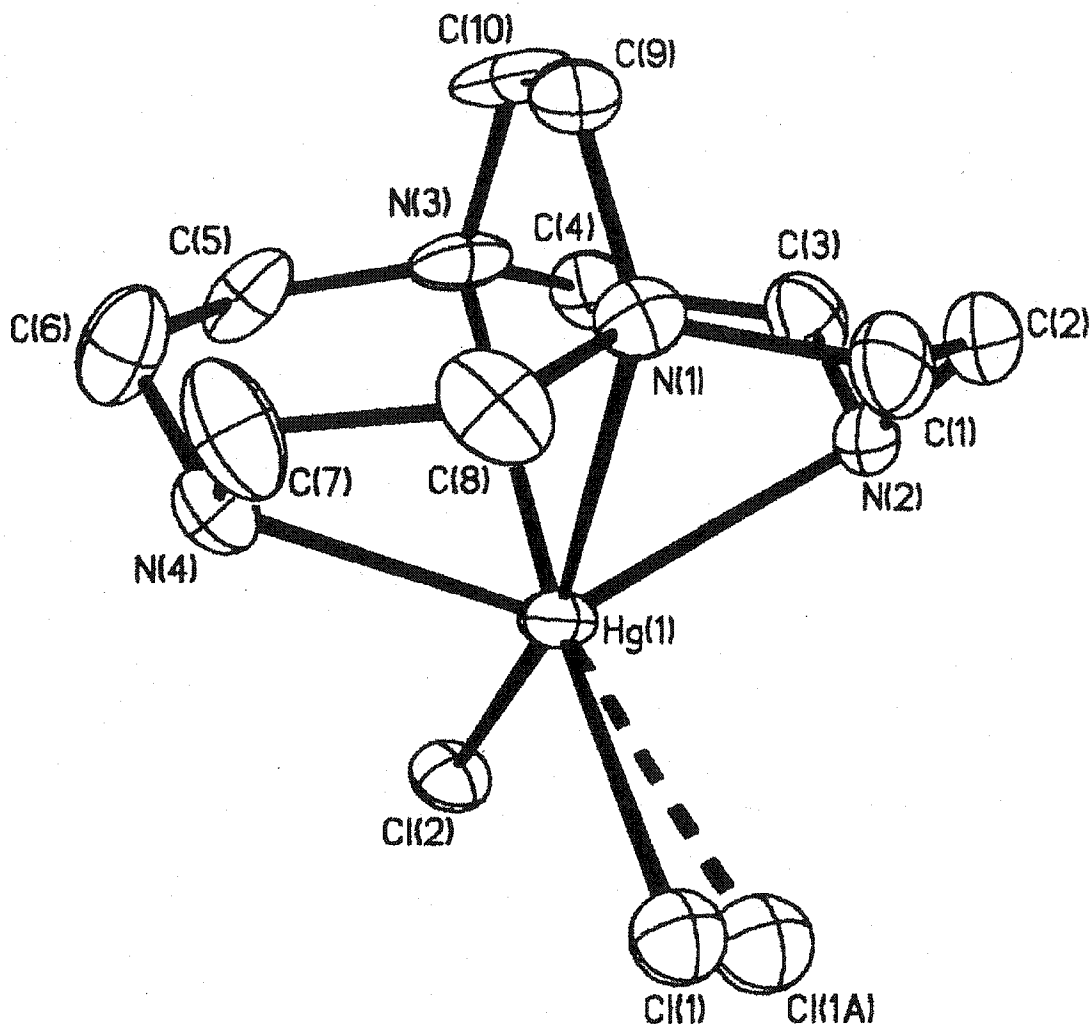


**Figure 2.40** An ORTEP view of the X-ray structure of  $\text{HgCl}_2 \cdot 2$  (123) showing one disordered terminal chloride.

Of the three  $\text{HgCl}_2$  complexes of macrocyclic tetraamines and their derivatives in the *Cambridge Crystallographic Database*,<sup>45(a),45(c),123</sup> only one has a *cis*-folded ligand conformation.<sup>45(c)</sup> Without a cross-bridging ethylene, this hexamethyl-cyclam complex has an axial N-Hg-N angle of  $156.53^\circ$  and equatorial N-Hg-N angle of  $89.45^\circ$ . Its secondary amine N(ax)-Hg bonds are corresponding shorter at only  $2.275\text{\AA}$ .

**Table 2.7(m)** Selected Bond Distances (Å) and Bond Angles (deg) in  $\text{HgCl}_2 \cdot 2$  (134).

Hg(1)-N(1)	2.568(9)	Hg(1)-N(2)	2.418(9)
Hg(1)-N(3)	2.572(7)	Hg(1)-N(4)	2.398(11)
Hg(1)-Cl(1)	2.556(6)	Hg(1)-Cl(1A)	2.547(11)
Hg(1)-Cl(2)	2.541(3)	Cl(1)-Cl(1A)	0.750(13)
N(2)-Hg(1)-N(4)	133.4(3)	N(1)-Hg(1)-N(2)	71.8(3)
N(1)-Hg(1)-N(3)	66.7(3)	N(1)-Hg(1)-N(4)	70.4(4)
N(2)-Hg(1)-N(3)	70.9(4)	N(3)-Hg(1)-N(4)	69.8(5)
N(1)-Hg(1)-Cl(1)	92.3(2)	N(2)-Hg(1)-Cl(1)	107.3(3)
N(3)-Hg(1)-Cl(1)	158.7(3)	N(4)-Hg(1)-Cl(1)	100.4(3)
N(1)-Hg(1)-Cl(1A)	100.0(3)	N(2)-Hg(1)-Cl(1A)	95.3(4)
N(3)-Hg(1)-Cl(1A)	163.0(4)	N(4)-Hg(1)-Cl(1A)	117.1(5)
N(1)-Hg(1)-Cl(2)	161.5(2)	N(2)-Hg(1)-Cl(2)	103.4(3)
N(3)-Hg(1)-Cl(2)	94.8(2)	N(4)-Hg(1)-Cl(2)	103.9(3)
Cl(2)-Hg(1)-Cl(1A)	98.2(3)	Cl(2)-Cl(1)-Cl(1)	106.08(18)
Cl(1A)-Hg(1)-Cl(1)	16.9(3)	Cl(1A)-Cl(1)-Hg(1)	80.9(10)
Cl(1)-Cl(1A)-Hg(1)	82.2(11)		

$(\text{HgCl}_2)_6 \cdot (2)_4$  (135). This structure contains two independent ligand 2-coordinated Hg(II) centers (**Figure 2.41** and **Figure 2.42**). Stoichiometrically, the ratio of the cationic

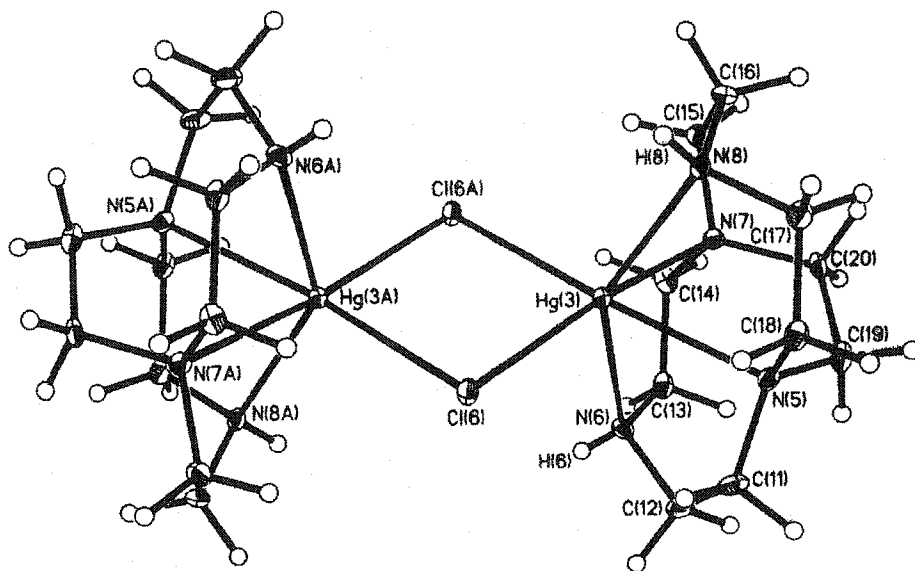


**Figure 2.41** Structure of the cationic  $[\text{Hg} \cdot 2(\mu\text{-Cl})]_2^{2+}$  part of  $(\text{HgCl}_2)_6 \cdot (2)_4$  (135), showing atomic labeling scheme.

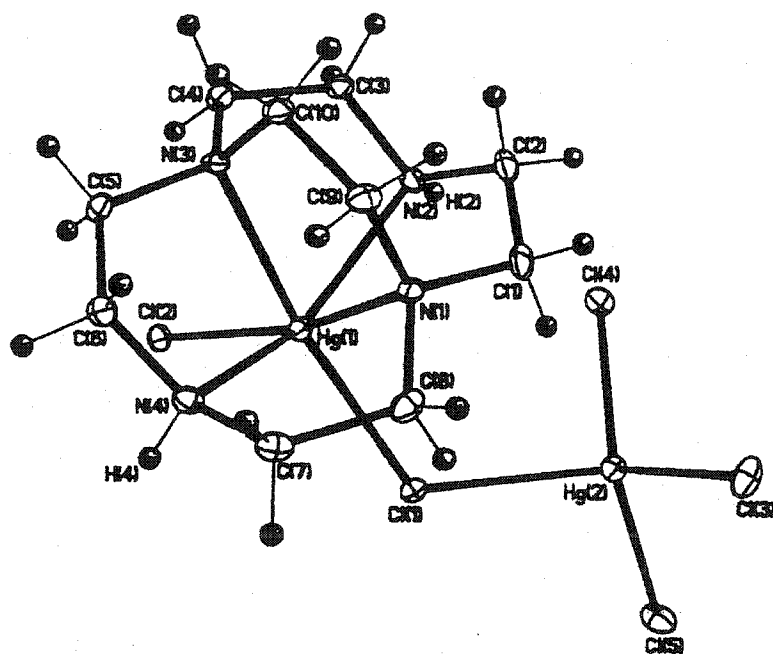


**Figure 2.42** X-ray Structure of the anionic  $[\text{Hg} \cdot 2\text{Cl}(\mu\text{-Cl})(\text{HgCl}_3)]^-$  part of  $(\text{HgCl}_2)_6 \cdot (2)_4$  (135), showing atomic labeling scheme.

Hg(II) unit in **Figure 2.41** to the anionic Hg(II) unit in **Figure 2.42** is 2:1. So  $(\text{HgCl}_2)_6 \cdot (\mathbf{2})_4$  can be better expressed by the formula  $[\text{Hg} \cdot \mathbf{2}(\mu\text{-Cl})]_2[\text{Hg} \cdot \mathbf{2}(\text{Cl})(\mu\text{-Cl})(\text{HgCl}_3)]_2$ . Similar to  $\text{HgCl}_2 \cdot \mathbf{2}$  and  $[\text{HgCl}_2(\mu\text{-1})]_2$ , there is no uncoordinated ionic chloride present in this structure. The most interesting part of this is the cationic Hg(II) center (**Figure 2.41**). This is the only example of a dimeric mercury(II) complex of any macrocyclic ligand bridged by one or two ancillary ligands. The axial N-Hg-N angle is  $138.82(14)^\circ$  and equatorial N-Hg-N angle is  $71.63(13)^\circ$ . The two secondary amine N(ax)-Hg bonds are  $2.407(4)\text{\AA}$  and  $2.444(4)\text{\AA}$  while the tertiary amine N(eq)-Hg distances are slightly lengthened to  $2.481(3)\text{\AA}$  and  $2.516(4)\text{\AA}$ . The distance between Hg and its bridging chloride is  $2.7693(11)\text{\AA}$ . The most closely-related structure in the literature is the dimeric  $[\text{Hg} \cdot \text{L}(\mu\text{-Cl})\text{Cl}]_2$  (L = 2-(2-pyridyl)quinoxaline).<sup>124</sup> The distances between two five-coordinate Hg(II) centers and one of two bridging chlorides are  $2.500(4)\text{\AA}$  and  $2.742(3)\text{\AA}$ . The anionic Hg(II) unit (**Figure 2.42**) in  $(\text{HgCl}_2)_6 \cdot (\mathbf{2})_4$  shows a Hg(II) center coordinated by four amine nitrogens from ligand **2**, one terminal chloride, and one bridging chloride from  $\text{HgCl}_4^{2-}$ . The N(ax)-Hg-N(ax) angle of  $135.50(14)^\circ$  and N(eq)-Hg-N(eq) angle of  $69.50(12)^\circ$  reflect an even poorer fit of Hg(II) in the coordinated **2** in this unit than in the cationic Hg(II) unit.

**Table 2.7(n)** Selected Bond Distances (Å) and Bond Angles (deg) in cationic  $[\text{Hg}\cdot 2(\mu\text{-Cl})]_2$  part of  $(\text{HgCl}_2)_6\cdot(2)_4$  (135).

Hg(3)-N(5)	2.468(4)	Hg(3)-N(6)	2.432(4)
Hg(3)-N(7)	2.428(3)	Hg(3)-N(8)	2.352(4)
Hg(3)-Cl(6)	2.4789(10)	Hg(3A)-Cl(6)	2.7963(11)
Cl(6A)-Hg(3)	2.7963(11)		
N(6)-Hg(3)-N(8)	138.82(14)	N(7)-Hg(3)-N(8)	72.30(18)
N(6)-Hg(3)-N(7)	76.63(13)	N(5)-Hg(3)-N(8)	75.78(13)
N(5)-Hg(3)-N(7)	71.63(13)	N(5)-Hg(3)-N(6)	70.98(13)
N(8)-Hg(3)-Cl(6)	118.95(10)	N(7)-Hg(3)-Cl(6)	168.65(9)
N(6)-Hg(3)-Cl(6)	94.51(10)	N(5)-Hg(3)-Cl(6)	108.39(9)
N(8)-Hg(3)-Cl(6A)	108.32(11)	N(7)-Hg(3)-Cl(6A)	89.71(9)
N(6)-Hg(3)-Cl(6A)	95.26(10)	N(5)-Hg(3)-Cl(6A)	158.98(9)
Cl(6)-Hg(3)-Cl(6A)	87.98(3)	Hg(3)-Cl(6)-Hg(3A)	92.02(3)

**Table 2.7(o)** Selected Bond Distances (Å) and Bond Angles (deg) in anionic  $[\text{Hg}\cdot 2\text{Cl}(\mu\text{-Cl})(\text{HgCl}_3)]^-$  part of  $(\text{HgCl}_2)_6\cdot(2)_4$  (135).

Hg(1)-N(1)	2.481(3)	Hg(1)-N(2)	2.407(4)
Hg(1)-N(3)	2.516(4)	Hg(1)-N(4)	2.444(4)
Hg(1)-Cl(1)	2.6271(11)	Hg(1)-Cl(2)	2.5059(10)
Hg(2)-Cl(1)	2.6439(11)	Hg(1)-Cl(3)	2.5275(11)
Hg(2)-Cl(5)	2.4287(13)	Hg(2)-Cl(4)	2.4233(12)
N(2)-Hg(1)-N(4)	135.50(14)	N(1)-Hg(1)-N(2)	74.07(13)
N(1)-Hg(1)-N(4)	71.63(13)	N(2)-Hg(1)-N(3)	70.71(13)
N(3)-Hg(1)-N(4)	73.01(13)	N(1)-Hg(1)-N(3)	69.50(12)
N(2)-Hg(1)-Cl(2)	108.40(10)	N(4)-Hg(1)-Cl(2)	99.50(9)
N(1)-Hg(1)-Cl(2)	162.84(9)	N(3)-Hg(1)-Cl(2)	94.94(9)
N(2)-Hg(1)-Cl(1)	105.86(10)	N(4)-Hg(1)-Cl(1)	103.81(10)
N(1)-Hg(1)-Cl(1)	97.76(9)	N(3)-Hg(1)-Cl(1)	167.24(9)
Cl(2)-Hg(1)-Cl(1)	97.79(4)	Cl(4)-Hg(2)-Cl(5)	129.32(4)
Cl(4)-Hg(2)-Cl(3)	110.77(4)	Cl(5)-Hg(2)-Cl(3)	100.93(5)
Cl(4)-Hg(2)-Cl(1)	97.21(4)	Cl(5)-Hg(2)-Cl(1)	105.75(4)

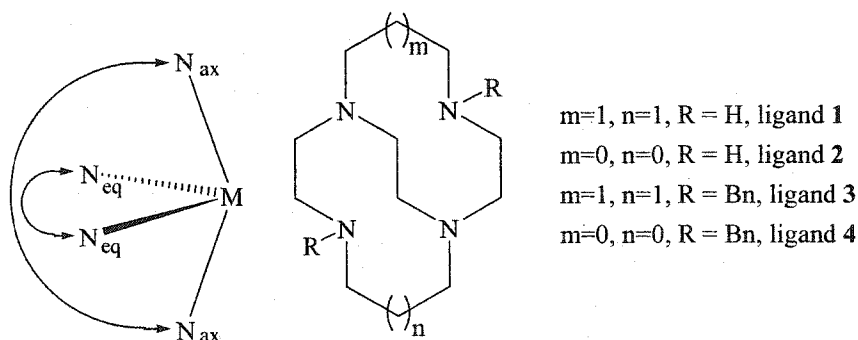
### 3.4 Summary of Structural Data.

With only a single exception, Zn(II), Cd(II), and Hg(II) complexes of these cross-bridged ligands **1-4** feature full  $\eta^4$ -N-coordination of the metal cations within the bicyclic tetraamine ligands' cleft in addition to two *cis*-ancillary ligands. A comparison of axial N-M-N angles and the equatorial N-M-N angles is listed in **Table 2.8**. Clearly, cross-bridged cyclam ligands **1** and **3** provide a better fit for octahedral Zn(II) than the smaller cross-bridged cyclen ligands **2** and **4**. This is best gauged by the axial N-Zn-N angles of between 169-174° for the former and 153-157° for the latter. A secondary indicator of this fit is the equatorial N-Zn-N angle which is between 84-85° for complexes of **1** and **3** but compressed to between 78-83° for **2** and **4** (**Table 2.8**). The *cis*-folded coordination conformation of **1** clearly favors smaller cations like Zn(II) compared to its cyclen analogue **2**.

Comparing structural data of ligand **2** complexes of ZnCl<sub>2</sub>, CdCl<sub>2</sub>, and HgCl<sub>2</sub>, the increased misfit of the two larger cations from the ligand cleft can be seen within their respective axial N-M-N angles: Zn (153-157°), Cd (137-139°), and Hg (133-139°). Parallel trends in the equatorial N-M-N angles are also observed: Zn (83°), Cd (70-72°), and Hg (67-72°). Concurrently the N(ax)-M distances increase from Zn (2.13Å) to Cd (2.32-2.40Å) to Hg (2.40-2.42Å) while the N(eq)-M bonds similarly lengthen from Zn (2.14Å) to Cd (2.44-2.50Å) to Hg (2.56-2.57Å). The ramification of this increasingly poor fit can be found directly in the decreased kinetic inertness of the respective complex in aqueous solution. These results provide confirmation of our original design of these cross-bridged ligands for selective complexation of small metal ions.

**Table 2.8** Comparison of Zn(II), Cd(II) and Hg(II) fit inside cross-bridged ligand clefts.

Complex	Axial N-M-N angle	Equatorial N-M-N angle
[Zn•1(OH <sub>2</sub> )(μ-Cl)ZnCl <sub>3</sub> ] (115)	173.5 (2)	84.9 (2)
[Zn•1(μ-Cl)] <sub>2</sub> Cl <sub>2</sub> •4CH <sub>3</sub> OH (116)	168.7 (3)	84.5 (2)
[Zn•1(μ-Cl)] <sub>2</sub> Cl <sub>2</sub> (116a)	168.3 (2)	83.4 (2)
Zn•3(μ-Cl) <sub>2</sub> -ZnCl <sub>2</sub> (120)	171.1 (2)	83.5 (3)
[Zn•2(H <sub>2</sub> O) <sub>2</sub> ](ClO <sub>4</sub> ) <sub>2</sub> (122)	156.8 (3)	83.08 (19)
ZnCl <sub>2</sub> •4 (124)	152.61 (9)	77.61 (8)
CdCl <sub>2</sub> •1 (125)	151.5 (6)	71.5 (4)
CdCl <sub>2</sub> •2 (129)	137.57 (7)	71.02 (7)
[Cd•2(η <sup>2</sup> -NO <sub>3</sub> ) <sub>2</sub> ] (131)	138.80 (19)	72.40 (17)
CdCl <sub>2</sub> •3 (128)	158.51 (13)	75.10 (14)
CdCl <sub>2</sub> •4 (132)	137.95 (11)	69.77 (11)
HgCl <sub>2</sub> •2 (134)	133.4 (3)	66.7 (3)
[Hg•2(μ-Cl)] <sub>2</sub> <sup>2+</sup> part of (HgCl <sub>2</sub> ) <sub>6</sub> •(2) <sub>4</sub> (134)	138.82 (14)	71.63 (13)
[Hg•2Cl(μ-Cl)(HgCl <sub>3</sub> )] <sup>-</sup> part of (HgCl <sub>2</sub> ) <sub>6</sub> •(2) <sub>4</sub> (134)	135.50 (14)	69.50 (12)



For the Zn and Cd complexes of ligand 1, cross-bridged cyclam, only inside-cavity metal complexes formed. So why can't Hg(II) fit into the molecular cleft of ligand 1? That this is not simply a kinetic phenomenon can be inferred from the observation that prolonged heating of either the reagents or the *exo*-[HgCl<sub>2</sub>(μ-1)]<sub>2</sub> complex in methanol did not result in formation of any such product. In the literature, there is no report of any simple macrocyclic tetraamine Hg(II) complex in which the tetraamine only coordinates in an η<sup>1</sup>-mode to the Hg(II) center.<sup>45(a),45(e),123</sup> It is likely that the transannular H-bonding



within this ligand cleft may be favored over a badly distended Hg(II) cation. The formation of dimeric Hg(II) centers that are doubly bridged by chlorides may also increase the preference for such a structure. Similarly, in the literature, a hexadentate diamine derivative of cyclam is fully coordinated to a Cd(II) center in its complex (73 in **Figure 1.26**).<sup>43(a)</sup> By contrast, in its mercury complex, at each end of the ligand, one nitrogen donor from the macrocyclic ring and one nitrogen from the amine arm together bridge a HgCl<sub>2</sub> unit to form dimercuric species (77 in **Figure 1.30**).<sup>45(b)</sup>

The X-ray structures of all three Hg(II) complexes of ligands **1** and **2** have showed no uncoordinated chloride. This confirms the propensity of Hg(II) to bind chloride rather than nitrogen and is consistent with literature precedents.<sup>45(b)</sup> This is also in agreement with the absence of any uncoordinated chloride in the lattice of any polyamine HgCl<sub>2</sub> complexes in the *Cambridge Crystallographic Database*.

## CHAPTER III

### Zn(II), Cd(II) AND Hg(II) COMPLEXES OF PENDANT-ARMED CROSS-BRIDGED TETRAAMINES LIGANDS 5-8

#### 1. General Comments on the Synthesis and Characterization of Zn(II), Cd(II) and Hg(II) Complexes of Ligands 5-8.

Thirteen Zn(II), Cd(II) and Hg(II) complexes of N,N'-dipendant-armed cross-bridged ligands, 5, 6, 7 and 8 (Figure 3.1) were synthesized and characterized by their IR (KBr),  $^1\text{H}$  and  $^{13}\text{C}\{^1\text{H}\}$  NMR spectral data, and CHN elemental analyses.

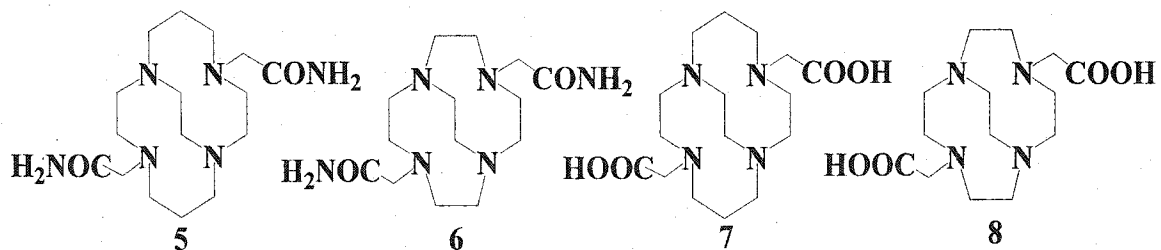


Figure 3.1 Pendant-armed cross-bridged ligands 5-8

Complexes  $[\text{Cd}\cdot(8\text{-}2\text{H})](\text{NaClO}_4)$  (147) and  $[\text{Hg}\cdot(7\text{-}2\text{H})](\text{K}_2\text{HgCl}_4)$  (148) were also characterized by chloride elemental analysis. Additional useful information to confirm the formation of Cd(II) and Hg(II) complexes of ligands 5-8 is from the observation of

$^1\text{H}$ - $^{111,113}\text{Cd}$ ,  $^{13}\text{C}$ - $^{111,113}\text{Cd}$ ,  $^1\text{H}$ - $^{199}\text{Hg}$ , or  $^{13}\text{C}$ - $^{199}\text{Hg}$  coupling satellites in their  $^1\text{H}$  or  $^{13}\text{C}\{^1\text{H}\}$  NMR spectra.

In general, these metal complexes were prepared by refluxing a methanol solution of the appropriate metal salt and an equivalent amount of a cross-bridged ligand for a period of several hours to several days. Crystals of the resulting complexes suitable for X-ray analyses were typically obtained by diethyl ether diffusion into a solution of the crude product in methanol. Interestingly, attempted crystallization of  $[\text{Hg}\cdot(7-2\text{H})](\text{K}_2\text{HgCl}_4)$  (**148**) from water yielded crystals whose structure actually showed a composition of  $[\text{Hg}\cdot(7-2\text{H})]_2(\text{HgCl}_2)_3$  (**148a**).

### 1.1 Synthesis of Zn(II) and Cd(II) Complexes of Ligands 5 and 6.

Zn(II) and Cd(II) complexes of diacetamide-armed cross-bridged ligands **5** and **6** were synthesized from the reactions of **5** (and **6**) with a hydrated metal salt in refluxing methanol. Diethyl ether diffusion into these methanol solutions produced crystals of these metal complexes. In the synthesis of  $[\text{Zn}\cdot\mathbf{5}](\text{ClO}_4)_2$  (**136**), the relative low purified yield (20%) was caused by the presence of about five percent organic impurity in ligand **5**. Several recrystallizations yielded this pure Zn(II) complex as needle-shaped crystals, on which X-ray analyses and CHN elemental analyses were carried out. Similarly,  $\text{Cd}(\text{ClO}_4)_2$  complex of **5** can be purified. The formation of the  $\text{Cd}(\text{ClO}_4)_2$  complex of **5** was indicated by the presence of doublet satellites around several  $^{13}\text{C}\{^1\text{H}\}$  resonances in its  $^{13}\text{C}\{^1\text{H}\}$  NMR spectrum in  $\text{D}_2\text{O}$  due to  $^{111,113}\text{Cd}$ - $^{13}\text{C}$  coupling. This will be discussed in detail in the NMR spectral discussion part. However, no CHN elemental analysis of this Cd(II) complex was obtained.

## 1.2 Synthesis of Zn(II), Cd(II) and Hg(II) Complexes of Ligands 7 and 8.

Ligands 7 and 8 are N,N'-dicarboxylate-armed derivatives of parent cross-bridged cyclam (1) and cyclen (2) respectively. Unlike ligands 1-6, equivalents of a base are necessary to neutralize these acidic protons in order to form metal complexes.

In the presence of an equivalent amount of aqueous sodium hydroxide, the reaction of a hydrated Zn(II) or Cd(II) salt with either ligand 7 or 8 yielded a clear solution. Diethyl ether diffusion into this solution yielded Zn(II) and Cd(II) complexes of ligands 7 and 8 as either crystals or micro-crystalline solid. CHN elemental analyses of both  $[\text{Zn}\cdot(7\text{-}2\text{H})](\text{NaNO}_3)$  (142) and  $[\text{Cd}\cdot(7\text{-}2\text{H})](\text{NaNO}_3)$  (146) indicated the presence of sodium hydroxide in these two complexes, consistent with the fact that their aqueous solutions are basic ( $>9$ ) when tested by pH paper. The complex  $[\text{Hg}\cdot(7\text{-}2\text{H})](\text{K}_2\text{HgCl}_4)$  (148) was formed even when an equivalent each of  $\text{HgCl}_2$  and  $7\cdot(\text{TFA})_2$  were used as reactants. Again, the preferred formation of such a complex is due to the high affinity of Hg(II) for chloride. Unlike  $\text{HgCl}_2$  complexes of ligands 1 and 2,  $[\text{Hg}\cdot(7\text{-}2\text{H})](\text{K}_2\text{HgCl}_4)$  (148) has good solubility in water and methanol. Resulting crystals grown from water were found by X-ray diffraction to be  $[\text{Hg}\cdot(7\text{-}2\text{H})]_2(\text{HgCl}_2)_3$ . Presumably because of the good solubility of potassium chloride in water,  $[\text{Hg}\cdot(7\text{-}2\text{H})](\text{K}_2\text{HgCl}_4)$  (148) apparently crystallized out as  $[\text{Hg}\cdot(7\text{-}2\text{H})]_2(\text{HgCl}_2)_3$  (148a) instead. These are the first examples for Cd(II) and Hg(II) complexes of carboxylate-armed macrocyclic tetraamines. Even though good-quality crystals of  $[\text{Cd}\cdot(7\text{-}2\text{H})](\text{NaClO}_4)$  (145) and  $[\text{Cd}\cdot(7\text{-}2\text{H})](\text{NaNO}_3)$  (146) were formed readily, neither of their crystal structures was structurally solved.

## 2. Spectral Data.

### 2.1 Infrared Spectra.

Typically two amide carbonyl bands ranging from 1650 to 1689  $\text{cm}^{-1}$  are found in the IR spectra (KBr) of Zn(II) and Cd(II) complexes of the amide-armed cross-bridged ligands **5** and **6** (Table 3.1). In addition to these two strong bands, medium-to-

**Table 3.1** Comparison of C=O stretches in the IR spectra of Zn(II), Cd(II) and Hg(II) complexes of ligands **5-8**.

Complex	$\nu_{\text{C=O}}$ ( $\text{cm}^{-1}$ )	Complex	$\nu_{\text{C=O}}$ ( $\text{cm}^{-1}$ )
[Zn• <b>5</b> ](ClO <sub>4</sub> ) <sub>2</sub>	1673, 1659	[Zn• <b>6</b> ](ClO <sub>4</sub> ) <sub>2</sub>	1682, 1663
[Zn• <b>6</b> ](NO <sub>3</sub> ) <sub>2</sub>	1683, 1656	Cd• <b>6</b> (ClO <sub>4</sub> ) <sub>2</sub>	1689, 1658
[Cd• <b>6</b> ( $\eta^1$ -NO <sub>3</sub> )](NO <sub>3</sub> )	1656, 1650	[Zn•( <b>7-2H</b> )](NaClO <sub>4</sub> )	1616, 1592
[Zn•( <b>7-2H</b> )](NaNO <sub>3</sub> )	1618, 1596	[Zn•( <b>8-2H</b> )](NaClO <sub>4</sub> )	1617 (br)
[Zn•( <b>8-2H</b> )](NaNO <sub>3</sub> )	1645, 1611	[Cd•( <b>7-2H</b> )](NaClO <sub>4</sub> )	1633, 1586
[Cd•( <b>7-2H</b> )](NaNO <sub>3</sub> )	1619, 1594	[Cd•( <b>8-2H</b> )](NaClO <sub>4</sub> )	1615, 1595
[Hg•( <b>7-2H</b> )](K <sub>2</sub> HgCl <sub>4</sub> )	1611, 1590		

weak bands around 1600  $\text{cm}^{-1}$  in these complexes can be assigned to NH or OH bending modes. These data are consistent with the reported coordinated amide carbonyl band of [Cu•**5**](ClO<sub>4</sub>)<sub>2</sub> at 1665  $\text{cm}^{-1}$ .<sup>69(a)</sup> For comparison, free ligand **5** has this band at 1685  $\text{cm}^{-1}$  while free ligand **6** has this band at 1675  $\text{cm}^{-1}$ .<sup>69(a),125(a)</sup> For the Zn(II), Cd(II) and Hg(II) complexes of the carboxylate-armed cross-bridged ligands **7** and **8**, two characteristic carboxylate bands ranging from 1586 to 1645  $\text{cm}^{-1}$  were observed. This is due to the presence of asymmetrical stretches of carboxylate groups since Deacon and Phillips concluded that coordinated carboxylate groups have asymmetrical stretches ranging from 1500-1675  $\text{cm}^{-1}$  and symmetrical stretches at lower than 1490  $\text{cm}^{-1}$ .<sup>125(b)</sup> These are

comparable to those reported for  $[\text{Cu}\cdot(7\text{-}2\text{H})](\text{NaClO}_4)$  at 1590 and 1616  $\text{cm}^{-1}$ .<sup>69(a)</sup> The presence of asymmetrical stretches of carboxylate groups indicates that the two coordinated carboxylate groups are different in the solid-state even though the X-ray structure of  $[\text{Zn}\cdot\mathbf{6}](\text{ClO}_4)_2$  shows that these two carboxylate pendant arms are equivalent because of its  $C_2$  symmetry (**Figure 3.23**, *vide infra*). The complex  $[\text{Zn}\cdot(8\text{-}2\text{H})](\text{NaClO}_4)$  (**143**), however, only showed a broad carboxylate band around 1617  $\text{cm}^{-1}$ . This may be a result of the overlapping of two bands. No IR absorption belonging to the COOH group between 1700 and 1740  $\text{cm}^{-1}$  was observed for any of these Zn(II), Cd(II) and Hg(II) complexes, further supporting metal coordination of their carboxylate groups.<sup>69(a)</sup>

## 2.2 Solution $^1\text{H}$ and $^{13}\text{C}\{^1\text{H}\}$ NMR Spectra.

Similar to Zn(II), Cd(II) and Hg(II) complexes of ligands 1-4, the  $^1\text{H}$  and  $^{13}\text{C}\{^1\text{H}\}$  NMR spectra of all thirteen Zn(II), Cd(II) and Hg(II) complexes of ligands 5-8 revealed only single species on the NMR time scale at room temperature. An exception is that both the  $^1\text{H}$  and  $^{13}\text{C}\{^1\text{H}\}$  NMR spectra of  $[\text{Cd}\cdot(8\text{-}2\text{H})](\text{NaClO}_4)$  (**147**) in  $\text{CD}_3\text{OD}$  showed only very broad resonances, which may imply presence of more than one species in intermediate exchange.

The  $^{13}\text{C}\{^1\text{H}\}$  NMR spectra of all characterized Zn(II), Cd(II) and Hg(II) complexes of cyclam-derived ligands 5 and 7 in solution at room temperature possess actual or time-averaged  $C_2$  symmetry as revealed by the presence of eight resonances out of a total sixteen carbons in both 5 and 7. All characterized Zn(II) and Cd(II) complexes of cyclen-derived ligands 6 and 8 including  $[\text{Cd}\cdot(8\text{-}2\text{H})](\text{NaClO}_4)$  (**144**) in  $\text{D}_2\text{O}$  exhibit a

higher-order  $C_{2v}$  solution symmetry at room temperature, as their  $^{13}\text{C}\{^1\text{H}\}$  NMR spectra featured only five carbon resonances out of fourteen total carbons in both **6** and **8**. A  $C_{2v}$  symmetry also resulted in the observation of the methylene protons in the pendant arms as a singlet in their  $^1\text{H}$  NMR spectra.

**(a) Zn(II) and Cd(II) Complexes of Ligand 5 and 6.**

Although neither a satisfactory CHN elemental analyses nor X-ray structural analysis was obtained for the  $\text{Cd}(\text{ClO}_4)_2$  complex of **5**, the formation of this complex was indicated by the presence of doublet satellites around five  $^{13}\text{C}$  resonances out of eight total ( $C_2$  symmetry) in its  $^{13}\text{C}\{^1\text{H}\}$  NMR spectrum in  $\text{D}_2\text{O}$  (**Figure 3.2(a)**). For

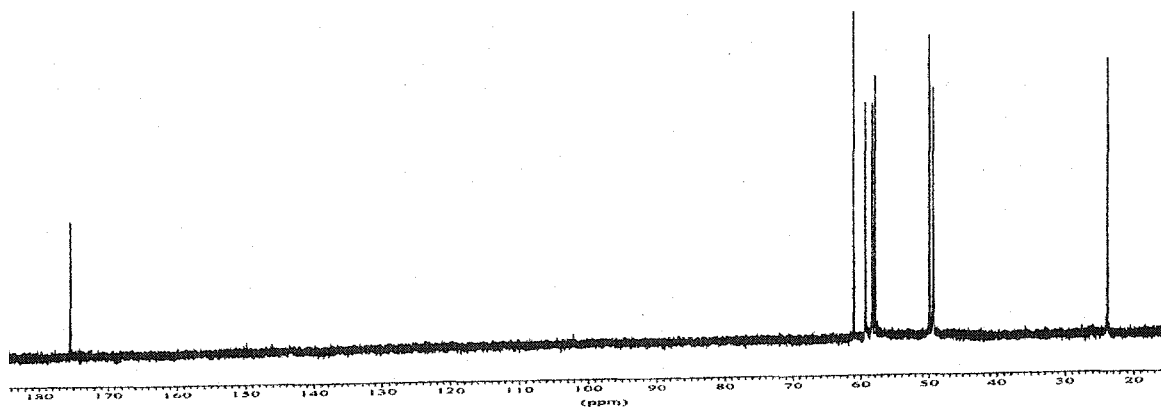


**Figure 3.2(a)** The  $^{13}\text{C}\{^1\text{H}\}$  NMR spectrum of the  $\text{Cd}(\text{ClO}_4)_2$  complex of **5** in  $\text{D}_2\text{O}$ .

example, the  $^{111,113}\text{Cd}-^{13}\text{C}$  satellites around the amide carbonyl  $^{13}\text{C}$  resonance have a coupling constant of 9 Hz (**Figure 3.2(b)**). The presence of these  $^{111,113}\text{Cd}-^{13}\text{C}$  satellites clearly suggests that the  $\text{Cd}(\text{II})$  center is coordinated by at least four amine nitrogen

donors from the hexadentate **5** in D<sub>2</sub>O on the NMR timescale even if the satellites around the amide carbonyl <sup>13</sup>C resonance are due to a <sup>3</sup>J coupling.

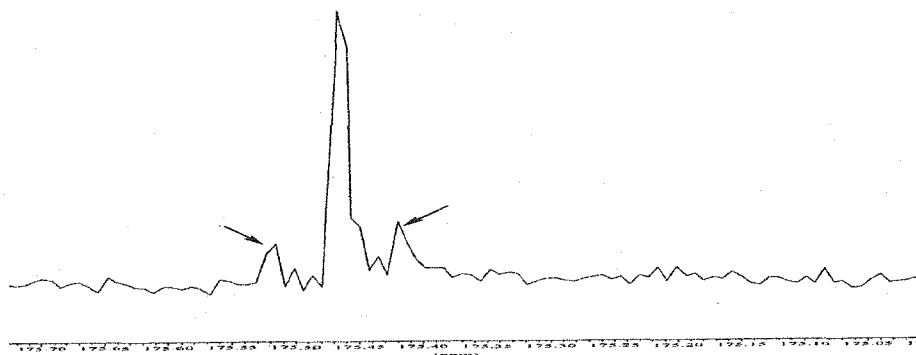


**Figure 3.2(b)** The carboxylate carbonyl resonance showing a doublet satellite (arrows) in the <sup>13</sup>C{<sup>1</sup>H} NMR spectrum of the Cd(ClO<sub>4</sub>)<sub>2</sub> complex of **5** in D<sub>2</sub>O.

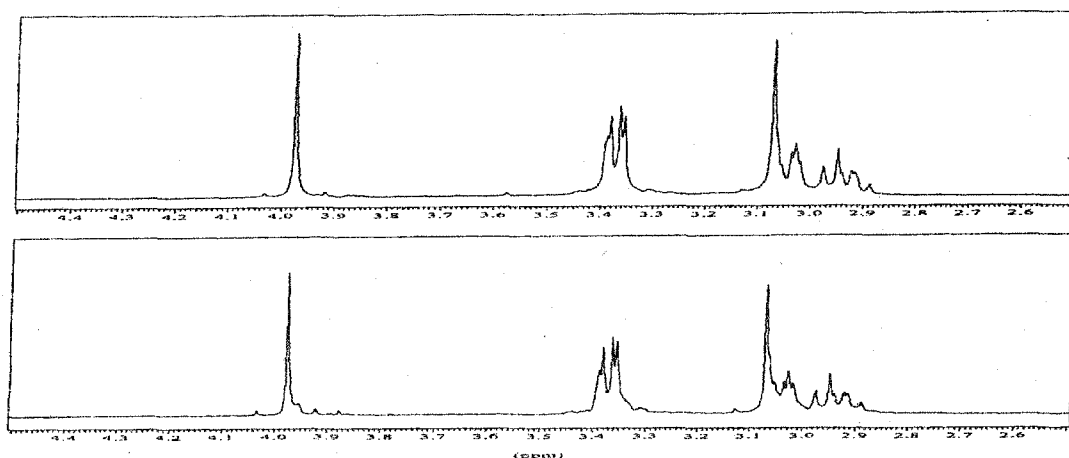


**Figure 3.3(a)** Comparison of <sup>1</sup>H NMR spectra of the two Zn(II) complexes of **6** in D<sub>2</sub>O. Top: [Zn•**6**](ClO<sub>4</sub>)<sub>2</sub>; bottom: [Zn•**6**](NO<sub>3</sub>)<sub>2</sub>.

In both D<sub>2</sub>O and methanol, [Zn•**6**](ClO<sub>4</sub>)<sub>2</sub> (**137**) and [Zn•**6**](NO<sub>3</sub>)<sub>2</sub> (**138**) show the same <sup>1</sup>H (**Figure 3.3 (a)** and **Figure 3.3(b)**) and <sup>13</sup>C{<sup>1</sup>H} NMR spectra, indicating a common solution structure. The largest chemical shift difference is only 0.02 ppm in



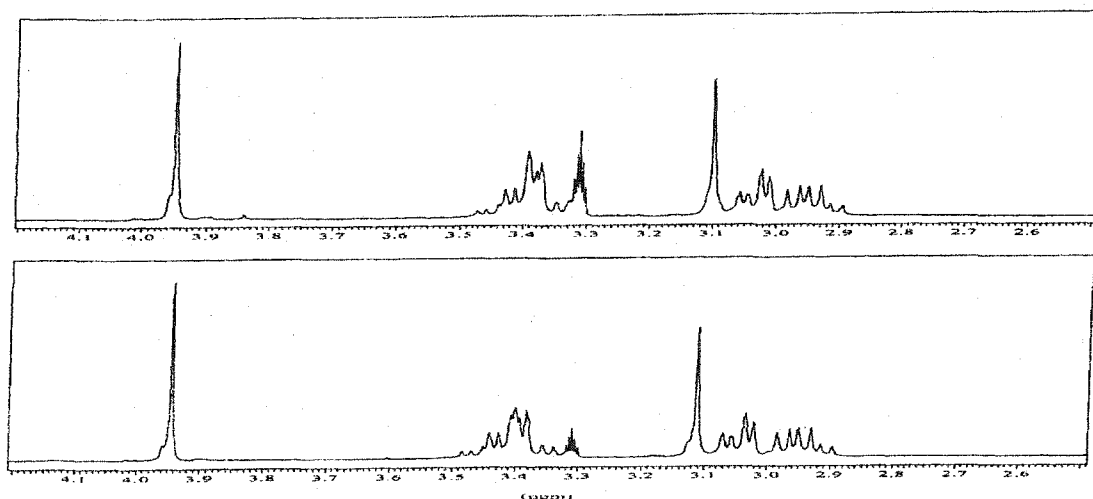


**Figure 3.3(b)** Comparison of  $^1\text{H}$  NMR spectra of the two Zn(II) complexes of **6** in  $\text{CD}_3\text{OD}$ . Top:  $[\text{Zn}\cdot\mathbf{6}](\text{NO}_3)_2$ ; bottom:  $[\text{Zn}\cdot\mathbf{6}](\text{ClO}_4)_2$ .

their proton NMR spectra and 0.02 ppm in their  $^{13}\text{C}\{^1\text{H}\}$  NMR spectra. Since the solid-state structure of  $[\text{Zn}\cdot\mathbf{6}](\text{ClO}_4)_2$  (**137**) (Figure 3.24, *vide infra*) shows that the Zn(II) is engulfed in the cavity formed by hexadentate **6**, the Zn(II) centers in both  $[\text{Zn}\cdot\mathbf{6}](\text{ClO}_4)_2$  and  $[\text{Zn}\cdot\mathbf{6}](\text{NO}_3)_2$  in either water or methanol are probably also fully coordinated. This is consistent with the kinetic stability of  $[\text{Zn}\cdot\mathbf{6}](\text{ClO}_4)_2$  being several orders of magnitude higher than of the parent cross-bridged cyclen Zn(II) complex,  $[\text{Zn}\cdot\mathbf{2}(\text{OH}_2)_2](\text{ClO}_4)_2$  (**122**) (*vide infra*). By contrast, the  $^1\text{H}$  NMR spectrum of  $\text{Cd}\cdot\mathbf{6}(\text{ClO}_4)_2$  (**139**) is significantly different from that of  $[\text{Cd}\cdot\mathbf{6}(\eta^1\text{-NO}_3)](\text{NO}_3)$  (**140**) in  $\text{CD}_3\text{OD}$  (Figure 3.4(a)). This suggests their different solution structures in methanol. This difference may be due to the different coordination numbers at Cd(II) because the X-ray structure of  $[\text{Cd}\cdot\mathbf{6}(\eta^1\text{-NO}_3)](\text{NO}_3)$  (Figure 3.25, *vide infra*) revealed that the Cd(II) center is seven-coordinated by four amino nitrogens and two carboxylate oxygens from ligand **6** as well as a monodentate nitrate.

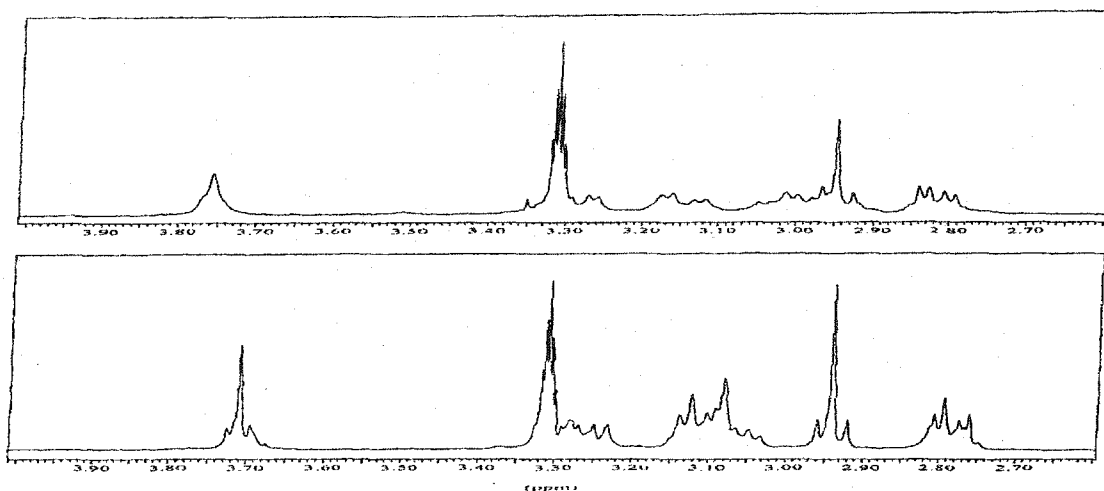


**Figure 3.4(a)**  $^1\text{H}$  NMR spectra of  $\text{Cd}\cdot\mathbf{6}(\text{ClO}_4)_2$  (top) and  $[\text{Cd}\cdot\mathbf{6}(\eta^1\text{-NO}_3)](\text{NO}_3)$  (bottom) in  $\text{CD}_3\text{OD}$ .

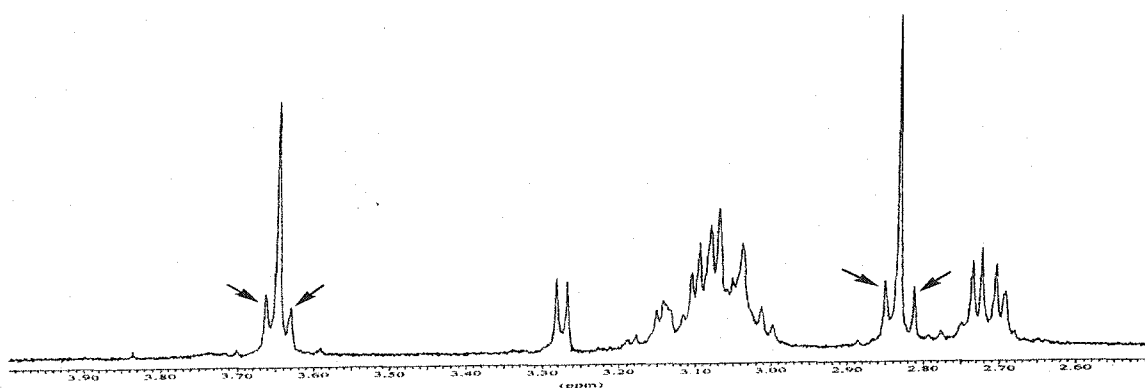


**Figure 3.4(b)**  $^1\text{H}$  NMR spectrum of  $[\text{Cd}\cdot\mathbf{6}(\eta^1\text{-NO}_3)](\text{NO}_3)$  in  $\text{CD}_3\text{CN}$ . The  $^{111,113}\text{Cd}$ - $^1\text{H}$  coupling satellites are marked by arrows. The downfield singlet belongs to two methylenes of the pendant arms while the upfield singlet belongs to the bridging ethylene.

The  $^1\text{H}$  NMR spectra of  $[\text{Cd}\cdot\mathbf{6}(\eta^1\text{-NO}_3)](\text{NO}_3)$  in both  $\text{CD}_3\text{OD}$  (**Figure 3.4(a)**) and  $\text{CD}_3\text{CN}$  (**Figure 3.4(b)**) show  $^{111,113}\text{Cd}$ - $^1\text{H}$  coupling satellites around both the methylene in the pendant arms and the bridging ethylene signals. The  $^1\text{H}$  NMR spectrum of  $\text{Cd}\cdot\mathbf{6}(\text{ClO}_4)_2$  in  $\text{CD}_3\text{CN}$  (**Figure 3.5**) shows similar coupling satellites around

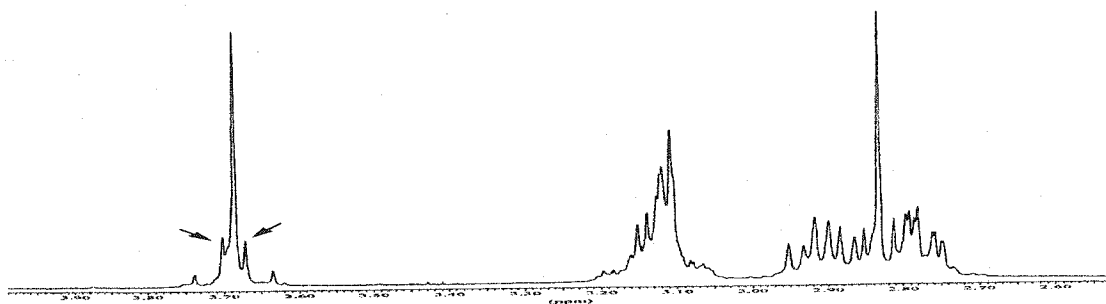


**Figure 3.5**  $^1\text{H}$  NMR spectrum of  $\text{Cd}\cdot 6(\text{ClO}_4)_2$  in  $\text{CD}_3\text{CN}$ . The  $^{111,113}\text{Cd}$ - $^1\text{H}$  coupling satellite is marked by arrows.

methylene in the pendant arms but those around the bridging ethylene resonance overlap with other resonances and are not detectable. These  $^3J$  coupling constants range from 10.6 Hz to 13.9 Hz. In the  $^{13}\text{C}\{^1\text{H}\}$  NMR spectrum of a saturated solution of  $\text{Cd}\cdot 6(\text{ClO}_4)_2$  (**139**) in  $\text{CD}_3\text{CN}$ , three sets of  $^{111,113}\text{Cd}$ - $^{13}\text{C}$  satellites with coupling constants between 3.2 to 12.1 Hz are observed. One of these appears at 176.27 ppm, the amide carbonyl resonance (**Figure 3.6**). This indicates that  $\text{Cd}(\text{II})$  is coordinated at least

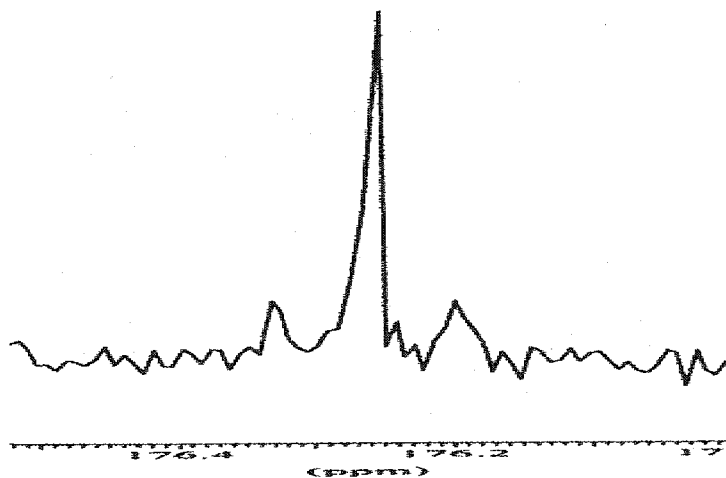


**Figure 3.6** A doublet satellite appears around the amide carbonyl resonance in the  $^{13}\text{C}\{^1\text{H}\}$  NMR spectrum of  $\text{Cd}\cdot 6(\text{ClO}_4)_2$  in  $\text{CD}_3\text{CN}$ .

by four amine nitrogen donors from this hexadentate ligand **6** in CD<sub>3</sub>CN. Surprisingly, the <sup>13</sup>C{<sup>1</sup>H} NMR spectrum of [Cd•**6**(η<sup>1</sup>-NO<sub>3</sub>)](NO<sub>3</sub>) in CD<sub>3</sub>OD has detectable <sup>111,113</sup>Cd-<sup>13</sup>C satellites only around its amide carbonyl resonance. The weak <sup>13</sup>C{<sup>1</sup>H} NMR spectrum of sparingly-soluble Cd•**6**(ClO<sub>4</sub>)<sub>2</sub> in CD<sub>3</sub>OD precludes the detection of any such <sup>111,113</sup>Cd-<sup>13</sup>C satellites.

**(b) Zn(II), Cd(II) and Hg(II) Complexes of Ligands 7 and 8.**

Similar to metal complexes of ligands **1** and **3**, all characterized Zn(II), Cd(II) and Hg(II) complexes of ligands **7** and **8** provided analogous upfield resonances patterns. The second-most upfield resonance can be assigned to the axial proton of the β-methylene in the six-membered chelate ring (β-CHH<sub>ax</sub>). A doublet of pentets (or a broad doublet) to the highest field belongs to the equatorial proton of the β-methylene in the six-membered chelate ring (β-CHH<sub>eq</sub>). [Zn•(7-2H)](NaClO<sub>4</sub>) (**141**) and [Zn•(7-2H)](NaNO<sub>3</sub>) (**142**) have a common aqueous solution structure because they have the same <sup>1</sup>H (Figure 3.7) and <sup>13</sup>C{<sup>1</sup>H} NMR spectra in D<sub>2</sub>O. As shown in the solid-state structure of [Zn•(7-2H)](NaClO<sub>4</sub>) (**141**) (Figure 3.26, *vide infra*), the six-coordinate Zn(II) was engulfed deeply in the cavity formed by the hexadentate **6**. This structure can account for the several orders of magnitude higher kinetic stability of [Zn•(7-2H)](NaClO<sub>4</sub>) compared to that of Zn•**1**(ClO<sub>4</sub>)<sub>2</sub> (**117**) (*vide infra*). We expect that such a structure of [Zn•(7-2H)](NaClO<sub>4</sub>) is also maintained in aqueous solution. This is likely also the case for the common aqueous solution species of [Zn•(8-2H)](NaClO<sub>4</sub>) (**143**) and [Zn•(8-2H)](NaNO<sub>3</sub>) (**144**). Figure 3.8 shows their <sup>1</sup>H NMR spectra in D<sub>2</sub>O. There is also no significant difference between the proton NMR spectra

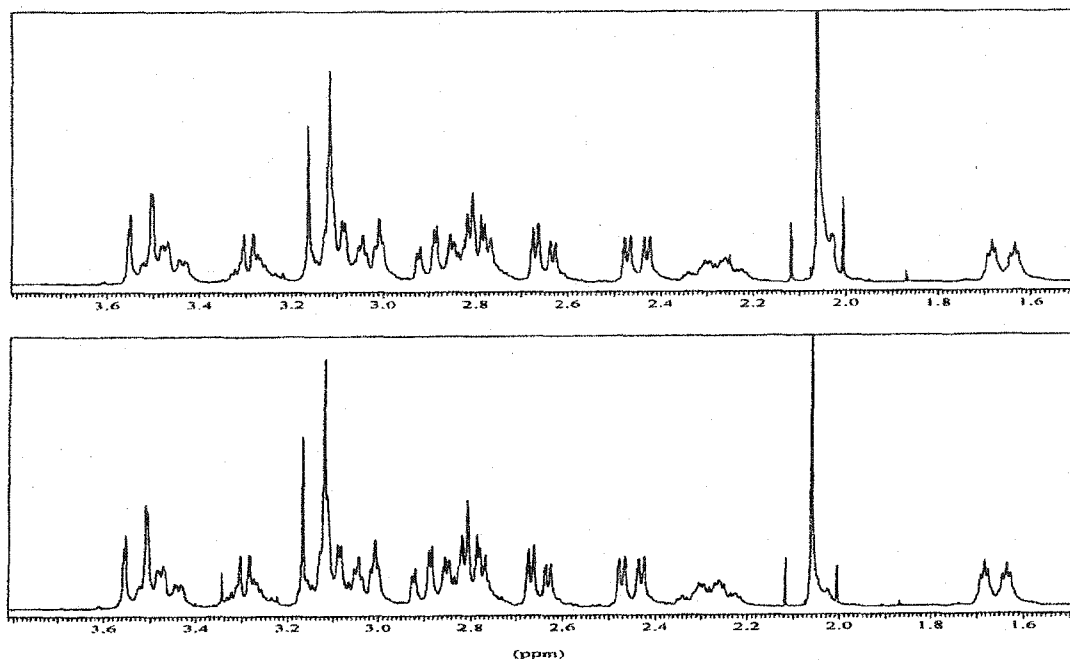


**Figure 3.7** Comparison of  $^1\text{H}$  NMR spectra of the two Zn(II) complexes of **7-2H** in  $\text{D}_2\text{O}$ . Top:  $[\text{Zn}\cdot(\mathbf{7-2H})](\text{NaClO}_4)$ . Bottom:  $[\text{Zn}\cdot(\mathbf{7-2H})](\text{NaNO}_3)$ . The large singlet around  $\delta$  2 is the reference  $\text{CH}_3\text{CN}$  resonance.

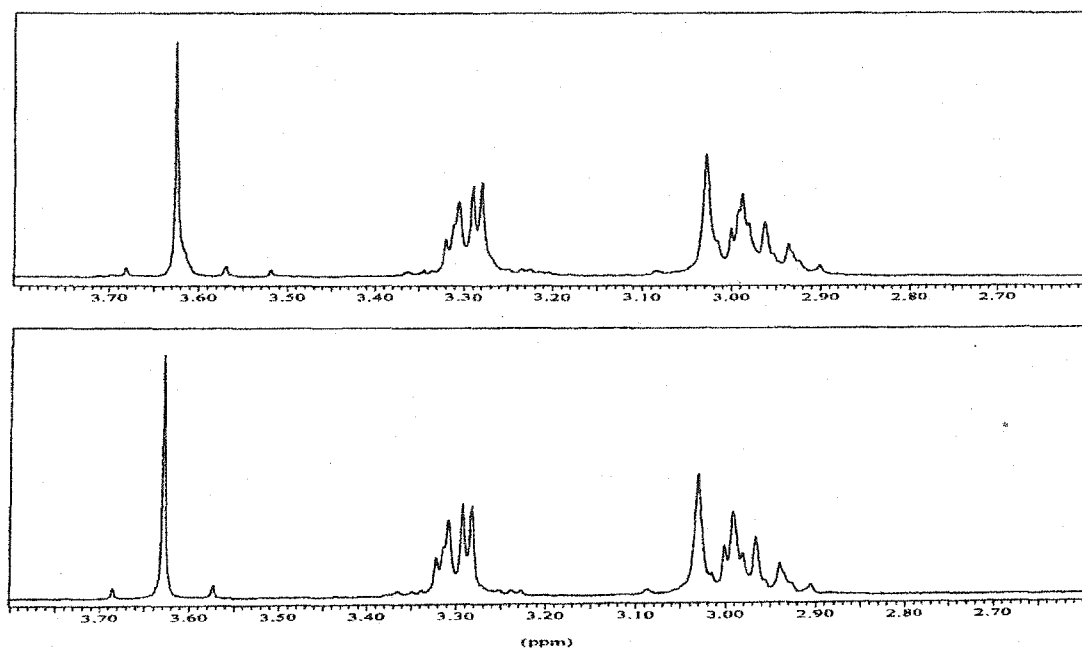


**Figure 3.8** Comparison of  $^1\text{H}$  NMR spectra of the two Zn(II) complexes of **8-2H** in  $\text{D}_2\text{O}$ . Top:  $[\text{Zn}\cdot(\mathbf{8-2H})](\text{NaClO}_4)$ . Bottom:  $[\text{Zn}\cdot(\mathbf{8-2H})](\text{NaNO}_3)$ .

of  $[\text{Cd}\cdot(7\text{-}2\text{H})](\text{NaClO}_4)$  (145) and  $[\text{Cd}\cdot(7\text{-}2\text{H})](\text{NaNO}_3)$  (146) (Figure 3.9) again, indicating a common aqueous solution species. No conclusion, however, can be drawn as to whether this species is six or seven coordinate at Cd(II).

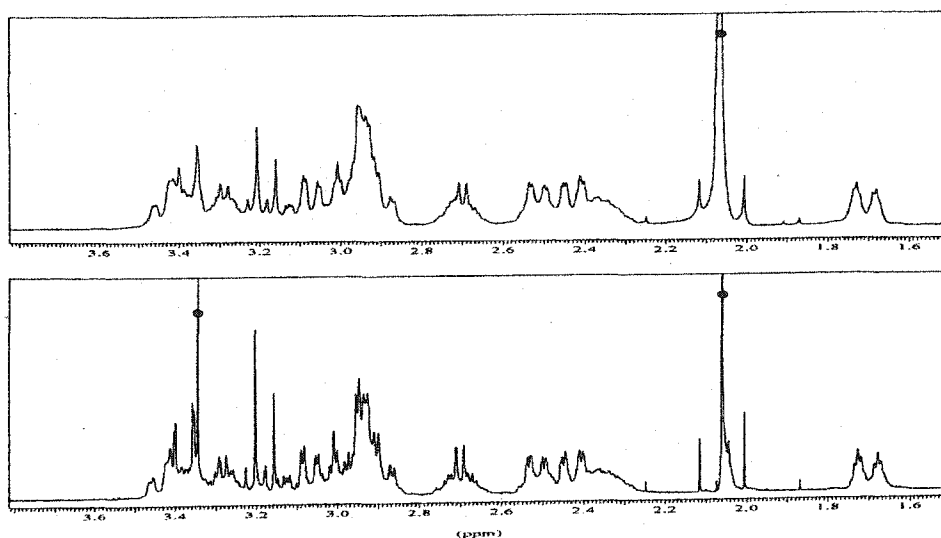


**Figure 3.9**  $^1\text{H}$  NMR spectra of  $[\text{Cd}\cdot(7\text{-}2\text{H})](\text{NaNO}_3)$  (top) and  $[\text{Cd}\cdot(7\text{-}2\text{H})](\text{NaClO}_4)$  (bottom) in  $\text{D}_2\text{O}$ . Solvents peaks are labeled by dots.

In  $\text{D}_2\text{O}$ , both  $[\text{Cd}\cdot(7\text{-}2\text{H})](\text{NaClO}_4)$  (142) and  $[\text{Cd}\cdot(7\text{-}2\text{H})](\text{NaNO}_3)$  (143) exhibit  $^{111,113}\text{Cd}\text{-}^{13}\text{C}$  satellites around four  $^{13}\text{C}$  resonances. These range from 6.0 to 12.0 Hz. Most importantly, the  $^{111,113}\text{Cd}\text{-}^{13}\text{C}$  satellites around the carboxylate carbon resonance are clearly present and give a coupling constant of 11 Hz (Figure 3.10). Even though no solid-state structure is available, the presence of these clearly confirms that the Cd(II) in both of these two cadmium(II) complexes are coordinated at least by four amine nitrogen donors from the hexadentate 7-2H in  $\text{D}_2\text{O}$ . In contrast to the relative well-resolved  $^1\text{H}$  and  $^{13}\text{C}\{^1\text{H}\}$  NMR spectra of these two Cd(II) complexes in  $\text{D}_2\text{O}$ , the proton NMR spectrum of  $[\text{Cd}\cdot(7\text{-}2\text{H})](\text{NaClO}_4)$  in  $\text{CD}_3\text{OD}$  (Figure 3.11(a)) gave rather broad

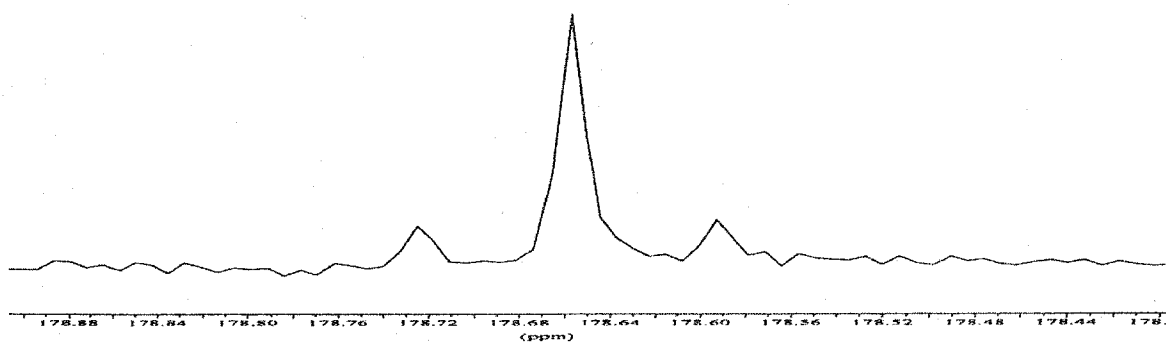


**Figure 3.10** The satellites around the carboxylate carbonyl resonance in the  $^{13}\text{C}\{^1\text{H}\}$  NMR spectrum of  $[\text{Cd}\cdot(7\text{-}2\text{H})](\text{NaNO}_3)$  in  $\text{D}_2\text{O}$ .

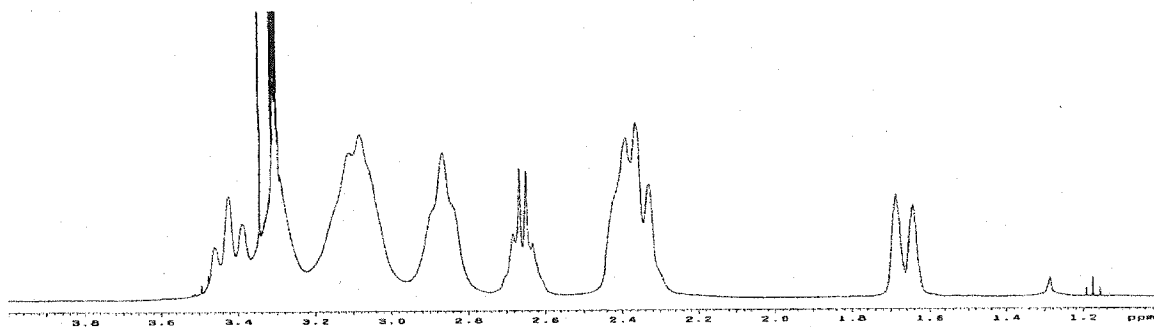


**Figure 3.11(a)**  $^1\text{H}$  NMR spectrum of  $[\text{Cd}\cdot(7\text{-}2\text{H})](\text{NaClO}_4)$  in  $\text{CD}_3\text{OD}$ .

resonances. In its  $^{13}\text{C}\{^1\text{H}\}$  NMR spectrum in the same solvent, only seven out of eight possible resonances from coordinated 7-2H are observed (**Figure 3.11(b)**). The missing resonance is probably overlapped either with the resonance at  $\delta$  62.20 or solvent peaks. The two  $^{13}\text{C}$  resonances at  $\delta$  65.68 and 52.70 (**Figure 3.11(b)**) from coordinated 7-2H in  $[\text{Cd}\cdot(7\text{-}2\text{H})](\text{NaClO}_4)$  are also quite broad. The broadening of both  $^1\text{H}$  and  $^{13}\text{C}\{^1\text{H}\}$  NMR spectra indicate a dynamic equilibrium around coordinated 7-2H in  $\text{CD}_3\text{OD}$ .

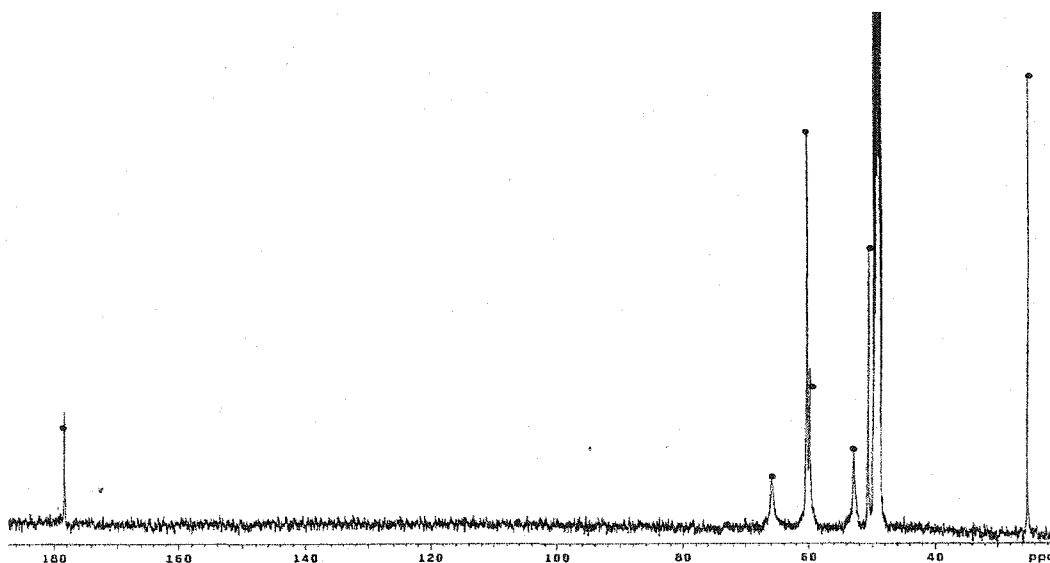


**Figure 3.11(b)**  $^{13}\text{C}\{^1\text{H}\}$  NMR spectrum of  $[\text{Cd}\cdot(7\text{-}2\text{H})](\text{NaClO}_4)$  in  $\text{CD}_3\text{OD}$ . The resonances assigned to this complex are marked by dots.

In its proton NMR spectrum in  $\text{D}_2\text{O}$  (**Figure 3.12**), complex  $[\text{Cd}\cdot(8\text{-}2\text{H})](\text{NaClO}_4)$  (**147**) shows satellites around both the methylene of both the pendant arm

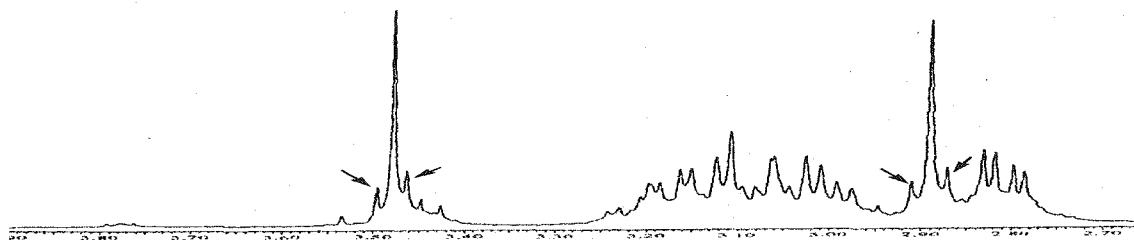


**Figure 3.12**  $^1\text{H}$  NMR spectrum of  $[\text{Cd}\cdot(8\text{-}2\text{H})](\text{NaClO}_4)$  in  $\text{D}_2\text{O}$ . The  $^{111,113}\text{Cd}\text{-}^1\text{H}$  satellites are marked by arrows.

and cross-bridging ethylene. Three  $^{13}\text{C}$  resonances out of five also show  $^{111,113}\text{Cd}\text{-}^{13}\text{C}$  satellites. Their coupling constants vary from these satellites vary from 6.0 to 15.3 Hz. Specifically, the satellites around the carboxylate carbon resonance have a coupling



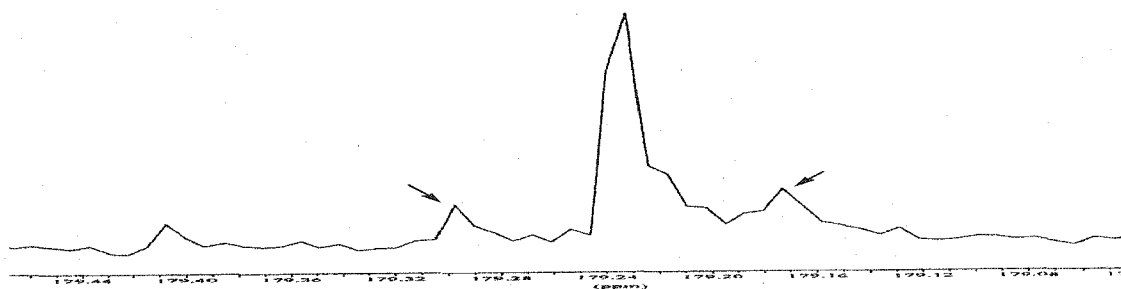


**Figure 3.13** Satellites around the carboxylate carbonyl resonance in the  $^{13}\text{C}\{^1\text{H}\}$  NMR spectrum of  $[\text{Cd}\cdot(8\text{-}2\text{H})](\text{NaClO}_4)$  in  $\text{D}_2\text{O}$ .

constant of 11.3 Hz (**Figure 3.13**). Again, these confirm that Cd(II) in this cadmium(II) complex is also coordinated at least by four amine nitrogen donors from the hexadentate **8-2H** in  $\text{D}_2\text{O}$ . This complex gives only very broad signals in both its proton (**Figure 3.14(a)**) and  $^{13}\text{C}\{^1\text{H}\}$  NMR spectra (**Figure 3.14(b)**) in  $\text{CD}_3\text{OD}$ , indicative of some intermediate dynamic exchange process.

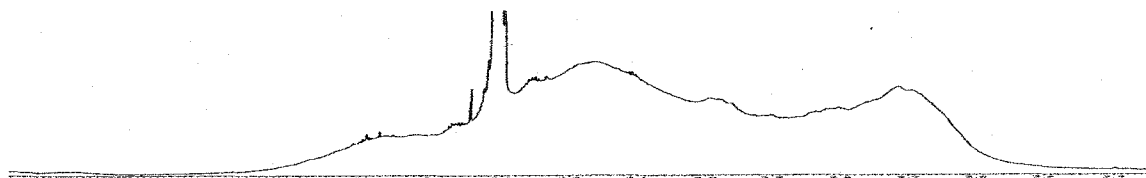


**Figure 3.14(a)**  $^1\text{H}$  NMR spectrum of  $[\text{Cd}\cdot(8\text{-}2\text{H})](\text{NaClO}_4)$  in  $\text{CD}_3\text{OD}$ .

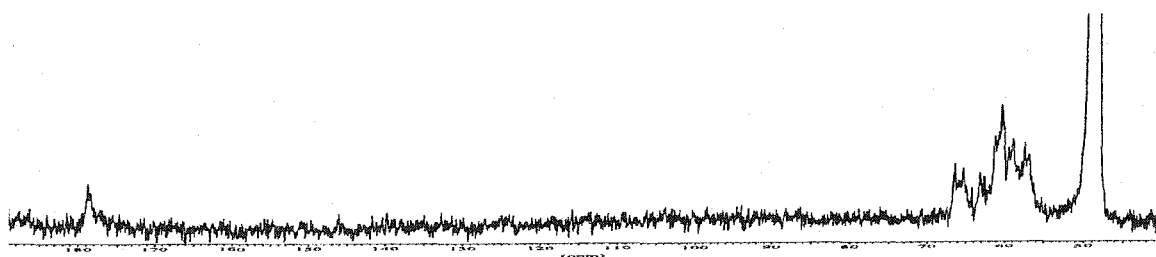


**Figure 3.14(b)**  $^{13}\text{C}\{^1\text{H}\}$  NMR spectrum of  $[\text{Cd}\cdot(8\text{-}2\text{H})](\text{NaClO}_4)$  in  $\text{CD}_3\text{OD}$ .

In the eight  $^{13}\text{C}\{^1\text{H}\}$  resonances of  $[\text{Hg}\cdot(7\text{-}2\text{H})](\text{K}_2\text{HgCl}_4)$  (148) in  $\text{D}_2\text{O}$  (Figure 3.15), seven including the carboxylate carbon resonance at  $\delta$  177.13 have detectable

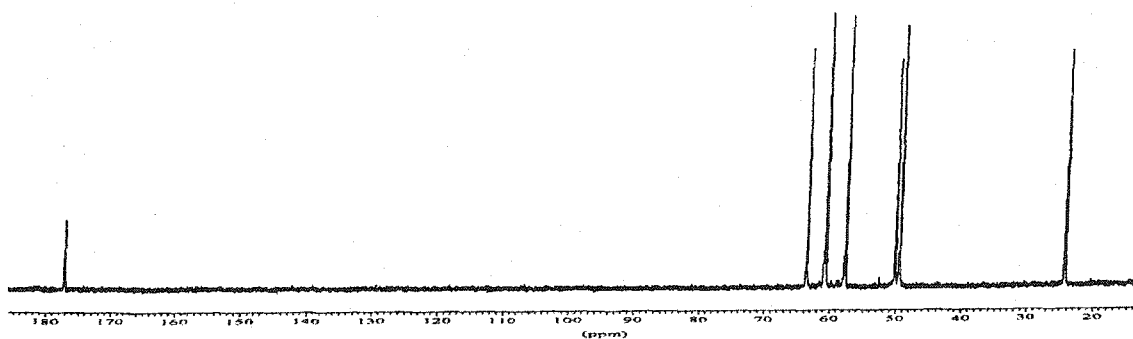


**Figure 3.15**  $^{13}\text{C}\{^1\text{H}\}$  NMR spectrum of  $[\text{Hg}\cdot(7\text{-}2\text{H})](\text{K}_2\text{HgCl}_4)$  in  $\text{D}_2\text{O}$ .

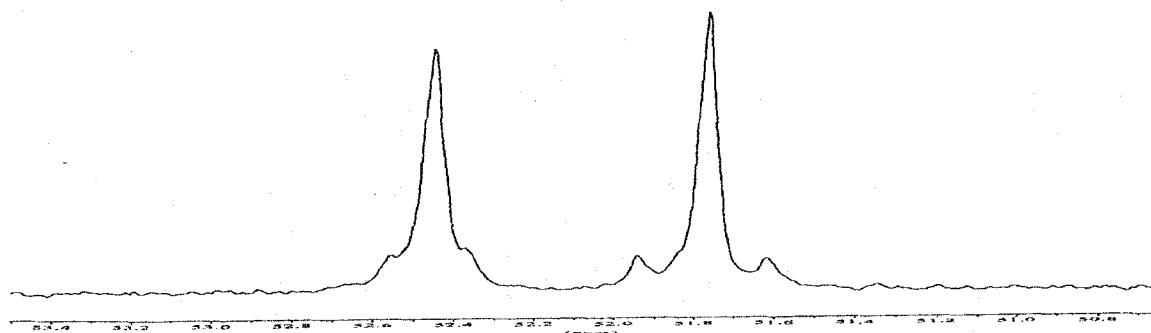


**Figure 3.16** Doublet satellites at the sides of both resonances in the  $^{13}\text{C}\{^1\text{H}\}$  NMR spectrum of  $[\text{Hg}\cdot(7\text{-}2\text{H})](\text{K}_2\text{HgCl}_4)$  in  $\text{D}_2\text{O}$ .

$^{199}\text{Hg}\text{-}^{13}\text{C}$  satellites with coupling constants between 16 to 36 Hz. **Figure 3.16** shows that the two  $^{13}\text{C}$  resonances in the  $\delta$  51-53 indeed have these features. Again, presence of these satellites confirms that at least four amine nitrogen donors from 7-2H are coordinated to the Hg(II) center. In  $\text{CD}_3\text{OD}$ , all  $^{13}\text{C}\{^1\text{H}\}$  resonances (except that at  $\delta$  49.58 overlapping with solvent peaks) have clearly detectable  $^{199}\text{Hg}\text{-}^{13}\text{C}$  satellites of between 11 to 30 Hz. These confirm that unlike the out-of-cleft complex formed by the

present ligand in  $[\text{HgCl}_2(\mu-1)]_2$  (**133**), an inside-cavity Hg(II) complex likely exists for  $[\text{Hg}\cdot(7-2\text{H})](\text{K}_2\text{HgCl}_4)$ . This is also consistent with the observation of metal-coordinated carboxylate bands in its solid-state IR (KBr) spectrum (Table 3.1). Indeed, the X-ray structure of  $[\text{Hg}\cdot(7-2\text{H})]_2(\text{HgCl}_2)_3$  (**148A**) (Figure 3.29, *vide infra*) supports this premise.

### 2.3 Variable-temperature $^1\text{H}$ and $^{13}\text{C}\{^1\text{H}\}$ NMR Spectral Studies in $\text{CD}_3\text{OD}$ .

All characterized Zn(II) and Cd(II) complexes of cyclen-derived ligands **6** and **8** exhibit a higher-order  $C_{2v}$  symmetry in solution at room temperature whereas the highest symmetry of their solid-state structures is only  $C_2$  (**136** in Figure 2.26). This indicates that these Zn(II) and Cd(II) complexes undergo some rapid dynamic process on the NMR time-scale. Two plausible mechanisms are shown for the Zn(II) complex of ligand **8-2H** (Figure 3.17). Lowering the temperature of these samples in  $\text{CD}_3\text{OD}$  may slow

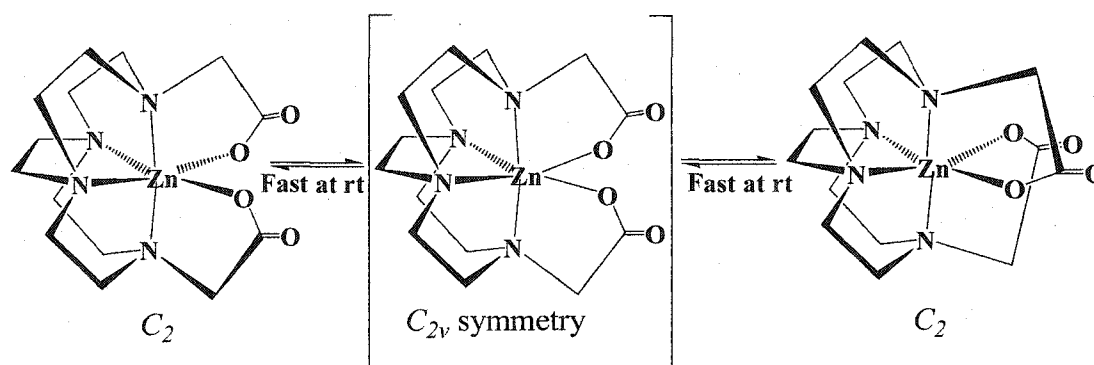


**Figure 3.17(a)** A possible non-dissociative mechanism for the averaged  $C_{2v}$  symmetry in the Zn(II) complex of **8-2H** in  $\text{CD}_3\text{OD}$ .

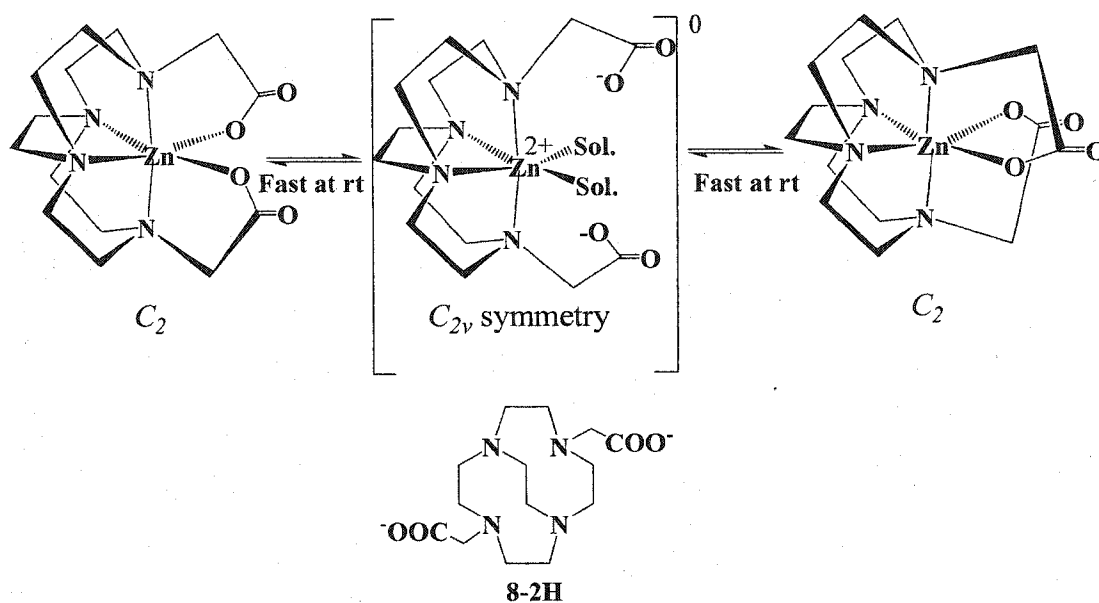


**Figure 3.17(b)** A dissociative mechanism for the averaged  $C_{2v}$  symmetry in the Zn(II) complex of **8-2H** in  $CD_3OD$ .

down this equilibrium (**Figure 3.17**) and result in a slow exchange  $C_2$  spectrum. Thus low temperature  $^1H$  (or  $^{13}C\{^1H\}$ ) NMR studies of these complexes were carried out in  $CD_3OD$ . Especially useful is the observed singlet assigned to the methylene protons on the pendant arms from coordinated **6** or **8-2H** at room temperature which should become an AB pattern at a low temperature. To begin with, low-temperature  $^1H$  NMR studies of both  $[Zn \cdot (7-2H)](NaClO_4)$  and  $[Cd \cdot (7-2H)](NaClO_4)$  in  $CD_3OD$  were performed.

The  $^1H$  NMR spectra of  $[Zn \cdot (7-2H)](NaClO_4)$  in  $CD_3OD$  at room temperature and at  $-80^\circ C$  are shown in **Figure 3.18** and these of  $[Cd \cdot (7-2H)](NaClO_4)$  in  $CD_3OD$  at room temperature and at  $-80^\circ C$  are shown in **Figure 3.19**. Broadening of both proton spectra indicate the slowing down of some dynamic process in both of these two complexes. Unfortunately, we were not able to reach the slow-exchange limit.

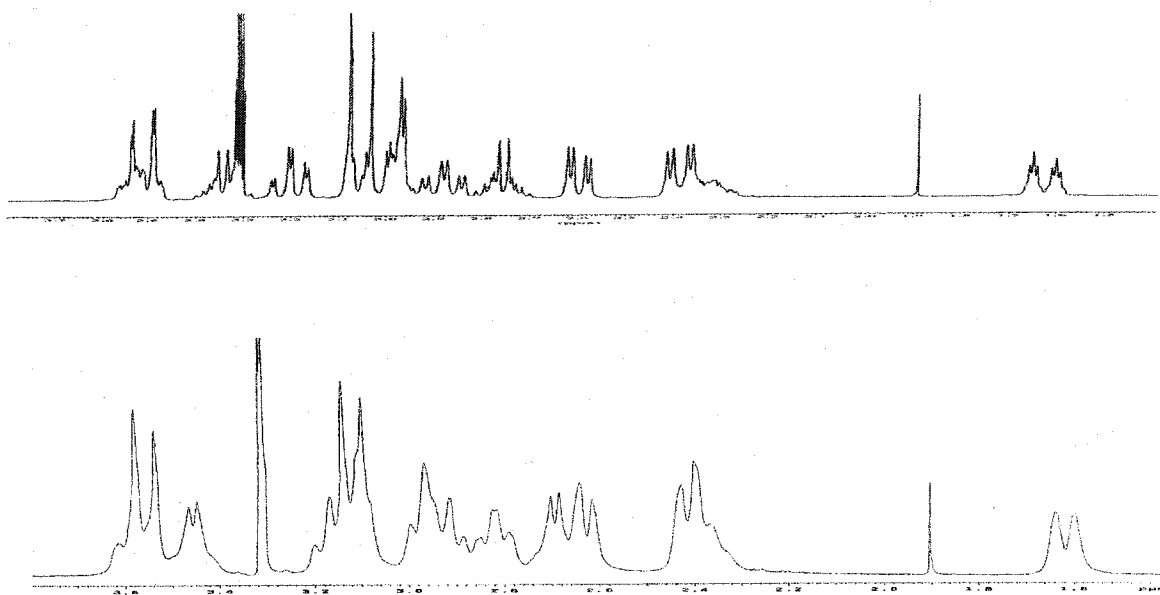


**Figure 3.18** Variable-temperature  $^1\text{H}$  NMR spectra of  $[\text{Zn}\cdot(7\text{-}2\text{H})](\text{NaClO}_4)$  in  $\text{CD}_3\text{OD}$  at room temperature (top) and at  $-80^\circ\text{C}$  (bottom).

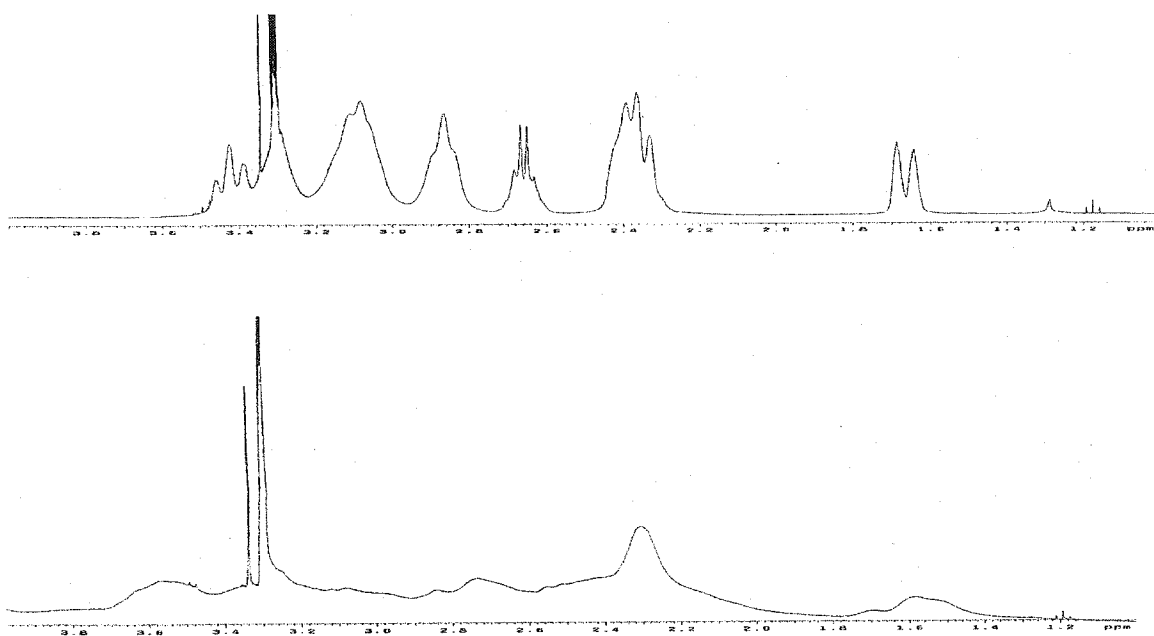


**Figure 3.19** Variable-temperature  $^1\text{H}$  NMR spectra of  $[\text{Cd}\cdot(7\text{-}2\text{H})](\text{NaClO}_4)$  in  $\text{CD}_3\text{OD}$  at room temperature (top) and at  $-80^\circ\text{C}$  (bottom).

The  $^1\text{H}$  NMR spectra of  $[\text{Zn}\cdot\mathbf{6}](\text{ClO}_4)_2$  in  $\text{CD}_3\text{OD}$  at both  $15^\circ\text{C}$  and at  $-80^\circ\text{C}$  are shown in **Figure 3.20**. Clearly, significant slowing of a dynamic process can again be seen. Again, no limiting spectrum was obtainable.

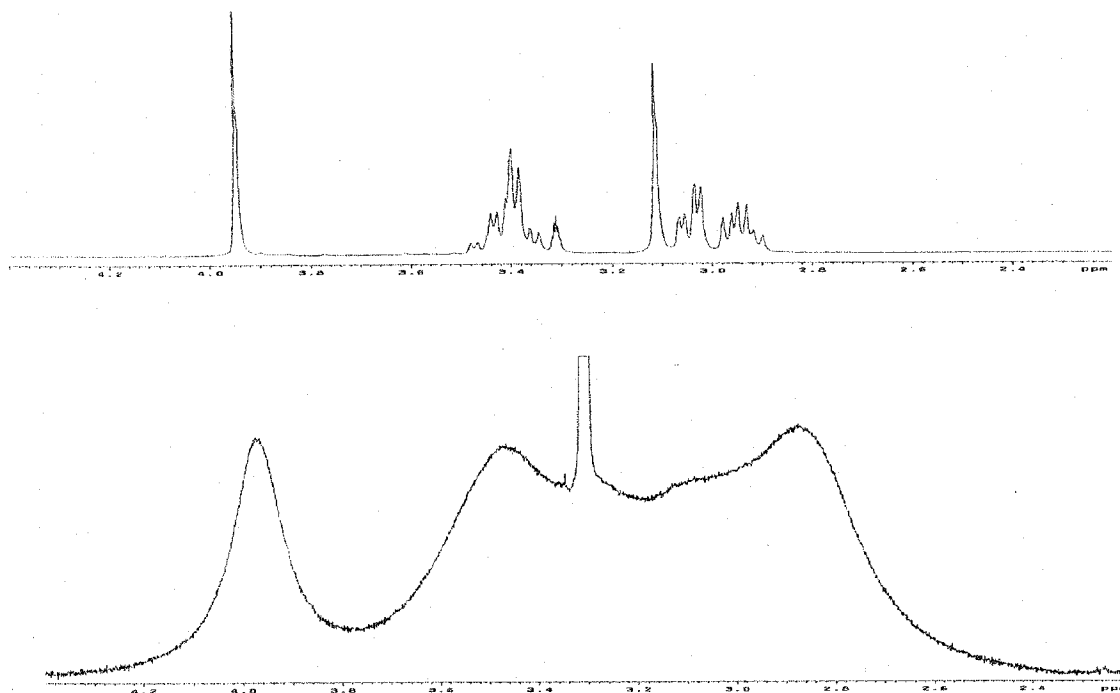


**Figure 3.20** Variable-temperature  $^1\text{H}$  NMR spectra of  $[\text{Zn}\cdot\mathbf{6}](\text{ClO}_4)_2$  in  $\text{CD}_3\text{OD}$  at  $15^\circ\text{C}$  (top) and at  $-80^\circ\text{C}$  (bottom).

The  $^1\text{H}$  NMR spectra of  $[\text{Zn}\cdot(\mathbf{8-2H})](\text{NaClO}_4)$  in  $\text{CD}_3\text{OD}$  at both room temperature and at  $-80^\circ\text{C}$  are shown in **Figure 3.21**. Interestingly, the observed singlet belonging to the methylene protons in the pendant arms at room temperature does resolve into an AB pattern at  $-80^\circ\text{C}$ . Further, we observed five carbon resonances (two of them are broad) from the  $^{13}\text{C}\{^1\text{H}\}$  NMR spectrum of  $[\text{Zn}\cdot(\mathbf{8-2H})](\text{NaClO}_4)$  in  $\text{CD}_3\text{OD}$  at room temperature and seven sharp  $^{13}\text{C}$  resonances at  $-80^\circ\text{C}$  (**Figure 3.22**).

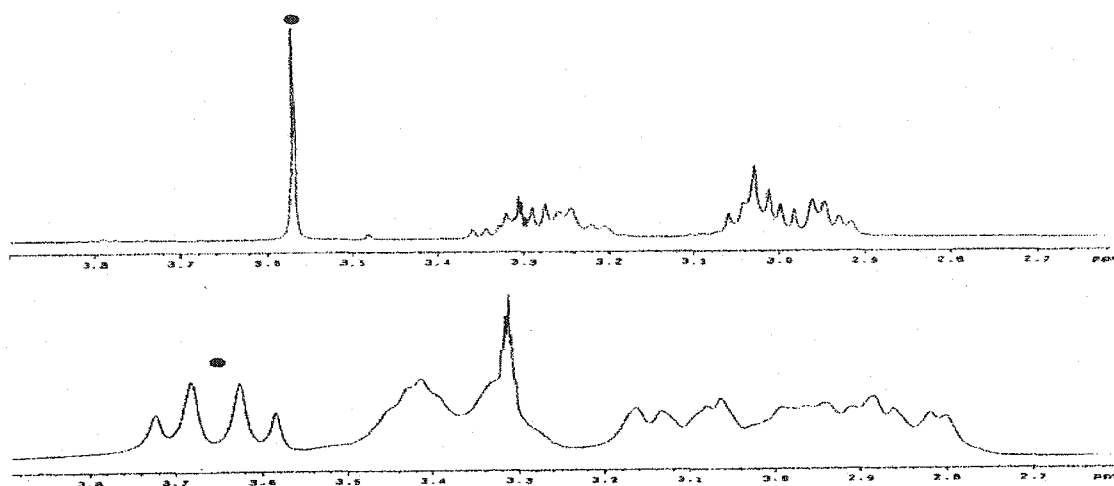


**Figure 3.21** Variable-temperature  $^1\text{H}$  NMR spectra of  $[\text{Zn}\cdot(8\text{-}2\text{H})](\text{NaClO}_4)$  in  $\text{CD}_3\text{OD}$  at room temperature (top) and at  $-80^\circ\text{C}$  (bottom). The resonances of the two methylene protons in the pendant arms are marked by dots.

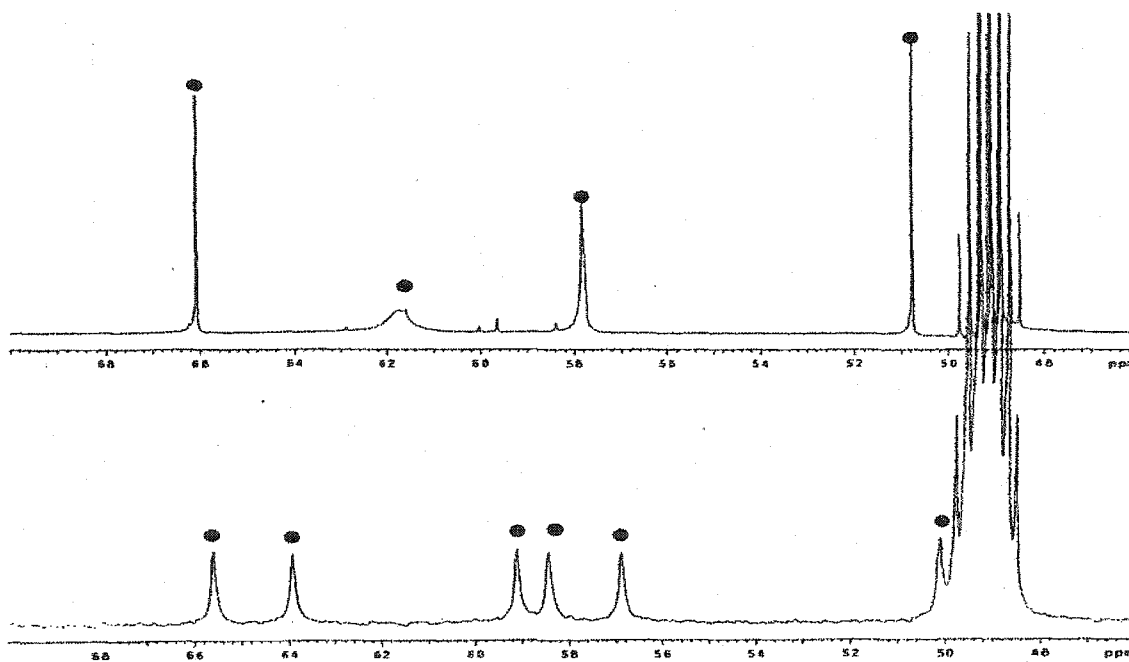


**Figure 3.22** Variable-temperature  $^{13}\text{C}\{^1\text{H}\}$  NMR spectra of  $[\text{Zn}\cdot(8\text{-}2\text{H})](\text{NaClO}_4)$  in  $\text{CD}_3\text{OD}$  at room temperature (top) and at  $-80^\circ\text{C}$  (bottom). The resonances from this complex are marked by dots.

Either a dissociative (**Figure 3.17(a)**) or non-dissociative (**Figure 3.17(b)**) mechanism can explain this dynamic process. Both can interconvert the  $C_2$  enantiomeric complex rapidly at room temperature to give averaged  $C_{2v}$  spectra. The latter process is analogous to a helicity twist to attain enantiomerization without bond rupture. A Zn(II) center with  $d^{10}$  configuration has no ligand-field stabilization energy, making this an attractive, low activation process.

### 3. X-ray Structural Data.

X-ray structures of  $[Zn\bullet 5](ClO_4)_2$  (**136**),  $[Zn\bullet 6](ClO_4)_2$  (**138**),  $[Cd\bullet 6(\eta^1-NO_3)](NO_3)$  (**140**),  $[Zn\bullet(7-2H)](NaClO_4)$  (**141**),  $[Zn\bullet(8-2H)](NaClO_4)$  (**143**) and  $[Hg\bullet(7-2H)]_2(HgCl_2)_3$  (**148a**) were determined. To date, structural data of  $[Zn\bullet(8-2H)](NaClO_4)$  (**143**) has not yet been available. Crystals of complexes suitable for X-ray analyses typically grew when their methanol solution was diffused with diethyl ether. A summary of relevant bond distances and angles of these metal complexes are listed in **Tables 3.2 (a-e)**.

$[Zn\bullet 5](ClO_4)_2$  (**136**). The crystal structure of this complex is shown in **Figure 3.23**. The Zn(II) center is fully enveloped by the cross-bridged tetraamine and its two pendant arms with a near-octahedral  $N_4O_2$  donor set. Similar to all characterized metal complexes of parent ligand **1**, the bicyclic tetraamine frame adopts the expected *cis*-folded configuration (*cis-V*) in this complex (**Figure 2.26**).<sup>69(a),72,77</sup> This Zn(II) center is deeply engulfed in the ligand cavity as shown by the  $N_{ax}-Zn-N_{ax}$  ( $N(2)-Zn-N(2A)$ )



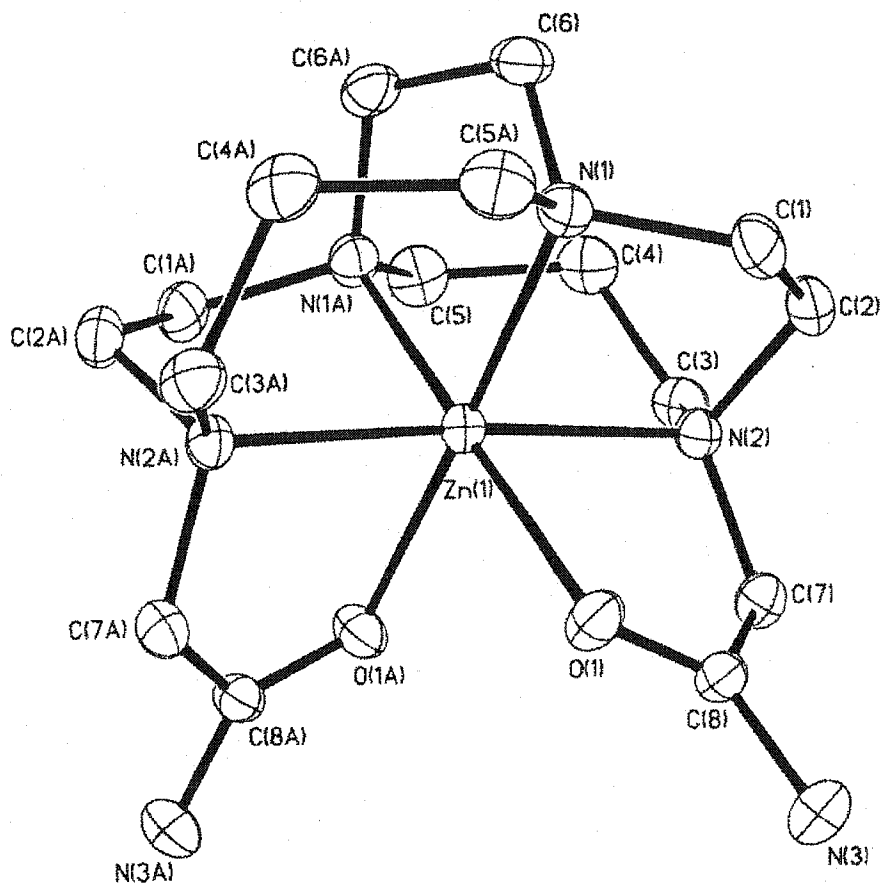


**Figure 3.23** X-ray structure of  $[\text{Zn}\cdot 5](\text{ClO}_4)_2$  (**136**) showing atomic labeling scheme.

angle of  $183.87(11)^\circ$  and the  $\text{N}(\text{eq})\text{-Zn-N}(\text{eq})$  ( $\text{N}(1)\text{-Zn-N}(1\text{A})$ ) angle of  $86.36(14)^\circ$ . Among reported 5- or 6-coordinated metal complexes of cross-bridged ligands,  $[\text{Cu}\cdot 7\text{Na}(\text{H}_2\text{O})\text{ClO}_4]_2(\text{H}_2\text{O})$  has the largest  $\text{N}_{\text{ax}}\text{-Cu-N}_{\text{ax}}$  bond angle of  $179.7(3)^\circ$  indicating an almost perfect fit inside the ligand.<sup>69(a)</sup> This  $\text{Zn}(\text{II})$  center is even deeper within the coordinated ligand cleft.

This  $\text{Zn}(\text{II})$  structure possesses a  $C_2$  symmetry. The two  $\text{Zn-N}(\text{ax})$  bondlengths of  $2.147(3) \text{ \AA}$  and  $\text{Zn-N}(\text{eq})$  bond distances of  $2.087(2) \text{ \AA}$  are significantly shorter than the

**Table 3.2(a)** Selected Bond Distances (Å) and Bond Angles (deg) in [Zn•5](ClO<sub>4</sub>)<sub>2</sub> (136).

Zn(1)-O(1)	2.099(2)	Zn(1)-O(1A)	2.099(2)
Zn(1)-N(1)	2.087(2)	Zn(1)-N(1A)	2.087(2)
Zn(1)-N(2)	2.147(3)	Zn(1)-N(2A)	2.147(3)
O(1)-Zn(1)-N(2A)	97.41(9)	O(1A)-Zn(1)-N(2)	97.41(9)
O(1)-Zn(1)-N(2)	79.71(9)	O(1A)-Zn(1)-N(2A)	79.71(9)
O(1)-Zn(1)-N(1A)	176.91(7)	O(1A)-Zn(1)-N(1)	176.91(7)
O(1)-Zn(1)-N(1)	94.35(11)	O(1A)-Zn(1)-N(1A)	94.35(11)
O(1)-Zn(1)-O(1A)	85.10(13)	N(2)-Zn(1)-N(2A)	183.87(11)
N(2)-Zn(1)-N(1)	85.48(9)	N(2A)-Zn(1)-N(1A)	85.48(9)
N(2A)-Zn(1)-N(1)	97.36(10)	N(2)-Zn(1)-N(1A)	97.36(10)
N(1)-Zn(1)-N(1A)	86.36(14)		

Zn-N bond distances in the six-coordinated Zn(II) complex of DOTAM (**65** in **Figure 1.21**), which range from 2.204(4) to 2.311(4) Å.<sup>164</sup> No X-ray structures of amide-armed cyclam complexes of Zn(II) have been updated. Comparing to the N(eq)-Zn bond distances of 2.185(4) Å in [Zn•1(μ-Cl)]<sub>2</sub>Cl<sub>2</sub>•4CH<sub>3</sub>OH (**116**) and of 2.124 (5)Å in Zn•3(μ-Cl<sub>2</sub>ZnCl<sub>2</sub>) (**120**), this Zn(II) complex appears to be a better fit (**Figure 1.57**). This is consistent with the larger N<sub>ax</sub>-Zn-N<sub>ax</sub> angle of 183.87(11)° in [Zn•5](ClO<sub>4</sub>)<sub>2</sub>

compared to  $168.4(3)^\circ$  in  $[\text{Zn}\cdot\mathbf{1}(\mu\text{-Cl})]_2\text{Cl}_2\cdot 4\text{CH}_3\text{OH}$  (**116**) and  $171.1(2)^\circ$  in  $\text{Zn}\cdot\mathbf{3}(\mu\text{-Cl}_2\text{ZnCl}_2)$  (**120**).

$[\text{Zn}\cdot\mathbf{6}](\text{ClO}_4)_2$  (**137**). The structure of this Zn(II) complex possesses a distorted octahedral  $\text{N}_4\text{O}_2$  donor set (**Figure 3.24**) similar to that of  $[\text{Zn}\cdot\mathbf{5}](\text{ClO}_4)_2$  (**136**). The

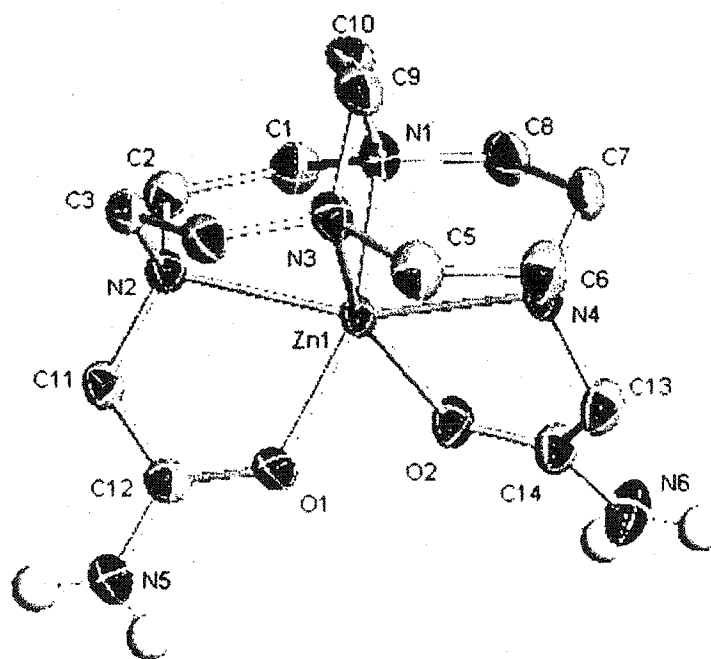


**Figure 3.24** X-ray structure of  $[\text{Zn}\cdot\mathbf{6}](\text{ClO}_4)_2$  (**138**) showing atomic labeling scheme.

smaller cross-bridged cyclen derivative, ligand **6**, is a poorer fit for the six-coordinate Zn(II). This is manifested in the increased distortion of the cation out from the bicyclic tetraamine cleft as the  $\text{N(ax)}\text{-Zn-N(ax)}$  angle is compressed to only  $159.14(10)^\circ$ . Again, the two  $\text{Zn-N(ax)}$  bond distances of  $2.172(3)$  and  $2.244(3)$  Å are slightly longer than the two  $\text{Zn-N(eq)}$  bond distances of  $2.076(3)$  and  $2.107(3)$  Å. Two different Zn-O bond

distances of 2.016(2) and 2.167(2) are found here. These bond distances are similar to those in the six-coordinated Zn(II) complex of DOTAM.<sup>40</sup>

**Table 3.2(b)** Selected Bond Distances (Å) and Bond Angles (deg) in [Zn•6](ClO<sub>4</sub>)<sub>2</sub> (137).

Zn(1)-O(1)	2.016(2)	Zn(1)-O(2)	2.167(2)
Zn(1)-N(1)	2.076(3)	Zn(1)-N(3)	2.107(3)
Zn(1)-N(2)	2.244(3)	Zn(1)-N(4)	2.172(3)
O(1)-Zn(1)-N(4)	117.38(10)	O(2)-Zn(1)-N(2)	118.58(9)
O(1)-Zn(1)-N(2)	78.75(9)	O(2)-Zn(1)-N(4)	77.53(9)
O(1)-Zn(1)-N(3)	100.39(11)	O(2)-Zn(1)-N(1)	96.24(10)
O(1)-Zn(1)-N(1)	157.07(10)	O(2)-Zn(1)-N(3)	158.02(10)
O(1)-Zn(1)-O(2)	86.54(10)	N(2)-Zn(1)-N(4)	159.14(10)
N(2)-Zn(1)-N(1)	79.97(10)	N(4)-Zn(1)-N(3)	80.79(10)
N(1)-Zn(1)-N(4)	85.35(10)	N(2)-Zn(1)-N(3)	83.34(10)
N(3)-Zn(1)-N(1)	85.48(11)		

[Cd•6(η<sup>1</sup>-NO<sub>3</sub>)](NO<sub>3</sub>) (140). This Cd(II) complex is coordinated fully by the hexadentate ligand **6** and a monodentate nitrate (**Figure 3.25**). This is the only known metal complex of a cross-bridged ligand with a coordination number of seven. The

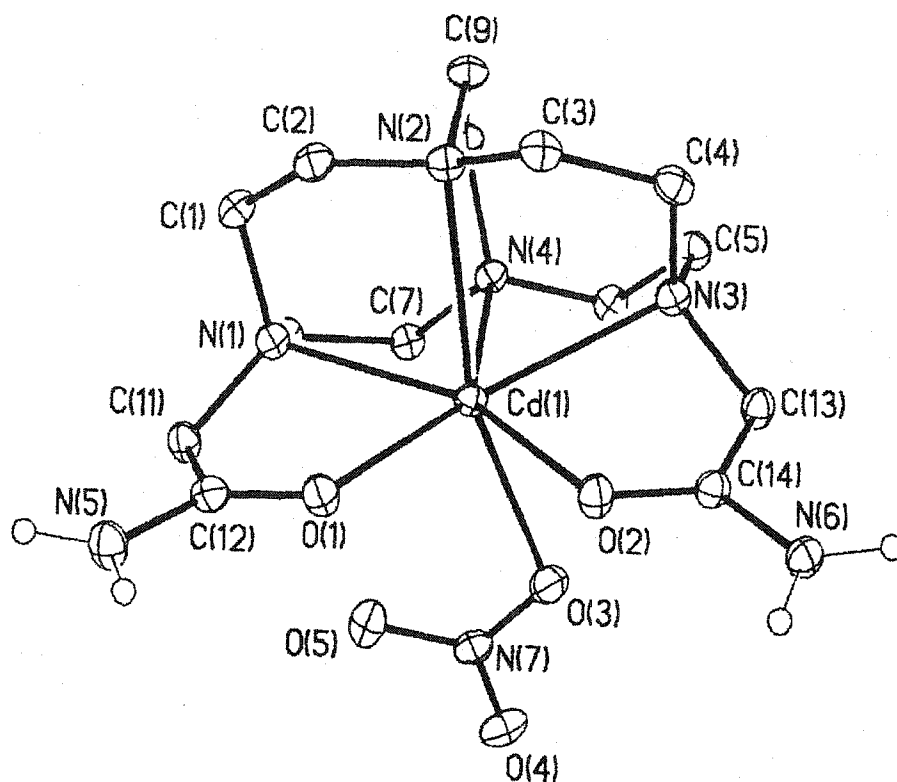


**Figure 3.25** X-ray structure of  $[\text{Cd}\cdot 6(\eta^1\text{-NO}_3)](\text{NO}_3)$  (**140**) showing atomic labeling scheme.

coordination geometry around cadmium can be described as the capped trigonal prism as the monodentate nitrate oxygen occupies the cap position. Similar to  $\text{CdCl}_2\cdot 2$  (**129**) and  $[\text{Cd}\cdot 2(\eta^2\text{-NO}_3)_2]$  (**131**), the axial N(1)-Cd-N(3) bond angle of  $137.5^\circ$  and equatorial N(2)-Cd-N(4) bond angle of  $71.8^\circ$  show how poorly the Cd(II) fit inside the coordinated ligand cleft. Four Cd(II)-N bond distances range from 2.408 to 2.456 Å, which are longer than two tertiary N-Cd(II) bond distances of 2.39 Å in  $[\text{Cd}\cdot 2(\eta^2\text{-NO}_3)_2]$  but shorter than the two tertiary N-Cd(II) bond lengths of 2.47 Å in  $\text{CdCl}_2\cdot 2$ . The average amide O-Cd(II) bond-length of 2.36 Å is similar to the two shorter amide O-Cd(II) bondlengths of 2.34 Å in  $[\text{Cd}(\text{II})\text{DOTAM}]^{2+}$  (**72** in **Figure 1.25**).<sup>40</sup>

**Table 2.8(c)** Selected Bond Distances (Å) and Bond Angles (deg) in [Cd•6( $\eta^1$ -NO<sub>3</sub>)](NO<sub>3</sub>) (140).

---

Cd(1)-N(1)	2.428(1)	Cd(1)-N(3)	2.456(2)
Cd(1)-N(2)	2.408(1)	Cd(1)-N(4)	2.416(1)
Cd(1)-O(1)	2.327(1)	Cd(1)-O(2)	2.395(1)
Cd(1)-O(3)	2.379(1)		
O(1)-Cd(1)-N(4)	143.51(5)	O(2)-Cd(1)-N(2)	103.61(5)
O(1)-Cd(1)-N(2)	98.84(5)	O(2)-Cd(1)-N(4)	141.07(5)
O(1)-Cd(1)-N(3)	138.17(5)	O(2)-Cd(1)-N(1)	145.96(5)
O(1)-Cd(1)-N(1)	71.63(5)	O(2)-Cd(1)-N(3)	68.73(4)
O(3)-Cd(1)-N(1)	113.12(5)	O(3)-Cd(1)-N(2)	158.33(5)
O(3)-Cd(1)-N(3)	91.51(5)	O(3)-Cd(1)-N(4)	91.32(5)
O(1)-Cd(1)-O(2)	75.04(4)	O(1)-Cd(1)-O(3)	102.78(5)
O(2)-Cd(1)-O(3)	80.71(5)	N(3)-Cd(1)-N(1)	137.47(5)
N(2)-Cd(1)-N(1)	75.27(5)	N(4)-Cd(1)-N(3)	73.50(5)
N(1)-Cd(1)-N(4)	71.89(5)	N(2)-Cd(1)-N(3)	71.00(5)
N(2)-Cd(1)-N(4)	71.84(5)		

---

[Zn•(7-2H)](NaClO<sub>4</sub>) (141). This Zn(II) complex is isostructural to the corresponding [Cu•(7-2H)Na(H<sub>2</sub>O)ClO<sub>4</sub>]<sub>2</sub>(H<sub>2</sub>O) (Figure 1.60). The Zn(II) center in this complex is also fully coordinated by four tetraamine nitrogens and two carboxylate oxygens from 7-2H in a near-octahedral manner (Figure 3.26). The N<sub>ax</sub>-Zn-N<sub>ax</sub> bond angle of 178.32(6)°

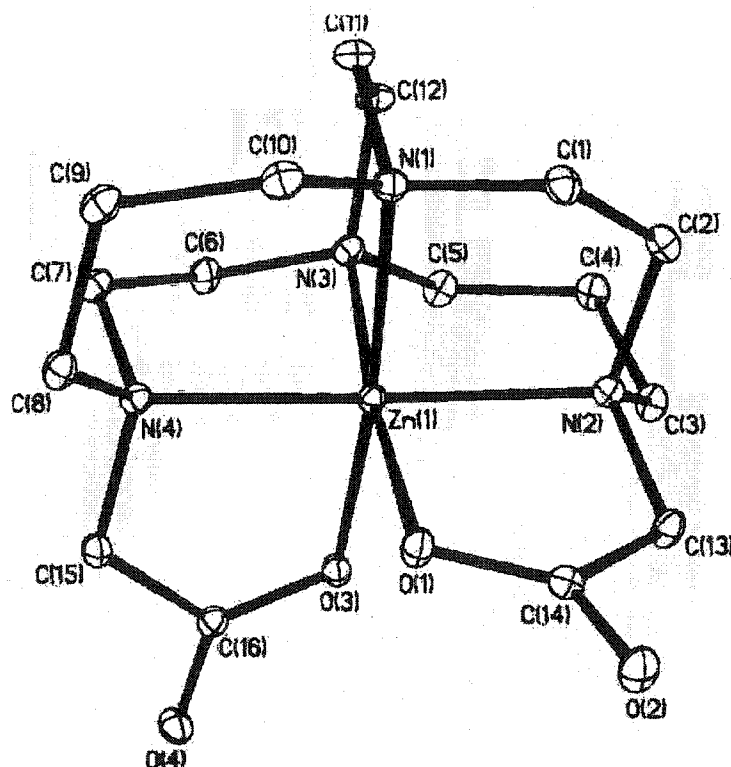


**Figure 3.26** X-ray structure of [Zn•(7-2H)](NaClO<sub>4</sub>) (141) showing atomic labeling scheme. Hydrogens bonded to carbons are omitted for clarity.

and the N(eq)-Zn-N(eq) bond angle of 83.84(6)° are also similar. Unlike both [Zn•5](ClO<sub>4</sub>)<sub>2</sub> and [Zn•6](ClO<sub>4</sub>)<sub>2</sub>, the Zn-N(ax) bond distance of 2.117(2) Å is slightly shorter than the two Zn-N(eq) bond distances of 2.158(2) Å. These are within the Zn(II)-N bondlengths ranging from 2.110 to 2.253 Å in the six-coordinated Zn(II) complexes of macrocyclic tetraamine carbamoyl ligands.<sup>137,164,165</sup> The two Zn-O bond distances of

2.0834(14) and 2.1103(13) Å are also within Zn(II)-O bondlengths of between 2.037 and 2.147 Å in these complexes.<sup>137,164,165</sup> The full structure of  $[\text{Zn} \cdot (7\text{-}2\text{H})](\text{NaClO}_4)$  includes sodium(I) cations coordinating to carboxylate oxygens from two different Zn(II) complex units in either mono or bidentate mode to form an infinite polymeric chain (Figure 3.27). Such an infinite Zn(II) coordination network may have potential application as a nonlinear optical material.<sup>126</sup>

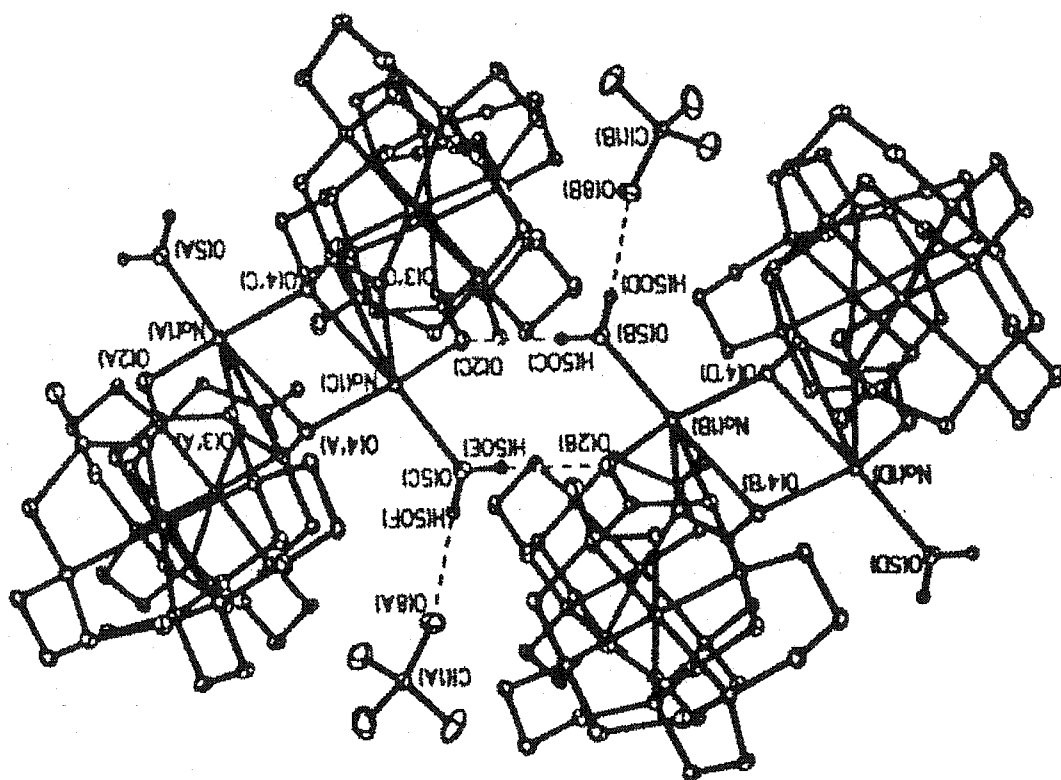


**Figure 3.27** Hydrogen bonding interactions in the crystal structure of  $[\text{Zn} \cdot (7\text{-}2\text{H})](\text{NaClO}_4)$  (141).



**Table 3.2(d)** Selected Bond Distances (Å) and Bond Angles (deg) in [Zn•(7-2H)](NaClO<sub>4</sub>)(141).

Zn(1)-O(1)	2.0834(14)	Zn(1)-O(3)	2.1103(13)
Zn(1)-N(1)	2.1557(16)	Zn(1)-N(3)	2.1598(16)
Zn(1)-N(2)	2.1172(16)	Zn(1)-N(4)	2.1162(16)
Na(1A)-O(2A)	2.3143(16)	Na(1A)-O(3'A)	2.5194(15)
Na(1A)-O(4'A)	2.5020(16)		
O(1)-Zn(1)-N(4)	97.88(6)	O(3)-Zn(1)-N(2)	98.45 (6)
O(1)-Zn(1)-N(2)	83.22(6)	O(3)-Zn(1)-N(4)	82.74(6)
O(1)-Zn(1)-N(3)	173.95(6)	O(3)-Zn(1)-N(1)	172.33(6)
O(1)-Zn(1)-N(1)	91.79(6)	O(3)-Zn(1)-N(3)	90.02(6)
O(1)-Zn(1)-O(3)	94.66(6)	N(2)-Zn(1)-N(4)	178.32(6)
N(2)-Zn(1)-N(1)	86.42(6)	N(4)-Zn(1)-N(3)	86.49(6)
N(1)-Zn(1)-N(4)	92.27(6)	N(2)-Zn(1)-N(3)	92.32(6)
N(3)-Zn(1)-N(1)	83.84(6)	Zn(1)-O(3)-Na(1A)	156.78(7)

[Zn•(8-2H)](NaClO<sub>4</sub>) (143). An X-ray structure of this complex (Figure 3.28) shows that Zn(II) center is also fully coordinated by four amine nitrogen donors and two

carboxylate oxygen atoms from **8-2H** in a distorted-octahedral geometry. Full structural data is not yet available at this time.

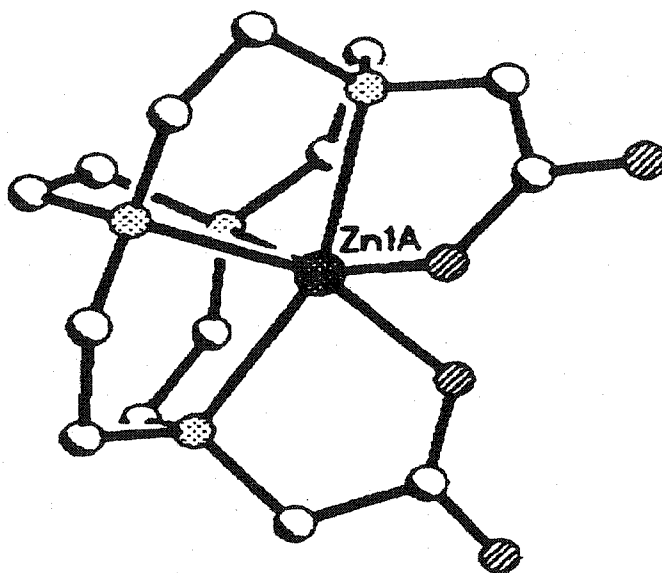


**Figure 3.28** X-ray structure of  $[\text{Zn}\cdot(\mathbf{8-2H})](\text{NaClO}_4)$  (**143**).

$[\text{Hg}\cdot(\mathbf{7-2H})]_2(\text{HgCl}_2)_3$  (**148a**). Unlike the out-of-cavity  $\text{HgCl}_2$  complex with parent cross-bridged cyclam **1** (**Figure 2.39**), the structure of this  $\text{Hg}(\text{II})$  complex of dicarboxylate pendant-armed cross-bridged cyclam derivative (**8**) shows an inside cavity  $\text{Hg}(\text{II})$  complex (**Figure 3.29**). Similar to all characterized  $\text{Zn}(\text{II})$  and  $\text{Cd}(\text{II})$  complexes of ligands **5-8**, the  $\text{Hg}(\text{II})$  center in this complex is fully enveloped by the cross-bridged tetraamine and its two pendant arms. Due to the larger size of  $\text{Hg}(\text{II})$ , the coordinated  $\text{Hg}(\text{II})$  center does not fit well in the cavity as indicated by the  $\text{N}_{\text{ax}}\text{-Hg-N}_{\text{ax}}$  angle of  $157.09(14)^\circ$  and the  $\text{N}(\text{eq})\text{-Hg-N}(\text{eq})$  angle of  $72.30(14)^\circ$ . This structure also features two independent but structurally similar  $\text{Hg}(\text{II})$  macrobicyclic units bridged by a third  $\text{Hg}(\text{II})$  through the carboxylate oxygen atoms. This bridging  $\text{Hg}(\text{II})$  is further coordinated to two terminal chlorides in a distorted square planar. Further, within each

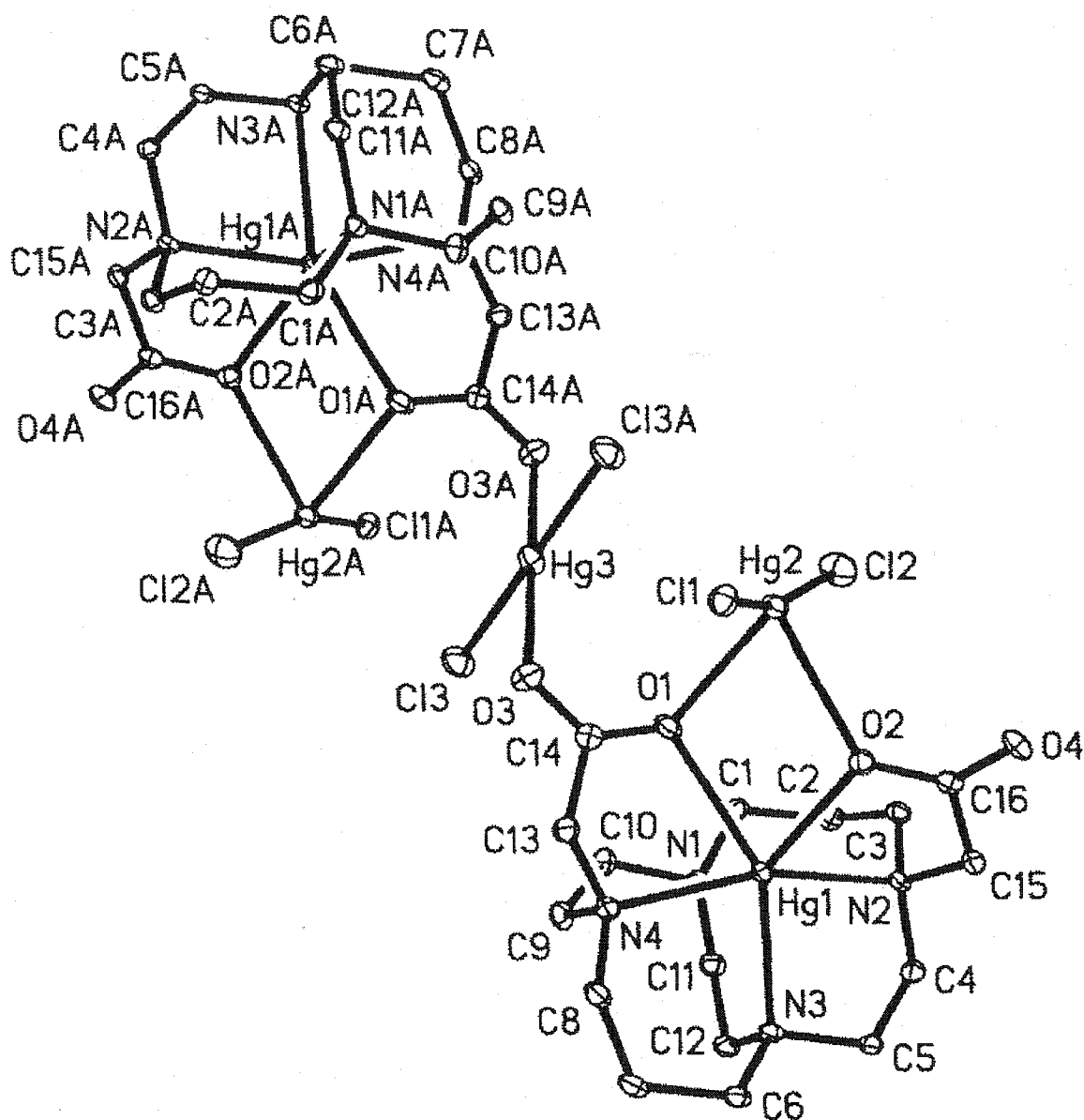


**Figure 3.29** X-ray structure of  $[\text{Hg}(\cdot(7\text{-}2\text{H}))_2(\text{HgCl}_2)_3$  (148a) showing atomic labeling scheme.

$[\text{Hg}(\text{II})\cdot(7\text{-}2\text{H})]$  units, an additional  $\text{HgCl}_2$  is chelated through two carboxylate oxygen atoms. This  $\text{Hg}(\text{II})$  atom adopts a distorted tetrahedral geometry with two terminal chlorides occupy the remaining coordinating sites.

**Table 3.2(e)** Selected Bond Distances (Å) and Bond Angles (deg) in [Hg•(7-2H)]<sub>2</sub>(HgCl<sub>2</sub>)<sub>3</sub> (148a).

Hg(1)-N(4)	2.331(4)	Hg(1)-N(1)	2.450(4)
Hg(1)-N(2)	2.344(4)	Hg(1)-N(3)	2.483(4)
Hg(1)-O(1)	2.537(4)	Hg(1)-O(2)	2.366(4)
Hg(2)-O(1)	2.464(4)	Hg(2)-O(2)	2.560(3)
Hg(3)-O(3)	2.594(4)	Hg(3)-O(3A)	2.594(4)
Hg(2)-Cl(1)	2.3081(13)	Hg(2)-Cl(2)	2.3023(15)
Hg(3)-Cl(3)	2.3007(16)	Hg(3)-Cl(3A)	2.3007(16)
N(2)-Hg(1)-N(4)	157.09(14)	N(3)-Hg(1)-N(1)	72.30(14)
N(1)-Hg(1)-N(4)	78.59(14)	N(2)-Hg(1)-N(3)	77.07(13)
N(1)-Hg(1)-N(2)	84.19(13)	N(3)-Hg(1)-N(4)	83.34(14)
O(1)-Hg(1)-N(4)	71.33(13)	O(3)-Hg(1)-N(2)	98.45 (6)
O(1)-Zn(1)-N(2)	83.22(6)	O(1)-Hg(1)-N(2)	121.79(13)
O(1)-Hg(1)-N(3)	147.98(13)	O(1)-Hg(1)-N(1)	83.50(13)
O(2)-Hg(1)-N(1)	129.96(13)	O(2)-Hg(1)-N(2)	71.60(12)
O(2)-Hg(1)-N(3)	138.78(13)	O(2)-Hg(1)-N(4)	131.26(13)
O(2)-Hg(1)-O(1)	74.10(12)	Cl(2)-Hg(2)-Cl(1)	161.50(6)
Cl(2)-Hg(2)-O(1)	102.97(10)	Cl(2)-Hg(2)-O(2)	94.59(9)
Cl(1)-Hg(2)-O(1)	94.64(9)	Cl(1)-Hg(2)-O(2)	96.21(8)
O(2)-Hg(2)-O(1)	72.09(13)	Cl(3)-Hg(3)-O(3)	86.16(10)

Cl(3)-Hg(3)-Cl(3A)	180.00(6)	Cl(3A)-Hg(3)-O(3)	93.84(10)
Cl(3)-Hg(3)-O(3A)	93.84(10)	Cl(3A)-Hg(3)-O(3A)	86.16(10)
O(3)-Hg(3)-O(3A)	180.00(9)		

---

The structure of this Hg(II) complex clearly indicates that the formation of the out-of-cavity complex  $[\text{HgCl}_2(\mu\text{-1})]_2$  (**133**) (**Figure 2.39**) is a result of the presence of two secondary amine hydrogens which maintained strong transannular hydrogen bonding within the ligand cleft. There have been no X-ray reports on the Hg(II) complexes of macrocyclic polyamine with one or more carboxylate pendant-arms.

#### Summary of Structural Data.

Those six Zn(II), Cd(II) and Hg(II) complexes of pendant-armed cross-bridged ligands **5-8** feature full  $\eta^4\text{-N}$ ,  $\eta^2\text{-O}$  coordination of the metal cations within the ligands clefts. So far, full structural data of  $[\text{Zn}(\mathbf{8-2H})](\text{NaClO}_4)$  is not yet available. A comparison of axial N-M-N angles and the equatorial N-M-N angles is listed in **Table 3.3**. Clearly, similar to parent ligands, cross-bridged cyclam derivatives **5** and **7-2H** provide a better fit for octahedral Zn(II) than the smaller cross-bridged cyclen derivatives **6** and **8-2H**. This is best gauged by the axial N-Zn-N angles of  $183.87^\circ$  and  $178.32(16)^\circ$  for the former and  $159.14(10)^\circ$  for  $[\text{Zn}(\mathbf{6})(\text{ClO}_4)_2]$  (**137**). However, unlike Zn(II) complexes of parent ligands **1** and **2**, the equatorial N-Zn-N angle which is

86.36(14)° and 83.84(6)° for Zn(II) complexes of cyclam-derived **5** and **7-2H** respectively is close to that of 85.48(11)° for [Zn•**6**](ClO<sub>4</sub>)<sub>2</sub>.

Comparison of the structural data of [Zn•**6**](ClO<sub>4</sub>)<sub>2</sub>(**137**) and [Cd•**6**(η<sup>1</sup>-NO<sub>3</sub>)](NO<sub>3</sub>)(**140**) clearly shows that the increased misfit of the larger cation. Their respective axial N-M-N angles are Zn (159.14(10)°) and Cd (137.5°). Parallel trends in the equatorial N-M-N angles are also observed for Zn (85.48(11)°) and Cd (71.8°). Similarly, comparison on the structural data of [Zn•(**7-2H**)](NaClO<sub>4</sub>)(**141**) and [Hg•(**7-2H**)]<sub>2</sub>(HgCl<sub>2</sub>)<sub>3</sub> (**148a**) again demonstrated this trend as their respective axial N-M-N angles are Zn (183.87(11)°) and Hg (157.09(14)°) while the equatorial N-M-N angles are Zn (86.36(14)°) and Hg (72.30(14)°). These data affirm the design purpose of these cross-bridged ligands with or without pendant-arms for selective complexation of smaller metal ions. Similar to any other Zn(II) and Cd(II) complexes of ligands **5-8**, a Hg(II) center has been shown to be fully coordinated by four tetraamine nitrogens and two carboxylate oxygens from **7** (**Figure 3.29**), albeit with substantial bond angle deviations from an idealized octahedral geometry.

**Table 3.3** Structural comparison of Zn(II), Cd(II) and Hg(II) complexes of ligands **5-8**.

Complex	Axial N-M-N angle	Equatorial N-M-N angle
[Zn• <b>5</b> ](ClO <sub>4</sub> ) <sub>2</sub> ( <b>136</b> )	183.87 (11)	86.36 (14)
[Zn• <b>6</b> ](ClO <sub>4</sub> ) <sub>2</sub> ( <b>138</b> )	159.14 (10)	85.48 (11)
[Cd• <b>6</b> (η <sup>1</sup> -NO <sub>3</sub> )](NO <sub>3</sub> ) ( <b>140</b> )	137.5	71.8
[Zn•( <b>7-2H</b> )](NaClO <sub>4</sub> ) ( <b>141</b> )	178.32 (6)	83.84 (6)
[Hg•( <b>7-2H</b> )] <sub>2</sub> (HgCl <sub>2</sub> ) <sub>3</sub> ( <b>148a</b> )	157.09 (14)	72.30 (14)

## CHAPTER IV

### Ga(III), In(III) AND Cu(II) COMPLEXES OF CROSS-BRIDGED LIGANDS 1-8

#### 1. Ga(III) and In(III) Complexes of Cross-bridged Ligands 1, 2, and 8.

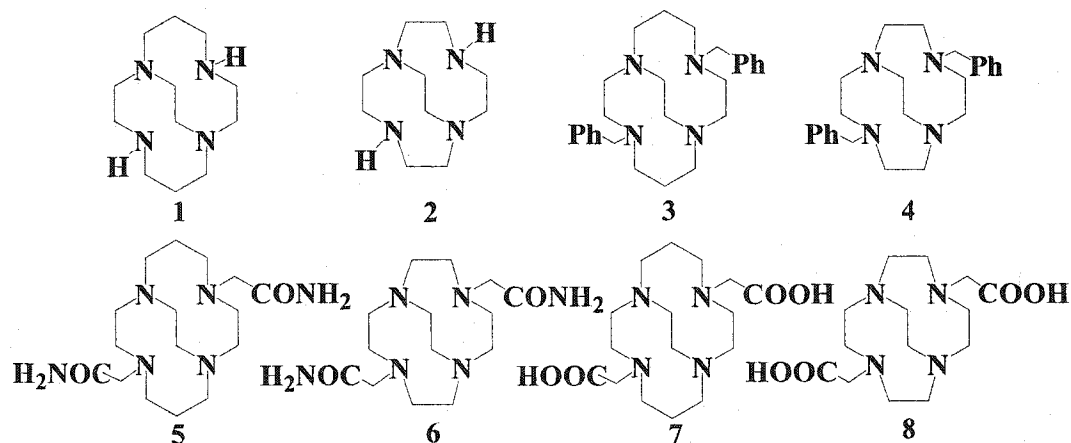
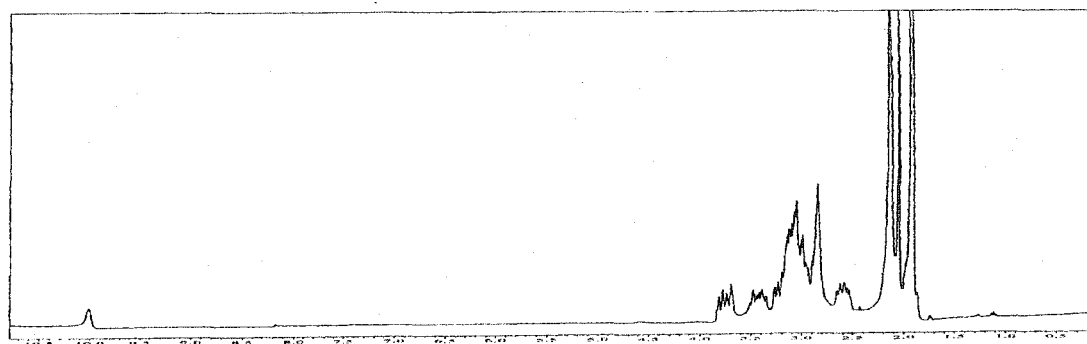


Figure 4.1 Cross-bridged ligands studied in Ga(III), In(III) and Cu(II) complexation.

#### 1.1. Synthesis and Characterization.

In the preparation of Ga(III) and In(III) coordination complexes, a persistent problem is that the precipitation of Ga(OH)<sub>3</sub> and In(OH)<sub>3</sub> may occur before the complexation process is complete.<sup>59</sup> The combination of this and the proton-sponge character of our cross-bridged ligands can easily lead to protonated ligand byproducts in the presence of moisture or any acidic proton sources. Early attempted complexations of

Ga(III) or In(III) salts with ligands **1** or **2** in the protic solvent methanol indeed produced this problem. For example, attempted complexation of InBr<sub>3</sub> with **2** in MeOH yielded some white precipitate from which pure [InBr<sub>2</sub>•**2**]Br (**152**) was isolable after several acetonitrile washings. However, Et<sub>2</sub>O diffusion into the mother liquor yielded a crystalline solid from which a proton NMR spectrum in CD<sub>3</sub>CN included a singlet resonance at δ 10 ppm (**Figure 4.2**). This indicates that protonated **2** was formed in the



**Figure 4.2** Proton NMR spectrum of the crystalline solid from [InBr<sub>2</sub>•**2**]Br synthesis in CD<sub>3</sub>CN.

attempted complexation. An attempted complexation of InBr<sub>3</sub> with **1** in methanol also yielded a mixture of complexed and protonated **1** as seen in its <sup>1</sup>H (**Figure 4.3(a)**) and <sup>13</sup>C{<sup>1</sup>H} NMR spectra in D<sub>2</sub>O. The characteristic resonance of protonated **1** at δ 2.53 in its proton NMR spectrum in **Figure 4.3(a)** can be compared with the proton NMR spectrum of protonated **1** (**Figure 4.3(a)**). A failed complexation between Ga(NO<sub>3</sub>)<sub>3</sub> hydrate and **1** in methanol yielded mainly protonated **1**(**Figure 4.3(b)**). Anhydrous reaction conditions were thus employed to prepare Ga(III) and In(III) complexes of cross-bridged cyclam (ligand **1**) and cross-bridged cyclen (ligand **2**). By avoiding moisture and using anhydrous acetonitrile as the reaction solvent, complexes [GaCl<sub>2</sub>•**1**]Cl (**149**) (68%,



yield),  $[\text{InBr}_2 \cdot \mathbf{1}]\text{Br}$  (**150**) (86%),  $[\text{GaCl}_2 \cdot \mathbf{2}]\text{Cl}$  (**151**) (53%), and  $[\text{InBr}_2 \cdot \mathbf{2}]\text{Br}$  (**152**) (60%) were isolated as confirmed by their CHN elemental analyses. In addition, three of these four Ga(III) and In(III) complexes were also characterized by X-ray analyses. These represent the first well-characterized gallium(III) and indium(III) halide complexes of any tetraamine.

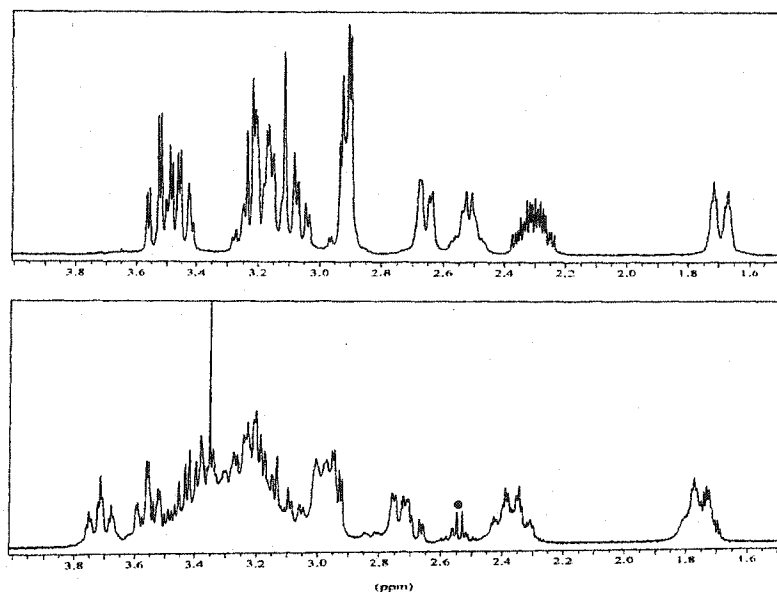


**Figure 4.3(a)** Top: Proton NMR spectrum of a protonated **1** in  $\text{D}_2\text{O}$ . Bottom: Proton NMR spectrum of an attempted complexation product of  $\text{InBr}_3$  with **1** in methanol in  $\text{D}_2\text{O}$ , in which the characteristic protonated **1** resonance is marked by a dot.

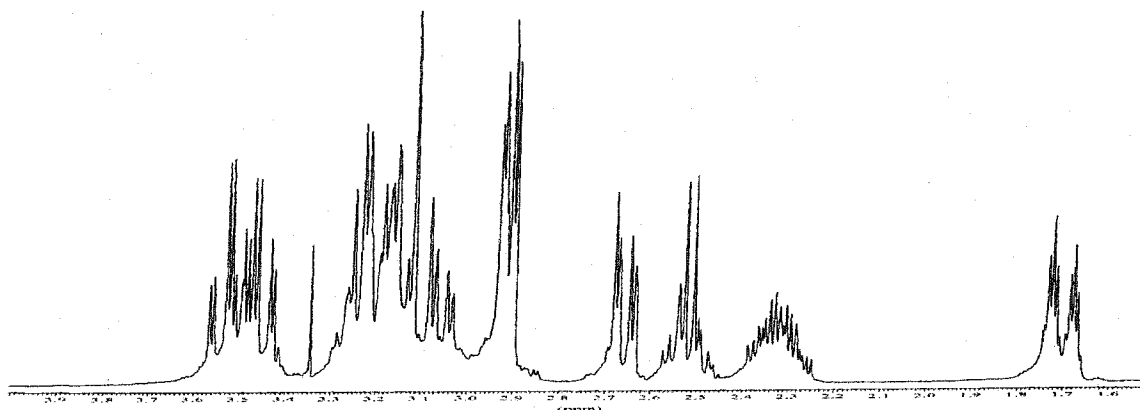


**Figure 4.3(b)** Proton NMR spectrum of an attempted complexation product between  $\text{Ga}(\text{NO}_3)_3$  hydrate and **1** in methanol ( $\text{D}_2\text{O}$ ).

Ligands **7** and **8** are N, N'-dicarboxylate pendant-armed derivatives of parent cross-bridged cyclam (**1**) and cross-bridged cyclen (**2**) respectively (**Figure 4.1**). Unlike ligands **1-6**, ligands **7** and **8** contain both carboxylate acidic protons and basic amines and they were synthesized as TFA salts. Equivalents of base are thus necessary to neutralize these acidic protons in order to facilitate the formation of metal complexes. In the presence of NaOAc base,  $[\text{Ga}\cdot(\mathbf{8-2H})](\text{NO}_3)$  (**153**) precipitated from the reaction mixture of  $\mathbf{8}\cdot\text{TFA}\cdot\text{H}_2\text{O}$  and  $\text{Ga}(\text{NO}_3)_3$  hydrate in MeOH after refluxing for several hours. Sodium acetate was chosen as the base for the following reason. Addition of a strong base such as sodium hydroxide into a solution containing  $\text{Ga}(\text{NO}_3)_3$  hydrate may cause the precipitation of  $\text{Ga}(\text{OH})_3$  whereas the weakly coordinating of acetate to Ga(III) can avoid this problem.<sup>22,59</sup>  $[\text{Ga}\cdot(\mathbf{8-2H})](\text{NO}_3)$  is soluble in  $\text{D}_2\text{O}$  and  $d_6$ -DMSO. Contrary to the relatively easy synthesis of  $[\text{Ga}\cdot(\mathbf{8-2H})](\text{NO}_3)$ , all attempted complexations of Ga(III) salts with  $\mathbf{7}\cdot(\text{TFA})_2$  have failed so far. For example, an attempted complexation of  $\text{Ga}(\text{NO}_3)_3$  hydrate with  $\mathbf{7}\cdot(\text{TFA})_2$  under similar reaction conditions yielded only a polymeric or oligomeric product as indicated by its poor solubility in  $\text{D}_2\text{O}$  and  $d_6$ -DMSO. The presence of ligand **7** in this is indicated by carboxylate carbonyl stretches at 1558, 1635, 1652, and 1685  $\text{cm}^{-1}$  in its IR (KBr) spectrum (**Figure 4.4**). Attempted complexation of  $\text{Ga}(\text{acac})_3$  with  $\mathbf{7}\cdot(\text{TFA})_2$  in the presence of a methanol solution of KOH (or NaOAc) did not yield an inside-cavity complex since both  $^1\text{H}$  and  $^{13}\text{C}\{^1\text{H}\}$  NMR spectra of the product in acidic  $\text{D}_2\text{O}$  are quite similar to those of  $\mathbf{7}\cdot(\text{HCl})_2$  (**Figure 4.5(a)** and **Figure 4.5(b)**).

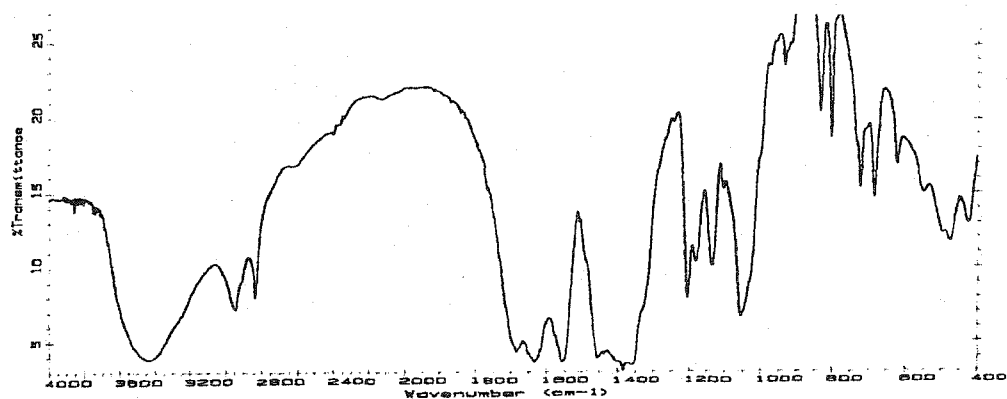


**Figure 4.4** IR (KBr) spectrum of the product of an attempted complexation of  $\text{Ga}(\text{NO}_3)_3$  hydrate with  $7 \cdot (\text{TFA})_2$

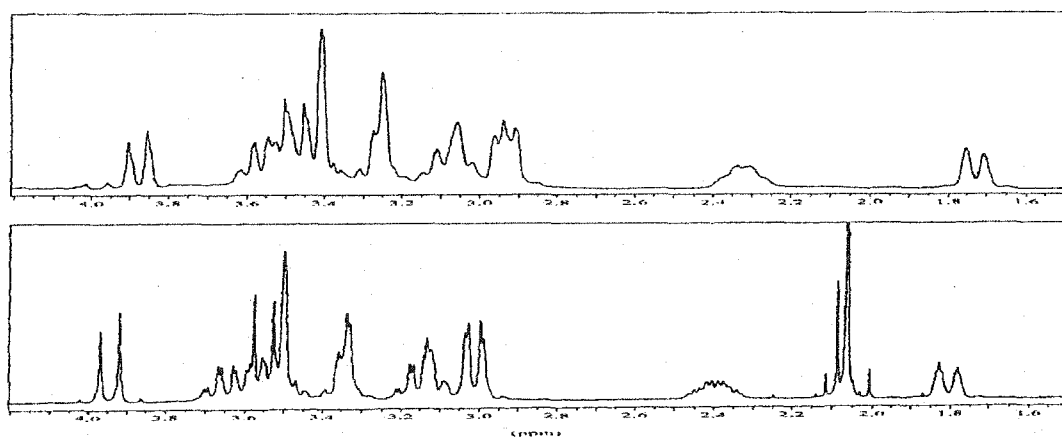


**Figure 4.5(a)** Top: Proton NMR spectrum of  $7 \cdot (\text{HCl})_2$  in  $\text{D}_2\text{O}$ . Bottom: Proton NMR spectrum of an attempted complexation product of  $\text{Ga}(\text{acac})_3$  with  $7 \cdot (\text{TFA})_2$  in  $\text{D}_2\text{O}$  (the singlet at  $\delta$  2.06 ppm is from  $\text{CH}_3\text{CN}$ ).

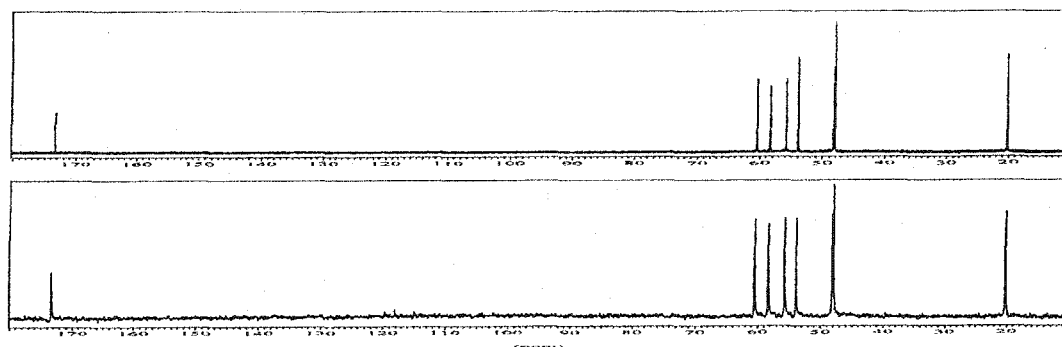


**Figure 4.5(b)** Top:  $^{13}\text{C}\{^1\text{H}\}$  NMR spectrum of  $7 \cdot (\text{HCl})_2$  in  $\text{D}_2\text{O}$ . Bottom:  $^{13}\text{C}\{^1\text{H}\}$  NMR spectrum of an attempted complexation product of  $\text{Ga}(\text{acac})_3$  with  $7 \cdot (\text{TFA})_2$  in  $\text{D}_2\text{O}$ .

## 1.2. Spectral Data.

### (a) Infrared Spectra.

In their IR(KBr) spectra, all four Ga(III) and In(III) complexes of ligands **1** and **2** have N-H stretches appearing between 3036 and 3137  $\text{cm}^{-1}$  (Table 4.1) which are significantly lower than those of Zn(II), Cd(II) and Hg(II) complexes of ligands **1** and **2**

**Table 4.1** NH stretches in the IR spectra of Ga(III) and In(III) complexes of ligands **1** and **2**.

Complex	$\nu_{\text{NH}}$ ( $\text{cm}^{-1}$ )		Complex	$\nu_{\text{NH}}$ ( $\text{cm}^{-1}$ )
$[\text{GaCl}_2 \cdot \mathbf{1}]\text{Cl}$	3137		$[\text{InBr}_2 \cdot \mathbf{1}]\text{Br}$	3116
$[\text{GaCl}_2 \cdot \mathbf{2}]\text{Cl}$	3049		$[\text{InBr}_2 \cdot \mathbf{2}]\text{Br}$	3036

(3216 and 3286  $\text{cm}^{-1}$ ) (Table 2.2) but similar to the N-H stretch of 3078  $\text{cm}^{-1}$  in the out-of-cavity complex  $[\text{HgCl}_2(\mu\text{-1})]_2$  (Table 2.2). Complex  $[\text{Ga} \cdot (\mathbf{8-2H})](\text{NO}_3)$  (**152**) shows two sharp and strong carboxylate bands at 1672 and 1692  $\text{cm}^{-1}$ . These two are higher than for the C=O stretches of Zn(II), Cd(II) and Hg(II) complexes with ligands **7-8** (Table 3.1). 1611 and 1645  $\text{cm}^{-1}$  are the two highest frequency carboxylate bands among these complexes.

### (b) Solution $^1\text{H}$ and $^{13}\text{C}\{^1\text{H}\}$ NMR Spectra.

Solution  $^1\text{H}$  and  $^{13}\text{C}\{^1\text{H}\}$  NMR spectra of the four Ga(III) and In(III) complexes of ligands **1** and **2** are discussed here. Similar to Zn(II) complexes of ligands **1** and **2** in  $\text{D}_2\text{O}$ , all these complexes display NH/ND exchange in  $\text{D}_2\text{O}$ . In  $\text{D}_2\text{O}$ ,  $[\text{GaCl}_2 \cdot \mathbf{1}]\text{Cl}$  (N-D complex) exhibited broad signals in both its  $^1\text{H}$  and  $^{13}\text{C}\{^1\text{H}\}$  NMR spectra (Figure 4.6(a))

and **Figure 4.6(b)**), which may be caused by dynamic exchanges involving chloride,  $D_2O$

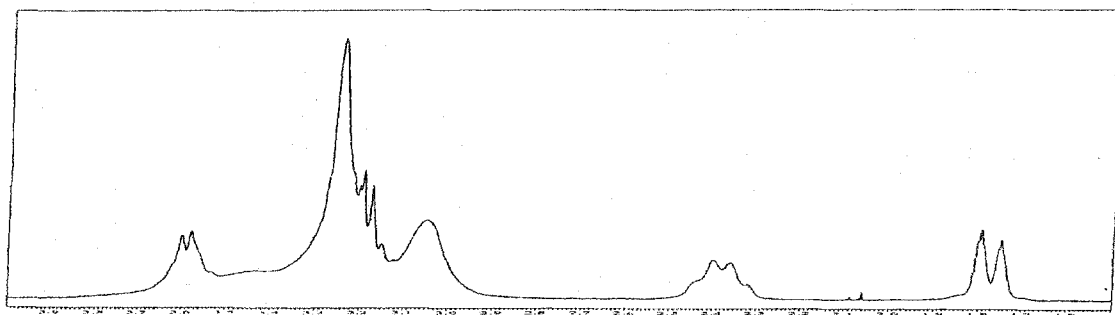


**Figure 4.6(a)** Proton NMR spectrum of  $[GaCl_2 \cdot 1]Cl$  (N-D complex) in  $D_2O$ .

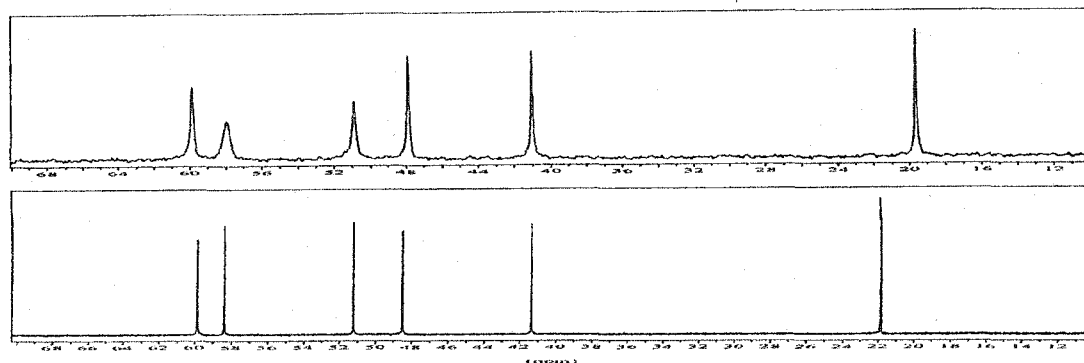


**Figure 4.6(b)** Top:  $^{13}C\{^1H\}$  NMR spectrum of  $[GaCl_2 \cdot 1]Cl$  (N-D complex) in  $D_2O$ . Bottom:  $^{13}C\{^1H\}$  NMR spectrum of  $[Zn \cdot 1(\mu-Cl)_2]Cl_2$  (**116a**) in  $D_2O$ .

and  $OD^-$  at the cation. For comparison, the sharp and well-resolved  $^{13}C\{^1H\}$  NMR spectrum of  $[Zn \cdot 1(\mu-Cl)_2]Cl_2$  (**116a**) is also shown in **Figure 4.6(b)**. Both the  $^1H$  and  $^{13}C\{^1H\}$  NMR spectra of  $[GaCl_2 \cdot 1]Cl$  in  $D_2O$  changed after the addition of acid. The  $^1H$  NMR spectrum of  $[GaCl_2 \cdot 1]Cl$  (N-D complex) in acidic  $D_2O$  (pD = 1.07,  $DClO_4$ ) is shown in **Figure 4.7**. Unlike the usual spin pattern of the most upfield resonance of a doublet of pentets around  $\delta$  1.6 of a coordinated cross-bridged cyclam (ligand **1**) and its derivatives, this spectrum shows two doublets of pentets at  $\delta$  1.84 and 1.76 (**Figure 4.8**). Since this Ga(III) complex is stable in acidic  $D_2O$  (pD = 1.07) for at least one year, these

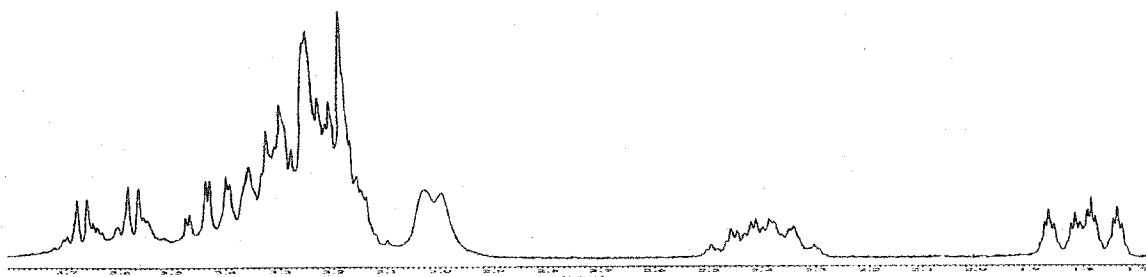


**Figure 4.7**  $^1\text{H}$  NMR spectrum of  $[\text{GaCl}_2\cdot\mathbf{1}]\text{Cl}$  (N-D complex) in acidic  $\text{D}_2\text{O}$  (pD = 1.07).

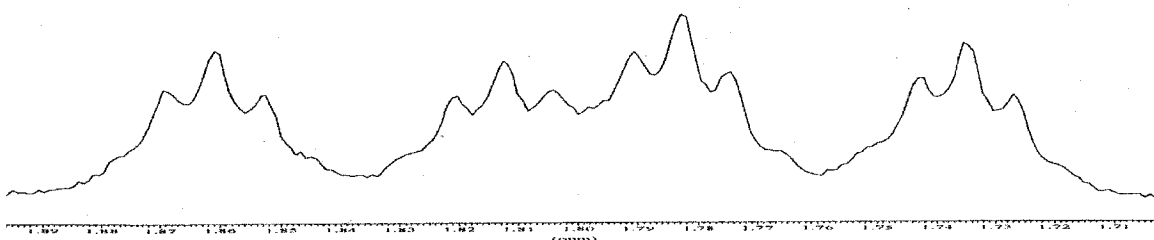


**Figure 4.8** Expansion of the two doublets of pentets at  $\delta$  1.84 and 1.76 in the  $^1\text{H}$  NMR spectrum of 0.015 M  $[\text{GaCl}_2\cdot\mathbf{1}]\text{Cl}$  (N-D complex) in acidic  $\text{D}_2\text{O}$  (pD = 1.07).

two separate doublets of pentets suggest that  $[\text{GaCl}_2\cdot\mathbf{1}]\text{Cl}$  can exist as two species in acidic  $\text{D}_2\text{O}$  in slow exchange on the NMR time scale. Consistent with this hypothesis, there are also two sets of  $^{13}\text{C}$  resonances for this Ga(III) complex (**Figure 4.9**). For example, the carbon  $\beta$  to amino nitrogens in coordinated  $\mathbf{1}$  appear as two distinct peaks at  $\delta$  19.7 and 19.4 (**Figure 4.10**). For clarity, these two Ga(III) species will be labeled Ga(III) complex **A** ( $^1\text{H}$  at  $\delta$  1.84) and Ga(III) complex **B** ( $^1\text{H}$  at  $\delta$  1.76) respectively. The  $\text{NH}/\text{ND}$  exchange also occurs for both as indicated by the fact that in a  $\text{NH}/\text{ND}$  complex mixture, a slightly different chemical shift is observed for the two  $^{13}\text{C}$  resonances around  $\delta$  48 and  $\delta$  41 for both species but not for the pure N-D complex (**Figure 4.9**). The assumption that complexes **A** and **B** are in slow exchange on the NMR time scale is

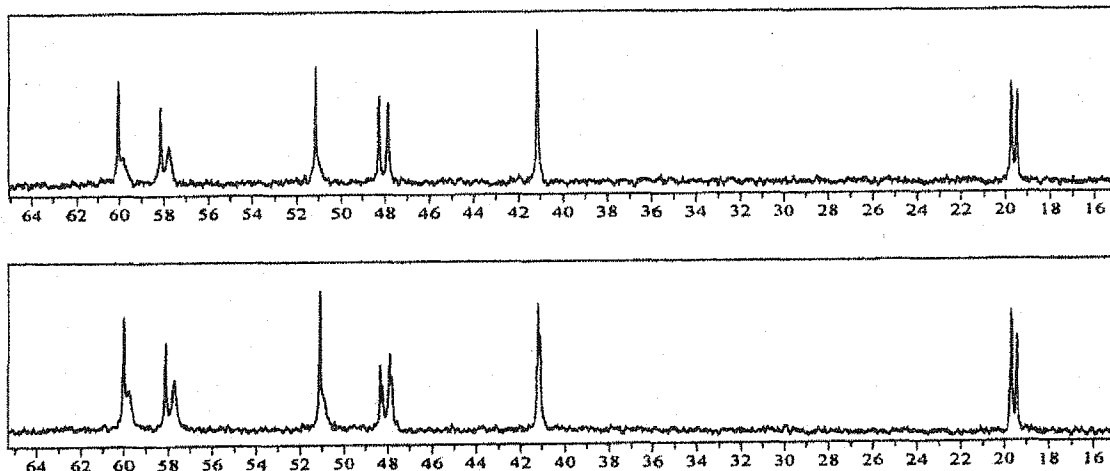


**Figure 4.9**  $^{13}\text{C}\{^1\text{H}\}$  NMR spectrum of 0.015 M  $[\text{GaCl}_2\cdot\mathbf{1}]\text{Cl}$  in acidic  $\text{D}_2\text{O}$  (pD = 1.07). Top: N-D complex. Bottom: a 1:1 N-H and N-D complex mixture.

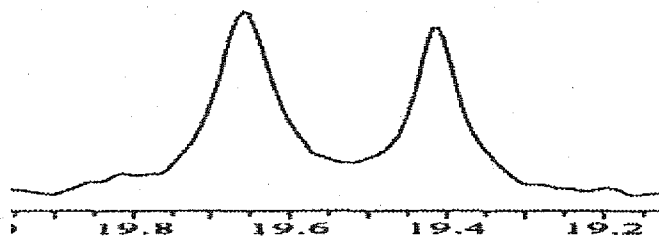


**Figure 4.10** Expansion of two peaks at  $\delta$  19.7 and 19.4 in the  $^{13}\text{C}\{^1\text{H}\}$  NMR spectrum of 0.015 M  $[\text{GaCl}_2\cdot\mathbf{1}]\text{Cl}$  (N-D complex) in acidic  $\text{D}_2\text{O}$  (pD = 1.07).

further supported by the changes of both  $^1\text{H}$  and  $^{13}\text{C}\{^1\text{H}\}$  NMR spectra upon addition of KCl. As shown in **Figure 4.11**, the increased KCl concentration increased the relative integration of the doublet of pentets at  $\delta$  1.76 while decreasing that at  $\delta$  1.84. This implies that the concentration of Ga(III) complex A decreased whereas that of Ga(III) complex B increased as the chloride anion concentration was increased. Since this increase of KCl concentration simultaneously increased the relative height of the  $^{13}\text{C}$  resonance at  $\delta$  19.7 relative to the one at  $\delta$  19.4 (**Figure 4.12**), we can assign  $\delta$  19.7 and 19.4 to complex B

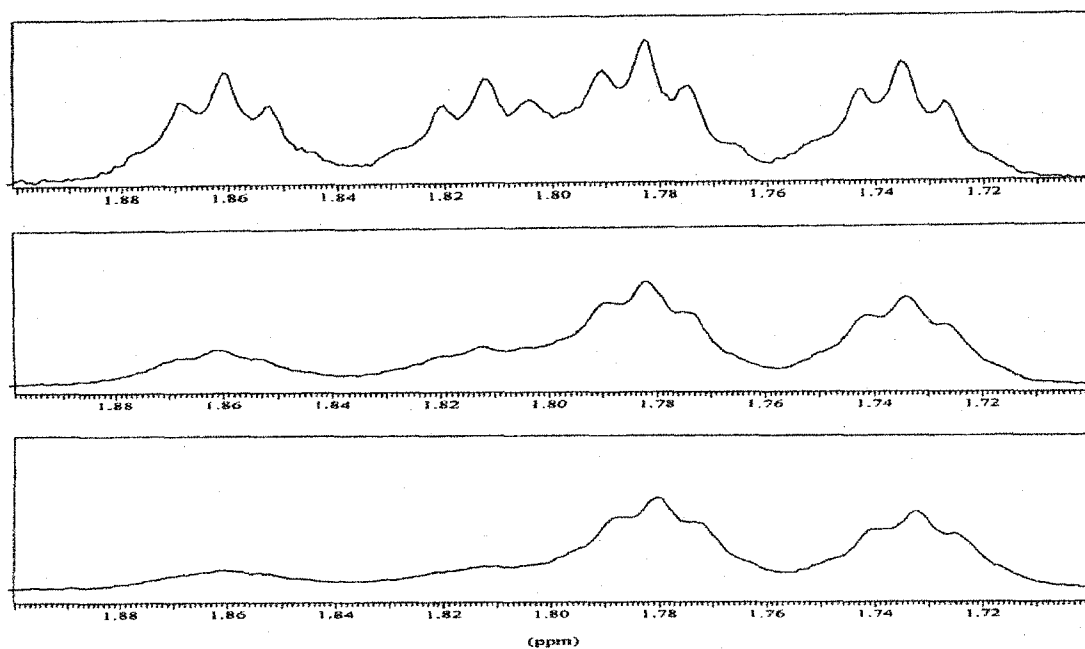


**Figure 4.11** Comparison of the changes of the two sets of proton doublet of pentets at  $\delta$  1.84 and 1.76 with increased KCl concentration (pD =1.07). Top: no KCl. Middle: 3 equivalents of KCl. Bottom: 9 equivalents of KCl.

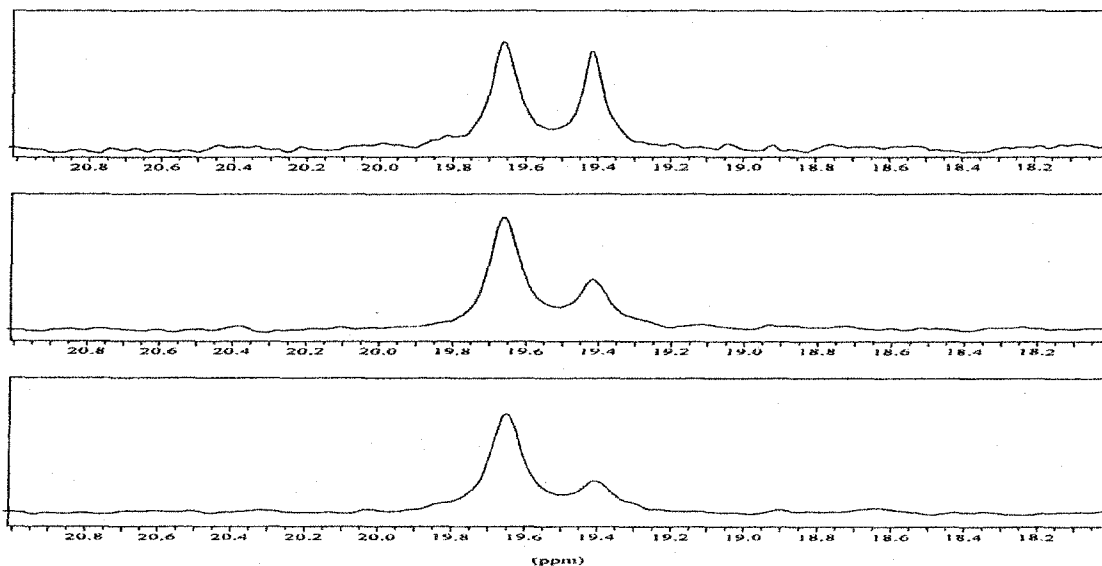


**Figure 4.12** Comparison of the changes of the two  $^{13}\text{C}\{^1\text{H}\}$  resonances at  $\delta$  19.7 and 19.4 with the increase of KCl concentration (pD =1.07). Top: no KCl. Middle: 3 equivalents of KCl. Bottom: 9 equivalents of KCl.



and complex **A** respectively. Since the relative intensity of the broader set of  $^{13}\text{C}$  resonances increased with  $[\text{KCl}]$  (Figure 4.13), one may speculate that complex **A** is more symmetrical than **B**. Complex **A** is then likely to be the more symmetrical species  $[\text{1-Ga}(\text{OH}_2)_2]^{3+}$  while complex **B** is probably the less symmetrical  $[\text{1-Ga}(\text{OH}_2)\text{Cl}]^{2+}$ . Confirmation of these conjectures will require much more detailed studies of the solution speciation.

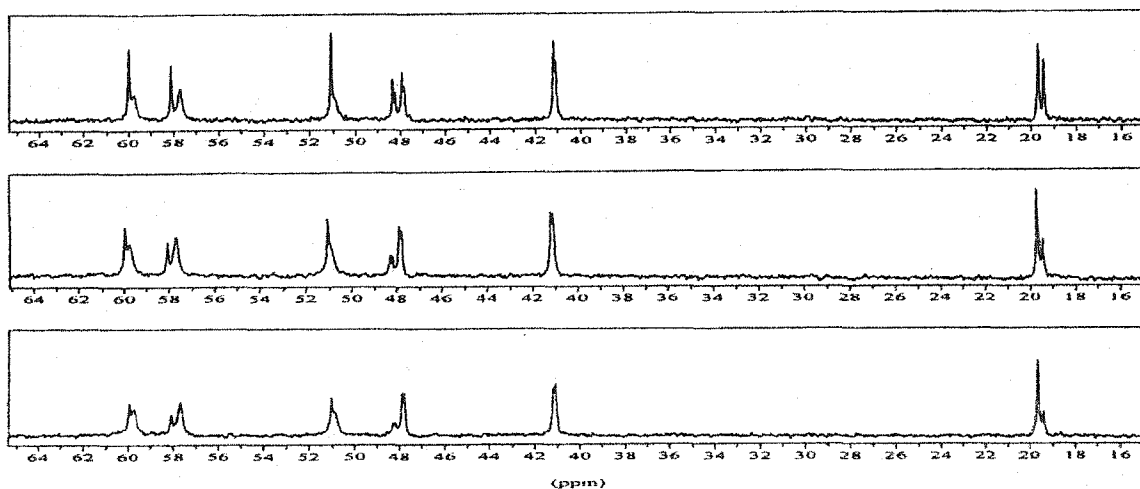


**Figure 4.13** Comparison of  $^{13}\text{C}\{^1\text{H}\}$  NMR spectral change of 0.015 M  $[\text{GaCl}_2\cdot\mathbf{1}]\text{Cl}$  (N-D complex) in acidic  $\text{D}_2\text{O}$  ( $\text{pD} = 1.07$ ) with the increase of  $\text{KCl}$  concentration. Top: no  $\text{KCl}$ . Middle: 3 equivalents of  $\text{KCl}$ . Bottom: 9 equivalents of  $\text{KCl}$ .

In  $\text{D}_2\text{O}$ ,  $[\text{InBr}_2\cdot\mathbf{1}]\text{Br}$  (N-D complex) existed as a major species and a minor species (10%) as indicated by its  $^1\text{H}$  and  $^{13}\text{C}\{^1\text{H}\}$  NMR spectra (Figure 4.14). In order to confirm whether there is equilibration between these species, a comparison of the  $^1\text{H}$  NMR spectra of 0.030 M, 0.018 M and 0.0030 M  $[\text{InBr}_2\cdot\mathbf{1}]\text{Br}$  in  $\text{D}_2\text{O}$  (Figure 4.15) were recorded to demonstrate that the relative ratios of these two species indeed changed as exemplified by the resonances between  $\delta$  1.6 to 1.8 and from  $\delta$  2.6 to 2.9.

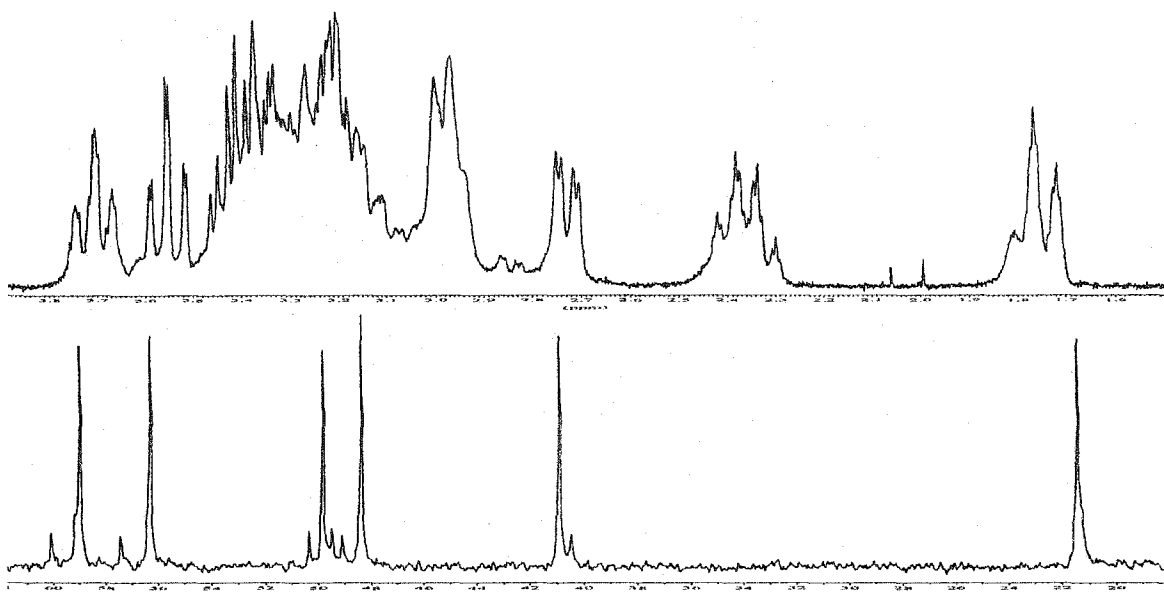


**Figure 4.14** Top: Proton NMR spectrum of  $[\text{InBr}_2 \cdot \mathbf{1}]\text{Br}$  (N-D complex) in  $\text{D}_2\text{O}$ . Bottom:  $^{13}\text{C}\{^1\text{H}\}$  NMR spectrum of this complex in  $\text{D}_2\text{O}$  (the small peak at  $\delta$  49.50 is the  $\text{CH}_3\text{OD}$  peak.).

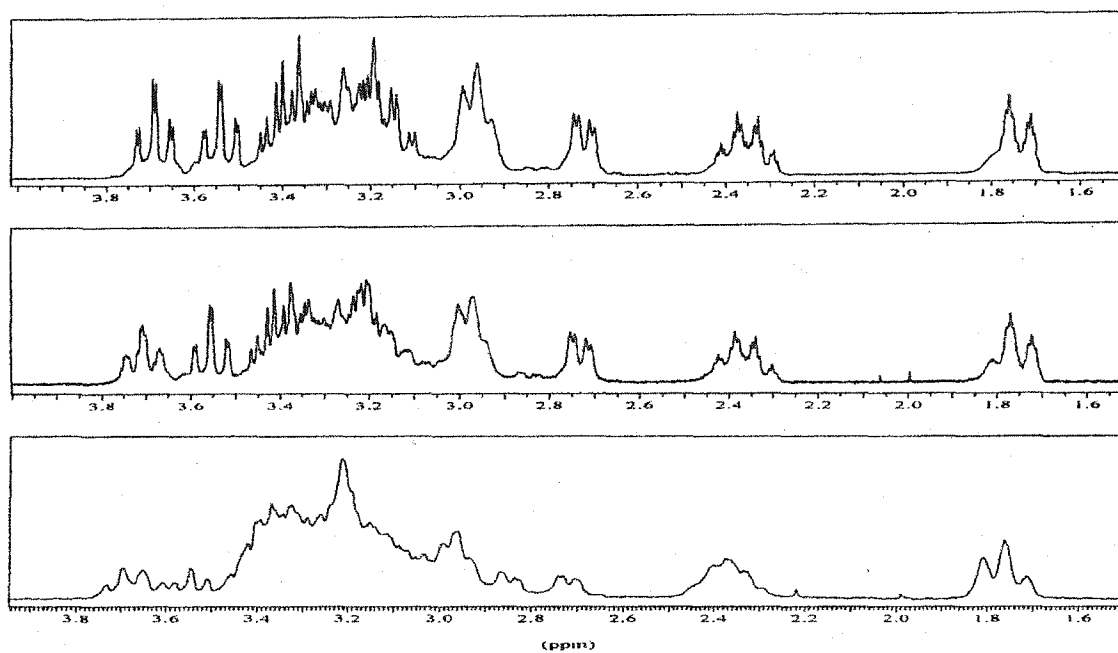


**Figure 4.15** Comparison of  $^1\text{H}$  NMR spectra of 0.030 M, 0.018 M and 0.0030 M  $[\text{InBr}_2 \cdot \mathbf{1}]\text{Br}$  in  $\text{D}_2\text{O}$ . Top: 0.030 M. Middle: 0.018 M. Bottom: 0.0030.

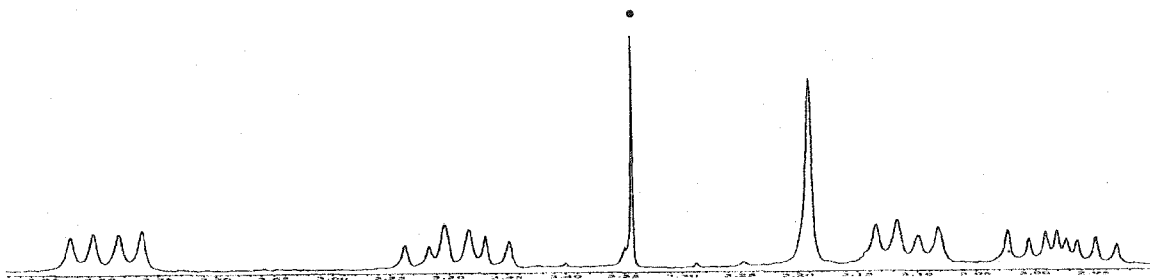


**Figure 4.16(a)** Proton NMR spectrum of  $[\text{InBr}_2 \cdot 2]\text{Br}$  (N-D complex) in  $\text{D}_2\text{O}$  (the singlet resonance labeled with a dot is the  $\text{CH}_3\text{OD}$  peak.).

By contrast, both  $^1\text{H}$  and  $^{13}\text{C}\{^1\text{H}\}$  NMR spectra of  $[\text{GaCl}_2 \cdot 2]\text{Cl}$  and  $[\text{InBr}_2 \cdot 2]\text{Br}$  (**Figure 4.16(a)** and **Figure 4.16(b)**) in  $\text{D}_2\text{O}$  showed only a species with  $C_{2v}$  symmetry on the NMR time scale.



**Figure 4.16(b)**  $^{13}\text{C}\{^1\text{H}\}$  NMR spectrum of  $[\text{InBr}_2 \cdot 2]\text{Br}$  (N-D complex) in  $\text{D}_2\text{O}$ .

In  $\text{CD}_3\text{CN}$ , all four Ga(III) and In(III) complexes give well-resolved  $^1\text{H}$  and  $^{13}\text{C}\{^1\text{H}\}$  NMR spectra except that no  $^{13}\text{C}\{^1\text{H}\}$  NMR spectrum of  $[\text{GaCl}_2 \cdot 2]\text{Cl}$  can be recorded due to its poor solubility. The six sharp carbon resonances in the  $^{13}\text{C}\{^1\text{H}\}$  NMR spectra of  $[\text{GaCl}_2 \cdot 1]\text{Cl}$  (**Figure 4.17**) and  $[\text{InBr}_2 \cdot 1]\text{Br}$  indicate their  $C_2$  symmetry on the NMR time scale. The three carbon resonances in the  $^{13}\text{C}\{^1\text{H}\}$  NMR spectrum of  $[\text{InBr}_2 \cdot 2]\text{Br}$  in  $\text{CD}_3\text{CN}$  (**Figure 4.18**) confirm its  $C_{2v}$  symmetry on the NMR time scale. Here, the appearance of cross-bridged ethylene as a singlet in the  $^1\text{H}$  NMR spectra of  $[\text{GaCl}_2 \cdot 2]\text{Cl}$  and  $[\text{InBr}_2 \cdot 2]\text{Br}$  (**Figure 4.19**) is also indicative of their  $C_{2v}$  symmetry.

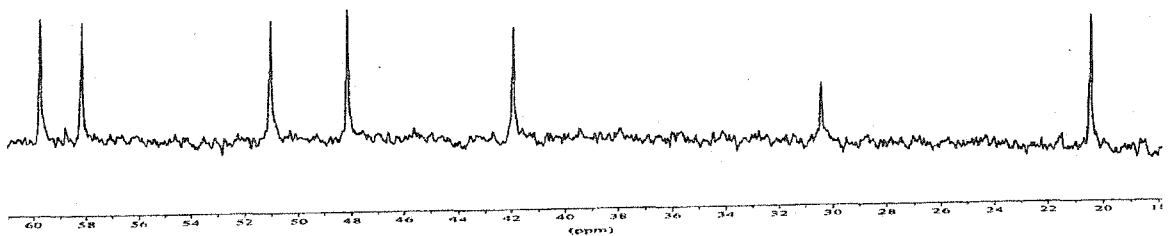


**Figure 4.17**  $^{13}\text{C}\{^1\text{H}\}$  NMR spectrum of  $[\text{GaCl}_2\cdot\mathbf{1}]\text{Cl}$  in  $\text{CD}_3\text{CN}$  (the shortest resonance at  $\delta$  30.8 is an impurity.).

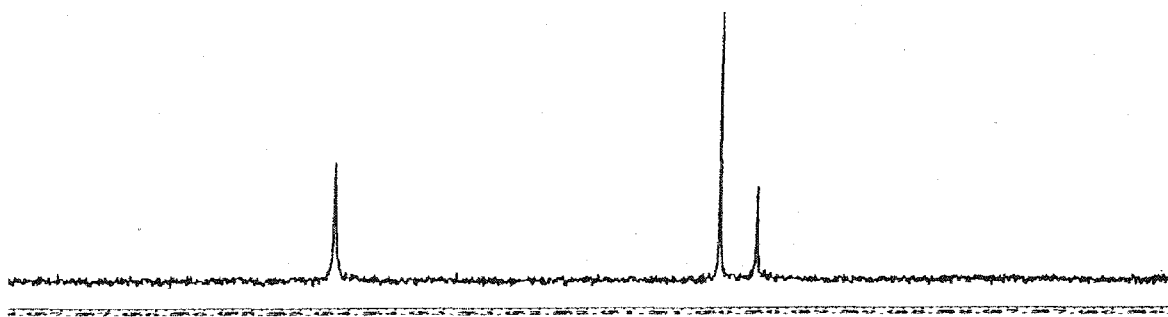


**Figure 4.18**  $^{13}\text{C}\{^1\text{H}\}$  NMR spectrum of  $[\text{InBr}_2\cdot\mathbf{2}]\text{Br}$  in  $\text{CD}_3\text{CN}$ .

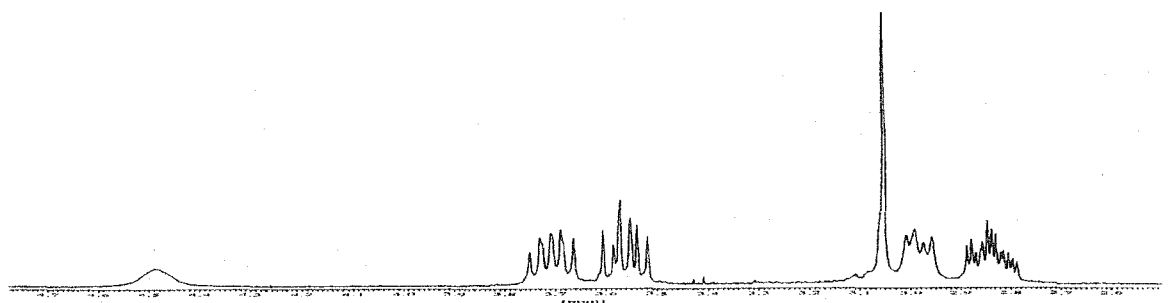


**Figure 4.19**  $^1\text{H}$  NMR spectrum of  $[\text{InBr}_2\cdot\mathbf{2}]\text{Br}$  in  $\text{CD}_3\text{CN}$ . The singlet of cross-bridged ethylene appears at  $\delta$  3.05.

The proton and  $^{13}\text{C}\{^1\text{H}\}$  NMR resonances of  $[\text{InBr}_2\cdot\mathbf{2}]\text{Br}$  in  $\text{CD}_3\text{CN}$  (**Figure 4.19** and **Figure 4.18**) can be assigned by a combination of 2D  $[^1\text{H},^1\text{H}]$  COSY and 2D  $[^1\text{H},^{13}\text{C}]$  HMQC NMR experiments. The 1-D proton NMR spectrum (**Figure 4.19**) is a first-order spectrum with a total of six well-resolved resonances from coordinated **2**. The broad singlet at  $\delta$  4.49 can be assigned to *NH* protons since it does not couple to any  $^{13}\text{C}$

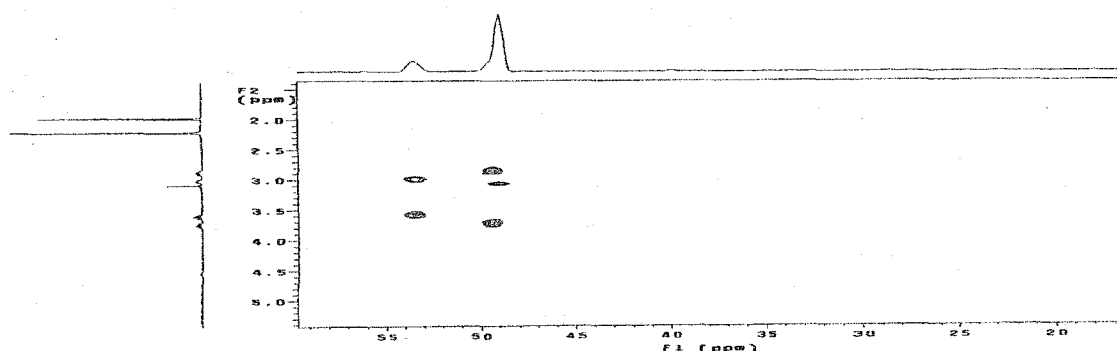


**Figure 4.20** A 2D [ $^1\text{H}$ ,  $^{13}\text{C}$ ] HMQC NMR spectrum of  $[\text{InBr}_2 \cdot 2]\text{Br}$  in  $\text{CD}_3\text{CN}$  (only  $^{13}\text{C}$  resonance images shown in the spectrum).

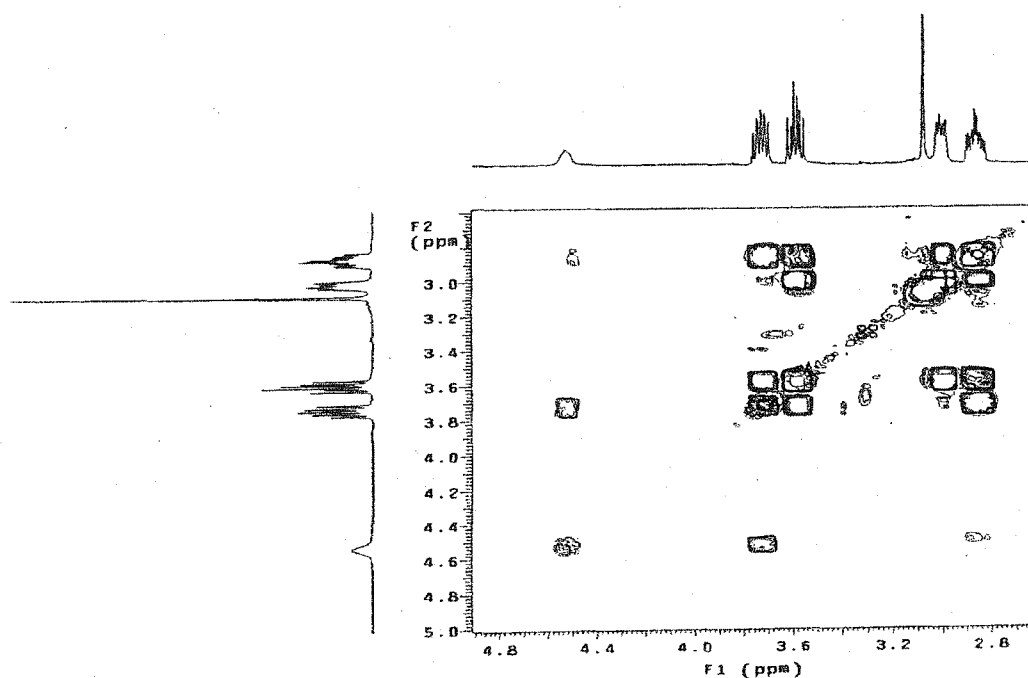


**Figure 4.21** A 2D [ $^1\text{H}$ ,  $^1\text{H}$ ] COSY spectrum of  $[\text{InBr}_2 \cdot 2]\text{Br}$  in  $\text{CD}_3\text{CN}$ .

resonances in the 2D [ $^1\text{H}$ ,  $^{13}\text{C}$ ] HMQC spectrum (**Figure 4.20**). 2D [ $^1\text{H}$ ,  $^1\text{H}$ ] COSY (**Figure 4.21**) reveals that the two multiplets at  $\delta$  3.71 and 2.84 are coupled to the N-H singlet at  $\delta$  4.49 so these two resonances belong to  $\text{H}_a$  and  $\text{H}_b$  (**Figure 4.22**). 2D [ $^1\text{H}$ ,  $^{13}\text{C}$ ] HMQC reveals that they are coupled to the  $^{13}\text{C}\{^1\text{H}\}$  resonance at  $\delta$  50.62. This carbon

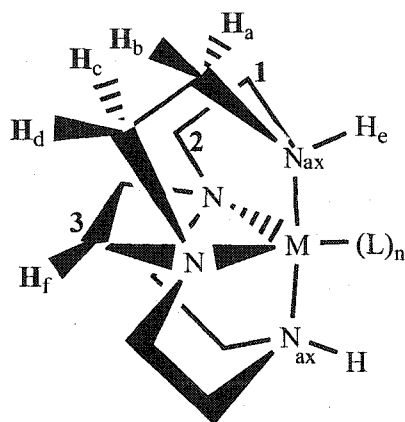


**Figure 4.22** Solution structure of  $[\text{InBr}_2 \cdot 2]\text{Br}$  with a  $C_{2v}$  symmetry. A total of six different resonances are expected in its  $^1\text{H}$  NMR spectrum.

resonance can thus be assigned to the one bonded to  $\text{H}_a$  and  $\text{H}_b$  (position 1 in **Figure 4.22**). The singlet at  $\delta$  3.05 does not show coupling to any other proton resonances so it can be assigned to the protons from bridging ethylene ( $\text{H}_f$ ). The  $^{13}\text{C}$  resonance at  $\delta$  50.62 showing coupling to this singlet can then be assigned to the bridging ethylene carbons (position 3 in **Figure 4.22**). The remaining unassigned  $^{13}\text{C}$  resonance at  $\delta$  54.65 can be assigned to position 2. Proton resonances at  $\delta$  3.56 and 3.05 do not couple to the singlet at  $\delta$  4.49 so these two belong to  $\text{H}_c$  and  $\text{H}_d$  in **Figure 4.22**. Consistent with this, they are also coupled to the  $^{13}\text{C}$  resonance at  $\delta$  54.65 assignable to position 2.

To assign the two proton resonances at  $\delta$  3.71 and 2.84 to  $\text{H}_a$  or  $\text{H}_b$ , we can check the coupling constants of these resonances. The resonance at  $\delta$  3.71 has a larger coupling constant of 7.6 Hz with the NH proton whereas the resonance at  $\delta$  2.84 has a smaller coupling constant of 3.4 Hz with the same NH proton. A model of this time-averaged  $C_{2v}$  In(III) complex shows that the dihedral angle between NH proton and  $\text{H}_a$  is around  $180^\circ$  and the dihedral angle between NH proton and  $\text{H}_b$  is between  $0$  to  $45^\circ$ . So the resonance at  $\delta$  3.71 probably belongs to the  $\text{H}_a$  protons while the resonance at  $\delta$  2.84 likely belongs

to the H<sub>b</sub> protons.

Unlike the C<sub>2v</sub> time-averaged symmetry of [Zn•(8-2H)](NaClO<sub>4</sub>) (143) observed in its solution NMR spectra at room temperature, complex [Ga•(8-2H)](NO<sub>3</sub>) (153) shows only C<sub>2</sub> symmetry. Such symmetry is indicated by the pendant-arm methylene giving an AB pattern (Figure 4.23) in its proton NMR spectrum as well as the presence of eight instead of five <sup>13</sup>C resonances. This indicates that at room temperature, there is no dynamic equilibration of this Ga(III) complex in D<sub>2</sub>O solution.

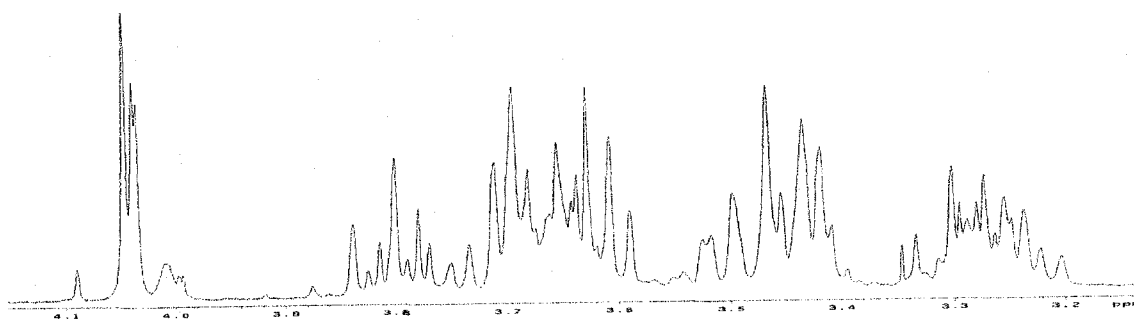


**Figure 4.23** <sup>1</sup>H NMR spectrum of Ga•(8-2H)](NO<sub>3</sub>) in D<sub>2</sub>O. The most downfield AB resonance belongs to the methylenes in the two pendant arms of 8-2H.

### 1.3 X-ray Structural Data.

X-ray structures of [GaCl<sub>2</sub>•1]Cl (149), [InBr<sub>2</sub>•1]Br (150), [InBr<sub>2</sub>•2]Br (152), and [Ga•(8-2H)](NO<sub>3</sub>) (153) were solved. Their relevant bond distances and angles are listed in Tables 4.2(a-d) individually.

[GaCl<sub>2</sub>•1]Cl (149) This complex has the cross-bridged ligand 1 in the distorted

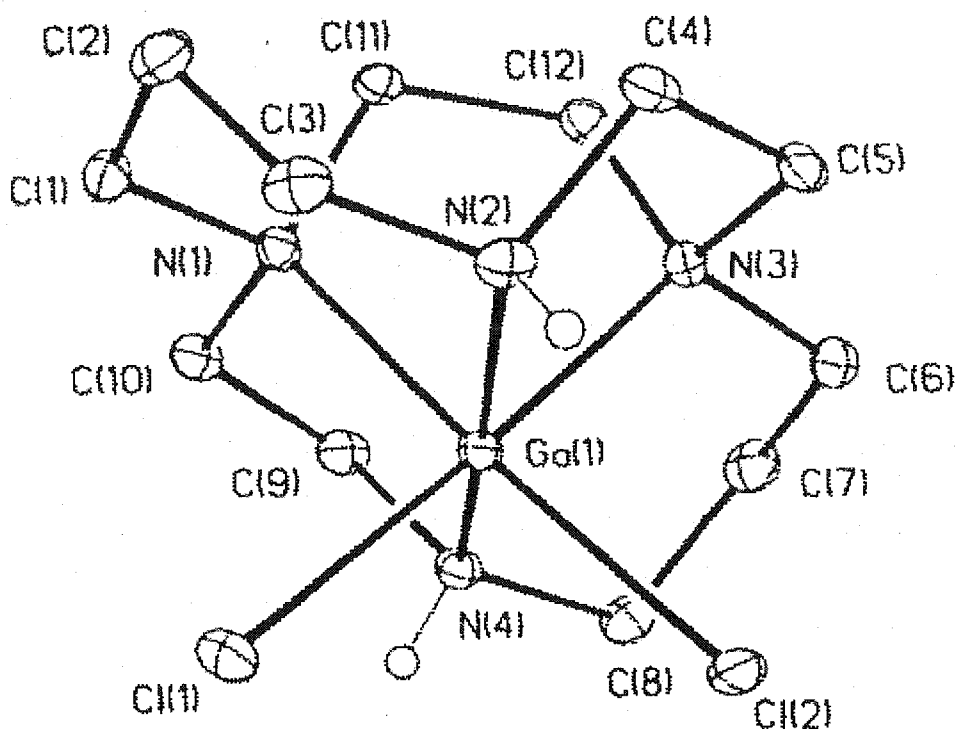


**Figure 4.24** X-ray structure of  $[\text{GaCl}_2 \cdot 1]\text{Cl}$  (149) showing atomic labeling scheme.

diamond lattice  $[2323]/[2323]$  *cis*-folded ligand conformation (**Figure 4.24**). Within the ligand molecular cleft, the Ga(III) has a slightly distorted octahedral coordination sphere as indicated by the axial N(2)-Ga-N(4) angle of  $169.3(1)^\circ$  and equatorial N(1)-Ga-N(3) angle of  $84.2(1)^\circ$ . The average secondary N(ax)-Ga bond length of  $2.08 \text{ \AA}$  is slightly shorter than the average tertiary N(eq)-Ga bond length of  $2.13 \text{ \AA}$ . There are limited structural studies of Ga(III) complexes of cyclam and its derivatives in the literature. Two known examples  $[\text{Ga}(\text{cyclam})]\text{PO}_4$  and  $[(\text{CH}_3)\text{Ga}(\text{cyclam})]\text{Cl}_2$  (**Figure 1.48**) have the *trans-III* ligand configuration. These have average amine N-Ga bond distances of  $2.05$  and  $2.08 \text{ \AA}$  respectively.

Ga-Cl bond distances of  $2.3227(6)$  and  $2.3184(6) \text{ \AA}$  are found in this Ga(III)



complex. These are slightly longer than the Ga-Cl bondlength of 2.265 (1) Å reported in six-coordinated  $[cis-Ga(Cl)_2(bipy)_2]^+[GaCl_4]^-$ .<sup>127</sup>

**Table 4.2(a)** Selected Bond Distances (Å) and Bond Angles (deg) in  $[GaCl_2 \cdot 1]Cl$  (149).

Ga(1)-N(1)	2.1323(16)	Ga(1)-N(2)	2.070(2)
Ga(1)-N(3)	2.1322(17)	Ga(1)-N(4)	2.088(2)
Ga(1)-Cl(1)	2.3227(6)	Ga(1)-Cl(2)	2.3184(6)
N(4)-Ga(1)-N(2)	169.33(7)	N(3)-Ga(1)-N(1)	84.17(7)
N(3)-Ga(1)-N(4)	88.20(7)	N(3)-Ga(1)-N(2)	83.93(7)
N(4)-Ga(1)-N(1)	83.80(7)	N(2)-Ga(1)-N(1)	88.23(7)
N(4)-Ga(1)-Cl(2)	95.94(5)	N(3)-Ga(1)-Cl(2)	9.42(5)
N(2)-Ga(1)-Cl(2)	91.46(5)	N(1)-Ga(1)-Cl(2)	175.59(5)
N(3)-Ga(1)-Cl(1)	177.02(5)	N(4)-Ga(1)-Cl(1)	92.37(5)
N(2)-Ga(1)-Cl(1)	95.13(5)	N(1)-Ga(1)-Cl(1)	92.98(5)
Cl(2)-Ga(1)-Cl(1)	91.43(2)		

**$[InBr_2 \cdot 1]Br$  (150)** The X-ray structure of this complex (**Figure 4.25**) reveals that two terminal bromides and four amino nitrogens from the ligand coordinate to this In(III) center. It has a distorted-octahedral coordination geometry with an axial N(4)-In-N(2) bond angle of 164.29(12)° and an equatorial N(1)-In-N(3) bond angle of 78.89(9)°. Comparison of these two bond angles with the analogous ones in  $[GaCl_2 \cdot 1]Cl$  reveals that

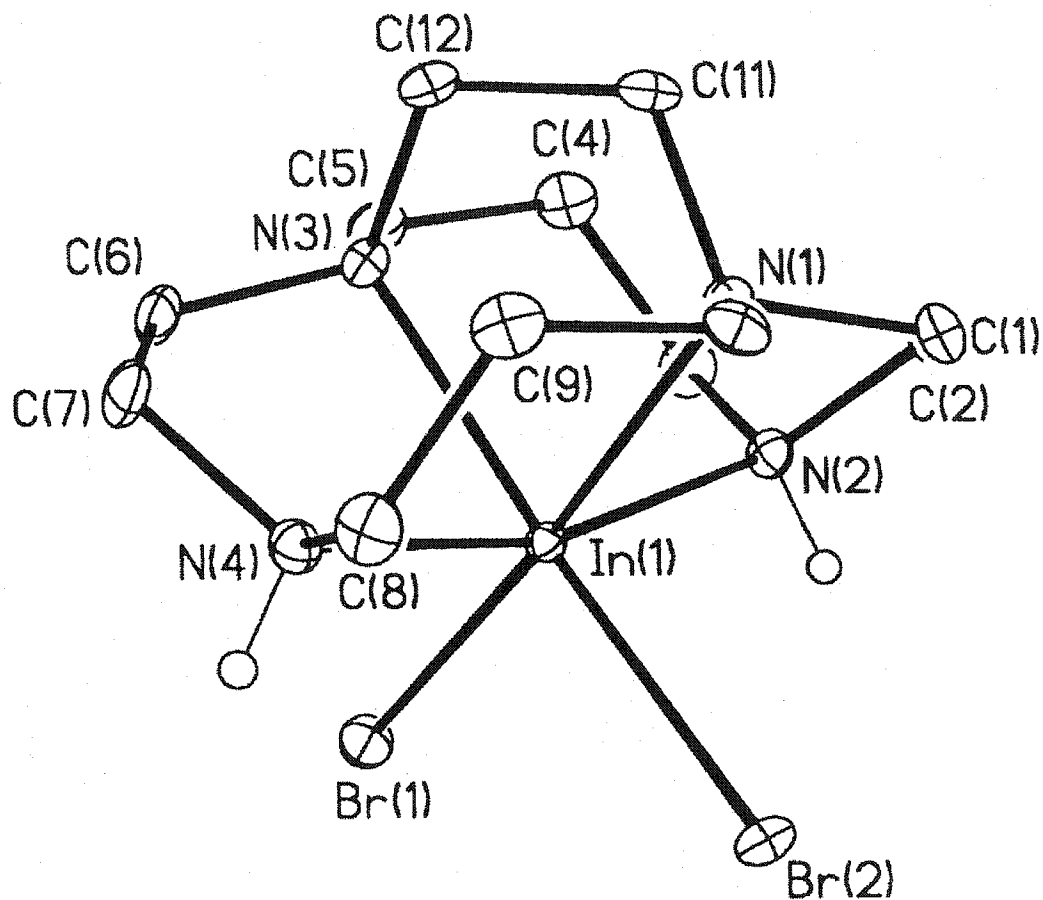


**Figure 4.25** X-ray structure of  $[\text{InBr}_2 \cdot \mathbf{1}]\text{Br}$  (150) showing atomic labeling scheme.

the larger In(III) does not fit as well as Ga(III) in the cleft formed by coordinated **1**. The axial and equatorial In-N bond distances are 2.26 and 2.31 Å respectively and the In-Br bond distance is 2.27 Å. There is no reported crystal structures of any In(III) complex with a  $\text{N}_4\text{X}_2$  donor set (X = halide). For comparison,  $[\text{InBr}_3(\text{Me}_3[9]\text{aneN}_3)]$  has a  $\text{N}_3\text{Br}_3$  coordination set<sup>128</sup> with the secondary In-N bond distances ranging from 2.338 (7) to 2.360 (7) Å and In-Br bond distances ranging from 2.5974 (11) to 2.6054 (11) Å.

**Table 4.2(b)** Selected Bond Distances (Å) and Bond Angles (deg) in [InBr<sub>2</sub>•1]Br (150).

In(1)-N(1)	2.309(3)	In(1)-N(2)	2.259(3)
In(1)-N(3)	2.306(3)	In(1)-N(4)	2.260(3)
In(1)-Br(1)	2.5806(4)	In(1)-Br(2)	2.6079(4)
N(4)-In(1)-N(2)	164.29(12)	N(3)-In(1)-N(1)	78.89(9)
N(3)-In(1)-N(4)	77.62(10)	N(3)-In(1)-N(2)	90.55(10)
N(4)-In(1)-N(1)	90.19(10)	N(2)-In(1)-N(1)	77.36(10)
N(4)-In(1)-Br(2)	95.14(7)	N(3)-In(1)-Br(2)	168.10(7)
N(2)-In(1)-Br(2)	94.82(7)	N(1)-In(1)-Br(2)	91.91(6)
N(3)-In(1)-Br(1)	94.39(7)	N(4)-In(1)-Br(1)	96.02(8)
N(2)-In(1)-Br(1)	95.05(8)	N(1)-In(1)-Br(1)	169.69(6)
Br(2)-In(1)-Br(1)	95.707(13)		

[InBr<sub>2</sub>•2]Br (152) Compared to that of [InBr<sub>2</sub>•1]Br, the pseudo-octahedral indium(III) coordination sphere here is even more distorted (**Figure 4.26**) with an axial N(2)-In-N(4) bond angle of only 144.0(1)° and equatorial N(1)-In-N(3) bond angle of 76.8(1)°. Again, this can be attributed to the smaller cleft of the coordinated cross-bridged cyclen **2** compared to that of cross-bridged cyclam **1**. The axial and equatorial In-N bond distances are 2.26 and 2.31 Å respectively which are similar to those of [InBr<sub>2</sub>•1]Br. Compared to the In-Br bond distance of 2.27 Å in [InBr<sub>2</sub>•1]Br, this complex has significantly longer In-Br distances of 2.57 Å.

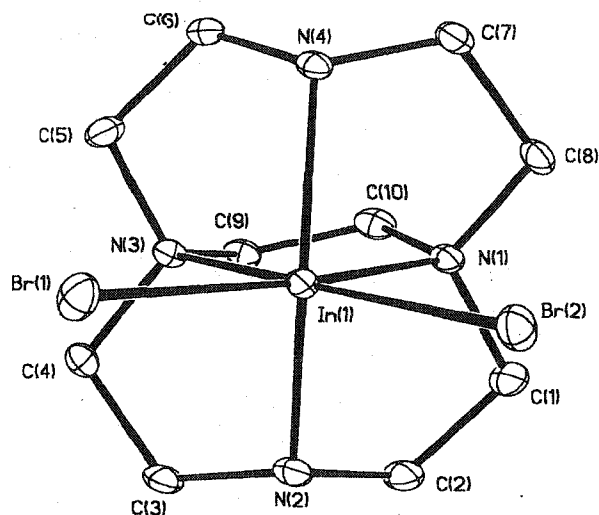


**Figure 4.26** X-ray structure of  $[\text{InBr}_2 \cdot 2]\text{Br}$  (**152**) showing atomic labeling scheme.

**Table 4.2(c)** Selected Bond Distances (Å) and Bond Angles (deg) in  $[\text{InBr}_2 \cdot 2]\text{Br}$  (**152**).

In(1)-N(1)	2.316(4)	In(1)-N(2)	2.277(3)
In(1)-N(3)	2.305(3)	In(1)-N(4)	2.254(3)
In(1)-Br(1)	2.5725(5)	In(1)-Br(2)	2.5653(5)
N(4)-In(1)-N(2)	143.95(12)	N(3)-In(1)-N(1)	76.78(12)
N(3)-In(1)-N(4)	77.81(11)	N(3)-In(1)-N(2)	74.17(11)
N(4)-In(1)-N(1)	74.31(11)	N(2)-In(1)-N(1)	77.55(12)
N(4)-In(1)-Br(2)	101.81(8)	N(3)-In(1)-Br(2)	171.65(9)
N(2)-In(1)-Br(2)	102.68(8)	N(1)-In(1)-Br(2)	95.04(8)
N(3)-In(1)-Br(1)	93.94(9)	N(4)-In(1)-Br(1)	101.13(8)
N(2)-In(1)-Br(1)	102.96(9)	N(1)-In(1)-Br(1)	170.27(8)
Br(2)-In(1)-Br(1)	94.316(18)		

[Ga•(8-2H)](NO<sub>3</sub>) (153) This structure (Figure 4.27) represents only the second X-ray of Ga(III) complexes of carboxylate pendant-armed tetraamines.<sup>66</sup> The Ga(III) center is engulfed in the cavity formed by the coordinated 8-2H in a N<sub>4</sub>O<sub>2</sub> donor set. The

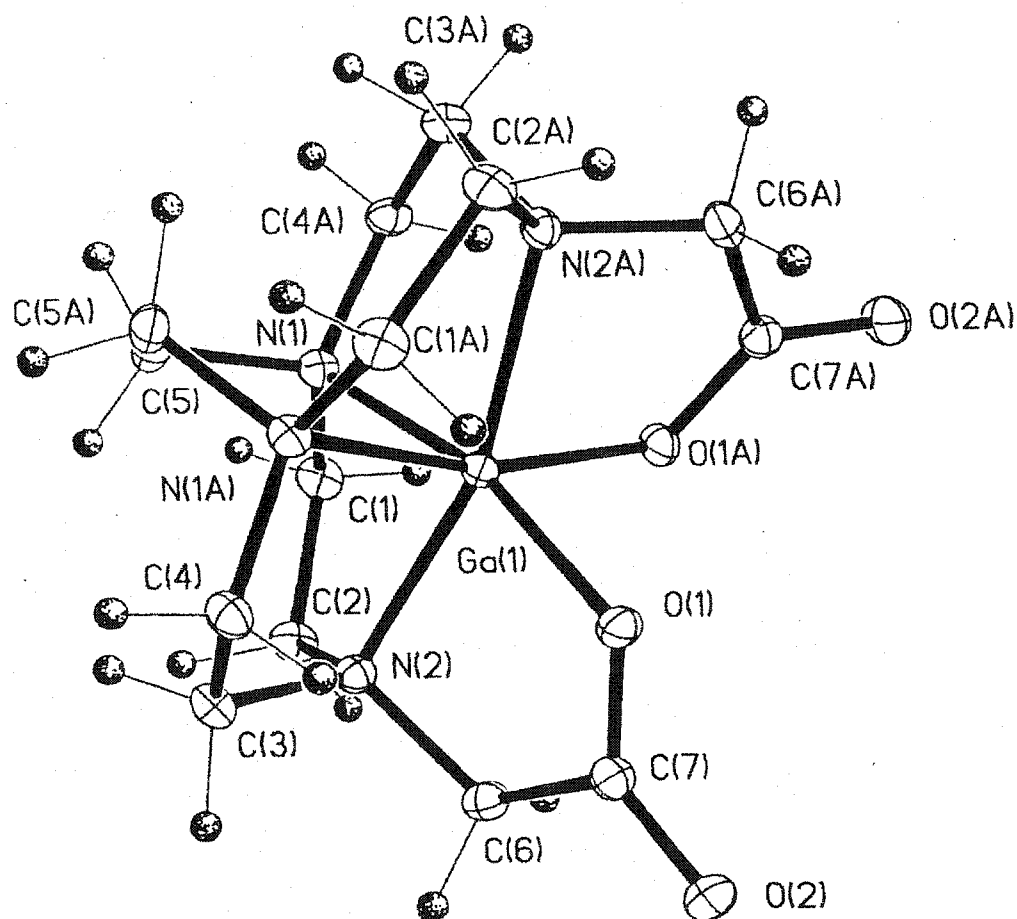


**Figure 4.27** X-ray structure of [Ga•(8-2H)](NO<sub>3</sub>) (153) showing atomic labeling scheme.

coordination sphere around Ga(III) is again a distorted octahedral with an axial N(2)-Ga-N(2A) angle of 164.56 (9)° and an equatorial N(1)-Ga-N(1A) angle of 86.24 (9)°. The axial Ga-N bond distance of 2.0780 (15) Å is slightly longer than the Ga-N(eq) bond

distance of 2.0461 (15) Å. In the literature, a Ga(III) complex of a tricarboxylate-armed cyclen derivative **106** also has a N<sub>4</sub>O<sub>2</sub> pseudo-octahedral geometry (**Figure 1.52**) with an axial N(3)-Ga-N(5) angle of 156.3 (2)° and an equatorial N(2)-Ga-N(4) angle of 105.6 (2)°. These bond angle differences imply that Ga(III) fits better in cross-bridged ligand **8-2H** than that in ligand **106**. Here, the axial Ga-N bond distance of 2.15 Å is also marginally longer than Ga-N(eq) bond distance of 2.13 Å. Two Ga(III)-O bondlengths of 1.904 (5) and 1.932 (4) Å are shorter than those of 1.9421 (13) Å found in [Ga•(**8-2H**)](NO<sub>3</sub>).

**Table 4.2(d)** Selected Bond Distances (Å) and Bond Angles (deg) in [Ga•(**8-2H**)](NO<sub>3</sub>) (**153**).

Ga(1)-O(1)	1.9421(13)	Ga(1)-O(1A)	1.9421(13)
Ga(1)-N(1)	2.0461(15)	Ga(1)-N(1A)	2.0461(15)
Ga(1)-N(2)	2.0780(15)	Ga(1)-N(2A)	2.0780(15)
O(1)-Ga(1)-N(2A)	107.90(6)	O(1A)-Ga(1)-N(2)	107.90(6)
O(1)-Ga(1)-N(2)	83.23(6)	O(1A)-Ga(1)-N(2A)	83.23(6)
O(1)-Ga(1)-N(1A)	93.60(6)	O(1A)-Ga(1)-N(1)	93.60(6)
O(1)-Ga(1)-N(1)	165.20(5)	O(1A)-Ga(1)-N(1A)	165.20(5)
O(1)-Ga(1)-O(1A)	90.28(8)	N(2)-Ga(1)-N(2A)	164.56(9)
N(2)-Ga(1)-N(1)	81.99(6)	N(2A)-Ga(1)-N(1A)	81.99(6)
N(2A)-Ga(1)-N(1)	86.75(6)	N(2)-Ga(1)-N(1A)	86.75(6)
N(1)-Ga(1)-N(1A)	86.24(9)		

### Summary of Structural Data.

X-ray structures of three Ga(III) and In(III) complexes with parent cross-bridged ligands **1** and **2** and the Ga(III) complex with the carboxylate derivative ligand **8** provide rare examples of Ga(III) and In(III) complexes of tetraamines and their derivatives. A comparison of their axial N-M-N angles and the equatorial N-M-N angles is listed in **Table 4.3**. similar to the trend shown in their Zn(II) complexes, cross-bridged cyclam **1** provides a better fit for octahedral In(III) than the smaller cross-bridged cyclen derivative **2**. This is best indicated by the axial N-In-N angles of  $164.29 (12)^\circ$  for the former and  $144.0 (1)^\circ$  for the latter.

Smaller Ga(III) fits better than In(III) in the cleft of complexed **1**. This is also shown by the axial N-Ga-N angles of  $169.3 (1)^\circ$  and the axial N-In-N angles of  $164.29 (12)^\circ$ . Consistent with this, the equatorial N-Ga-N bond angle of  $84.2 (1)^\circ$  in the former is closer to  $90^\circ$  compared to that of  $78.89 (9)^\circ$  in the latter.

Comparison of the axial and equatorial bond angles of  $[\text{Ga}(\mathbf{8-2H})](\text{NO}_3)$  and the Ga(III) complex of a tricarboxylate-armed cyclen derivative **106** (**Figure 1.52**) revealed that our cross-bridged cyclen provide a better fit for Ga(III) than this cyclen derivative. This structural difference may imply the higher kinetic stability of  $[\text{Ga}(\mathbf{8-2H})](\text{NO}_3)$  than the Ga(III) complex of a tricarboxylate-armed cyclen derivative **106**. However, the larger axial N-Ga-N angles of  $169.3 (1)^\circ$  in Ga(III) complex of parent cross-bridged cyclam  $[\text{GaCl}_2 \cdot \mathbf{1}]\text{Cl}$  (**Table 4.3**) indicated that gallium complex of the dicarboxylate pendant-armed cross-bridged cyclam,  $[\text{Ga}(\mathbf{7-2H})]^+$ , will be the most interesting target for further work in this field.

**Table 4.3** Comparison of Ga(III) and In(III) 'fit' inside cross-bridged ligand clefts

Complex	Axial N-M-N angle	Equatorial N-M-N angle
[GaCl <sub>2</sub> •1]Cl ( <b>149</b> )	169.33 (7)	84.17 (7)
[InBr <sub>2</sub> •1]Br ( <b>150</b> )	164.29 (12)	78.89 (9)
[InBr <sub>2</sub> •2]Br ( <b>152</b> )	143.95 (12)	76.78 (12)
[Ga•(8-2H)](NO <sub>3</sub> ) ( <b>153</b> )	164.56 (9)	86.24 (9)



## 2. Cu(II) Complexes of Ligands 1-4.

### 2.1 Preparation and Characterization of Copper Complexes.

Seven new copper complexes of cross-bridged ligands **1-4** were synthesized and characterized by their IR (KBr) and UV-Vis spectral data as well as CHN elemental analyses. All of these Cu(II) complexes were synthesized by the reaction of CuCl<sub>2</sub> or Cu(ClO<sub>4</sub>)<sub>2</sub>•6H<sub>2</sub>O with the specific ligand.

As reported in the literature,<sup>69(a)</sup> we had previously synthesized complex Cu(**1**)(ClO<sub>4</sub>)<sub>2</sub>. The reaction of Cu(ClO<sub>4</sub>)<sub>2</sub>•6H<sub>2</sub>O with **1** in MeOH afforded a blue solution which upon evaporating and recrystallization from 95% aq. ethanol/ether formed Cu(**1**)(ClO<sub>4</sub>)<sub>2</sub>. The X-ray structure of Cu(**1**)(ClO<sub>4</sub>)<sub>2</sub> exhibits a five-coordinate Cu(II) geometry (**Figure 1.58**).<sup>69(a)</sup> Interestingly, slight variation of this procedure yielded a new complex Cu<sub>2</sub>(OH)(**1**)<sub>2</sub>(ClO<sub>4</sub>)<sub>3</sub>(H<sub>2</sub>O) (**154**). Here after the reaction of Cu(ClO<sub>4</sub>)<sub>2</sub>•6H<sub>2</sub>O with **1** in MeOH to afford a dark-blue solution, diethyl ether vapor diffusion yielded crystalline Cu<sub>2</sub>(OH)(**1**)<sub>2</sub>(ClO<sub>4</sub>)<sub>3</sub>(H<sub>2</sub>O). This complex was characterized by CHN and chloride elemental analyses. Since several Cu(II) complexes of **1** show a coordination number of five,<sup>69(a)</sup> a possible structure of Cu<sub>2</sub>(OH)(**1**)<sub>2</sub>(ClO<sub>4</sub>)<sub>3</sub>(H<sub>2</sub>O) may be a dimeric Cu(II) complex bridged by a hydroxide group, in which each Cu(II) center has a coordination number of 5. This proposed structure is similar to the reported X-ray structures of Cu<sub>2</sub>(μ-OH)(tren)<sub>2</sub>(ClO<sub>4</sub>)<sub>3</sub>(H<sub>2</sub>O)<sup>129</sup> and Cu<sub>2</sub>(μ-OH)(2,2'-bipyridine)<sub>4</sub>(ClO<sub>4</sub>)<sub>3</sub>(H<sub>2</sub>O).<sup>130</sup>

$[\text{Cu} \cdot 2(\mu\text{-Cl})]_2\text{Cl}_2$  (155) and  $\text{Cu}(2)(\text{ClO}_4)_2$  (156) were synthesized in reasonable yields by the reaction of 2 with the respective Cu(II) salt in ethanol. These two copper(II) complexes were also readily formed in methanol. Recrystallization of  $\text{Cu}(2)(\text{ClO}_4)_2$  from methanol yielded a methanol-coordinated  $[\text{Cu}(2)(\text{CH}_3\text{OH})(\text{ClO}_4)] (\text{ClO}_4)$  complex (Figure 4.39, *vide infra*). Synthesis or recrystallization of  $\text{Cu}(1)(\text{ClO}_4)_2$  and  $\text{Cu}(2)(\text{ClO}_4)_2$  from MeCN did not yield a Cu(II) complex of 2 with a coordinated MeCN in the solid state since no  $\text{C}\equiv\text{N}$  stretch around  $2300\text{ cm}^{-1}$  can be observed in their IR (KBr) spectra (Figure 4.28 and Figure 4.29).<sup>133</sup>

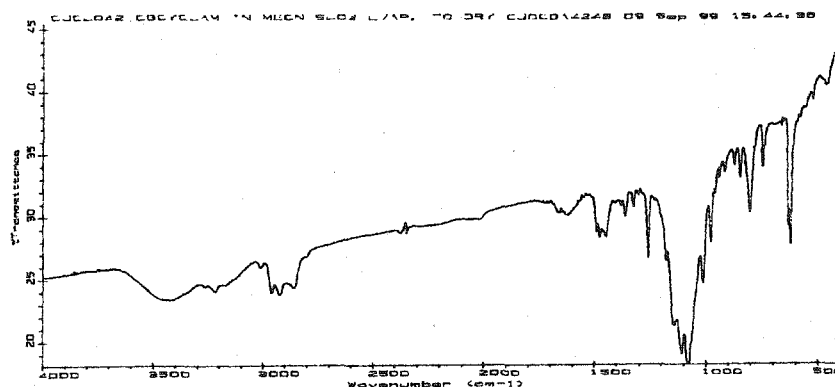


Figure 4.28 IR (KBr) spectrum of recrystallized (MeCN)  $\text{Cu}(1)(\text{ClO}_4)_2$ .

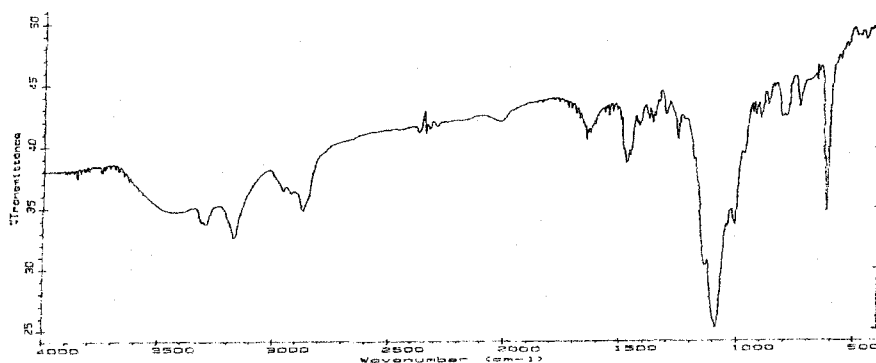
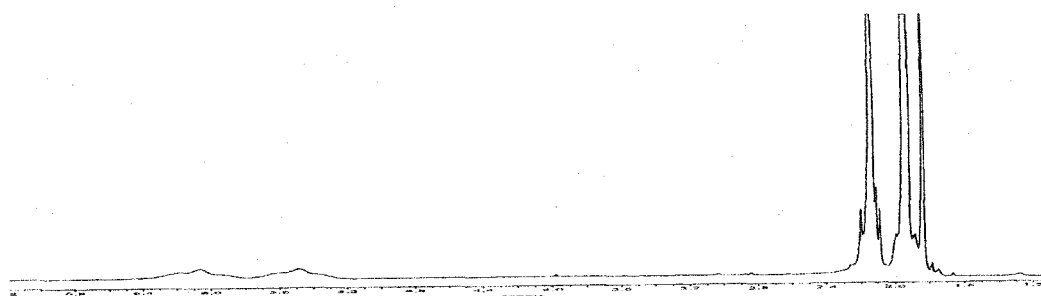


Figure 4.29 IR (KBr) spectrum of recrystallized (MeCN)  $\text{Cu}(2)(\text{ClO}_4)_2$ .

Cu(II) complexes of the N, N'-dibenzyl cross-bridged ligands **3** and **4**, CuCl<sub>2</sub>•**4** (**158**) and Cu(**3**)(ClO<sub>4</sub>)<sub>2</sub> (**157**) were also readily prepared in MeOH. The synthesis of Cu(**4**)(ClO<sub>4</sub>)<sub>2</sub> (**160**), however, was not straightforward. In an attempted synthesis, an unexpected carbonate-bridged copper(II) complex, [Cu<sub>2</sub>(μ-η<sup>1</sup>:η<sup>2</sup>-CO<sub>3</sub>)(**4**)<sub>2</sub>](ClO<sub>4</sub>)<sub>2</sub> (**159**) was isolated and characterized by CHN elemental analyses and X-ray analysis. The formation of this complex was due to the adsorbance of CO<sub>2</sub> from the air. One possibility is that ligand **4** adsorbed CO<sub>2</sub> from air due to its high basicity. Due to the hygroscopic nature of **4**, this liquid tertiary polyamine could have absorbed moisture from air, and then reacted with carbon dioxide in the presence of water.<sup>131</sup> Another possibility is that this carbonate complex was formed by the absorbance of CO<sub>2</sub> from air during the slow ether diffusion process. In another attempted synthesis of Cu(**4**)(ClO<sub>4</sub>)<sub>2</sub>, a mixture of equal equivalents of ligand **4** and Cu(ClO<sub>4</sub>)<sub>2</sub>•6H<sub>2</sub>O in MeOH were refluxed for one and half days. Solvent methanol was then removed to afford a blue solid. This was redissolved in MeCN to form a deep dark-blue solution. After refluxing for eight hours, this solution became black. Diethyl ether vapor diffusion into this solution provided a mixture of a white solid and a black solid. Sublimation of this residue provided colorless crystals. A <sup>1</sup>H NMR spectrum of these colorless crystals in CD<sub>3</sub>CN (**Figure 4.30**)



**Figure 4.30** A <sup>1</sup>H NMR spectrum of colorless crystals obtained from an attempted recrystallization of Cu(**1**)(ClO<sub>4</sub>)<sub>2</sub> from refluxing MeCN (NMR solvent is CD<sub>3</sub>CN.).

confirmed that these crystals were acetamide. This indicated that acetonitrile was hydrolyzed to acetamide in the presence of a Cu(II) complex of **4**. A possible mechanism for this process could be similar to the one shown in **Scheme 1.11**.<sup>47</sup> Acetonitrile is thus not a suitable reaction solvent in this case.

Cu(**4**)(ClO<sub>4</sub>)<sub>2</sub> was eventually synthesized and characterized by CHN elemental analyses. Its synthetic procedure is similar to that of [Cu<sub>2</sub>(μ-η<sup>1</sup>:η<sup>2</sup>-CO<sub>3</sub>)(**4**)<sub>2</sub>](ClO<sub>4</sub>)<sub>2</sub> except for the pre-drying of ligand **4** and Cu(ClO<sub>4</sub>)<sub>2</sub>•6H<sub>2</sub>O under vacuum. This reduced the amount of moisture as well as any adsorbed CO<sub>2</sub>.

Unlike Cu(**1**)(ClO<sub>4</sub>)<sub>2</sub> and Cu(**2**)(ClO<sub>4</sub>)<sub>2</sub>, in the presence of acetonitrile both Cu(**4**)(ClO<sub>4</sub>)<sub>2</sub> and Cu(**3**)(ClO<sub>4</sub>)<sub>2</sub> formed acetonitrile-coordinated Cu(II) complexes, [Cu(**3**)(CH<sub>3</sub>CN)](ClO<sub>4</sub>)<sub>2</sub> and Cu(**4**)(CH<sub>3</sub>CN)<sub>2</sub>(ClO<sub>4</sub>)<sub>2</sub>. The formation of Cu(**3**)(CH<sub>3</sub>CN)(ClO<sub>4</sub>)<sub>2</sub> was confirmed by its IR spectral data and X-ray structure determination whereas the isolation of Cu(**4**)(CH<sub>3</sub>CN)<sub>2</sub>(ClO<sub>4</sub>)<sub>2</sub> was supported by IR spectral data and CHN elemental analyses.

## 2.2 Infrared Spectra.

In the IR (KBr) spectrum of Cu<sub>2</sub>(OH)(**1**)<sub>2</sub>(ClO<sub>4</sub>)<sub>3</sub>(H<sub>2</sub>O) (**154**) (**Figure 4.31**), a slightly broadened N-H stretching band at 3270 cm<sup>-1</sup> is essentially the same as that of Cu(**1**)(ClO<sub>4</sub>)<sub>2</sub> (**Figure 4.32**).<sup>69(a)</sup> However, consistent with its composition, an additional very broad OH stretching band at 3537 cm<sup>-1</sup> can be observed in the IR spectrum (KBr) of Cu<sub>2</sub>(OH)(**1**)<sub>2</sub>(ClO<sub>4</sub>)<sub>3</sub>(H<sub>2</sub>O) whereas a much weaker OH stretching band is found for

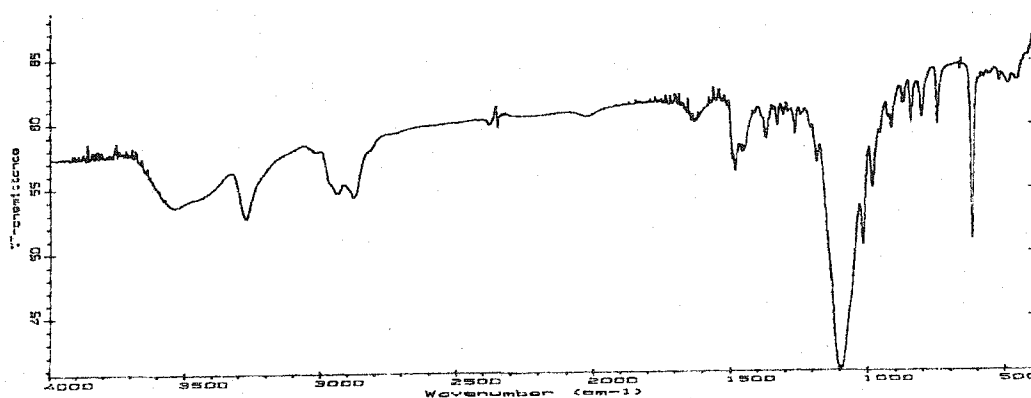


**Figure 4.31** The IR (KBr) spectrum of  $\text{Cu}_2(\text{OH})(\mathbf{1})_2(\text{ClO}_4)_3(\text{H}_2\text{O})$ .

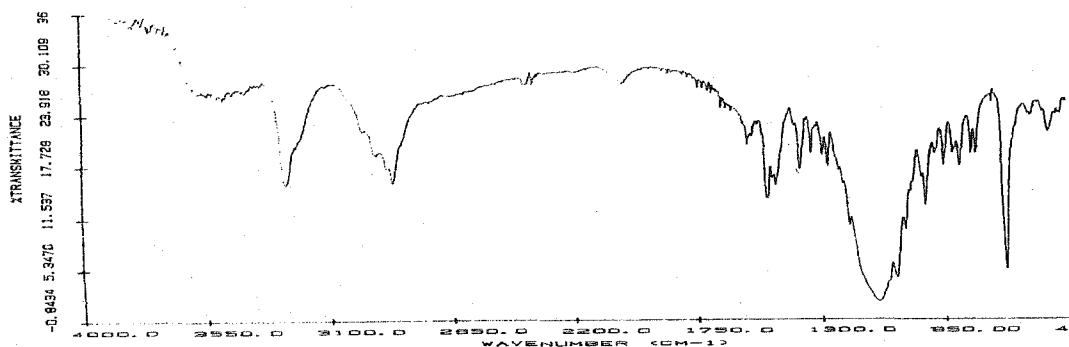


**Figure 4.32** The IR (KBr) spectrum of  $\text{Cu}(\mathbf{1})(\text{ClO}_4)_2$ .

$\text{Cu}(\mathbf{1})(\text{ClO}_4)_2$  (**Figure 4.32**). Compared to the broadened and complicated perchlorate bands of  $\text{Cu}(\mathbf{1})(\text{ClO}_4)_2$  centered at  $1090\text{ cm}^{-1}$ , the only single strong perchlorate band for  $\text{Cu}_2(\text{OH})(\mathbf{1})_2(\text{ClO}_4)_3(\text{H}_2\text{O})$  at  $1096\text{ cm}^{-1}$  is formed in the range  $900\text{--}1300\text{ cm}^{-1}$ . This indicates that in  $\text{Cu}_2(\text{OH})(\mathbf{1})_2(\text{ClO}_4)_3(\text{H}_2\text{O})$ , probably no perchlorate coordinates to the metal center<sup>132</sup> whereas one oxygen atom from a perchlorate in  $\text{Cu}(\mathbf{1})(\text{ClO}_4)_2$  likely coordinates to the copper(II) center as confirmed by its X-ray structure. The presence of two NH stretches at  $3150$  and  $3180\text{ cm}^{-1}$  in the IR spectrum (KBr) of  $[\text{Cu}\cdot\mathbf{2}(\mu\text{-Cl})]_2\text{Cl}_2$  indicate the nonequivalence of the two NHs in complexed **2** at least in the solid-state.

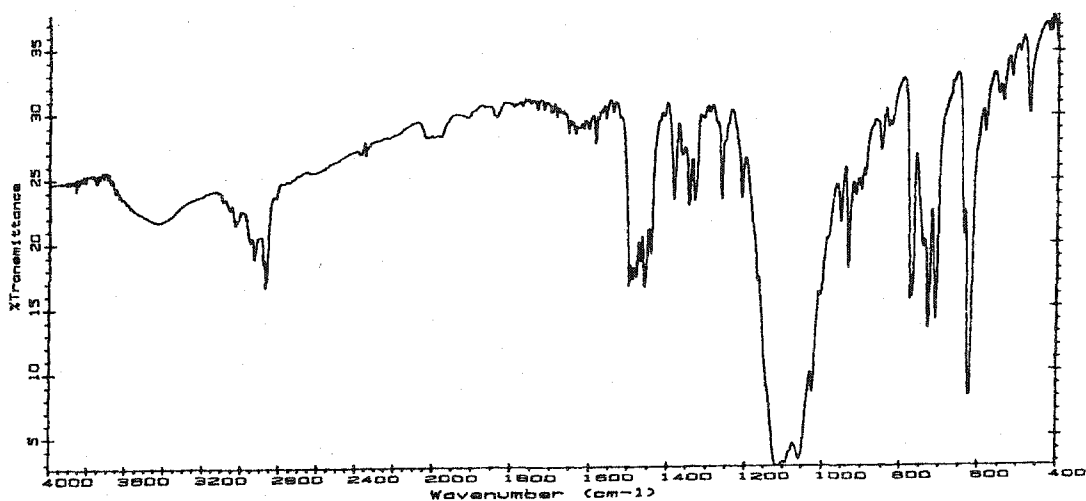


**Figure 4.33** The IR (KBr) spectrum of  $\text{Cu}(3)(\text{ClO}_4)_2$ .

In the IR spectrum of  $\text{Cu}(3)(\text{ClO}_4)_2$  (**Figure 4.33**), two strong and broadened perchlorate bands are observed at  $1055$  and  $1097\text{ cm}^{-1}$ . Based on this<sup>132</sup> and the fact that there is no solvent present in this complex according to its CHN elemental analyses, it is proposed that at least one of these two perchlorates is coordinated to the Cu(II) center. Consistent with the fact that no perchlorate coordinates to the Cu(II) center in  $[\text{Cu}(3)(\text{CH}_3\text{CN})](\text{ClO}_4)_2$  (**Figure 4.34(a)**), only a strong ionic perchlorate band appears at  $1086\text{ cm}^{-1}$  within the range  $900\text{--}1300\text{ cm}^{-1}$ . The coordination of acetonitrile to this Cu(II) center is indicated by the presence of two  $\nu_{\text{C}\equiv\text{N}}$  at  $2285$  and  $2314\text{ cm}^{-1}$  (**Figure 4.34(a)**). In the literature, Karlin has reported an acetonitrile  $\nu_{\text{C}\equiv\text{N}}$  at  $2300\text{ cm}^{-1}$  in the IR spectrum (nujol) of a dimeric 5-coordinated Cu(II) polyamine complex.<sup>133</sup> A strong and relatively-sharp band at  $1089\text{ cm}^{-1}$  in the range  $900\text{--}1300\text{ cm}^{-1}$  can be seen in the IR (KBr) spectrum of  $\text{Cu}(4)(\text{CH}_3\text{CN})_2(\text{ClO}_4)_2$  (**Figure 4.34(b)**). This indicates that no perchlorate is coordinated to the Cu(II). The observation of two  $\nu_{\text{C}\equiv\text{N}}$  bands at  $2333$  and  $2305\text{ cm}^{-1}$  is indicative of the acetonitrile coordination.

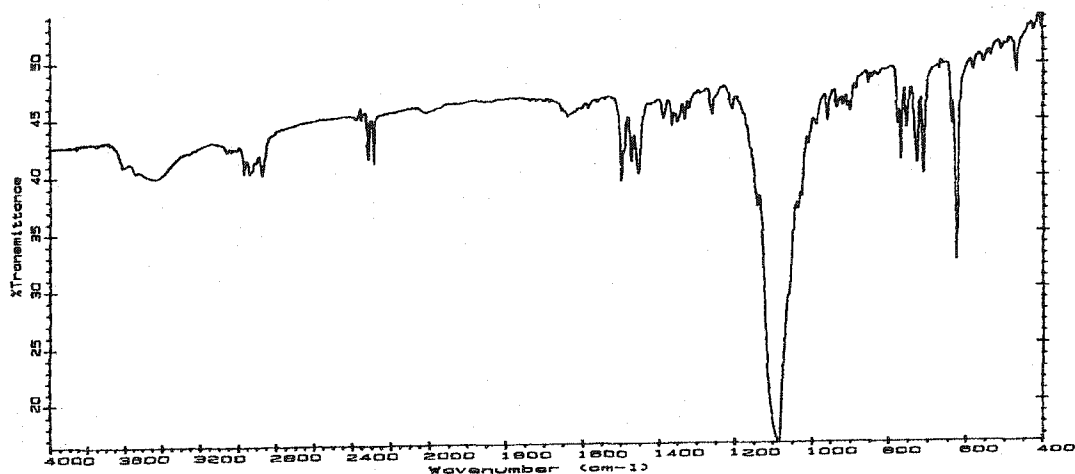


Figure 4.34(a) The IR (KBr) spectrum of  $[\text{Cu}(3)(\text{CH}_3\text{CN})](\text{ClO}_4)_2$ .

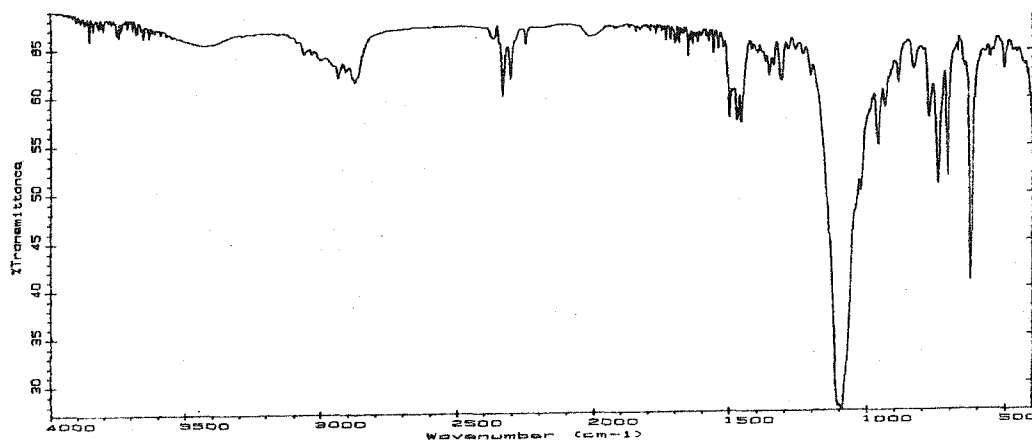
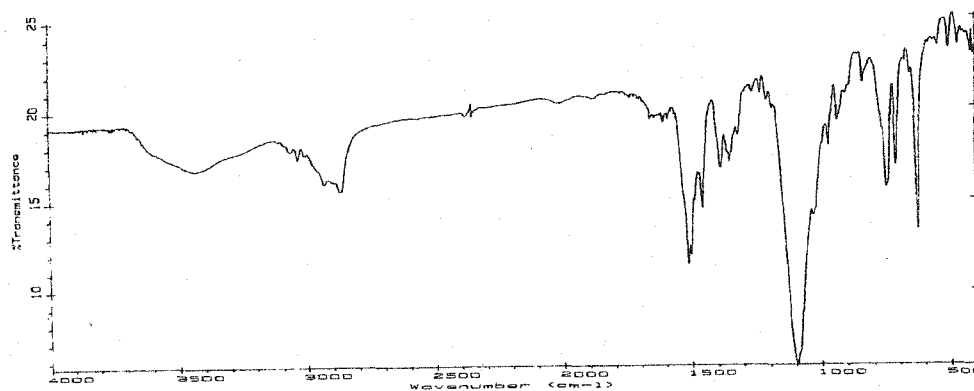
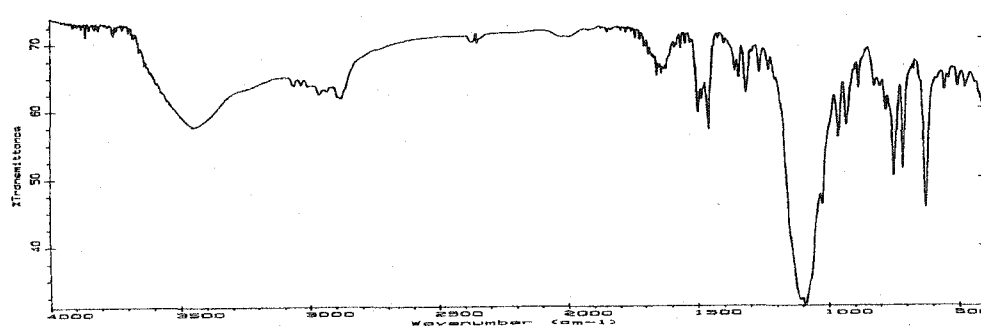


Figure 4.34(b) The IR (KBr) spectrum of  $\text{Cu}(4)(\text{CH}_3\text{CN})_2(\text{ClO}_4)_2$ .

Two relatively-strong bands at  $1506$  and  $1496\text{ cm}^{-1}$  in the IR (KBr) spectrum of  $[\text{Cu}_2(\mu\text{-}\eta^1\text{:}\eta^2\text{-CO}_3)(4)_2](\text{ClO}_4)_2$  (Figure 4.35(a)) suggest the presence of the C=O group whereas no such strong bands was observed in the spectrum of  $\text{Cu}(4)(\text{ClO}_4)_2$  (Figure 4.35(b)). In the literature,  $[\text{Cu}_2(\mu\text{-}\eta^1\text{:}\eta^2\text{-CO}_3)(\text{L})_2(\text{H}_2\text{O})](\text{CF}_3\text{SO}_3)_2$  ( $\text{L}=1,4,7\text{-trisisopropyl-}1,4,7\text{-triazacyclononane}$ ) featuring the same carbonate coordination mode has these two bands at  $1539$  and  $1476\text{ cm}^{-1}$ .<sup>134</sup> This was consistent with the the X-ray structure of



**Figure 4.35(a)** The IR (KBr) spectrum of  $[\text{Cu}_2(\mu\text{-}\eta^1:\eta^2\text{-CO}_3)(4)_2](\text{ClO}_4)_2$ .



**Figure 4.35(b)** The IR (KBr) spectrum of  $\text{Cu}(4)(\text{ClO}_4)_2$ .

$[\text{Cu}_2(\mu\text{-}\eta^1:\eta^2\text{-CO}_3)(4)_2](\text{ClO}_4)_2$  (**Figure 4.42**, *vide infra*) in which a bridging carbonate featuring both unidentate and bidentate coordination modes was found. A strong and relatively-sharp perchlorate band at  $1095\text{ cm}^{-1}$  was consistent with the presence of only ionic perchlorates in this complex.

### 2.3 Electronic Spectra.

Solution electronic spectra of the described copper complexes are summarized in **Table 4.4**. Except that of  $\text{Cu}_2(\text{OH})(1)_2(\text{ClO}_4)_3(\text{H}_2\text{O})$ , these d-d transitions are found as



**Table 4.4** Summary of electronic spectral data for the copper complexes of ligands 1-4.

Complex	$\lambda_{\max}$ ( $\epsilon$ , $M^{-1}cm^{-1}$ )	Complex	$\lambda_{\max}$ ( $\epsilon$ , $M^{-1}cm^{-1}$ )
$Cu_2(OH)(1)_2(ClO_4)_3$ ( $H_2O$ ) in MeCN	584 nm (151), 904 (71)	$Cu_2(OH)(1)_2(ClO_4)_3$ ( $H_2O$ ) in water	595 nm (93), 958 (69)
$[Cu \cdot 2(\mu-Cl)]_2Cl_2$ in water	640 nm (72)	$Cu(2)(ClO_4)_2$ in water	635 nm (76)
$Cu(3)(ClO_4)_2$ in MeCN	623 nm (129)	$CuCl_2 \cdot 4$ in MeCN	710 nm (85)
$[Cu_2(\mu^1-\mu^2-CO_3)(4)_2]$ $(ClO_4)_2$ in MeCN	660 nm (148)	$Cu(4)(ClO_4)_2$ in MeCN	647 nm (162)
$[Cu_2(\mu^1-\mu^2-CO_3)(4)_2]$ $(ClO_4)_2$ in MeOH	687 nm (187)	$Cu(4)(ClO_4)_2$ in MeOH	657 nm (94)

broad bands between 623 and 710 nm. The electronic spectrum of  $Cu_2(OH)(1)_2(ClO_4)_3$  ( $H_2O$ ) shows two bands at 584 and 904 nm in acetonitrile (**Figure 4.36**) and two bands at 595 and 958 nm in water. This is significantly different from that of  $Cu(1)(ClO_4)_2$  in which only a band at 567 nm can be observed in acetonitrile. This suggests that in solution, hydroxide remains still partially or fully coordinated to the former Cu(II) center.

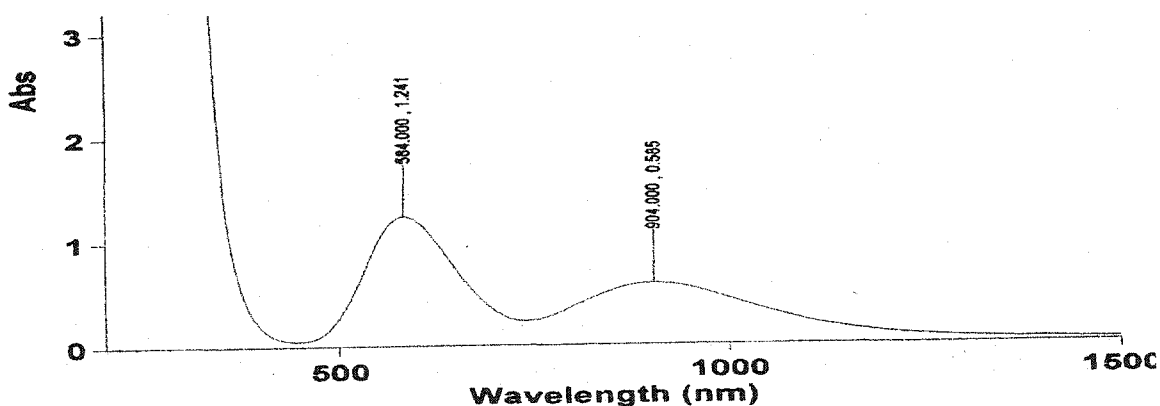


**Figure 4.36** The electronic spectrum of  $Cu_2(OH)(1)_2(ClO_4)_3$  ( $H_2O$ ) in acetonitrile.

In  $H_2O$ , diluted  $[Cu \cdot 2(\mu-Cl)]_2Cl_2$  (**155**) (0.0024 M) has a maximum at 640 nm ( $\epsilon = 72 M^{-1}cm^{-1}$ ) in its electronic spectrum (**Figure 4.37(a)**) while  $Cu(2)(ClO_4)_2$  (**156**) has a

similar maximum at 635 nm ( $\epsilon = 76 \text{ M}^{-1}\text{cm}^{-1}$ ) (Figure 4.37(b)). This suggests that they may have a common aqueous solution species, probably  $[\text{Cu}(\text{H}_2\text{O})_6]^{2+}$ .

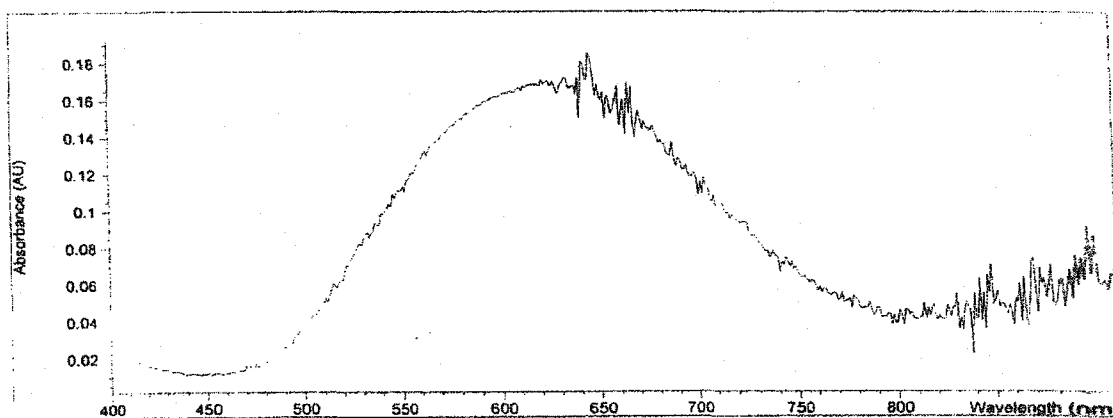


Figure 4.37(a) The electronic spectrum of  $[\text{Cu}\cdot 2(\mu\text{-Cl})]_2\text{Cl}_2$  in water.

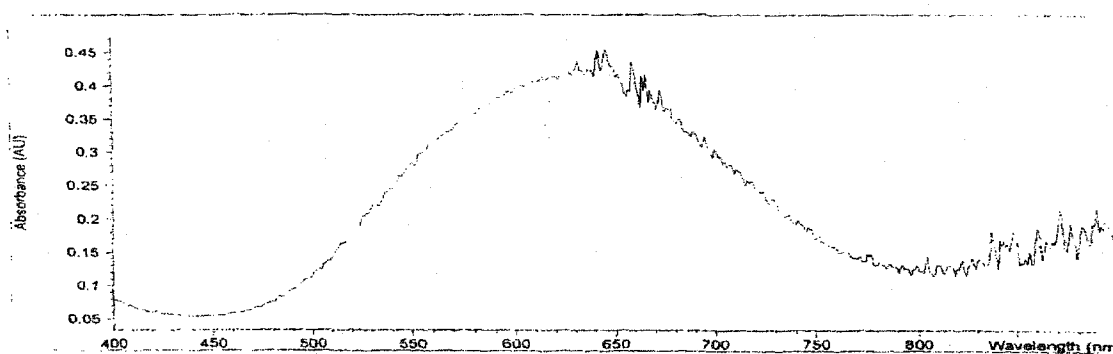


Figure 4.37(b) The electronic spectrum of  $\text{Cu}(2)(\text{ClO}_4)_2$  in water.

In MeCN,  $\text{CuCl}_2\cdot 4$  has a longer wavelength d-d maximum at 710 nm compared to that of  $[\text{Cu}\cdot 3\text{Cl}]\text{Cl}(\text{H}_2\text{O})$  at 680 nm. Similarly,  $\text{Cu}(4)(\text{ClO}_4)_2$  has a longer wavelength d-d maximum at 647 nm compared to that of  $\text{Cu}\cdot 3(\text{ClO}_4)_2$  at 623 nm.<sup>69(a)</sup> This indicates that ligand 3 has a strong ligand field towards Cu(II) than ligand 4.

## 2.4 X-ray Structural Data.

X-ray structures of  $[\text{Cu}\cdot 2(\mu\text{-Cl})]_2\text{Cl}_2$  (**155**),  $[\text{Cu}(2)(\text{CH}_3\text{OH})(\text{ClO}_4)](\text{ClO}_4)$  (**156a**),  $[\text{Cu}(3)(\text{CH}_3\text{CN})](\text{ClO}_4)_2$  (**157a**),  $\text{CuCl}_2\cdot 4$  (**158**) and  $[\text{Cu}_2(\mu\text{-}\eta^1:\eta^2\text{-CO}_3)(4)_2](\text{ClO}_4)_2$  (**159**) were successfully solved. Their relevant bond distances and angles are listed in **Tables 4.5(a-e)**.

**$[\text{Cu}\cdot 2(\mu\text{-Cl})]_2\text{Cl}_2$  (**155**):** The structure of this Cu(II) complex shows a centrosymmetric dimeric Cu(II) complex with each Cu(II) adopting a distorted octahedral geometry (**Figure 4.38**). The distance between these two copper atoms is 3.9038(7) Å. The N(ax)-

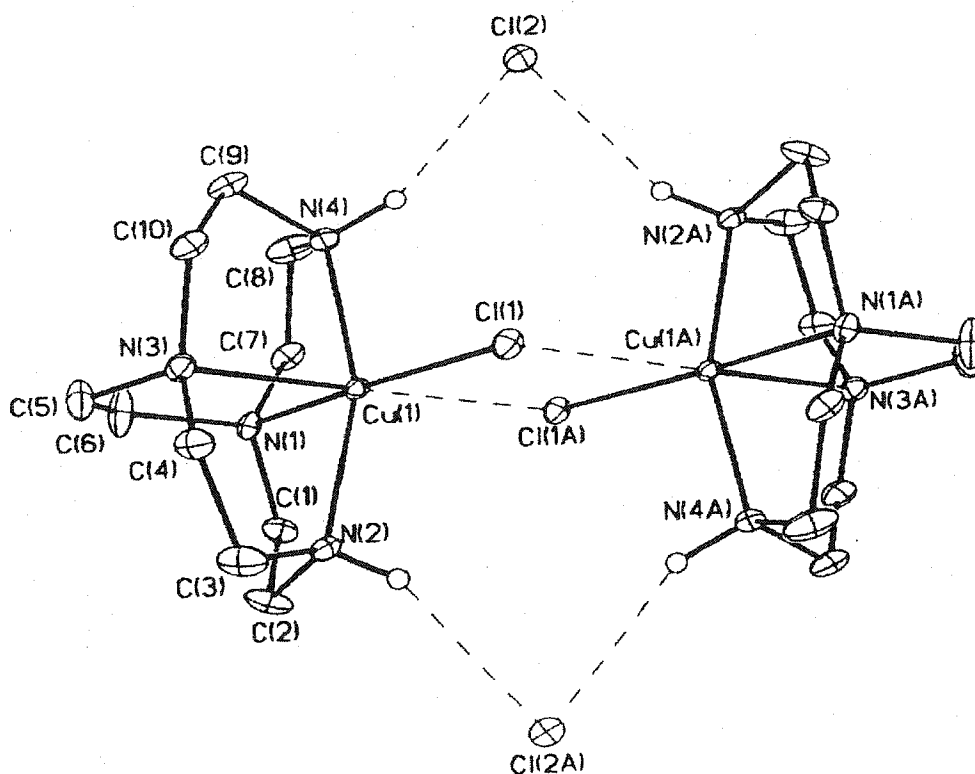


**Figure 4.38** X-ray structure of  $[\text{Cu}\cdot 2(\mu\text{-Cl})]_2\text{Cl}_2$  (**155**) showing atomic labeling scheme.

**Table 4.5(a)** Selected Bond Distances (Å) and Bond Angles (deg) in  $[\text{Cu}\cdot 2(\mu\text{-Cl})]_2\text{Cl}_2$  (155) (Hydrogen bonding interactions are included.).

Cu(1)-N(1)	2.037(2)	Cu(1)-N(3)	2.197(2)
Cu(1)-N(2)	2.073(2)	Cu(1)-N(4)	2.050(2)
Cu(1)-Cl(1)	2.2842(8)	Cu(1)-Cl(1A)	2.893
N4---Cl(2)	3.362(3)	N2A---Cl(2)	3.299(3)
N(4)-Cu(1)-N(2)	160.37(11)	N(1)-Cu(1)-N(3)	85.35(9)
N(1)-Cu(1)-N(2)	83.87(10)	N(3)-Cu(1)-N(2)	81.46(10)
N(1)-Cu(1)-N(4)	82.33(10)	N(3)-Cu(1)-N(4)	83.57(10)
N(1)-Cu(1)-Cl(1)	174.13(7)	N(3)-Cu(1)-Cl(1)	100.50(7)
N(4)-Cu(1)-Cl(1)	97.94(7)	N(2)-Cu(1)-Cl(1)	97.21(7)
Cl(1A)-Cu(1)-Cl(1)	82.8	H(2A)-Cl(2)-H(4)	75.1

Cu-N(ax) angle is  $160.37(11)^\circ$  and the N(eq)-Cu-N(eq) angle is  $85.35(9)^\circ$ . Among four Cu(1)-N distances, one N(eq)-Cu (Cu(1)-N(3)) bond distance of  $2.197(4)$  Å is significantly longer than the other three Cu(1)-N bondlengths which range from 2.04 to 2.07 Å. This dimer has an inversion center with very unsymmetrical bridging Cu(1)-Cl bond distances of 2.28 Å and 2.89 Å. Such long Cu(1)-N(3) and Cu(1)-Cl(1A) distances in *trans* to each other are clearly due to the Jahn-Teller distortion. For comparison, five-coordinate  $[\text{Cu}\cdot 1\text{Cl}]\text{Cl}(\text{H}_2\text{O})_3$  showed Cu(1)-N bondlengths ranging from 2.00 to 2.14 Å and Cu-Cl bond distance of 2.30 Å.<sup>69(a)</sup> In the literature, there are more than thirty Cu-Cl

bond distances longer than 3.0 Å<sup>134</sup> with the longest of 3.44 Å.<sup>135(a-e)</sup> For example, a dimeric copper complex of diethylenetriamine with two bridging chlorides has a Cu-Cl bond distance of 3.02 Å.<sup>135(c)</sup> This is the one of several reported dichloride-bridged Cu(II) complexes of polyamines.<sup>135(c),136</sup>

**[Cu(2)(CH<sub>3</sub>OH)(ClO<sub>4</sub>)](ClO<sub>4</sub>) (156a):** Unlike five-coordinate Cu(II) complexes of parent cross-bridged cyclam and its derivatives **3**, **107**, and **111**,<sup>69(a),74,78</sup> this complex of the smaller cross-bridged cyclen, ligand **2**, has a six coordinate geometry (**Figure 4.39**).

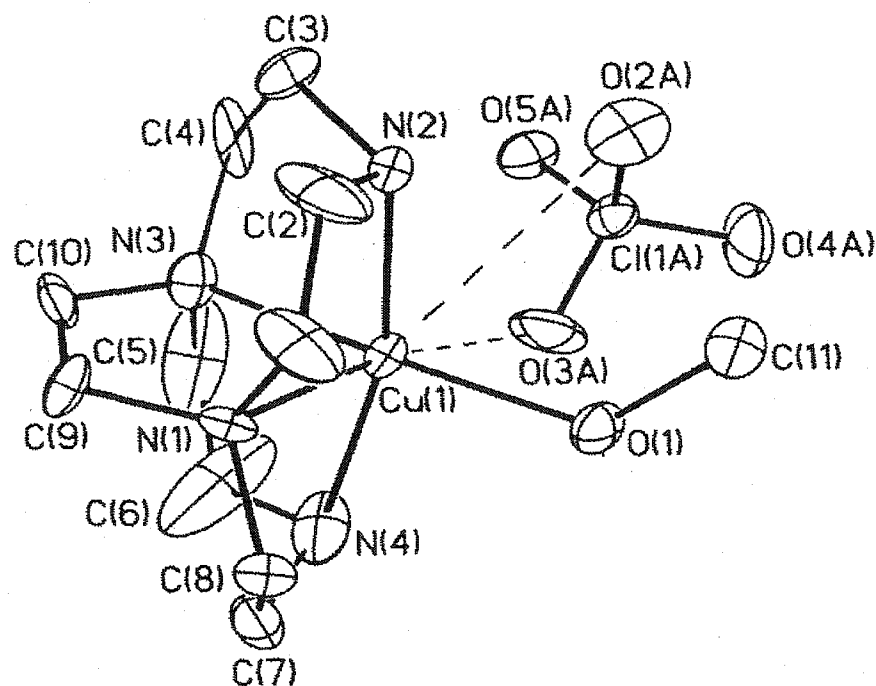


**Figure 4.39** X-ray structure of [Cu(2)(CH<sub>3</sub>OH)(ClO<sub>4</sub>)](ClO<sub>4</sub>) (**156a**) showing atomic labeling scheme.

The Cu(II) atom is coordinated by four amino nitrogen donors from the macrocycle ligand together with one methanol oxygen and one monodentate perchlorate oxygen in a distorted octahedron. This is indicated by the axial N(2)-Cu-N(4) bond angle of 165.3(5)°

**Table 4.5(b)** Selected Bond Distances (Å) and Bond Angles (deg) in [Cu(2)(CH<sub>3</sub>OH)](ClO<sub>4</sub>)<sub>2</sub> (156a).

Cu(1)-N(1)	2.167(9)	Cu(1)-N(3)	2.030(11)
Cu(1)-N(2)	2.024(12)	Cu(1)-N(4)	2.079(14)
Cu(1)-O(1)	2.019(9)	Cu(1)-O(2)	3.483(14)
Cu(1)-O(3)	2.741(14)		
N(4)-Cu(1)-N(2)	165.3(5)	N(1)-Cu(1)-N(3)	84.7(4)
N(1)-Cu(1)-N(2)	85.0(4)	N(3)-Cu(1)-N(2)	84.5(5)
N(1)-Cu(1)-N(4)	84.8(5)	N(3)-Cu(1)-N(4)	84.1(6)
N(1)-Cu(1)-O(1)	102.6(4)	N(2)-Cu(1)-O(1)	97.3(4)
N(3)-Cu(1)-O(1)	172.6(4)	N(4)-Cu(1)-O(1)	95.2(5)
N(1)-Cu(1)-O(2)	150.8(3)	N(2)-Cu(1)-O(2)	66.5(4)
N(3)-Cu(1)-O(2)	98.0(4)	N(4)-Cu(1)-O(2)	124.4(5)
N(1)-Cu(1)-O(3)	167.2(3)	N(2)-Cu(1)-O(3)	107.8(4)
N(3)-Cu(1)-O(3)	95.7(4)	N(4)-Cu(1)-O(3)	82.6(5)
O(1)-Cu(1)-O(2)	76.3(4)	O(2)-Cu(1)-O(3)	41.9(3)
O(1)-Cu(1)-O(3)	76.9(4)		

and equatorial N(1)-Cu-N(3) bond angle of 84.7(4)°. Again, one N(eq)-Cu (Cu-N(1)) bond distance of 2.167(9) Å is significantly longer than the other three Cu(1)-N bondlengths which range from 2.030(11) to 2.079(14) Å. The coordinating of only one

oxygen from perchlorate is indicated by the single O(perchlorate)-Cu distance of 2.741(14) Å under 3.4 Å. This perchlorate Cu-O(3) distance is significantly longer than that of 2.166(6) Å in [Cu(1)(ClO<sub>4</sub>)]ClO<sub>4</sub> (Figure 1.58). Such long Cu-N(1) and Cu-O(3) distances in *trans* sites are again due to the Jahn-Teller distortion.

The methanol O(1)-Cu bond distance in this Cu(II) complex is 2.019(9) Å. There is no literature data on the methanol-coordinated Cu(II) complexes of tetraamines. However, a numerous Cu(II) complexes with coordinated MeOH in a N<sub>4</sub>O mode are available.<sup>137(a-i)</sup> These have longer methanol O-Cu bond distances ranging from 2.24 to 2.54 Å.

[Cu(3)(CH<sub>3</sub>CN)](ClO<sub>4</sub>)<sub>2</sub> (157a): This structure (Figure 4.40) has the same [Cu(3)(CH<sub>3</sub>CN)]<sup>2+</sup> fragment as that of [Cu(II)•3(MeCN)](PF<sub>6</sub>)<sub>2</sub> (Figure 1.65).<sup>78</sup> This has acetonitrile in the fifth coordinate position and an axial N(3)-Cu-N(4) bond angle of 177.79(19)° and equatorial N(1)-Cu-N(2) bond angle of 88.37(19)° whereas the same N<sub>ax</sub>-Cu-N<sub>ax</sub> bond angle and a different N<sub>eq</sub>-Cu-N<sub>eq</sub> bond angle of 86.96(10)° were reported for [Cu(II)(MeCN)•3](PF<sub>6</sub>)<sub>2</sub>. The Cu(II) atom has a slightly distorted square-pyramidal coordination geometry as indicated by an Addison and Reedjik's τ-parameter of 0.1515.<sup>138</sup> The acetonitrile and three nitrogen atoms from the cross-bridged ligand occupy the equatorial position while N(1) is apical. The four Cu(II)-N distances are within the range between 2.020(5) and 2.127(5) Å.

The bond distance between the acetonitrile nitrogen atom and Cu is 2.020(5) Å which is essentially the same as that in [Cu(II)•3(MeCN)](PF<sub>6</sub>)<sub>2</sub>. In the literature, several 6-coordinate Cu(II) complexes of cyclam and cyclam derivatives with two coordinated

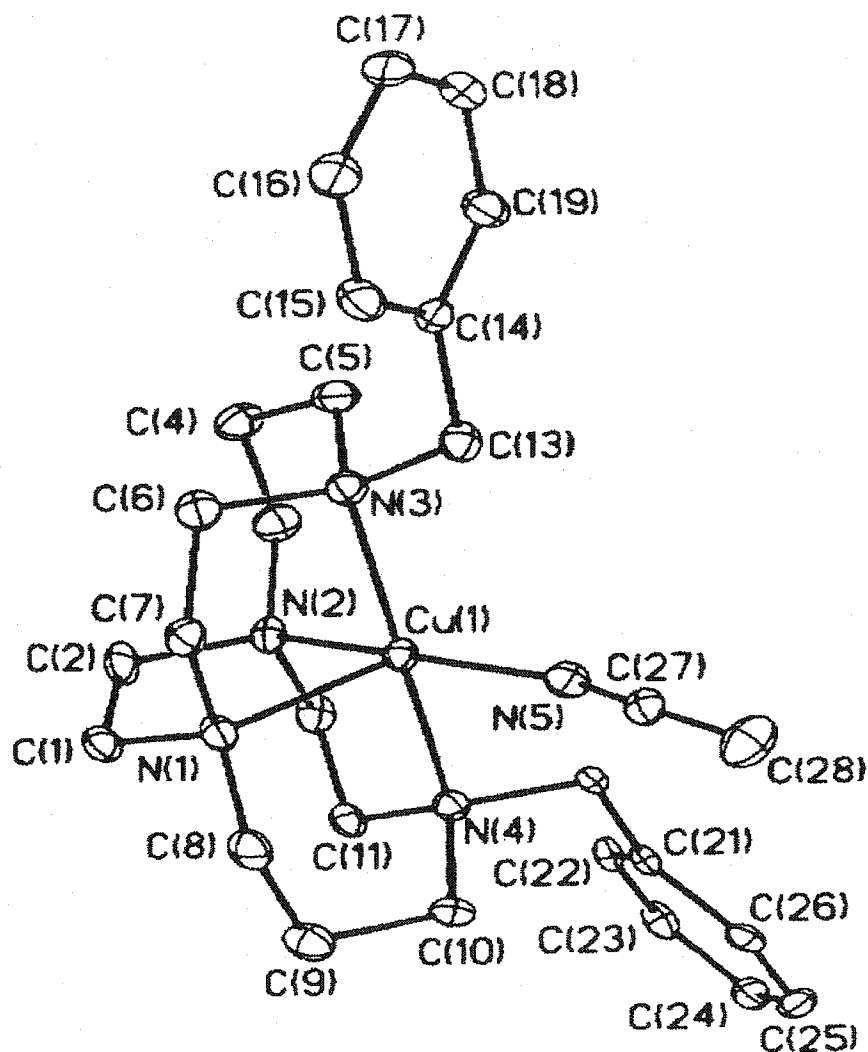


**Figure 4.40** X-ray structure of  $[\text{Cu}(\text{3})(\text{CH}_3\text{CN})](\text{ClO}_4)_2$  (**157a**) showing atomic labeling scheme.

acetonitriles in *trans* positions have been reported.<sup>50(a),139(a),139(b)</sup> The bond distances between acetonitrile nitrogen and copper in these complexes are all essentially the same (2.6 Å). Two five-coordinate Cu(II) complexes of cyclam derivatives with a coordinating acetonitrile have also been reported.<sup>50(k),51(h)</sup> The Cu-N bond distances in these two complexes are 2.17 and 2.48 Å, which are also substantially longer than that in  $[\text{Cu}(\text{3})(\text{CH}_3\text{CN})](\text{ClO}_4)_2$ .



**Table 4.5(c)** Selected Bond Distances (Å) and Bond Angles (deg) in [Cu(3)(CH<sub>3</sub>CN)](ClO<sub>4</sub>)<sub>2</sub> (**157a**).

Cu(1)-N(1)	2.130(5)	Cu(1)-N(3)	2.127(5)
Cu(1)-N(2)	2.058(5)	Cu(1)-N(4)	2.082(5)
Cu(1)-N(5)	2.020(5)		
N(4)-Cu(1)-N(3)	177.79(19)	N(1)-Cu(1)-N(2)	88.37(19)
N(2)-Cu(1)-N(5)	168.7(2)	N(4)-Cu(1)-N(5)	88.42(19)
N(2)-Cu(1)-N(4)	84.82(19)	N(3)-Cu(1)-N(5)	92.98(19)
N(2)-Cu(1)-N(3)	93.5(2)	N(1)-Cu(1)-N(5)	101.1(2)
N(1)-Cu(1)-N(4)	93.45(19)	N(1)-Cu(1)-N(3)	87.97(19)

**CuCl<sub>2</sub>•4** (**158**): The crystal structure of this Cu(II) complex is shown in **Figure 4.41**. One terminal chloride and four nitrogen atoms from the macrobicyclic ligand coordinate to Cu(II) atom. This complex has an axial N(2)-Cu-N(4) bond angle of 167.9(3)° and equatorial N(1)-Cu-N(3) bond angle of 81.0(3)° whereas the Cu(II) complex of the cross-bridged cyclam analogue, [Cu(3)Cl]Cl(H<sub>2</sub>O) (**Figure 1.59**) has axial N(1)-Cu-N(8) bond angle of 176.0(2)° and equatorial N(4)-Cu-N(11) bond angle of 86.1(1)°. <sup>69(a)</sup> Clearly, Cu(II) fits better in the latter cross-bridged cyclam derivative compared to its cyclam analogue. Three short tertiary amine nitrogen-Cu bond lengths ranging between 2.047(8) and 2.080(7) Å were observed. The fourth nitrogen-Cu bond of 2.197(7) Å is significantly N(3) at the apex as indicated by an Addison and Reedjik  $\tau$ -parameter of only 0.013.

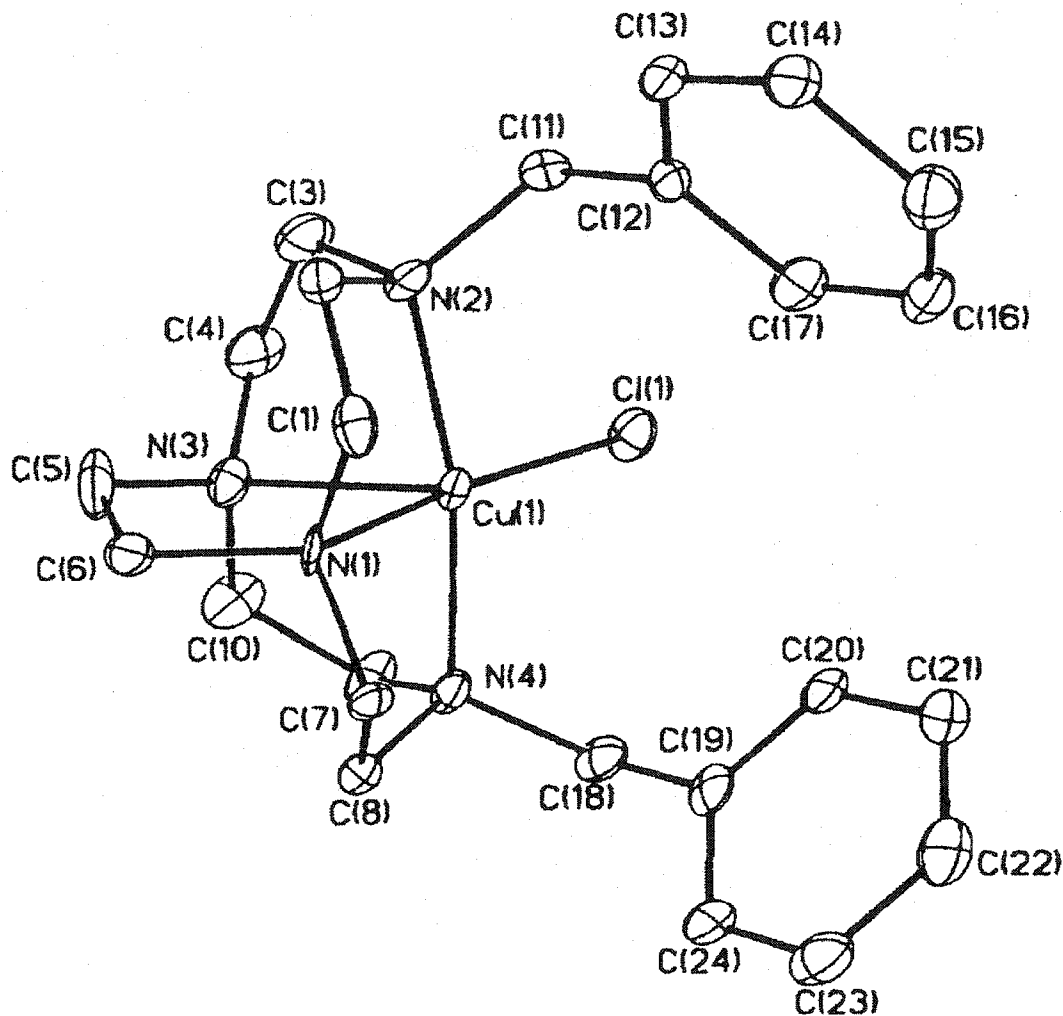


**Figure 4.41** X-ray structure of  $\text{CuCl}_2 \cdot 4$  (158) showing atomic labeling scheme.

The Cu(II)-Cl bond distance of 2.251(3) Å is slightly shorter than that of 2.296 Å found in  $[\text{Cu}(3)\text{Cl}]\text{Cl}(\text{H}_2\text{O})$  (Figure 1.59).<sup>69(a)</sup> Several five-coordinate Cu(II) complexes of cyclen derivatives with a terminal chloride in the fifth coordination position have been reported.<sup>54(a),54(e),54(r-t)</sup> Their longer Cu-Cl bond distances range from 2.37 to 2.43 Å while the Cu-N bond distances range from 2.026 to 2.144 Å.

**Table 4.5(d)** Selected Bond Distances (Å) and Bond Angles (deg) in CuCl<sub>2</sub>•4 (**158**).

Cu(1)-N(1)	2.080(7)	Cu(1)-N(3)	2.197(7)
Cu(1)-N(2)	2.079(7)	Cu(1)-N(4)	2.047(8)
Cu(1)-Cl(1)	2.251(3)		
N(4)-Cu(1)-N(2)	167.9(3)	N(1)-Cu(1)-N(3)	81.0(3)
N(1)-Cu(1)-N(2)	86.1(3)	N(1)-Cu(1)-N(4)	85.8(3)
N(3)-Cu(1)-N(4)	85.9(3)	N(2)-Cu(1)-N(3)	84.0(3)
N(1)-Cu(1)-Cl(1)	168.7(2)	N(2)-Cu(1)-Cl(1)	95.0(2)
N(3)-Cu(1)-Cl(1)	110.3(2)	N(4)-Cu(1)-Cl(1)	94.7(2)

[Cu<sub>2</sub>(μ-η<sup>1</sup>:η<sup>2</sup>-CO<sub>3</sub>)(4)<sub>2</sub>](ClO<sub>4</sub>)<sub>2</sub> (**159**): The structure of this dimeric copper complex features η<sup>1</sup>:η<sup>2</sup>-bridging carbonate and η<sup>4</sup>-coordinating bicycle tetraamines **4b** (Figure 4.42). At two copper(II) centers, Cu(1) is in a distorted octahedral N<sub>4</sub>O<sub>2</sub> environment whereas Cu(2) adopts a square-pyramidal geometry as indicated by its Addison and Reedjik's τ-parameter of 0.099. The distortion of the octahedral geometry around Cu(1) is indicated by the axial N(3)-Cu(1)-N(4) bond angle of only 155.70(16)° and the chelate O(1)-Cu(1)-O(2) bond angle of only 66.44(16)°. Unlike the structures of **155**, **156a**, **157a**, and **158**, N(ax)-Cu(1) bondlengths of 2.399(5) and 2.421(5) Å are significantly longer than the N(eq)-Cu(1) bondlength of 1.999(5) and 2.018(5) Å and related N-Cu bondlengths in **155**, **156a**, **157a**, and **158**. These longer bond distances in the axial

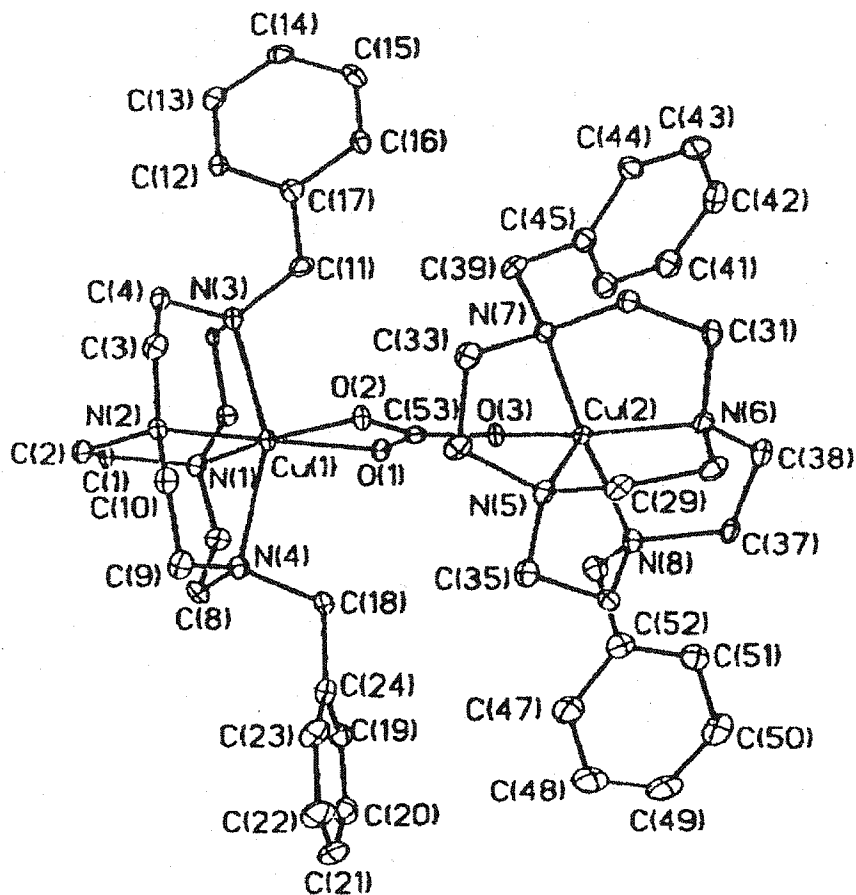


**Figure 4.42** X-ray structure of  $[\text{Cu}_2(\mu\text{-}\eta^1:\eta^2\text{-CO}_3)(4)](\text{ClO}_4)_2$  (**159**) showing atomic labeling scheme.

positions are again caused by the Jahn-Teller distortion along the axial N(3) and N(4) sites.

Cu(2) in the square-pyramidal coordination geometry is coordinated by four nitrogen atoms from the macrobicyclic and one monodenate carbonate oxygen. According to our standard definition, it has an axial N(7)-Cu-N(8) bond angle of  $165.6(2)^\circ$  and equatorial N(5)-Cu-N(6) bond angle of  $84.13(19)^\circ$ . Four amine N-Cu bond distances range from 2.034(5) to 2.158(5) Å. Again, the amine nitrogen N(5) opposite the vacant sixth site has the longest bond distance of 2.158(5) Å.

**Table 4.5(e)** Selected Bond Distances (Å) and Bond Angles (deg) in [Cu<sub>2</sub>(μ-η<sup>1</sup>:η<sup>2</sup>-CO<sub>3</sub>)(4)<sub>2</sub>](ClO<sub>4</sub>)<sub>2</sub> (**159**).

Cu(1)-N(1)	2.018(5)	Cu(1)-N(3)	2.421(5)
Cu(1)-N(2)	1.999(5)	Cu(1)-N(4)	2.399(5)
Cu(2)-N(5)	2.158(5)	Cu(2)-N(6)	2.034(5)
Cu(2)-N(7)	2.080(5)	Cu(2)-N(8)	2.124(5)
Cu(1)-O(1)	1.977(4)	Cu(1)-O(2)	2.028(4)
Cu(2)-O(3)	1.933(4)		
N(4)-Cu(1)-N(3)	155.70(16)	N(1)-Cu(1)-N(2)	86.59(19)
N(7)-Cu(2)-N(8)	165.6(2)	N(5)-Cu(2)-N(6)	84.13(19)
N(2)-Cu(1)-N(4)	79.58(18)	N(1)-Cu(1)-N(4)	81.57(19)
N(2)-Cu(1)-N(3)	83.41(18)	N(1)-Cu(1)-N(3)	80.21(18)
N(6)-Cu(2)-N(7)	86.41(19)	N(6)-Cu(2)-N(8)	82.40(19)
N(5)-Cu(2)-N(7)	83.42(19)	N(5)-Cu(2)-N(8)	86.50(19)
N(1)-Cu(1)-O(1)	102.98(18)	N(2)-Cu(1)-O(1)	170.15(18)
N(3)-Cu(1)-O(1)	100.36(16)	N(4)-Cu(1)-O(1)	99.29(16)
N(1)-Cu(1)-O(2)	169.39(18)	N(2)-Cu(1)-O(2)	103.96(18)
N(3)-Cu(1)-O(2)	101.86(16)	N(4)-Cu(1)-O(2)	99.00(17)
N(6)-Cu(2)-O(3)	159.65(19)	N(7)-Cu(2)-O(3)	99.60(18)
N(8)-Cu(2)-O(3)	93.98(18)	N(5)-Cu(2)-O(3)	115.75(17)
O(1)-Cu(1)-O(2)	66.44(16)		

The tridentate carbonate has two slightly longer chelate O-Cu bond lengths of 1.977(4) and 2.028(4) Å and a slightly shorter monodentate carbonate O-Cu bond length of 1.933(4) Å. Such a dimeric copper complex featuring an  $\eta^1:\eta^2$ -bridging carbonate is rare for Cu(II) polyamine complexes. The only other literature example is the complex  $[\text{Cu}_2(\mu\text{-}\eta^1:\eta^2\text{-CO}_3)(\text{L})_2(\text{H}_2\text{O})](\text{CF}_3\text{SO}_3)_2$  (L=1,4,7-triisopropyl-1,4,7-triazacyclononane) in which two five-coordinate copper atoms are bridged by a carbonate. It has chelating O-Cu bond lengths of 1.967(3) and 2.036(2) Å and a monodentate carbonate O-Cu bond lengths of 1.967(2) Å. The amine nitrogen-Cu bond distances range from 2.036(2) and 2.228(3) Å. There is another example of a Cu(II) carbonate complex with a cross-bridged ligand. It is a trinuclear Cu(II) complex with a  $\mu_3$ -carbonate,  $[(\text{Cu}\cdot\mathbf{112})_3(\mu_3\text{-CO}_3)](\text{ClO}_4)_4(\text{H}_2\text{O})_2$ <sup>90</sup> (Figure 4.43). Its three equivalent Cu(II) atoms have N(ax)-Cu-N(ax) bond angles of 169.0(2)° and equatorial N(eq)-Cu-N(eq) bond angles of 98.0(2)°. All the monodentate carbonate O-Cu bond lengths are 2.001(11) Å.

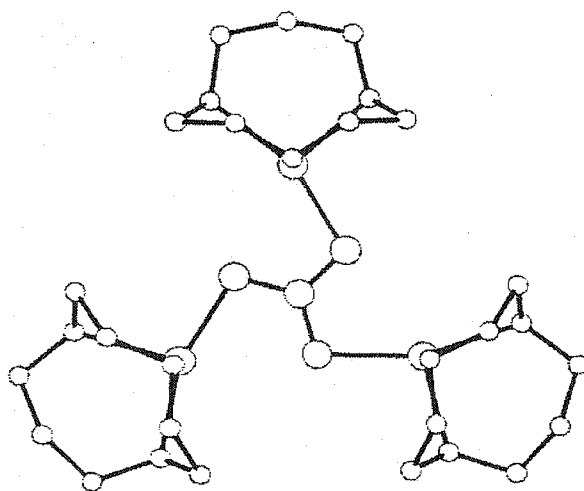


**Figure 4.43** X-ray structure of  $[(\text{Cu}\cdot\mathbf{112})_3(\mu_3\text{-CO}_3)](\text{ClO}_4)_4(\text{H}_2\text{O})_2$  from reference 90.

### Summary of Structural Data.

These five copper complexes of cross-bridged ligands **2**, **3**, and **4** showed coordination numbers of five or six. A summary of their axial N-Cu-N bond angles and equatorial N-Cu-N bond angles is listed in **Table 4.6**. Together with the data in **Table 1.1**, five or six-coordinate Cu(II) complexes of cross-bridged cyclam and its derivatives, ligands **1**, **3**, **107**, and **111** thus have the axial N-Cu-N angles ranging from 175.16(13) to 179.7(3)° and the equatorial N-Cu-N bond angles ranging from 84.8(1) to 88.5(3)°. By comparison, Cu(II) complexes of cross-bridged cyclen and its derivatives, ligands **1**, **3**, **107**, and **111** have their axial N-Cu-N angles from 155.70(16) to 167.9(3)° and equatorial N-Cu-N bond angles ranging from 81.0(3) to 86.59(19)°. Similar to the case for zinc, these structural data confirm that the smaller cross-bridged cyclen and its derivatives are not as good a fit for Cu(II) as cross-bridged cyclam and its derivatives. Consistent with this, this structural trend is paralleled in their kinetic stabilities in acidic solution (*vide infra*). The Cu(II) complex of cross-bridged cyclam is at least several orders of magnitude more inert than the copper(II) complex of cross-bridged cyclen.

**Table 4.6** Summary of axial N-Cu-N angles and equatorial N-McuN angles in Cu(II) complexes of cross-bridged ligands **2**, **3** and **4**.

Complex	Axial N-Cu-N angle	Equatorial N-Cu-N angle
$[\text{Cu}\cdot\mathbf{2}(\mu\text{-Cl})_2]\text{Cl}_2$	160.37 (11)	85.35 (9)
$[\text{Cu}(\mathbf{2})(\text{CH}_3\text{OH})(\text{ClO}_4)](\text{ClO}_4)$	165.3 (5)	84.7 (4)
$[\text{Cu}(\mathbf{3})(\text{CH}_3\text{CN})](\text{ClO}_4)_2$	177.79 (19)	88.37 (19)
$\text{CuCl}_2\cdot\mathbf{4}$	167.9 (3)	81.0 (3)
Five-coordinate Cu(II) in $[\text{Cu}_2(\mu\text{-}\eta^1\text{:}\eta^2\text{-CO}_3)(\mathbf{4})_2](\text{ClO}_4)_2$	165.6 (2)	84.13 (19)
Six-coordinate Cu(II) in $[\text{Cu}_2(\mu\text{-}\eta^1\text{:}\eta^2\text{-CO}_3)(\mathbf{4})_2](\text{ClO}_4)_2$	155.70 (16)	86.59 (19)

### 3. Cu(II) Complexes of Ligands 5-8

#### 3.1 Preparation and Characterization of Copper Complexes.

Six copper complexes of four N,N'-dipendant-armed cross-bridged ligands, **5**, **6**, **7** and **8** (Figure 3.1) were synthesized and characterized by their IR (KBr) and UV-Vis spectral data and CHN elemental analyses.

In the synthesis of  $[\text{Cu}\cdot\mathbf{5}](\text{NO}_3)_2$  (**161**), no purified yield can be obtained due to the presence of about five percent organic impurity in ligand **5**. Several recrystallizations yielded this pure Cu(II) complex as needle-shaped crystals, on which X-ray analyses and CHN elemental analyses were carried out.  $[\text{Cu}\cdot\mathbf{6}](\text{ClO}_4)_2$  (**162**) and  $[\text{Cu}\cdot\mathbf{6}](\text{NO}_3)_2$  (**163**) were formed readily by the reaction of the respective hydrated metal salt with **6** in MeOH.

$[\text{Cu}\cdot(\mathbf{8-2H})](\text{NaClO}_4)$  (**165**) and  $[\text{Cu}\cdot(\mathbf{8-2H})](\text{NaNO}_3)$  (**166**) were synthesized by the same method. The reaction of  $\text{Cu}(\text{ClO}_4)_2\cdot 6\text{H}_2\text{O}$  or  $\text{Cu}(\text{NO}_3)_2\cdot 3\text{H}_2\text{O}$  with  $\mathbf{8}\cdot\text{TFA}\cdot\text{H}_2\text{O}$  in the presence of equivalents of aqueous sodium hydroxide yielded a blue solution. Diethyl ether diffusion into this solution yielded  $[\text{Cu}\cdot(\mathbf{8-2H})](\text{NaClO}_4)$  (or  $[\text{Cu}\cdot(\mathbf{8-2H})](\text{NaNO}_3)$ ) as blue crystals. To study its kinetic stability, solution IR spectral and solution capillary electrophoresis studies, complex  $[\text{Cu}\cdot(\mathbf{7-2H})](\text{NaClO}_4)(\text{NaCF}_3\text{COO})_{0.5}(\text{H}_2\text{O})_{1.5}$  (**164**) was synthesized more than ten times using the a similar procedure to make previous-reported  $[\text{Cu}\cdot(\mathbf{7-2H})\text{Na}(\text{H}_2\text{O})\text{ClO}_4]_2(\text{H}_2\text{O})$ .<sup>69(a)</sup> The only difference is the use of  $\mathbf{7}\cdot(\text{TFA})_2$  as the reactant instead of  $\mathbf{7}\cdot(\text{HCl})_4$ . The formation of  $[\text{Cu}\cdot(\mathbf{7-2H})](\text{NaClO}_4)(\text{NaCF}_3\text{COO})_{0.5}(\text{H}_2\text{O})_{1.5}$  is indicated by its CHN elemental results. It is essentially the same as the reported  $[\text{Cu}\cdot(\mathbf{7-2H})\text{Na}(\text{H}_2\text{O})\text{ClO}_4]_2(\text{H}_2\text{O})$ .<sup>69(a)</sup>



### 3.2 Infrared Spectra.

Similar to their Zn(II) and Cd(II) analogues, typically two strong carbonyl bands ranging from 1595 to 1685  $\text{cm}^{-1}$  were observed from the IR (KBr) spectra recorded on Cu(II) complexes of the carbamoyl or carboxylate cross-bridged ligands **5**, **6**, **7** and **8** (Table 4.7). Again, this is due to the presence of asymmetrical stretches of carboxylate

**Table 4.7** Summary of C=O stretches in the IR spectra of Cu(II) complexes of ligands **5-8**.

Complex	$\nu_{\text{C=O}}$ ( $\text{cm}^{-1}$ )	Complex	$\nu_{\text{C=O}}$ ( $\text{cm}^{-1}$ )
[Cu• <b>5</b> ](NO <sub>3</sub> ) <sub>2</sub>	1678	[Cu• <b>6</b> ](ClO <sub>4</sub> ) <sub>2</sub>	1682, 1661
[Cu• <b>6</b> ](NO <sub>3</sub> ) <sub>2</sub>	1685, 1670	[Cu•(7-2H)](NaClO <sub>4</sub> ) (NaCF <sub>3</sub> COO) <sub>1.5</sub>	1624, 1595
[Cu•(8-2H)](NaClO <sub>4</sub> )	1624, 1595	[Cu•(8-2H)](NaNO <sub>3</sub> )	1638, 1595

groups since Phillips reviewed that coordinated carboxylate groups have the asymmetrical stretches ranging from 1500-1675  $\text{cm}^{-1}$  and the symmetrical stretches is lower than 1490  $\text{cm}^{-1}$ .<sup>125(b)</sup> However, in the IR (KBr) spectrum of [Cu•**5**](NO<sub>3</sub>)<sub>2</sub> (**161**) (Figure 4.44), only one strong carbonyl band is observed at 1678  $\text{cm}^{-1}$ . In the range of

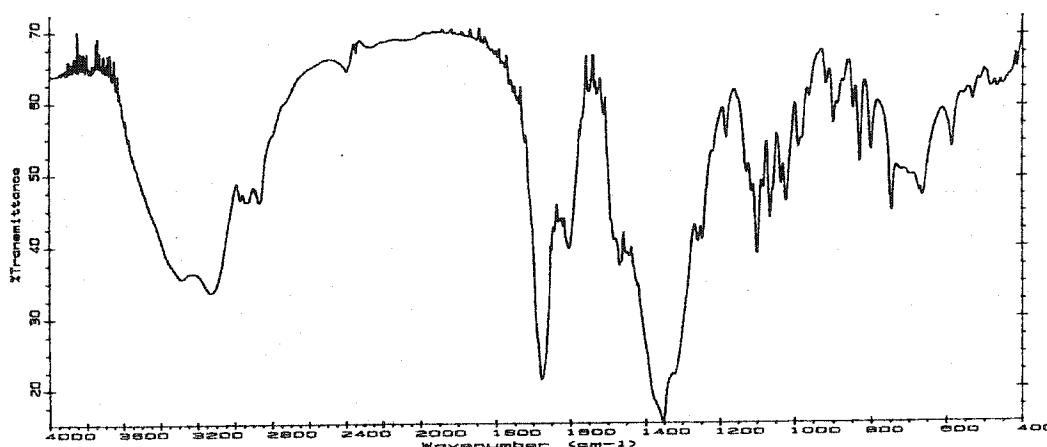


**Figure 4.44** The IR (KBr) spectrum of [Cu•**5**](NO<sub>3</sub>)<sub>2</sub> (**161**).

1500 to 1800  $\text{cm}^{-1}$ , a medium intensity band at 1606  $\text{cm}^{-1}$  probably belongs to either NH or OH bending. For comparison, the coordinated amide-carbonyl band of  $[\text{Cu}\cdot\mathbf{5}](\text{ClO}_4)_2$  appears at 1665  $\text{cm}^{-1}$ .<sup>69(a)</sup> Even though the solid-state structure of  $[\text{Cu}\cdot\mathbf{6}](\text{ClO}_4)_2$  showed three independent Cu(II) centers with different coordination geometries (**Figure 4.49**, **Figure 4.50** and **Figure 4.51**, *vide infra*), the IR spectrum of this complex showed only two strong carbonyl bands at 1682 and 1661  $\text{cm}^{-1}$  (**Figure 4.45**). This is probably due to crystal solvent loss as a result of the vacuum-drying of this copper complex before the spectral work.

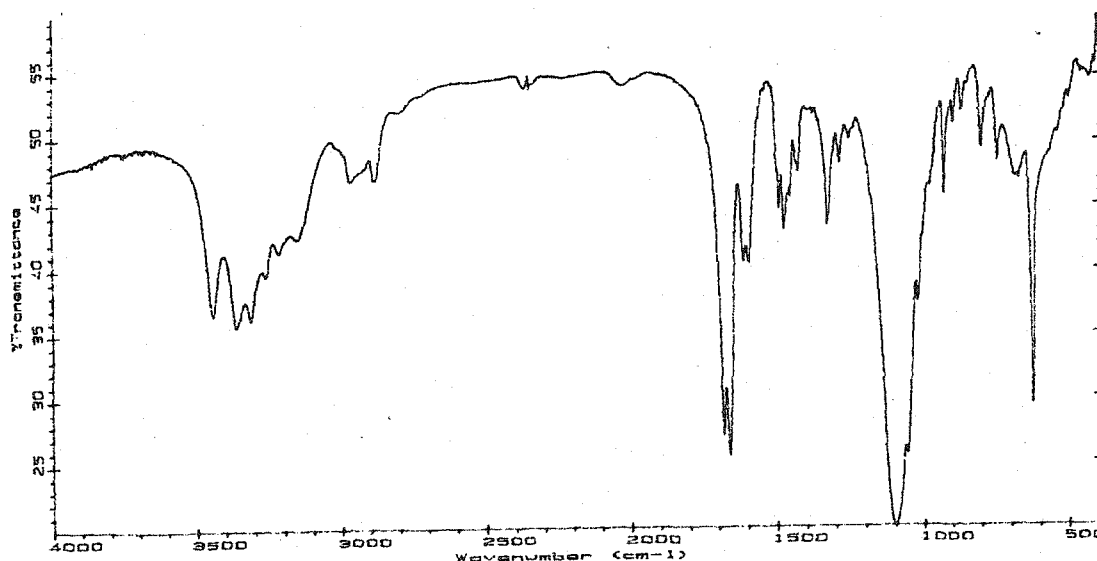


**Figure 4.45** The IR (KBr) spectrum of  $[\text{Cu}\cdot\mathbf{6}](\text{ClO}_4)_2$  (**162**).

### 3.3 Electronic Spectra.

Solution electronic spectra of the described copper complexes are summarized in **Table 4.8**. These d-d transitions are found as broad bands between 620 and 647 nm in water. For examples, the UV-Vis spectrum of  $[\text{Cu}\cdot\mathbf{6}](\text{ClO}_4)_2$  in water shows a band at

627 nm (Figure 4.46) and that of  $[\text{Cu}\cdot(8\text{-}2\text{H})](\text{NaClO}_4)$  in water has a band at 642 nm (Figure 4.47).

**Table 4.8** Summary of electronic spectral data for the copper complexes of ligands 5-8.

Complex	$\lambda_{\text{max}}$ ( $\epsilon, \text{M}^{-1}\text{cm}^{-1}$ )	Complex	$\lambda_{\text{max}}$ ( $\epsilon, \text{M}^{-1}\text{cm}^{-1}$ )
$[\text{Cu}\cdot 5](\text{NO}_3)_2$ in water	625 nm (34)	$[\text{Cu}\cdot 6](\text{ClO}_4)_2$ in MeCN	637 nm (89)
$[\text{Cu}\cdot 6](\text{NO}_3)_2$ in water	627 nm (66)	$[\text{Cu}\cdot 6](\text{ClO}_4)_2$ in water	627 nm (96)
$[\text{Cu}\cdot(7\text{-}2\text{H})](\text{NaClO}_4)$ $(\text{NaCF}_3\text{COO})_{1.5}$ in water	620 nm (43)	$[\text{Cu}\cdot(8\text{-}2\text{H})](\text{NaClO}_4)$ in water	642 nm (75)
$[\text{Cu}\cdot(7\text{-}2\text{H})](\text{NaClO}_4)$ $(\text{NaCF}_3\text{COO})_{1.5}$ in HCl	623 nm (47)	$[\text{Cu}\cdot(8\text{-}2\text{H})](\text{NaClO}_4)$ in MeCN	736 nm (84)
$[\text{Cu}\cdot(8\text{-}2\text{H})](\text{NaNO}_3)$ in water	647 nm (57)		

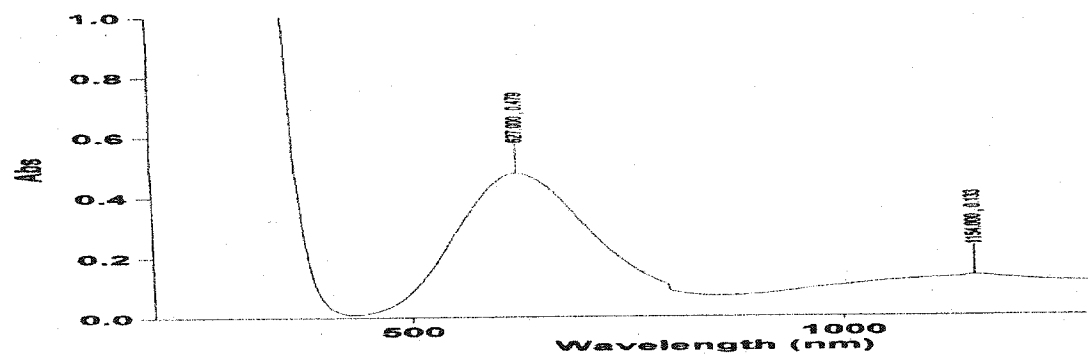


**Figure 4.46** The UV-Vis spectrum of  $[\text{Cu}\cdot 6](\text{ClO}_4)_2$  in water.

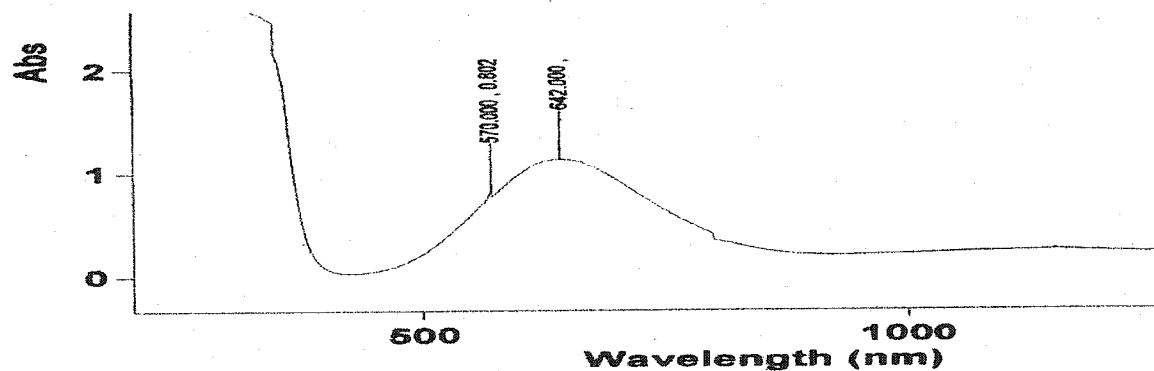


**Figure 4.47** The UV-Vis spectrum of  $[\text{Cu}\cdot(8\text{-}2\text{H})](\text{NaClO}_4)$  in water.

Aqueous solution electronic spectra of complexes  $[\text{Cu}\cdot\mathbf{6}](\text{ClO}_4)_2$  and  $[\text{Cu}\cdot\mathbf{6}](\text{NO}_3)_2$  both show a band at 627 nm. However, this has an  $\epsilon$  value of  $96 \text{ M}^{-1}\text{cm}^{-1}$  and  $66 \text{ M}^{-1}\text{cm}^{-1}$  respectively. Such a discrepancy is probably due to their different aqueous solution speciation or due to instrument instability. Similarly, the UV-Vis spectrum of  $[\text{Cu}\cdot(\mathbf{8}\text{-}\mathbf{2H})](\text{NaClO}_4)$  in water has a band at 642 nm ( $75 \text{ M}^{-1}\text{cm}^{-1}$ ) whereas that of  $[\text{Cu}\cdot(\mathbf{8}\text{-}\mathbf{2H})](\text{NaNO}_3)$  has a band at 647 nm ( $57 \text{ M}^{-1}\text{cm}^{-1}$ ).

### 3.4 X-ray Structural Data.

X-ray structures of  $[\text{Cu}\cdot\mathbf{5}](\text{NO}_3)_2$  (**161**),  $[\text{Cu}\cdot\mathbf{6}](\text{ClO}_4)_2$  (**162**) and  $[\text{Cu}\cdot(\mathbf{8}\text{-}\mathbf{2H})](\text{NaNO}_3)$  (**166**) were solved. Full structural data have not yet become available for  $[\text{Cu}\cdot(\mathbf{8}\text{-}\mathbf{2H})](\text{NaNO}_3)$ . The relevant bond distances and angles of the other two Cu(II) complexes are listed in **Tables 4.9(a-d)**. Interestingly, three independent Cu(II) centers with different coordination geometries in the X-ray structure of  $[\text{Cu}\cdot\mathbf{6}](\text{ClO}_4)_2$  are found. These three Cu(II) centers include a five-coordinate Cu(1) with MeOH hydrogen bonding, five-coordinate Cu(2) center, as well as a six-coordinate Cu(3). Their bond distances and angles are thus listed separately in the table **Tables 4.9**.

**$[\text{Cu}\cdot\mathbf{5}](\text{NO}_3)_2$  (161)** Similar to the X-ray structure of  $[\text{Zn}\cdot\mathbf{5}](\text{ClO}_4)_2$  (**Figure 3.23**), ligand **5** in  $[\text{Cu}\cdot\mathbf{5}](\text{NO}_3)_2$  holds Cu(II) within its molecular cleft with  $\text{N}_4\text{O}_2$  donors (**Figure 4.48**). Similar to all characterized metal complexes of parent ligand **1**, the bicyclic tetraamine ligand also adopts the *cis*-folded ligand configuration in this copper complex.<sup>69(a),72,77</sup>

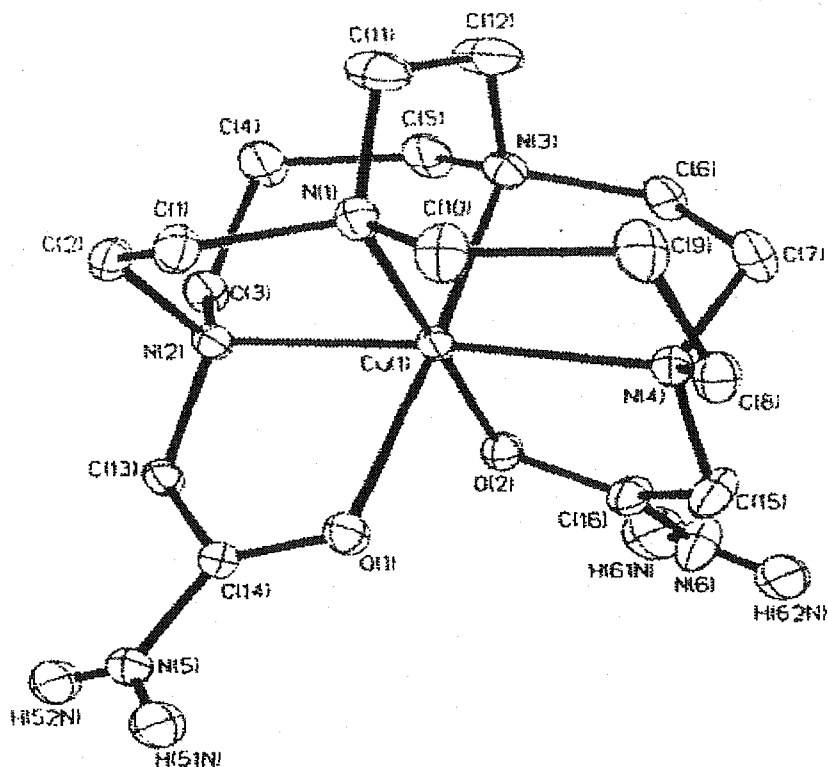


**Figure 4.48** X-ray structure of  $[\text{Cu}\cdot\mathbf{5}](\text{NO}_3)_2$  (**161**) showing atomic labeling scheme.

This Cu(II) center is deeply engulfed in the cavity as shown by the  $\text{N}_{\text{ax}}\text{-Cu-N}_{\text{ax}}$  ( $\text{N}(2)\text{-Cu-N}(4)$ ) angle of  $174.38(8)^\circ$  and the  $\text{N}(\text{eq})\text{-Cu-N}(\text{eq})$  ( $\text{N}(1)\text{-Cu-N}(3)$ ) angle of  $86.93(9)^\circ$ . For comparison,  $[\text{Zn}\cdot\mathbf{5}](\text{ClO}_4)_2$  (**Figure 3.23**) has an obtuse  $\text{N}_{\text{ax}}\text{-Zn-N}_{\text{ax}}$  bond angle of  $183.87(11)^\circ$  and a  $\text{N}(\text{eq})\text{-Zn-N}(\text{eq})$  angle of  $86.36(14)^\circ$ . The related Cu(II) complex of dicarboxylate pendant-armed cross-bridged cyclam,  $[\text{Cu}\cdot(\mathbf{7}\text{-}2\text{H})\text{Na}(\text{H}_2\text{O})\text{ClO}_4]_2(\text{H}_2\text{O})$  (**Figure 1.60**) has a slightly larger  $\text{N}_{\text{ax}}\text{-Cu-N}_{\text{ax}}$  bond angle of  $179.7(3)^\circ$ .<sup>69(a)</sup>

Unlike  $[\text{Zn}\cdot\mathbf{5}](\text{ClO}_4)_2$ , this Cu(II) complex does not possess a  $C_2$  symmetry. This is explained by one Cu-N(ax) bondlength, Cu-N(3) of  $2.178(2)$  Å which is significantly longer than the other three Cu-N bondlengths which are between  $2.043(2)$  and  $2.061(2)$  Å. Consequently, the bond distance between copper and the amide oxygen *trans* to N(3),

**Table 4.9(a)** Selected Bond Distances (Å) and Bond Angles (deg) in [Cu•5](NO<sub>3</sub>)<sub>2</sub> (161).

Cu(1)-N(1)	2.043(2)	Cu(1)-N(2)	2.044(2)
Cu(1)-N(3)	2.178(2)	Cu(1)-N(4)	2.061(2)
Cu(1)-O(1)	2.2643(18)	Cu(1)-O(2)	2.0423(19)
N(2)-Cu(1)-N(4)	174.38(8)	N(1)-Cu(1)-N(3)	86.93(9)
N(1)-Cu(1)-N(2)	86.98(8)	N(2)-Cu(1)-N(3)	98.50(8)
N(1)-Cu(1)-N(4)	97.44(8)	N(3)-Cu(1)-N(4)	85.24(8)
N(1)-Cu(1)-O(1)	90.86(8)	N(3)-Cu(1)-O(1)	177.64(8)
N(4)-Cu(1)-O(1)	95.86(7)	N(2)-Cu(1)-O(1)	80.56(7)
N(1)-Cu(1)-O(2)	179.09(8)	N(3)-Cu(1)-O(2)	92.28(8)
N(4)-Cu(1)-O(2)	82.93(8)	N(2)-Cu(1)-O(2)	92.70(8)
O(1)-Cu(1)-O(2)	89.93(7)		

O(1)-Cu is 2.2643(18) Å which is significantly longer than the other amide O(2)-Cu bond distance of 2.0423(19) Å. Again, this elongation is due to the Jahn-Teller distortion in an octahedral copper complex. Several X-ray structures of Cu(II) complexes with amide pendant-armed cyclam derivatives have been reported.<sup>57(a),57(i),57(j)</sup> These Cu(II) complexes also adopt a distorted octahedral geometry but cyclam derivatives in them all have a *trans*-III configuration. Their amide oxygen(2)-Cu bond distances range from 2.29 to 2.36 Å. The bond distances between the four equatorial nitrogen donors and Cu(II) vary from 2.04 to 2.15 Å. In the literature, a Cu(II) complex of a bis(acetamido)-

pendant armed dibenzocyclam has been also reported.<sup>53(d)</sup> The copper atom in this complex is octahedrally coordinated by this hexadentate ligand in a *cis*-folded configuration. The distortion of this from full octahedral geometry is indicated by its  $N_{ax}$ -Cu- $N_{ax}$  bond angle of  $176.5(2)^\circ$  and  $N(eq)$ -Cu- $N(eq)$  bond angle of  $101.3(2)^\circ$ .

**The Five-coordinate Cu(2) center in  $[Cu\cdot 6](ClO_4)_2$  (162).** The X-ray structure of this Cu(II) center (**Figure 4.49**) shows that it is only penta-coordinated by the hexadentate ligand **6** since one of two amide-pendant arms remains uncoordinated. The coordination geometry around copper is again a square pyramid with the longer apical

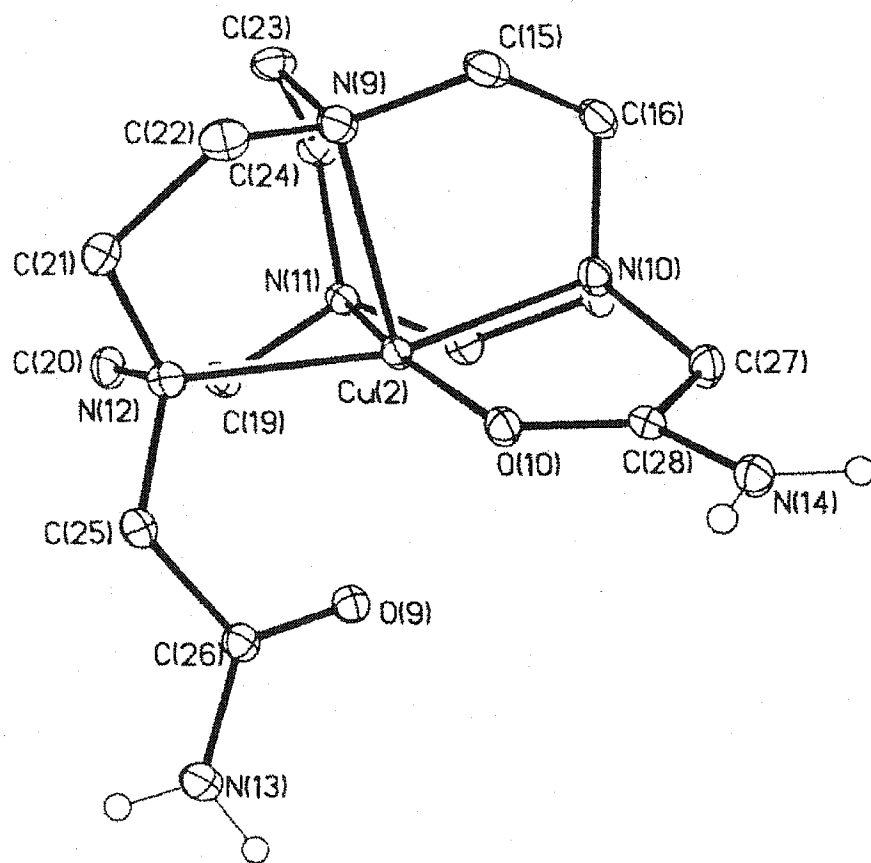


**Figure 4.49** X-ray structure of the five-coordinate Cu(2) center in  $[Cu\cdot 6](ClO_4)_2$  (162) showing atomic labeling scheme.

N(9)-Cu bondlength of 2.1763(19) Å as indicated by an Addison and Reedjik's  $\tau$ -parameter of 0.012.<sup>138</sup> The other three N-Cu(II) bond distances range from 1.97 to 2.06 Å while the coordinated amide oxygen-Cu bondlength is 1.9576(14) Å. According to our definition, this complex has an  $N_{ax}$ -Cu- $N_{ax}$  (N(10)-Cu-N(12)) bond angle of 165.80(7)° and an  $N_{eq}$ -Cu- $N_{eq}$  bond angle of 87.01(7)°. In the literature, a copper complex of an octadentate ligand 1,4,7,10-tetrakis(2-carbamoyl)ethyl-1,4,7,10-tetraazacyclododecane also shows a square pyramidal geometry with the amide oxygen from a pendant arm in the apical position.<sup>54(n)</sup> The coordinated amide oxygen-Cu bond distance is 2.137(3) Å and the four N-Cu distances are between 2.017(3)-2.072(3) Å.

**Table 4.9(b)** Selected Bond Distances (Å) and Bond Angles (deg) of the five-coordinate Cu(II) center in [Cu•6](ClO<sub>4</sub>)<sub>2</sub> (**162**).

Cu(2)-N(9)	2.1763(19)	Cu(2)-N(10)	2.0593(17)
Cu(2)-N(11)	1.9686(18)	Cu(2)-N(12)	2.1021(19)
Cu(2)-O(10)	1.9576(14)		
N(10)-Cu(2)-N(12)	165.80(7)	N(9)-Cu(2)-N(11)	87.01(7)
N(10)-Cu(2)-N(11)	84.58(7)	N(11)-Cu(2)-N(12)	87.60(7)
N(9)-Cu(2)-N(10)	85.91(7)	N(9)-Cu(2)-N(12)	81.86(7)
N(9)-Cu(2)-O(10)	100.49(7)	N(10)-Cu(2)-O(10)	84.82(6)
N(11)-Cu(2)-O(10)	166.53(7)	N(12)-Cu(2)-O(10)	104.43(6)



The Five-coordinate Cu(1) center involving MeOH hydrogen bonding in  $[\text{Cu}\cdot\mathbf{6}](\text{ClO}_4)_2$  (162). Again, the X-ray structure of this Cu(II) center (Figure 4.50) shows that it is only penta-coordinated by the hexadentate ligand **6**. Unlike the other five-

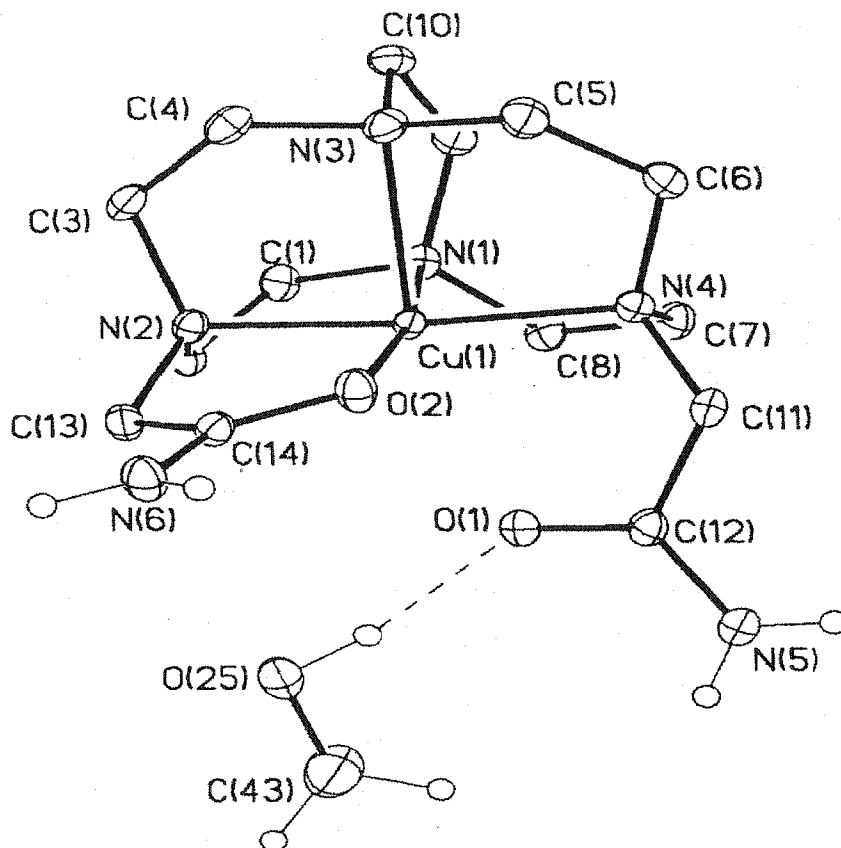


**Figure 4.50** X-ray structure of the five-coordinate Cu(1) center with MeOH hydrogen bonding in  $[\text{Cu}\cdot\mathbf{6}](\text{ClO}_4)_2$  (162) showing atomic labeling scheme.

coordinate center, this uncoordinated amide oxygen is hydrogen-bonded by a methanol solvent. Again, the coordination geometry around this copper(II) remains a square pyramid as indicated by an Addison and Reedjik's  $\tau$ -parameter of 0.033, the longest nitrogen-Cu bond distance of 2.1935(15) Å (Cu(1)-N(3)) is in the apical position. Its  $\text{N}_{\text{ax}}\text{-Cu-N}_{\text{ax}}$  bond angle of 173.02(8)° is significantly larger than that of 165.80(7)° in the

first five-coordinate Cu(II) center whereas the  $N_{eq}\text{-Cu-}N_{eq}$  bond angle of  $80.66(7)^\circ$  is significantly smaller than that of  $87.01(7)^\circ$  in the first five-coordinate Cu(II) center.

**Table 4.9(c)** Selected Bond Distances (Å) and Bond Angles (deg) of the five-coordinate Cu(II) center involving MeOH hydrogen bonding in  $[\text{Cu}\cdot\mathbf{6}](\text{ClO}_4)_2$  (**162**).

Cu(1)-N(1)	2.0439(18)	Cu(1)-N(2)	1.9696(17)
Cu(1)-N(3)	2.1935(15)	Cu(1)-N(4)	1.9885(18)
Cu(1)-O(2)	2.0223(16)		
N(2)-Cu(1)-N(4)	173.02(8)	N(1)-Cu(1)-N(3)	80.66(7)
N(1)-Cu(1)-N(2)	87.92(7)	N(2)-Cu(1)-N(3)	88.34(7)
N(1)-Cu(1)-N(4)	85.62(8)	N(3)-Cu(1)-N(4)	88.00(7)
N(1)-Cu(1)-O(2)	171.06(7)	N(3)-Cu(1)-O(2)	98.51(7)
N(4)-Cu(1)-O(2)	103.27(7)	N(2)-Cu(1)-O(2)	83.16(7)

**The Six-coordinate Cu(3) center in  $[\text{Cu}\cdot\mathbf{6}](\text{ClO}_4)_2$  (**162**).** Similar to all characterized Zn(II), Cd(II) and Hg(II) complexes of ligands **5-8**, this Cu(II) center in  $[\text{Cu}\cdot\mathbf{6}](\text{ClO}_4)_2$  is fully enveloped by the cross-bridged tetraamine and its two pendant arms in a distorted-octahedral  $N_4O_2$  donor set (**Figure 4.51**). It has a  $N_{ax}\text{-Cu-}N_{ax}$  bond angle of  $162.20(7)^\circ$  and  $N_{eq}\text{-Cu-}N_{eq}$  bond angle of  $87.47(7)^\circ$ . Four macrobicyclic tetraamine nitrogen-Cu bond distances vary from 1.9625(18) to 2.172(2) Å and two amide oxygen-Cu bonds are 2.2306(16) to 1.9542(15) Å respectively. The longest

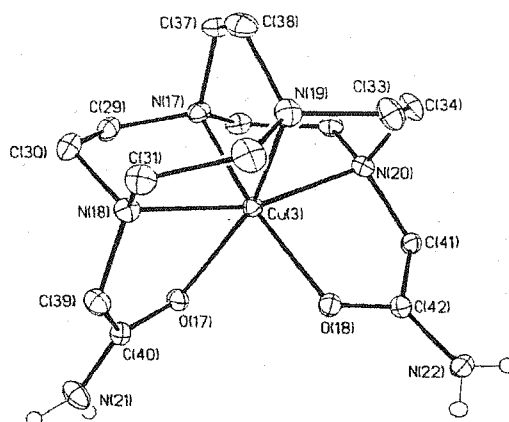


**Figure 4.51** X-ray structure of the six-coordinate Cu(3) center in  $[\text{Cu}^*6](\text{ClO}_4)_2$  (**162**) showing atomic labeling scheme.

**Table 4.9(d)** Selected Bond Distances (Å) and Bond Angles (deg) of the six-coordinate Cu(II) center in  $[\text{Cu}^*6](\text{ClO}_4)_2$  (**162**).

Cu(3)-N(17)	1.9625(18)	Cu(3)-N(18)	2.172(2)
Cu(3)-N(19)	2.1556(19)	Cu(3)-N(20)	2.0926(18)
Cu(3)-O(17)	2.2306(16)	Cu(3)-O(18)	1.9524(15)
N(18)-Cu(3)-N(20)	162.20(7)	N(17)-Cu(3)-N(19)	87.47(7)
N(17)-Cu(3)-N(20)	84.03(7)	N(19)-Cu(3)-N(20)	84.56(7)
N(17)-Cu(3)-N(18)	85.80(7)	N(18)-Cu(3)-N(19)	80.42(7)
N(17)-Cu(3)-O(17)	94.65(7)	N(18)-Cu(3)-O(17)	76.79(6)
N(19)-Cu(3)-O(17)	156.87(7)	N(20)-Cu(3)-O(17)	118.56(6)
N(17)-Cu(3)-O(18)	167.62(7)	N(18)-Cu(3)-O(18)	106.45(6)
N(19)-Cu(3)-O(18)	96.21(7)	N(20)-Cu(3)-O(18)	84.55(7)
O(17)-Cu(3)-O(18)	86.61(6)		

macrobicyclic tetraamine nitrogen-Cu bond distance of 2.172(2) Å (Cu-N(18)) and the longer amide oxygen-Cu bond distance of 2.2306(16) Å are not *trans* to each other. In the literature, the only Cu(II) complex of any carbamoyl cyclen derivative is the five-coordinate copper complex of 1,4,7,10-tetrakis(2-carbamoylethyl)-1,4,7,10-tetraazacyclododecane mentioned above.<sup>54(n)</sup>

[Cu•(8-2H)](NaNO<sub>3</sub>) (166) The X-ray structure of this complex (Figure 4.52) shows that the Cu(II) atom is also fully coordinated by four amine nitrogen donors and two carboxylate oxygen atoms from 8-2H in a distorted-octahedral N<sub>4</sub>O<sub>2</sub> donor set. Its structural data are not yet available.

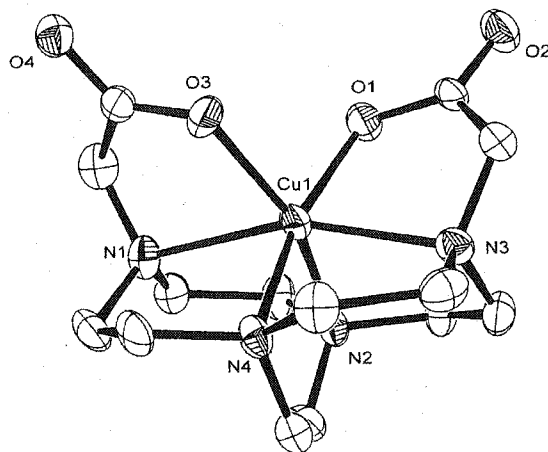


Figure 4.52 X-ray structure of [Cu•(8-2H)](NaNO<sub>3</sub>) (166).

### Summary of Structural Data.

The X-ray structure of [Cu•5](NO<sub>3</sub>)<sub>2</sub> shows a distorted octahedral geometry around copper whereas that of [Cu•6](ClO<sub>4</sub>)<sub>2</sub> showed three different Cu(II) centers in

either a distorted-octahedral or a square pyramidal coordination geometry. A summary of their axial N-Cu-N bond angles and the equatorial N-Cu-N bond angles is listed in **Table 4.10**. As indicated by the  $N_{ax}$ -Cu- $N_{ax}$  bond angles and the  $N_{eq}$ -Cu- $N_{eq}$  bond angles of  $[Cu\cdot 5](NO_3)_2$  and the Six-coordinate Cu(3) center in  $[Cu\cdot 6](ClO_4)_2$ , Cu(II) fits much better in the cross-bridged cyclam derivative ligand **5** than in the smaller cyclen analogue **6**.

The  $N_{ax}$ -Cu- $N_{ax}$  bond angles of the three different Cu(II) centers in  $[Cu\cdot 6](ClO_4)_2$  vary from  $162.20(7)^\circ$  to  $173.02(8)^\circ$  and their  $N_{eq}$ -Cu- $N_{eq}$  bond angles from  $80.66(7)^\circ$  to  $87.47(7)^\circ$ . This indicates some degree of flexibility for this pendant-armed cross-bridged ligand.

**Table 4.10** Summary of axial N-Cu-N angles and equatorial N-Cu-N angles in Cu(II) complexes of cross-bridged ligands **5** and **6**.

Complex	Axial N-Cu-N angle	Equatorial N-Cu-N angle
$[Cu\cdot 5](NO_3)_2$	174.38(8)	86.93(9)
Five-coordinate Cu(1) center involving MeOH hydrogen bonding in $[Cu\cdot 6](ClO_4)$	173.02(8)	80.66(7)
Five-coordinate Cu(2) center in $[Cu\cdot 6](ClO_4)$	165.80(7)	87.01(7)
Six-coordinate Cu(3) center in $[Cu\cdot 6](ClO_4)$	162.20(7)	87.47(7)

## CHAPTER V

# KINETIC STABILITY STUDIES OF METAL COMPLEXES OF CROSS-BRIDGED LIGANDS

### 1. Introduction

Acid-promoted dissociation studies of many main group and transition metal complexes of polyamines have been reported.<sup>140(a-h)</sup> For example, Kaden *et al.* have reported the acid decomplexation studies of Ni(II), Cu(II), Co(II), Zn(II) and In(III) complexes of cyclam and cyclen derivatives.<sup>140(c-f)</sup> Chung reviewed the kinetics and mechanism of the dissociation reactions of open-chain and macrocyclic tetraamine copper complexes.<sup>140(a)</sup> In a very recent paper,<sup>140(b)</sup> Hermann *et al.* summarized the kinetic data on acid decomplexation of Cu(II) complexes with macrocyclic tetraamines.

As expected from the Irving-Williams series, Cu(II) complexes with nitrogen donor ligands are typically found to be more stable than Zn(II) complexes by several orders of magnitude.<sup>141</sup> It can thus be expected that a more acidic solution is necessary to decomplex a copper complex compared to its zinc analogue. Due to the high basicity (proton-sponge activity) of our cross-bridged ligands, protonated cross-bridged ligands form quickly as the kinetically-controlled products in their complexation with a metal ion whereas the completion of a complexation process takes much longer time.<sup>77,81,84</sup>

Therefore, determination of the thermodynamic stability constants of their metal complexes in aqueous solution is not routine.<sup>81,84</sup> Thus we have been interested in the relative kinetic stability studies in acidic solution of selected metal complexes with cross-bridged ligands. These metal ions include Zn(II), Cd(II), Hg(II), Ga(III), In(III) and Cu(II). The kinetic inertness of selected diamagnetic Zn(II), Cd(II), Hg(II), Ga(III) and In(III) complexes can be readily monitored in buffered D<sub>2</sub>O solutions by NMR spectroscopy whereas distinct d-d transition maxima are expected for complexed and decomplexed Cu(II). The kinetics of the process can thus be followed spectrophotometrically in the UV-Vis region (370-800 nm).

## 2. Results and Discussion

The ligands included in these studies are shown in **Figure 5.1**.

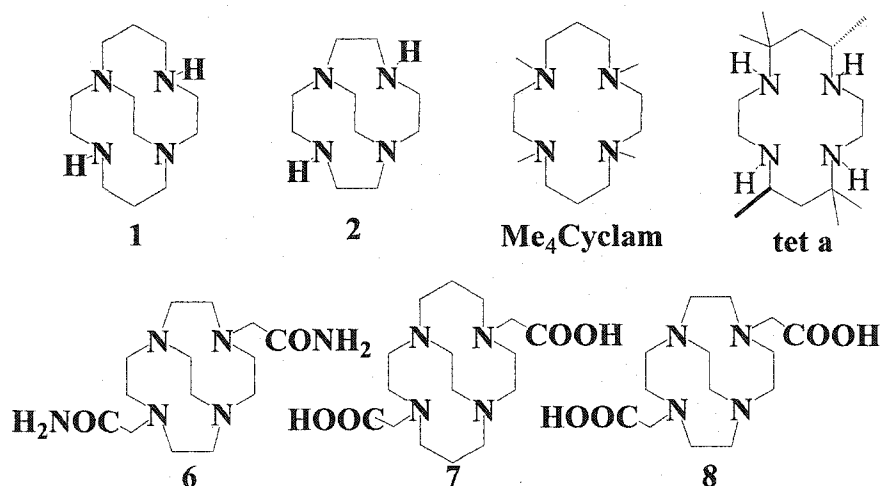


**Figure 5.1** Cross-bridged ligands and other ligands used in kinetic stability studies.

### 2.1 Relative Kinetic Inertness of Ga(III) and In(III) Complexes

All the kinetic studies were carried out using proton NMR spectroscopy at room

temperature (22°C).  $[\text{InBr}_2 \cdot \mathbf{2}]\text{Br}$  (**152**) is the most labile among the four characterized Ga(III) and In(III) complexes of ligands **1** and **2**. Among these structurally-characterized complexes, this indium complex should therefore have the poorest fit inside the ligand cavity. This poor fit is confirmed by its smaller axial N-M-N and equatorial N-M-N angles in its solid-state structure (Table 4.3). Figure 5.2 shows its  $^1\text{H}$  NMR spectra

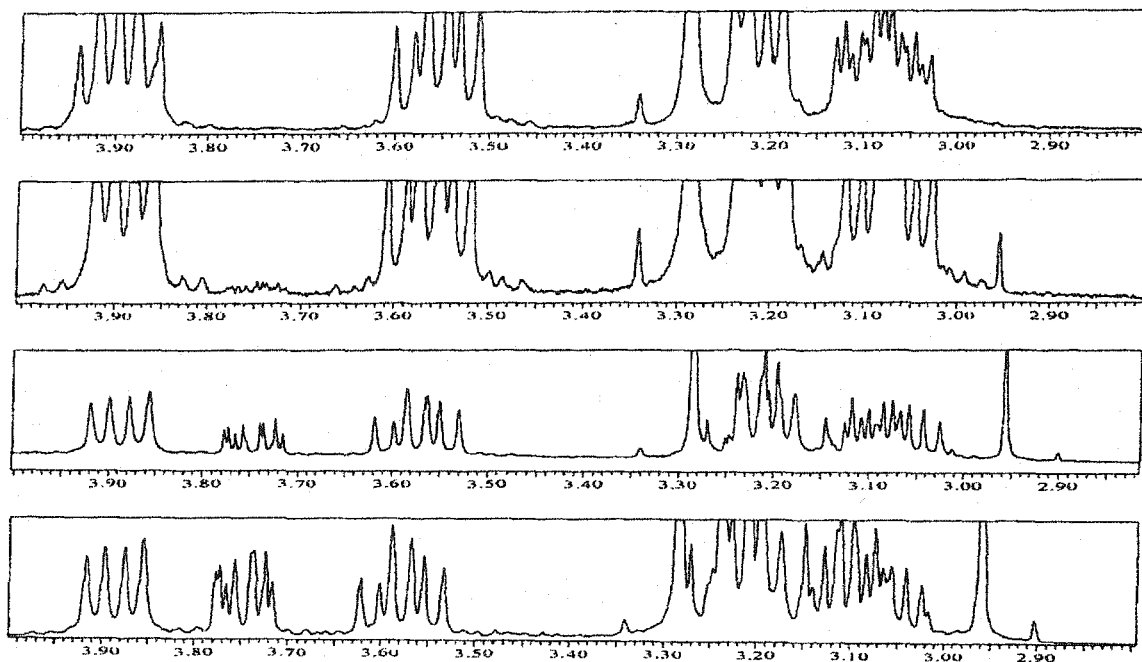


**Figure 5.2**  $^1\text{H}$  NMR spectra recorded at different time periods for  $[\text{InBr}_2 \cdot \mathbf{2}]\text{Br}$  was dissolved in  $\text{D}_2\text{O}$ . From the top to the bottom one: Spectrum one -- Immediately after complex was dissolved in  $\text{D}_2\text{O}$ ; Spectrum two -- 5 days later; Spectrum three -- 3 months later; Spectrum four -- 6 months later.

recorded in  $\text{D}_2\text{O}$  as a function of time. The ddd multiplet between  $\delta$  3.70-3.80 and the singlet at  $\delta$  2.96 belong to protonated **2**. As indicated by the increased amount of protonated **2** with time, decomplexation occurred. For example, the second spectrum in Figure 5.2 was recorded after five days. Integration indicates that about five percent of protonated **2** was present.



In contrast, no  $^1\text{H}$  NMR-detectable decomplexation of  $[\text{InBr}_2\cdot\mathbf{1}]\text{Br}$  (**150**) occurred even after this complex was kept in  $\text{D}_2\text{O}$  at room temperature for twelve days and then at

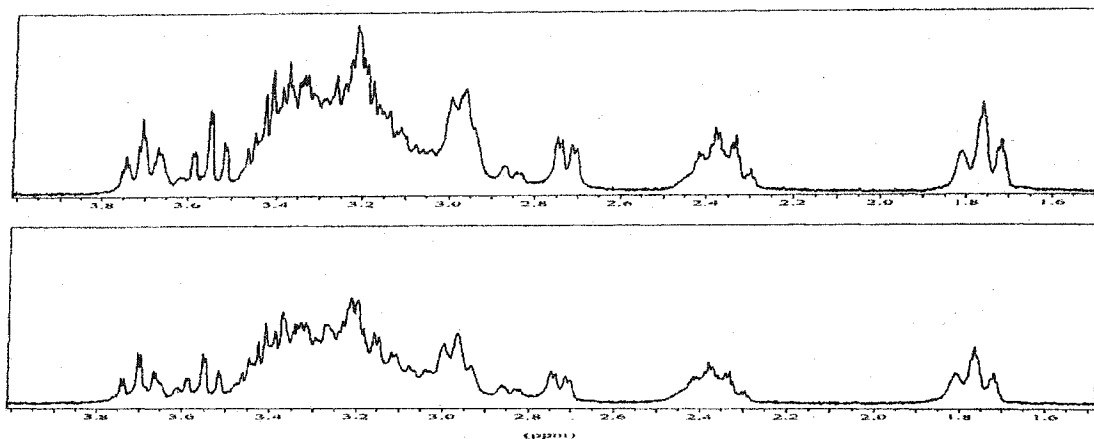


**Figure 5.3**  $^1\text{H}$  NMR spectra recorded after  $[\text{InBr}_2\cdot\mathbf{1}]\text{Br}$  was dissolved in  $\text{D}_2\text{O}$ . Top: Immediately after this complex was dissolved in  $\text{D}_2\text{O}$ ; Bottom: After 2 days at room temperature then  $80^\circ\text{C}$  for 12 days.

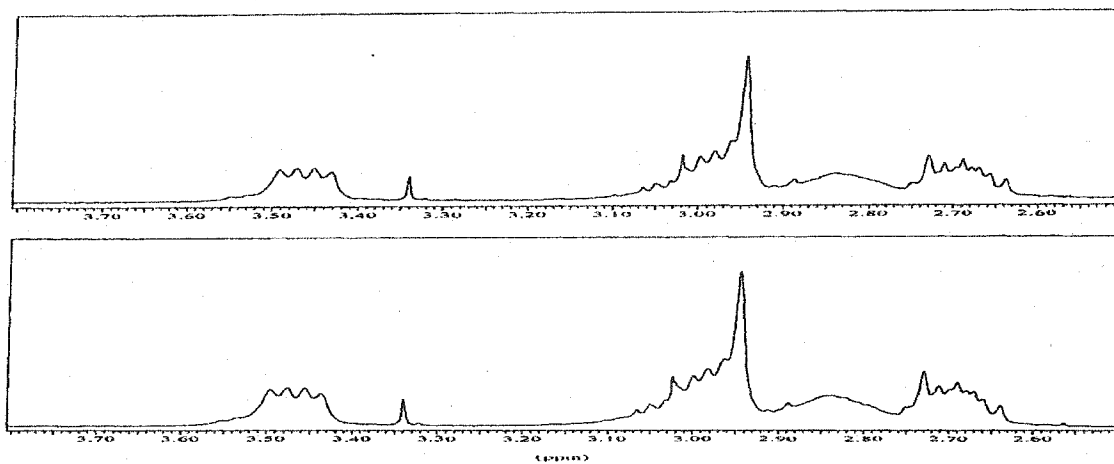


**Figure 5.4**  $^1\text{H}$  NMR spectra recorded after  $[\text{GaCl}_2\cdot\mathbf{2}]\text{Cl}$  was dissolved in  $\text{D}_2\text{O}$ . Top: Immediately after this complex was dissolved in  $\text{D}_2\text{O}$ . Bottom: After 46 days at room temperature.

$80^\circ\text{C}$  for additional twenty days (**Figure 5.3**). Similarly, no  $^1\text{H}$  NMR-detectable decomplexation of  $[\text{GaCl}_2\cdot\mathbf{2}]\text{Cl}$  (**151**) was observed even after 46 days at r.t. (**Figure 5.4**).  $[\text{GaCl}_2\cdot\mathbf{1}]\text{Cl}$  (**149**) is also stable in  $\text{D}_2\text{O}$  for months. More interestingly, this complex

is even stable in acidic D<sub>2</sub>O (pD = 1.07, HClO<sub>4</sub>) for at least one year and eight months (Figure 5.5). However, due to the poor solubility of both [InBr<sub>2</sub>•1]Br and [InBr<sub>2</sub>•2]Br in acidic D<sub>2</sub>O, no kinetic studies on the acidic decomplexation of these complexes were possible.

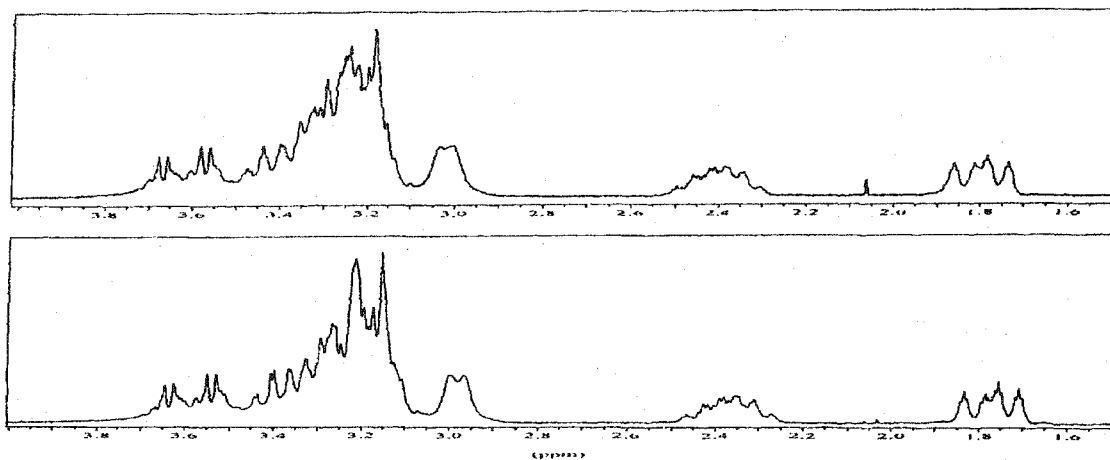


**Figure 5.5** <sup>1</sup>H NMR spectra after [GaCl<sub>2</sub>•1]Cl was dissolved in acidic D<sub>2</sub>O (pD = 1.07, HClO<sub>4</sub>). Top one: Immediately after this complex was dissolved in D<sub>2</sub>O. Bottom: After one year and eight months at room temperature.

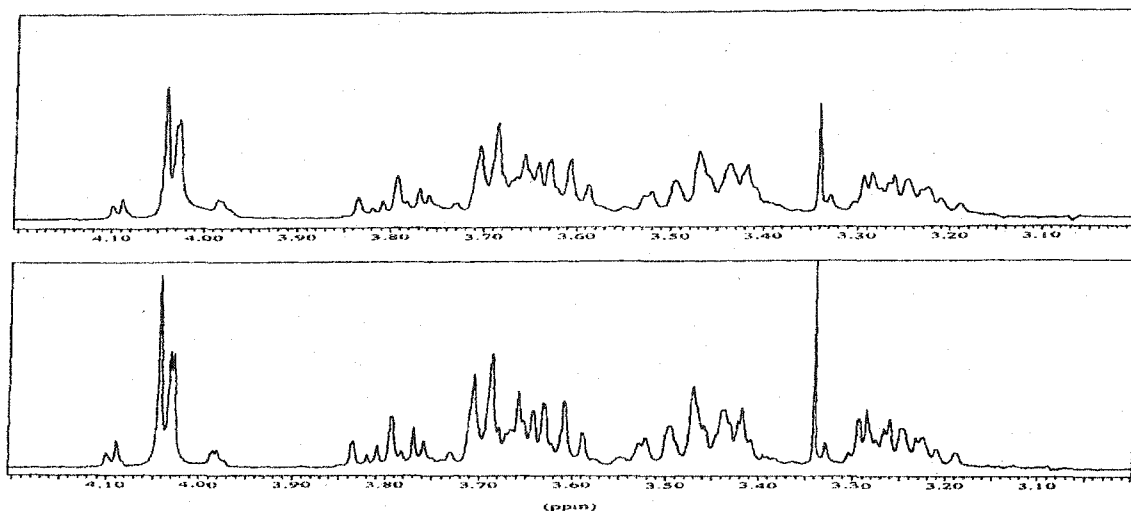


**Figure 5.6** <sup>1</sup>H NMR spectra after [Ga•(8-2H)](NO<sub>3</sub>) was dissolved in acidic D<sub>2</sub>O (pD = 1.07, HCl). Top one: Immediately after complex was dissolved in D<sub>2</sub>O. Bottom: After seven months at room temperature.

Finally, complex  $[\text{Ga}(\mathbf{8-2H})](\text{NO}_3)$  (**153**) was found to be stable in acidic  $\text{D}_2\text{O}$  ( $\text{pD} = 1.07$ ,  $\text{HCl}$ ) for at least seven months (**Figure 5.6**).

## 2.2 Relative Kinetic Inertness of Zn(II), Cd(II) and Hg(II) Complexes

The kinetic studies discussed here were typically carried out at  $36.8(1)^\circ\text{C}$  by using a constant-temperature water-bath. Comparative half-lives of these pseudo-first-order decomplexation processes for selected Zn(II), Cd(II) and Hg(II) complexes of ligands **1** and **2** are shown in **Table 5.1** and **Table 5.2**. For reference, the acid decomplexation data of  $\text{Zn}(\text{NO}_3)_2 \cdot (\text{Me}_4\text{Cyclam})$  (**168**) are also included. Proton NMR spectra of these complexes recorded at time intervals were used to monitor their decomplexation process in acidic  $\text{D}_2\text{O}$ . For these decomplexation studies with metal complex concentrations ranging between 0.020 and 0.030 M (**Table 5.1** and **Table 5.2**), if only protonated ligand was detected within the time needed to record the first  $^1\text{H}$  NMR spectrum of a decomplexation process, a pseudo-first order rate law is assumed and the  $^1\text{H}$  NMR detection limit of three percent of the initial complexed ligand is also assumed to obtain the half-life of this process. If an equilibrium between protonated and complexed ligand was reached within the time needed to record the first  $^1\text{H}$  NMR spectrum of a decomplexation process, a pseudo-first order rate law is also assumed to obtain the upper limit of the half-life of this process and the ratio of protonated to complexed ligand at the equilibrium is used to calculate the half-life of this decomplexation process. If no decomplexation was observable within the measured period, a pseudo-first-order rate law is assumed to obtain a lower limit of the half-life.

**Table 5.1** Acid decomplexation data for Zn(II) and Cd(II) complexes of ligands **1** and **2**, [Zn•**6**](ClO<sub>4</sub>)<sub>2</sub>, and Zn(NO<sub>3</sub>)<sub>2</sub>•(Me<sub>4</sub>Cyclam) in D<sub>2</sub>O at pD 5.0.

Complex	Half-life (minutes)	Complexed L / Protonated L at Equilibrium	Time to reach this equilibrium
Zn(NO <sub>3</sub> ) <sub>2</sub> • <b>1</b>	2.4(1) x 10 <sup>3</sup>	1.0 : 0.57	< 4 days
Cd(NO <sub>3</sub> ) <sub>2</sub> • <b>1</b>	< 3	only protonated <b>1</b>	< 16 minutes
Zn(NO <sub>3</sub> ) <sub>2</sub> •(Me <sub>4</sub> Cyclam)	< 3	1.0 : 9.1	< 7 minutes
[Zn(OH <sub>2</sub> ) <sub>2</sub> • <b>2</b> ](ClO <sub>4</sub> ) <sub>2</sub>	< 16	1.0 : 1.0	< 16 minutes
[Cd(η <sup>2</sup> -NO <sub>3</sub> ) <sub>2</sub> • <b>2</b> ]	< 1	only protonated <b>2</b>	< 5 minutes
[Zn• <b>6</b> ](ClO <sub>4</sub> ) <sub>2</sub>	1.1 x 10 <sup>4</sup>	1.0 : 0.38	< 8 days

[Zn]<sub>i</sub> or [Cd]<sub>i</sub> = 0.020 to 0.030 M, HOAc/NaOAc (1.0 M), 36.8(1)°C, I = 1.0 M, NaCF<sub>3</sub>SO<sub>3</sub>.

**Table 5.2** Acid decomplexation data for Zn(II), Cd(II), and Hg(II) complexes of ligands **1** and **2** and Zn(NO<sub>3</sub>)<sub>2</sub>•(Me<sub>4</sub>Cyclam) in buffered D<sub>2</sub>O at pD 5.9.

Complex	Half-life (minutes)	Complexed L / Protonated L at Equilibrium	Time to reach this equilibrium
Zn(NO <sub>3</sub> ) <sub>2</sub> • <b>1</b>	> 1.0 x 10 <sup>6</sup>	-----	-----
Cd(NO <sub>3</sub> ) <sub>2</sub> • <b>1</b>	3.1(1) x 10 <sup>3</sup>	protonated <b>1</b> > 85%	-----
[HgCl <sub>2</sub> (μ- <b>1</b> )] <sub>2</sub>	< 3	only protonated <b>1</b>	< 15 minutes
[Cd(η <sup>2</sup> -NO <sub>3</sub> ) <sub>2</sub> • <b>2</b> ]	< 8	-----	< 8 minutes
HgCl <sub>2</sub> • <b>2</b>	< 10	-----	< 10 minutes

[Zn]<sub>i</sub> or [Cd]<sub>i</sub> = 0.020 to 0.030 M, [Hg]<sub>i</sub> = a saturated solution, MES (1.0 M), 36.8(1)°C, I = 1.0 M, NaCF<sub>3</sub>SO<sub>3</sub> (----- no data available).

For the Zn(II), Cd(II) and Hg(II) complexes of ligand **1**, changes upon hydrolysis at the most upfield doublet of pentets assignable to the equatorial proton of the β-methylene unit are well-resolved and allowed quantitation of the decomplexation process

(Figure 5.7). As shown by the data in these tables, the observed relative kinetic inertness

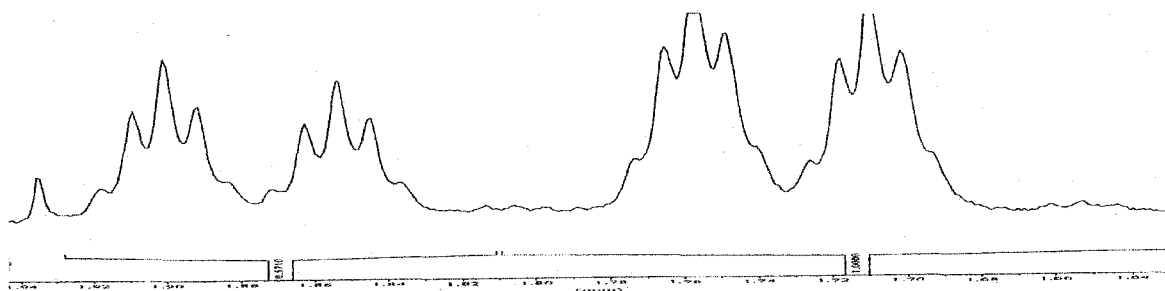


**Figure 5.7** The most upfield doublets of pentets in the  $^1\text{H}$  NMR spectrum of  $\text{Cd}(\text{NO}_3)_2 \cdot \mathbf{1}$  in buffered  $\text{D}_2\text{O}$  (pD = 5.9, MES). On the left is protonated  $\mathbf{1}$  and on the right is complexed  $\mathbf{1}$ .

of these complexes at pD 5.0 and 5.9 is in the expected order of  $\text{Zn}(\text{II}) > \text{Cd}(\text{II}) \gg \text{Hg}(\text{II})$ . Unlike any other  $\text{Zn}(\text{II})$ ,  $\text{Cd}(\text{II})$  and  $\text{Hg}(\text{II})$  complexes of either ligand  $\mathbf{1}$  or  $\mathbf{2}$ , the decomplexation of  $[\text{HgCl}_2(\mu\text{-}\mathbf{1})]_2$  occurred immediately after it was dissolved in  $\text{D}_2\text{O}$  as indicated by the presence of protonated  $\mathbf{1}$  in all proton NMR spectra of this complex in  $\text{D}_2\text{O}$ . Within 15 minutes, complex  $[\text{HgCl}_2(\mu\text{-}\mathbf{1})]_2$  was completely decomplexed in buffered acidic  $\text{D}_2\text{O}$  (pD = 5.9, buffer MES (4-morpholineethanesulfonic acid monohydrate)). The half-life of this decomplexation is thus less than 3 minutes if we assume the  $^1\text{H}$  NMR detection limit of three percent. Under the same conditions,  $\text{Cd}(\text{NO}_3)_2 \cdot \mathbf{1}$  has a pseudo-first-order reaction half-life of  $3.1(1) \times 10^3$  minutes (**Figure 5.8**) which was obtained from three parallel runs ( $R^2 > 0.990$ ) whereas  $\text{Zn}(\text{NO}_3)_2 \cdot \mathbf{1}$  has a half-life of  $> 1.0 \times 10^6$  minutes. The slight deviation of kinetic data in the end time in **Figure 5.8** is probably due to the approaching to the equilibrium between complexed and protonated ligand. At a pD of 5.0 (HOAc/NaOAc), only protonated  $\mathbf{1}$  was detected for  $\text{Cd}(\text{NO}_3)_2 \cdot \mathbf{1}$  as soon as this complex was dissolved whereas  $\text{Zn}(\text{NO}_3)_2 \cdot \mathbf{1}$  has a half-life of

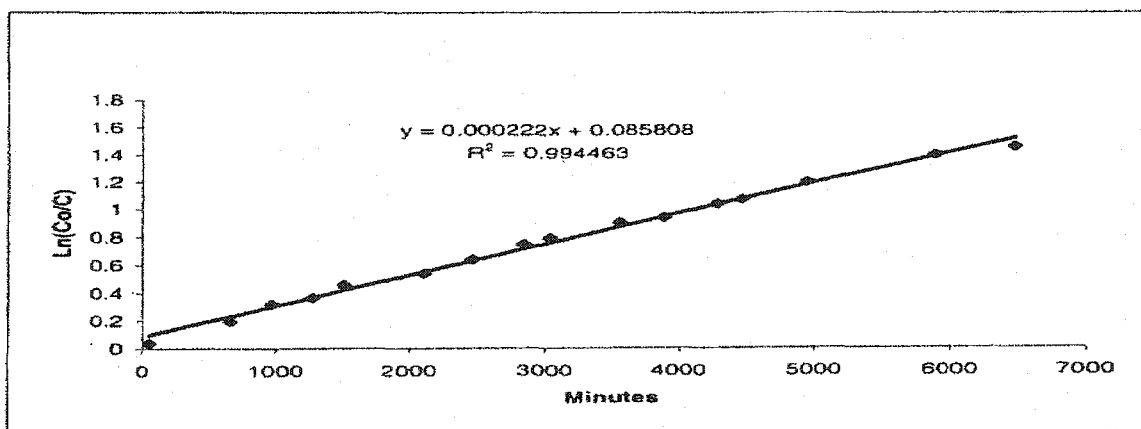


**Figure 5.8** A typical kinetic plot of  $\ln(C_0/C)$  vs time ( $t$ ) in the acid decomplexation of  $\text{Cd}(\text{NO}_3)_2 \cdot 1$  in buffered  $\text{D}_2\text{O}$ .  $[\text{Cd}]_i = 0.020 \text{ M}$ ,  $\text{pD} = 5.9$ ,  $\text{MES} (1.0 \text{ M})$ ,  $36.8(1)^\circ\text{C}$ ,  $I = 1.0 \text{ M}$ ,  $\text{NaCF}_3\text{SO}_3$ .

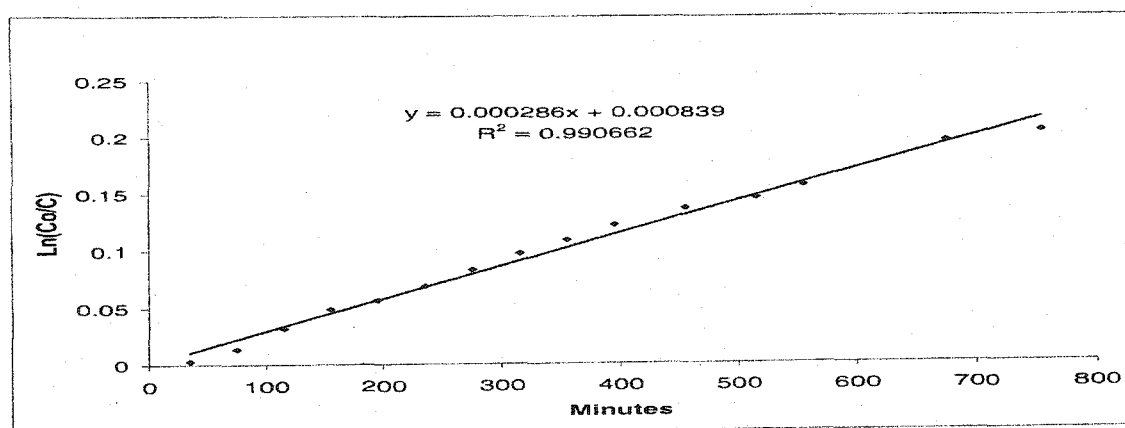


**Figure 5.9** A typical kinetic plot of  $\ln(C_0/C)$  vs time ( $t$ ) in the acid decomplexation of  $\text{Zn}(\text{NO}_3)_2 \cdot 1$  in buffered  $\text{D}_2\text{O}$ .  $[\text{Cd}]_i = 0.020 \text{ M}$ ,  $\text{pD} = 5.0$ ,  $\text{HOAc/NaOAc} (1.0 \text{ M})$ ,  $36.8(1)^\circ\text{C}$ ,  $I = 1.0 \text{ M}$ ,  $\text{NaCF}_3\text{SO}_3$ .

$2.4(1) \times 10^3$  minutes which was also obtained from three parallel runs ( $R^2 > 0.990$ ) (Figure 5.9). This is consistent with their solid-state structural trend. The *exo*-coordination mode of the  $\text{Hg}(\text{II})$  complex undoubtedly renders it significantly less inert than the fully *endo*-coordinated  $\text{Zn}(\text{II})$  and  $\text{Cd}(\text{II})$  analogues. As  $\text{Zn}(\text{II})$  fits much better than the larger  $\text{Cd}(\text{II})$  inside cross-bridged cyclam (ligand 1) (Table 2.8),  $\text{Zn}(\text{NO}_3)_2 \cdot 1$  is found to be at least 800 times kinetically more inert than  $\text{Cd}(\text{NO}_3)_2 \cdot 1$  (Table 5.1).

Thermodynamically, the ratio of complexed to protonated ligand **1** at equilibrium is 1.0 : 0.57 in the acid decomplexation product of  $\text{Zn}(\text{NO}_3)_2 \cdot \mathbf{1}$  whereas only protonated **1** was detected in the acid decomplexation product of  $\text{Cd}(\text{NO}_3)_2 \cdot \mathbf{1}$ . Complex  $[\text{HgCl}_2(\mu\text{-}\mathbf{1})]_2$  completely decomplexed at  $\text{pD} = 5.9$ . Therefore,  $\text{Zn}(\text{NO}_3)_2 \cdot \mathbf{1}$  is at least twenty times more stable thermodynamically than the  $\text{Cd}(\text{II})$  and  $\text{Hg}(\text{II})$  complexes of **1**.

The equilibrium between complexed and protonated  $\text{Me}_4\text{Cyclam}$  was reached in seven minutes as indicated by the  $^1\text{H}$  NMR spectra of  $\text{Zn}(\text{NO}_3)_2 \cdot (\text{Me}_4\text{Cyclam})$  run in buffered  $\text{D}_2\text{O}$  ( $\text{pD} = 5.0$ ). The major species is protonated  $\text{Me}_4\text{Cyclam}$  (90%) as indicated by the major methyl singlet at  $\delta$  2.58 belonging to protonated ligand and the minor methyl singlet at  $\delta$  2.54 belonging to complexed ligand (the middle spectrum in **Figure 5.10**). More clearly, the ratio of the singlet at  $\delta$  2.58 to the singlet at  $\delta$  2.54 decreased in the spectrum in a less acidic solution ( $\text{pD} = 5.9$ , MES). The upper limit of the half-life for

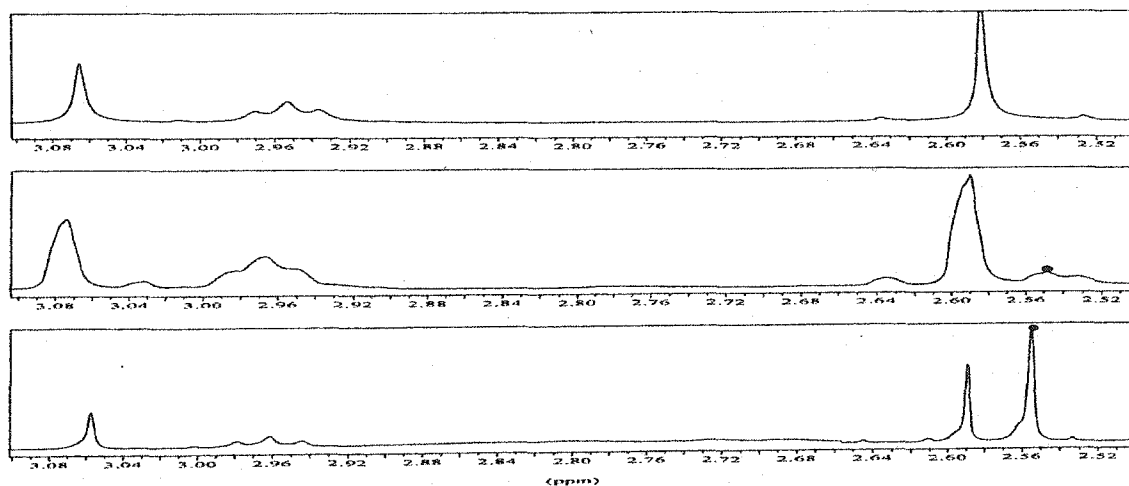


**Figure 5.10** Comparison of  $^1\text{H}$  NMR spectra of  $\text{Me}_4\text{Cyclam}$  in buffered  $\text{D}_2\text{O}$  ( $\text{pD} = 5.0$ ,  $\text{HOAc}/\text{NaOAc}$ ) (Top spectrum),  $\text{Zn}(\text{NO}_3)_2 \cdot (\text{Me}_4\text{Cyclam})$  in buffered  $\text{D}_2\text{O}$  ( $\text{pD} = 5.0$ ,  $\text{HOAc}/\text{NaOAc}$ ), (Middle spectrum), and  $\text{Zn}(\text{NO}_3)_2 \cdot (\text{Me}_4\text{Cyclam})$  in buffered  $\text{D}_2\text{O}$  ( $\text{pD} = 5.9$ , MES), (Bottom spectrum). The singlet with the dot belongs to complexed  $\text{Me}_4\text{Cyclam}$ .

this process at pD =5.0 is thus calculated at three minutes. Therefore, the zinc complex of cross-bridged cyclam,  $\text{Zn}(\text{NO}_3)_2 \cdot \mathbf{1}$ , is at least 800 times more inert than this  $\text{Zn}(\text{II})$   $\text{Me}_4\text{cyclam}$  analogue.

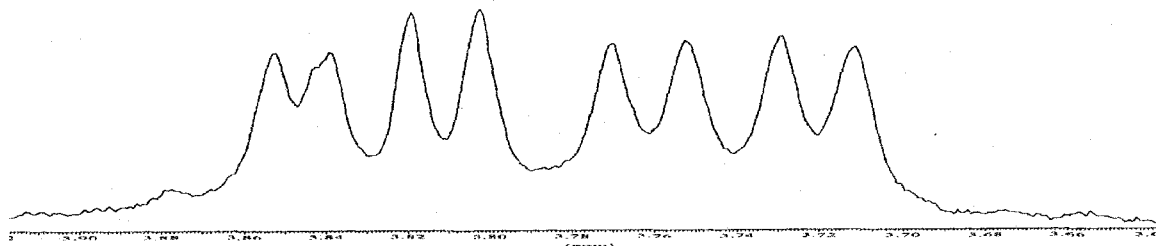


**Figure 5.11** The two most downfield doublet of doublets in the  $^1\text{H}$  NMR spectrum of  $[\text{Zn}(\text{OH}_2)_2 \cdot \mathbf{2}](\text{ClO}_4)_2$  in buffered  $\text{D}_2\text{O}$  (pD =5.0, HOAc/NaOAc). The left doublet belongs to protonated  $\mathbf{2}$  and the right dd belongs to complexed  $\mathbf{2}$ .

For complexes of ligand  $\mathbf{2}$ , changes at the most downfield doublet of doublets upon decomplexation are well-resolved in buffered  $\text{D}_2\text{O}$  (pD =5.0) (**Figure 5.11**). As shown in **Table 5.1**, compared to  $\text{Zn}(\text{NO}_3)_2 \cdot \mathbf{1}$ ,  $[\text{Zn}(\text{OH}_2)_2 \cdot \mathbf{2}](\text{ClO}_4)_2$  is at least 150 times more labile. The proton NMR spectrum recorded in 16 minutes after  $[\text{Zn}(\text{OH}_2)_2 \cdot \mathbf{2}](\text{ClO}_4)_2$  was dissolved in  $\text{D}_2\text{O}$  indicated that the equilibrium between complexed and protonated ligand  $\mathbf{2}$  was reached. The ratio of complexed to protonated ligand  $\mathbf{2}$  is 1.0 to 1.0. The half-life of this acid decomplexation is thus less than 16 minutes. By contrast, the spectrum recorded as soon as  $[\text{Cd}(\eta^2\text{-NO}_3)_2 \cdot \mathbf{2}]$  was dissolved in this solution showed only protonated  $\mathbf{2}$  (**Figure 5.12**). Therefore,  $[\text{Zn}(\text{OH}_2)_2 \cdot \mathbf{2}](\text{ClO}_4)_2$  is at least fifteen times thermodynamically more stable than  $[\text{Cd}(\eta^2\text{-NO}_3)_2 \cdot \mathbf{2}]$ .

In 1.0 M MES buffer solution (pD =5.9), however, the strong proton resonances from the buffer MES overlapped with this most downfield doublet of doublets from  $\mathbf{2}$ . For example, the proton NMR spectrum of  $[\text{Cd}(\eta^2\text{-NO}_3)_2 \cdot \mathbf{2}]$  in this buffer shows mainly the resonances from MES (relatively strong) and protonated  $\mathbf{2}$  between  $\delta$  2.7 and 4.0



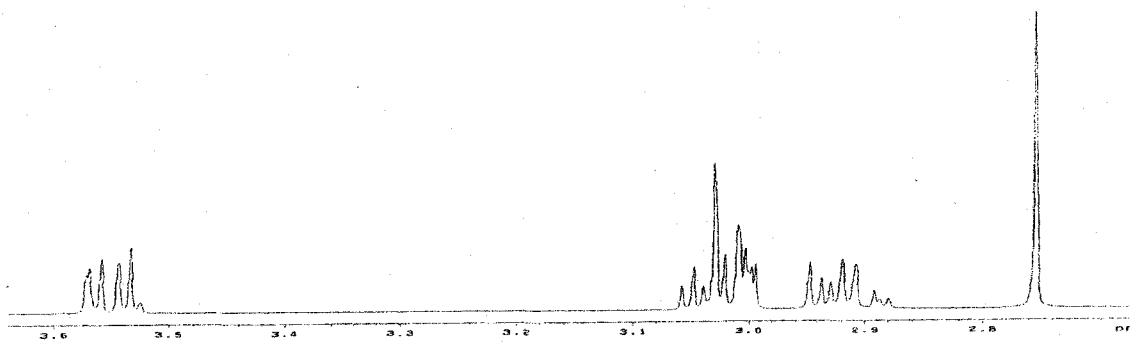


**Figure 5.12**  $^1\text{H}$  NMR spectrum of  $[\text{Cd}(\eta^2\text{-NO}_3)_2 \cdot 2]$  in buffered  $\text{D}_2\text{O}$  (pD = 5.0, HOAc/NaOAc). It is the same as that of protonated **2** in this buffer.

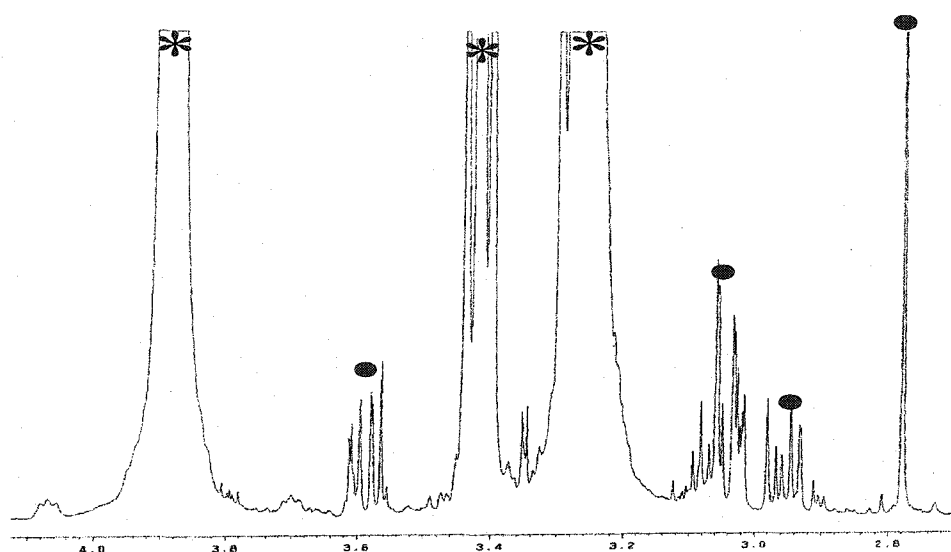


**Figure 5.13**  $^1\text{H}$  NMR spectrum of  $[\text{Cd}(\eta^2\text{-NO}_3)_2 \cdot 2]$  in buffered  $\text{D}_2\text{O}$  (pD = 5.9, MES). The resonances with asterisks belong to the buffer MES whereas those with dots are assigned to protonated **2**.

(**Figure 5.13**). Therefore, the relative integrations between the buffer and protonated **2** in the proton NMR spectra as well as the  $^{13}\text{C}\{^1\text{H}\}$  NMR spectra of these Cd(II) and Hg(II) complexes were used to determine the progress of this decomplexation process. Since the two proton NMR spectra of  $\text{HgCl}_2 \cdot 2$  recorded after it is kept in this buffer for 10 minutes and 2 days showed the same integration ratio of the resonance at  $\delta$  3.89 from MES to that of the singlet at  $\delta$  2.78 from protonated **2** (**Figure 5.14** and **Figure 5.15**) and protonated **2**

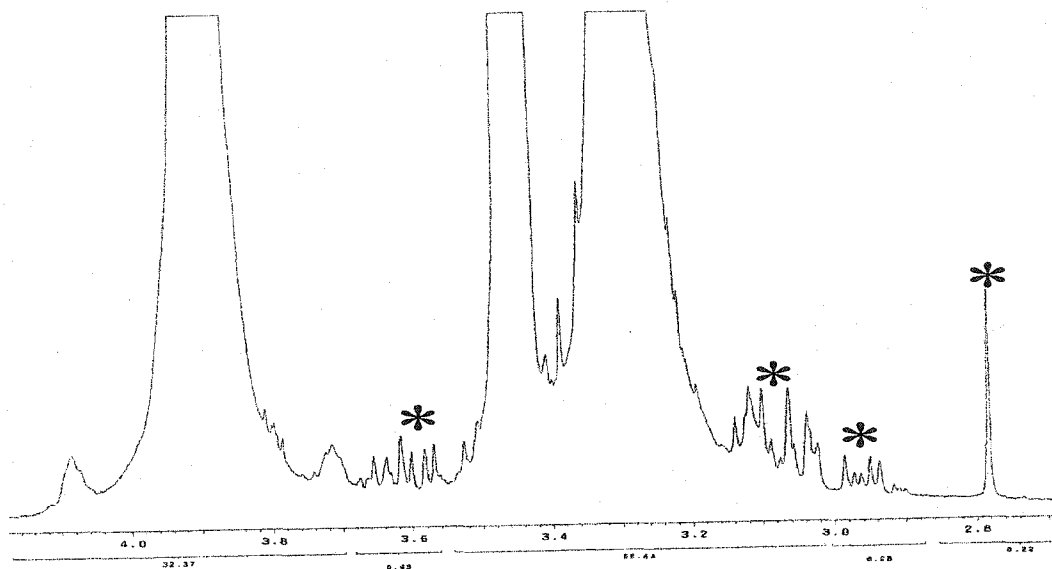


**Figure 5.14**  $^1\text{H}$  NMR spectrum of  $\text{HgCl}_2 \cdot 2$  in buffered  $\text{D}_2\text{O}$  (pD = 5.9, MES) recorded 14 minutes after this complex was dissolved. The resonances marked with asterisks belong to protonated **2**. The integration values are shown below the scale.

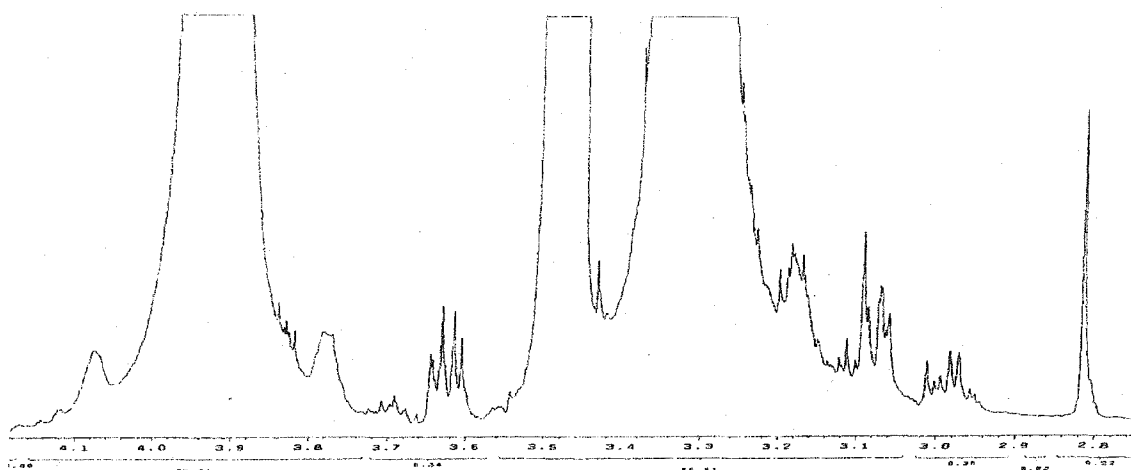


**Figure 5.15**  $^1\text{H}$  NMR spectrum of  $\text{HgCl}_2 \cdot 2$  in buffered  $\text{D}_2\text{O}$  (pD = 5.9, MES) recorded 163 minutes after dissolving. The integration values are shown below the scale.

is the only major species in its decomplexation product as indicated by its proton and  $^{13}\text{C}\{^1\text{H}\}$  NMR spectrum in this buffer, this decomplexation half-life is shorter than 10 minutes. Similarly, the half-life of acid decomplexation of  $[\text{Cd}(\eta^2\text{-NO}_3)_2 \cdot 2]$  in buffered  $\text{D}_2\text{O}$  (pD = 5.9, MES) is shorter than 8 minutes. Because  $\text{Cd}(\text{NO}_3)_2 \cdot 1$  has a half-life of

$3.1(1) \times 10^3$  minutes in the same buffer, its kinetic inertness is at least 300 times higher than analogous Cd(II) and Hg(II) complexes of cross-bridged cyclen **2** (Table 5.1).

Since the equilibrium between complexed and protonated ligand **2** reached a 1.0 to 1.0 ratio in buffered D<sub>2</sub>O (pD = 5.0, HOAc/NaOAc), an additional experiment was carried out to see whether complex  $[\text{Zn}(\text{OH}_2)_2 \cdot \mathbf{2}](\text{ClO}_4)_2$  can be formed from protonated **2** and  $\text{Zn}(\text{ClO}_4)_2 \cdot 6\text{H}_2\text{O}$  under these conditions. To protonated **2** in buffered D<sub>2</sub>O (pD = 5.0, HOAc/NaOAc), two crystals of  $\text{Zn}(\text{ClO}_4)_2 \cdot 6\text{H}_2\text{O}$  were added. After this solution was kept in a 36.8(1)<sup>o</sup>C bath for 49 minutes, the proton NMR spectrum of this solution was significantly changed (Figure 5.16) as both complexed and protonated ligand **2** were detected in a 1.3:1.0 ratio. A second <sup>1</sup>H NMR spectrum run after this solution was kept at 36.8(1)<sup>o</sup>C for 28 days showed no further changes. This indicates that the equilibrium between complexed and protonated ligand **2** was reached within 49 minutes at 36.8<sup>o</sup>C. This suggests the possibility of obtaining thermodynamic stability constant of this complex by potentiometric titration.

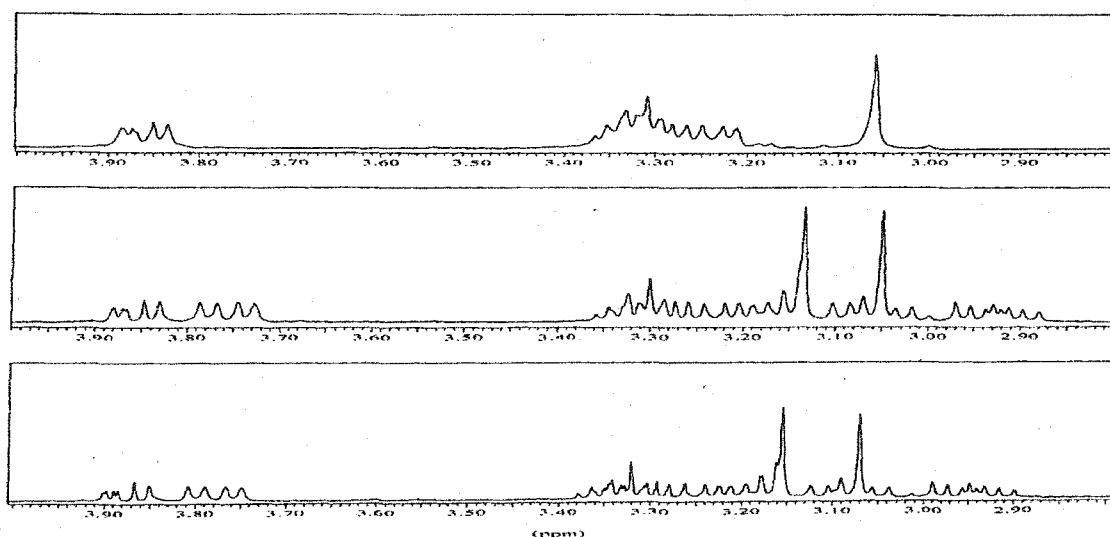


**Figure 5.16** Comparison of <sup>1</sup>H NMR spectra of protonated **2** in buffered D<sub>2</sub>O (pD = 5.0, HOAc/NaOAc) (Top spectrum), protonated **2** plus two crystals of  $\text{Zn}(\text{ClO}_4)_2 \cdot 6\text{H}_2\text{O}$  after 49 minutes at 36.8(1)<sup>o</sup> (Middle spectrum) and 28 days (Bottom).

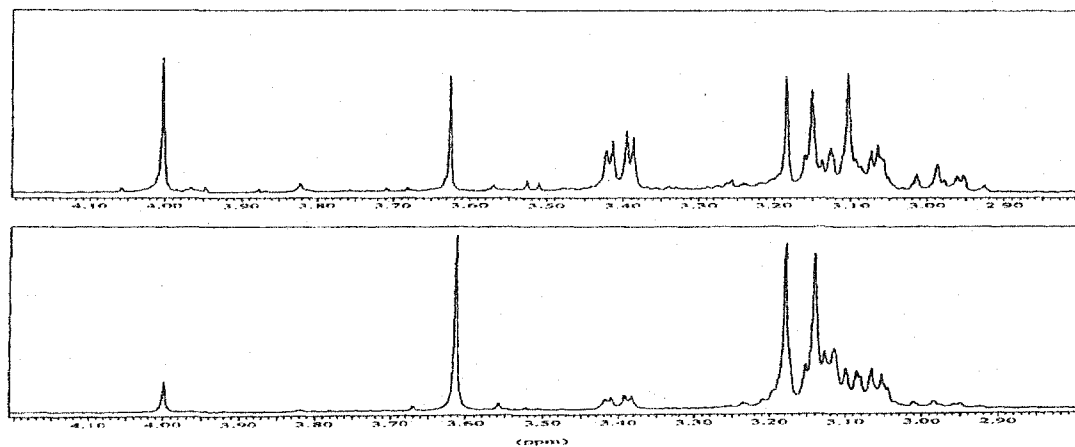


**Figure 5.17** Top:  $^1\text{H}$  NMR spectrum of  $[\text{Zn}\cdot\mathbf{6}](\text{ClO}_4)_2$  in buffered  $\text{D}_2\text{O}$  (pD = 5.0, HOAc/NaOAc) at equilibrium; Bottom: Spectrum of a mixture of  $[\text{Zn}\cdot\mathbf{6}](\text{ClO}_4)_2$  in buffered  $\text{D}_2\text{O}$  (pD = 5.0, HOAc/NaOAc) at equilibrium and excess protonated  $\mathbf{6}$ .

Ligand  $\mathbf{6}$  is the dicarbamoyl pendant-armed cross-bridged cyclen. Changes in the most downfield singlet assignable to the methylene protons from the pendant arms upon decomplexation are well-resolved and allowed quantitation of the  $[\text{Zn}\cdot\mathbf{6}](\text{ClO}_4)_2$  decomplexation process (top spectrum in **Figure 5.17**). The comparison of the proton NMR spectra of this complex before and after the addition of protonated ligand enabled us to assign the singlet at  $\delta$  4.00 to complexed  $\mathbf{6}$  and the singlet at 3.61 to protonated  $\mathbf{6}$  (**Figure 5.17**). Since the kinetic data collected near the equilibrium deviated from the pseudo-first order behavior (**Figure 5.18(a)**), only the first three data points were used to calculate this half-life (**Figure 5.18(b)**). From this, we can confirm that indeed this zinc complex is at least 600 times more inert than the Zn(II) complex of parent cross-bridged cyclen  $\mathbf{2}$  (**Table 5.1**). To further show that the acid decomplexation of this complex also follows a pseudo-first-order rate law, a more acidic  $\text{D}_2\text{O}$  solution (pD = 4.2) was used. Consistently, the first seven data points collected also show a pseudo-first-order reaction behavior (**Figure 5.19**).

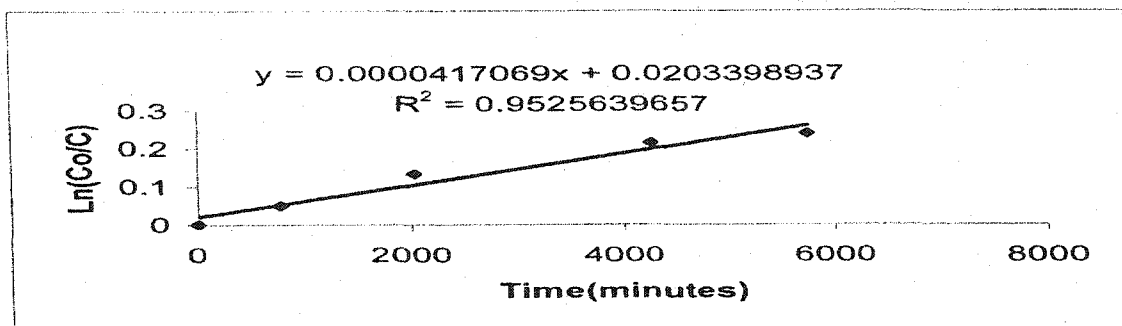


**Figure 5.18(a)** A kinetic plot of  $\ln(C_0/C)$  vs time ( $t$ ) in the acid decomplexation of  $[\text{Zn}\cdot 6](\text{ClO}_4)_2$  in buffered  $\text{D}_2\text{O}$ .  $[\text{Zn}]_i = 0.020 \text{ M}$ ,  $\text{pD} = 5.0$ ,  $\text{HOAc}/\text{NaOAc}$  (1.0 M),  $36.8(1)^\circ\text{C}$ ,  $I = 1.0 \text{ M}$ ,  $\text{NaCF}_3\text{SO}_3$ .

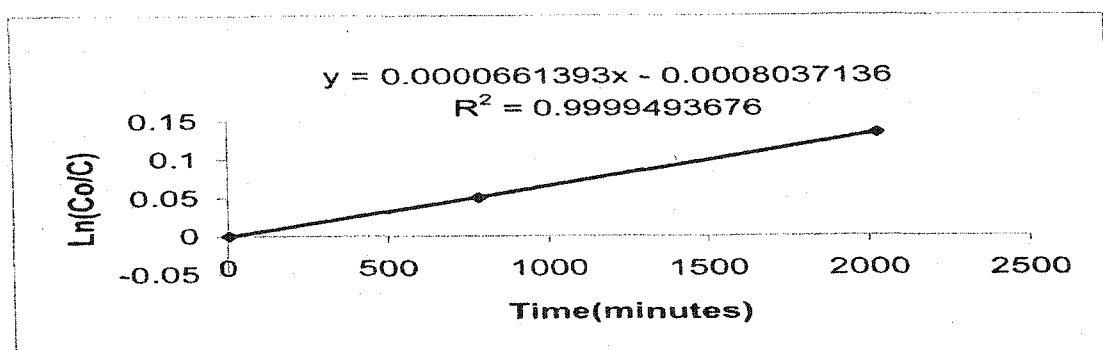


**Figure 5.18(b)** A kinetic plot of  $\ln(C_0/C)$  vs time ( $t$ ) in the acid decomplexation of  $[\text{Zn}\cdot 6](\text{ClO}_4)_2$  in buffered  $\text{D}_2\text{O}$  excluding two data points collected after 3000 minutes.  $[\text{Zn}]_i = 0.020 \text{ M}$ ,  $\text{pD} = 5.0$ ,  $\text{HOAc}/\text{NaOAc}$  (1.0 M),  $36.8(1)^\circ\text{C}$ ,  $I = 1.0 \text{ M}$ ,  $\text{NaCF}_3\text{SO}_3$ .

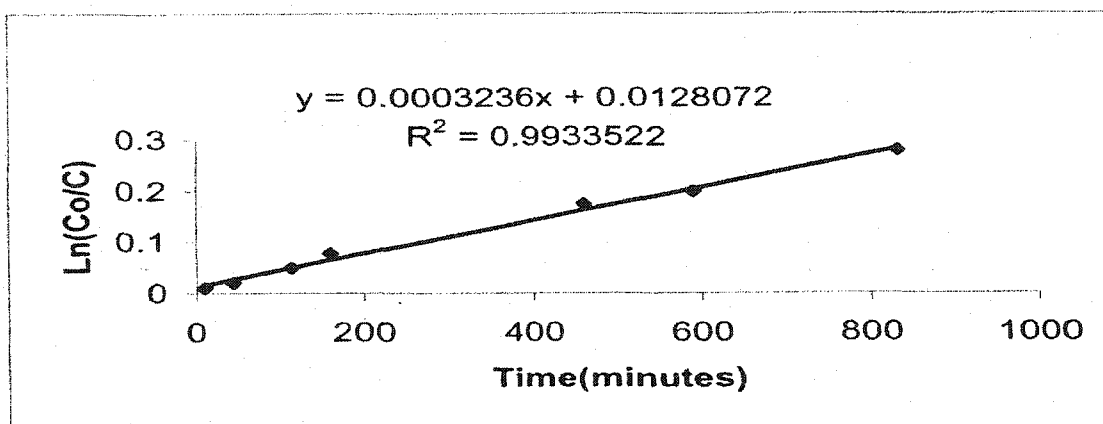


**Figure 5.19** A kinetic plot of  $\ln(C_0/C)$  vs time ( $t$ ) in the acid decomplexation of  $[\text{Zn}\cdot 6](\text{ClO}_4)_2$  in buffered  $\text{D}_2\text{O}$ .  $[\text{Zn}]_i = 0.020 \text{ M}$ ,  $\text{pD} = 4.2$ ,  $\text{HCOOH}/\text{HCOONa}$  (1.0 M),  $36.8(1)^\circ\text{C}$ ,  $I = 1.0 \text{ M}$ ,  $\text{NaCF}_3\text{SO}_3$ .

In order to compare our data with Springborg's reported kinetic data (Table 1.3),<sup>76</sup> the decomplexation of  $\text{Zn}(\text{NO}_3)_2 \cdot \mathbf{1}$  in acidic  $\text{D}_2\text{O}$  (5 M HCl) was carried out at room temperature ( $22^\circ\text{C}$ ). Within 11 minutes,  $\text{Zn}(\text{NO}_3)_2 \cdot \mathbf{1}$  was completely decomplexed in this medium (Figure 5.20). Since only relative noisy  $^1\text{H}$  NMR spectra were recorded (Figure 5.20), a detection limitation of five percent is used. The half-life of this acid

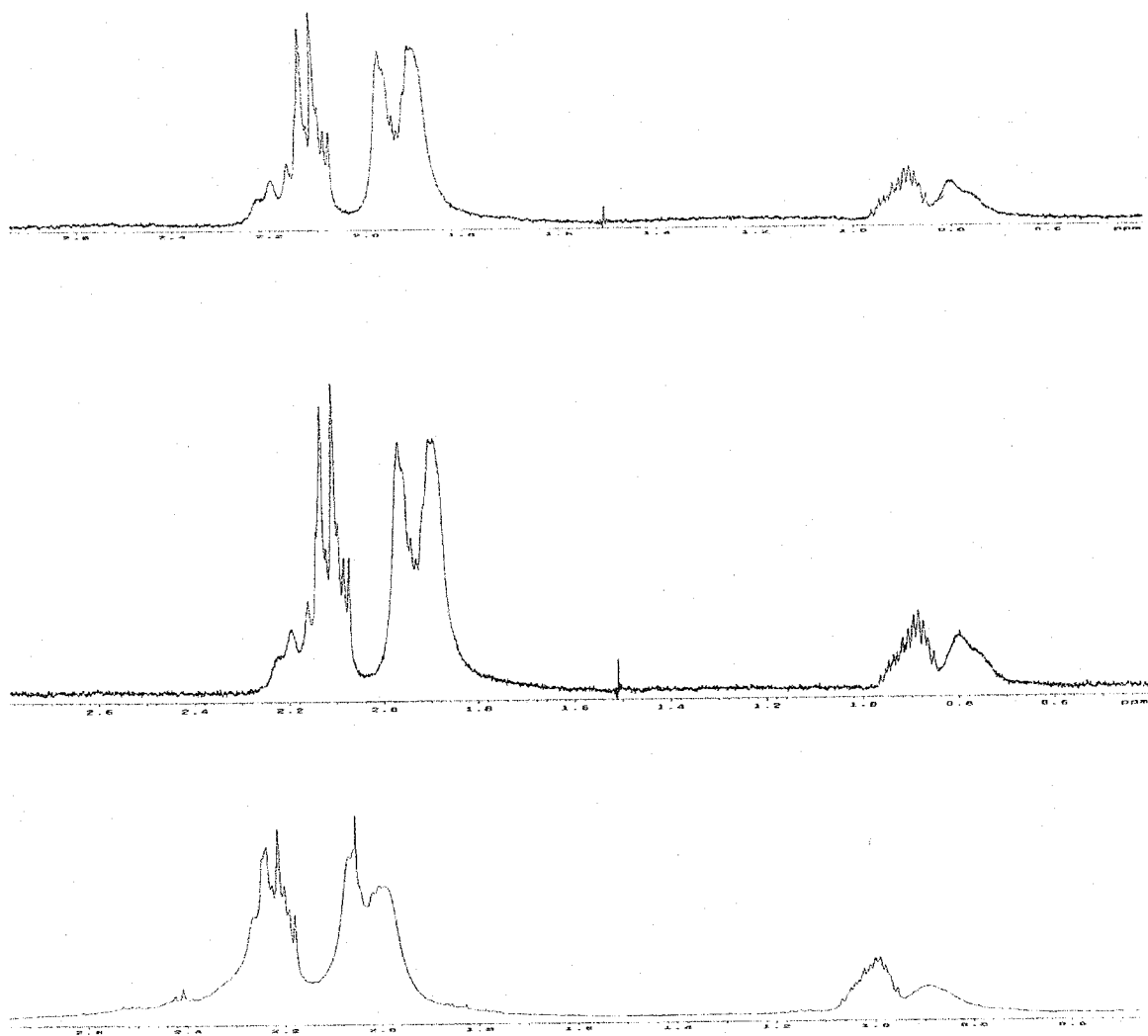


**Figure 5.20** Top:  $^1\text{H}$  NMR spectrum of  $\text{Zn}(\text{NO}_3)_2 \cdot \mathbf{1}$  in acidic  $\text{D}_2\text{O}$  (5 M HCl) obtained 11 minutes after the complex was dissolved. Middle:  $^1\text{H}$  NMR spectrum of  $\text{Zn}(\text{NO}_3)_2 \cdot \mathbf{1}$  in acidic  $\text{D}_2\text{O}$  (5 M HCl) obtained 92 minutes after the complex was dissolved. Bottom:  $^1\text{H}$  NMR spectrum of protonated  $\mathbf{1}$  in acidic  $\text{D}_2\text{O}$  (5 M HCl).

decomplexation process is thus less than three minutes. For comparison, under similar conditions, Springborg's Zn(II) complex of a homologous trimethylene-cross-bridged tetraamine,  $[\text{Zn}\cdot\mathbf{114}]^{2+}$  was reported to have a half-life of 72 minutes (Table 1.3).<sup>88</sup>

Unlike the out-of-cavity  $\text{HgCl}_2$  complex of cross-bridged cyclam **1** which decomplexed in  $\text{D}_2\text{O}$  within minutes, no detectable decomplexation was observed for the Hg(II) complex of the dicarboxylate pendant-armed cross-bridged cyclam derivative **7**,  $[\text{Hg}\cdot(\mathbf{7-2H})](\text{K}_2\text{HgCl}_4)$  (**148**), in  $\text{D}_2\text{O}$  after 48 days (Figure 5.21).

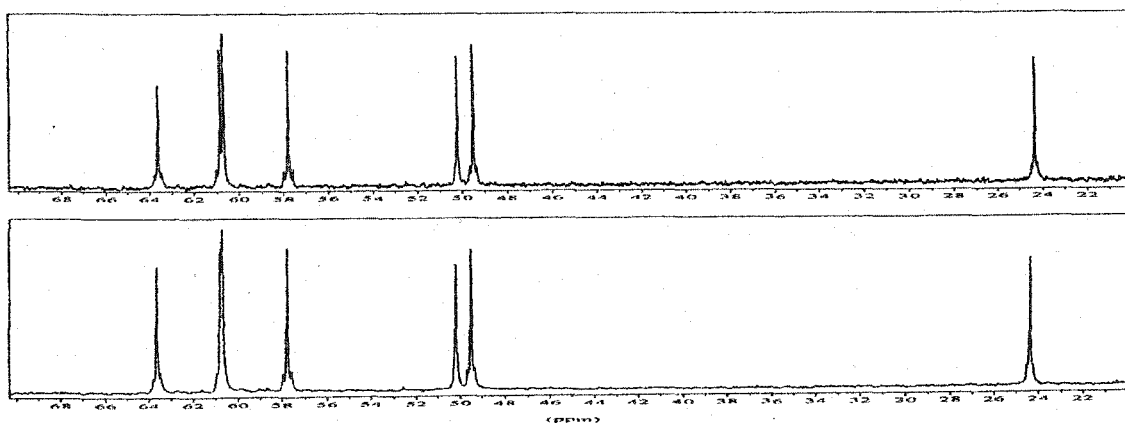


**Figure 5.21** Top:  $^{13}\text{C}\{^1\text{H}\}$  NMR spectrum of  $[\text{Hg}\cdot(\mathbf{7-2H})](\text{K}_2\text{HgCl}_4)$  (**148**) after it was kept in  $\text{D}_2\text{O}$  for 48 days. Bottom:  $^{13}\text{C}\{^1\text{H}\}$  NMR spectrum of  $[\text{Hg}\cdot(\mathbf{7-2H})](\text{K}_2\text{HgCl}_4)$  (**148**) immediately after it was dissolved in  $\text{D}_2\text{O}$ .

Complex  $[\text{Zn}\cdot(\mathbf{7-2H})](\text{NaClO}_4)$  was also found to be stable in acidic  $\text{D}_2\text{O}$  (pD = 5.0, HOAc/NaOAc,  $I = 1.0$  M,  $\text{NaCF}_3\text{SO}_3$ ) at  $36.8^\circ$  for at least 79 days as indicated by the unchanged  $^1\text{H}$  NMR spectra in Figure 5.22. The presence of only complexed **7-2H** is further supported by its  $^{13}\text{C}\{^1\text{H}\}$  NMR spectrum (Figure 5.23). The half-life of this acidic decomplexation is thus longer than 1800 days ( $2.6 \times 10^6$  minutes). Therefore, the kinetic inertness of this complex is at least 1000 times that of  $\text{Zn}(\text{NO}_3)_2\cdot\mathbf{1}$  (**118**). Such dramatically-increased kinetic inertness is a direct result of the added dicarboxylate pendant arms.

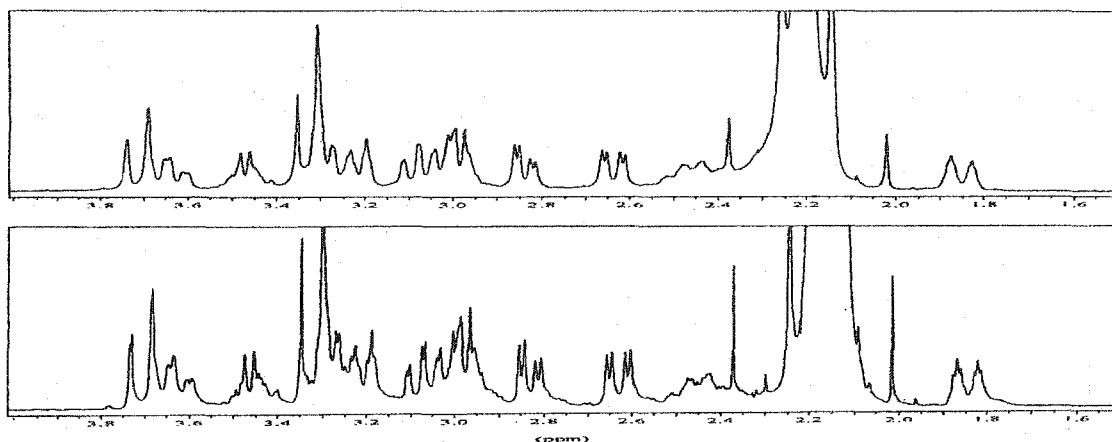


**Figure 5.22** Top:  $^1\text{H}$  NMR spectrum of  $\text{Zn}\cdot(7-2\text{H})](\text{NaClO}_4)$  in acidic  $\text{D}_2\text{O}$  (pD = 5.0, HOAc/NaOAc) as soon as it was dissolved in this solution. Bottom:  $^1\text{H}$  NMR spectrum of  $\text{Zn}\cdot(7-2\text{H})](\text{NaClO}_4)$  in acidic  $\text{D}_2\text{O}$  (pD = 5.0, HOAc/NaOAc) after 70 days. The strong resonance at  $\delta$  2.15 belongs to the buffer.

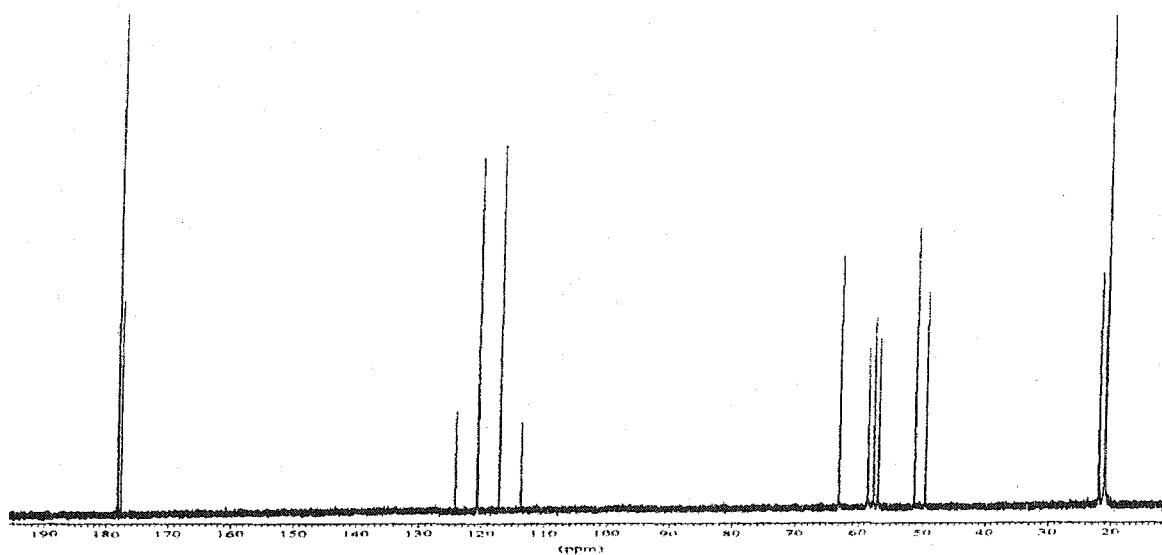


**Figure 5.23**  $^{13}\text{C}\{^1\text{H}\}$  NMR spectrum of  $\text{Zn}\cdot(7-2\text{H})](\text{NaClO}_4)$  in acidic  $\text{D}_2\text{O}$  (pD = 5.0, HOAc/NaOAc) after 70 days (only resonances of complex  $\text{Zn}\cdot(7-2\text{H})](\text{NaClO}_4)$ , acetic acid, and  $\text{NaCF}_3\text{SO}_3$  were detected).

It can thus be concluded that the kinetic stabilities of these complexes follow this order:  $[\text{Zn}\cdot(7-2\text{H})](\text{NaClO}_4) > [\text{Zn}\cdot 6](\text{ClO}_4)_2 > \text{Zn}(\text{NO}_3)_2\cdot 1 \gg \text{Cd(II) complex of ligand 1, Zn(II), Cd(II) and Hg(II) complexes of ligand 2, and Zn}(\text{NO}_3)_2\cdot(\text{Me}_4\text{Cyclam}) > [\text{HgCl}_2(\mu-1)]_2$ .



### 2.3 Preliminary Results on Relative Kinetic Inertness of Cu(II) Complexes

The kinetic studies for all Cu(II) complexes were carried out in 5 N HCl at room temperature (22°C) by UV-Vis spectroscopy. Comparative pseudo-first-order half-lives are shown in Table 5.3. Since all copper complexes of cross-bridged ligands show d-d maxima ranging from 595 to 647 nm in water except that Cu<sub>2</sub>(OH)(1)<sub>2</sub>(ClO<sub>4</sub>)<sub>3</sub> has a band at 595 nm and an additional band at 958 nm, we assumed that the d-d transitions of those

**Table 5.3** Acid decomplexation data for Cu(II) complexes of cross-bridged ligands and the reference copper complex of ligand **tet a** in 5N HCl.\*

Complex	Half-life (hours)	Complex	Half-life (hours)
Cu <sub>2</sub> (OH)(1) <sub>2</sub> (ClO <sub>4</sub> ) <sub>3</sub> (H <sub>2</sub> O)	6.5(5) x 10 <sup>2</sup>	[Cu•(7-2H)](NaClO <sub>4</sub> ) (NaCF <sub>3</sub> COO) <sub>0.5</sub> (H <sub>2</sub> O) <sub>1.5</sub>	> 2.5 x 10 <sup>4</sup>
[Cu•2(μ-Cl)] <sub>2</sub> Cl <sub>2</sub>	<< 1.0	[Cu•(8-2H)](NaClO <sub>4</sub> )	<< 1.0
[Cu•6](ClO <sub>4</sub> ) <sub>2</sub>	<< 1.0	Cu( <b>tet a</b> )(ClO <sub>4</sub> ) <sub>2</sub>	2.4(2) x 10 <sup>3</sup>

\* Detailed reaction conditions are included in the experimental section of this chapter.

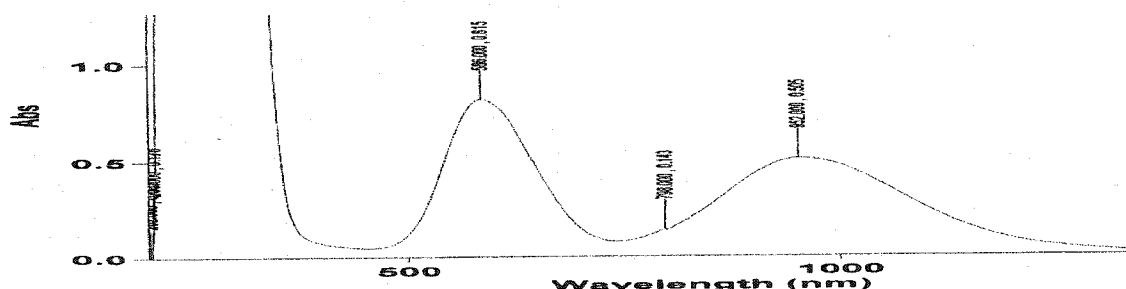


**Figure 5.24** The electronic spectrum of Cu<sub>2</sub>(OH)(1)<sub>2</sub>(ClO<sub>4</sub>)<sub>3</sub> (H<sub>2</sub>O) in aqueous 5N HCl ([Cu]<sub>i</sub> = 0.020 M).

Cu(II) complexes (Table 5.3) in 5 N HCl would be in a similar range. Indeed, Cu<sub>2</sub>(OH)(1)<sub>2</sub>(ClO<sub>4</sub>)<sub>3</sub> (154) has a band at 587 nm and an additional band at 958 nm in 5N HCl (Figure 5.24). Since the decomplexation product CuCl<sub>x</sub><sup>2-x</sup> has broad bands used to monitor the around 905 nm (Figure 5.25), the decrease in the absorbance of the band at

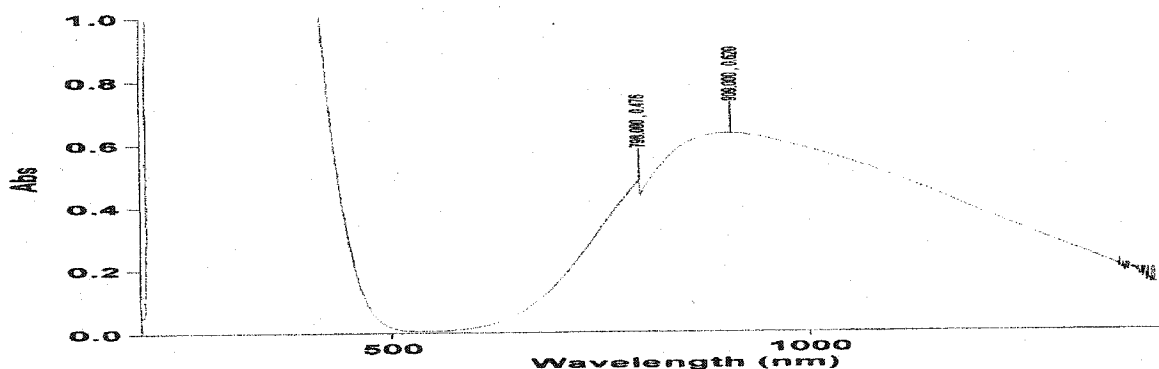


**Figure 5.25** The electronic spectrum of 0.00905 M  $\text{CuCl}_2$  in aqueous 5N HCl. The spike at 798 nm is due to the instrument.

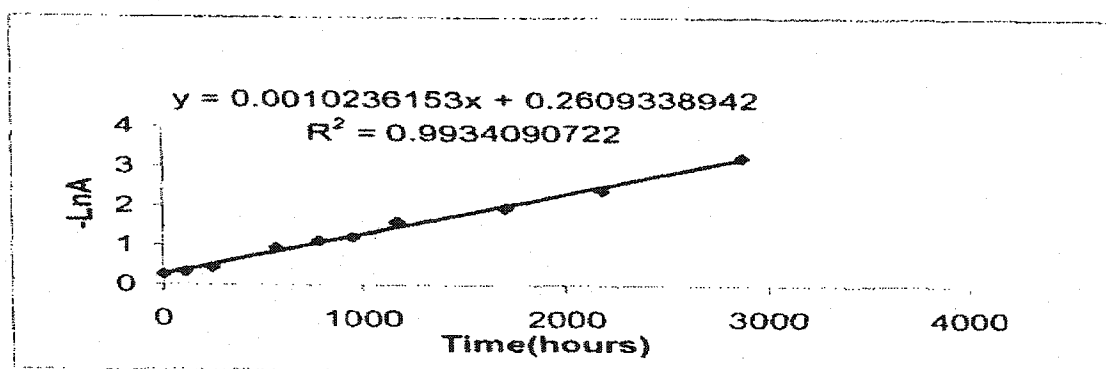


**Figure 5.26** A plot of  $-\ln A$  vs time ( $t$ ) in the acid decomplexation of  $\text{Cu}_2(\text{OH})(1)_2(\text{ClO}_4)_3$  in 5N HCl.  $[\text{Cu}]_i = 0.020$  M.

587 nm was kinetic process. A half-life of  $6.5(5) \times 10^2$  hours was then calculated from the data obtained from three parallel runs ( $R^2 > 0.985$ ) (Figure 5.26). For comparison, under similar conditions, the Cu(II) complex of Springborg's homologous trimethylene-cross-bridged tetraamine,  $[\text{Cu}\cdot\mathbf{114}]^{2+}$ , has a half-life of  $8.4(1) \times 10^2$  hours (Table 1.3).<sup>88</sup> Complex  $[\text{Cu}\cdot(7\text{-}2\text{H})](\text{NaClO}_4)(\text{NaCF}_3\text{COO})_{0.5}(\text{H}_2\text{O})_{1.5}$  (164) has a d-d transition band at 623(2) nm in 5 N HCl (Figure 5.27) which is very similar to its maximum at 620 nm in water. However, this copper complex is so stable in 5 N HCl that the data collected during six months from three parallel runs did not result in any significant change. Due to this long period of data collection, the maximum absorbance of this copper complex in

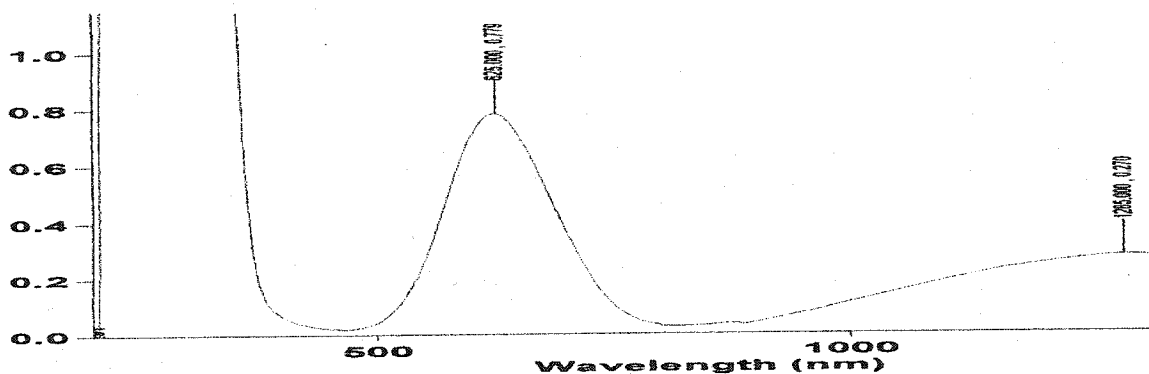


**Figure 5.27** The electronic spectrum of  $[\text{Cu}\cdot(7-2\text{H})](\text{NaClO}_4)(\text{NaCF}_3\text{COO})_{0.5}(\text{H}_2\text{O})_{1.5}$  in aqueous 5N HCl ( $[\text{Cu}] = 0.016 \text{ M}$ ).

water was used as a reference standard. All absorbance data collected during this period were corrected using the absorbance of this copper complex in water as a reference and shown in **Table 5.4(a-c)**. Using the lowest absorbance of 0.590 in these tables and the highest starting absorbance of 0.775, the low-limit of its acid decomplexation half-life can be estimated to be  $2.5 \times 10^4$  hours.

In 5N HCl, by contrast, copper complexes of cross-bridged cyclen **1** and its pendant-armed derivatives **6** and **8** decomplexed so fast that no band from 500 to 700 nm in the spectra were observed within 3 minutes (**Figure 5.28**, **Figure 5.29**, and **Figure 5.30**). Instead, only a strong broad band around 905 nm belonging to the decomplexation

**Table 5.4(a)** Acid decomplexation data for  $[\text{Cu}\cdot(7-2\text{H})](\text{NaClO}_4)(\text{NaCF}_3\text{COO})_{0.5}(\text{H}_2\text{O})_{1.5}$  in 5N HCl (First Run).  $\lambda_{\text{max}} = 624(1) \text{ nm}$ .

Time (hours)	Absorbance (A) before calibration	Absorbance (A) after calibration	Time (hours)	Absorbance (A) before calibration	Absorbance (A) after calibration
288	0.775	-----	2060	0.666	0.862
552	0.765	0.765	2566	0.590	0.685
816	0.747	0.743	4248	0.730	0.777
1224	0.763	0.773			

\* ----- No data available

**Table 5.4(b)** Acid decomplexation data for  $[\text{Cu}\cdot(7\text{-}2\text{H})](\text{NaClO}_4)(\text{NaCF}_3\text{COO})_{0.5}(\text{H}_2\text{O})_{1.5}$  in 5N HCl (Second Run).  $\lambda_{\text{max}} = 624(1)$  nm.

Time (hours)	Absorbance (A) before calibration	Absorbance (A) after calibration	Time (hours)	Absorbance (A) before calibration	Absorbance (A) after calibration
288	0.763	-----	2061	0.599	0.775
553	0.747	0.747	2565	0.603	0.700
817	0.756	0.751	4248	0.725	0.771
1223	0.777	0.787			

\* ----- No data available.

**Table 5.4(c)** Acid decomplexation data for  $[\text{Cu}\cdot(7\text{-}2\text{H})](\text{NaClO}_4)(\text{NaCF}_3\text{COO})_{0.5}(\text{H}_2\text{O})_{1.5}$  in 5N HCl (Third Run).  $\lambda_{\text{max}} = 623(2)$  nm.

Time (hours)	Absorbance (A) before calibration	Absorbance (A) after calibration	Time (hours)	Absorbance (A) before calibration	Absorbance (A) after calibration
289	0.764	-----	2060	0.602	0.779
552	0.752	0.752	2565	0.629	0.730
817	0.770	0.765	3141	0.600	0.794
823	0.775	0.770	4248	0.698	0.743
1224	0.759	0.769			

\* ----- No data available.

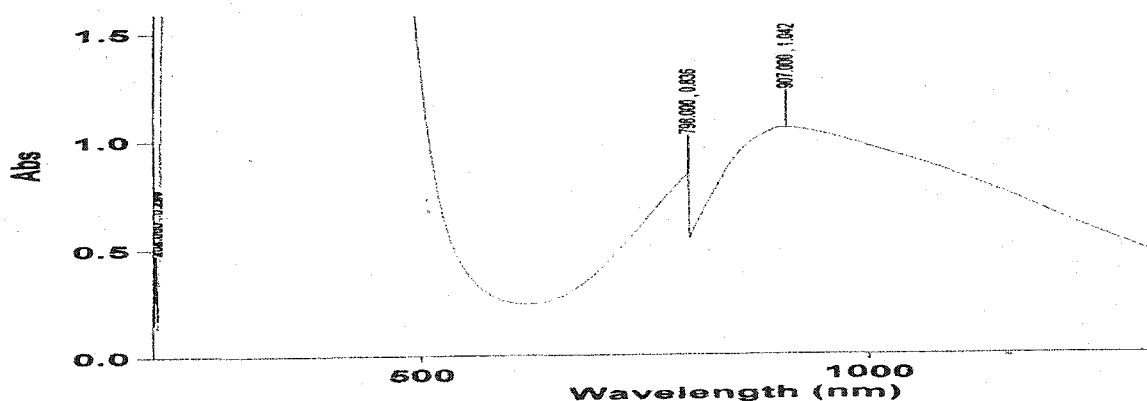


**Figure 5.28** The electronic spectrum of  $[\text{Cu}\cdot 2(\mu\text{-Cl})]_2\text{Cl}_2$  after 2 minutes in aqueous 5N HCl ( $[\text{Cu}]_i = 0.011$  M).

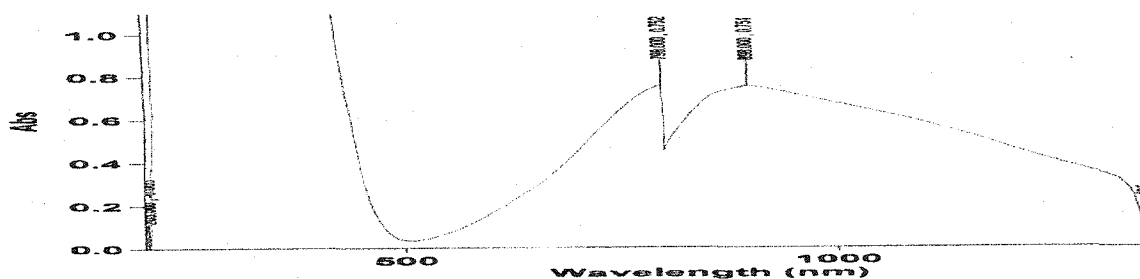


**Figure 5.29** The electronic spectrum of  $[\text{Cu}\cdot(8\text{-}2\text{H})](\text{NaClO}_4)$  after 2 minutes in aqueous 5N HCl ( $[\text{Cu}]_i = 0.018 \text{ M}$ ).

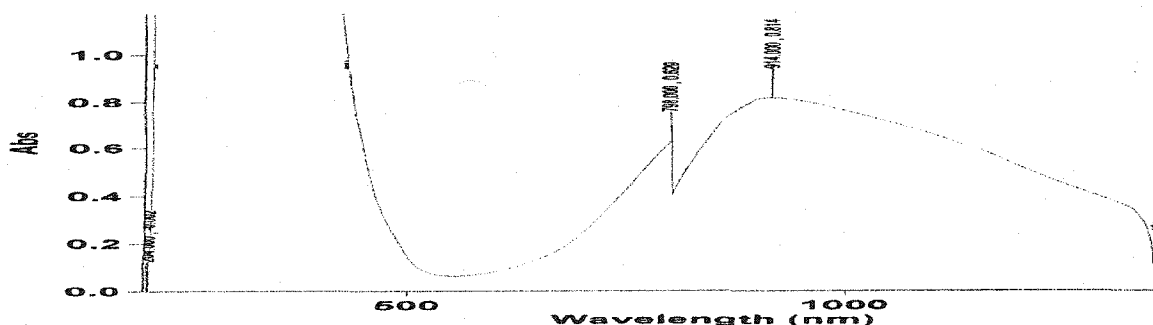


**Figure 5.30** The electronic spectrum of  $[\text{Cu}\cdot 6](\text{ClO}_4)_2$  after 3 minutes in aqueous 5N HCl ( $[\text{Cu}]_i = 0.011 \text{ M}$ ).

product  $\text{CuCl}_x^{2-x}$  appeared. Further, spectra recorded about 60 minutes later were almost the same (**Figure 5.31** and **Figure 5.32**). The half-lives of  $[\text{Cu}\cdot 2(\mu\text{-Cl})_2\text{Cl}_2]$  (**155**),  $[\text{Cu}\cdot(8\text{-}2\text{H})](\text{NaClO}_4)$  (**165**), and  $[\text{Cu}\cdot 6](\text{ClO}_4)_2$  (**162**) are thus all far less than an hour. For comparison, the decomplexation of the most-stable isomer in the Cu(II) complex of the ligand **tet a**, red-isomer  $\text{Cu}(\text{tet a})(\text{ClO}_4)_2$ , in 5N HCl was also monitored by the d-d transition band at 518 nm. A half-life of  $2.4(2) \times 10^4$  hours was then calculated from the data obtained from three parallel runs ( $R^2 > 0.970$ ) (**Figure 5.33**). This is significantly longer than previously reported half-life of 528 hours in 6.1 N HCl at  $25^\circ\text{C}$  in the literature.<sup>140(f)</sup>

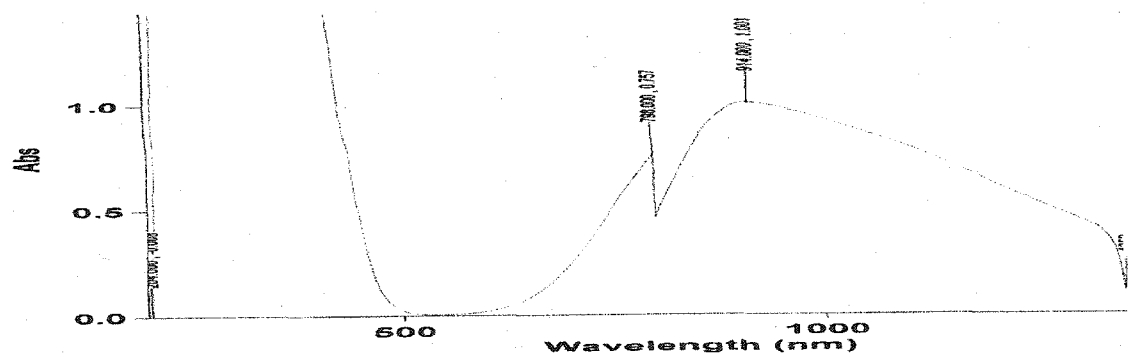


**Figure 5.31** The electronic spectrum of  $[\text{Cu}\cdot(8-2\text{H})](\text{NaClO}_4)$  after 63 minutes in aqueous 5N HCl ( $[\text{Cu}]_i = 0.018 \text{ M}$ ).

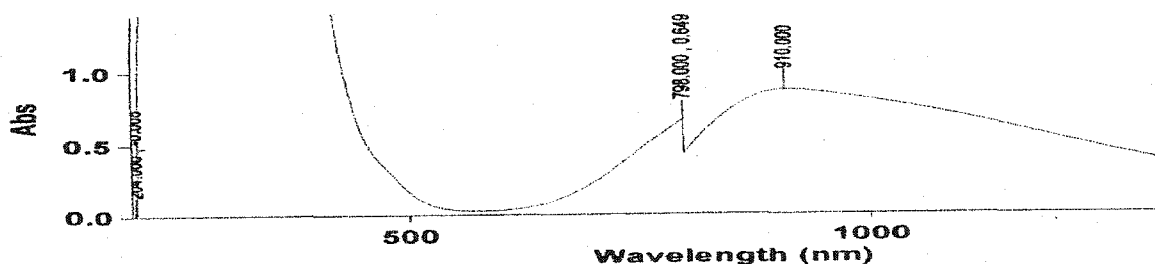


**Figure 5.32** The electronic spectrum of  $[\text{Cu}\cdot 6](\text{ClO}_4)_2$  after 52 minutes in aqueous 5N HCl ( $[\text{Cu}]_i = 0.011 \text{ M}$ ).

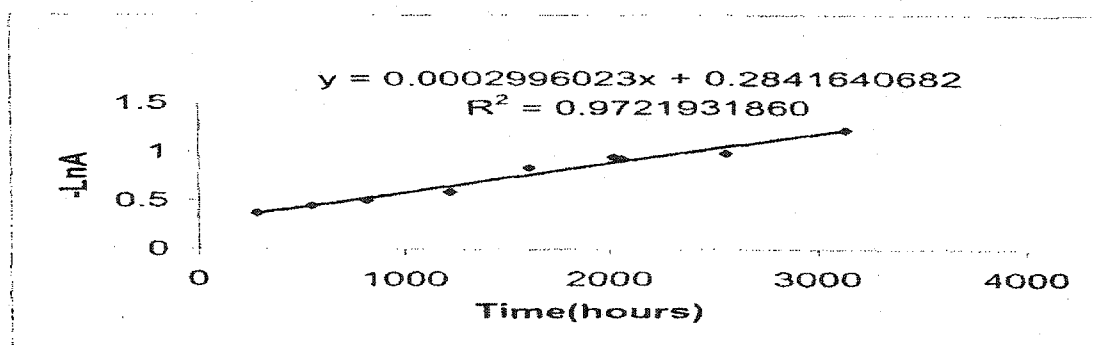


**Figure 5.33** A kinetic plot of  $-\ln A$  vs time ( $t$ ) in the acid decomplexation of red-isomer  $\text{Cu}(\text{tet a})(\text{ClO}_4)_2$  in 5N HCl.  $[\text{Cu}]_i = 0.051 \text{ M}$ .

It can therefore be concluded that the kinetic inertness of these complexes follow the order:  $[\text{Cu}\cdot(7-2\text{H})](\text{NaClO}_4)(\text{NaCF}_3\text{COO})_{0.5}(\text{H}_2\text{O})_{1.5} > \text{red-isomer } \text{Cu}(\text{tet a})(\text{ClO}_4)_2 > \text{Cu}_2(\text{OH})(1)_2(\text{ClO}_4)_3 \gg [\text{Cu}\cdot(8-2\text{H})](\text{NaClO}_4), [\text{Cu}\cdot 6](\text{ClO}_4)_2, \text{ and } [\text{Cu}\cdot 2(\mu\text{-Cl})_2\text{Cl}_2.$

### 3. Experimental for Kinetic Studies.

#### (1) Zn(II), Cd(II), Hg(II), Ga(III) and In(III) Complexes

Proton NMR spectra of these complexes recorded at time intervals were used to monitor their decomplexation process in either D<sub>2</sub>O or acidic D<sub>2</sub>O. The pD of a D<sub>2</sub>O solution can be calculated using the empirical formula  $pD = pH \text{ (meter reading)} + 0.40$ .<sup>48(e)</sup> Acidic D<sub>2</sub>O include buffered solutions, HClO<sub>4</sub> or HCl in D<sub>2</sub>O (pD = 1.07), and 5 M HCl in D<sub>2</sub>O. A solution containing one of the complexes was kept in a sealed NMR tube or small vial with a cap and parafilm. Zn(II), Cd(II) and Hg(II) complexes with concentrations between 0.020 and 0.030 M were generally used for these studies. For complexes of ligand **1**, changes upon hydrolysis at the most upfield doublet of pentets assignable to the equatorial proton of the  $\beta$ -methylene unit are well-resolved and allowed quantitation of the decomposition process. For complexes of ligand **2**, changes upon decomplexation at the most downfield doublet of doublets is well-resolved between complexed and protonated ligand **2** and allowed quantitation of the decomposition process. Samples were kept in thermostated baths at 36.8(1)°C throughout the studies on zinc, cadmium and mercury complexes in buffered D<sub>2</sub>O solutions. For a pD of 5.0, a 1.0 M acetic acid/sodium acetate buffer system was used, while for pD 5.9, a 1.0 M MES (4-morpholine-ethanesulfonic acid) buffer was used. Sodium trifluoromethylsulfonate was used to maintain all solution ionic strengths at  $I = 1.0$  M according to the literature method.<sup>142</sup> Three parallel experiments were carried out for any collected kinetic data on the Zn(II), Cd(II) and Hg(II) complexes of ligands **1** and **2**. However, if no detectable decomplexation of a complex occurred after it was dissolved in a buffer for at least

several days, two parallel experiments were carried out. If the decomplexation is complete immediately after a complex was dissolved in a buffer, two parallel experiments were also carried out. The  $^1\text{H}$  NMR detection limit of three percent is assumed for the metal complexes used for these studies with concentrations between 0.020 and 0.030 M. For Zn(II), Cd(II) and Hg(II) complexes of other cross-bridged ligands, only a single kinetic run was collected for each complex. Likewise for the Ga(III) and In(III) complexes. If  $\text{D}_2\text{O}$ ,  $\text{HClO}_4$  in  $\text{D}_2\text{O}$  ( $\text{pD} = 1.07$ ), or 5 M HCl in  $\text{D}_2\text{O}$  was used as the decomplexation medium, the kinetic studies were carried out at air-conditioned room temperature ( $22(3)^\circ\text{C}$ ).

## (2) Cu(II) Complexes

Decomplexation kinetics were followed by monitoring changes in the d-d transitions of the UV-Vis region (450-650 nm). In order to make our data comparable to the literature data,<sup>76</sup> 5 N HCl in deionized water was used as the acid source. All Cu(II) complexes of cross-bridged ligands were made according to the synthetic procedure described in the experimental part. The 5N HCl solution containing each of these complexes was kept in a small vial and sealed with parafilm. Kinetic data were generally collected from at least three parallel runs. However, for very fast decomplexations, only one experiment was carried out. The copper complexes used for these studies have concentrations between 0.011 and 0.018 M except for  $\text{Cu}_2(\text{OH})(\mathbf{1})_2(\text{ClO}_4)_3(\text{H}_2\text{O})$  (**154**) which was either 0.0020 or 0.0030 M. The reference complex  $\text{Cu}(\text{tet } \mathbf{a})(\text{ClO}_4)_2$  was synthesized according to the literature method.<sup>143</sup> A concentration of 0.051 M was used for this acid decomplexation study.



## Experimental Section:

### General Methods and Materials.

Unless indicated otherwise, 1-D  $^1\text{H}$  and  $^{13}\text{C}\{^1\text{H}\}$  NMR spectra were recorded at 360.13 and 90.56 MHz respectively (Bruker AM-360). Acetonitrile was generally used as an internal standard for NMR spectra in  $\text{D}_2\text{O}$  solutions; the methyl resonance was set at  $\delta$  2.06 and  $\delta$  1.70 for  $^1\text{H}$  and  $^{13}\text{C}\{^1\text{H}\}$  spectra respectively. Proton *COSY*, *gCOSY*, *NOESY*, *gHSQC*, and *HMQC* NMR experiments were performed at 400 or 500 MHz (Varian Inova-400 or 500).  $^{113}\text{Cd}$  NMR spectra were recorded at 90 MHz (JEOL FX90Q). Variable-temperature  $^1\text{H}$  and  $^{13}\text{C}\{^1\text{H}\}$  NMR spectral studies were carried out at 400 MHz (Varian Inova-400) in which a methanol chemical shift thermometer (0.03% conc. HCl in MeOH) was used to monitor the temperature of the probe. IR spectra were recorded as KBr pellets on a Nicolet MX-1 FT Spectrophotometer. Elemental analyses were obtained from the University of New Hampshire University Instrumentation Center or Atlantic Microlab, Inc., Norcross, GA. Reactions were run under a nitrogen atmosphere with magnetic stirring in standard Schlenk glassware. Bulk solvent removal was by rotary evaporation under reduced pressure and trace volatile removal from solids was by vacuum pump. Solvents except for acetonitrile were used as purchased. Acetonitrile was dried over a  $\text{CaH}_2/\text{KOH}$  mixture.

Cross-bridged ligands **1-4** (Figure 1.36) were prepared as described previously.<sup>19,69</sup> In the synthesis of Ga(III) and In(III) complexes of ligands **1** and **2**,

ligands **1** and **2** were kept under nitrogen after being sublimated under vacuum. Cross-bridged ligands **5**, **6**, **7**, and **8** were prepared according to our group's methods.<sup>19,69,125(a)</sup> Ligand **5** was synthesized only once by a slight modification of our group's method. However, the resulting **5** was only about 95% pure and was used for complexation with metal salts. Because of the synthetic routes,<sup>69,125(a)</sup> ligand **7** was made as  $7 \cdot (\text{TFA})(\text{H}_2\text{O})_{0.5}$  and ligand **8** was isolated as  $8 \cdot (\text{TFA})_2(\text{H}_2\text{O})$ . In the synthesis of ligand **8**, by the avoiding of any moisture from air and trace water from solvents, ligand **8** was isolated as  $8 \cdot (\text{TFA})_2$  as indicated by its CHN elemental results. Standard aqueous 1.0N NaOH solution and standard 0.505N KOH solution in methanol were purchased from Aldrich. Metal salts were obtained commercially and used without further purification. Anhydrous  $\text{GaCl}_3$  and anhydrous  $\text{InBr}_3$  were stored in a  $\text{N}_2$ -filled glovebox. Recrystallizations of any metal complexes were carried out in closed containers without special precautions to exclude moisture or air.

**[Zn•1(OH<sub>2</sub>)(μ-Cl)ZnCl<sub>3</sub>] (115):** To a MeOH solution (4 mL) of  $\text{ZnCl}_2$  (70.9 mg, 0.520 mmol), 0.056 mL of deionized  $\text{H}_2\text{O}$  was added. To this clear solution, a MeOH solution (3 mL) of **1** (56.2 mg, 0.248 mmol) was added. This solution became cloudy after stirring for 1 minute and was then refluxed for 14 hours. The white precipitate was centrifuged out and washed by MeOH (2x4 mL). Removal of residual solvent yielded 95.7 mg (75%) of a white solid. IR (KBr): 3434 ( $\nu_{\text{OH}}$ ), 3264, 3252  $\text{cm}^{-1}$  ( $\nu_{\text{NH}}$ ).  $^1\text{H}$  NMR in  $D_2\text{O}$  (0.043 M solution):  $\delta$  3.51 (2H, broad t,  $J \sim 8$  Hz, NH), 2.80-3.22 (18H, m), 2.56-2.70 (2H, broad m), 2.16-2.32 (2H, m,  $\beta\text{-CHH}_{ax}$ ), 1.56 (2H, broad dp,  $J = 17.0, 2.8$  Hz,  $\beta\text{-CH}_{eq}\text{H}$ );  $^{13}\text{C}\{^1\text{H}\}$  data in  $D_2\text{O}$  (0.043 M solution):  $\delta$  59.83, 58.37, 51.21, 48.46, 41.32, 21.81.

Anal. Calcd. for  $Zn_2Cl_4C_{12}H_{28}N_4O$ : C, 27.88; H, 5.46; N, 10.84%. Found: C, 27.98; H, 5.35; N, 10.70%.

**[Zn•1( $\mu$ -Cl)]<sub>2</sub>Cl<sub>2</sub>•4CH<sub>3</sub>OH (116):** To a refluxing solution of ligand **1** (52 mg, 0.23 mmol) in 4 mL of methanol was added a methanol solution of ZnCl<sub>2</sub> (31 mg, 0.23 mmol) in 5 mL methanol. This was refluxed overnight to give a clear solution. After cooling to room temperature, diethyl ether diffusion into this solution yielded 63 mg (75%) of clear X-ray-quality crystals. CHN elemental analyses were carried out on these crystals after vacuum-drying. IR (KBr): 3216 cm<sup>-1</sup>( $\nu_{NH}$ ). <sup>1</sup>H NMR data for the [Zn(**1**)( $\mu$ -Cl)]<sub>2</sub>Cl<sub>2</sub> complex in D<sub>2</sub>O (0.050 M solution):  $\delta$  3.51 (2H, broad t,  $J \sim 9$  Hz, NH), 2.79-3.22 (18H, m), 2.61-2.68 (2H, broad m), 2.16-2.32 (2H, m,  $\beta$ -CHH<sub>ax</sub>), 1.56 (2H, broad dp,  $J = 16.9$ , 2.8 Hz,  $\beta$ -CH<sub>eq</sub>H); in CD<sub>3</sub>OD (0.017 M solution):  $\delta$  3.69 (2H, broad t,  $J \sim 9$  Hz, NH), 3.48 (2H, tt,  $J = 13.2$ , 3.0 Hz), 3.18-3.29 (4H, m), 3.14 (2H, td,  $J = 12.1$ , 5.9 Hz), 2.72-3.07 (10H, m), 2.48 (2H, dd,  $J = 11.7$ , 3.6 Hz), 2.30 (2H, dtt, 16.6, 13.4, 3.3 Hz,  $\beta$ -CHH<sub>ax</sub>), 1.56 (2H, broad dp,  $J = 16.9$ , 2.9 Hz,  $\beta$ -CH<sub>eq</sub>H); in CD<sub>3</sub>OD (0.050 M solution at 500 MHz):  $\delta$  3.77 (2H, broad t,  $J \sim 9$  Hz, NH), 3.52 (2H, tt,  $J = 13.2$ , 3.0 Hz), 3.22-3.32 (4H, m, including AA' of AA'XX'), 3.16 (2H, td,  $J = 12.8$ , 5.5 Hz), 2.92-3.06 (4H, m), 2.88 (2H, d,  $J \sim 13$ Hz), 2.82 (2H, d,  $J \sim 12$  Hz), 2.70-2.78 (2H, XX' of AA'XX'), 2.48 (2H, dd,  $J = 11.7$ , 3.6 Hz), 2.30 (2H, dtt, 16.6, 13.4, 3.3 Hz,  $\beta$ -CHH<sub>ax</sub>), 1.56 (2H, broad dp,  $J = 16.9$ , 2.9 Hz,  $\beta$ -CH<sub>eq</sub>H); in CD<sub>3</sub>OD (0.017 M N-D complex): 3.47 (2H, td,  $J = 13.1$ , 2.9 Hz), 3.18-3.29 (4H, m), 3.14 (2H, td,  $J = 13$ , 5.3 Hz), 2.72-3.06 (10H, m), 2.48 (2H, ddd,  $J = 12.0$ , 3.8, 1.1 Hz), 2.29 (2H, dtt, 19.7, 13.4, 3.2 Hz,  $\beta$ -CHH<sub>ax</sub>), 1.56 (2H, broad dp,  $J = 16.9$ , 2.9 Hz,  $\beta$ -CH<sub>eq</sub>H); in CD<sub>3</sub>OD (0.050 M N-D complex at 500

MHz): 3.52 (2H, td,  $J = 13.3, 2.8$  Hz), 3.22-3.32 (4H, m, including AA' of AA'XX'), 3.16 (2H, td,  $J = 12.8, 5.3$  Hz), 3.01 (2H, td,  $J = 13.5, 4.3$  Hz), 2.90-2.96 (2H, m), 2.87 (2H, broad d,  $J = 12.5$  Hz), 2.81 (2H, broad d,  $J = 12.5$  Hz), 2.69-2.78 (2H, XX' of AA'XX'), 2.48 (2H, broad dd,  $J = 12.0, 4.0$  Hz), 2.31 (2H, dtt, 16.5, 13.0, 3.0 Hz,  $\beta$ -CHH<sub>ax</sub>), 1.53 (2H, broad dp,  $J = 16.5$  Hz, 3.0 Hz,  $\beta$ -CH<sub>eq</sub>H); in CD<sub>3</sub>CN:  $\delta$  3.65 (2H, tt,  $J = 12.7, 3.0$  Hz), 3.47 (2H, td,  $J = 12.8, 2.7$  Hz), 3.41 (2H, td,  $J = 12.2, 6.8$  Hz), 3.15 (2H, br m, shift dependent on amount of water in solvent, NH), 3.02-3.15 (2H, AA' of AA'XX', cross-bridging CH<sub>2</sub>CH<sub>2</sub>), 2.81-2.91 (4H, m), 2.72 (2H, dp,  $J = 12.6, 1.6$  Hz), 2.55-2.66 (4H, m including XX' of AA'XX'), 2.23 (2H, dd,  $J = 3.8, 1.5$  Hz), 2.04-2.20 (2H, dtt overlapping with water peak,  $J = 16.7, 13.4, 3.3$  Hz,  $\beta$ -CHH<sub>ax</sub>), 1.42 (2H, dp,  $J = 16.6, 2.8$  Hz,  $\beta$ -CH<sub>eq</sub>H); <sup>13</sup>C{<sup>1</sup>H} data in D<sub>2</sub>O (0.050 M solution):  $\delta$  59.86, 58.40, 51.22, 48.49, 41.34, 21.82; in CD<sub>3</sub>OD (0.017 M solution):  $\delta$  59.99, 59.84, 52.03, 48.67 (overlapped with the methanol peaks), 42.55, 22.76; in CD<sub>3</sub>OD (0.050 M solution at 125.7 MHz):  $\delta$  60.04, 59.77, 51.98, 48.49, 42.60, 22.66; in CD<sub>3</sub>OD (0.017 M N-D complex):  $\delta$  59.99, 59.83, 52.02, 48.57 (overlapped with the methanol peaks), 42.44, 22.74; in CD<sub>3</sub>OD (0.050 M N-D complex at 125.7 MHz):  $\delta$  60.05, 59.74, 51.98, 48.35, 42.51, 22.63; <sup>13</sup>C data in CD<sub>3</sub>CN:  $\delta$  59.17, 58.95, 51.49, 47.70, 42.13, 22.63. Anal. Calcd. for ZnCl<sub>2</sub>(C<sub>12</sub>H<sub>26</sub>N<sub>4</sub>)•0.5H<sub>2</sub>O: C, 38.78; H, 7.32; N, 15.07%. Found: C, 39.06; H, 7.19; N, 14.99%.

**Zn•1(ClO<sub>4</sub>)<sub>2</sub> (117):** To a solution of ligand 1 (82 mg, 0.36 mmol) in 5 mL methanol was added a 2 mL methanol solution of Zn(ClO<sub>4</sub>)<sub>2</sub>•6H<sub>2</sub>O (141 mg, 0.38 mmol). After 1 day of refluxing then cooling, diethyl ether vapor diffusion yielded 164 mg (92%) of colorless

crystals. IR (KBr): 3286  $\text{cm}^{-1}$  ( $\nu_{\text{NH}}$ ).  $^1\text{H}$  NMR in  $D_2O$   $\delta$  3.50 (2H, broad t,  $J = 9$  Hz NH), 2.81-3.19 (18H, m), 2.61-2.66 (2H, broad m), 2.16-2.32 (2H, m,  $\beta\text{-CHH}_{ax}$ ), 1.56 (2H, dp,  $J = 17.1$  Hz, 2.8 Hz,  $\beta\text{-CHH}_{eq}$ ); in  $CD_3OD$  (0.020 M):  $\delta$  3.91 (2H, broad t,  $J = 8$  Hz, NH), 3.19 (2H, tt,  $J = 13.1, 2.9$  Hz), 2.83-3.16 (16H, m), 2.61-2.70 (2H, m), 2.24-2.41 (2H, m,  $\beta\text{-CHH}_{ax}$ ), 1.60 (2H, broad dp,  $J = 16.9, 3.0$  Hz,  $\beta\text{-CH}_{eq}\text{H}$ ); in  $CD_3CN$ :  $\delta$  3.35 (2H, broad s, NH), 3.19 (2H, tt,  $J = 13.2, 2.9$  Hz), 2.64-3.13 (16H, m), 2.52-2.62 (2H, m), 2.07-2.21 (2H, m,  $\beta\text{-CHH}_{ax}$ ), 1.51 (2H, broad dp,  $J = 16.8, 2.8$  Hz,  $\beta\text{-CH}_{eq}\text{H}$ );  $^{13}\text{C}\{^1\text{H}\}$  data in  $D_2O$ :  $\delta$  59.88, 58.42, 51.22, 48.51, 41.34, 21.81; in  $CD_3OD$ : 61.00, 59.20, 52.39, 49.94, 42.47, 22.77; in  $CD_3CN$ :  $\delta$  60.02, 59.10, 51.64, 48.57, 42.09, 22.27. Anal. Calcd. for  $[\text{Zn}(\text{C}_{12}\text{H}_{26}\text{N}_4)](\text{ClO}_4)_2$ : C, 29.38; H, 5.34; N, 11.42%. Found: C, 29.76; H, 5.51; N, 11.44%.

**Zn•1(NO<sub>3</sub>)<sub>2</sub> (118):** To a solution of ligand 1 (226 mg, 0.998 mmol) in 2 mL methanol was added a methanol solution (4 mL) of  $\text{Zn}(\text{NO}_3)_2 \cdot 6\text{H}_2\text{O}$  (304 mg, 1.02 mmol). After a day of reflux, a clear solution was obtained. Diethyl ether was diffused in at room temperature to give 408 mg (98%) of colorless crystalline product. IR (KBr): 3255  $\text{cm}^{-1}$  ( $\nu_{\text{NH}}$ ).  $^1\text{H}$  NMR data in  $D_2O$ :  $\delta$  3.51 (2H, br t,  $J = 8$  Hz, NH), 3.13 (2H, tt,  $J = 13.1, 2.9$  Hz), 2.80-3.04 (16H, m), 2.60-2.65 (2H, broad m), 2.16-2.32 (2H, m,  $\beta\text{-CHH}_{ax}$ ), 1.56 (2H, dp,  $J = 16.9, 2.8$  Hz,  $\beta\text{-CHH}_{eq}$ ); in  $CD_3OD$  (0.020M):  $\delta$  4.10 (2H, broad s, NH), 3.22 (2H, tt,  $J = 13.2, 2.8$  Hz), 3.10-3.21 (2H, m), 2.85-3.07 (14H, m, including 4H, AA' and BB' of AA'BB'), 2.61-2.65 (2H, br m), 2.22-2.41 (2H, m,  $\beta\text{-CHH}_{ax}$ ), 1.58 (2H, broad dp,  $J = 16.8, 2.9$  Hz,  $\beta\text{-CH}_{eq}\text{H}$ ); in  $CD_3CN$ :  $\delta$  3.88 (2H, broad s, NH), 3.23 (2H, tt,  $J = 13.3, 3.0$  Hz), 3.04-3.15 (2H, AA' of AA'XX'), 2.81-3.03 (14H, m), 2.70-2.81 (2H, XX'

of AA'XX'), 2.52-2.56 (2H, m), 2.17 (2H, dtt,  $J = 16.4, 13.1, 3.3$  Hz,  $\beta$ -CHH<sub>ax</sub>), 1.50 (2H, broad dp,  $J = 16.8, 2.9$  Hz,  $\beta$ -CH<sub>eq</sub>H); <sup>13</sup>C{<sup>1</sup>H} in D<sub>2</sub>O:  $\delta$  59.90, 58.43, 51.24, 48.53, 41.35, 21.83; in CD<sub>3</sub>OD:  $\delta$  61.04, 59.74, 52.24, 48.93, 42.35, 22.79; in CD<sub>3</sub>CN:  $\delta$  60.34, 59.47, 51.52, 48.65, 41.82, 22.38. Anal. Calcd. for Zn(C<sub>12</sub>H<sub>26</sub>N<sub>4</sub>)(NO<sub>3</sub>)<sub>2</sub>: C, 34.67; H, 6.30; N, 20.21%. Found: C, 34.56; H, 6.31; N, 19.96%.

**ZnCl<sub>2</sub>•3 (119):** In a glovebox, 45 mg (0.33 mmol) of anhydrous ZnCl<sub>2</sub> and 134 mg (0.330 mmol) of ligand **3** were transferred into a Schlenk flask. This sealed flask was then evacuated for about half an hour. Under N<sub>2</sub> protection and with stirring, 15 mL of MeCN (anhydrous) was added into the Schlenk flask to form a cloudy solution. After this was refluxed for 3 days, the white precipitate was centrifuged off and washed with dry benzene (2x8 mL) and acetone (2x8 mL). The removal of residual solvents in *vacuo* gave 158 mg (88%) of ZnCl<sub>2</sub>•3 as a white powder. <sup>1</sup>H NMR data in D<sub>2</sub>O:  $\delta$  7.33-7.47 (10H, m, phenyl), 4.24 and 3.93 (4H, AB,  $J = 14.2$  Hz, CH<sub>2</sub>Ph), 2.58-3.46 (20H, m), 2.16-2.25 (2H, m,  $\beta$ -CHH<sub>ax</sub>), 1.67 (2H broad d,  $J \sim 17$  Hz,  $\beta$ -CHH<sub>eq</sub>); in *d*<sub>6</sub>-DMSO:  $\delta$  7.28-7.42 (10H, m, phenyl), 4.37 and 3.99 (4H, AX,  $J = 14.1$  Hz, CH<sub>2</sub>Ph), 3.23-3.44 (8H, m, overlapped with the water signal), 2.78 (2H, broad t,  $J \sim 14$  Hz), 2.43-2.66 (6H, m, overlapped with DMSO), 2.30 (4H, broad t,  $J \sim 9$ Hz), 2.10 (2H, broad q,  $J \sim 14$  Hz,  $\beta$ -CHH<sub>ax</sub>), 1.50 (2H, broad d,  $J \sim 17$  Hz,  $\beta$ -CH<sub>eq</sub>H); <sup>13</sup>C{<sup>1</sup>H} in D<sub>2</sub>O:  $\delta$  133.35, 131.79, 129.21, 128.90, 58.77, 58.06 (two resonances overlapped), 54.26, 50.70, 42.78, 22.37; in *d*<sub>6</sub>-DMSO:  $\delta$  132.60, 132.26, 128.01, 127.93, 58.14 (two resonances overlapped), 57.33, 52.98, 48.97, 41.88, 22.00. Anal. Calcd. for ZnCl<sub>2</sub>C<sub>26</sub>H<sub>38</sub>N<sub>4</sub>: C, 57.52; H, 7.06; N, 10.32%. Found: C, 57.33; H, 6.85; N, 10.14%.

**Zn•3(μ-Cl)<sub>2</sub>-ZnCl<sub>2</sub> (120):** In a glovebox, 53 mg (0.19 mmol) of anhydrous ZnCl<sub>2</sub> and 79 mg (0.19 mmol) of ligand **3** were transferred to a Schlenk flask. The sealed flask was evacuated for about half an hour. Under N<sub>2</sub> protection, 15 mL of anhydrous MeCN was added and the resulting cloudy solution was refluxed for 3 days. Then the white precipitate was centrifuged off and washed by toluene (5 mL) and ethanol (8 mL). The removal of residual solvents *in vacuo* gave 120 mg of Zn•3(μ-Cl)<sub>2</sub>ZnCl<sub>2</sub> (92%) as a white powder. <sup>1</sup>H NMR data in D<sub>2</sub>O: δ 7.34-7.49 (10H, m, phenyl), 4.24 and 3.94 (4H, AX, *J* = 14.0 Hz, CH<sub>2</sub>Ph), 2.58-3.45 (20H, m), 2.10-2.29 (2H, m, β-CHH<sub>ax</sub>, overlapped with the CH<sub>3</sub>CN peak), 1.67 (2H broad d, *J* ~ 18 Hz, β-CHH<sub>eq</sub>); in *d*<sub>6</sub>-DMSO: δ 7.29-7.43 (10H, m, phenyl), 4.35 and 3.97 (4H, AX, *J* = 14.2 Hz, CH<sub>2</sub>Ph), 3.20-3.42 (8H, m, overlapped with water signal), 2.80 (2H, broad t, *J* ~ 14 Hz), 2.44-2.66 (6H, m, overlapped with the DMSO peaks), 2.32 (4H, broad t, *J* ~ 11 Hz), 2.11 (2H, broad q, *J* ~ 16 Hz, β-CHH<sub>ax</sub>), 1.50 (2H, broad d, *J* ~ 17 Hz, β-CH<sub>eq</sub>H); <sup>13</sup>C{<sup>1</sup>H} in D<sub>2</sub>O: δ 133.35, 131.80, 129.20, 128.90, 58.77, 58.11, 58.01, 54.26, 50.69, 42.82, 22.38; in *d*<sub>6</sub>-DMSO: 132.61, 132.11, 128.02, 127.96, 58.07, 57.26, 57.23, 52.93, 48.97, 41.81, 21.91. Anal. Calcd. for Zn<sub>2</sub>Cl<sub>4</sub>C<sub>26</sub>H<sub>38</sub>N<sub>4</sub>: C, 45.98; H, 5.64; N, 8.25 %. Found: C, 46.14; H, 5.60; N, 8.28%.

**ZnCl<sub>2</sub>•2 (121):** An amount of 41 mg (0.21 mmol) of ligand **2** and 29 mg (0.21 mmol) of ZnCl<sub>2</sub> were placed in a Schlenk flask. Under N<sub>2</sub> protection, 10 ml of absolute MeOH was added and this solution was refluxed for 10 hours forming a clear solution with a small amount of white precipitate which was centrifuged off from the methanol solution. Et<sub>2</sub>O vapor diffusion into this solution yielded needle crystals. These crystals were washed by acetone and dissolved in MeOH. Et<sub>2</sub>O vapor diffusion into this solution yielded 44.5 mg

needle-like crystals (64%). This complex is not soluble in MeCN and  $\text{CHCl}_3$ . IR (KBr):  $3186\text{ cm}^{-1}(\nu_{\text{NH}})$ .  $^1\text{H}$  NMR in  $D_2O$  (0.02 M solution, MeOH as internal reference):  $\delta$  3.78 (2H, broad s, NH), 3.52-3.61 (4H, m), 2.95 (4H, s, cross-bridging  $\text{CH}_2\text{CH}_2$ ), 2.93-3.01 (4H, m), 2.89 (4H, td,  $J = 11.9, 6.4$  Hz), 2.76 (4H, br dddd,  $J = 15, 11, 9, 4$  Hz); in  $CD_3OD$  (0.0066 M solution):  $\delta$  3.92 (2H, broad s, NH), 3.54 (4H, ddd,  $J = 14.5, 9.3, 7.1$  Hz), 3.17 (4H, td,  $J = 11.6, 7.3$  Hz), 2.93 (4H, s, cross-bridging  $\text{CH}_2\text{CH}_2$ ), 2.81 (4H, dd,  $J = 11.9, 6.1$  Hz), 2.69-2.79 (4H, m); in  $D_2O$  (0.02 M N-deuterated complex, both MeOH and MeCN as internal references):  $\delta$  3.56 (4H, dd,  $J = 14.5, 6.2$  Hz), 2.94 (4H, s, cross-bridging  $\text{CH}_2\text{CH}_2$ ), 2.84-2.98 (8H, m), 2.74 (4H, ddd,  $J = 14.9, 11.4, 6.5$  Hz); in  $CD_3OD$  (0.0066 M solution):  $\delta$  3.54 (4H, dd,  $J = 14.8, 7.2$  Hz), 3.15 (4H, td,  $J = 11.7, 7.4$  Hz), 2.93 (4H, s, cross-bridging  $\text{CH}_2\text{CH}_2$ ), 2.82 (4H, dd,  $J = 11.7, 5.9$  Hz), 2.74 (4H, ddd,  $J = 14.6, 11.6, 5.9$  Hz); in  $d_6$ -DMSO:  $\delta$  4.09 (2H, broad s, NH) 3.27-3.44 (4H, m, overlapping with the  $\text{H}_2\text{O}$  peak), 3.02-3.15 (4H, m), 2.77 (4H, s, cross-bridging  $\text{CH}_2\text{CH}_2$ ), 2.39-2.67 (8H, m, overlapping with the DMSO peak);  $^{13}\text{C}\{^1\text{H}\}$  NMR of N-deuterated complex in  $D_2O$  (0.02 M solution):  $\delta$  56.36, 50.67, 50.34; in  $CD_3OD$  (0.0066 M N-deuterated complex):  $\delta$  57.26, 51.77, 51.21; in  $d_6$ -DMSO:  $\delta$  55.45, 49.62, 49.34. Anal. Calcd. for  $\text{ZnCl}_2(\text{C}_{10}\text{H}_{22}\text{N}_4)$ : C, 35.90; H, 6.63; N, 16.74%. Found: C, 35.86; H, 6.79; N, 16.55%.

**$[\text{Zn}\cdot 2(\text{OH}_2)_2](\text{ClO}_4)_2$  (122)**: A MeOH solution (4 mL) of ligand **2** (56.8 mg, 0.287 mmol) was mixed with a MeOH solution (6 mL) of  $\text{Zn}(\text{ClO}_4)_2\cdot 6\text{H}_2\text{O}$  (109.8 mg, 0.295 mmol). This reaction mixture was refluxed for one day to afford a clear solution.  $\text{Et}_2\text{O}$  vapor diffusion into this solution yielded 106 mg (80%) of colorless crystals. IR (KBr): 3198,  $3173\text{ cm}^{-1}(\nu_{\text{NH}})$ .  $^1\text{H}$  NMR in  $D_2O$  (MeOH as internal reference):  $\delta$  3.76 (2H, broad s, NH),



3.52-3.61 (4H, m), 2.95 (4H, s, cross-bridging  $CH_2CH_2$ ), 2.93-3.00 (4H, m), 2.89 (4H, td,  $J = 11.7, 6.5$  Hz), 2.76 (4H, br dddd,  $J = 16, 12, 7, 4$  Hz); in  $CD_3OD$ :  $\delta$  4.22 (2H, broad s, NH), 3.53-3.69 (4H, m), 3.00 (4H, s, cross-bridging  $CH_2CH_2$ ), 2.93-3.03 (4H, m), 2.79-2.89 (8H, m); N-deuterated complex in  $D_2O$  (MeOH as internal reference): 3.56 (4H, dd,  $J = 11.7, 6.5$  Hz), 2.95 (4H, s, cross-bridging  $CH_2CH_2$ ), 2.93-3.00 (4H, m), 2.88 (4H, td,  $J = 11.8, 6.7$  Hz), 2.75 (4H, ddd,  $J = 14.8, 11.6, 6.3$  Hz); N-deuterated complex in  $CD_3OD$ :  $\delta$  3.54-3.66 (4H, m), 2.99 (4H, s, cross-bridging  $CH_2CH_2$ ), 2.93-3.03 (4H, m), 2.77-2.93 (8H, m); in  $CD_3CN$ :  $\delta$  3.43-3.60 (6H, m), 2.79-2.96 (10H, m), 2.64 (4H, br dddd,  $J = 16, 12, 7, 4$  Hz);  $^{13}C\{^1H\}$  in  $D_2O$ :  $\delta$  56.42, 50.69, 50.50;  $D_2O$  (N-deuterated complex, MeOH as internal reference):  $\delta$  56.40, 50.70, 50.38; in  $CD_3CN$ :  $\delta$  56.75, 51.27, 50.86; in  $CD_3OD$ : 57.38, 51.68, 51.56; in  $CD_3OD$  (N-D complex): 57.39, 51.55, 51.53. Anal. Calcd. For  $ZnCl_2C_{10}H_{22}N_4O_8 \cdot 2.5H_2O$ : C, 23.66; H, 5.36; N, 11.04%. Found: C, 23.55; H, 5.32; N, 10.94%.

**$Zn \cdot 2(NO_3)_2$  (123):** To a solution of ligand **2** (105 mg, 0.528 mmol) in 5 mL of MeOH was added a MeOH solution (6 mL) of  $Zn(NO_3)_2 \cdot 6H_2O$  (157 mg, 0.528 mmol). The resulting clear solution was refluxed for two hours.  $Et_2O$  vapor diffusion into this clear solution yielded 174 mg (85%) of colorless crystals. IR (KBr): 3199, 3173  $cm^{-1}$  ( $\nu_{NH}$ ).  $^1H$  NMR in  $D_2O$ :  $\delta$  3.78 (2H, broad s, NH), 3.52-3.62 (4H, m), 2.94 (4H, s, cross-bridging  $CH_2CH_2$ ), 2.93-3.00 (4H, m), 2.88 (4H, td,  $J = 11.8, 6.5$  Hz), 2.74 (4H, br dddd,  $J = 16, 12, 7, 4$  Hz); N-deuterated complex in  $D_2O$ :  $\delta$  3.56 (4H, dd,  $J = 14.6, 6.4$  Hz), 2.94 (4H, s, cross-bridging  $CH_2CH_2$ ), 2.93-3.00 (4H, m), 2.88 (4H, td,  $J = 11.8, 6.7$  Hz), 2.75 (4H, ddd,  $J = 14.7, 11.5, 6.3$  Hz); in  $CD_3OD$ :  $\delta$  4.10 (2H, broad s, NH), 3.53-3.62 (4H, m),

2.96 (4H, s, cross-bridging  $CH_2CH_2$ ), 2.90-2.98 (8H, m), 2.74-2.87 (4H, m); N-deuterated complex in  $CD_3OD$ :  $\delta$  3.59 (2H, dd, 5.3, 1.8 Hz), 3.55 (2H, t, 3.8 Hz), 2.96 (4H, s, cross-bridging  $CH_2CH_2$ ), 2.89-2.99 (8H, m), 2.73-2.88 (4H, m); in  $CD_3CN$ :  $\delta$  3.50-3.61 (4H, m), 3.46 (2H, broad s, NH), 2.82-2.96 (12H, m), 2.65 (4H, dddd,  $J = 16, 12, 7, 4$  Hz);  $^{13}C\{^1H\}$  in  $D_2O$  (N-D complex):  $\delta$  56.43, 50.72, 50.39; in  $CD_3OD$  (N-D complex):  $\delta$  57.57, 51.38, 51.29; in  $CD_3CN$ :  $\delta$  57.56, 51.02 (include two overlapping resonances); Anal. Calcd. For  $Zn(NO_3)_2C_{10}H_{22}N_4 \cdot 0.5H_2O$ : C, 30.28; H, 5.84; N, 21.18%. Found: C, 30.62; H, 6.30; N, 20.94%.

**ZnCl<sub>2</sub>•4 (124):** Method one: To a solution of ligand **4** (133 mg, 0.350 mmol) in absolute MeOH (5 mL), a MeOH solution (6 mL) of ZnCl<sub>2</sub> (47.8 mg, 0.351 mmol) was added dropwise. The resulting solution was refluxed for 15 hours to yield a very cloudy solution. This white precipitate was centrifuged out and dried *in vacuo* to give a white powder (102 mg) which was washed with CHCl<sub>3</sub>. Evaporation of this CHCl<sub>3</sub> extract solution yielded pure ZnCl<sub>2</sub>•4 (47.3 mg, 26%). Crystals suitable for X-ray analysis were grown by ether vapor diffusion into a chloroform solution of this complex.  $^1H$  NMR in  $CDCl_3$ :  $\delta$  7.28-7.38 (10H, m, phenyl), 4.62 (4H, s,  $CH_2Ph$ ), 4.15 (4H, br td,  $J = 12, 6$  Hz), 3.61-3.67 (4H, m), 2.86 (4H, s, cross-bridging  $CH_2CH_2$ ), 2.53-2.64 (8H, m); in  $D_2O$  (a saturated solution): 7.45-7.54 (10H, br m, phenyl), 4.12 (4H, s,  $CH_2Ph$ ), 3.68 (4H, dd,  $J = 15.3, 6.1$  Hz), 3.14-3.23 (4H, m), 2.99 (4H, br s, cross-bridging  $CH_2CH_2$ ), 2.94-3.06 (4H, m), 2.76-2.88 (4H, m);  $^{13}C\{^1H\}$  in  $CDCl_3$ :  $\delta$  135.95, 131.14, 128.56, 127.85, 61.13, 56.01, 55.84, 52.41; in  $D_2O$ : 134.96, 131.60, 129.33, 129.07, 59.45, 55.81, 55.52, 51.07. Anal.

Calcd. for  $\text{ZnCl}_2\text{C}_{24}\text{H}_{34}\text{N}_4$ : C, 55.99; H, 6.66; N, 10.88%. Found: C, 55.44; H, 6.74; N, 10.79%. Anal. Calcd. for  $\text{ZnCl}_2\text{C}_{24}\text{H}_{34}\text{N}_4(\text{H}_2\text{O})_{0.5}$ : C, 55.03; H, 6.73; N, 10.70%.

Method 2: 103 mg (0.272 mmol) of **4** and 37 mg of  $\text{ZnCl}_2$  (0.27 mmol) were weighed in a glovebox. The sealed flask was taken out of the glovebox and kept in vacuo for about half an hour. Under  $\text{N}_2$  protection, 10 mL of absolute MeOH was added into the Schlenk flask by using a syringe to form a clear solution that was refluxed for 10 hours. A white precipitate formed was centrifuged from this MeOH solution and washed by MeOH (5 mL). The removal of residual solvents in vacuo gave a white powder (110.1 mg, 77%).  $^1\text{H}$  NMR spectrum of this white powder in  $\text{CDCl}_3$  showed only the same  $^1\text{H}$  NMR spectrum as that of  $\text{ZnCl}_2\cdot\mathbf{4}$ .

**$\text{CdCl}_2\cdot\mathbf{1}$  (125)**: To a refluxing suspension of  $\text{CdCl}_2$  (112 mg, 0.611 mmol) in 8 mL methanol was added a solution of ligand **1** (139 mg, 0.612 mmol) in methanol (8 mL). After refluxing overnight, a clear solution was formed. At room temperature, diethyl ether was diffused in to yield 154 mg (61%) of colorless crystals. IR (KBr): 3248, 3220  $\text{cm}^{-1}$  ( $\nu_{\text{NH}}$ ).  $^1\text{H}$  NMR in  $D_2O$  (0.1 M solution, MeOH and MeCN as internal reference):  $\delta$  3.48 (2H, broad s, NH), 3.21 (2H, tt,  $J = 13.0, 2.6$  Hz), 2.79-3.12 (16H, m), 2.40-2.55 (2H, m), 2.26 (2H, dtt,  $J = 15.9, 13.1, 2.7$  Hz,  $\beta\text{-CH}_{\text{ax}}\text{H}$ ), 1.57 (2H, broad d,  $J = 17$  Hz,  $\beta\text{-CH}_{\text{eq}}\text{H}$ ); in  $D_2O$  (N-D complex): 3.19 (2H, td,  $J = 13.1, 2.4$  Hz), 2.80-3.12 (16H, m), 2.41-2.57 (2H, m), 2.27 (2H, dtt,  $J = 16.8, 13.1, 2.7$  Hz,  $\beta\text{-CH}_{\text{ax}}\text{H}$ ), 1.57 (2H, broad d,  $J = 17$  Hz,  $\beta\text{-CH}_{\text{eq}}\text{H}$ ); in  $\text{CDCl}_3$ :  $\delta$  3.69 (4H, tt,  $J = 13.1, 2.8$  Hz), 3.64 (2H, td,  $J = 10.4, 2.1$  Hz), 3.52 (2H, td,  $J = 13.0, 4.5$  Hz), 3.08 (2H, ddd,  $J = 13.4, 7.6, 4.4$  Hz), 2.91-3.04 (4H, m), 2.58-2.88 (8H, m), 2.19-2.30 (2H, m), 2.11 (2H, qp,  $J = 13.1, 2.7$  Hz), 1.57 (2H,

broad dp,  $J = 16.6, 2.7$  Hz);  $^{13}\text{C}\{^1\text{H}\}$  data of N-D complex in  $D_2O$ :  $\delta$  59.79, 58.59 ( $^{111}\text{Cd}$ ,  $^{113}\text{Cd}$  satellites,  $J = 7.3$  Hz), 49.86 ( $^{111}\text{Cd}$ ,  $^{113}\text{Cd}$  satellites,  $J = 11.3$  Hz), 49.35 ( $^{111}\text{Cd}$ ,  $^{113}\text{Cd}$  satellites,  $J = 7$  Hz), 40.94, 22.94 ( $^{111}\text{Cd}$ ,  $^{113}\text{Cd}$  satellites,  $^3J = 7.3$  Hz); in  $CDCl_3$ :  $\delta$  58.61 ( $^{111}\text{Cd}$ ,  $^{113}\text{Cd}$  satellites,  $J = 5$  Hz), 58.37, 49.90 ( $^{111}\text{Cd}$ ,  $^{113}\text{Cd}$  satellites,  $J = 9.3$  Hz), 48.24 ( $^{111}\text{Cd}$ ,  $^{113}\text{Cd}$  satellites,  $J = 5.3$  Hz), 41.24, 23.26 ( $^{111}\text{Cd}$ ,  $^{113}\text{Cd}$  satellites,  $^3J = 6.6$  Hz).  $^{113}\text{Cd}\{^1\text{H}\}$  NMR chemical shift of 0.10 M  $\text{CdCl}_2 \cdot \mathbf{1}$  in  $D_2O$ :  $\delta$  326 (ref. to 3M  $\text{CdSO}_4$  in  $D_2O$ : -3 ppm). Anal. Calcd. for  $\text{CdCl}_2(\text{C}_{12}\text{H}_{26}\text{N}_4)$ : C, 35.18; H, 6.40; N, 13.68%. Found: C, 34.79; H, 6.55; N, 13.34%.

**$\text{Cd} \cdot \mathbf{1}(\text{NO}_3)_2$  (126)**: A solution of  $\text{Cd}(\text{NO}_3)_2 \cdot 4\text{H}_2\text{O}$  (58.1 mg, 0.188 mmol) in 2 mL of methanol was mixed with a methanol solution (8 mL) of ligand **1** (44.7 mg, 0.197 mmol). The resulting solution was refluxed overnight to afford a clear solution.  $\text{Et}_2\text{O}$  vapor diffusion into this yielded 74.2 mg (85%) of colorless crystals of the complex. IR (KBr):  $3259\text{ cm}^{-1}$  ( $\nu_{\text{NH}}$ ).  $^1\text{H}$  NMR in  $D_2O$  (0.03 M):  $\delta$  3.74 (2H, broad s, NH), 2.88–3.15 (16H, m), 2.78 (2H, td,  $J = 12.9, 5.0$  Hz), 2.54–2.62 (2H, m), 2.17–2.35 (2H, m,  $\beta\text{-CH}_{\text{ax}}\text{H}$ ), 1.60 (2H, broad dp,  $J = 17$  Hz, 3 Hz,  $\beta\text{-CH}_{\text{eq}}\text{H}$ ); in  $CD_3\text{CN}$ :  $\delta$  3.15 (2H, tt,  $J = 13.1, 2.9$  Hz), 2.66–3.11 (18H, m), 2.31–2.40 (2H, m), 2.13–2.27 (2H, m, overlapped with the water peak), 1.51 (2H, broad dp,  $J = 16.9, 2.8$  Hz,  $\beta\text{-CH}_{\text{eq}}\text{H}$ ); in  $CDCl_3$ :  $\delta$  3.34 (2H, tt,  $J = 13.3, 2.4$  Hz), 2.84–3.21 (12H, m), 2.65–2.81 (6H, m), 2.31 (2H, dd,  $J = 12.2, 4.3$  Hz), 2.07 (2H, br qp,  $J = 13, 3$  Hz,  $\beta\text{-CH}_{\text{ax}}\text{H}$ ), 1.52 (2H, broad d,  $J = 17$  Hz,  $\beta\text{-CH}_{\text{eq}}\text{H}$ );  $^{13}\text{C}\{^1\text{H}\}$  in  $D_2O$ :  $\delta$  60.27, 58.70 ( $^{111}\text{Cd}$ ,  $^{113}\text{Cd}$  satellites,  $J = 6.6$  Hz), 49.99, 49.97 ( $^{111}\text{Cd}$ ,  $^{113}\text{Cd}$  satellites,  $J = 10.6$  Hz), 41.02, 22.93 ( $^{111}\text{Cd}$ ,  $^{113}\text{Cd}$  satellites,  $^3J = 8.6$  Hz); in  $CD_3\text{CN}$ :  $\delta$  60.38, 59.71 ( $^{111}\text{Cd}$ ,  $^{113}\text{Cd}$  satellites,  $J = 6.4$  Hz), 50.60 ( $^{111}\text{Cd}$ ,  $^{113}\text{Cd}$  satellites,  $J = 10.2$  Hz), 50.00

( $^{111}\text{Cd}$ ,  $^{113}\text{Cd}$  satellites,  $J = 7.0$  Hz), 41.89, 23.77 ( $^{111}\text{Cd}$ ,  $^{113}\text{Cd}$  satellites,  $^3J = 7.6$  Hz); in  $\text{CDCl}_3$ :  $\delta$  59.46, 58.64 ( $^{111}\text{Cd}$ ,  $^{113}\text{Cd}$  satellites,  $J = 6.6$  Hz), 50.12 ( $^{111}\text{Cd}$ ,  $^{113}\text{Cd}$  satellites,  $J = 10.6$  Hz), 48.97 ( $^{111}\text{Cd}$ ,  $^{113}\text{Cd}$  satellites,  $J = 6.6$  Hz), 41.23, 23.17 ( $^{111}\text{Cd}$ ,  $^{113}\text{Cd}$  satellites,  $^3J = 8.0$  Hz).  $^{113}\text{Cd}\{^1\text{H}\}$  NMR chemical shift of 0.10 M  $\text{Cd}(\text{NO}_3)_2 \cdot \mathbf{1}$  in  $\text{D}_2\text{O}$ :  $\delta$  262 (ref. to 3M  $\text{CdSO}_4$  in  $\text{D}_2\text{O}$ : -3 ppm). Anal. Calcd. for  $\text{CdC}_{12}\text{H}_{26}\text{N}_6\text{O}_6$ : C, 31.14; H, 5.66; N, 18.16%. Found: C, 31.08; H, 5.67; N, 18.01%.

**$\text{Cd} \cdot \mathbf{1}(\text{ClO}_4)_2$  (127):** To a solution of  $\text{Cd}(\text{ClO}_4)_2 \cdot 6\text{H}_2\text{O}$  (60 mg, 0.14 mmol) in 2 mL of methanol was added a methanol solution (6 mL) of ligand **1** (33 mg, 0.14 mmol). The resulting solution was refluxed overnight to afford a clear solution.  $\text{Et}_2\text{O}$  vapor diffusion into this yielded 59 mg (63 %) of colorless crystals. IR (KBr):  $3284\text{ cm}^{-1}$  ( $\nu_{\text{NH}}$ ).  $^1\text{H}$  NMR (0.13M) in  $\text{D}_2\text{O}$  (MeOH internal reference):  $\delta$  3.72 (2H br s, NH), 2.88–3.19 (16H, m), 2.78 (2H, td,  $J = 12.9, 5.0$  Hz), 2.54–2.63 (2H, m), 2.28 (2H, dt,  $J = 16.2, 10.7, 4.9$  Hz,  $\beta\text{-CH}_{\text{ax}}\text{H}$ ), 1.63 (2H, br d,  $J = 17$  Hz,  $\beta\text{-CH}_{\text{eq}}\text{H}$ ); in  $\text{CD}_3\text{CN}$ :  $\delta$  3.41 (2H, br, NH), 3.11 (2H, tt,  $J = 13.2, 2.5$  Hz), 2.72–3.07 (16H, m), 2.47–2.56 (2H, m), 2.12–2.27 (2H, m,  $\beta\text{-CH}_{\text{ax}}\text{H}$ ), 1.56 (2H, br dp,  $J = 18, 3$  Hz,  $\beta\text{-CH}_{\text{eq}}\text{H}$ );  $^{13}\text{C}\{^1\text{H}\}$  in  $\text{D}_2\text{O}$  (MeOH internal reference):  $\delta$  60.29, 58.72 ( $^{111}\text{Cd}$ ,  $^{113}\text{Cd}$  satellites,  $J = 6.0$  Hz), 50.03, 49.96, 41.02, 22.92 ( $^{111}\text{Cd}$ ,  $^{113}\text{Cd}$  satellites,  $^3J = 8$  Hz); in  $\text{CD}_3\text{CN}$ :  $\delta$  60.18, 59.14 ( $^{111}\text{Cd}$ ,  $^{113}\text{Cd}$  satellites,  $J = 6$  Hz), 50.18 ( $^{111}\text{Cd}$ ,  $^{113}\text{Cd}$  satellites,  $J = 11$  Hz), 49.79 ( $^{111}\text{Cd}$ ,  $^{113}\text{Cd}$  satellites,  $J = 7$  Hz), 41.45 ( $^{111}\text{Cd}$ ,  $^{113}\text{Cd}$  satellites,  $J = 4$  Hz), 23.20 ( $^{111}\text{Cd}$ ,  $^{113}\text{Cd}$  satellites,  $^3J = 8$  Hz).  $^{113}\text{Cd}\{^1\text{H}\}$  NMR chemical shift of 0.13 M  $\text{Cd}(\text{ClO}_4)_2 \cdot \mathbf{1}$  in  $\text{D}_2\text{O}$ :  $\delta$  267 (ref. to 3M  $\text{CdSO}_4$  in  $\text{D}_2\text{O}$ : -3 ppm). Anal. Calcd. for  $\text{Cd}(\text{ClO}_4)_2(\text{C}_{12}\text{H}_{26}\text{N}_4)$ : C, 26.81; H, 4.87; N, 10.42%. Found: C, 26.66; H, 4.82; N, 10.00%.

**CdCl<sub>2</sub>•3 (128):** Amounts of 73.6 mg (0.402 mmol) of CdCl<sub>2</sub> and 164 mg (0.403 mmol) of ligand **3** were dried *in vacuo* overnight in a Schlenk flask. Then under N<sub>2</sub> protection and with stirring, 10 mL of MeCN (anhydrous) was added by a syringe to form a cloudy solution. After this solution was refluxed for 3 days, the white precipitate was centrifuged off and washed with more MeCN (2x10 mL). Drying of the residue gave 182 mg (77%) of CdCl<sub>2</sub>•**3** as a white powder <sup>1</sup>H NMR in CDCl<sub>3</sub>: δ 7.22-7.37 (10H, m, Ph), 4.65 and 4.39 (4H, AB, *J* = 14.6 Hz), 3.93 (2H, br t, *J* = 12 Hz), 3.60-3.74 (4H, m), 2.78-2.93 (6H, m), 2.51-2.67 (6H, m), 2.23 (2H, broad dd, *J* = 13, 2 Hz), 1.92 (2H, broad q, *J* = 14 Hz), 1.54-1.70 (2H, m, overlapped with the solvent peaks); <sup>13</sup>C{<sup>1</sup>H} in CDCl<sub>3</sub>: δ 132.81, 132.58 (<sup>111</sup>Cd, <sup>113</sup>Cd satellites, <sup>3</sup>*J* = 6 Hz), 128.18, 128.04, 59.61 (<sup>111</sup>Cd, <sup>113</sup>Cd satellites, *J* = 8 Hz), 58.95, 56.23, 54.41 (<sup>111</sup>Cd, <sup>113</sup>Cd satellites, *J* = 5 Hz), 49.50 (<sup>111</sup>Cd, <sup>113</sup>Cd satellites, *J* = 11.9 Hz), 42.88, 24.69 (<sup>111</sup>Cd, <sup>113</sup>Cd satellites, *J* = 6 Hz). Anal. Calcd. for CdCl<sub>2</sub>(C<sub>26</sub>H<sub>38</sub>N<sub>4</sub>): C, 52.94; H, 6.49; N, 9.50%. Found: C, 53.18; H, 6.28; N, 9.52%.

**CdCl<sub>2</sub>•2 (129):** A mixture of CdCl<sub>2</sub> (43.0 mg, 0.235 mmol) and ligand **2** (47.1 mg, 0.238 mmol) was dried *in vacuo* for 1 hour. Then under N<sub>2</sub> protection, 23 mL of anhydrous MeOH was added to this mixture. The resulting solution was refluxed for 2 days to afford a clear solution. Et<sub>2</sub>O vapor diffusion into this clear solution yielded 54.9 mg (61%) of colorless crystals. IR (KBr): 3248 cm<sup>-1</sup> (ν<sub>NH</sub>). <sup>1</sup>H NMR of N-D complex in D<sub>2</sub>O (0.045 M solution): δ 3.56 (4H, dd, *J* = 15.1 Hz, 6.2 Hz), 2.87 (4H, s, cross-bridging CH<sub>2</sub>CH<sub>2</sub>, <sup>111</sup>Cd, <sup>113</sup>Cd satellites, <sup>3</sup>*J* = 25 Hz), 2.80-3.04 (8H, m), 2.73 (4H, br ddd, *J* = 15, 12, 5 Hz); in CD<sub>3</sub>OD (0.022 M): δ 3.90 (2H, broad s, NH), 3.46-3.58 (4H, m), 3.28-3.38 (4H, m, overlapped with the methanol peaks), 2.86 (4H, s, cross-bridging CH<sub>2</sub>CH<sub>2</sub>, <sup>111</sup>Cd,

$^{113}\text{Cd}$  satellites,  $^3J = 11.6$  Hz), 2.65-2.77 (8H, m); N-H complex in  $\text{CD}_3\text{OD}$  (0.022 M N-D complex):  $\delta$  3.47-3.57 (4H, m), 3.24-3.38 (4H, m, overlapped with the methanol peaks), 2.86 (4H, s, cross-bridging  $\text{CH}_2\text{CH}_2$ ,  $^{111}\text{Cd}$ ,  $^{113}\text{Cd}$  satellites,  $^3J = 11.6$  Hz), 2.65-2.76 (8H, m); in  $\text{CD}_3\text{CN}$ :  $\delta$  3.38-3.57 (8H, m), 3.00 (2H, s, NH), 2.75 (4H, s, cross-bridging  $\text{CH}_2\text{CH}_2$ ,  $^{111}\text{Cd}$ ,  $^{113}\text{Cd}$  satellites,  $^3J = 10.6$  Hz), 2.50-2.65 (8H, m);  $^{13}\text{C}\{^1\text{H}\}$  in  $\text{D}_2\text{O}$  (0.045 M N-D complex):  $\delta$  57.15 ( $^{111}\text{Cd}$ ,  $^{113}\text{Cd}$  satellites,  $J = 8.6$  Hz), 50.64, 48.14 ( $^{111}\text{Cd}$ ,  $^{113}\text{Cd}$  satellites,  $J = 14.6$  Hz); in  $\text{CD}_3\text{OD}$  (0.022 M N-D complex):  $\delta$  57.82 ( $^{111}\text{Cd}$ ,  $^{113}\text{Cd}$  satellites,  $J = 9.9$  Hz), 51.60, 49.44 (overlapped with the methanol signals); in  $\text{CD}_3\text{CN}$ :  $\delta$  57.45 ( $^{111}\text{Cd}$ ,  $^{113}\text{Cd}$  satellites,  $J = 9$  Hz), 51.72, 49.20 ( $^{111}\text{Cd}$ ,  $^{113}\text{Cd}$  satellites,  $J = 13$  Hz). Anal. Calcd. for  $\text{CdCl}_2\text{C}_{10}\text{H}_{22}\text{N}_4$ : C, 31.47; H, 5.81; N, 14.68%. Found: C, 31.41; H, 5.85; N, 14.49%.

**$\text{Cd}\cdot 2(\text{ClO}_4)_2$  (130):** Absolute MeOH (15 mL) was added to a mixture of  $\text{Cd}(\text{ClO}_4)_2\cdot 6\text{H}_2\text{O}$  (255 mg, 0.608 mmol) and ligand **2** (121 mg, 0.0610 mmol). The resulting cloudy solution was refluxed for 2 days to afford a clear solution.  $\text{Et}_2\text{O}$  vapor diffusion into this yielded 226 mg (68 %) of colorless crystals. IR (KBr):  $3260\text{ cm}^{-1}$  ( $\nu_{\text{NH}}$ ).  $^1\text{H}$  NMR of N-deuterated complex in  $\text{D}_2\text{O}$  (MeOH internal reference):  $\delta$  3.52-3.63 (4H, m), 2.72-2.99 (12H, m), 2.88 (4H, s, cross-bridging  $\text{CH}_2\text{CH}_2$ );  $^1\text{H}$  NMR of N-deuterated complex in  $\text{CD}_3\text{OD}$ :  $\delta$  3.53-3.68 (4H, m), 2.76-3.01 (12H, m), 2.93 (4H, s, cross-bridging  $\text{CH}_2\text{CH}_2$ ); in  $\text{CD}_3\text{CN}$ :  $\delta$  3.40-3.64 (6H, m, including br NH), 2.74-2.94 (8H, m), 2.80 (4H, s, cross-bridging  $\text{CH}_2\text{CH}_2$ ), 2.61-2.72 (4H, m);  $^{13}\text{C}\{^1\text{H}\}$  in  $\text{D}_2\text{O}$  (N-D complex, MeOH internal reference):  $\delta$  57.60 ( $^{111}\text{Cd}$ ,  $^{113}\text{Cd}$  satellites,  $J = 7$  Hz), 50.69, 47.86 ( $^{111}\text{Cd}$ ,  $^{113}\text{Cd}$  satellites,  $J = 14.6$  Hz); in  $\text{CD}_3\text{OD}$  (N-D complex):  $\delta$  58.62 ( $^{111}\text{Cd}$ ,  $^{113}\text{Cd}$  satellites,  $J = 8.6$

Hz), 51.74, 48.81; in  $CD_3CN$ :  $\delta$  57.81 ( $^{111}Cd$ ,  $^{113}Cd$  satellites,  $J \sim 10$  Hz), 51.25, 48.48 ( $^{111}Cd$ ,  $^{113}Cd$  satellites,  $J = 15.2$  Hz). Anal. Calcd. for  $CdCl_2C_{10}H_{22}N_4O_8 \cdot 2H_2O$ : C, 22.01; H, 4.80; N, 10.27%. Found: C, 21.84; H, 4.78; N, 10.14%.

[ $Cd \cdot 2(\eta^2-NO_3)_2$ ] (131): Amounts of 22.6 mg (0.0732 mmol) of  $Cd(NO_3)_2 \cdot 4H_2O$  and 14.5 mg (0.0731 mmol) of **2** were dissolved together in 7 mL of MeOH to form a clear solution. This was refluxed for 23 hours. Needle-like crystals formed after  $Et_2O$  vapor diffusion into this MeOH solution. After drying *in vacuo*, 17.6 mg (54%) of these crystals were obtained. IR (KBr):  $3292\text{ cm}^{-1}$  ( $\nu_{NH}$ ),  $1442$ ,  $1298\text{ cm}^{-1}$  (br,  $\nu_{NO}$ );  $^1H$  NMR of N-deuterated complex in  $D_2O$  (0.020 M solution, MeOH internal reference):  $\delta$  3.52-3.65 (4H, m), 2.71-3.00 (12H, m), 2.88 (4H, s, cross-bridging  $CH_2CH_2$ ); N-H complex in  $CD_3OD$  (0.020 M solution):  $\delta$  4.11(2H, broad t,  $J = 10$  Hz, NH), 3.55 (4H, dddd with shoulders due to coupling to  $^{111,113}Cd$ ,  $J = 16.4$  Hz, 11.4 Hz, 5.1 Hz, 1.9 Hz), 2.84-2.95 (8H, m), 2.90 (4H, s, cross-bridging  $CH_2CH_2$ ), 2.79 (4H, dddd,  $J = 17.4$  Hz, 11.4 Hz, 5.4 Hz, 3.2 Hz); N-deuterated complex in  $CD_3OD$  (0.020 M solution):  $\delta$  3.54 (4H, ddd with shoulders due to coupling to  $^{111,113}Cd$ ,  $J = 14.4$  Hz, 4.4 Hz, 1.8 Hz), 2.84-2.95 (8H, m), 2.90 (4H, s, cross-bridging  $CH_2CH_2$ ), 2.78 (4H, ddd,  $J = 17.2$  Hz, 11.1 Hz, 5.8 Hz); in  $CD_3CN$ :  $\delta$  3.43-3.56 (4H, m), 3.09 (2 H, broad s, NH), 2.94 (4H, td,  $J = 12.2$  Hz, 6.7 Hz), 2.58-2.85 (8H, m), 2.79 (4H, s, cross-bridging  $CH_2CH_2$ );  $^{13}C\{^1H\}$  in  $D_2O$  (0.020 M N-D complex, MeOH internal reference):  $\delta$  57.57 ( $^{111}Cd$ ,  $^{113}Cd$  satellites,  $J \sim 8$  Hz), 50.69, 47.93 ( $^{111}Cd$ ,  $^{113}Cd$  satellites,  $J = 14$  Hz); in  $CD_3OD$  (0.020 M N-D complex):  $\delta$  58.62 ( $^{111}Cd$ ,  $^{113}Cd$  satellites,  $J \sim 9$  Hz), 51.47, 49.11 (overlapped with the solvent peaks). Anal. Calcd. for  $CdC_{10}H_{22}N_6O_6 \cdot 0.2Et_2O$ : C, 28.86; H, 5.38; N, 18.69%. Found: C, 28.81; H,



5.37; N, 18.69%. The presence of Et<sub>2</sub>O in the sample for CHN analyses was supported by its <sup>1</sup>H and <sup>13</sup>C{<sup>1</sup>H} NMR spectra in CD<sub>3</sub>CN.

**CdCl<sub>2</sub>•4 (132):** Amounts of 61.8 mg (0.337 mmol) of CdCl<sub>2</sub> and 125.9 mg (0.333 mmol) of ligand **4** were dried *in vacuo* overnight in a Schlenk flask. Then under N<sub>2</sub> protection and with stirring, 15 mL of anhydrous MeCN was added to give a cloudy solution. After this cloudy solution was refluxed for 3 days, the white precipitate was centrifuged off from the solution and washed with MeCN (2x6 mL) and dried to give 117.9 mg (63%) of CdCl<sub>2</sub>•4 as a white powder. <sup>1</sup>H NMR in CDCl<sub>3</sub>: δ 7.31-7.40 (10H, m, phenyl), 4.47 (4H, s, CH<sub>2</sub>Ph), 4.05 (2H, t, *J* = 13.3 Hz), 4.03 (2H, t, *J* = 11.6 Hz), 3.61-3.71 (4H, m), 2.80 (4H, s, cross-bridging CH<sub>2</sub>CH<sub>2</sub>, <sup>111</sup>Cd, <sup>113</sup>Cd satellites, <sup>3</sup>*J* = 11.6 Hz), 2.60-2.71 (8H, m); <sup>13</sup>C{<sup>1</sup>H} in CDCl<sub>3</sub>: δ 135.39 (<sup>111</sup>Cd, <sup>113</sup>Cd satellites, <sup>3</sup>*J* = 5.3 Hz), 130.61, 128.75, 128.04, 61.20, 56.77, 55.99, 47.13 (<sup>111</sup>Cd, <sup>113</sup>Cd satellites, *J* = 14 Hz). Anal. Calcd. for CdCl<sub>2</sub>C<sub>24</sub>H<sub>34</sub>N<sub>4</sub>: C, 51.30; H, 6.10; N, 9.97%. Found: C, 51.41; H, 5.93; N, 9.85%.

**[HgCl<sub>2</sub>(μ-1)]<sub>2</sub> (133):** To a solution of **1** (32.5 mg, 0.144 mmol) in absolute MeOH (5 mL), a MeOH solution (7 mL) of HgCl<sub>2</sub> (38.0 mg, 0.140 mmol) was added dropwise. The resulting solution was refluxed for five days to yield a clear solution. The diffusion of Et<sub>2</sub>O vapor into this solution yielded block-shaped crystals (47.3 mg, 68%). IR (KBr): 3078 cm<sup>-1</sup> (ν<sub>NH</sub>). <sup>1</sup>H NMR of N-D complex in D<sub>2</sub>O: δ 3.34 (2H, td, *J* = 13.0, 2.6 Hz), 3.23 (2H, broad dd, *J* = 15, 4 Hz), 2.82-3.13 (14H, m), 2.58 (2H, ddd, *J* = 12.5, 4.0, 1.1 Hz), 2.30 (2H, dt, *J* = 17.1, 12.5, 2.6 Hz, β-CH<sub>ax</sub>H), 1.62 (2H, broad dm, *J* = 17.4 Hz,

$\beta$ - $CH_{eq}H$ ); in  $CD_3OD$ :  $\delta$  3.52 (2H, td,  $J = 13.1, 2.8$  Hz), 3.23-3.3 (2H, m, overlapped with solvent), 2.92-3.12 (10H, m), 2.75-2.86 (2H, m), 2.69 (2H, broad d,  $J = 13$  Hz), 2.24-2.44 (4H, m), 1.52 (2H, br dp,  $J = 17, 3$  Hz);  $^{13}C\{^1H\}$  in  $D_2O$ :  $\delta$  60.88, 58.68, 51.06, 50.02, 40.82, 23.60; in  $CD_3OD$  (at 125.7 MHz):  $\delta$  60.63, 59.70 ( $^{199}Hg$  satellites,  $J = 42$  Hz), 50.76 ( $^{199}Hg$  satellites,  $J = 28$  Hz), 50.12 ( $^{199}Hg$  satellites,  $J = 27$  Hz), 41.41, 24.42 ( $^{199}Hg$  satellites,  $^3J = 25$  Hz). Anal. Calcd. for  $HgCl_2(C_{12}H_{26}N_4)$ : C, 28.95; H, 5.26; N, 11.25%. Found: C, 28.96; H, 5.23; N, 11.14%.

**HgCl<sub>2</sub>•2 (134)**: Amounts of 54 mg (0.199 mmol) of  $HgCl_2$  and 44 mg (0.222 mmol) of **2** were weighed in a glovebox and transferred into a Schlenk flask. Under nitrogen protection, 10 mL of anhydrous MeOH was added. This solution was refluxed for 12 hours to yield a clear solution from which clear needle-like crystals grew after  $Et_2O$  vapor diffusion. Removal of residual solvent from these crystals afforded 80.5 mg of  $HgCl_2\cdot 2$  (86%). IR (KBr):  $3240\text{ cm}^{-1}$  ( $\nu_{NH}$ ).  $^1H$  NMR of N-deuterated complex in  $D_2O$  (MeOH internal reference):  $\delta$  3.73 (4H, dd,  $J = 13.6, 5.6$  Hz,  $^{199}Hg$  satellites,  $J \sim 53$  Hz), 2.95 (4H, s, cross-bridging  $CH_2CH_2$ ), 2.73-3.03 (12H, m); in  $CD_3OD$  (500 MHz):  $\delta$  3.60 (4H, dd,  $J = 14.8, 6.5$  Hz;  $^{199}Hg$  satellites,  $J \sim 41$  Hz), 3.24 (4H, dt,  $J = 12, 7$  Hz), 2.88 (4H, s, cross-bridging  $CH_2CH_2$ ,  $^{199}Hg$  satellites,  $^3J = 44$  Hz), 2.72 (4H, ddd,  $J = 15.0, 11.8, 5.2$  Hz), 2.63 (4H, dd,  $J = 12.0, 5.5$  Hz,  $^{199}Hg$  satellites,  $J = 55$  Hz); in  $CD_3CN$ :  $\delta$  3.44-3.56 (4H, m), 3.37 (4H, dt,  $J = 11, 7$  Hz), 2.96 (2H, NH), 2.76 (4H, s, cross-bridging  $CH_2CH_2$ ,  $^{199}Hg$  satellites,  $^3J = 40$  Hz), 2.41-2.65 (8H, m);  $^{13}C\{^1H\}$  in  $D_2O$  (MeOH internal reference):  $\delta$  57.72 ( $^{199}Hg$  satellites,  $J = 42.9$  Hz), 49.57, 47.02 ( $^{199}Hg$  satellites,  $J \sim 40$  Hz); in  $CD_3OD$  (at 125.7 MHz):  $\delta$  58.51 ( $^{199}Hg$  satellites,  $J = 46$  Hz), 51.60, 48.62 ( $^{199}Hg$

satellites,  $J = 40$  Hz); in  $CD_3CN$ :  $\delta$  57.40, 51.11, 47.51. Anal. Calcd. for  $HgCl_2C_{10}H_{22}N_4$ : C, 25.57; H, 4.72; N, 11.93%. Found: C, 25.60; H, 4.82; N, 11.73%.

**$(HgCl_2)_6 \cdot (2)_4$  (135)**: Amounts of 52.5 mg (0.193 mmol) of  $HgCl_2$  and 38.0 mg (0.192 mmol) of **2** were weighed in air and transferred into a Schlenk flask. This mixture was kept in vacuum for 12 minutes. Then under nitrogen protection, 14 mL of anhydrous MeOH was added to form a clear solution. This solution was refluxed for 11 hours to yield a solution from which a mixture of clear crystals and a white precipitate fell out when cooled to room temperature. After standing under nitrogen for 4 days, the mixture of clear crystals and the white precipitate were separated from this solution and dried (36.1 mg). This mixture was redissolved in MeOH and ether vapor diffusion into this solution still yielded a mixture of clear crystals and a white precipitate. An X-ray structural determination of these crystals revealed that they have the composition of  $(HgCl_2)_6 \cdot (2)_4$ . IR (KBr):  $3262\text{ cm}^{-1}$  (b,  $\nu_{NH}$ ).  $^1H$  NMR in  $CD_3CN$  (NH/ND complex mixture):  $\delta$  3.52–3.67 (4H, m), 3.09–3.30 (5.2–5.5 H, m, including NH), 2.81 (4H, s, cross-bridging  $CH_2CH_2$ ,  $^{199}Hg$  satellites,  $^3J = 40$  Hz), 2.57–2.70 (8H, m), 2.21 (3H, 1:1:1 triplet, HOD,  $J = 1.0$  Hz); in  $d_6$ -DMSO:  $\delta$  4.34 (2H, broad t,  $J = 9.6$  Hz; NH), 3.27–3.49 (4H, m, overlapped with solvent peaks), 3.07 (4H, dt,  $J = 11.4, 6.6$  Hz), 2.76 (4H, s, cross-bridging  $CH_2CH_2$ ,  $^{199}Hg$  satellites,  $^3J = 41$  Hz), 2.49–2.67 (8H, m, overlapped with solvent peaks);  $^{13}C\{^1H\}$  in  $CD_3CN$ :  $\delta$  57.54, 50.46, 50.34, 47.17; in  $d_6$ -DMSO:  $\delta$  56.10 ( $^{199}Hg$  satellites,  $J = 44$  Hz), 49.06 ( $^{199}Hg$  satellites,  $J = 11$  Hz), 45.63 ( $^{199}Hg$  satellites,  $J = 5$  Hz).

**[Zn•5](ClO<sub>4</sub>)<sub>2</sub> (136):** To a MeOH solution (5 mL) of **5**•(H<sub>2</sub>O)<sub>0.5</sub> (46.3 mg, 0.132 mmol) which was about 95% pure, a MeOH solution (6 mL) of Zn(ClO<sub>4</sub>)<sub>2</sub>•6H<sub>2</sub>O (50.3 mg, 0.135 mmol) was added. This resulting solution was refluxed for 27 hours to form a very cloudy solution. This solution was then centrifuged to remove the white precipitate. Et<sub>2</sub>O vapor diffusion into this supernatant yielded 52.9 mg of a white solid, which was recrystallized from acetone and washed by CHCl<sub>3</sub>. Then it was redissolved in MeCN and ether diffused into this solution to form pure [Zn•5](ClO<sub>4</sub>)<sub>2</sub> as needle-shaped crystals (15.6 mg, 20%). IR (KBr): 3442, 3337, 3293 and 3232 cm<sup>-1</sup> (ν<sub>OH</sub> and ν<sub>NH</sub>), 1673, 1659 cm<sup>-1</sup> (ν<sub>C=O</sub>), 1590 cm<sup>-1</sup> (w, NH<sub>2</sub> bending). <sup>1</sup>H NMR in CD<sub>3</sub>CN: δ 7.31(2H, s, NH<sub>2</sub>), 6.94 (2H, s, NH<sub>2</sub>), 3.66 (2H, br A of AB in CH<sub>2</sub>CONH<sub>2</sub> arms), 3.47 (2H, B of AB in CH<sub>2</sub>CONH<sub>2</sub> arms), 3.35-3.44 (2H, m), 3.15-3.29 (4H, m), 3.08 (4H, broad td, *J* = 12.9, 2.4 Hz), 2.59-2.87 (10H, m), 2.17-2.31 (2H, m, β-CHH<sub>ax</sub>), 1.68 (2H, dp, *J* = 17.6, 2.5 Hz, β-CH<sub>eq</sub>H); <sup>13</sup>C {<sup>1</sup>H} data in CD<sub>3</sub>CN: δ 176.88, 62.13, 60.68, 59.71, 58.53, 52.35, 51.52, 23.80. Anal. Calcd. for ZnC<sub>16</sub>H<sub>32</sub>N<sub>6</sub>O<sub>2</sub>(ClO<sub>4</sub>)<sub>2</sub>: C, 31.78; H, 5.33; N, 13.90%. Found: C, 31.99; H, 5.39; N, 13.78%.

**[Zn•6](ClO<sub>4</sub>)<sub>2</sub> (137):** A mixture of ligand **6**•H<sub>2</sub>O (74.1 mg, 0.224 mmol) in MeOH (5mL) and Zn(ClO<sub>4</sub>)<sub>2</sub>•6H<sub>2</sub>O (84.0 mg, 0.226 mmol) in MeOH (2 mL) was refluxed for one day. After cooling to room temperature, needle-shaped crystals (53.0 mg) grew out and were centrifuged from this solution. Ether was diffused into the supernatant to produce another 27.2 mg of colorless crystals. The combined yield was 62%. IR (KBr): 3413, 3370, 3296, 3241 cm<sup>-1</sup> (ν<sub>NH</sub> or OH), 1682(s), 1663(s) cm<sup>-1</sup> (ν<sub>C=O</sub> stretches) 1597 (medium) cm<sup>-1</sup> (OH or NH<sub>2</sub> bending). <sup>1</sup>H NMR of N-deuterated complex in CD<sub>3</sub>OD:

$\delta$  3.94 (4H, s,  $\text{CH}_2\text{COND}_2$ ), 3.32-3.49 (8H, m), 3.11 (4H, s, cross-bridging  $\text{CH}_2\text{CH}_2$ ), 3.05 (4H, dd,  $J = 12.1, 4.8$  Hz), 2.94 (4H, td,  $J = 12.3, 7.1$  Hz); in  $\text{CD}_3\text{OD}$  ( $-80^\circ\text{C}$  at 400 MHz):  $\delta$  3.97 (4H, broad s,  $\text{CH}_2\text{COND}_2$ ), 2.50-3.70 (20H, m); in  $\text{D}_2\text{O}$  (400 MHz):  $\delta$  3.98 (4H, s,  $\text{CH}_2\text{COND}_2$ ), 3.38 (8H, br dd,  $J = 9.4, 3.0$  Hz), 3.07 (4H, s, cross-bridging  $\text{CH}_2\text{CH}_2$ ), 2.89-3.06 (8H, m); in  $\text{CD}_3\text{CN}$  (partially N-deuterated complex):  $\delta$  7.42 (1.5H, s,  $\text{NH}_2$ ), 7.08 (1.5H, s,  $\text{NH}_2$ ), 3.86 (4H, s,  $\text{CH}_2\text{CONH}_2$ ), 3.21-3.38 (8H, m), 2.99 (4H, s, cross-bridging  $\text{CH}_2\text{CH}_2$ ), 2.96-3.04 (4H, m), 2.81 (4H, td,  $J = 12.1, 7.7$  Hz);  $^{13}\text{C}\{^1\text{H}\}$  NMR in  $\text{CD}_3\text{OD}$  (N-D complex):  $\delta$  177.90, 63.08, 61.73, 57.81, 50.58; in  $\text{D}_2\text{O}$  (N-D complex):  $\delta$  177.09, 62.27, 60.98, 56.73, 49.98; in  $\text{CD}_3\text{CN}$  (partially N-deuterated complex):  $\delta$  177.49 (N-H complex), 177.40 (N-D complex), 62.84 (N-H complex), 62.80 (N-D complex), 61.49, 57.30 (N-H complex), 57.28 (N-D complex), 50.01. Anal. Calcd. for  $\text{ZnCl}_2\text{C}_{14}\text{H}_{28}\text{N}_6\text{O}_{10}$ : C, 29.16; H, 4.89; N, 14.57%. Found: C, 29.23; H, 4.98; N, 14.31%.

**[Zn·6](NO<sub>3</sub>)<sub>2</sub> (138):** A mixture of ligand  $6\cdot\text{H}_2\text{O}$  (67.1 mg, 0.203 mmol) and  $\text{Zn}(\text{NO}_3)_2\cdot 6\text{H}_2\text{O}$  (62.4 mg, 0.210 mmol) in MeOH (22 mL) was refluxed for 16 hours. After cooling to room temperature, this solution was diffused with  $\text{Et}_2\text{O}$  vapor to yield 90.4 mg (89%) of colorless crystals. IR (KBr): 3331, 3129  $\text{cm}^{-1}$  ( $\nu_{\text{NH or OH}}$ ), 1683 (s), 1656 (s)  $\text{cm}^{-1}$ , ( $\nu_{\text{C=O}}$  stretches), 1601 (medium)  $\text{cm}^{-1}$  (OH or  $\text{NH}_2$  bending).  $^1\text{H}$  NMR of N-deuterated complex in  $\text{CD}_3\text{OD}$ :  $\delta$  3.95 (4H, s,  $\text{CH}_2\text{COND}_2$ ), 3.32-3.49 (8H, m), 3.10 (4H, s, cross-bridging  $\text{CH}_2\text{CH}_2$ ), 3.03 (4H, dd,  $J = 12.6, 4.0$  Hz), 2.94 (4H, td,  $J = 12.2, 7.2$  Hz); in  $\text{D}_2\text{O}$ :  $\delta$  3.98 (4H, s,  $\text{CH}_2\text{COND}_2$ ), 3.37 (8H, br dd,  $J = 9.3, 2.9$  Hz), 3.07 (4H, s, cross-bridging  $\text{CH}_2\text{CH}_2$ ), 2.88-3.09 (8H, m); in  $\text{CD}_3\text{CN}$  (partially N-deuterated

complex):  $\delta$  7.97 (1.6H, s,  $\text{NH}_2$ ), 7.22 (1.6H, s,  $\text{NH}_2$ ), 3.88 (4H, s,  $\text{CH}_2\text{CONH}_2$ ), 3.16-3.39 (8H, m), 2.97 (4H, s, cross-bridging  $\text{CH}_2\text{CH}_2$ ), 2.91-3.06 (4H, m), 2.82 (4H, td,  $J = 12.3, 7.6$  Hz);  $^{13}\text{C}\{^1\text{H}\}$  NMR in  $\text{CD}_3\text{OD}$  (N-D complex):  $\delta$  177.90, 63.08, 61.71, 57.83, 50.59; in  $\text{D}_2\text{O}$  (N-D complex):  $\delta$  177.09, 62.26, 60.97, 56.73, 49.89. Anal. Calcd. for  $\text{ZnC}_{14}\text{H}_{28}\text{N}_8\text{O}_8$ : C, 33.51; H, 5.62; N, 22.33%. Found: C, 33.36; H, 5.51; N, 22.56%.

**$\text{Cd}(\text{ClO}_4)_2 \cdot 6$  (139):** To a MeOH solution (5mL) of  $\text{Cd}(\text{ClO}_4)_2 \cdot 6\text{H}_2\text{O}$  (78.4 mg, 0.187 mmol), a solution of ligand  $6 \cdot \text{H}_2\text{O}$  (55.5 mg, 0.168 mmol) in MeOH (15 mL) was added. This resulting solution was refluxed for 1.5 days. After cooling to room temperature, this solution was diffused with  $\text{Et}_2\text{O}$  vapor to yield 72.1 mg (67%) of colorless crystals. IR (KBr): 3430, 3353, 3299, 3240  $\text{cm}^{-1}$  ( $\nu_{\text{NH or OH}}$ ), 1689 (s), 1658 (s)  $\text{cm}^{-1}$ , ( $\nu_{\text{C=O}}$  stretches), 1606 (medium)  $\text{cm}^{-1}$  (OH or  $\text{NH}_2$  bending).  $^1\text{H}$  NMR of N-deuterated complex in  $\text{CD}_3\text{OD}$ :  $\delta$  3.76 (4H, s,  $\text{CH}_2\text{COND}_2$ ), 3.24-3.37 (4H, m, overlapped with methanol peaks), 3.15 (4H, broad dd,  $J = 16.0, 5.2$  Hz), 2.95 (4H, s, cross-bridging  $\text{CH}_2\text{CH}_2$ ), 2.89-3.06 (4H, m), 2.82 (4H, broad dd,  $J = 12.2, 4.7$  Hz); NH complex in  $\text{CD}_3\text{CN}$  (saturated):  $\delta$  7.13 (2H, s,  $\text{NH}_2$ ), 6.85 (2H, s,  $\text{NH}_2$ ), 3.69 (4H, s,  $\text{CH}_2\text{CONH}_2$ ,  $^{111}\text{Cd}$ ,  $^{113}\text{Cd}$  satellites,  $J = 10.9$  Hz), 3.03-3.21 (8H, m), 2.83 (4H, s, cross-bridging  $\text{CH}_2\text{CH}_2$ ,  $^{111}\text{Cd}$ ,  $^{113}\text{Cd}$  satellites,  $J = 14.9$  Hz), 2.91 (4H, td,  $J = 12.1, 6.7$  Hz), 2.77 (4H, ddd,  $J = 12.4, 4.2, 1.3$  Hz);  $^{13}\text{C}\{^1\text{H}\}$  NMR in  $\text{CD}_3\text{OD}$  (N-D complex):  $\delta$  176.92, 63.25, 61.02, 58.31, 48.23; in  $\text{CD}_3\text{CN}$ :  $\delta$  176.27 ( $^{111}\text{Cd}$ ,  $^{113}\text{Cd}$  satellites,  $J = 12.1$  Hz), 62.49, 60.58 ( $^{111}\text{Cd}$ ,  $^{113}\text{Cd}$  satellites,  $J \sim 3$  Hz), 57.54 ( $^{111}\text{Cd}$ ,  $^{113}\text{Cd}$  satellites,  $J = 15.9$  Hz), 47.50. Anal. Calcd. for  $\text{CdC}_{14}\text{H}_{28}\text{N}_6\text{O}_2(\text{ClO}_4)_2(\text{H}_2\text{O})$ : C, 26.20; H, 4.71; N, 13.10%. Found: C, 26.59; H, 4.95; N, 12.67%.

**[Cd•6( $\eta^1$ -NO<sub>3</sub>)](NO<sub>3</sub>) (140):** A mixture of ligand 6•H<sub>2</sub>O (89.8 mg, 0.272 mmol) and Cd(NO<sub>3</sub>)<sub>2</sub>•4H<sub>2</sub>O (84.4 mg, 0.274 mmol) in MeOH (9 mL) was refluxed for two days. After cooling to room temperature, needle-shaped crystals (65.9 mg) grew out and were centrifuged from solution. This solution was then diffused with Et<sub>2</sub>O vapor to produce another 9.5 mg of colorless crystals. The combined weight of crystalline product is 75.4 mg (49%). IR (KBr): 3348, 3304, 3151 cm<sup>-1</sup> ( $\nu_{\text{NH or OH}}$ ), 1656 (s), 1650 (s) cm<sup>-1</sup> ( $\nu_{\text{C=O}}$ ), 1611 cm<sup>-1</sup> (medium, OH or NH bending). <sup>1</sup>H NMR of a saturated N-deuterated complex in CD<sub>3</sub>OD:  $\delta$  3.71 (4H, s, CH<sub>2</sub>COND<sub>2</sub>, <sup>111</sup>Cd, <sup>113</sup>Cd satellites,  $J$  = 11.1 Hz), 3.21-3.33 (4H, m, overlapped with solvent peaks), 3.02-3.15 (8H, m), 2.94 (4H, s, cross-bridging CH<sub>2</sub>CH<sub>2</sub>, <sup>111</sup>Cd, <sup>113</sup>Cd satellites,  $J$  = 14.1 Hz), 2.74-2.83 (4H, m); N-H/N-D complex in CD<sub>3</sub>CN:  $\delta$  6.95 (0.74H, s, NH<sub>2</sub>), 6.66 (1.0H, s, NH<sub>2</sub>), 3.65 (4H, s, CH<sub>2</sub>CONH<sub>2</sub>, <sup>111</sup>Cd, <sup>113</sup>Cd satellites,  $J$  = 11.6 Hz), 2.98-3.18 (12H, m), 2.83 (4H, s, cross-bridging CH<sub>2</sub>CH<sub>2</sub>, <sup>111</sup>Cd, <sup>113</sup>Cd satellites,  $J$  = 13.9 Hz), 2.71 (4H, broad dd,  $J$  = 11.2, 4.4 Hz); <sup>13</sup>C{<sup>1</sup>H} in CD<sub>3</sub>OD (a saturated N-D complex):  $\delta$  177.04 (<sup>111</sup>Cd, <sup>113</sup>Cd satellites,  $J$  = 11.3 Hz), 63.41, 61.11, 58.29, 48.57. Anal. Calcd. for CdC<sub>14</sub>H<sub>28</sub>N<sub>8</sub>O<sub>4</sub>(H<sub>2</sub>O)<sub>0.5</sub>: C, 30.14; H, 5.24; N, 20.09%. Found: C, 29.95; H, 5.25; N, 19.96%.

**[Zn•(7-2H)](NaClO<sub>4</sub>) (141):** **Method 1:** To a MeOH solution (6 mL) of 7•(TFA)<sub>2</sub> (105.6 mg, 0.185 mmol), a MeOH solution (6 mL) of Zn(ClO<sub>4</sub>)<sub>2</sub>•6H<sub>2</sub>O (72.6 mg, 0.195 mmol) was added. This resulting solution was refluxed to form a very cloudy solution. To this cloudy solution, 0.75 mL of an aqueous NaOH (0.9864 N) solution was added and the reaction mixture was refluxed for 1.5 days. The white precipitate was then centrifuged off from this reaction solution. Et<sub>2</sub>O vapor diffusion into this supernatant

yielded 55.3 mg (56%) of a white solid. **Method 2:** To a 95% aqueous EtOH solution (25 mL) of  $7 \cdot (\text{TFA})_{2.8}$  (231.8 mg, 0.350 mmol), a 95% aqueous EtOH solution (8 mL) of  $\text{Zn}(\text{ClO}_4)_2 \cdot 6\text{H}_2\text{O}$  (131.8 mg, 0.354 mmol) was added. This mixture was stirred at room temperature for 1 hour to form a very cloudy solution. To this cloudy solution, 1.08 mL of an aqueous NaOH (0.970 N) solution was added and refluxed for 30 hours. This resulting 95% aqueous EtOH solution was then centrifuged off from the white precipitate. Et<sub>2</sub>O vapor diffusion into this supernatant yielded 165.3 mg (88%) of a white solid. IR (KBr): 3568, 3363 cm<sup>-1</sup> (ν<sub>OH</sub>), 1616, 1592 cm<sup>-1</sup> (ν<sub>C=O</sub>). <sup>1</sup>H NMR in D<sub>2</sub>O: δ 3.40-3.57 (4H, m, including A of AX from CH<sub>2</sub>COO arms), 3.30 (2H, AA' of AA'XX'), 2.97-3.18 (8H, m, including X of AX from CH<sub>2</sub>COO arms), 2.88 (2H, td, *J* = 13.0, 2.8 Hz), 2.72-2.86 (4H, m), 2.65 (2H, dd, *J* = 13.4, 4.3 Hz), 2.45 (2H, dd, *J* = 14.8, 4.4 Hz), 2.20-2.35 (2H, m, β-CHH<sub>ax</sub>), 1.66 (2H, dp, *J* = 17.1, 3.0 Hz, β-CH<sub>eq</sub>H); in CD<sub>3</sub>OD: δ 3.46-3.57 (4H, m, including A of AB in CH<sub>2</sub>COO arms), 3.34 (2H, AA' of AA'XX'), 3.20 (2H, td, *J* = 12.6, 2.7 Hz), 3.02-3.09 (4H, m, including B of AB in CH<sub>2</sub>COO arms), 2.94-3.01 (4H, m), 2.88 (2H, td, *J* = 13.7, 4.6 Hz), 2.76 (2H, XX' of AA'XX'), 2.60 (2H, dd, *J* = 13.2, 3.9 Hz), 2.39 (2H, dd, *J* = 15.0, 4.4 Hz), 2.25-2.43 (2H, m), 1.63 (2H, dp, *J* = 17.2, 2.9 Hz, β-CH<sub>eq</sub>H); CD<sub>3</sub>CN: δ 3.63 (2H, dd, 16.9, 1.4 Hz, A of AX from CH<sub>2</sub>COO arms), 3.25-3.40 (4H, m), 3.17 (2H, td, *J* = 12.9, 2.8 Hz), 3.03 (2H, td, *J* = 12.9, 2.7 Hz), 2.94 (2H, d, *J* = 12.4 Hz), 2.70-2.89 (4H, m, including X of AX from CH<sub>2</sub>COO arms), 2.45-2.58 (4H, m), 2.25 (2H, dd, *J* = 14.5, 4.2 Hz), 2.11-2.23 (2H, m, overlapped with DOH peak), 1.66 (2H, dp, *J* = 17.2, 2.9 Hz, β-CH<sub>eq</sub>H); in CD<sub>3</sub>OD (-80°C at 400 MHz): δ 3.39-3.64 (6H, m), 3.04-3.22 (6H, m), 2.76-3.01 (6H, m), 2.61-2.70 (4H, m), 2.31-2.46 (4H, m), 1.62 (2H, broad d, *J* = 15.2 Hz, β-CH<sub>eq</sub>H); <sup>13</sup>C{<sup>1</sup>H} data in D<sub>2</sub>O: δ 178.95, 64.28, 59.85,



58.87, 58.17, 52.60, 50.97, 23.32; in  $CD_3OD$ : 177.94, 65.48, 60.69, 59.50, 59.39, 53.35, 51.69, 24.40; in  $CD_3CN$ :  $\delta$  177.85, 64.52, 59.69, 59.53, 58.45, 53.19, 51.09, 24.12. Anal. Calcd. for  $ZnC_{16}H_{28}N_4O_4NaClO_4(H_2O)_{0.5}$ : C, 35.77; H, 5.44; N, 10.43%. Found: C, 35.59; H, 5.67; N, 10.05%.

**[Zn•(7-2H)](NaNO<sub>3</sub>)<sub>3</sub> (142):** To a MeOH solution (6 mL) of **7•(TFA)<sub>2</sub>** (106.3 mg, 0.186 mmol), was added a MeOH solution (6 mL) of  $Zn(NO_3)_2 \cdot 6H_2O$  (62.3 mg, 0.209 mmol). This resulting solution was refluxed to form a slightly cloudy solution. To this solution, aqueous NaOH (0.970 N, 0.77 mL) was added and refluxed for 1.5 days. A small amount of white precipitate was then centrifuged off to yield a clear supernatant. Et<sub>2</sub>O vapor diffusion into this supernatant yielded 91.7 mg (71%) of a white solid. IR (KBr): 3430  $cm^{-1}$ , 3263  $cm^{-1}$  ( $\nu_{OH}$ ), 1618, 1596  $cm^{-1}$  ( $\nu_{C=O}$ ). <sup>1</sup>H NMR in  $D_2O$ :  $\delta$  3.40-3.57 (4H, m, including A of AX from  $CH_2COO$  arms), 3.30 (2H, AA' of AA'XX'), 2.97-3.18 (8H, m, including X of AX from  $CH_2COO$  arms), 2.89 (2H, td,  $J = 13.0, 2.8$  Hz), 2.72-2.86 (4H, m), 2.65 (2H, dd,  $J = 13.4, 4.3$  Hz), 2.45 (2H, dd,  $J = 14.8, 4.4$  Hz), 2.20-2.35 (2H, m), 1.66 (2H, dp,  $J = 17.1, 3.0$  Hz,  $\beta-CH_{eq}H$ ); <sup>13</sup>C{<sup>1</sup>H} data in  $D_2O$ :  $\delta$  179.01, 64.28, 59.87, 58.90, 58.19, 52.61, 50.99, 23.35. Anal. Calcd. for  $ZnC_{16}H_{28}N_4O_4(NaNO_3)_3(NaOH)_{0.5}(H_2O)_{0.5}$ : C, 27.86; H, 4.31; N, 14.21%. Found: C, 27.94; H, 4.02; N, 13.89%.

**[Zn•(8-2H)](NaClO<sub>4</sub>) (143):** To a MeOH solution (10 mL) of **8•TFA•H<sub>2</sub>O** (113.3 mg, 0.265 mmol), was added 0.818 mL of an aqueous solution of NaOH (0.970 N) to form a clear solution. A MeOH solution (6 mL) of  $Zn(ClO_4)_2 \cdot 6H_2O$  (100.4 mg, 0.270 mmol) was then added. After refluxing for 2 days, this MeOH solution was centrifuged off from

some precipitate. Et<sub>2</sub>O vapor diffusion into this supernatant yielded 106.4 mg (71%) of a white crystalline solid. IR (KBr): 1617 cm<sup>-1</sup> (broad) (ν<sub>C=O</sub>). <sup>1</sup>H NMR in D<sub>2</sub>O: δ 3.63 (4H, s, CH<sub>2</sub>COO), 3.20-3.37 (8H, m), 3.03 (4H, s, cross-bridging CH<sub>2</sub>CH<sub>2</sub>), 2.89-3.08 (8H, m); <sup>1</sup>H NMR in CD<sub>3</sub>OD (400 MHz): δ 3.61 (4H, s, CH<sub>2</sub>COO), 3.20-3.41 (8H, m), 3.07 (4H, s, cross-bridging CH<sub>2</sub>CH<sub>2</sub>), 2.91-3.15 (8H, m); in CD<sub>3</sub>OD at -80<sup>0</sup>C (400 MHz): δ 3.65 (4H, AB, CH<sub>2</sub>COO), 3.24-3.48 (8H, m), 2.72-3.19 (12H, m); <sup>13</sup>C{<sup>1</sup>H} data in D<sub>2</sub>O: δ 179.03, 64.94, 61.10 (br), 56.83, 49.95; in CD<sub>3</sub>OD: δ 177.85, 66.11, 61.77 (broad), 57.85, 50.80; CD<sub>3</sub>OD at -80<sup>0</sup>C: δ 178.59, 65.62, 63.93, 59.12, 58.55, 56.89, 49.78. Anal. Calcd. for ZnC<sub>14</sub>H<sub>24</sub>N<sub>4</sub>O<sub>4</sub>(NaClO<sub>4</sub>)<sub>1.5</sub>: C, 29.95; H, 4.31; N, 9.98%. Found: C, 30.05; H, 4.68; N, 9.81%.

**[Zn•(8-2H)](NaNO<sub>3</sub>) (144):** To a clear solution of Zn(NO<sub>3</sub>)<sub>2</sub>•6H<sub>2</sub>O (60.8 mg, 0.204 mmol) in MeOH (6 mL), a MeOH solution (6 mL) of 8•TFA•H<sub>2</sub>O (82.8 mg, 0.193 mmol) was added to form a clear solution. An amount of 0.60 mL aqueous NaOH (0.970 N) was then added to form a clear solution. After refluxing for 2 days, this MeOH solution was centrifuged off from some white precipitate. Et<sub>2</sub>O vapor diffusion into this supernatant yielded 47.9 mg (38%) of a white crystalline solid. IR (KBr): 1645, 1611 cm<sup>-1</sup> (ν<sub>C=O</sub>). <sup>1</sup>H NMR in D<sub>2</sub>O: δ 3.63 (4H, s, CH<sub>2</sub>COO), 3.21-3.38 (8H, m), 3.03 (4H, s, cross-bridging CH<sub>2</sub>CH<sub>2</sub>), 2.89-3.08 (8H, m); <sup>13</sup>C{<sup>1</sup>H} data in D<sub>2</sub>O: δ 179.08, 64.94, 61.12, 56.84, 49.97. Anal. Calcd. for ZnC<sub>14</sub>H<sub>24</sub>N<sub>4</sub>O<sub>4</sub> (NaNO<sub>3</sub>)<sub>3</sub>(H<sub>2</sub>O)<sub>1.5</sub>: C, 25.49; H, 4.13; N, 14.86%. Found: C, 25.20; H, 3.92; N, 15.00%.

**[Cd•(7-2H)](NaClO<sub>4</sub>) (145):** To a MeOH solution (7 mL) of Cd(ClO<sub>4</sub>)<sub>2</sub>•6H<sub>2</sub>O (61.0 mg, 0.145 mmol), a MeOH solution (7 mL) of 7•(TFA)<sub>2</sub> (76.5 mg, 0.134 mmol) was added to form a clear solution. To this solution, 0.553 mL of an aqueous NaOH (0.970 N) solution was added and refluxed for one and a half days. The MeOH solution was diffused with Et<sub>2</sub>O vapor to yield 60.3 mg (76%) of a white solid. IR (KBr): 1633, 1586 cm<sup>-1</sup> (ν<sub>C=O</sub>). <sup>1</sup>H NMR in D<sub>2</sub>O: δ 2.85-3.48 (18H, m, including AX of CH<sub>2</sub>COO), 2.70 (2H, XX' of AA'XX'), 2.51 (2H, br dd, *J* = 13, 3 Hz), 2.43 (2H, dd, *J* = 15.2, 2.7 Hz), 2.26-2.45 (2H, m), 1.70 (2H, dp, *J* = 17.7, 3.0 Hz, β-CH<sub>eq</sub>H); in CD<sub>3</sub>OD (400 MHz): δ 3.32-3.49 (6H, m, overlapped with solvent peaks), 2.98-3.21 (8H, m), 2.87 (4H, broad s), 2.66 (2H, broad AA' or XX' of AA'XX'), 2.26-2.48 (6H, broad m), 1.66 (2H, broad d, *J* = 17.2 Hz, β-CH<sub>eq</sub>H); <sup>13</sup>C{<sup>1</sup>H} data in D<sub>2</sub>O: δ 178.66 (<sup>111</sup>Cd, <sup>113</sup>Cd satellites, *J* = 12.0 Hz), 64.40 (<sup>111</sup>Cd, <sup>113</sup>Cd satellites, *J* = 8.6 Hz), 59.48, 59.46, 58.58, 51.75, 49.78 (<sup>111</sup>Cd, <sup>113</sup>Cd satellites, *J* = 11.3 Hz), 24.02 (<sup>111</sup>Cd, <sup>113</sup>Cd satellites, *J* = 6.0 Hz); in CD<sub>3</sub>OD (100.5 MHz): δ 178.24, 65.68 (broad), 60.20, 59.66, 52.70 (broad), 50.53, 25.08. Anal. Calcd. for CdC<sub>16</sub>H<sub>28</sub>N<sub>4</sub>O<sub>4</sub>(NaClO<sub>4</sub>)(H<sub>2</sub>O): C, 32.39; H, 5.10; N, 9.44%. Found: C, 32.41; H, 5.10; N, 9.53%.

**[Cd•(7-2H)](NaNO<sub>3</sub>) (146):** To a MeOH solution (6 mL) of Cd(NO<sub>3</sub>)<sub>2</sub>•4H<sub>2</sub>O (37.4 mg, 0.121 mmol), a MeOH solution (6 mL) of 7•(TFA)<sub>2</sub> (60.6 mg, 0.106 mmol) was added to form a clear solution into which aqueous NaOH (0.970 N, 0.44 mL) was added and refluxed for sixteen hours. This MeOH solution was then centrifuged off from some white precipitate. Et<sub>2</sub>O vapor diffusion into this supernatant yielded 49.2 mg (78%) of a white solid. IR (KBr): 1619, 1594 cm<sup>-1</sup> (ν<sub>C=O</sub>). <sup>1</sup>H NMR in D<sub>2</sub>O: δ 2.85-3.48 (18H, m),

2.70 (2H, AA' or XX' of AA'XX'), 2.51 (2H, dd,  $J = 13.4, 2.4$  Hz), 2.43 (2H, dd,  $J = 15, 3$  Hz), 2.26-2.50 (2H, m), 1.70 (2H, dp,  $J = 17.7, 3.0$  Hz,  $\beta$ -CH<sub>eg</sub>H);  $^{13}\text{C}\{^1\text{H}\}$  data in  $D_2O$ :  $\delta$  178.66 ( $^{111}\text{Cd}, ^{113}\text{Cd}$  satellites,  $J = 11.9$  Hz), 64.39 ( $^{111}\text{Cd}, ^{113}\text{Cd}$  satellites,  $J = 8.6$  Hz), 59.47, 59.44, 58.59, 51.73, 49.78 ( $^{111}\text{Cd}, ^{113}\text{Cd}$  satellites,  $J = 10.6$  Hz), 24.02 ( $^{111}\text{Cd}, ^{113}\text{Cd}$  satellites,  $J = 6.6$  Hz). Anal. Calcd. for  $\text{CdC}_{16}\text{H}_{28}\text{N}_4\text{O}_4(\text{NaNO}_3)(\text{NaOH})(\text{H}_2\text{O})$ : C, 32.25; H, 5.24; N, 11.75%. Found: C, 32.66; H, 5.25; N, 11.61%.

**[Cd•(8-2H)](NaClO<sub>4</sub>) (147):** To a clear mixture of  $8\cdot\text{TFA}\cdot\text{H}_2\text{O}$  (89.0 mg, 0.208 mmol) and  $\text{Cd}(\text{ClO}_4)_2\cdot 6\text{H}_2\text{O}$  (94.8 mg, 0.226 mmol) in 15 mL MeOH, 0.64 mL of an aqueous solution of NaOH (0.970 N) was added to form a cloudy solution. After refluxing for 7 hours, some white precipitate was centrifuged off. Et<sub>2</sub>O vapor diffusion into this supernatant yielded 73 mg (61%) of a white crystalline solid. IR (KBr): 1615, 1595 cm<sup>-1</sup> ( $\nu_{\text{C=O}}$ ).  $^1\text{H}$  NMR in  $D_2O$ :  $\delta$  3.48 (4H, s, CH<sub>2</sub>COO<sub>2</sub>,  $^{111}\text{Cd}, ^{113}\text{Cd}$  satellites,  $J = 11.6$  Hz), 2.94-3.26 (12H, m), 2.89 (4H, s, cross-bridging CH<sub>2</sub>CH<sub>2</sub>,  $^{111}\text{Cd}, ^{113}\text{Cd}$  satellites,  $J = 13.7$  Hz), 2.81 (4H, broad dd,  $J = 12.1, 4.4$  Hz); in CD<sub>3</sub>OD:  $\delta$  2.51-3.71 (very broad m);  $^{13}\text{C}\{^1\text{H}\}$  data in  $D_2O$  (MeCN external reference):  $\delta$  179.23 ( $^{111}\text{Cd}, ^{113}\text{Cd}$  satellites,  $J = 11.3$  Hz), 64.95 ( $^{111}\text{Cd}, ^{113}\text{Cd}$  satellites,  $J = 6.0$  Hz), 60.58, 57.32, 47.63 ( $^{111}\text{Cd}, ^{113}\text{Cd}$  satellites,  $J = 15.3$  Hz); in CD<sub>3</sub>OD:  $\delta$  176-180 (broad signals), 55-68 (broad signals). Anal. Calcd. for  $\text{CdC}_{14}\text{H}_{24}\text{N}_4\text{O}_4(\text{NaClO}_4)(\text{H}_2\text{O})_{1.5}$ : C, 29.28; H, 4.74; N, 9.76; Cl, 6.27%. Found: C, 29.31; H, 4.70; N, 9.65; Cl, 5.96%.

**[Hg•(7-2H)](K<sub>2</sub>HgCl<sub>4</sub>) (148):** To a MeOH solution (10 mL) of HgCl<sub>2</sub> (86.4 mg, 0.318 mmol), a MeOH solution (7 mL) of  $7\cdot(\text{TFA})_2$  (82.3 mg, 0.144 mmol) was added to form

a clear solution. A volume of 0.44 mL of a MeOH solution of KOH (0.505 N) was added into this solution to form a clear solution. This was refluxed for 27 hours, then centrifuged to remove some white precipitate. Et<sub>2</sub>O vapor diffusion into this supernatant yielded 104.5 mg (75%) of a white crystalline solid. IR (KBr): 1611, 1590 cm<sup>-1</sup> (ν<sub>C=O</sub>). <sup>1</sup>H NMR in D<sub>2</sub>O: δ 2.80-3.51 (20H, m), 2.66 (2H, dd, *J* = 15, 3 Hz), 2.57 (2H, dd, *J* = 13, 3 Hz), 2.31-2.50 (2H, m), 1.73 (2H, broad d, *J* = 17.7 Hz, β-CH<sub>eq</sub>H); in CD<sub>3</sub>OD: δ 3.10-3.40 (12H, m, overlapped with methanol solvent peaks, including AB of CH<sub>2</sub>COO arms), 2.89-3.07 (4H, m), 2.73 (2H, dd, *J* = 12.2, 3.7 Hz), 2.65 (2H, dt, *J* = 12.7, 2.7 Hz), 2.47 (2H, dd, *J* = 14.9, 2.5 Hz), 2.17-2.41 (4H, m), 1.62 (2H, broad d, *J* = 16.4 Hz, β-CH<sub>eq</sub>H); <sup>13</sup>C{<sup>1</sup>H} data in D<sub>2</sub>O: δ 177.13 (<sup>199</sup>Hg satellites, *J* = ~ 34 Hz), 63.64 (<sup>199</sup>Hg satellites, *J* = 31.2 Hz), 60.78 (<sup>199</sup>Hg satellites, *J* ~ 31 Hz), 60.69, 57.75 (<sup>199</sup>Hg satellites, *J* = 35.8 Hz), 50.18 (<sup>199</sup>Hg satellites, *J* = 16.6 Hz), 49.50 (<sup>199</sup>Hg satellites, *J* = 29.9 Hz), 24.34 (<sup>199</sup>Hg satellites, *J* = 25.9 Hz); in CD<sub>3</sub>OD: δ 177.30 (<sup>199</sup>Hg satellites, *J* ~ 19 Hz), 65.17 (<sup>199</sup>Hg satellites, *J* = 17.9 Hz), 61.15 (<sup>199</sup>Hg satellites, *J* = 11.3 Hz), 60.03 (<sup>199</sup>Hg satellites, *J* = 17.9 Hz), 57.94 (<sup>199</sup>Hg satellites, *J* = 29.9 Hz), 50.72 (<sup>199</sup>Hg satellites, *J* = 23.2 Hz), 49.58 (overlapped with solvent peaks), 25.53 (<sup>199</sup>Hg satellites, *J* = 21.9 Hz). Anal. Calcd. for Hg<sub>2</sub>C<sub>32</sub>H<sub>56</sub>N<sub>8</sub>O<sub>8</sub>Hg<sub>3</sub>Cl<sub>6</sub>: C, 19.98; H, 2.93; N, 5.83, Cl, 14.75%. Found: C, 20.35; H, 3.23; N, 5.69; Cl, 14.21%.

[GaCl<sub>2</sub>•1]Cl (149): Anhydrous GaCl<sub>3</sub> (42 mg, 0.24 mmol) and ligand 1 (47 mg, 0.21 mmol) were transferred into a Schlenk flask in a glovebox with a nitrogen atmosphere. Then the Schlenk flask was sealed and taken out of the glovebox. Under N<sub>2</sub> protection, dry acetonitrile (8 mL) was added through a syringe. This cloudy MeCN solution was

refluxed for 2 days to give a white precipitate which was isolated by filtration, washed with MeCN, and dried to give 58 mg (68%) of the product as a white powder. X-ray crystals were grown by slow evaporation of an acetonitrile solution of the complex. IR (KBr): 3577, 3379  $\text{cm}^{-1}$  ( $\nu_{\text{OH}}$ ), 3137  $\text{cm}^{-1}$  ( $\nu_{\text{NH}}$ ), 1643  $\text{cm}^{-1}$  (OH bending).  $^1\text{H}$  NMR data in  $D_2O$ :  $\delta$  5.37 (br s, NH), 2.91-3.86 (20H, br m,  $\alpha\text{-CH}_2$ ), 2.26-2.51 (2H, br m,  $\beta\text{-CHH}_{ax}$ ), 1.70-1.82 (2H, br dm,  $J = 17$  Hz,  $\beta\text{-CH}_{eq}\text{H}$ ); in acidic  $D_2O$  (0.15 M N-D complex) ( $pD = 0.67$ ,  $\text{HClO}_4$ ): 3.11-3.73 (18H, br m), 3.01 (2H, br d,  $J = 12$  Hz), 2.28-2.52 (2H, br m,  $\beta\text{-CHH}_{ax}$ ), 1.84 (1H, dp,  $J = 17.5, 3.0$  Hz,  $\beta\text{-CH}_{eq}\text{H}$  of Ga(III) Complex A), 1.76 (1H, dp,  $J = 17.2, 2.8$  Hz,  $\beta\text{-CH}_{eq}\text{H}$  of Ga(III) Complex B); in  $CD_3CN$ :  $\delta$  4.28 (2H, br s, NH), 3.81 (2H, tt,  $J = 13.4, 3.0$  Hz), 3.60 (2H, td,  $J = 13.1, 3.0$  Hz), 3.32-3.53 (4H, m), 2.90-3.21 (8H, m), 2.77-2.87 (2H, dm,  $J = 12.4$  Hz), 2.70 (2H, dd,  $J = 12.6, 4.8$  Hz), 2.10-2.33 (2H, m overlapping with solvent peak,  $\beta\text{-CHH}_{ax}$ ), 1.62 (2H, dm,  $J = 16.9$  Hz,  $\beta\text{-CH}_{eq}\text{H}$ );  $^{13}\text{C}\{^1\text{H}\}$  data in  $D_2O$  (N-D complex):  $\delta$  59.85 (br), 57.83 (br), 50.91 (br), 47.87 (br), 41.05 (br), 19.61 (br); in acidic  $D_2O$  (0.15 M N-D complex) ( $pD = 0.67$ ,  $\text{HClO}_4$ ): 60.04 (Complex A), 59.76 (br, Complex B), 58.12 (Complex A), 57.75 (br, Complex B), 51.09 (from both Complexes A and B), 48.23 (Complex A), 47.83 (Complex B), 41.11 (both Complexes A and B), 19.65 (Complex B), 19.41 (Complex A); in  $CD_3CN$ :  $\delta$  60.02, 58.43, 51.32, 48.44, 42.21, 20.75. Anal. Calcd. for  $\text{GaCl}_3(\text{C}_{12}\text{H}_{26}\text{N}_4) \cdot 0.5\text{H}_2\text{O}$ : C, 35.03; H, 6.61; N, 13.62%. Found: C, 34.94; H, 6.54; N, 13.39%.

**[InBr<sub>2</sub>•1]Br (150):** Anhydrous InBr<sub>3</sub> (72 mg, 0.20 mmol) and ligand 1 (46 mg, 0.20 mmol) were transferred into a Schlenk flask in a glovebox with a nitrogen atmosphere. Then the Schlenk flask was sealed and taken out of the glovebox. Under N<sub>2</sub> protection,

dry acetonitrile (11 mL) was added through a syringe. This cloudy MeCN solution was refluxed for 2 days to give a white precipitate which was isolated by filtration, washed with MeCN, and dried to give 65 mg of the product. Diffusion of ether into the filtrate gave an additional 38 mg of the product as needle crystals for a combined yield of 86%. IR (KBr): 3587, 3415  $\text{cm}^{-1}$  ( $\nu_{\text{OH}}$ ), 3116  $\text{cm}^{-1}$  ( $\nu_{\text{NH}}$ ), 1635  $\text{cm}^{-1}$  (OH bending).  $^1\text{H}$  NMR data in  $D_2O$  (0.18 mM):  $\delta$  5.18 (br s with shoulders at 5.32 and 5.26, NH), 3.64-3.78 (2H, tm,  $J = 13.6$  Hz), 3.56 (2H, td,  $J = 12.8, 2.1$  Hz), 2.92-3.49 (14H, m), 2.73 (2H, br dd,  $J = 13.1, 4.3$  Hz), 2.26-2.48 (2H, m,  $\beta\text{-CHH}_{ax}$ ), 1.69-1.89 (2H, dm with shoulder at 1.81,  $J = 17.1$  Hz,  $\beta\text{-CH}_{eq}\text{H}$ ); in  $CD_3CN$ :  $\delta$  4.14 (2H, br s, NH), 3.67 (2H, tt,  $J = 13.5, 2.9$  Hz), 3.57 (2H, td,  $J = 13.1, 2.4$  Hz), 3.39 (2H, td,  $J = 13.2, 5.3$  Hz), 3.16-3.33 (4H, m), 2.96-3.12 (4H, m), 2.83-2.93 (2H, dm,  $J = 13$  Hz), 2.57-2.66 (2H, dm,  $J = 11$  Hz), 2.26 (2H, dtt,  $J = 16.4, 13.1, 3.0$  Hz,  $\beta\text{-CHH}_{ax}$ ), 1.68 (2H, dp,  $J = 17.6, 3.0$  Hz,  $\beta\text{-CH}_{eq}\text{H}$ );  $^{13}\text{C}\{^1\text{H}\}$  data in  $D_2O$  (N-D complex):  $\delta$  60.05 (minor), 59.12 (minor), 5.95, 57.40 (minor), 56.28, 50.31 (minor), 49.79, 49.43 (minor), 49.05 (minor), 48.35, 40.88, 40.33 (minor), 21.43, 21.31 (minor), 21.21 (minor); in  $CD_3CN$ :  $\delta$  59.33, 57.33, 50.22, 49.05, 41.78, 22.16; in  $d_6\text{-DMSO}$ :  $\delta$  57.72, 55.63, 48.48, 47.66, 40.13, 20.53. Anal. Calcd. for  $\text{InBr}_3(\text{C}_{12}\text{H}_{26}\text{N}_4)\cdot 0.5\text{H}_2\text{O}$ : C, 24.43; H, 4.61; N, 9.50%. Found: C, 24.35; H, 4.30; N, 9.28%.

**[GaCl<sub>2</sub>•2]Cl (151):** Under nitrogen protection, a cloudy solution of a mixture of anhydrous GaCl<sub>3</sub> (69 mg, 0.39 mmol) and ligand **2** (82 mg, 0.41 mmol) in acetonitrile (15 mL) were refluxed to give a white precipitate. After filtration and drying, 136.5 mg of a white precipitate was obtained. An amount of 39 mg of this white precipitate was

dissolved in MeOH (18 mL) to form a clear solution. Ether diffusion into this solution yielded 23 mg of white crystalline solid (53%). IR (KBr): 3049  $\text{cm}^{-1}$ ( $\nu_{\text{NH}}$ ).  $^1\text{H}$  NMR in  $D_2O$  (N-D complex):  $\delta$  3.77 (4H, dd,  $J = 14.3, 7.0$  Hz), 3.30 (4H, dd,  $J = 12.2, 6.4$  Hz), 3.25 (4H, s, cross-bridging  $\text{CH}_2\text{CH}_2$ ), 3.06-3.21 (4H, br m), 2.99 (4H, ddd,  $J = 14.8, 11.3, 6.9$  Hz); in  $\text{CD}_3\text{CN}$ :  $\delta$  4.58 (br s, NH) 3.68 (4H, dt,  $J = 14.9, 8.3$  Hz), 3.54 (4H, ddd,  $J = 12.0, 11.2, 8.1$  Hz), 3.08 (4H, s, cross-bridging  $\text{CH}_2\text{CH}_2$ ), 3.00-3.12 (4H, br m), 2.81 (4H, dddd,  $J = 14.8, 11.0, 6.8, 3.9$  Hz);  $^{13}\text{C}\{^1\text{H}\}$  NMR of N-deuterated complex in  $D_2O$ :  $\delta$  54.97 (br), 51.60 (br), 49.16 (br). Anal. Calcd. for  $\text{GaCl}_3(\text{C}_{10}\text{H}_{22}\text{N}_4)\text{H}_2\text{O}$ : C, 30.61; H, 6.16; N, 14.28%. Found: C, 30.59; H, 6.14; N, 14.31%.

**[InBr<sub>2</sub>•2]Br (152):** Under nitrogen protection, a cloudy solution of a mixture of anhydrous InBr<sub>3</sub> (57 mg, 0.16 mmol) and ligand **2** (32 mg, 0.14 mmol) in acetonitrile (15 mL) were refluxed to give a white precipitate. This was filtered off, washed with more acetonitrile, and dried to give 44 mg of the product. Diffusion of diethyl ether into the filtrate gave an additional 10 mg of the product for a combined yield of 60%. Crystals suitable for X-ray analyses were obtained from slow evaporation of an acetonitrile solution of the product. IR (KBr): 3036  $\text{cm}^{-1}$ ( $\nu_{\text{NH}}$ ).  $^1\text{H}$  NMR in  $D_2O$  (N-D complex):  $\delta$  3.80 (4H, dd,  $J = 15.0, 7.3$  Hz), 3.49 (4H, td,  $J = 12.3, 7.4$  Hz), 3.19 (4H, s, cross-bridging  $\text{CH}_2\text{CH}_2$ ), 3.11 (4H, br dd,  $J = 12.1, 6.3$  Hz), 2.98 (4H, ddd,  $J = 15.1, 11.8, 6.3$  Hz); in  $\text{CD}_3\text{CN}$ :  $\delta$  4.49 (2H, br s, NH) 3.71 (4H, ~dt,  $J = 15.4, 7.6$  Hz), 3.56 (4H, td,  $J = 12.0, 7.5$  Hz), 3.05 (4H, s, cross-bridging  $\text{CH}_2\text{CH}_2$ ), 2.98 (4H, br dd,  $J = 12.4, 6.1$  Hz), 2.84 (4H, dddd,  $J = 15.0, 11.6, 6.3, 3.4$  Hz);  $^{13}\text{C}\{^1\text{H}\}$  NMR of N-deuterated complex in



$D_2O$ :  $\delta$  54.03, 49.74, 49.69; in  $CD_3CN$ :  $\delta$  54.65, 50.62, 50.23. Anal. Calcd. for  $InBr_3(C_{10}H_{22}N_4)$ : C, 21.73; H, 4.01; N, 10.13%. Found: C, 21.67; H, 4.09; N, 10.05%.

**[Ga•(8-2H)](NO<sub>3</sub>) (153)**: To a MeOH solution (14 mL) of **8•TFA•H<sub>2</sub>O** (66.4 mg, 0.155 mmol), a solution of Ga(NO<sub>3</sub>)<sub>3</sub> hydrate (38.6 mg, 0.15 mmol) in MeOH (6 mL) was added to form a clear solution. Anhydrous NaOAc (46.3 mg, 0.55 mmol) in MeOH (7 mL) was then added in two portions. After refluxing for 2 days, a white precipitate formed and was centrifuged off. This white precipitate was dried (41.9 mg, 62%) and dissolved in a H<sub>2</sub>O (2.6 mL) / MeOH (3.2 mL) mixture. Et<sub>2</sub>O/MeOH (1:1) vapor diffusion into this H<sub>2</sub>O/MeOH solution yielded crystals suitable for X-ray analyses. IR (KBr): 1692 (s), 1672 (s) cm<sup>-1</sup> ( $\nu_{C=O}$ ), 1363 (s), 1351 (s), 1339 (s), 1299 (s), 1284 (s) cm<sup>-1</sup> (broad) ( $\nu_{NO_3}$ ). <sup>1</sup>H NMR in  $D_2O$ :  $\delta$  4.04 (4H, AB, CH<sub>2</sub>COO), 3.57-3.85 (10H, m), 3.38-3.54 (6H, m), 3.18-3.31 (4H, s, cross-bridging CH<sub>2</sub>CH<sub>2</sub>); <sup>13</sup>C{<sup>1</sup>H} data in  $D_2O$ :  $\delta$  174.89, 64.07, 63.67, 57.11, 57.09, 54.87, 51.78; in  $d_6$ -DMSO:  $\delta$  169.92, 63.65, 61.92, 56.21, 55.35, 54.06, 50.25. Anal. Calcd. For GaC<sub>14</sub>H<sub>24</sub>N<sub>4</sub>O<sub>4</sub>(NO<sub>3</sub>): C, 37.86; H, 5.45; N, 15.77%. Found: C, 37.82; H, 5.45; N, 15.75%.

**Cu<sub>2</sub>(OH)(1)<sub>2</sub>(ClO<sub>4</sub>)<sub>3</sub>(H<sub>2</sub>O) (154)**: To a solution of ligand **1** (110.3 mg, 0.487 mmol) in methanol (8 mL) was added a 12 mL methanol solution of Cu(ClO<sub>4</sub>)<sub>2</sub>•6H<sub>2</sub>O (184.0 mg, 0.497 mmol). A dark-blue methanol solution formed. After one day of refluxing, diethyl ether vapor diffusion into this solution yielded 85.5 mg (38%) of blue crystals. Electronic spectrum (CH<sub>3</sub>CN):  $\lambda_{max}$  ( $\epsilon$ ) = 584 nm (151 M<sup>-1</sup>cm<sup>-1</sup>), 904 (71); (H<sub>2</sub>O):  $\lambda_{max}$  ( $\epsilon$ ) = 595 nm (93 M<sup>-1</sup>cm<sup>-1</sup>), 958 (69). IR (KBr): 3537 (br  $\nu_{OH}$ ), 3270 ( $\nu_{NH}$ ), 1096 (strong,  $\nu_{ClO_4}$ ) cm<sup>-1</sup>.

Anal. Calcd. for  $\text{Cu}_2(\text{OH})(\text{C}_{12}\text{H}_{26}\text{N}_4)_2(\text{ClO}_4)_3 (\text{H}_2\text{O})$ : C, 31.57; H, 6.07; N, 12.27; Cl, 11.65%. Found: C, 31.84; H, 6.27; N, 12.05, Cl, 11.21% .

**[Cu•2( $\mu$ -Cl)]<sub>2</sub>Cl<sub>2</sub> (155):** To a mixture of 28 mg (0.14 mmol) of ligand 2 and 19 mg (0.14 mmol) of CuCl<sub>2</sub>, 5 mL of absolute EtOH was added to form a dark-blue solution. This solution was refluxed overnight. Et<sub>2</sub>O vapor diffusion into this solution yielded blue crystalline solid (40 mg, 85%). X-ray crystals were obtained from diethyl ether vapor diffusion into a MeOH solution of it. Electronic spectrum (H<sub>2</sub>O):  $\lambda_{\text{max}}$  ( $\epsilon$ ) = 275 nm (3,620 M<sup>-1</sup>cm<sup>-1</sup>), 640 nm (72 M<sup>-1</sup>cm<sup>-1</sup>). IR (KBr): 3448 (br,  $\nu_{\text{OH}}$ ), 3180, 3150 cm<sup>-1</sup> ( $\nu_{\text{NH}}$ ). Anal. Calcd. for  $\text{CuCl}_2(\text{C}_{10}\text{H}_{22}\text{N}_4)(\text{H}_2\text{O})_{0.25}$ : C, 35.61; H, 6.72; N, 16.61%. Found: C, 35.57; H, 6.42; N, 16.47%.

**Cu(2)(ClO<sub>4</sub>)<sub>2</sub> (156):** To a solution of ligand 2 (36.8 mg, 0.19 mmol) in 5 mL absolute ethanol was added Cu(ClO<sub>4</sub>)<sub>2</sub>•6H<sub>2</sub>O (68.8 mg, 0.19 mmol). After refluxing for half an hour, some blue crystalline solid formed and was centrifuged off from a dark-blue solution. This dark-blue solution was then diffused with Et<sub>2</sub>O to yield needle-shaped crystals (64.2 mg, 72%). Crystals suitable for X-ray analyses were grown out from a methanol solution. The X-ray structure of these crystals showed a Cu(II) complex with a composition of [Cu(2)(CH<sub>3</sub>OH)(ClO<sub>4</sub>)](ClO<sub>4</sub>) (156a). Electronic spectrum (H<sub>2</sub>O):  $\lambda_{\text{max}}$  ( $\epsilon$ ) = 635 nm (76 M<sup>-1</sup>cm<sup>-1</sup>). IR (KBr): 3425 (br,  $\nu_{\text{OH}}$ ), 3299 cm<sup>-1</sup> (slightly br,  $\nu_{\text{NH}}$ ), 1104 cm<sup>-1</sup> (br,  $\nu_{\text{ClO}_4}$ ); IR of crystals grown from MeOH (KBr): 3420 (br,  $\nu_{\text{OH}}$ ), 3314, 3282 (slightly br,  $\nu_{\text{NH}}$ ), 1098 cm<sup>-1</sup> (very br,  $\nu_{\text{ClO}_4}$ ). Anal. Calcd. for  $[\text{Cu}(\text{C}_{10}\text{H}_{22}\text{N}_4)](\text{H}_2\text{O})_{0.5}(\text{ClO}_4)_2$ : C, 25.57; H, 4.94; N, 11.93%. Found: C, 25.76; H, 5.19; N, 11.58%.

**Cu(3)(ClO<sub>4</sub>)<sub>2</sub> (157):** To a solution of ligand 3 (70 mg, 0.172 mmol) in 2 mL methanol was added a methanol solution (4 mL) of Cu(ClO<sub>4</sub>)<sub>2</sub>•6H<sub>2</sub>O (56 mg, 0.151 mmol). A cloudy pale-blue solution was formed. After 2 days of refluxing followed by cooling, a dark blue solid formed and was separated from this methanol solution and dried to yield 96 mg (81%) of a blue solid which is soluble in MeCN and DMF, slightly soluble in MeOH, and insoluble in CHCl<sub>3</sub> and t-butanol. Blue crystals suitable for X-ray analyses were obtained by the slow evaporation of a MeCN solution containing this solid. The X-ray structure of these crystals showed a Cu(II) complex with a composition of [Cu(3)(CH<sub>3</sub>CN)](ClO<sub>4</sub>)<sub>2</sub> (**157a**). Electronic spectrum (CH<sub>3</sub>CN): λ<sub>max</sub> (ε) = 340 nm (12400 M<sup>-1</sup>cm<sup>-1</sup>), 623 (129); (a saturated solution in CH<sub>3</sub>OH): λ<sub>max</sub> = 324, 648 nm. IR (KBr) of the blue solid: 1097 cm<sup>-1</sup> (broad, ν<sub>ClO<sub>4</sub></sub>), 1055 (strong and broad, ν<sub>ClO<sub>4</sub></sub>). IR (KBr) of X-ray-crystals: 2314 (ν<sub>C≡N</sub>), 2286 (ν<sub>C≡N</sub>), 1086 cm<sup>-1</sup> (strong, ν<sub>ClO<sub>4</sub></sub>). Anal. Calcd. for CuC<sub>26</sub>H<sub>38</sub>N<sub>4</sub>(ClO<sub>4</sub>)<sub>2</sub>: C, 46.68; H, 5.72; N, 8.37%. Found: C, 46.33; H, 5.85; N, 8.26%.

**CuCl<sub>2</sub>•4 (158):** To a solution of ligand 4 (202 mg, 0.533 mmol) in absolute MeOH (6 mL), a MeOH solution (5 mL) of CuCl<sub>2</sub> (72.8 mg, 0.541 mmol) was added. A cloudy blue solution formed was refluxed for 9.5 hours to yield a dark-blue solution and some brown precipitate. This dark-blue solution was centrifuged off from the brown precipitate and diffused with diethyl ether to give dark blue crystals (191.6 mg, 68%). Electronic spectrum (CH<sub>3</sub>CN): λ<sub>max</sub> (ε) = 710 nm (85 M<sup>-1</sup>cm<sup>-1</sup>). IR (KBr) of the blue-crystals: 3398 cm<sup>-1</sup> (br, ν<sub>OH</sub>). Anal. Calcd. for CuCl<sub>2</sub>C<sub>24</sub>H<sub>34</sub>N<sub>4</sub> (H<sub>2</sub>O): C, 54.28; H, 6.83; N, 10.55%. Found: C, 54.07; H, 7.04; N, 10.36%.

**Unexpected synthesis of  $[\text{Cu}_2(\mu\text{-}\eta^1\text{:}\eta^2\text{-CO}_3)(4)_2](\text{ClO}_4)_2$  in an attempted synthesis of  $\text{Cu}(4)(\text{ClO}_4)_2$  (159):** To a solution of ligand 4 (107 mg, 0.283 mmol) in 4 mL methanol was added a methanol solution (6 mL) of  $\text{Cu}(\text{ClO}_4)_2 \cdot 6\text{H}_2\text{O}$  (108 mg, 0.291 mmol). A cloudy pale-blue solution was formed. After 1.5 days of refluxing, a dark-blue solution formed was separated from a brown precipitate. Diethyl ether vapor diffusion into this solution yielded blue crystals suitable for X-ray analyses as well as some colorless crystals. The blue crystals (66.8 mg, 40 %) were collected manually. Electronic spectrum (MeOH):  $\lambda_{\text{max}} (\epsilon) = 295 \text{ nm} (9986 \text{ M}^{-1}\text{cm}^{-1}), 687 (187)$ ; MeCN:  $\lambda_{\text{max}} (\epsilon) = 660 \text{ nm} (148 \text{ M}^{-1}\text{cm}^{-1})$ . IR (KBr) of the blue-crystals: 3420 (br,  $\nu_{\text{OH}}$ ), 1506, 1496 (strong,  $\nu_{\text{C=O}}$ ), 1095  $\text{cm}^{-1}$  (strong,  $\nu_{\text{OC14}}$ ). IR (KBr) of the brown precipitate: 2500  $\text{cm}^{-1}$  (br). Anal. Calcd. for  $\text{Cu}_2\text{C}_{48}\text{H}_{68}\text{N}_8(\text{CO}_3)(\text{ClO}_4)_2(\text{H}_2\text{O})_{1.5}$ : C, 50.30; H, 6.12; N, 9.58%. Found: C, 50.09; H, 5.91; N, 9.51%.

**$\text{Cu}(4)(\text{ClO}_4)_2$  (160):** A mixture of ligand 4 (69.7 mg, 0.184 mmol) and  $\text{Cu}(\text{ClO}_4)_2 \cdot 6\text{H}_2\text{O}$  (75.4 mg, 0.203 mmol) were dried in vacuum for about an hour. Then under nitrogen, 10 mL of methanol was added to this mixture. A cloudy pale-blue solution was formed immediately. After one day of refluxing, a dark-blue precipitate (64.7 mg, 51%) was separated from a dark blue solution. Some of this dark-blue precipitate was dissolved in MeCN to form a dark-blue solution. Diethyl ether vapor diffusion into this solution yielded blue block-shaped crystals. Electronic spectrum ( $\text{CH}_3\text{OH}$ ) of the dark-blue precipitate:  $\lambda_{\text{max}} (\epsilon) = 301 \text{ nm} (3735 \text{ M}^{-1}\text{cm}^{-1}), 657 \text{ nm} (94 \text{ M}^{-1}\text{cm}^{-1})$ . Electronic spectrum ( $\text{CH}_3\text{CN}$ ) of the blue crystals:  $\lambda_{\text{max}} (\epsilon) = 304 \text{ nm} (1184 \text{ M}^{-1}\text{cm}^{-1}), 647 \text{ nm} (162 \text{ M}^{-1}\text{cm}^{-1})$ . IR (KBr) of the dark-blue precipitate: 1108  $\text{cm}^{-1}$

(strong,  $\nu_{\text{ClO}_4}$ ), 1091 (strong,  $\nu_{\text{ClO}_4}$ ). IR (KBr) of the blue crystals: 2333 ( $\nu_{\text{C}\equiv\text{N}}$ ), 2305 ( $\nu_{\text{C}\equiv\text{N}}$ ), 1102  $\text{cm}^{-1}$  (strong,  $\nu_{\text{ClO}_4}$ ), 1089  $\text{cm}^{-1}$  (strong,  $\nu_{\text{ClO}_4}$ ). Anal. Calcd. for the dark-blue precipitate,  $\text{CuC}_{24}\text{H}_{34}\text{N}_4(\text{ClO}_4)_2(\text{H}_2\text{O})_{2.5}$ : C, 42.02; H, 5.73; N, 8.17%. Found: C, 41.98; H, 5.57; N, 7.91%. Anal. Calcd. for the dark-blue crystals,  $\text{CuC}_{24}\text{H}_{34}\text{N}_4(\text{ClO}_4)_2(\text{CH}_3\text{CN})_2$ : C, 46.51; H, 5.58; N, 11.62%. Found: C, 46.30; H, 5.60; N, 11.31%.

**[Cu•5](NO<sub>3</sub>)<sub>2</sub> (161):** A mixture of **5**•(H<sub>2</sub>O)<sub>0.5</sub> (136.9 mg, 0.392 mmol) and Cu(NO<sub>3</sub>)<sub>2</sub>•3H<sub>2</sub>O (95.8 mg, 0.397 mmol) in MeOH (16 mL) was refluxed for 17 hours to form a dark-blue MeOH solution and some bluish brown precipitate. This MeOH solution was then centrifuged off from the bluish brown precipitate. Et<sub>2</sub>O vapor diffusion into this MeOH solution yielded 138.7 mg of a blue crystalline solid, which was dissolved in H<sub>2</sub>O/MeOH mixture (1:1) and diffused by acetone vapor to form blue crystals. Electronic spectrum (H<sub>2</sub>O):  $\lambda_{\text{max}}$  ( $\epsilon$ ) = 286 nm (1348 M<sup>-1</sup>cm<sup>-1</sup>), 625 (34). IR (KBr): 3285, 3139  $\text{cm}^{-1}$  ( $\nu_{\text{OH}}$  and  $\nu_{\text{NH}}$ ), 1678 (s) ( $\nu_{\text{C}=\text{O}}$ ), 1604 (medium)  $\text{cm}^{-1}$ . Anal. Calcd. for  $\text{CuC}_{16}\text{H}_{32}\text{N}_6\text{O}_2(\text{NO}_3)_2\text{H}_2\text{O}$ : C, 35.19; H, 6.28; N, 20.52%. Found: C, 34.93; H, 6.24; N, 20.32%.

**[Cu•6](ClO<sub>4</sub>)<sub>2</sub> (162):** A mixture of ligand **6**•H<sub>2</sub>O (16.8 mg, 0.0508 mmol) and Cu(ClO<sub>4</sub>)<sub>2</sub>•6H<sub>2</sub>O (22.1 mg, 0.0596 mmol) in MeOH (11 mL) was refluxed for 1 day. After cooling to room temperature, this solution was diffused with Et<sub>2</sub>O vapor to yield 21.0 mg (72%) of blue crystals. Electronic spectrum (CH<sub>3</sub>CN):  $\lambda_{\text{max}}$  ( $\epsilon$ ) = 637 nm (89 M<sup>-1</sup>cm<sup>-1</sup>); H<sub>2</sub>O:  $\lambda_{\text{max}}$  ( $\epsilon$ ) = 627 nm (96 M<sup>-1</sup>cm<sup>-1</sup>). IR (KBr): 3439, 3359, 3309, 3256  $\text{cm}^{-1}$  ( $\nu_{\text{OH}}$  and  $\nu_{\text{NH}}$ ), 1682(s), 1661 (s)  $\text{cm}^{-1}$  ( $\nu_{\text{C}=\text{O}}$ ), 1612 (medium), 1593 (medium)  $\text{cm}^{-1}$  ( $\nu_{\text{C}=\text{O}}$  or

NH<sub>2</sub> bending). Anal. Calcd. for CuCl<sub>2</sub>C<sub>14</sub>H<sub>28</sub>N<sub>6</sub>O<sub>10</sub>: C, 29.25; H, 4.91; N, 14.62%. Found: C, 29.09; H, 5.19; N, 14.59%.

**[Cu•6](NO<sub>3</sub>)<sub>2</sub> (163):** A mixture of ligand **6**•H<sub>2</sub>O (65.5 mg, 0.198 mmol) and Cu(NO<sub>3</sub>)<sub>2</sub>•3H<sub>2</sub>O (48.4 mg, 0.200 mmol) in MeOH (9 mL) was refluxed for 26 hours. After cooling to room temperature, this clear dark-blue solution was diffused with Et<sub>2</sub>O vapor to yield 58.7 mg (58%) of blue crystals. Electronic spectrum (H<sub>2</sub>O): λ<sub>max</sub> (ε) = 627 nm (66 M<sup>-1</sup>cm<sup>-1</sup>). IR (KBr): 3293, 3138 (broad) (ν<sub>OH</sub> and ν<sub>NH</sub>), 1685 (s), 1670 (s) cm<sup>-1</sup> (ν<sub>C=O</sub>), 1619 cm<sup>-1</sup> (ν<sub>C=O</sub> or NH<sub>2</sub> bending). Anal. Calcd. for CuC<sub>14</sub>H<sub>28</sub>N<sub>6</sub>O<sub>2</sub>(NO<sub>3</sub>)<sub>2</sub>(H<sub>2</sub>O)<sub>0.5</sub>: C, 33.04; H, 5.74; N, 22.02%. Found: C, 33.44; H, 5.82; N, 21.92%.

**[Cu•(7-2H)](NaClO<sub>4</sub>)(NaCF<sub>3</sub>COO)<sub>0.5</sub>(H<sub>2</sub>O)<sub>1.5</sub> (164):** To a cloudy mixture of **7**•(TFA)<sub>2</sub>•H<sub>2</sub>O (289.9 mg, 0.4926 mmol) and Cu(ClO<sub>4</sub>)<sub>2</sub>•6H<sub>2</sub>O (182.5 mg, 0.4926 mmol) in 95% aqueous ethanol solution (36 mL), an aqueous solution of NaOH (0.9864 N, 2.00 mL) was added to form a slightly cloudy blue solution which was refluxed for 2 days. After a small amount of precipitate was centrifuged off, Et<sub>2</sub>O vapor diffusion into this solution yielded 217.5 mg (71%) of blue crystals. Electronic spectrum (H<sub>2</sub>O): λ<sub>max</sub> (ε) = 620 (43 M<sup>-1</sup>cm<sup>-1</sup>); (5 M HCl): λ<sub>max</sub> (ε) = 623 nm (47 M<sup>-1</sup>cm<sup>-1</sup>). IR (KBr): 3422 (br) (ν<sub>OH</sub>), 1624 (br, s), 1595 (br, s) (ν<sub>C=O</sub>). Anal. Calcd. for CuC<sub>16</sub>H<sub>28</sub>N<sub>4</sub>O<sub>4</sub>(NaClO<sub>4</sub>)(NaCF<sub>3</sub>COO)<sub>0.5</sub>(H<sub>2</sub>O)<sub>1.5</sub>: C, 32.86; H, 5.03; N, 9.02%. Found: C, 32.94; H, 5.26; N, 9.13%.

**[Cu•(8-2H)](NaClO<sub>4</sub>) (165):** To a MeOH solution (5 mL) of Cu(ClO<sub>4</sub>)<sub>2</sub>•6H<sub>2</sub>O (57.0 mg, 0.154 mmol), a mixture of a MeOH solution (7 mL) of **8**•TFA•H<sub>2</sub>O (64.3 mg, 0.150

mmol) and an aqueous solution of NaOH (0.970 N, 0.460 mL) was added to form a clear blue solution which was refluxed for 2 hours. After some precipitate was centrifuged off, diethyl ether vapor diffusion into this yielded 79.6 mg (98%) of a blue crystalline solid. Electronic spectrum (H<sub>2</sub>O):  $\lambda_{\max}(\epsilon) = 642 \text{ nm}$  ( $75 \text{ M}^{-1}\text{cm}^{-1}$ ); CH<sub>3</sub>CN:  $\lambda_{\max}(\epsilon) = 736 \text{ nm}$  ( $84 \text{ M}^{-1}\text{cm}^{-1}$ ). IR (KBr): 3422 (br) ( $\nu_{\text{OH}}$ )  $\text{cm}^{-1}$ , 1624 (s), 1595 (s) ( $\nu_{\text{C=O}}$ )  $\text{cm}^{-1}$ . Anal. Calcd. for CuC<sub>14</sub>H<sub>24</sub>N<sub>4</sub>O<sub>4</sub> (NaClO<sub>4</sub>)(H<sub>2</sub>O)<sub>2.5</sub>: C, 30.95; H, 5.38; N, 10.31%. Found: C, 30.89; H, 5.03; N, 10.12%.

**[Cu•(8-2H)](NaNO<sub>3</sub>) (166):** To a blue MeOH (25 mL) solution of Cu(NO<sub>3</sub>)<sub>2</sub>•3H<sub>2</sub>O (53.6 mg, 0.222 mmol) and 8•TFA•H<sub>2</sub>O (89.0 mg, 0.208 mmol), an aqueous solution of NaOH (0.970 N, 0.64 mL) was added to form a clear blue solution which was refluxed for 8 hours. After some precipitate was centrifuged off, Et<sub>2</sub>O vapor diffusion into 3/5 of this MeOH solution yielded 26.5 mg (38%) of blue block-shaped crystals. Electronic spectrum (H<sub>2</sub>O):  $\lambda_{\max}(\epsilon) = 647 \text{ nm}$  ( $57 \text{ M}^{-1}\text{cm}^{-1}$ ); CH<sub>3</sub>CN (a saturated solution):  $\lambda_{\max}(A) = 270 \text{ nm}$  ( $A = 0.950$ ), 760 ( $A = 0.037$ ). IR (KBr): 1638 (s), 1595 (s) ( $\nu_{\text{C=O}}$ )  $\text{cm}^{-1}$ . Anal. Calcd. for CuC<sub>14</sub>H<sub>24</sub>N<sub>4</sub>O<sub>4</sub> (NaNO<sub>3</sub>)<sub>2</sub>(H<sub>2</sub>O)<sub>0.5</sub>: C, 30.30; H, 4.54; N, 15.14; F, 0 %. Found: C, 30.60; H, 4.15; N, 14.85, F, < 0.25%.

**[Ni(μ-Cl)•1]<sub>2</sub>Cl<sub>2</sub> (167):** To a solution of ligand **1** (36.1mg, 0.159 mmol) in 8 mL of methanol was added a methanol solution of NiCl<sub>2</sub> (21.2 mg, 0.163 mmol) in 8 mL methanol. This was refluxed for three days to give a red solution. After cooling to room temperature, solvent was removed to yield a light red solid. This solid was washed by toluene and dried to yield [Ni•1(μ-Cl)]<sub>2</sub>Cl<sub>2</sub> (39.0 mg, 76%) as indicated by its CHN

elemental analyses. Crystals suitable for X-ray analyses were obtained from slow evaporation of a MeOH solution of the product. Electronic spectrum (CH<sub>3</sub>OH):  $\lambda_{\max}$  ( $\epsilon$ ) = 360 nm (37 M<sup>-1</sup>cm<sup>-1</sup>), 541 (13), 910 (17); (H<sub>2</sub>O):  $\lambda_{\max}$  = 515, 850 nm. IR (KBr): 3379 (br,  $\nu_{\text{OH}}$ ), 3240 and 3203 cm<sup>-1</sup> ( $\nu_{\text{NH}}$ ). Anal. Calcd. for NiCl<sub>2</sub>(C<sub>12</sub>H<sub>26</sub>N<sub>4</sub>)•0.5H<sub>2</sub>O: C, 39.49; H, 7.46; N, 15.35%. Found: C, 39.65; H, 7.30; N, 15.12%.

**Zn(NO<sub>3</sub>)<sub>2</sub>•(Me<sub>4</sub>Cyclam) (168):** To a solution of ligand **9** (235.4 mg, 0.918 mmol) in 2 mL of MeOH was added a MeOH solution (5 mL) of Zn(NO<sub>3</sub>)<sub>2</sub>•6H<sub>2</sub>O (281.1 mg, 0.945 mmol). The resulting clear solution was refluxed for 1 day. Et<sub>2</sub>O vapor diffusion into this clear solution yielded 398.3 mg (97%) of colorless needle-like crystals. <sup>1</sup>H NMR in D<sub>2</sub>O:  $\delta$  3.19 (4H, td,  $J$  = 12.8, 1.5 Hz), 2.49-3.07 (12H, m), 2.55 (12H, s, CH<sub>3</sub>), 2.33 (2H, qm,  $J$  = 14.2 Hz), 1.72 (2H, dp,  $J$  = 16.8, 2.0 Hz); in CD<sub>3</sub>CN:  $\delta$  3.27 (4H, broad t,  $J$  = 12.9 Hz), 2.55-2.84 (12H, m), 2.51 (12H, s, CH<sub>3</sub>), 2.16-2.33 (2H, qm, including one H<sub>2</sub>O peak), 1.61-1.71 (2H, m); <sup>13</sup>C{<sup>1</sup>H} in D<sub>2</sub>O:  $\delta$  61.12, 56.84, 44.19, 21.32; in CD<sub>3</sub>CN:  $\delta$  62.07, 57.91, 45.72, 22.79; Anal. Calcd. for Zn(NO<sub>3</sub>)<sub>2</sub>C<sub>14</sub>H<sub>32</sub>N<sub>4</sub>: C, 37.72; H, 7.23; N, 18.85%. Found: C, 37.63; H, 7.16; N, 19.26%.



## LIST OF REFERENCES:

1. Izatt R. M. and Christensen, J. J. *Synthetic Multidentate Macrocyclic Compounds*, Eds. Academic Press, 1978.
2. Pedersen, C. J. *J. Am. Chem. Soc.*, **1967**, *89*, 2495-2496.
3. Lehn, J. M. *Acc. Chem. Res.* **1978**, *11*, 49-57.
4. Curtis, N. F. *J. Chem. Soc.*, **1960**, 4409-4413.
5. Busch, D. H. *Acc. Chem. Res.* **1978**, *11*, 392-400.
6. Martell, A. E.; Smith, R. M. *Critical Stability Constants*, Volume 1-6, Plenum Press, New York, 1974-1989.
7. Meyer, M.; Dahaoui-Gindrey, V.; Lecomte, C.; Guillard, R. *Coord. Chem. Rev.*, **1998**, *178*, 1313-1405.
8. Wainwright, P. K. *Coord. Chem. Rev.*, **1997**, *166*, 35-90.
9. Heeg, J. M.; Jurisson, S. S. *Acc. Chem. Res.* **1999**, *32*, 1053-1060.
10. Dovinova, I.; Paulikova, H.; Rauko, P.; Hunakova, L.; Hanusovska, E.; Tibenska, E. *Toxicology in Vitro*, **2002**, *16(5)*, 491-498.
11. Richert, d. E.; Lewis, J. S.; Anderson, C. J. *Coord. Chem. Rev.*, **1999**, *184*, 3-66.
12. Williams, N. H.; Takasaki, B.; Wall, M.; Chin, J. A. *Acc. Chem. Res.* **1999**, *32*, 485-493.
13. Wainwright, K. P. *Advances in Inorganic Chemistry*, **2001**; Vol. 52, pp 293-335.
14. Aoki, S.; Zulkefi, M.; Shiro, M.; Kimura, E. *Proc. Nat. Acad. Sci. USA*, **2002**, *99*, 4894-4899.
15. Aoki, S.; Shiro, M.; Koike, T.; Kimura, E. *Chem.-Eur. J.* **2002**, *8*, 929-939.
16. Aoki, S.; Shiro, M.; Koike, T.; Kimura, E. *J. Am. Chem. Soc.* **2000**, *122*, 576-584.
17. Fabbrizzi, L.; Licchelli, M.; Pallavicini, P. *Acc. Chem. Res.* **1999**, *32*, 846-853.

18. Weisman, G. R.; Rogers, M. E.; Wong, E. H.; Jasinski, J. P.; Paight, E. S. *J. Am. Chem. Soc.*, **1990**, *112*, 8604.
19. Weisman, G. R.; Wong, E. H.; Hill, D. C.; Rogers, M. E.; Reed, D. P.; Calabrese, J. C. *J. Chem. Soc. Chem. Commun.*, **1996**, 947.
20. Bosnich, B.; Poon, C. K.; Tobe, M. L. *Inorg. Chem.* **1965**, *4*, 1102-1108.
21. Donnelly, A. M.; Zimmer, M. *Inorg. Chem.* **1999**, *38*, 1650-1658.
22. (a) Martell, A. E.; Hancock, R. D. *Metal Complexes in Aqueous Solutions*, Plenum Press, New York, 1996, p 97-147. (b) Bucher, C.; Duval, E.; Espinosa, E.; Barbe, J.; Verpeaux, J.; Amatore, C.; Guilard, R. *Eur. J. Inorg. Chem.* **2001**, 1077-1079. (c) Schonherr, T. S.; Weber, E.; Seichter, W. *Z. Anorg. Allg. Chem.* **2001**, *627*, 2420. (d) Kickelbick, G.; Pintauer, T.; Matyjaszewski, K. *New J. Chem.* **2002**, *26*, 462. (e) Maimon, E.; Zilbermann, I.; Golub, G.; Ellem, A.; Shames, A. I.; Cohen, H.; Meyerstein, D. *Inorg. Chim. Acta.* **2001**, *324*, 65.
23. (a) Ito, T.; Kato, M.; Ito, H. *Bull. Chem. Soc. Jpn.* **1984**, *57*, 2634-2640. (b) Porai-Koshits, M. A.; Antsyshkina, A. S.; Shevchenko, Y. N.; Yashina, N. I.; Vavava, F. B. *Zh. Neorg. Khim.* **1994**, *139*, 4351. (c) Tyson, T. A.; Hodgson, K. O.; Hedman, B.; Clark, G. R. *Acta Crystallogr.* **1990**, *C40*, 1638. (d) Riesen, A.; Zehnder, M.; Kaden, T. A. *Acta Crystallogr.* **1991**, *C47*, 531. (e) Choi, K.; Chun, K. M.; Suh, II. *Main Group Metal Chemistry*, **1998**, *21*, 623. (f) Choi, K.-Y. *J. Chem. Cryst.* **1999**, *29*, 1015. (g) Alcock, N. W.; Berry, A.; Moore, P. *Acta Crystallogr.* **1992**, *C48*, 16. (h) Antsyshkina, A. S.; Porai-Koshits, M. A.; Saidov, B. I.; Mal'tseva, N. N.; Kedrova, N. S.; Ostrikoval, V. N. *Zh. Neorg. Khim.* **1991**, *136*, 2291. (i) Kato, M.; Ito, T. *Inorg. Chem.* **1985**, *24*, 504-508. (j) Choi, K.-Y. *Polyhedron* **1998**, *17*, 1975-1982. (k) Comba, P.; Luther, S. M.; Maas, O.; Pritzkow, H.; Vielfort, A. *Inorg. Chem.* **1991**, *40*, 2335. (l) Choi, K.-Y.; Suh, II-H.; Kim, J. *Polyhedron* **1997**, *16*, 1783-1786.
24. (a) Choi, K.; Kim, D. W.; Suh, II. *Bull. Korean Chem. Soc.* **1998**, *19*, 135. (b) Hu, H.; Sun, H.; You, X.; Huan, X. *Acta Crystallogr.* **1996**, *C52*, 1946. (c) Choi, K.-Y. *Polyhedron* **1997**, *16*, 2073. (d) Pickardt, J.; Staub, B.; Gong, G. T. *Z. Kristallogr.* **1994**, *209*, 554. (e) Davis, P. J.; Taylor, M. R.; Wainwright, K. P. *J. Chem. Soc. Chem. Commun.* **1998**, 827.
25. (a) Alcock, N. W.; Herron, N.; Moore, P. *J. Chem. Soc. Dalton Trans.* **1978**, 1282. (b) Kato, M.; Ito, T. *Inorg. Chem.* **1985**, *24*, 509-514. (c) Panneerselvam, K.; Lu, T.; Chi, T.; Tung, S.; Chung, C. *Anai. Sci.* **1999**, *15*, 205.

26. (a) Liang, X.; Parkinson, J. A.; Parsons, S.; Weishäupl, M.; Gould, R. O.; Paisey, S. J.; Park, H.-S.; Hunter, T. M.; Blindauer, C. A.; Parsons, S.; Salder, P. *J. Am. Chem. Soc.* **2002**, *124*, 9105-9112. (b) Plenio, H.; Aberie, C.; Shihadeh, Y. A.; Lloris, J.M.; Martinez-Manez, R.; Pardo, T.; Soto, T. *Chem.-Eur. J.* **2001**, *7*, 2848-2861. (c) Choi, K.; Suh, H. *Main Group Metal Chemistry*, **1999**, *22*, 123-126. (d) Bernhardt, P. V.; Moore, E. G.; Riley, M. J. *Inorg. Chem.* **2002**, *41*, 3025-3031. (e) Malinovskii, S. T.; Simonov, Y. A.; Nazarenko, A. Y.; Pinaeva, S. G. *Zh. Struki. Khim.* (Russ.) **1988**, *129*, 128-132.
27. Kato, M.; Ito, T. *Bull. Chem. Soc. Jpn.* **1986**, *59*, 285-294.
28. Kimura, E.; Kurosaki, H.; Koike, T.; Toriumi, K. *Journal of Inclusion Phenomena and Molecular Recognition in Chemistry* **1992**, *12*, 377-87.
29. (a) Schrod, A.; Neubrand, A.; van Eldik, R. *Inorg. Chem.* **1997**, *36*, 4579-4584. (b) Koike, T.; Kajitani, S.; Nakamura, I.; Kimura, E.; Shiro, M. *J. Am. Chem. Soc.* **1995**, *117*, 1210-1219. (c) Koike, T.; Watanabe, T.; Aoki, S.; Kimura, E.; Shiro, M. *J. Am. Chem. Soc.* **1996**, *118*, 12696-12703. (d) Shionoya, M.; Kimura, E.; Shiro, M. *J. Am. Chem. Soc.* **1993**, *115*, 6730-6737. (e) Kimura, E.; Gotoh, T.; Koike, T.; Shiro, M. *J. Am. Chem. Soc.* **1999**, *121*, 1267-1274. (f) Aoki, S.; Iwaida, K.; Hanamoto, N.; Shiro, M.; Kimura, E. *J. Am. Chem. Soc.* **2002**, *124*, 5256-5257. (g) Kimura, E.; Aoki, S.; Koike, T.; Shiro, M. *J. Am. Chem. Soc.* **1997**, *119*, 3068. (h) Pariya, C.; Chi, T.-Y.; Mishra, T. K.; Chung, C.-S. *Inorg. Chem. Commun.* **2002**, *5*, 119. (i) Kobayashi, K.; Shionoya, M.; Kimura, E.; Tsuboyama, K.; Tsuboyama, S. *Anal. Sci.* **1995**, *11*, 1029. (j) Marsh, R. E. *Acta Crystallogr.* **1999**, *B55*, 931. (k) Kimura, E.; Kitamura, H.; Koike, T.; Shiro, M. *J. Am. Chem. Soc.* **1997**, *119*, 10909. (l) Bu, X.; Cao, X.; Yuan, M.; Wan, X.; Chen, R. *Jie Gou Hua Xue* (Chin.) (*J. Struct. Chem.*) **1996**, *115*, 499.
30. (a) Norate, G. M.; Vaira, M. D.; Mazzi, S.; Stoppioni, P. *Inorg. Chem.* **1990**, *29*, 2822. (b) Vaira, M. D.; Mani, F.; Stoppioni, P. *J. Chem. Soc. Dalton Trans.* **1998**, 1879-1884. (c) Aoki, S.; Kawatani, H.; Kimura, E.; Shiro, M. *J. Am. Chem. Soc.* **2001**, *123*, 1123-1132.
31. Kimura, E.; Kikuta, E. *JBIC* **2000**, *5*, 139-155.
32. Kimura, E. *Progress in Inorganic Chemistry*, **1994**, *41*, 443-91.
33. Kimura, E.; Koike, T. *Comm. Inorg. Chem.*, **1991**, *11*, 285-301.
34. Kimura, E. *Acc. Chem. Res.* **2001**, *34*, 171-179.
35. Kim, E. E.; Wyckoff, H. W. *J. Mol. Biol.* **1991**, *218*, 449-464.

36. Kimura, E.; Kodama, Y.; Koike, T.; Shiro, M. *J. Am. Chem. Soc.* **1995**, *117*, 8304-8311.
37. Kimura, E.; Gotoh, T.; Aoki, S.; Shiro, M. *Inorg. Chem.* **2002**, *41*, 3239-3248.
38. Zhang, X.; van Eldik, R. *Inorg. Chem.* **1995**, *34*, 5606-5614.
39. (a) Kimura, E.; Ikeda, T.; Shionoya, M.; *Pure & Appl. Chem.* **1997**, *115*, 6730-6737. (b) Shiro, M.; Honda, Y.; Kimura, E. *J. Am. Chem. Soc.* **1998**, *120*, 10018-10026. (c) Kimura, E.; Kikuchi, M.; Kitamura, H.; Koike, T. *Chem. Eur. J.* **1999**, *5*, 3113-3123. (d) Aoki, S.; Shiro, M.; Koike, T.; Kimura, E. *J. Am. Chem. Soc.* **2000**, *122*, 576-584. (e) Kimura, E.; Katsube, N.; Koike, T.; Shiro, M.; Aoki, S. *Supramol. Chem.* **2002**, *14*, 95-102.
40. Maumela, H.; Hancock, R. D.; Carlton, L.; Reibenspies, J. H.; Wainwright, K. P. *J. Am. Chem. Soc.* **1995**, *117*, 6698-6707.
41. Weeks, J. M.; Taylor, M. R.; Wainwright, K. P. *J. Chem. Soc. Dalton Trans.* **1997**, 317.
42. (a) Smith, C. B.; Stephens, A. K. W.; Wallwork, K.S.; Lincoln, S. F.; Taylor, M. R.; Wainwright, K. P. *Inorg. Chem.* **2002**, *41*, 1093. (b) Smith, C. B.; Wallwork, K.S.; Weeks, J. M.; Buntine, M. A.; Lincoln, S. F.; Taylor, M. R.; Wainwright, K. P. *Inorg. Chem.* **1999**, *41*, 4986. (c) Smith, C. B.; Stephens, A. K. W.; Wallwork, K.S.; Lincoln, S. F.; Taylor, M. R.; Wainwright, K. P. *Acta. Crystallogr.* **2000**, *C56*, 28. (d) Smith, C. B.; Lincoln, S. F.; Taylor, M. R.; Wainwright, K. P. *Acta. Crystallogr.* **2002**, *E58*, m33. (e) Variz, M. D.; Mani, F.; Menicatti, M.; Morassi, R.; Stoppioni, P. *Polyhedron* **1997**, *16*, 3585.
43. (a) Bernhardt, P. V.; Comba, P.; Hambley, T. W.; Lawrance, G. A.; Varnagy, K. *J. Chem. Soc. Dalton Trans.* **1992**, 355. (b) Liang, X.; Parkinson, J. A.; Parsons, S.; Weishaupl, M.; Salder, P. J. *Inorg. Chem.* **2002**, *41*, 4539-4547. (c) Ito, H.; Ito, T. *Acta. Crystallogr.* **1985**, *C41*, 1598. (d) Choi, K.-Y.; Suh, M.; Kim, J.; Choo, G.-H.; Suh, H. Ng, S. W. *Main Group Metal Chemistry* **2001**, *24*, 119. (e) Dong, Y.; Farquhar, S.; Gloe, K.; Lindoy, L.; Rumel, B. R.; Turner, P.; Wichmann, K. *J. Chem. Soc. Dalton Trans.* **2003**, 1558-1566.
44. (a) Yamaguchi, T.; Yamazaki, F.; Ito, T. *J. Am. Chem. Soc.* **1999**, *121*, 7405. (b) Shihadeh, Y. A.; Benito, A.; Iloris, J. M.; Martinez-Manez, R.; Pardo, T.; Soto, J.; Marcos, M. D. *J. Chem. Soc. Dalton Trans.* **2000**, 1199.
45. (a) Alcock, N. W.; Curson, E. H.; Herron, N.; Moore, P. *J. Chem. Soc. Dalton Trans.* **1979**, 1987. (b) Lye, P. G.; Lawrance, G. A.; Maeder, M.;

- Skelton, B. W.; Wen, H.; White, A. H. *J. Chem. Soc. Dalton Trans.* **1994**, 793. (c) Burke, M. R.; Richardson, M. F. *Inorg. Chim. Acta.* **1983**, 69, 29.
46. (a) Chin, J. *Acc. Chem. Res.* **1991**, 24, 145. (b) Williams, N. H.; Takasaki, B.; Wall, M.; Chin, J. A. *Acc. Chem. Res.* **1999**, 32, 485-493. (c) Buckingham, A. D.; Clark, R. C. *Metal Ions in Biological Systems* **2001**, 38, 43-102.
47. Kim, J.-H.; Britten, J.; Chin, J. *J. Am. Chem. Soc.* **1993**, 115, 3618-3622.
48. (a) Buckingham, D. A.; Clark, C. R.; Rogers, A. J.; Simpson, J. *Inorg. Chem.* **1995**, 34, 3646-3657. (b) Buckingham, D.; Clark, C. R.; Rogers, A. J. *Inorg. Chim. Acta* **1995**, 240, 125-134. (c) Clark, C. R.; Buckingham, D. A. *Inorg. Chim. Acta* **1997**, 254, 339-343. (d) Buckingham, D. A.; Clark, C. R.; Rogers, A. J. *Inorg. Chem.* **1997**, 36, 3791-3793. (e) Buckingham, A. D.; Clark, R. C.; Rogers, A. J. *J. Am. Chem. Soc.* **1997**, 119, 4050-4058. (f) Buckingham, D. A.; Clark, C. R.; Rogers, A. J.; Simpson, J. *Aust. J. Chem.* **1998**, 51, 461-469. (g) Buckingham, D. A.; Clark, C. R.; Rogers, A. J.; Simpson, J. *Inorg. Chem.* **1998**, 37, 3497-3504. (h) Brasch, N. E.; Buckingham, D. A.; Clark, C. R.; Rogers, A. J.; Simpson, J. *Inorg. Chem.* **1998**, 37, 4865-4871. (i) Andrea, J.; Buckingham, D. A.; Rogers, A. J.; Blackman, G. A.; Clark, C. R. *Inorg. Chem.* **2000**, 39, 4769-4775.
49. Wilkinson, S. R.; Gillard, R. D.; McCleverty, J. A. *Comprehensive Coordination Chemistry*, Pergamon Press, 1987, vol.5, p533.
50. (a) Scott, M. J.; Holm, R. H. *J. Am. Chem. Soc.* **1994**, 116, 11357. (b) Kang, S.-G.; Kim, S.-J.; Jeong, J. H. *Polyhedron* **1998**, 17, 3227. (c) Kato, M.; Ito, T. *Bull. Chem. Soc. Jpn.* **1986**, 59, 285-294. (d) Bernhardt, P. V.; Sharpe, P. C. *Inorg. Chem.* **2000**, 39, 2020. (e) Bulach, V.; Mandon, D.; Fisher, J.; Weiss, R.; Bil, E.; Butzlaff, C.; Trautwein, A. X. *New J. Chem.* **1994**, 18, 709. (f) Esley, J.; Arif, M.; Bates, P. A.; Hursthouse, M. B. *J. Mol. Struct.* **1990**, 220, 1. (g) Lu, T.-H.; Tahirov, T. H.; Liu, Y.-L.; Chung, C.-S.; Huang, C.-C.; Hong, Y.-S. *Acta. Crystallogr.* **2002**, C52, 1093. (h) Emsley, J.; Arif, M.; Bates, P. A.; Hursthouse, M. B. *J. Chem. Soc. Chem. Commun.*, **1988**, 1387. (i) Aneetha, H.; Lai, Y.-H.; Lin, S.-C.; Panneerselvam; Lu, T.-H.; Chung, C.-S. *J. Chem. Soc. Dalton Trans.* **1999**, 2885. (j) Lawrance, G. A.; Skelton, B. W.; White, A. H.; Comba, P. *Aust. J. Chem.* **1986**, 39, 1101. (k) Bernhardt, P. V.; Moore, E. G.; Riley, M. J. *Inorg. Chem.* **2001**, 40, 5799. (l) Willett, R. D.; Vij, A. *J. Chem. Cryst.* **2000**, 30, 399. (m) Ochiai, E.-I.; Rettig, S. J.; Trotter, J. *Can. J. Chem.* **1978**, 56, 267. (n) Bernhardt, P. V.; Sharpe, P. C. *Inorg. Chem.* **1998**, 37, 1629.
51. (a) Lu, T.-H.; Wu, D.-T.; Chung, C.-S. *J. Chem. Soc. Dalton Trans.* **1999**, 1986. (b) Lee, T.-J.; Lee, T.-Y.; Hong, C.-Y.; Wu, D.-T.; Chung, C.-S. *Acta. Crystallogr.* **1986**, C42, 999. (c) Maimon, E.; Zilbermann, I.; Golub, G.; Ellem, A.; Shames, A. I.; Cohen, H.; Meyerstein, D. *Inorg. Chim. Acta.* **2001**,

- 324, 65. (d) Harrowfield, J. M.; Sargeson, A. M.; Skelton, B. W.; White, A. *H. Aust. J. Chem.* **1994**, *47*, 181. (e) Lu, T. -H.; Shui, W.-Z.; Tung, S.-F.; Chi, T.-Y.; Liao, F.; Chung, C. -S. *Acta. Crystallogr.* **1998**, *C54*, 1071. (f) Tahirov, T. H.; Lu, T.-H.; Liao, F.-L.; Wang, S.-L.; Chen, B.-H.; Chi, T.-Y.; Chung, C. -S. *Acta. Crystallogr.* **1996**, *C52*, 2687. (g) Oberholzer, M. R.; Neuburger, M.; Zehnder, M.; Kaden, T. A. *Helv. Chim. Acta.* **1995**, *78*, 505. (h) Comba, P.; Jurisic, P.; Lampeka, Y. D.; Peters, A.; Prikhod'ko, A. I.; Pritzkow, H. *Inorg. Chim. Acta.* **2001**, *324*, 99.
52. (a) Lu, T.-H.; Lin, S.-C.; Aneetha, H.; Panneerselvam, K.; Chung, C.-S. *J. Chem. Soc. Dalton Trans.* **1999**, 3385. (b) Kowallick, R.; Neuburger, M.; Zehnder, M.; Kaden, T. A. *Helv. Chim. Acta.* **1997**, *80*, 948. (c) Patrick, G.; Ngwenya, M. P.; Dobson, S. M.; Hancock, R. D. *J. Chem. Soc. Dalton Trans.* **1991**, 1295. (d) Lancashire, R. J.; Newman, P. D. *J. Coord. Chem.* **1995**, *34*, 339.
53. (a) Hughey, J. L.; Fawcett, T. G.; Rudich, S. M.; Lalancette, R. A.; Potenza, J. A.; Schugar, H. *J. Am. Chem. Soc.* **1979**, *101*, 2617. (b) Bernhardt, P. V.; Bramley, R.; Engelhardt, L. M.; Harrowfield, J. M.; Hockless, D. C. R.; Korybut-Daskiewicz, B. R.; Krausz, E. R.; Morgan, T.; Sargeson, A. M.; Skelton, B. W.; White, A. H. *Inorg. Chem.* **1995**, *34*, 3589. (c) John, E.; Bharadwaj, P. K.; Potenza, J. A.; Schugar, H. *J. Inorg. Chem.* **1986**, *25*, 3065. (d) Matted, R.; Voet, U.Z. *Naturforsch. B., Chem. Sci.* **1999**, 321.
54. (a) DeSimone, R. E.; Blinn, E. L.; Mucker, K. F. *Inorg. Nuclear Chem. Lett.* **1980**, *16*, 23. (b) Kong, D.; Qin, C.; Meng, L.; Xie, Y. *Bioorg. Med. Chem. Lett.* **1999**, *9*, 1087. (c) Jin, X.; Jiang, Y.; Zhang, S. *Jiegou Huaxue (Chin.)* **1992**, *11*, 343. (d) Dapporto, P.; Fusi, V.; Micheloni, M.; Palma, P.; Paoli, P.; Pontellini, R. *Inorg. Chim. Acta.* **1998**, *275*, 168. (e) Brunner, U.; Neuburger, M.; Zehnder, M.; Kaden, T. A. *Supramol. Chem.* **1993**, *2*, 103. (f) Bu, X.; Chen, W.; Fang, Y.; Lu, S.; Wang, C.; Zhang, R. *Acta. Chem. Scand.* **1998**, *52*, 813. (g) Yeung, W.; Wong, W.; Zuo, J.; Lau, T. *J. Chem. Soc. Dalton Trans.* **2000**, 629. (h) Lu, T. -H.; Lin, J.-L.; Liao, W.-J.; Chung, C. -S. *Acta. Crystallogr.* **1997**, *C53*, 1598. (i) Clay, R.; Murrar-Rust, P.; Murray-Rust, J. *Acta. Crystallogr.* **1979**, *C35*, 1894. (j) Bazzicalupi, C.; Bencini, A.; Bianchi, A.; Fusi, V.; Giorgi, C.; Paoletti, B.; Valtancoli, B. *Acta. Crystallogr. J. Chem. Soc. Dalton Trans.* **1994**, 3581. (k) Antipin, M. Y.; Baranov, A. P.; Kabachnik, M. I.; Pisareva, S. A.; Polikarpov, Y. M.; Sinyacskaya, E. I.; Struchkov, Y. T.; Tsimbal, L. B. *Heteroat. Chem.* **1996**, 229. (l) De Sousa, A. S.; Hancock, R. d.; Reibenspies, J. H. *J. Chem. Soc. Dalton Trans.* **1997**, 939. (m) Webb, R. L.; Mino, M. L.; Blinn, E. L.; Pinkerton, A. A. *Inorg. Chem.* **1993**, *32*, 1396. (n) Kong, D.; Xie, Y. *Polyhedron* **2000**, *19*, 1527. (o) Bu, X.; Cao, X.; Zhang, W.; Zhang, R.; Clifford, T. *Transition Met. Chem.* **1997**, *22*, 513. (p) Kim, S.-Y.; Jung, I.-S.; Lee, E.; Kim, J.; Sakamoto, S.; Yamaguchi, K.; Kim, K. *Angew. Chem. Int. Ed. Engl.* **2001**, *40*, 2119. (r) Sakurai, T.;

- Kobayashi, K.; Hasegawa, A.; Tsuboyama, S.; Tsboyama, K. *Acta Crystallogr.* **1982**, C38, 107. (s) Sakurai, T.; Kobayashi, K.; Masuda, H.; Tsuboyama, S.; Tsboyama, K. *Acta Crystallogr.* **1983**, C39, 334. (t) Kobayashi, K.; Sakurai, T.; Hasegawa, A.; Tsuboyama, S.; Tsboyama, K. *Acta Crystallogr.* **1982**, C38, 1154.
55. Bencini, A.; Bianchi, A.; Borselli, A.; Chimichi, S.; Ciampolini, M.; Dapporto, P.; Micheloni, M.; Nardi, N.; Paol, P.; Valtancoli, B. *Inorg. Chem.* **1990**, 29, 3282-3286.
56. (a) Riesen, A.; Zehnder, M.; Kaden, T. A. *Helv. Chim. Acta.* **1986**, 69, 2067. (b) Riesen, A.; Zehnder, M.; Kaden, T. A. *J. Chem. Soc. Chem. Commun.*, **1985**, 1336. (c) Riesen, A.; Zehnder, M.; Kaden, T. A. *Helv. Chim. Acta.* **1986**, 69, 2074. (d) Barbaro, P.; Bianchini, C.; Capannesi, G.; Luca, L. D.; Laschi, F.; Petroni, D.; Slavadori, P. A.; Vacca, A.; Vizza, F. *J. Chem. Soc. Dalton Trans.* **2002**, 2393.
57. (a) Espinosa, E.; Meyer, M.; Berard, D.; Guilard, R. *Acta Crystallogr.* **2002**, C58, m119. (b) Chapman, J.; Ferguson, G.; Gallagher, J. F.; Jennings, M. C.; Parker, D. *J. Chem. Soc. Dalton Trans.* **1992**, 345. (c) Riesen, A.; Zehnder, M.; Kaden, T. A. *Acta Crystallogr.* **1988**, C44, 1740. (d) Moi, M. K.; Yanuck, M.; Deshpande, S. V.; Hope, H.; DeNardo, S. J.; Meares, C. F. *Inorg. Chem.* **1987**, 26, 3458. (e) Helps, I. M.; Parker, D.; Chapman, J.; Ferguson, G. *J. Chem. Soc. Chem. Commun.*, **1988**, 1094. (f) Belsky, V. K.; Streltsova, N. R.; Kuzmina, E. N.; Nazarenko, A. Y. *Polyhedron* **1993**, 12, 831. (g) Bernhardt, Sharpe, P. C. *Inorg. Chem.* **2000**, 39, 2020. (h) Chen, L.; Thompson, L. K.; Bridson, J. N.; Xu, J.; Ni, S.; Guo, R. *Can. J. Chem.* **1993**, 71, 1805. (i) Choi, K.-Y.; Lee, H.-H.; Park, B.-B.; Kim, J.-H.; Kim, J.; Kim, M.-W.; Ryu, J.-W.; Suh, M.; Suh, I.-H. *Polyhedron* **2001**, 20, 2003. (j) Choi, K.-Y.; Kim, Y.-S.; Coo, G.-H.; Kim, J.-G.; Suh, I.-H. *Acta Crystallogr.* **2001**, C57, 1014. (k) Riesen, A.; Zehnder, M.; Kaden, T. A. *Acta Crystallogr.* **1988**, C44, 1740. (l) Choi, K.-Y.; Suh, I.-H.; Kim, J.-G.; Park, Y.-S.; Jeong, S.-II.; Kim, II.-K.; Hong, C.-P.; Choi, S.-N. *Polyhedron* **1999**, 18, 3013. (m) Bucher, C.; Duval, E.; Barbe, J.-M.; Verpeaux, J. -N.; Amatore, C.; Guilard, R. *C. R. Acad. Sci. Ser.IIc:Chim.* **2000**, 3, 21. (n) Studer, M.; Riesen, A.; Kaden, T. A. *Acta Crystallogr.* **1990**, C46, 741. (o) Kurosaki, H.; Bucher, C.; Espinosa, E.; Barbe, J.-M.; Guilard, R. *Inorg. Chim. Acta.* **2001**, 322, 145.
58. Kumar, K.; Tweedle, M. F.; Malley, M. F.; Gougoutas, J. Z. *Inorg. Chem.* **1995**, 34, 6472.
59. Anderson, J. C.; Welch, J. M. *Chem. Rev.* **1999**, 99, 2219-2234.
60. Sun, X.; Wuest, M.; Kovacs, Z.; Sherry, A. D.; Motekaitis, R.; Wang, Z.; Martell, A. E.; Welch, M. J.; Anderson, C. J. *JBIC*, **2003**, 8, 217-225.

61. (a) Coward, K. M.; Jones, A. C.; Steiner, A.; Bickley, J. F.; Smith, L. M.; Pemble, M. E. *J. Chem. Soc. Dalton Trans.* **2001**, 41. (b) Coward, K. M.; Jones, A. C.; Steiner, A.; Bickley, J. F.; Pemble, M. E.; Boag, N. M.; Rushworth, S. A.; Smith, L. M. *J. Mater. Chem.* **2000**, *10*, 1875. (c) Wragg, D. S.; Hix, G. B.; Morris, R. E. *J. Am. Chem. Soc.* **1998**, *120*, 6822-6823.
62. (a) Lee, B.; Moise, F.; Pennington, W. T.; Robinson, G. H. *J. Coord. Chem.* **1992**, *26*, 187-197. (b) Lee, B.; Pennington, W. T.; Robinson, G. H.; Rogers, R. D. *J. Organomet. Chem.* **1990**, *396*, 269. (c) Robinson, G. H.; Pennington, W. T.; Lee, B.; Self, M. F.; Hrcir, D. C. *Inorg. Chem.* **1990**, *30*, 809. (d) Khasnis, D. V.; Zhang, H.; Lattman, M. *Organometallics* **1992**, 3748.
63. (a) Wessels, T.; McCusker, L. B.; Ch, B.; Reinert, P.; Patarin, J. *Microporous Mesoporous Mater.* **1998**, *23*, 67. (b) Reinert, P.; Patarin, J.; Marler, B. *Eur. J. Solid state Inorg. Chem.* **1998**, *35*, 389.
64. Taylor, M. J.; Tuck, D. G.; Victoriano, L. *J. Chem. Soc. Dalton Trans.* **1981**, 928-932.
65. Riesen, A.; Kaden, T. A.; Ritter, W.; Macke, H. R. *J. Chem. Soc. Chem. Commun.* **1989**, 460-462.
66. Heppeler, A.; Froidevaux, S.; Macke, H. R. *Chem. Eur. J.* **1999**, *5*, 1974-1981.
67. (a) Clarke, E. T.; Martell, A. E. *Inorg. Chim. Acta.* **1991**, *190*, 37-46. (b) Mishra, A. K.; Chatal, J.-F. *New J. Chem.* **2001**, *25*, 336-339.
68. (a) Wainwright, K. P. *Inorg. Chem.* **1980**, *19*, 1396-1398. (b) Ramasubba, a.; Wainwright, K. P. *J. Chem. Soc., Chem. Commun.* **1982**, 277-8.
69. (a) Wong, E. H.; Weisman, G. R.; Hill, D. C.; Reed, D. P.; Rogers, M.E.; Condon, J. P.; Fagan, M. A.; Calabrese, J. C.; Lam, K. C.; Guzei, I. A.; Rheingold, A. L. *J. Am. Chem. Soc.* **2000**, *122*, 10561-10572. (b) Peng, Y., Weisman, R. W., Wong, E. H. Unpublished results.
70. Bencini, A.; Bianchi, A.; Bazzicalupi, C.; Ciampolini, M.; Fusi, V.; Michelini, M.; Nardi, N.; Paoli, P.; Valtancoli, B. *Supramol. Chem.*, **1994**, *3*, 141.
71. Miyahara, Y.; Tanaka, Y.; Amimoto, K.; Akazawa, T.; Sakuragi, T.; Kobayashi, H.; Kubota, K.; Suenaga, M.; Koyama H.; Inazu, T. *Angew. Chem., Int. Ed.*, **1999**, *38*, 956.
72. Niu, W.; Wong, E. H.; Weisman, G. R.; Lam, K.-C.; Rheingold, A. L. *Inorg. Chem. Commun.* **1999**, *2*, 361.



73. Hubin, T. J.; McCormick, J. M.; Collinson, S. R.; Alcock, N. W.; Busch, D. H. *Chem. Commun.* **1998**, 1675-1676.
74. Hubin, T. J.; McCormick, J. M.; Alcock, N. W.; Clase, H. J.; Busch, D. H. *Inorg. Chem.* **1999**, *38*, 4435-4446.
75. Hubin, T. J.; McCormick, J. M.; Collinson, S. R.; Buchalova, M.; Perkins, C. M.; Alcock, N. W.; Kahol, P. K.; Raghunathan, A.; Busch, D. H. *J. Am. Chem. Soc.* **2000**, *122*, 2512-2522.
76. Springborg, J. J. *Chem. Soc. Dalton Trans.* **2003**, 1653-1665.
77. Niu, W.; Wong, E. H.; Weisman, G. R.; Sommer, R. D.; Rheingold, A. L. *Inorg. Chem. Commun.* **2002**, *5*, 1-4.
78. Hubin, T. J.; Alcock, N. W.; Busch, D. H. *Acta. Crystallogr.* **1999**, *C55*, 1404-1406.
79. Hubin, T. J.; Alcock, N. W.; Busch, D. H. *Acta. Crystallogr.* **2000**, *C56*, 37-39.
80. Hubin, T. J.; McCormick, J. M.; Alcock, N. W.; Busch, D. H. *Inorg. Chem.* **2001**, *40*, 435-444.
81. Hubin, T. J.; Alcock, N. W.; Clase, H.; Busch, D. H. *Supramol. Chem.* **2001**, *13*, 261-276.
82. Alcock, N. W.; Clase, H.; Seib, L. L.; Busch, D. H. *Inorg. Chim. Acta* **2002**, *337*, 91-102.
83. Hubin, T. J.; McCormick, J. M.; Collinson, S. R.; Alcock, N. W.; Clase, H. J.; Busch, D. H. *Inorg. Chim. Acta* **2003**, *337*, 76-86.
84. Sun, X.; Wuest, M.; Weisman, G. R.; Wong, E. H.; Reed, D. P.; Boswell, C. A.; Motekaitis, R.; Martell, A. E.; Welch, M. J.; Anderson, C. J. *J. Med. Chem.*, **2002**, *45*, 469.
85. Busch, d. H.; Collinson, S. R.; Hubin, T. J. Catalysts and Methods for Catalytic Oxidation. WO 98/39098, Sept. 11, 1998.
86. Busch, d. H.; Collinson, S. R.; Hubin, T. J. Labeque, R.; Williams, B. K.; Johnston, J. P.; Kitko, D. J.; Burkett-St. Laurent, J. C. T. R.; Perkins, C. M. Bleach Compositions. WO 98/39406, Sept. 11, 1998.

87. Springborg, J.; Nielsen, B.; Olsen, C. E.; Søtofte, I. *J. Chem. Soc. Perkin Trans. 2*, **1999**, 2701.
88. Broge, L.; Pretzmann, U.; Nielsen, B.; Søtofte, I.; Olsen, C. E.; Springborg, J. *Inorg. Chem.* **2001**, *40*, 2323-2334.
89. Springborg, J.; Søtofte, I. *Acta. Chem. Scand.* **1997**, *51*, 357.
90. Springborg, J.; Glerup, J.; Søtofte, I. *Acta. Chem. Scand.* **1997**, *51*, 832.
91. Sanzenbacher, R.; Søtofte, I.; Springborg, J. *Acta Chem. Scand.*, **1999**, *53*, 457.
92. Broge, L.; Søtofte, I.; Olsen, C. E.; Springborg, J. *Inorg. Chem.*, **2001**, *40*, 3124.
93. Bencini, A.; Bianchi, A.; Bazzicalupi, C.; Ciampolini, M.; Dapporto, P.; Fusi, V.; Michelini, M.; Nardi, N.; Paoli, P.; Valtancoli, B. *J. Chem. Soc., Perkin Trans. 2*, **1993**, 115.
94. Bencini, A.; Bianchi, A.; Bazzicalupi, C.; Ciampolini, M.; Dapporto, P.; Fusi, V.; Michelini, M.; Nardi, N.; Paoli, P.; Valtancoli, B. *J. Chem. Soc., Perkin Trans. 2*, **1993**, 715.
95. Bencini, A.; Bianchi, A.; Borselli, A.; Ciampolini, M.; Michelini, M.; Paoli, P.; Valtancoli, B.; Dapporto, E.; Garcia-Espana, E.; Ramirez, J. A. *J. Chem. Soc., Perkin Trans. 2*, **1990**, 209.
96. Brandès, S.; Denat, F.; Lacour, S.; Rabiet, F.; Barbette, F.; Pullumbi, P.; Guillard, R. *Eur. J. Chem. Soc., Perkin Trans. 1*, **1998**, 639.
97. Brandès, S.; Lacour, S.; Denat, F.; Rabiet, F.; Barbette, F.; Pullumbi, P.; Guillard, R. *Eur. J. Org. Chem.*, **1998**, 2349.
98. Springborg, J.; Kofod, P.; Olsen, C. E.; Toftlund, H.; Søtofte, I. *Acta. Chem. Scand.* **1995**, *49*, 547.
99. Bebout, D. C.; Ehmann, D. E.; Trinidad, J. C.; Crahan, K. K. *Inorg. Chem.* **1997**, *36*, 4257-4264.100.
100. Bebout, D. C.; DeLanoy, A. E.; Ehmann, D. E.; Kastner, M. E.; Parrish, D. A.; Butcher, R. J. *Inorg. Chem.* **1998**, *37*, 2952-2959.
101. Bebout, D. C.; Bush II, J. F.; Crahan, K. K.; Kastner, M. E.; Parrish, D. A. *Inorg. Chem.* **1998**, *37*, 4641-4646.

102. Bebout, D. C.; Stokes, S. W.; Butcher, R. J. *Inorg. Chem.* **1999**, *38*, 1126-1133.
103. Bebout, D. C.; Bush II, J. F.; Crahan, K. K.; Butcher, R. J. *Inorg. Chem.* **2002**, *41*, 2529-2536.
104. Meyerstein, D. *Coord. Chem. Rev.*, **1999**, *185-186*, 141-147.
105. (a) Munakata, M.; Kitagawa, S.; Yagi, F. *Inorg. Chem.* **1986**, *25*, 964-970. (b) Ratilainen, J.; Airola, K.; Kolehmainen, E.; Rissanen, K. *Chem. Ber.* **1997**, *130*, 1353-1359. (c) Franklin, G. W.; Riley, D.; Neumann, W. L. *Coord. Chem. Rev.*, **1998**, *174*, 133-146. (d) Sanchiz, J.; Esparza, P.; Dominguez, S.; Mederos, A.; Saysell, D.; Sanchez, A.; Ruano, R.; Arrieta, J. M. *J. Chem. Soc. Dalton Trans.* **2001**, 1559-1565. (e) Summers, M. *Coord. Chem. Rev.*, **1988**, *86*, 43-134.
106. Darensbourg, D. J.; Niezgodna, S. A.; Holtcamp, M. W.; Draper, J. D.; Reibenspies, J. H. *Inorg. Chem.* **1997**, *36*, 2426-2432.
107. Rodesiler, P. F.; Turner, R. W.; Charles, N. G.; Griffith, E. A. H.; Amma, E. L. *Inorg. Chem.* **1984**, *23*, 999-1004.
108. Dale, J. In *Topics in Stereochemistry*; Alliger, N. L., Eliel, E. L., Eds.; Wiley-Interscience: New York, 1976; Vol. 9, pp 199-270.
109. Silver, G. C.; Gantzel, P.; Trogler, W. C. *Inorg. Chem.* **1995**, *34*, 2487-2489.
110. Follner, H. *Z. Anorg. Allg. Chem.* **1972**, *387*, 43.
111. Muller, B.; Ruf, M.; Vahrenkamp, H. *Z. Angew. Chem., Int. Ed. Engl.* **1994**, *33*, 2089.
112. Vahrenkamp, H. *Acc. Chem. Res.* **1999**, *32*, 589-596.
113. Chen, X.-M.; Yao, Y.-X.; Xu, Z.-T.; Shi, K. P.; Xu, Y.-J. *Polyhedron* **1995**, *14*, 1195.
114. (a) Sekutof, A.; D. G.; Stucky, G. D. *Inorg. Chem.* **1975**, *14*, 2192. (b) Cotton, F. A.; Duraj, S. A.; Extine, M. W.; Lewis, G. E.; Roth, W. J.; Schmulbach, C. D.; Schwotzer, W. *Chem. Commun.* **1983**, 1377. (c) Ivakina, L. V.; Bel'skii, V. K.; Strel'sova, N. R.; Storozhenko, P. A.; Bulychev, B. N. *Zh. Strukt. Khim. (Russ. J. Struct. Chem.)* **1989**, *30*, 161-163. (d) Bel'sky, V. K.; Strel'tsova, N. R.; Bulychev, B. M.; Storozhenko, P. A.; Ivakina, L. V.; Gorbunov, A. I. *Inorg. Chim. Acta.* **1989**, *164*, 211. (e) Doxsee, K. M.; Hagadom, J. R.; Weakley, T. J. R. *Inorg. Chem.* **1994**, *33*, 2600. (f) Bremer, J.; Wegner, R.; Krebs, B. *Z. Anorg. Allg. Chem.* **1995**, *621*, 1123.

115. Kikuchi, M.; Murata, M.; Katsube, N.; Koike, T.; Kimura, E. *J. Am. Chem. Soc.* **1999**, *121*, 5426-5436.
116. Hu, N-H.; Liu, Y.-S. *Acta Crystallogr.* **1991**, *C47*, 2324-2326.
117. Baggio, R.; Baggio, S.; Pardo, M. I.; Garland, M. T. *Acta Crystallogr.* **1996**, *C52*, 820-823.
118. (a) Strasdeit, H.; Saak, W.; Pohl, S.; Driessen, W. L.; Reedijk, J. *Inorg. Chem.* **1988**, *27*, 1557. (b) Paap, F.; Erdonmez, A.; Driessen, W. L.; Reedijk, J. *Acta Crystallogr.* **1986**, *C42*, 783. (c) Castro, J. A.; Romero, J.; Garica-Vazquez, J. A.; Macias, A.; Sousa, A.; Englert, U. *Acta Crystallogr.* **1994**, *C50*, 369. (d) Wang, H.; Xiong, R.; Chen, H.; Huang, X.; You, X. *Acta Crystallogr.* **1996**, *C52*, 1658.
119. Ratilainen, J.; Airola, K.; Frohlich, R.; Nieger, M.; Rissanen, K. *Polyhedron* **1999**, *18*, 2265.
120. Strasdeit, H.; Pohl, S. *Z. Naturforsch., Teil B* **1988**, *43*, 1579.
121. (a) Bell, N. A.; Goldstein, M.; Jones, T.; Nowell, I. W. *Inorg. Chim. Acta.* **1980**, *43*, 87. (b) Gonzalez-Duarte, P.; Leiva, A.; March, R.; Pons, J.; Clegg, W.; Sloans, X.; Alvarez-Larena, A.; Piniella, J. F. *Polyhedron* **1998**, *17*, 1591. (c) Ercan, I.; Ercan, F.; Arici, C.; Atakol, O. *Acta Crystallogr.* **2002**, *C58*, m137.
122. Cotton, F. A.; Wilkinson, G. *Advanced Inorganic Chemistry (Fourth edition)*, Cooper, R. S., Ed.; Wiley-VCH Publisher, Inc; pp604-605.
123. Alcock, N. W.; Curzon, E. H.; Moore, P. J. *J. Chem. Soc. Dalton Trans.* **1984**, 2813-2820.
124. Kasselouri, S.; Garoufis, A.; Paschalidou, S.; Perlepes, S. P.; Butler, I. S.; Hadjiliadis, N. *Inorg. Chim. Acta.* **1994**, *227*, 129-136.
125. (a) Condon, J. S. M.S. Thesis, University of New Hampshire, 2002. (b) Deacon, G. B.; Phillips, R. J. *Coord. Chem. Rev.*, **1980**, *33*, 227-250.
126. Evans, O. R.; Lin, W. *Acc. Chem. Res.* **2002**, *35*, 511-522.
127. Restivo, R.; Palenik, G. J. *J. Chem. Soc. Dalton Trans.* **1972**, 341-344.
128. Willey, G. R.; Aris, D. R.; Haslop, J. V.; Erington, W. *Polyhedron* **2001**, *20*, 423-429.

129. Duan, C.; Lu, Z.; You, X.; *Trans. Metal Chem.* **1998**, *23*, 77-79.
130. Haddad, M. S.; Wilson, S. R.; Hodgson, D. J.; Hendrickson, D. N. *J. Am. Chem. Soc.* **1981**, *103*, 384-391.
131. Gomes, M. T.; Barros, C. M.; Santana-Marques, M. G.; Oliverira, J. A. *Can. J. Chem.* **1999**, *77*, 401-408.
132. Nakamoto, K. *Infrared spectra of Inorganic and Coordination Compounds*; Willey: New York, 1971, p176.
133. Lee, D., Murthy, N. N., Karlin, K. D. *Inorg. Chem.*, **1997**, *36*, 5785-5792.
134. Schneider, J. L.; Young, Jr., V. G.; Tolman, W. B. *Inorg. Chem.*, **1996**, *35*, 5410.
135. (a) Chandrasekhar, V.; Kingsley, S. *Angew. Chem., Int. Ed.*, **2000**, *39*, 2320. (b) Wilson, J. C.; Verweij, P. D.; Driessen, W. L.; Reedijk, J. *Inorg. Chim. Acta* **1992**, *192*, 219. (c) Willett, R. D. *Acta. Crystallogr.* **2001**, *E57*, m605. (d) Bukowska-Strzyzewska, M.; Maniukiewicz, W. *J. Crystallogr. Spectrosc. Res.* **1992**, *22*, 43 (e) Garland, M. T.; Grandjea, D.; Spodine, e.; Atria, A. M.; Manzur, J. *Acta. Crystallogr.* **1988**, *C44*, 1209. (f) Hatfield W. E.; ter Haar, L. W.; Olmstead, M. M.; Musker, W. K. *Inorg. Chem.* **1986**, *25*, 558.
136. Rodriguez, M.; Llobet, A.; Corbella, M.; Martell, A. E.; Reibenspies, J. *Inorg. Chem.* **1999**, *38*, 2328.
137. (a) Luneau, D.; Oshio, H.; Okawa, H.; Koikawa, M.; Kida, S. *Bull. Chem. Soc. Jpn.* **1990**, *63*, 2212. (b) Pajunen, A.; Camara, F.; Dominques-Vera, J. M.; Colacio, E. *Acta. Crystallogr.* **2000**, *C56*, e49. (c) Ackermann, J.; Meyer, F.; Kaifer, E.; Pritzkow, H. *Chem. Eur. J.* **2002**, *8*, 247. (d) Fritsky, I. O.; Ott, R.; Pritzkow, H.; Kramer, R. *Chem. Eur. J.* **2001**, *7*, 1221. (e) Fleming, J. S.; Mann, K. L. V.; Couchman, S. M.; Jeffery, J. C.; McCleverty, J. A.; Ward, M. D. *J. Chem. Soc. Dalton Trans.* **1998**, 2047. (f) Akitsu, T.; Komorita, S.; Kushi, Y.; Li, C.; Kanehisa, N.; Kai, Y. *Bull. Chem. Soc. Jpn.* **1997**, *70*, 821. (g) Mann, K. L. V.; Psillakis, E.; Jeffery, J. C.; Rees, L. H.; Harden N. M.; McCleverty, J. A.; Ward, M. D.; Gatteschi, D.; Totti, F.; Mabbs, F. E.; McInnes, E. J. L.; Riedi, P. C.; Smith, G. M. *J. Chem. Soc. Dalton Trans.* **1999**, 339. (h) Humphrey, E. R.; Mann, K. L. V.; Reeves, Z. R.; Behrendt, A.; Jeffery, J. C.; Maher, J. P.; McCleverty, J. A.; Ward, M. D. *New J. Chem.* **1999**, *23*, 417. (i) Bergerhoff, G.; Weber, R.; Cieslik, M.; Fingerhuth, M.; Lindner, J.; Padberg, H. J. *Z. Anorg. Allg. Chem.* **1999**, *625*, 1592.
138. Addison, A. W.; Rao, T.; Reedijk, J.; van Rijn, J.; Verschoor, G. C. *J. Chem. Soc. Dalton Trans.* **1984**, 1349.

139. (a) Oshio, H. *Inorg. Chem.*, **1993**, *32*, 4123. (b) Kim, J.-C.; Fettingner, J. C.; Kim, Y.-II. *Inorg. Chim. Acta* **1999**, *286*, 67.
140. (a) Lan, W.; Chung, C. *J. Chin. Chem. Soc.* **1992**, *39*, 577-582. (b) Kotek, J.; Lubal, P.; Hermann, P.; Cisarova, I.; Lukes, I.; Godula, T.; Svobodova, I.; Taborsky, P.; Havel, J. *Chem.-Eur. J.* **2003**, *9*, 233. (c) Oberholzer, M. R.; Siegfried, L. C.; Kaden, T. A. *Inorg. Chim. Acta* **1996**, *246*, 41-45. (d) Cai, H.; Kaden, T. A. *Helv. Chim. Acta* **1994**, *77*, 383-98. (e) Hertli, L.; Kaden, T. A. *Helv. Chim. Acta* **1974**, *57*, 1328. (f) Kaden, T. A. *Helv. Chim. Acta* **1970**, *53*, 617-632. (g) Margerum, D. W.; Rorabacher, D. B. Clarke, J. F. G., Jr. *Inorg. Chem.* **1963**, *2*, 667-677. (f) Cabbiness, D. K.; Margerum, D. W. *J. Am. Chem. Soc.* **1969**, *91*, 6540-6541. (h) Cabbiness, D. K.; Margerum, D. W. *J. Am. Chem. Soc.* **1970**, *92*, 2151-2153.
141. Fahrni, C. J.; O' Halloran, T. V. *J. Am. Chem. Soc.* **1999**, *121*, 1448-11458.
142. (a) [Http://www.bi.umist.ac.uk/users/mjfrbn/buffers/makebuf.asp](http://www.bi.umist.ac.uk/users/mjfrbn/buffers/makebuf.asp). (b) [Http://www.public.asu.edu/~laserweb/woodbury/classes/chm467/samplelab/SAMPLAB.html](http://www.public.asu.edu/~laserweb/woodbury/classes/chm467/samplelab/SAMPLAB.html). Checking date: 2003, June, 17.
143. Clay, R.; Murray-Rust, J.; Murray-Rust, P. *J. Chem. Soc. Dalton Trans.* **1979**, 1135.

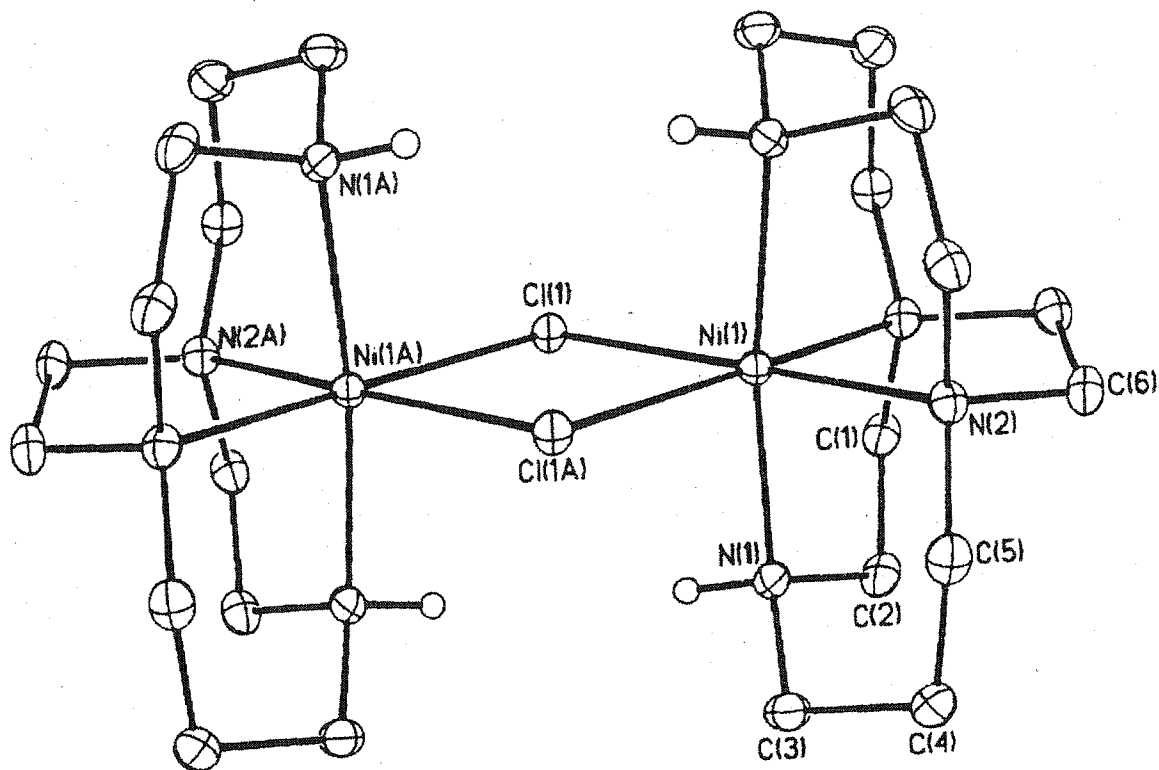
## Appendix

**Appendix Table** Selected Bond Distances (Å) and Bond Angles (deg) in  
[Ni•1(μ-Cl)]<sub>2</sub>Cl<sub>2</sub> (Hydrogen bonding interactions are included.).

---

Ni(1)-N(1)	2.090(3)	Ni(1)-N(1A)	2.090(3)
Ni(1)-N(2)	2.095(3)	Ni(1)-N(2A)	2.095(3)
Ni(1)-Cl(1)	2.4793(8)	Ni(1)-Cl(1A)	2.4793(8)
Ni(1A)-Cl(1)	2.4794(8)	H(N1)---Cl(2A)	2.27(6)
<hr/>			
N(1)-Ni(1)-N(1A)	172.67(13)	N(1)-Ni(1)-N(2A)	84.68(10)
N(1)-Ni(1)-N(2)	89.99(10)	N(1A)-Ni(1)-N(2)	84.68(10)
N(2A)-Ni(1)-N(2)	86.64(14)	N(1A)-Ni(1)-N(2A)	89.99(10)
N(1)-Ni(1)-Cl(1A)	95.24(8)	N(1A)-Ni(1)-Cl(1A)	90.24(8)
N(2A)-Ni(1)-Cl(1A)	178.25(7)	N(2)-Ni(1)-Cl(1A)	95.11(8)
Cl(1A)-Ni(1)-Cl(1)	83.15(4)	Ni(1)-Cl(1)-Ni(1A)	96.85(4)

---



**Appendix Figure** Structure of the  $[\text{Ni}(\mu\text{-Cl})\cdot\mathbf{1}]_2^{2+}$  dimer in  $[\text{Ni}(\mu\text{-Cl})\cdot\mathbf{1}]_2\text{Cl}_2$  (**167**) showing atomic labeling scheme. Hydrogens bonded to carbons are omitted for clarity.